GEOLOGICAL SURVEY OF CANADA
COMMISSION GÉOLOGIQUE DU CANADA

PAPER/ÉTUDE
90-1D

CURRENT RESEARCH, PART D
INTERIOR PLAINS AND ARCTIC CANADA

RECHERCHES EN COURS, PARTIE D
PLAINES INTÉRIEURES ET RÉGION ARCTIQUE DU CANADA

Energy, Mines and Resources Canada
Énergie, Mines et Ressources Canada

THE ENERGY OF OUR RESOURCES, THE POWER OF OUR IDEAS
L'ÉNERGIE DE NOS RESSOURCES, NOTRE FORCE CRÉATRICE

NOTICE TO LIBRARIANS AND INDEXERS

The Geological Survey's Current Research series contains many reports comparable in scope and subject matter to those appearing in scientific journals and other serials. Most contributions to Current Research include an abstract and bibliographic citation. It is hoped that these will assist you in cataloguing and indexing these reports and that this will result in a still wider dissemination of the results of the Geological Survey's research activities.

AVIS AUX BIBLIOTHÉCAIRES ET PRÉPARATEURS D'INDEX

La série Recherches en cours de la Commission géologique paraît une fois par année; elle contient plusieurs rapports dont la portée et la nature sont comparables à ceux qui paraissent dans les revues scientifiques et autres périodiques. La plupart des articles publiés dans Recherches en cours sont accompagnés d'un résumé et d'une bibliographie, ce qui vous permettra, nous l'espérons, de cataloguer et d'indexer ces rapports, d'ou une meilleure diffusion des résultats de recherche de la Commission géologique.

GEOLOGICAL SURVEY OF CANADA
COMMISSION GÉOLOGIQUE DU CANADA
PAPER/ÉTUDE 90-1D

CURRENT RESEARCH, PART D
INTERIOR PLAINS AND ARCTIC CANADA

RECHERCHES EN COURS, PARTIE D
PLAINES INTÉRIEURES ET RÉGION ARCTIQUE DU CANADA

1990

90-05178/

© Minister of Supply and Services Canada 1990

Available in Canada through

authorized bookstore agents and other bookstores

or by mail from

Canadian Government Publishing Centre
Supply and Services Canada
Ottawa, Canada K1A 0S9

and from

Geological Survey of Canada offices:

601 Booth Street
Ottawa, Canada K1A 0E8

3303-33rd Street N.W.
Calgary, Alberta T2L 2A7

100 West Pender Street
Vancouver, British Columbia V6B 1R8

A deposit copy of this publication is also available
for reference in public libraries across Canada

Cat. No. M44-90/1D
ISBN 0-660-55685-5

Cover Photo
For description see
Fig. 3 p. 59

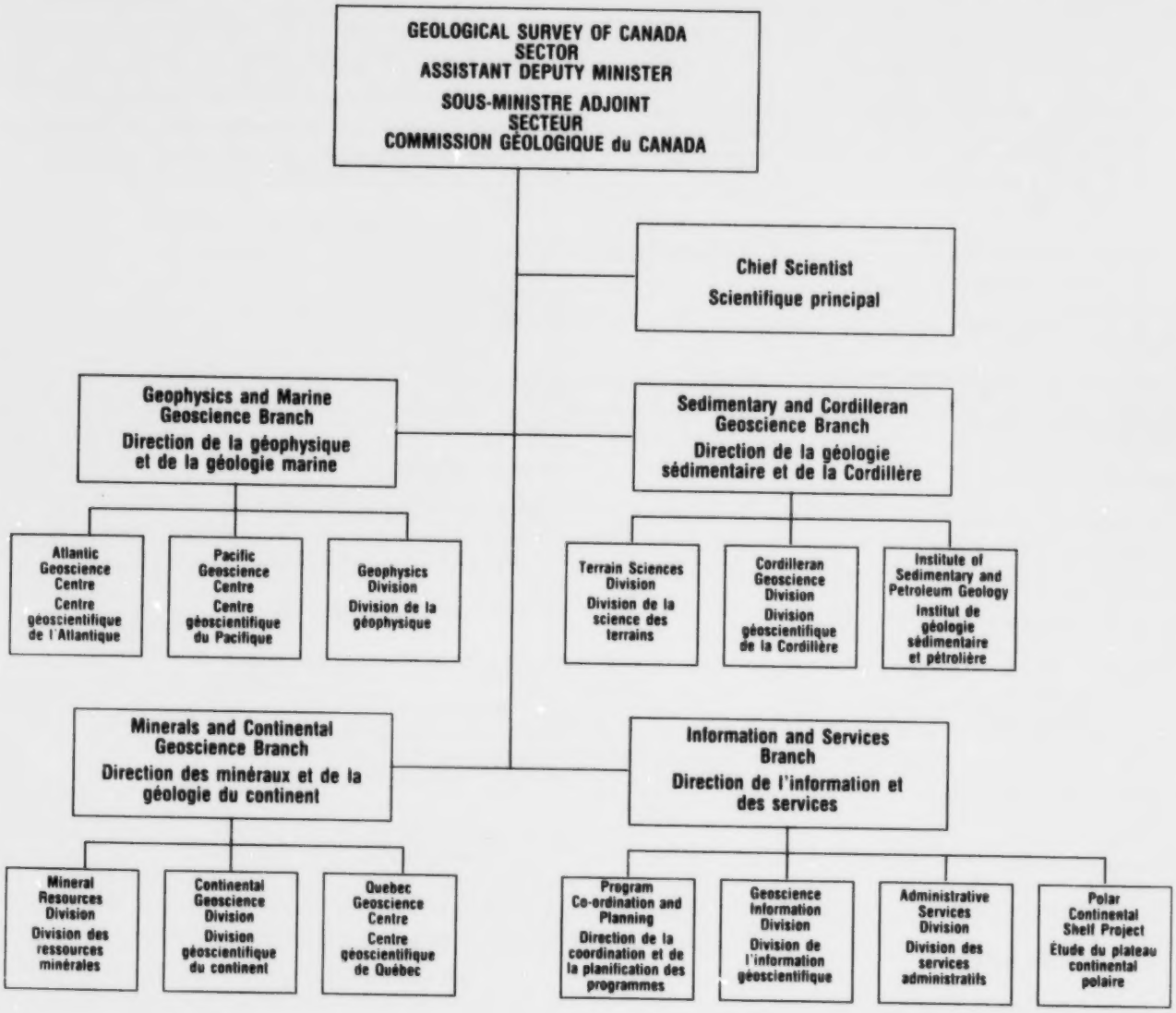
GEOLOGICAL SURVEY OF CANADA
SECTOR
ASSISTANT DEPUTY MINISTER
SOUS-MINISTRE ADJOINT
SECTEUR
COMMISSION GÉOLOGIQUE du CANADA
Chief Scientist
Scientifique principal
Geophysics and Marine Geoscience Branch
Direction de la géophysique et de la géologie marine
Sedimentary and Cordilleran Geoscience Branch
Direction de la géologie sédimentaire et de la Cordillère
Atlantic Geoscience Centre
Centre géoscientifique de l'Atlantique
Pacific Geoscience Centre
Centre géoscientifique du Pacifique
Geophysics Division
Division de la géophysique
Terrain Sciences Division
Division de la science des terrains
Cordilleran Geoscience Division
Division géoscientifique de la Cordillère
Institute of Sedimentary and Petroleum Geology
Institut de géologie sédimentaire et pétrolière
Minerals and Continental Geoscience Branch
Direction des minéraux et de la géologie du continent
Information and Services Branch
Direction de l'information et des services
Mineral Resources Division
Division des ressources minérales
Continental Geoscience Division
Division géoscientifique du continent
Quebec Geoscience Centre
Centre géoscientifique de Québec
Program Co-ordination and Planning
Direction de la coordination et de la planification des programmes
Geoscience Information Division
Division de l'information géoscientifique
Administrative Services Division
Division des services administratifs
Polar Continental Shelf Project
Étude du plateau continental polaire

Separates

A limited number of separates of the papers that appear in this volume are available by direct request to the individual authors. The addresses of the Geological Survey of Canada offices follows:

601 Booth Street,
OTTAWA, Ontario
K1A 0E8
(FAX: 613-996-9990)

Institute of Sedimentary and Petroleum Geology,
3303-33rd Street N.W.,
CALGARY, Alberta
T2L 2A7
(FAX: 403-292-5377)

Cordilleran Division,
100 West Pender Street,
VANCOUVER, B.C.
V6B 1R8
(FAX: 604-666-1124)

Pacific Geoscience Centre
P.O. Box 6000,
9860 Saanich Road
SIDNEY, B.C.
V8L 4B2
(FAX: 604-356-6565)

Atlantic Geoscience Centre
Bedford Institute of Oceanography,
P.O. Box 1006,
DARTMOUTH, N.S.
B2Y 4A2
(FAX: 902-426-2256)

Québec Geoscience Centre
Institut national de la recherche scientifique
Complexe scientifique
2700, rue Einstein
C.P. 7500
Ste-Foy, Quebec
G1V 4C7
(FAX: 418-654-2695)

When no location accompanies an author's name in the title of a paper, the Ottawa address should be used.

Tirés à part

On peut obtenir un nombre limité de « tirés à part » des articles qui paraissent dans cette publication en s'adressant directement à chaque auteur. Les adresses des différents bureaux de la Commission géologique du Canada sont les suivantes:

601, rue Booth
OTTAWA Ontario
K1A 0E8
(facsimilé: 613-996-9990)

Institut de géologie sédimentaire et pétrolière
3303-33rd St. N.W.,
CALGARY Alberta
T2L 2A7
(facsimilé: 403-292-5377)

Division de la Cordillère
100 West Pender Street,
VANCOUVER, Colombie-Britannique
V6B 1R8
(facsimilé: 604-666-1124)

Centre géoscientifique du Pacifique
B.P. 6000,
9860 Saanich Road
SIDNEY Colombie-Britannique
V8L 4B2
(facsimilé: 604-356-6565)

Centre géoscientifique de l'Atlantique
Institut océanographique de Bedford
B.P. 1006
DARTMOUTH Nouvelle-Écosse
B2Y 4A2
(facsimilé: 902-426-2256)

Centre geoscientifique de Québec
Institut national de la recherche scientifique
Complexe scientifique
2700, rue Einstein
C.P. 7500
Ste-Foy Quebec
G1V 4C7
(facsimilé: 418-654-2695)

Lorsque l'adresse de l'auteur ne figure pas sous le titre d'un document, on doit alors utiliser l'adresse d'Ottawa.

CONTENTS

1 | R. MACNAB, J. VERHOEF, and S.P. SRIVASTAVA
A compilation of magnetic data from the Arctic and North Atlantic oceans

11 | C.D. HARDWICK, J.B. NELSON, L. THORNING, M.E. BOWER, D.L. MARCOTTE, D. FORSYTH, R. MACNAB, and D. TESKEY
Procedures and preliminary results of an aeromagnetic survey in the Lincoln Sea

17 | B.V. SANFORD and A.C. GRANT
New findings relating to the stratigraphy and structure of the Hudson Platform

31 | P.B. HOLMAN and R.L. GRASTY
An airborne gamma-ray soil survey in southern Manitoba

37 | H. QING and E. MOUNTJOY
Petrography and diagenesis of the Middle Devonian Presqu'île barrier: implications on formation of dissolution vugs and breccias at Pine Point and adjacent subsurface, District of Mackenzie

47 | R.N. RANDELL and G.M. ANDERSON
The geology of the Polaris carbonate-hosted Zu-Pb deposit, Canadian Arctic Archipelago

55 | I. MCMARTIN and D.A. ST-ONGE
Lake Wisconsinan deglaciation of the area south of Dolphin and Union Strait, northern District of Mackenzie

67 | D.A. HODGSON
Were erratics moved by glaciers or icebergs to Prince Patrick Island, western Arctic Archipelago, Northwest Territories?

71 | P.A. EGGINGTON and D.A. HODGSON
Preliminary assessment of selected drainage basins in western Fosheim Peninsula, Ellesmere Island, as sites for global change studies

79 | D.S. LEMMEN
Surficial materials associated with glacial Lake McConnell, southern District of Mackenzie

85 | M. WOO, K.L. YOUNG, and S.A. EDLUND
1989 observations of soil, vegetation, and microclimate and effects on slope hydrology, Hot Weather Creek basin, Ellesmere Island, Northwest Territories

95 | R.G. DECHESNE and E.W. MOUNTJOY
Geology of the Lucerne east-half map area, Rocky Mountain Main Ranges, Alberta and British Columbia

101 | M. SAVARD, B. BEAUCHAMP, and J. VEIZER
Petrography of silica in upper Paleozoic carbonates of the Sverdrup Basin, Canadian Arctic

111 | R. MCFARLANE and F. GOODARZI
A photoacoustic infrared spectroscopic study to determine variations of the chemical structures of samples from weathered outcrops and fresh coals from Western Canada

115 | B. BEAUCHAMP and J. LAMIRANDE
The BP Graham C-52 well and upper Paleozoic subsurface stratigraphy in the Canadian Arctic

123 | L.D. STASIUK and K.G. OSADETZ
The life cycle and phyletic affinity of *Gloeocapsomorpha prisca* Zalessky 1917 from Ordovician rocks in the Canadian Williston Basin

139 C.A. WALLACE and B. BEAUCHAMP
Field investigation of the Mount Bayley Formation, a Lower Permian evaporite in the Canadian Arctic

147 H.P. TRETTIN and G.S. NOWLAN
Middle Ordovician sedimentary and volcanic rocks at Fire Bay, Emma Fiord, northwestern Ellesmere Island

153 K.G. OSADETZ, F. GOODARZI, L.R. SNOWDON, P.W. BROOKS, and S. FAYERMAN
Winnepegosis Pinnacle Reef play in Williston Basin, Saskatchewan and North Dakota oil compositions and effects of oil-based drilling muds on exploration geochemistry

165 K.G. OSADETZ, D.E. PEARSON and L.D. STASIUK
Paleogeothermal gradients and changes in the geothermal gradient field of the Alberta Plains

179 P.H. BENHAM and E.T. BURDEN
Stratigraphy of Cretaceous-Tertiary rocks of North Bylot Trough, Bylot Island, N.W.T.

187 T. GENTZIS, F. GOODARZI, and K. LALI
Petrographic study of Upper Cretaceous brackish-water coal from Vesta Mine, east-central Alberta

195 T. GENTZIS, F. GOODARZI, and T. JERZYKIEWICZ
Petrology of the Arbour and Val d'Or coal seams at Coalspur, Alberta

201 D.N. SKIBO, K.G. OSADETZ, and F. GOODARZI
Models of organic maturation and hydrocarbon potential: application to Lougheed Island drillholes, Sverdrup Basin, Canadian Arctic Islands

213 A.D. ARKHANGELSKAYA, D.C. MCGREGOR, and J.B. RICHARDSON
Correlation of the lower Middle Devonian *Elenisporis biformis* spore subzone in Arctic Canada and the U.S.S.R.

A compilation of magnetic data from the Arctic and North Atlantic oceans

R. Macnab, J. Verhoef, and S.P. Srivastava
Atlantic Geoscience Centre

Macnab, R., Verhoef, J., and Srivastava, S.P. A compilation of magnetic data from the Arctic and North Atlantic oceans; in Current Research, Part D, Geological Survey of Canada, Paper 90-1 D, p. 1-9, 1990.

Abstract

The production of accurate magnetic anomaly maps and detailed plate reconstruction studies require good quality magnetic data. To meet these needs in the Arctic and North Atlantic oceans, a project has been initiated to assemble all available marine and aeromagnetic observations from international sources. When assembled, the data will be critically assessed, adjusted, and merged to create a coherent digital database. By late 1991, contributors should receive preliminary versions of the resulting maps, as well as copies of the final database for their prior and exclusive use. By late 1992, maps and the database should be available to the general public.

Résumé

Pour produire des cartes exactes des anomalies magnétiques et réaliser des reconstitutions détaillées des plaques, il faut disposer de bonnes données magnétiques. Pour répondre à ces besoins dans les océans Arctique et Atlantique Nord, un projet a été mis sur pied pour rassembler toutes les observations marines et aéromagnétiques recueillies par différents organismes internationaux. Ces données seront évaluées, corrigées et fusionnées dans une base de données numériques cohérente. D'ici la fin de 1991, les organismes y ayant contribué devraient recevoir des versions préliminaires des cartes produites ainsi que des exemplaires de la base de données finale qu'ils seront les premiers à utiliser de façon exclusive. Quant au grand public, il devrait avoir accès aux cartes et à la base de données avant la fin de 1992.

INTRODUCTION

A compilation of magnetic data has been initiated in order to assemble all available marine and aeromagnetic observations from international sources, and to produce a coherent digital database for the Arctic and North Atlantic oceans and adjacent continental areas.

On completion, the database will be used for the production of accurate magnetic anomaly maps; in addition, a gridded computer readable version will be publicly released. Of particular significance to the geoscientific community, the database will be an important resource for quantitative interpretations that bear on plate tectonic reconstructions, the structure and development of continental margins, and the history of seafloor spreading.

PLATE RECONSTRUCTIONS AND MAGNETIC DATA

Plate reconstructions offer a powerful method for investigating the structure and development of the Earth's crust along continental margins and over the ocean floor. In a typical reconstruction experiment, the relative positions and motions of two or more plates are modelled backward in time to close the intervening oceans, and to re-unite plate margins that were conjugate in the past.

By studying carefully the relative motions between plates and how well they fit together when rejoined, investigators can learn much about the geological and tectonic processes involved in the breakup of continents and the formation of oceanic crust. For instance: many sedimentary

Figure 1. The Arctic Ocean and North Atlantic Ocean basins. The two basins are linked tectonically, having been formed by the breakup of Pangea and the spreading apart of the Eurasian and North American plates.

basins on continental margins owe their origin and development to patterns of crustal rifting and stretching associated with continental breakup; climate, glaciation, sea level, and sedimentation were all impacted by changes in global ocean circulation that arose from the creation of new seafloor.

Plate reconstructions are based on the locations of seafloor isochrons and poles of rotation, both derived from detailed magnetic anomaly maps. Isochrons are identified by matched pairs of lineated magnetic anomalies: each pair delineates a strip of seafloor that formed along the axis of an ancient spreading centre, to be subsequently split and forced aside by new ocean floor. A pole of rotation is a property of motion over a spherical surface: the displacements of tectonic plates, and hence the locations of their poles of rotation, can be determined by analysis of patterns of transform faults that appear as offsets in seafloor magnetic lineations.

THE ARCTIC AND NORTH ATLANTIC OCEANS

The Arctic and North Atlantic oceans (Fig. 1) were created by the breakup of Pangea into the North American and Eurasian plates. The histories of the two ocean basins and their respective evolutions are therefore strongly interrelated, and cannot be explained in isolation.

The Arctic Mid Ocean Ridge and the Mid Atlantic Ridge are joined structurally through a chain of spreading centres that runs the length of the Norwegian-Greenland Sea, and across Iceland. In the eastern Arctic, the development of the Eurasian Basin and its margins is closely tied to the evolutionary history of the North Atlantic (Jackson et al., 1982). In the more poorly mapped Western Arctic, the development of Canada Basin and its margins is still conjectural (Vogt et al., 1982).

South of the Azores around 36°N, the tectonic history of the North Atlantic is complicated by the separate motions of the African plate. While this region is under intensive scientific scrutiny (Klitgord and Schouten, 1986), it is beyond the scope of the present study.

THE NEED FOR A BETTER DATABASE

Recent work focusing on the continental margin and seafloor off eastern Canada has demonstrated the importance of a good quality magnetic database in order to carry out detailed and accurate interpretations (Srivastava et al., 1988a, 1988b; Verhoef et al., 1989). To lend itself to rigorous analysis, the database needs to be accurate, coherent, and well distributed. Unfortunately, such a database does not exist for the whole of the Arctic and North Atlantic oceans: while the magnetic field has been mapped to varying degrees of quality and densities of coverage in many areas, all the available observations have never been assembled and organized in a critical scientific fashion to produce a uniform body of information with known properties.

The primary reason for the database project, therefore, is to develop an important and much-needed resource for scientific analysis and interpretation. A secondary reason is to create a focal point for international investigators who are interested in the tectonic problems of the Arctic and North Atlantic oceans, and for whom the exchange of data can provide both an opportunity and an incentive to trade scientific ideas.

BACKGROUND TO THE COMPILATION PROJECT

In many respects, the project is an outgrowth of a recent undertaking to prepare a digital database of magnetic observations on the continental margin of Eastern Canada (Verhoef and Macnab, 1987). During that activity, many data handling procedures and software tools were developed and refined for the efficient manipulation, display, and analysis of large digital data sets.

The project assembled nearly three million data points collected on 91 cruises, as well as grids from over a dozen aeromagnetic surveys, and produced a coherent data set gridded at a spacing of 0.05° latitude and longitude. The new database covers land and marine areas of Eastern Canada from the northern limit of the Sohm Abyssal Plain to the southern Lincoln Sea (Fig. 2).

The experience gained from that project, the exposure to many potentially useful data sets outside the area of immediate interest, and the scientific spinoffs from the new database (see for example: Srivastava et al., 1988a, 1988b; Woodside and Verhoef, 1989) kindled plans to enlarge the compilation activity to include all of the North Atlantic Ocean, the Arctic Ocean, and adjacent continental areas. An added incentive was the existence of a comparable compilation of magnetic data from a large area in the eastern Atlantic (Verhoef et al., 1986).

Accordingly, an announcement was prepared and widely circulated throughout the international geophysical community, explaining the rationale for the enlarged compilation project and spelling out the procedures to be followed (Macnab et al., 1988). Also, individuals and organizations were invited to participate by contributing data, or by getting directly involved in different aspects of the data handling process.

To promote participation from as broad a sector of the community as possible, several benefits to participants were identified: among others, these included significant opportunities for exchanges with other scientists who share similar interests, as well as prior and exclusive use of the new database and the preliminary magnetic anomaly maps.

The response to this invitation has been encouraging: so far, 20 organizations in 11 countries (see Table 1) have provided or offered data. Most data assembled so far have come directly from contributing organizations, with the remainder provided from the archives of data distribution centres.

Figure 2. Distribution of marine magnetic data points assembled for the compilation of magnetic data over the continental margin of eastern Canada.

METHODOLOGY

As outlined in Figure 3, there are four phases to the compilation project:

Phase 1 Data acquisition and cataloguing;

Phase 2 Editing and correcting of individual data sets;

Phase 3 Gridding and merging of all data sets, with application of further refinements to the final grid;

Phase 4 Reporting, map production, and data dissemination.

The individual boxes in Figure 3 represent separate tasks that require different procedures and software tools; except for Phase 1, all were developed and tested during the earlier compilation project over the continental margin of eastern Canada; they have been described in some detail by Macnab et al. (1987), and by Verhoef and Macnab (1987).

Phase 1 activities have necessitated the development of improved methods for cataloguing and managing the large amounts of digital data that are involved. Essentially, the approach entails the use of the ORACLE database management system to create and maintain an on-line **index** of data sets (the data sets themselves are too voluminous to store on line). Controlled by a series of search filters, the retrieval process extracts descriptions of the data sets that match requirements, and initiates a procedure for fetching the appropriate files from off-line storage. For more information on the data management aspects of the compilation project, see Verhoef et al. (1990).

Depending on how they were provided by project contributors, individual data sets may be in one of two forms in Phase 2: grids, or time series of observations along ship tracks or aircraft flight lines. In time series form, each data set typically refers to a single marine or aeromagnetic survey; in grid form, a data set may represent a compilation of several surveys. Individual data sets are assessed for suitability and accuracy; this involves various display and statistical operations, followed if necessary by editing and correction.

In Phase 3, all data sets are gridded or regridded to a common matrix, using procedures and weighting functions most appropriate to the distribution and frequency content of the data. A feature of the technique permits subsequent revisions to the grid through removal or addition of individual data sets or track segments, without the necessity of reprocessing all the original data sets. This is accomplished by retaining for each mesh point the three quantities used to compute the final grid value at that point: the number of original data points within the grid cell, the summation of the weight function used in that particular gridding operation, and the summation of the values of the contributing data points multiplied by the weighting function.

Table 1. Contributing organizations

The following laboratories and institutions have provided or offered magnetic data to the compilation project:

Bullard Laboratories, Cambridge University, Cambridge, UK

Bundesanstalt fur Geowissenschaften und Rohstoffe, Hannover, Federal Republic of Germany

Centro de Geofisica da Universidade de Lisboa, Lisbon, Portugal

Geological Survey of Canada, Dartmouth and Ottawa, Canada

Grant Institute of Geology, University of Edinburgh, Edinburgh, Scotland

Gronlands Geologiske Undersogelse, Copenhagen, Denmark

IFREMER Centre de Brest, Brest, France

Institut du physique du globe de Paris, Université de Paris VI, Paris, France

Institute of Oceanographic Sciences, Wormley, UK

Lamont Doherty Geological Observatory, Palisades, USA

National Geophysical Data Center, Boulder, CO, USA

Norges Geologiske Undersokelse, Trondheim, Norway

Raunvisindastofnun Haskolans, Reykjavik, Iceland

Scripps Institution of Oceanography, La Jolla, USA

Sveriges Geologiska Undersokning, Uppsala, Sweden

U.S. Geological Survey, Woods Hole, USA

U.S. Naval Oceanographic Office, Bay St. Louis, USA

U.S. Naval Research Laboratory, Washington, USA

Vening Meinesz Laboratorium, Utrecht, The Netherlands

Woods Hole Oceanographic Institution, Woods Hole, USA

The final step in Phase 3 involves the merging of gridded data sets, with several factors considered in the choice of method: density and quality of original observations, areal coverage, levelling problems, etc. Contiguous data grids are butt-fitted, while overlapping grids may be averaged or trimmed to fit. Gaps and seams are handled through appropriate extrapolation and filtering; levelling corrections, where applied, consist of simple planar shifts, ramp functions, or adjustments to fitted surfaces. Other corrections may be applied at this time, such as decorrugation to minimize mislevelling between parallel ship tracks.

In Phase 4, the final merged grid will be used to produce preliminary coloured maps and other graphic representations of the magnetic anomaly field: selected profiles in regions of special tectonic interest, shaded relief plots, etc. All aspects of the project will be fully documented: data sources, error corrrections, filtering and gridding techniques, merging procedures, and results of statistical and spectral analyses. Organizations that have contributed data to the project will receive pre-publication copies of the magnetic anomaly maps, as well as computer-readable copies of the final gridded database. When the final maps are printed and distributed to the public, the gridded data set will be similarly released.

Interspersed with the steps outlined above, and to capitalize on their time and space distribution, the assembled data sets will be analyzed to assess the accuracy and behaviour of magnetic field models embodied in the International Geomagnetic Reference Field (IGRF). A similar study carried out during the compilation project off eastern Canada revealed deficiencies in the IGRF's modelled time-dependent components in the northwest Atlantic (Verhoef and Macnab, 1987).

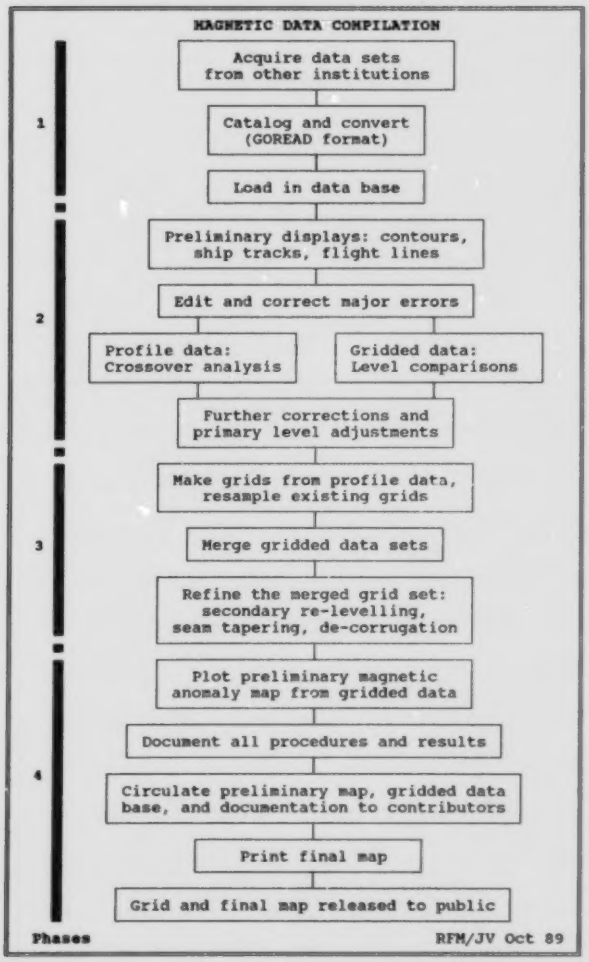

Figure 3. Principal operations in the magnetic data compilation project. The phases are discussed in the text.

PROJECT TIMETABLE

While there is considerable overlap between the two, data compilations in the Arctic and North Atlantic oceans are being handled as separate subprojects. Right from the outset, the existence of numerous data sets and partial compilations (not to mention well developed working contacts between North American and European investigators) place the North Atlantic compilation at a more advanced stage than the Arctic compilation. In the project's timing and organization, this will be reflected by a lag of six to twelve months in the Arctic compilation; this extra time will be used to identify possible new sources of Arctic data, to develop new contacts in the polar geoscientific community, and to negotiate exchanges of data.

Project milestones and projected completion dates are shown in Table 2.

Table 2. Project timetable

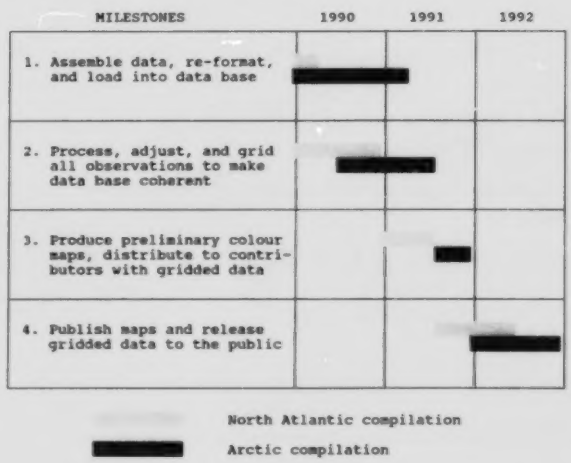

PRESENT STATUS OF THE COMPILATION PROJECT

A partial distribution of the data assembled to date for the North Atlantic compilation is shown in Figure 4, while a preliminary shaded relief map of the magnetic anomaly is shown in Figure 5. This represents an estimated accumulation of 9 000 000 marine data points, 7 000 000 aeromagnetic points, and over a dozen gridded data sets that cover areas of various sizes. A partial distribution of the Arctic data points is shown in Figure 6.

ACKNOWLEDGMENTS

This project has benefitted substantially from the contributions of many individuals and organizations. At the Atlantic Geoscience Centre, competent and enthusiastic assistance in software development and data processing is rendered by Gordon Oakey, Keh-Gong Shih, Karl Usow, and Peter Hull. Members of the Geophysical Data Centre of the Geophysics Division of the GSC have contributed data, software, computer support services, and general expertise.

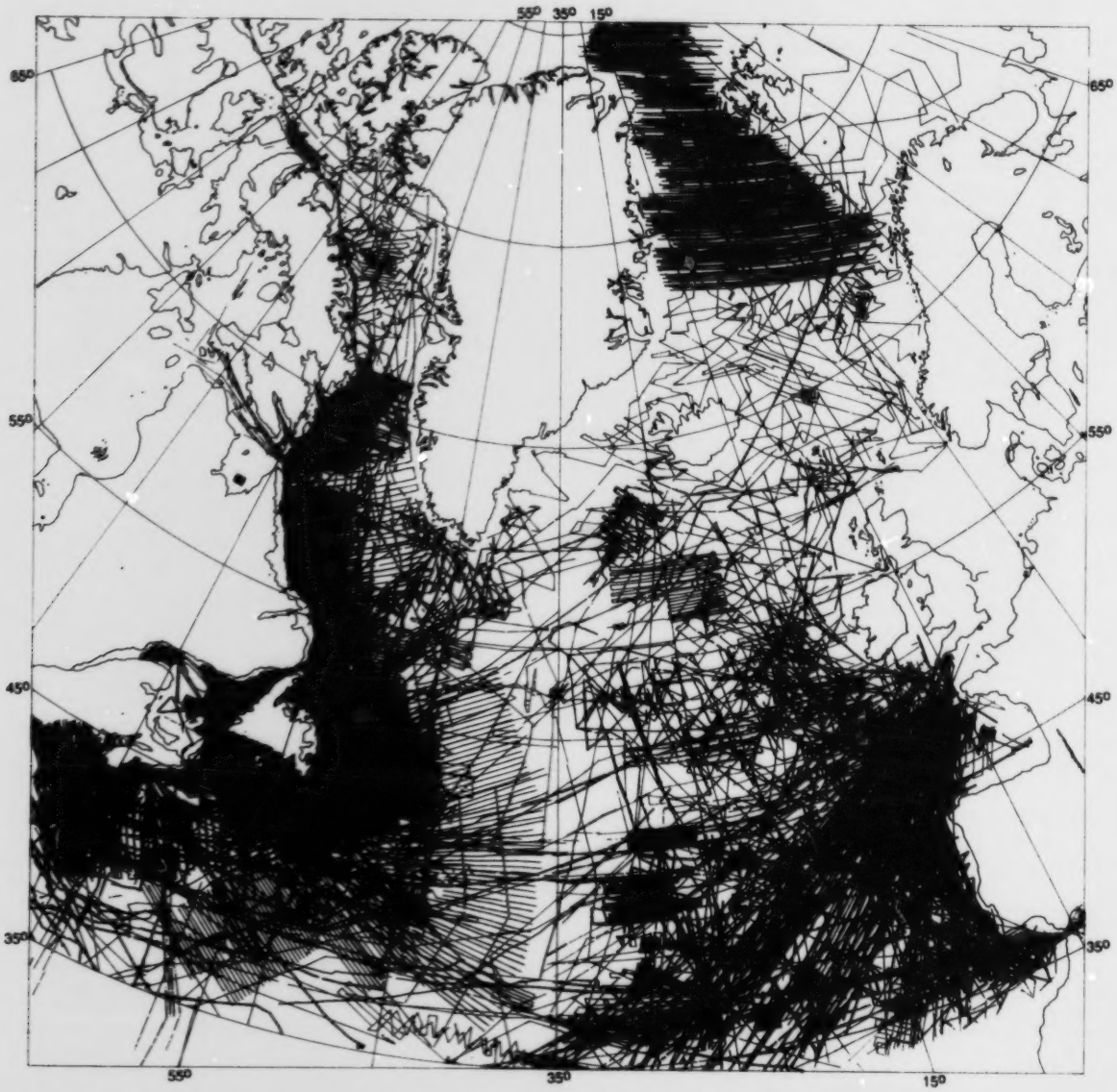

Figure 4. Partial distribution of marine and aeromagnetic data holdings currently in hand for the North Atlantic.

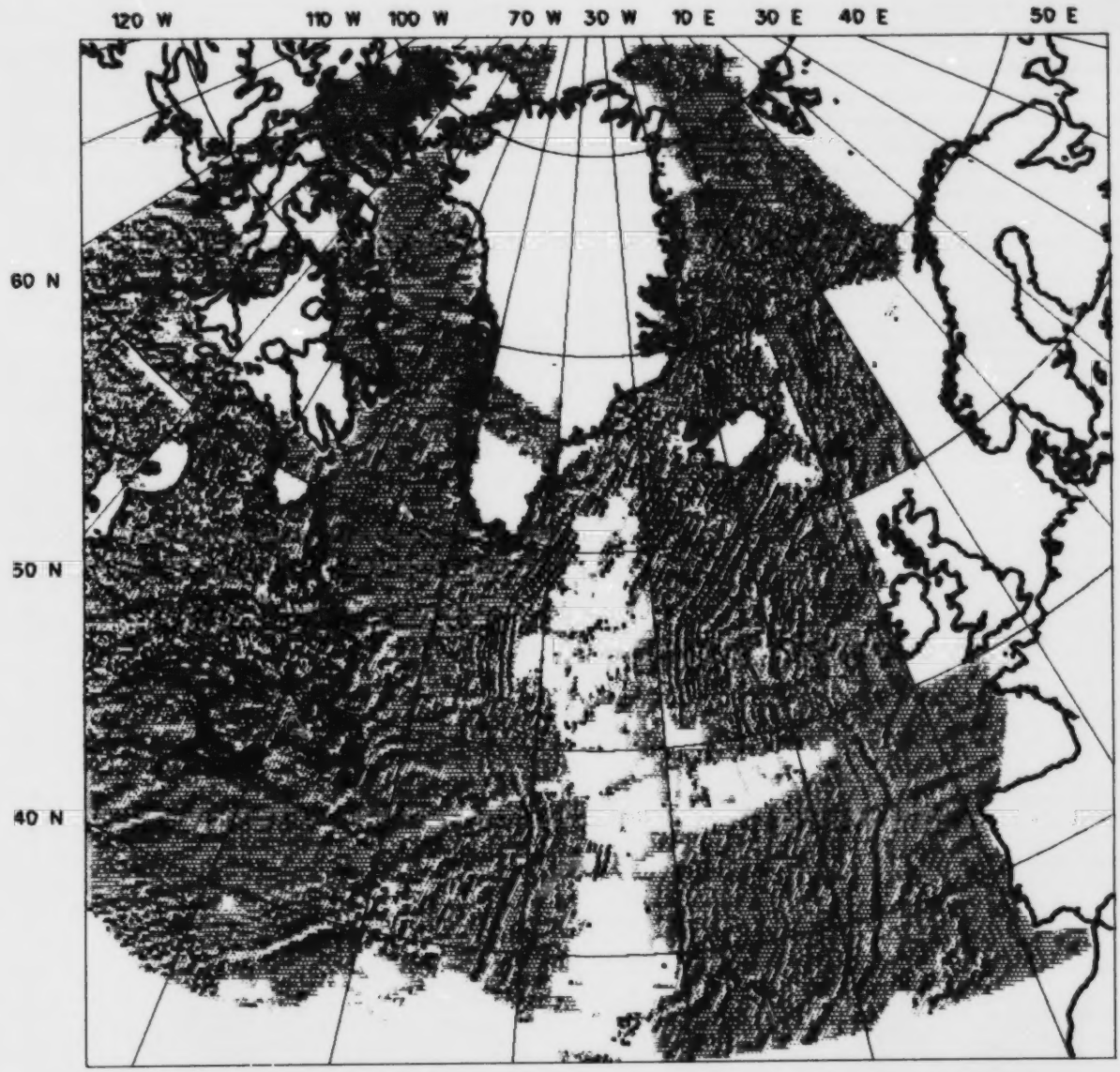

Figure 5. Preliminary shaded relief map portraying the unadjusted magnetic anomaly over the North Atlantic, illuminated from the west.

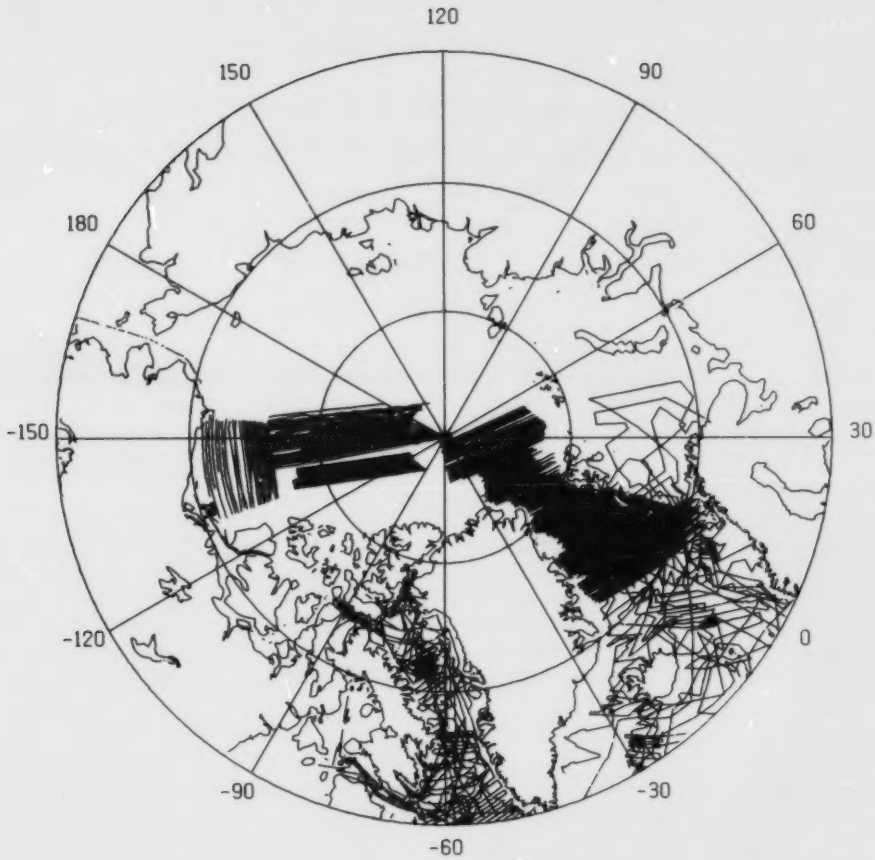

Figure 6. Partial distribution of marine and aeromagnetic data holdings currently in hand for the Arctic.

Important components of the project software were developed at the Vening Meinesz Laboratorium of the University of Utrecht. Staff and management of the external institutions listed in Table 1 have demonstrated support for the project by contributing data and by participating in useful discussions.

BIBLIOGRAPHY

Jackson, H.R., Reid, I., and Falconer, R.K.H.
1982: Crustal structure near the Arctic Mid-Ocean Ridge; Journal of Geophysical Research, v. 87, p. 1773-1783.

Klitgord, K.D. and Schouten, H.
1986: Plate kinematics of the central Atlantic; *in* The Geology of North America, Volume M, The Western North Atlantic Region, edited by P.R. Vogt and B.E. Tucholke, Geological Society of America.

Macnab, R., Verhoef, J., and Srivastava, S.P.
1988: Announcement and invitation to participate: compilation of magnetic data in the Arctic and North Atlantic oceans; unpublished circular, Atlantic Geoscience Centre, Geological Survey of Canada, 14 p.

Macnab, R., Verhoef, J., and Woodside, J.
1987: Techniques for the display and editing of marine potential field data; *in* Current Research, Part A, Geological Survey of Canada, Paper 87-1A, p. 865-875.

Srivastava, S.P., Verhoef, J., and Macnab, R.
1988a: Results from a detailed aeromagnetic survey across the northeast Newfoundland margin, Part I: Spreading anomalies and the relationship between magnetic anomalies and the ocean continent boundary; Marine and Petroleum Geology, v. 5, p. 306-323.

1988b: Results from a detailed aeromagnetic survey across the northeast Newfoundland margin, Part II: Early opening of the North Atlantic between the British Isles and Newfoundland; Marine and Petroleum Geology, v. 5, p. 324-337.

Verhoef, J. and Macnab, R.
1987: Magnetic data over the continental margin of eastern Canada: preparation of a data base and construction of a 1:5 million magnetic anomaly map; Geological Survey of Canada, Open File 1504, 95 p.

Verhoef, J., Collette, B.J., Miles, P.R., Searle, R.C., Sibuet, J.-C., and Williams, C.A.
1986: Magnetic anomalies in the northeast Atlantic Ocean (35-50°N); Marine Geophysical Researches, v. 8, p. 1-25.

Verhoef, J., Macnab, R., Oakey, G.O., Usow, K., and Hull, P.
1990: A technique for cataloguing and retrieving large sets of marine magnetic and aeromagnetic data; *in* Current Research, Part A, Geological Survey of Canada, Paper 90-1A, p. XX-YY.

Verhoef, J., Roest, W.R., and Srivastava, S.P.
1989: Plate reconstructions and gridded data: a new tool in deciphering correlations across oceans; EOS Transactions of the American Geophysical Union, v. 70, p. 609.

Vogt, P.R., Taylor, P.T., Kovacs, L.C., and Johnson, G.L.
1982: The Canada Basin: aeromagnetic constraints on structure and evolution; *in* Structure of the Arctic, edited by G.L. Johnson and J.F. Sweeney, Tectonophysics, v. 89, p. 295-336.

Woodside, J. and Verhoef, J.
1989: Geological and tectonic framework of eastern Canada as inferred from potential field imagery; Geological Survey of Canada, Paper 88-26, 33 p.

Procedures and preliminary results of an aeromagnetic survey in the Lincoln Sea

C.D. Hardwick[1], J.B. Nelson[2], L. Thorning[3], M.E. Bower[1], D.L. Marcotte[1], D. Forsyth[4], R. Macnab[5], and D. Teskey[6]

Hardwick, C.D., Nelson, J.B., Thorning, L., Bower, M.E., Marcotte, D.L., Forsyth, D., Macnab, R., and Teskey, D., Procedures and preliminary results of an aeromagnetic survey in the Lincoln Sea; in Current Research, Part D, Geological Survey of Canada, Paper 90-1 D, p. 11-16, 1990.

Abstract

In a joint project involving three Federal Government agencies and the Government of Greenland, the Convair 580 operated by the National Aeronautical Establishment collected 10 742 line kilometres of high resolution aeromagnetic data in the Lincoln Sea. With a line spacing of 4 km maintained under rigorous navigation control, the new data represent a significant improvement over the regional information that was previously available. Even with its limited coverage, the survey has permitted the accurate delineation of part of a zone of high amplitude, short wavelength anomalies in the northern Lincoln Sea.

Résumé

Dans le cadre d'un projet mixte auquel participent trois organismes du gouvernement fédéral et le gouvernement du Groenland, le Convair 580 exploité par l'Établissement national d'aéronautique a recueilli des données aéromagnétiques de haute résolution sur 10 742 kilomètres linéaires dans la mer de Lincoln. Suivant un espacement des trajectoires rigoureusement contrôlé de 4 km, les nouvelles données marquent une amélioration importante par rapport aux renseignements régionaux jusqu'à maintenant disponibles. Malgré sa couverture limitée, le levé a permis de délimiter avec exactitude une partie d'une zone d'anomalies à courte longueur d'onde et à forte amplitude dans le nord de la mer de Lincoln.

[1] National Aeronautical Establishment, Ottawa, Ont
[2] Defence Research Establishment Pacific, Victoria, BC
[3] Gronlands Geologiske Undersolgese, Copenhagen, Denmark
[4] Continental Geoscience Division, Ottawa, Ont
[5] Atlantic Geoscience Centre, Dartmouth, NS
[6] Geophysics Division, Ottawa, Ont

INTRODUCTION

A knowledge of the crustal structure of the Lincoln Sea north of Ellesmere Island and northwest Greenland is critical to understanding the development of the Alpha and Lomonosov ridges, adjustments between Ellesmere Island and Greenland, and the controversial developments along Nares Strait.

In this region, however, data have been insufficient to address the basic tectonic questions of continental breakup, ocean ridge and basin formation, and seafloor evolution. Prior to 1989, the only data consisted of widely spaced aeromagnetic lines flown over part of the area by the U.S. Navy in 1975 (Kovacs et al., 1985); while failing to resolve relationships between major tectonic features, these regional data do suggest that there is a significant zone of short wavelength, high amplitude anomalies in the Lincoln Sea. This signature is very different from that expected for the major ridges, intervening basins, and shelf areas that extend into the Lincoln Sea.

To gather data that would permit investigators to address these and other issues, a high resolution aeromagnetic survey was undertaken in May 1989 to map a portion of the Lincoln Sea (Figure 1). A total of 10 742 line kilometres were flown in an operation that combined the resources of three agencies of the Government of Canada: the Defence Research Establishment Pacific (DREP), the National Aeronautical Establishment (NAE), and the Geological Survey of Canada (GSC). A fourth agency, the Geological Survey of Greenland (GGU), provided field and data processing assistance in a related operation that yielded four low altitude transits totalling 2450 line kilometres and extending between Alert, Northwest Territories and Thule, Greenland.

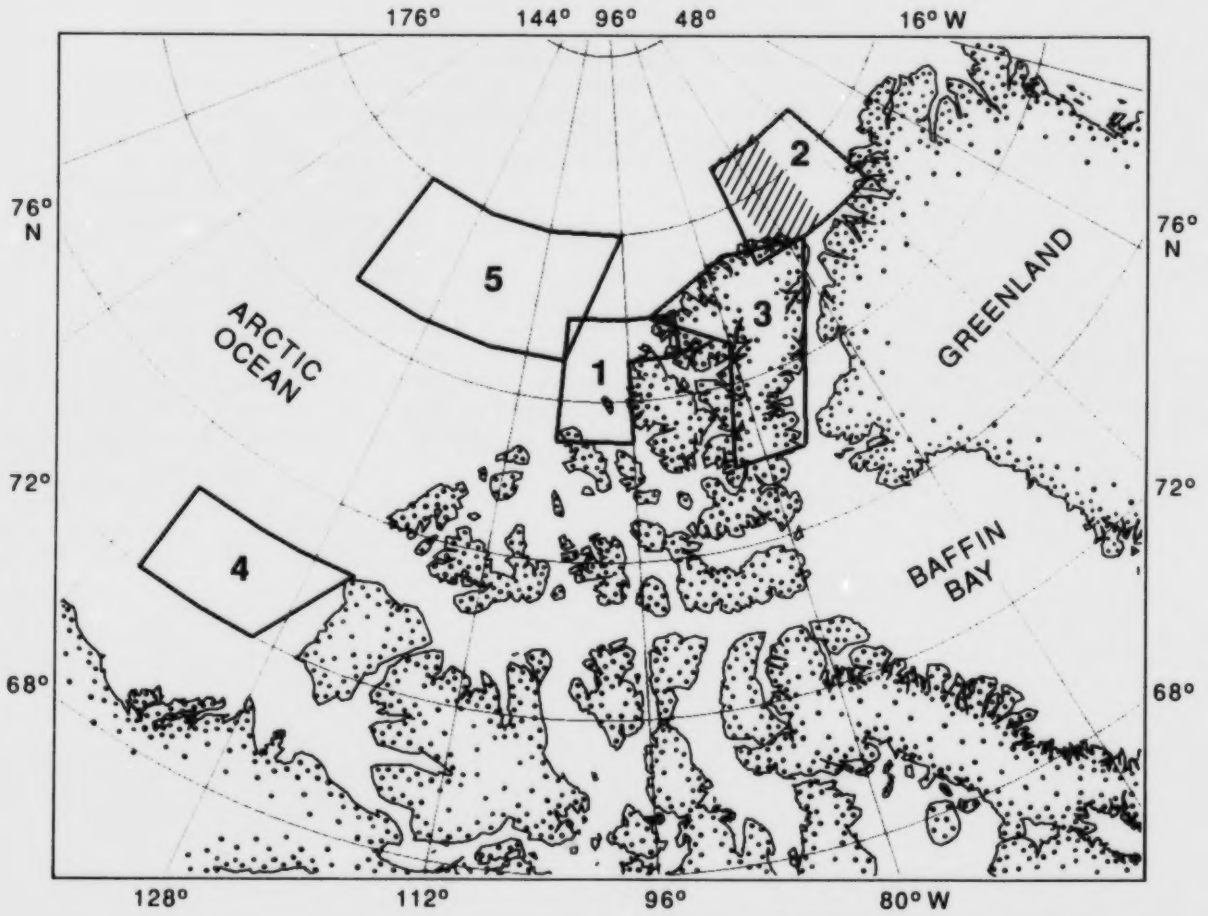

Figure 1. The location of the 1989 NAE-DREP-GSC aeromagnetic survey is shown by the stippled area. Thirty-seven lines were flown in a north-south direction at a spacing of 4 km; for most lines, aircraft height over both land and water was 305 m. Other numbered boxes in the figure outline known gaps in the aeromagnetic coverage of Canada's polar continental margin.

SURVEY INSTRUMENTATION AND PROCEDURES

The survey was carried out using the NAE Convair 580. This aircraft has an operating range of approximately 1700 km for low level surveys in the Arctic, and is equipped with specially developed navigation systems for extended over-water operations in remote areas. The main base of operation was located in Thule, Greenland, with Alert, Northwest Territories serving as a fuelling stop.

The main survey lines were flown with a spacing of 4 km in a north-south direction over a length of about 300 km, crossing known structural trends at an angle of approximately 60°. Four tie lines were flown in an east-west direction, positioned in areas of low magnetic gradient. Except for the westernmost line, aircraft height throughout the survey was held to 305 m (constant altitude over water, draped over land). The westernmost line was flown at 1981 m over land, on account of mountainous terrain. Over the sea, height was determined by radar altimeter; for the draped portions of the survey over land, barometric altitude was the primary reference, with altimeter corrections derived by radar while flying over sea ice.

Aircraft magnetic compensation was carried out in a low gradient area north of Alert at an altitude of 10 000 feet. One compensation was done at the start of the project and two on the last survey flight. Compensation manœuvres consisted of rolls and pitches covering the entire flight envelope of the aircraft, including 35° bank turns.

Navigation was done by an integrated system that combined in a real time error state Kalman filter the outputs from a Marconi Model CMA 786 GPS receiver, a Litton Model LTN91 inertial navigator, Doppler radar, a VLF/Omega receiver, and a barometric altimeter. It had been intended to use a ground-based GPS receiver to provide differential range corrections for the airborne GPS data, but as will be explained below, problems with the airborne and ground-based GPS equipment made this impossible.

Data timing was controlled by a rubidium standard, which was also used as a reference for VLF navigation. All real time navigation processing was performed on a MicroVAX 3200. Optimally estimated master positions were updated internally every 1/8 second and logged every 10 seconds. The navigation package included a guidance program that stored end points of proposed survey lines, calculated great circle routes, and displayed cross-track steering errors to the pilots. For each line that passed over land, visual "on tops" were recorded on the aircraft's video system over identifiable surface features.

The Convair was equipped with three Scintrex Model VIAW optically-pumped Cesium magnetometers, one mounted on each wingtip and one at the tip of the tail fin. With total field measured at the port wingtip, the three-sensor array produced vertical gradient and horizontal gradient data, both perpendicular and parallel to the flight path. A vector magnetometer measured dip angle and declination. Magnetic observations were logged 8 times per second on a 9-track magnetic tape transport controlled by a Perkin-Elmer 7/32 computer.

A specially-established base station at Alert consisted of a GPS receiver for differential navigation, a magnetometer for monitoring diurnal variations, and a desktop computer for instrument control and data logging. The current state of the diurnal variation was reviewed at the beginning of each day, in considering whether or not to fly on that particular day. Once airborne, survey personnel could monitor the variation through communication with the base station. Typically, the field often changed by over 100 nT during the several hours that the Convair was aloft (Fig. 2).

The Convair also performed several experiments for the Atmospheric Environment Service of the Department of the Environment, observing size and distribution of aerosol particles, measuring ozone concentration, and collecting air samples.

DATA PROCESSING

Preliminary field processing was performed with MAGIC (a package developed at DREP primarily for analysis of magnetic data) as a first look for quality control, and to identify lines that needed to be reflown. Following each day's flight, data were transferred from 9-track tape to disc on a desktop computer; subsequent reduction and inspection of the data in the form of stacked profiles were generally carried out within 24 hours of acquisition.

Preliminary post-processing at the NAE facility in Ottawa has consisted of:

a) Removal of noise spikes in the magnetic data and interpolation through occasional 4-second gaps caused by data logger errors.
b) Recompensation for certain lines. There are several reasons for this procedure: for example, in light cloud, the aircraft anti-ice system had to be operated, which caused shifts in the DC baselines of all the magnetic quantities. Different compensation coefficients had to be applied during these periods.
c) Navigation reflies, consisting of refining the real-time track calculated on the survey lines. In the navigation filter, the GPS positions were given considerable authority compared to the other navigation data. However, it turned out that the CMA-786 receivers did not perform well in the high Arctic.[1] Although the survey flights were timed to coincide with favourable satellite constellation windows, the receivers often would not converge to a solution. Usually, when they did converge, the solution appeared to be correct, but at times, the data were erroneous **with no indication** to this effect. Thus, the filter would be pushed off position. Once it became clear that this was happening, the GPS was only fed into the solution by manual intervention; also, procedures were modified to incorporate visual on-tops as supplements to the solution.

The refly task consisted of screening all GPS fixes for reasonableness, and incorporating only the good ones in the solution. At the same time, all the usable on-tops were

[1] NAE has been involved with Canadian Marconi in the flight testing of their GPS receivers for several years, and considerable effort has been expended in tuning their tracking filters.

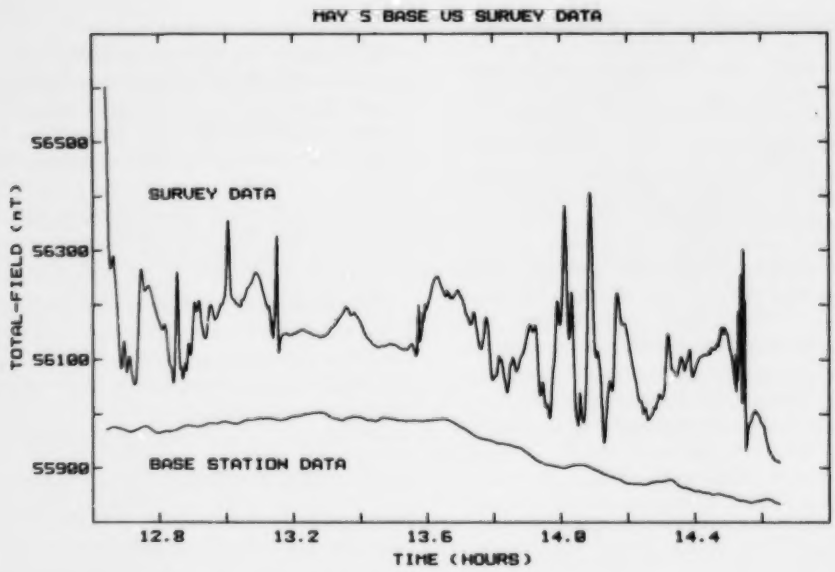

Figure 2. During the Convair's mapping flights, a stationary base magnetometer recorded the magnetic field at Alert, Northwest Territories in order to monitor disturbances caused by diurnal variation. The lower line in this plot represents the output of that base magnetometer during one particular flight; the upper line indicates the magnetic field (offset by 100 nT for clarity) observed concurrently aboard the Convair. Clearly, the variation of the magnetic field distorts the short wavelength anomalies recorded over the Lincoln Sea; the temporal disturbance appears as a long wavelength spatial feature in the total field.

included in the solution, yielding an estimated positional accuracy[2] of 81 m. The final filtered flight line should pass smoothly through the on-top points. The navigation database so generated offers the additional advantage of fine tuning certain error model parameters in the Kalman filter for future surveys.

Future processing at NAE will include use of the measured horizontal gradient to enhance the total field gridding process and possibly, in conjunction with DREP, generation of the vertical gradient from the horizontal components to compare with the directly measured vertical gradient.

Concurrent with the navigation reprocessing being carried out at NAE, the despiked magnetometer outputs were gridded and contoured at DREP to reveal severe levelling problems attributed to diurnal variations of the Earth's magnetic field. To determine corrections for the diurnal variation at Alert, readings from the base station magnetometer were averaged over the duration of the survey; the average was then subtracted from the individual observations, and the residuals so derived were subtracted from the flight line data. This first-order adjustment procedure significantly reduced the levelling problems. With improved estimates of the navigation, it is expected that the levelling problems will be further reduced. Thus, base station magnetometer observations appear to provide reliable diurnal variation corrections for data collected on offshore flights in this particular region.

Figure 3 shows a contour plot of the data after preliminary processing and correction for diurnal variations. Some depth to source analysis has been performed at DREP with MAGMOD3, the computer-fitting software obtained from GEOSOFT, Inc. For a given magnetic profile, this package models the shape of a dyke or prism to generate the theoretical anomaly that most closely matches the observed anomaly. Four groups of anomalies have been analyzed with this software, yielding the preliminary evaluations of Table 1.

[2] Final analysis of the overall accuracy is not yet complete. The "ground truth" points are the on-tops which depend on three different maps. An apparent co-ordinate offset between Greenland and Canadian maps has to be evaluated before final accuracy statistics can be derived.

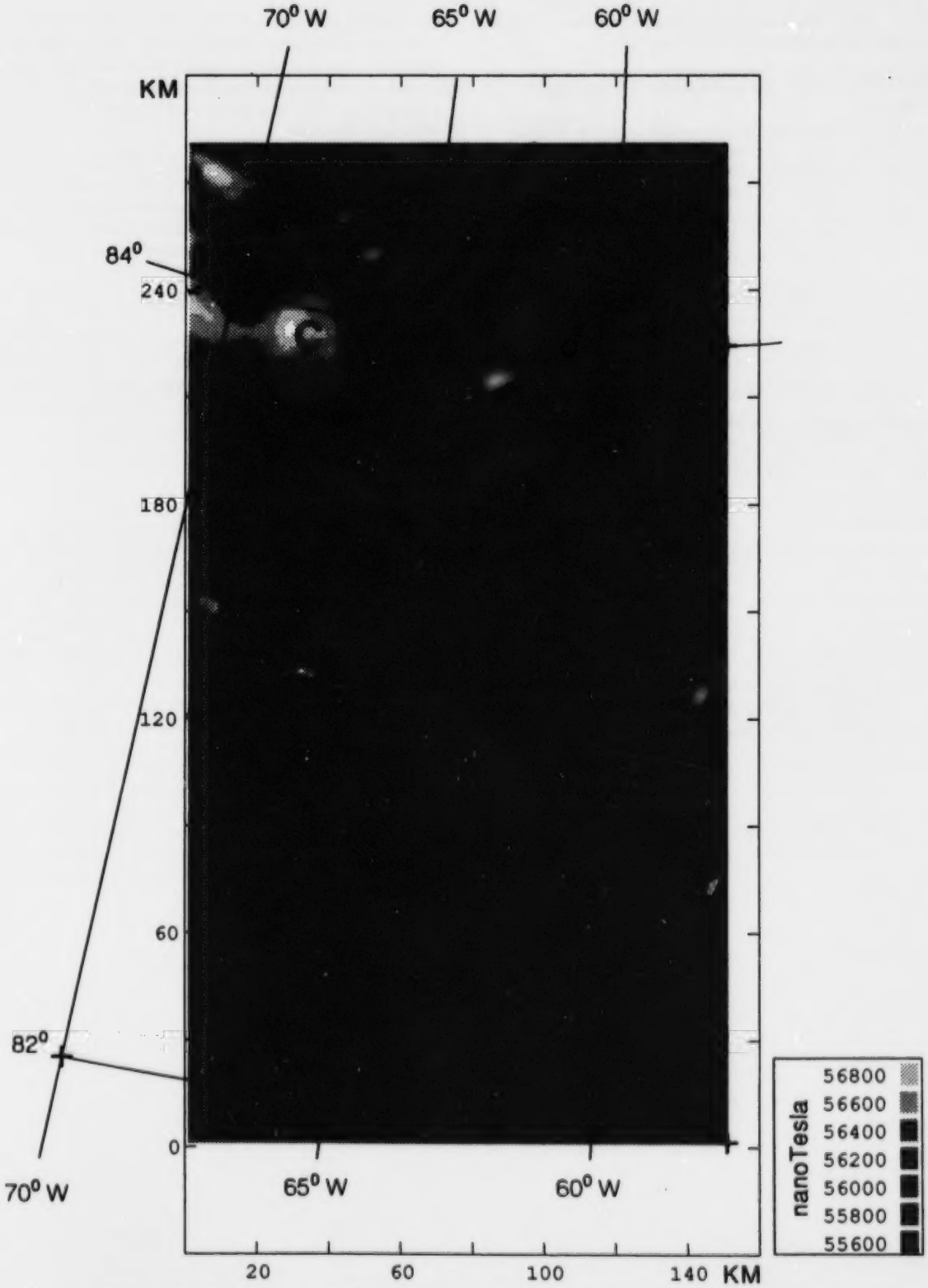

Figure 3. Contour plot of Lincoln Sea aeromagnetic survey data after preliminary processing and removal of diurnal variations (units are in nanoTesla). Labels identify anomalies used in preliminary estimates of depth to basement (see Table 1).

Table 1. Preliminary evaluation of aeromagnetic anomalies in estimating depth to source (see Fig. 3)

LOCATION (Fig. 3)	COMMENTS
A	Depth to source <400 m below sea surface. Location matches Wegener Fracture Zone (Kovacs, 1982). May be due to faulting in the magnetic basement.
B	Depth to source <500 m below sea surface. Dip = 130°-145°, k = 0.006 Caused by intrusive dykes?
C	Depth to source about 4000 m. Kovacs (1982) identified as edge of continental crust.
D	Depth to source about 1400 m below sea surface. Associated with seafloor spreading?

As with previous Convair expeditions, the final data set will be archived in the National Geophysical Data Centre operated by the Geophysics Division of the GSC.

CONCLUSIONS

The 1989 aeromagnetic data have limited coverage, but their high resolution clearly illustrates the abrupt termination of the zone of short wavelength anomalies in the northern Lincoln Sea, while showing long wavelength, low amplitude anomalies in the broad crustal transition zone off Ellesmere Island. More high resolution data are needed over the oceanic area to help determine whether the change to higher amplitude, shorter wavelength anomalies in the northern Lincoln Sea is caused by fundamental variations on oceanic or transitional crust, or by an unrecognized zone of intrusive, possibly volcanic activity. More data are also required over Ellesmere Island, which has little magnetic coverage; better mapping here would provide additional constraints for interpretations on the nature of the continent to ocean transition.

An eastward continuation of the 1989 survey is planned for 1990, in the expectation that it will provide more clues as to the nature of the sedimentary section that thickens shoreward, the role of the Greenland Plate, and the controversial structure beneath northern Nares Strait.

ACKNOWLEDGMENTS

We are indebted to the pilots and crew of the NAE Convair, who had to operate for long hours under sometimes difficult conditions. We are grateful also for the support and encouragement received from Dr. Robin Riddihough, GSC Chief Scientist.

BIBLIOGRAPHY

Kovacs, L.C.
1982: Motion along Nares Strait recorded in the Lincoln Sea: aeromagnetic evidence; *in* Nares Strait and the Drift of Greenland: A Conflict in Plate Tectonics, edited by P.R. Dawes and J.W. Kerr, Meddelelser om Gronland, Geoscience 8, p. 275-290.

Kovacs, L.C., Bernero, C., Johnson, G.L., Pilger, Jr., R.H., Srivastava, S.P., Taylor, P.T., Vink, G.E., and Vogt, P.R.
1985: Residual magnetic anomaly chart of the Arctic Ocean region; Chart MC-53, Geological Society of America, Boulder, Colorado.

New findings relating to the stratigraphy and structure of the Hudson Platform[1]

B.V. Sanford[2] and A.C. Grant[3]

Sanford, B.V. and Grant, A.C., New findings relating to the stratigraphy and structure of the Hudson Platform; in Current Research, Part D, Geological Survey of Canada, Paper 90-1D, p. 17-30, 1990.

Abstract

Marine and onshore investigations of Hudson Platform in 1985 to 1988 necessitate major revisions to the geology of this region. The new data provide better resolution of subsurface structure and areal distribution of Ordovician to Devonian rock units both onshore and offshore. New findings also include identification of Cretaceous rocks in central Hudson Bay and in the deeper channels of eastern Hudson Strait, Evans Strait, and Foxe Channel. Fieldwork on southwestern Baffin Island and subsurface studies of Hudson Bay Lowlands enabled improved lithostratigraphic classification of the Ordovician succession, and better definition of the stratigraphy and distribution of Ordovician "oil shale" units. Several new names are informally proposed for Ordovician rock units in Foxe Basin and the Akpatok Island region of Ungava Basin.

Résumé

Les recherches réalisées en mer et sur le littoral de la plate-forme d'Hudson, de 1985 à 1988, se traduiront par des révisions importantes de la géologie de cette région. Les nouvelles données donnent une meilleure résolution de la structure de subsurface et une meilleure répartition spatiale des unités rocheuses datant de l'Ordovicien au Dévonien, tant sur le littoral qu'au large. Les nouvelles données ont également permis d'identifier des roches crétacées dans le centre de la baie d'Hudson et dans les chenaux profonds de l'est du détroit d'Hudson, du détroit d'Evans et du chenal Fox. Les travaux sur le terrain dans le sud-ouest de l'île de Baffin et les études souterraines des basses terres de la baie d'Hudson ont permis d'améliorer la classification lithostratigraphique de la succession ordovicienne et de mieux définir la stratigraphie et la répartition des unités ordoviciennes de « shale pétrolifère ». Plusieurs nouveaux noms non officiels ont été proposés pour désigner les unités rocheuses d'âge ordovicien dans le bassin de Foxe et dans la région de l'île Akpatok dans le bassin d'Ungava.

---

[1] Contribution to Frontier Geoscience Program

[2] Continental Geoscience Division, Ottawa

[3] Atlantic Geoscience Centre, Dartmouth, NS

INTRODUCTION

Hudson Platform embraces some 1.5 million km^2 of Paleozoic and Mesozoic terranes. Principal onshore-offshore basinal tectonic elements are the Moose River, Hudson Bay, and Foxe basins (Fig. 1). Three aulocogen-style basins underlie eastern Hudson and Evans straits, and Foxe Channel, herein referred to as Ungava, Evans Strait, and Southampton basins respectively.

The age and lithological composition of the Paleozoic (Cambrian to Devonian) and Mesozoic (Jurassic to Cretaceous) sequences are illustrated in Figures 2, 3 and 4. Cambrian to Lower Silurian rocks are contained in Foxe Basin, and Middle to Upper Ordovician strata in the Hudson Strait-Ungava Bay segment of the platform. The oldest Paleozoic strata in Hudson Bay and Moose River basins are Late Ordovician in age, and these are succeeded by relatively complete Silurian and Devonian sequences, overlain locally by Jurassic and/or Cretaceous strata.

An orthogonal arch system oriented northeast and northwest borders and intersects the Hudson Platform (Fig. 1). Uplift of most of these elements took place near the close of the Early Silurian. Intensive vertical movements of some of the arches also occurred in the Early Devonian and again in the Early Cretaceous. Block faulting in the Cretaceous was associated with deposition of marine clastics in Ungava, Southampton, Evans Strait, and Foxe basins in a seaway that connected with Labrador Shelf to the east, and presumably with a Cretaceous seaway in the Interior Platform across the Severn Arch to the west (see Fig. 8).

This paper summarizes the more significant contributions to the geology of Hudson Platform that derive from analyses of industry and government seismic and borehole data, and onshore fieldwork in 1988. These findings include: identification of Cretaceous strata in various basins of the platform; more accurate stratigraphic definition and distribution of Ordovician "oil shale" units; informal naming of several newly defined rock units in Foxe and Ungava basins; identification of oil and gas exploration plays; and more precise mapping generally of Paleozoic and Mesozoic rock units throughout the Hudson Platform.

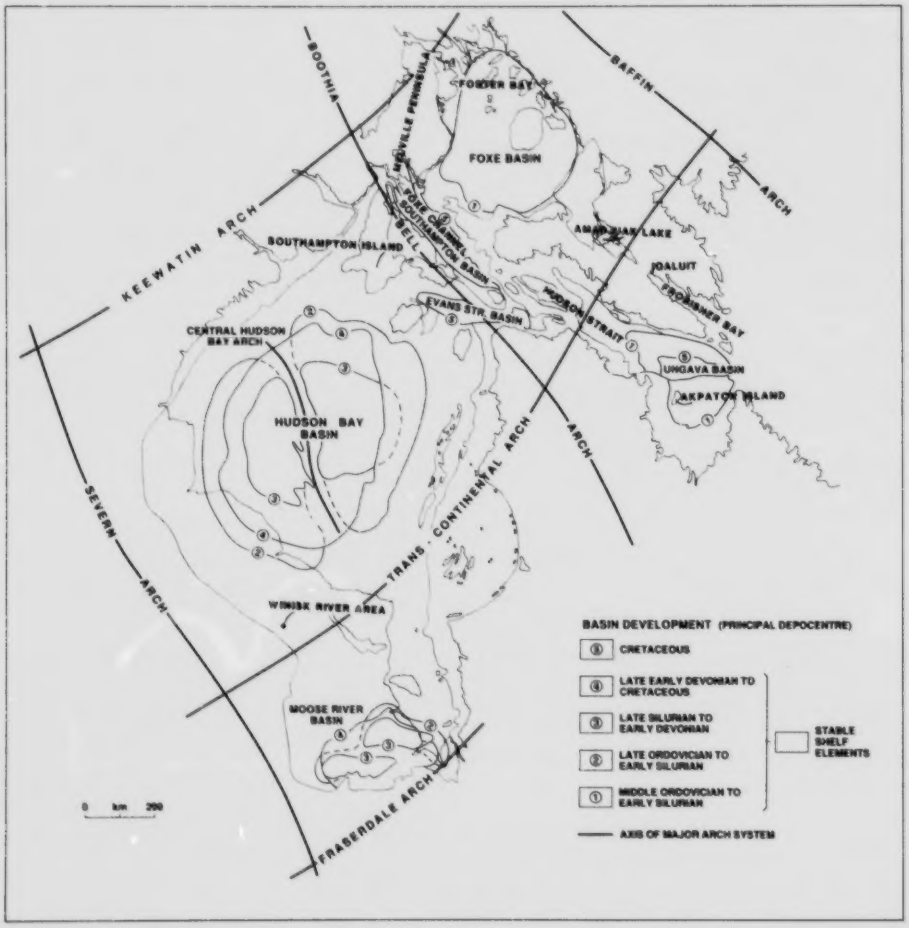

Figure 1. Index map of Hudson Platform showing tectonic elements and localities referred to in text.

REGIONAL GEOLOGY

Moose River Basin

Stratigraphic information from recent boreholes by government and industry in the Moose River Basin (R. Bezys, pers. comm., 1989) has necessitated major revision to the published geological map of the region by Sanford and Norris (1975). Some of the revisions (Fig. 4) involve changes in the distribution of Middle to Upper Devonian and Middle Jurassic to Lower Cretaceous rock units, mostly in the central part of the basin. New bathymetric data are the basis for revised mapping of Ordovician and Silurian rock units in the James Bay region. Other sources of data were Larsson and Stearn (1986), Telford and Long (1986), and Telford (1988).

Precambrian basement configuration and timing of movements beneath Moose River Basin (Fig. 1, 6) are more complex than previously thought (e.g., Wade et al., 1977). Block faulting associated with rejuvenation of the Fraserdale Arch was intensive in the Early Silurian, and segmented the region into two subbasins. Although much smaller in scale, the structural style of these movements was identical to the segmentation of Hudson Bay Basin near the close of the Early Silurian. As in Hudson Bay Basin, the deeper subbasins in Moose River Basin, once initiated, were filled by clastics and evaporites during ensuing Late Silurian to Devonian time. For the remainder of the Devonian and in the Cretaceous the basin subsided as a single tectonic entity (Fig. 1).

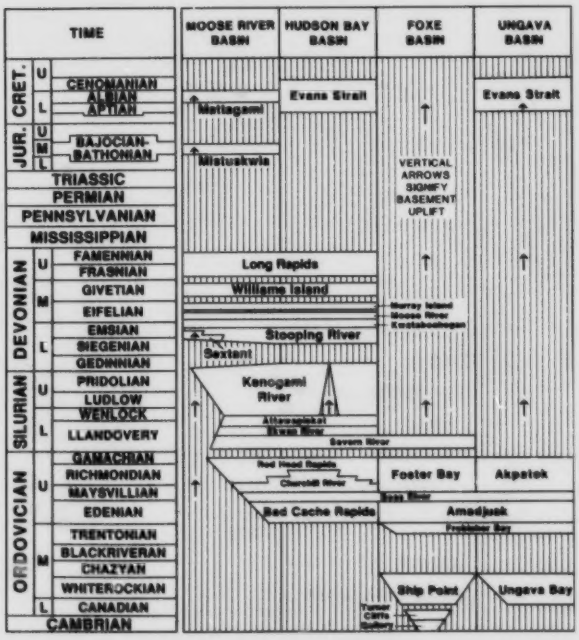

Figure 2. Time-stratigraphic framework of Paleozoic and Mesozoic sequences.

Hudson Bay Basin

Analysis of single channel seismic data and borehole data acquired in 1986 and 1987 (Grant and Sanford, 1988), in conjunction with detailed bathymetry, has enabled more definitive mapping of Phanerozoic rock units. For example, it has been possible to identify and determine the distribution, thickness, and probable composition (Fig. 4, 5, 8) of Cretaceous strata beneath central Hudson Bay. The ring-shaped distribution of these beds closely follows the Devonian Moose River Formation, and their preservation is due at least in part to structural depression in this formation caused by salt dissolution and collapse.

The Cretaceous beds, up to 150 m thick, are interpreted from seismic profiles to be sands and shales. Paleontological analysis of residue from a borehole in north-central Hudson Bay (McGregor, 1987) confirmed a Cretaceous age, more precisely defined as Aptian to Cenomanian by R.A. Fensome (pers. comm. 1989). As these beds are better developed (up to 1000 m) in nearby Evans Strait, the informal name Evans Strait formation is applied to all marine Cretaceous strata in Hudson Platform (Fig. 4, 8).

A significant new finding in Hudson Bay Basin relates to regional distribution of the Boas River Formation (oil shale) and its stratigraphic relationship with older and younger Ordovician strata (Fig. 2 - 5, 9, 11). This unit, originally identified and named by Sanford (in Heywood and Sanford, 1976; see also MacAuley, 1986; Dewing et al., 1987; McCracken and Nowlan, in press), was long thought to be confined to Southampton Island. It has now been identified in boreholes and outcrop over a much wider segment of Hudson Platform. Only a thin veneer is recognized in offshore wells on higher structural anomalies; the unit may be best developed in regionally deeper parts of the basin. The extended southward distribution of the unit is confirmed in boreholes in Hudson Bay Lowlands, particularly in the Winisk River area. Core from one of these holes (54° 30' 30" N, 87° 31' 00" W) encountered 9.8 m of black to dark brown bituminous limestone representative of the Boas River "oil shale" interval.

In the original definition of the Boas River Formation, Sanford (in Heywood and Sanford, 1976) described the exposed lower gradational contact with the Bad Cache Rapids, but assumed a disconformable contact with the overlying Churchill River Group, in the absence of the latter at the Boas River type section. Drill cores in the Winisk River area of Hudson Bay Lowlands indicate the oil shale interval is conformable and gradational with the Bad Cache Rapids below and Churchill River above. This relationship would appear to prevail elsewhere in Hudson Bay Lowlands and offshore where the Boas River Formation is recognized in the subsurface.

The thin "oil shale" interval that occurs locally near the top of the Red Head Rapids Formation on Southampton Island, as reported by Nelson and Johnson (1976), Dewing et al. (1987), and McCracken and Nowlan (1989) has not been recognized in any boreholes elsewhere in the Hudson Bay Basin.

Analysis of industry multichannel seismic data calibrated by deep stratigraphic tests has enabled more precise mapping of the fault pattern of the Central Hudson Bay Arch (Fig. 7), and more accurate assessment of the structural framework of the basin generally (Fig. 1, 5, 6); see also Dingwall (1986), Roksandic (1987), Sanford (1987) and Thorpe (1988). The timing and tectonic movements of the Central Hudson Bay Arch and corresponding basin development can be readily seen in Figures 1 and 5. The two basement tests (Netsiq and Beluga) completed in 1985, in conjunction with multichannel seismic data, indicate the presence of an arch system prior to inception of the Hudson Bay Basin. This feature underwent major rejuvenation and block faulting near the close of the Early Silurian. In response to vertical movements of the arch, sedimentation was substantially accelerated but confined to subbasins east and west of its axis. As the subbasins filled with Upper Silurian to Lower Devonian evaporites, they ceased to develop as separate tectonic entities and merged into a single basin for the remainder of Devonian time and during the Cretaceous.

The highest structural segment of the Central Hudson Bay Arch was tested by I.G.C. Sogepet et al. Netsiq N-O1 in 1985 (Fig. 5, 7). There, upper Middle Devonian Williams Island Formation rests unconformably on Lower Silurian Ekwan River Formation. The absence of Upper Silurian to lower Middle Devonian strata records the hiatus in sedimentation that prevailed on this segment of the arch following the Early Silurian orogenic episode.

In striking contrast to the boreholes on the arch, the 1985 Trillium et al. Beluga O-23 borehole in the adjacent subbasin encountered more than 800 m of halite and minor shales and carbonates of the Upper Silurian to Lower Devonian Kenogami River Formation (Fig. 5, 7). The accelerated subsidence of the peripheral subbasins during this period

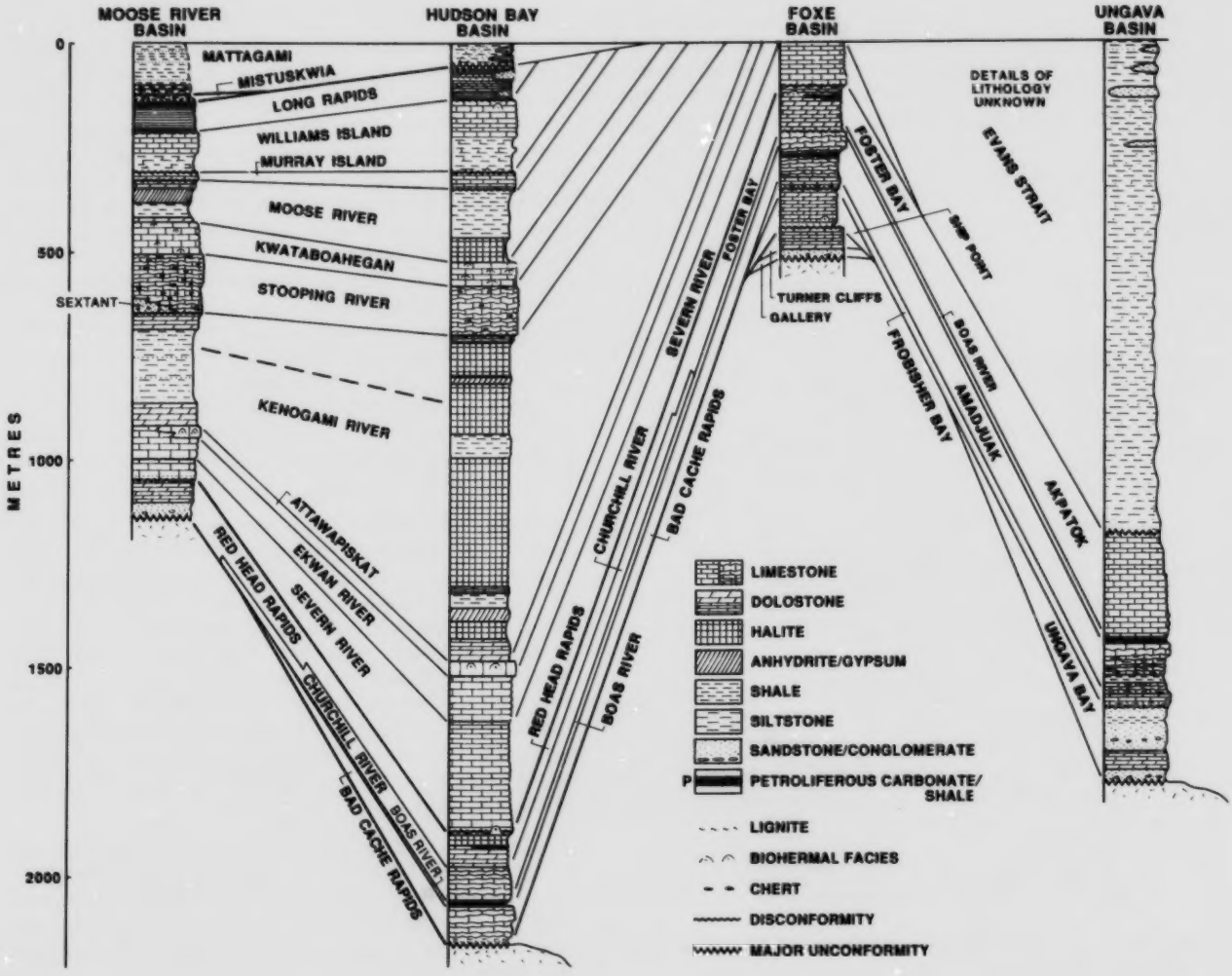

Figure 3. Lithostratigraphical framework of Paleozoic and Mesozoic sequences.

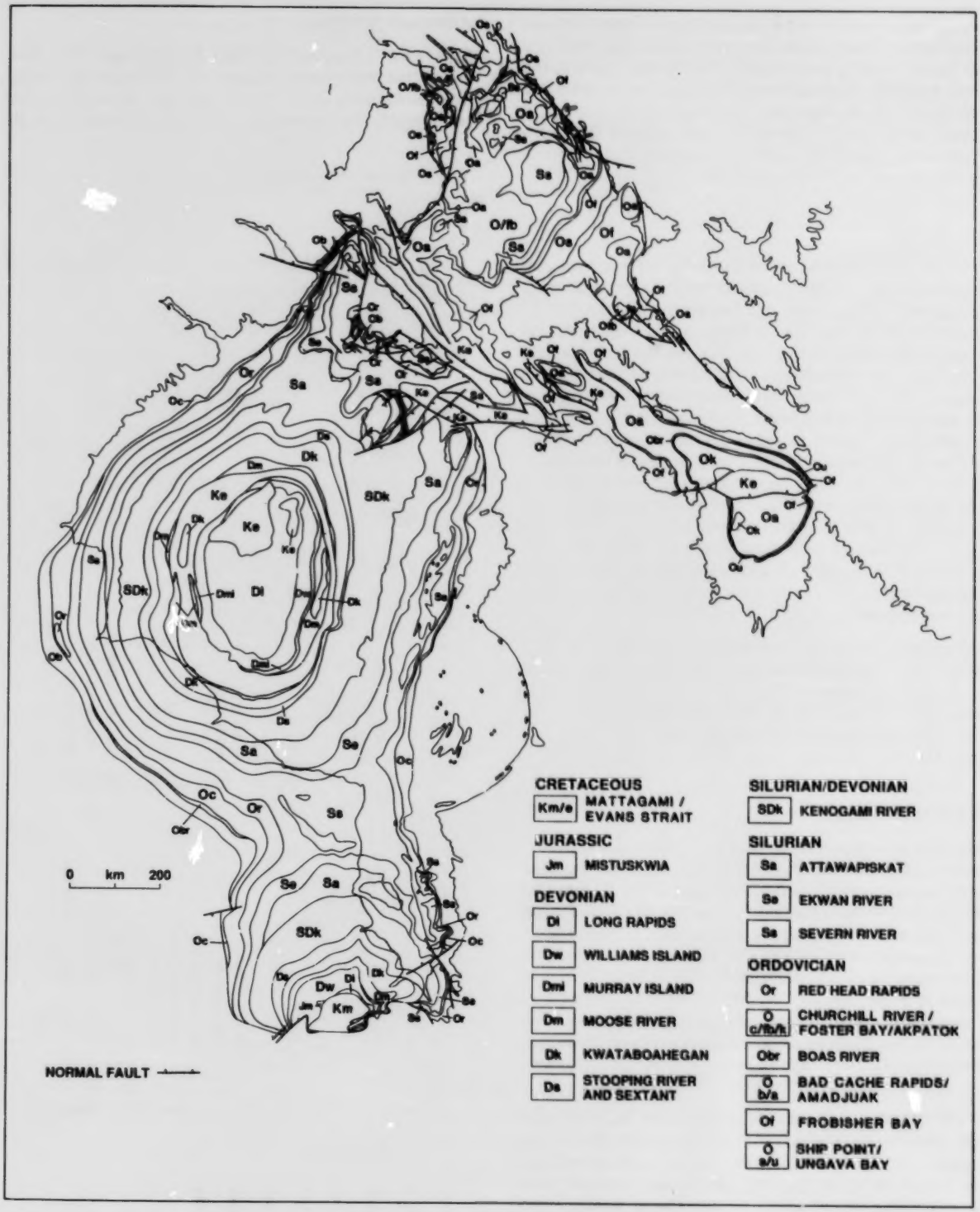

Figure 4. Geological map of Hudson Platform.

corresponds to similar rapid development of the Michigan and Allegheny basins of the western St. Lawrence Platform, and basins forming peripheral to the Boothia Arch in the Arctic Platform. Although the mechanism for the basin and arch epeirogeny is unknown, the similarity in timing and intensity of the widely separated events suggests they were in some way related to orogeny in progress along the continental margins of North America.

Foxe Basin

Cambrian and Ordovician rocks along the northern and western margins of Foxe Basin and on adjacent islands were mapped by Trettin (1975) and in part by Sanford (1977). Extrapolation of bedrock geology offshore is based on revised bathymetric contouring. The southeastern segment of the basin that extends into southwestern Baffin Island is composed of Ordovician rocks preserved in a half-graben downdropped to the southwest. This area was visited briefly in 1986 by N.J. McMillan and G. MacAulay of the Geological Survey of Canada. An important outcome of their investigation was the identification of oil shale deposits (MacAuley, 1987) within the Ordovician succession, and recognition of their hydrocarbon source rock potential. During the following field season (1987) the same area was visited by B.V. Sanford, A.C. Grant, and A. McCracken, who examined the rocks in some detail and mapped them on a reconnaissance scale.

To clarify the Ordovician stratigraphy of southwestern Baffin Island and adjacent areas of Foxe Basin, new names are informally proposed for the three rock units that stratigraphically succeed the Ship Point Formation (Fig. 2, 3, 9). The new names in ascending stratigraphic order are Frobisher Bay, Amadjuak, and Foster Bay formations.

Frobisher Bay formation

This name is proposed for 15 m of grey, thin to thick, evenly bedded limestone that disconformably succeeds the Ship Point Formation over much of Foxe Basin, but overlaps the latter in southwestern Baffin Island to lie unconformably on the Precambrian. The beds are well exposed at many localities, but are most accessible along the Jordan River some 25 km above its mouth on Frobisher Bay. The selected type section is at 63° 59' 15'' N, 69° 10' 00'' W, where 5 m of strata are exposed in a narrow gorge of the river. The beds here, and elsewhere in Foxe Basin, contain distinctive *Gonioceras* and *Labyrinthites* fauna (Bolton, 1977), indicative of a late Middle Ordovician Trentonian age.

The beds here referred to as the Frobisher Bay formation were described by Sanford (1977) as unit 1 of the Bad Cache Rapids Formation on Melville Peninsula. As these rocks are now known to be lithologically and faunally distinct from the succeeding strata, unit 1 of Bad Cache Rapids is no longer considered a valid term as applied to this region, and its use should be discontinued.

Amadjuak formation

This name is proposed for the limestones and shaly limestones that conformably succeed the Frobisher Bay formation throughout Foxe Basin, and are in turn overlain conformably by bituminous and reefy limestones of the

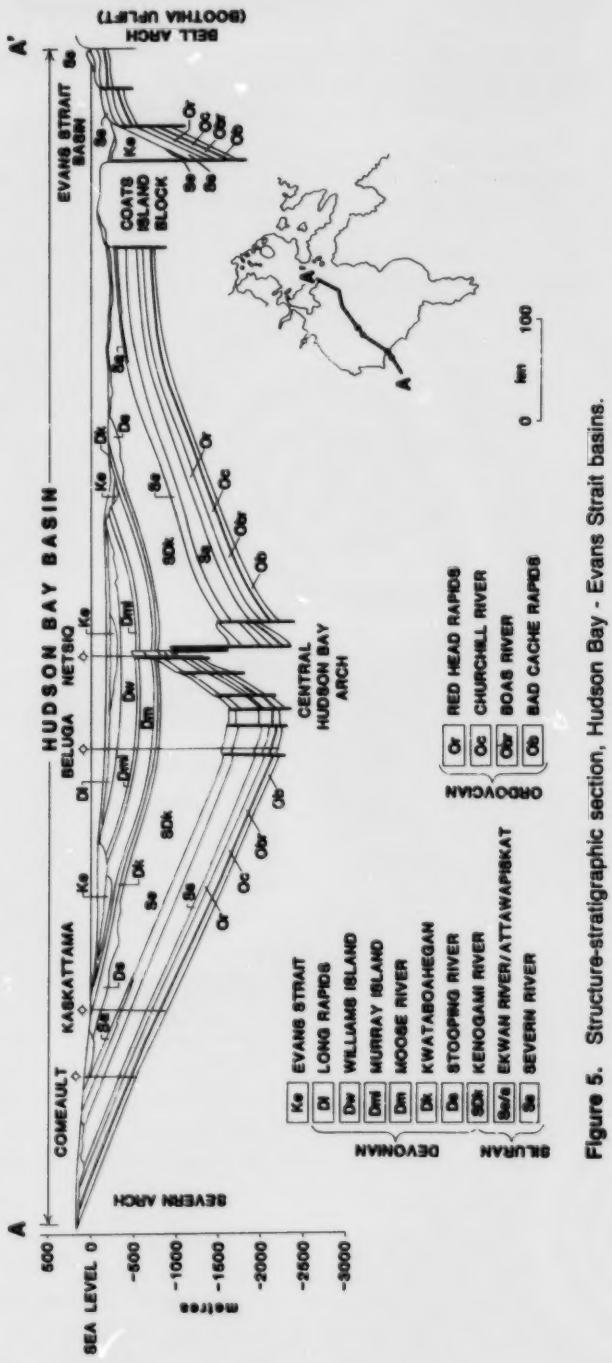

Figure 5. Structure-stratigraphic section, Hudson Bay - Evans Strait basins.

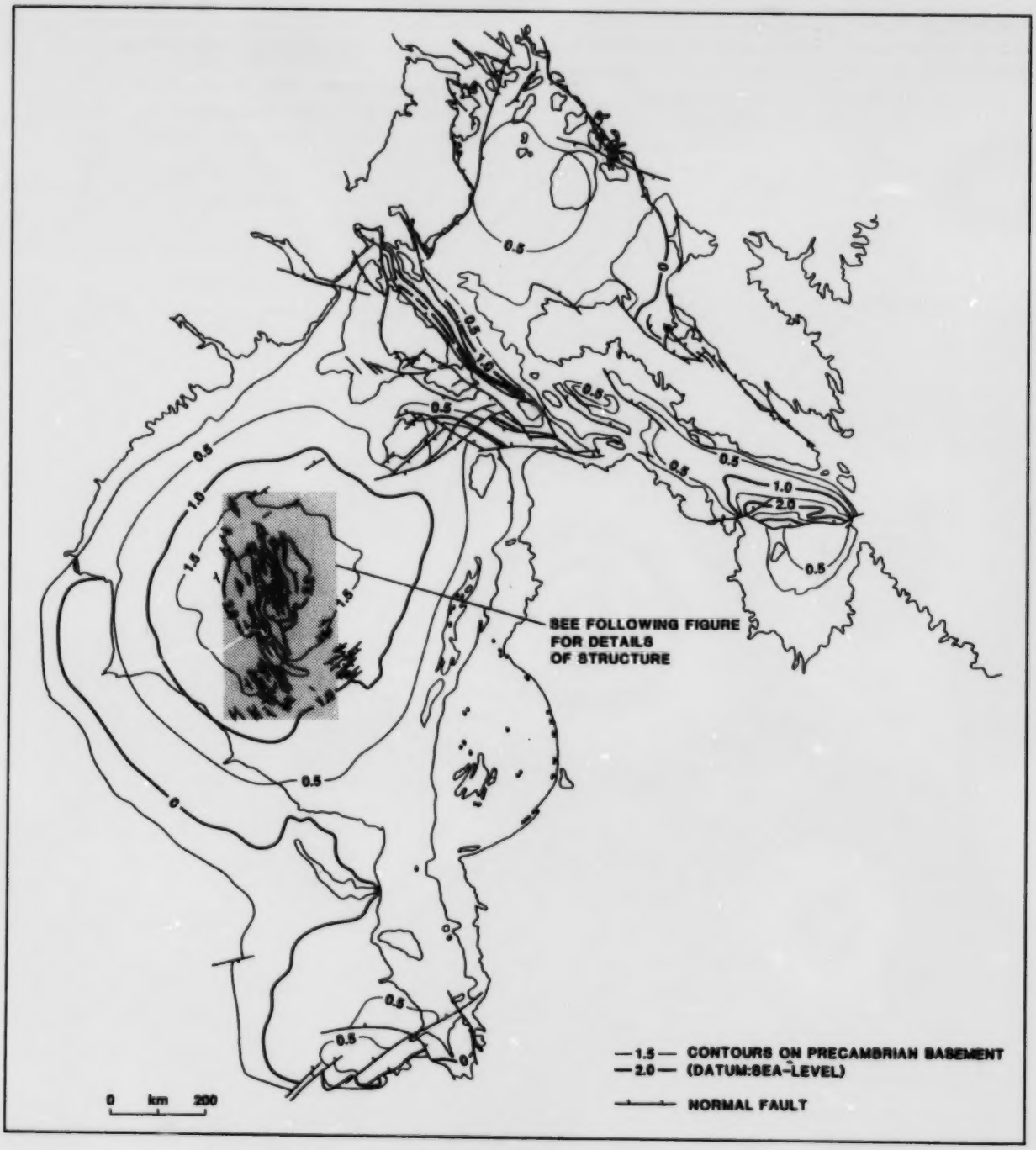

Figure 6. Regional structural framework of Hudson Platform.

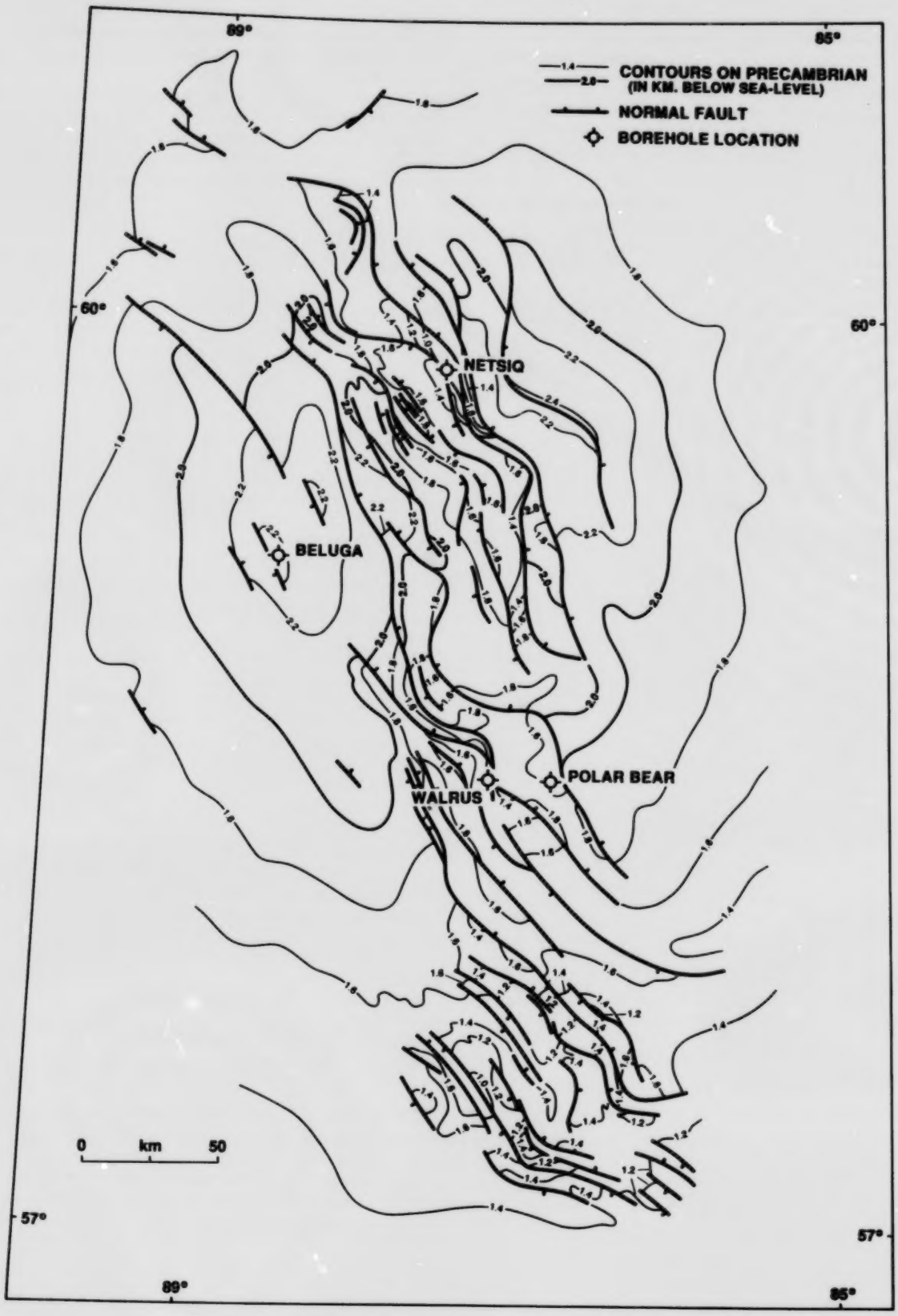

Figure 7. Details of basement structure, central Hudson Bay.

Foster Bay formation. The beds, up to 100 m thick, consist of a lower unit of nodular, flaggy, and rubbly weathered thin bedded limestones and interbedded shales, capped by resistant, massive, nodular bedded dolomitic limestones, the latter wherever present forming an abrupt escarpment. The strata are grey-brown to dark brown in colour, and weather to a characteristic mottled grey and yellowish orange. The rocks are well exposed on Baffin Island, particularly in the Amadjuak Lake region and on Melville Peninsula. The most readily accessible strata occur at Silliman's Fossil Mount, 23 km due west of Iqaluit (63° 45' 00'' N, 68° 56' 45'' W), and it is selected as the type section. Here, 54 m of thin bedded limestones and shale interbeds are capped by 16 m of resistant weathering limestones at the top of the formation.

The lower thin, flaggy, argillaceous to shaly and nodular beds of the Amadjuak formation contain the "oil shale" interbeds described by MacAuley (1987). The best known development is in cliff sections of a large Paleozoic outlier immediately west of Jordan River, approximately 25 km above its mouth.

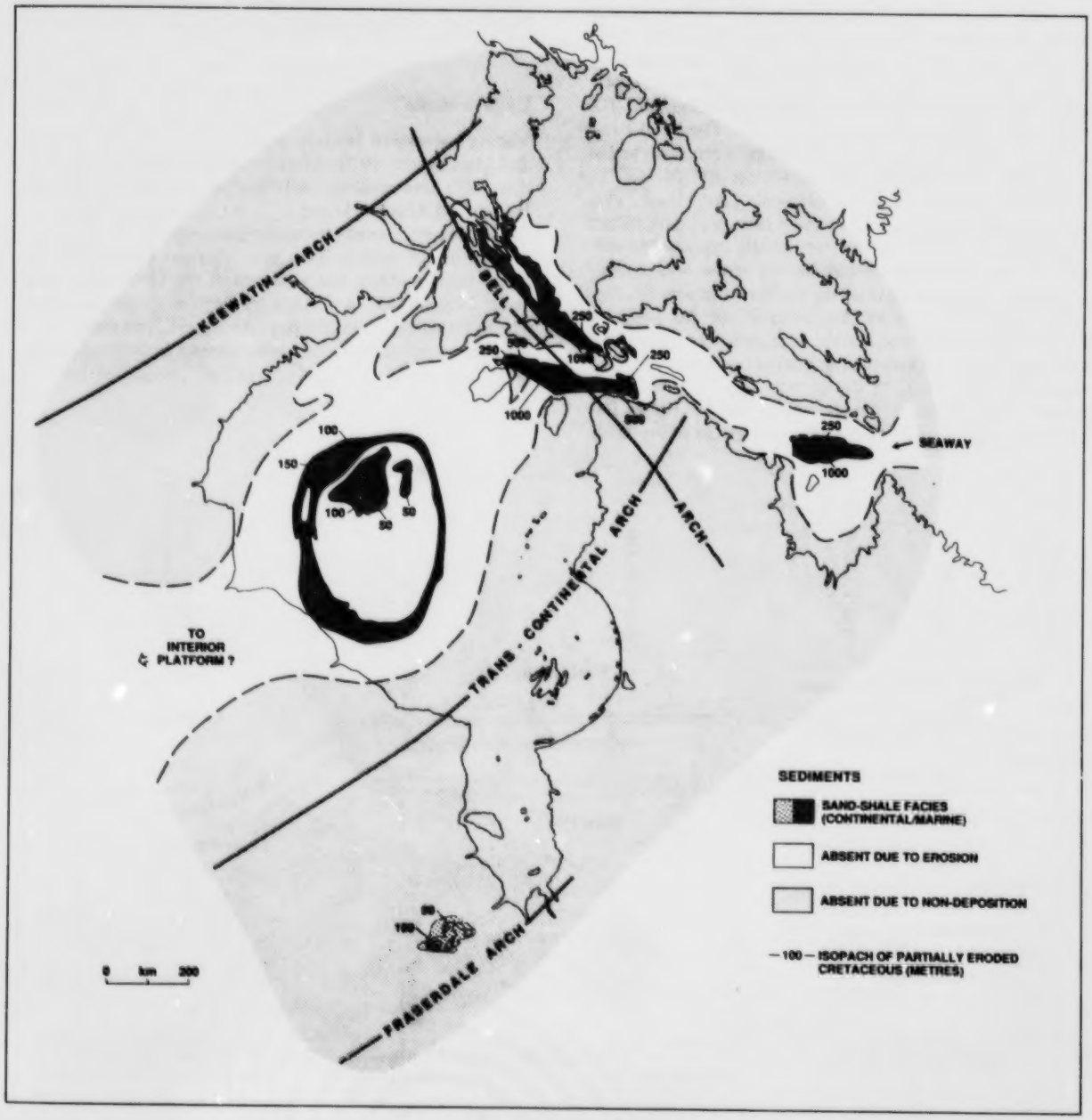

Figure 8. Cretaceous deposition in Hudson Platform.

The Amadjuak formation contains the distinctive *Receptaculites* and *Maclurites* fauna, which along with several coral and cephalopod genera relate these beds to the "Arctic Ordovician" Red River fauna (Bolton, 1977). The beds are roughly equivalent to the Bad Cache Rapids Group of the Hudson Bay Lowlands, and are thus assumed to be of Late Ordovician Edenian age.

Foster Bay formation

This name is proposed for the succession of brown and tan, thin platy, uniformly bedded limestones and dolomitic limestones conformably overlying the Amadjuak formation and succeeded by the Early Silurian Severn River Formation in central Foxe Basin. Only remnants of the formation occur on southwestern Baffin Island and Melville Peninsula (Fig. 4) where 9 and 10 m of strata have been recorded respectively. The formation probably reaches a thickness of 100 m or more in the central part of the basin. The basal strata in contact with the Amadjuak formation were observed at one locality in Foxe Basin, in a stream cut (65° 01' 45" N, 72° 27' 55" W) immediately southwest of Amadjuak Lake. Here the initial beds of the formation consist of dark brown bituminous limestones. As they are poorly exposed, no estimate of the thickness of bituminous strata was readily obtainable. They undoubtedly occupy the same approximate stratigraphic position as the Boas River oil shale of Southampton Island, and if their distribution in Foxe Basin were to be firmly documented that name could apply to these strata. The upper part of the section contains small algal masses (thrombolites?), which suggest that the Foster Bay formation may be reefal in this eastern segment of the basin.

The formation is best exposed as an isolated remnant on Melville Peninsula (Sanford, 1977) some 15 km west of Foster Bay, and that area (Fig. 4) is here considered the type locality. The thin uniformly bedded dolostones are interreefal strata to bioherms that occur in great profusion throughout the formation. As the lower beds of the Foster Bay are not exposed, the presence or otherwise of Boas River bituminous strata is unknown.

Foster Bay strata have many lithological characteristics in common with the Red Head Rapids Formation of the Hudson Bay Basin, but would appear to occupy a broader stratigraphic interval embracing it, as well as the underlying Churchill River Group. A similar correlation is implied by Bolton (1977) based on paleofavositid corals and other fossils (Fig. 2).

Ungava Basin

Marine surveys of Hudson Strait and Ungava Bay (Grant and Manchester, 1970; Maclean et al., 1986), in conjunction with stratigraphic information from the Premium Homestead Akpatok Island L-26 borehole (Workum et al., 1976) have been used to piece together the Ordovician succession in this region. Two new informal names are proposed for the oldest and youngest of the Ordovician rock units, Ungava Bay and Akpatok formations respectively. The intervening Frobisher Bay, Amadjuak, and Boas River formations are used in the same context as in Foxe Basin (Fig. 3, 4, 9).

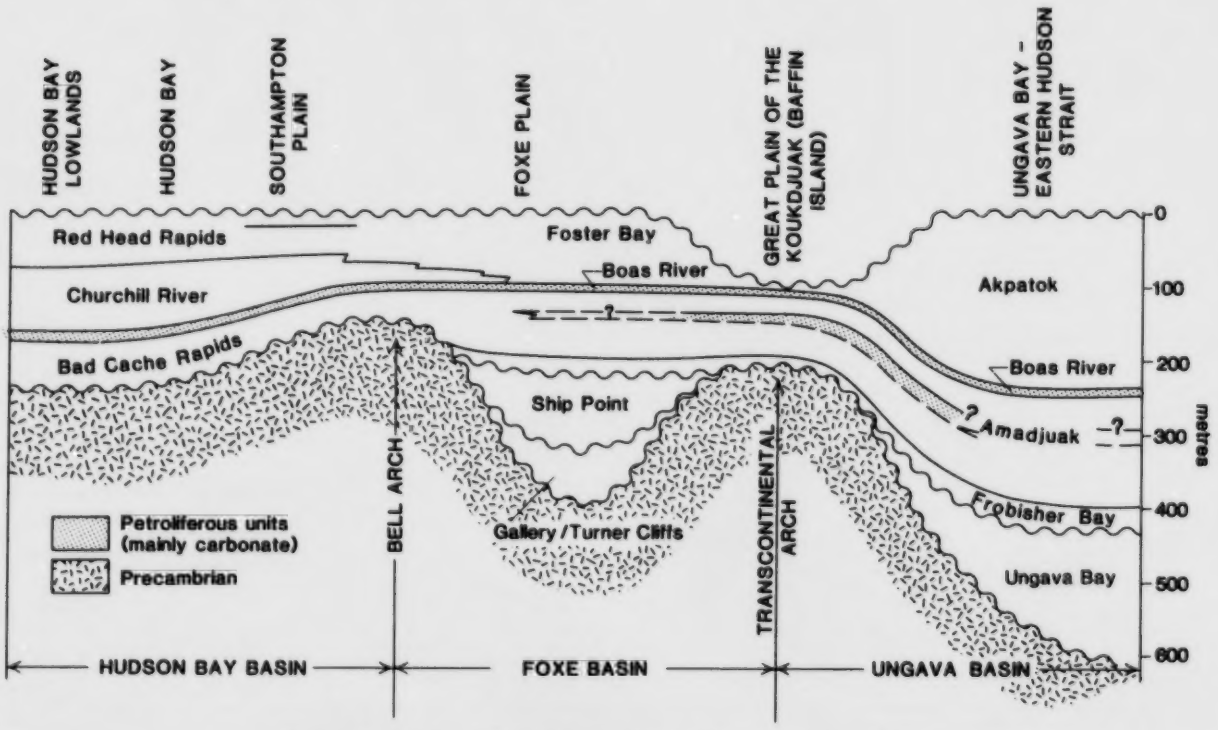

Figure 9. Stratigraphic relationships of Ordovician succession.

Ungava Bay formation

This name is proposed for the orthoquartzitic sandstones and interbedded limestones and dolostones lying unconformably on the Precambrian and disconformably succeeded by limestones of the Frobisher Bay formation. The beds are early Middle Ordovician Whiterockian age (Barnes, *in* Workum et al., 1976), roughly equivalent to the Ship Point Formation of Foxe Basin and Arctic Platform. They are not exposed onshore but were encountered between 172.3 and 354.3 m in the Premium Homestead well on the western shore of Akpatok Island (60° 25' 40'' N, 68° 20' 30'' W).

Succeeding the Ungava Bay formation are limestones and minor shales of the Frobisher Bay formation (26.3 m), followed by the Amadjuak formation (146 m). Only the upper (resistant) beds of the Amadjuak formation are exposed near the base of the escarpment that forms Akpatok Island. Approximately 5 m of brown bituminous limestones overlie the Amadjuak formation, and as these are lithologically similar and occupy approximately the same stratigraphic position as the Boas River Formation of Hudson Bay Basin, that name is tentatively applied in this region of the Hudson Platform.

Akpatok formation

This name is proposed for the 240+ m of thin, uniformly bedded limestone and shale that succeed the Boas River Formation on Akpatok Island, and underlie much of eastern

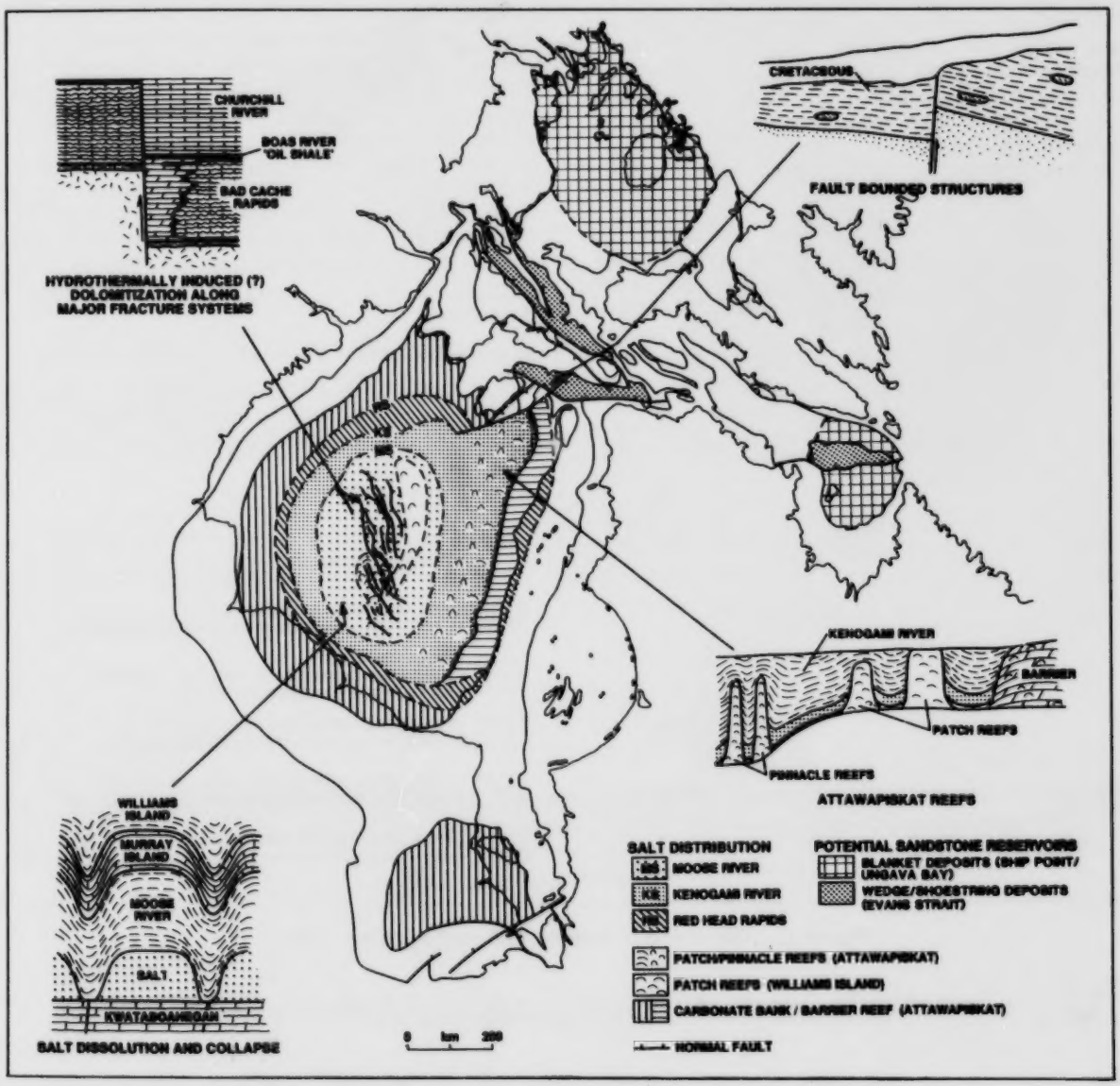

Figure 10. Potential hydrocarbon trapping mechanisms (exploration plays).

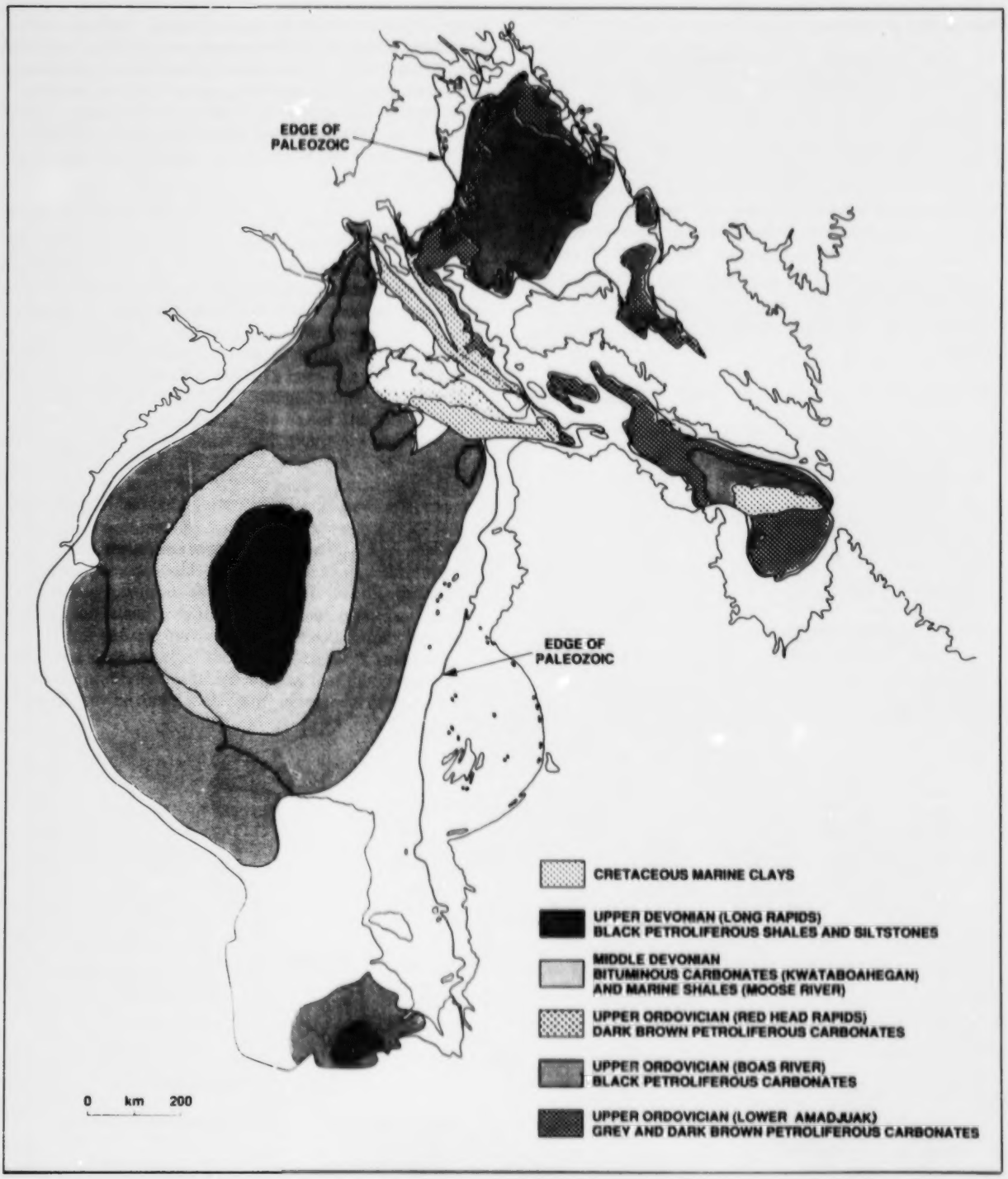

Figure 11. Distribution of potential hydrocarbon source rocks.

Hudson Strait (Fig. 4). Their precise age is not known: they are undoubtedly Late Ordovician, but can only be assumed to be the same general age as the Churchill River Group of Hudson Bay Lowlands (Bolton, *in* Workum et al., 1976), presumably Maysvillian to Richmondian.

The Ordovician rock units beneath eastern Hudson Strait and Ungava Bay (Fig. 2 - 4, 9) have weathering characteristics that enable them to be identified and mapped with the aid of single channel seismic data and contoured hydrographic charts. The upper resistant limestones of the Amadjuak formation form a major escarpment above the recessive weathering beds of the lower Amadjuak and underlying friable sandstones of the Ungava Bay formation.

Cretaceous deposits in Evans Strait, Southampton, and Ungava basins

Marine investigations in Ungava (MacLean et al., 1986), Evans Strait, and Southampton basins (Grant and Sanford, 1988) have established the presence of thick sand/shale wedges of Cretaceous age, informally referred to as Evans Strait formation (Fig. 2, 3, 5, 8). Its presence is based on seismic signature and correlation with Hudson Bay Basin, and the profound unconformity of the strata with Paleozoic and Precambrian rocks. The beds are more than 1000 m thick in Evans Strait and Ungava basins, and possibly in excess of 2000 m in parts of Southampton Basin beneath Foxe Channel.

Oil and gas exploration plays and source rock potential

A variety of "exploration plays" prevail in Hudson Platform, and a few of the more significant are illustrated in Figure 10. The basal orthoquartzitic sandstones of Cambrian to Early Ordovician age (Gallery and Ship Point formations), and early Middle Ordovician Ungava Bay formation have excellent reservoir potential. These sandstones, if found in fault-bounded blocks in combination with overlying oil shale deposits in the Amadjuak formation, could offer fair potential as an oil and gas exploration play in various parts of Foxe Basin and eastern Hudson Strait.

Cretaceous rocks in fault-bounded basins beneath Foxe Channel and Evans Strait may also represent an exploration target. Source rocks, including the Boas River, Red Head Rapids (?), and basal shaly limestones of the Amadjuak/Bad Cache Rapids may underlie these basins (Fig. 11). They are not large, but if these basins have long histories of restricted circulation, then the possibility for occurrence of source rocks may be enhanced.

Ordovician limestones in the Great Lakes region of Canada and United States, partly equivalent to the Bad Cache Rapids Group of Hudson Bay Basin, have yielded large volumes of oil and gas in structures that have been repeatedly faulted and dolomitized. Block-faulted structures, including those along the Central Hudson Bay Arch (Fig. 7, 10), should thus be reassessed with drilling emphasis on the downdropped side of the tilted blocks where more intensive dolomitization is likely to have occurred.

Marine surveys in 1987 suggest that Attawapiskat reefs are best developed in the eastern part of the Hudson Bay Basin (Fig. 10). Basinward progression from barrier to patch and pinnacle reef zones should be further investigated to determine if the bioherms are sufficiently developed to offer oil and gas potential deeper in the basin.

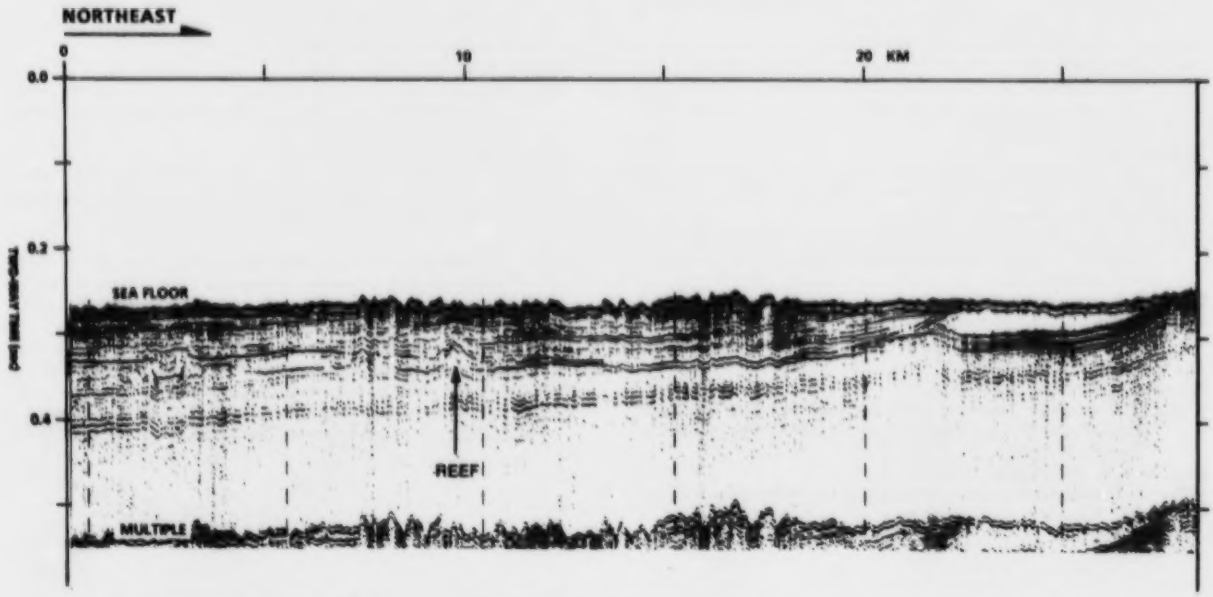

Figure 12. Single channel seismic profile of interpreted Williams Island reefs in east-central Hudson Bay (e.g. 10 km and 0.32 sec).

Evaporite deposits occur in all systems from Ordovician to Devonian, and the widespread occurrence of salt collapse structures represent an excellent potential trapping mechanism. Some of these (Fig. 10) closely resemble the Devonian structures in the Michigan Basin that contain much of the oil produced from that system.

Single channel seismic profiles (Fig. 12) demonstrate the presence of Williams Island reefs in the east-central part of Hudson Bay Basin (Fig. 10). The individual structures are relatively small but numerous, and could conceivably represent suitable trapping mechanisms for oil and gas.

The paucity of hydrocarbon source rocks has long been regarded as a major detriment to oil and gas exploration in the Hudson Platform. The number and distribution of rock units that contain some, albeit uncertain potential, as shown in Figure 11, are probably more significant than previously thought. The widespread distribution of Boas River oil shales, for example, throughout the Hudson Bay Basin is a new revelation which could have important ramifications on future oil and gas exploration in the region.

ACKNOWLEDGMENTS

We gratefully acknowledge generous assistance from H.W. Josenhans, chief scientist on the 1986 and 1987 cruises to Hudson Bay. We thank T.E. Bolton for advice on stratigraphic nomenclature of various parts of the Hudson Platform, and A. Edwards and K.D. McAlpine for helpful review of the manuscript.

REFERENCES

Bolton, T.E.
1977: Ordovician megafauna, Melville Peninsula, southeastern District of Franklin; *in* Geology of Ordovician rocks, Melville Peninsula and region, southeastern District of Franklin, T.E. Bolton, B.V. Sanford, M.J. Copeland, C.R. Barnes, and J.K. Rigby, Geological Survey of Canada, Bulletin 269, p. 23-75.

Dewing, K., Copper, P., and Hamilton, S.M.
1987: Preliminary report on the stratigraphic position of oil shales in the lower Paleozoic of Southampton Island, Northwest Territories; *in* Current Research, Part A, Geological Survey of Canada, Paper 87-1A, p. 883-888.

Dingwall, R.G.
1986: The exploration of Hudson Bay; *in* Proceedings of the Ontario Petroleum Institute Annual Meeting, London, Ontario, p. 1-41.

Grant, A.C. and Manchester, K.S.
1970: Geophysical investigations in the Ungava Bay-Hudson Strait region of Northern Canada; Canadian Journal of Earth Sciences, v. 7, p. 1062-1076.

Grant, A.C. and Sanford, B.V.
1988: Bedrock geological mapping and basin studies in the Hudson Bay region; *in* Current Research, Part B, Geological Survey of Canada, Paper 88-1B, p. 287-296.

Heywood, W.W. and Sanford, B.V.
1976: Geology of Southampton, Coats and Mansel islands, District of Keewatin, Northwest Territories; Geological Survey of Canada, Memoir 382, 35 p.

Larsson, S.Y. and Stearn, C.W.
1986: Silurian stratigraphy of the Hudson Bay lowland of Quebec; Canadian Journal of Earth Sciences, v. 23, p. 288-299.

MacAuley, G.
1986: Geochemistry of the Boas River oil shale, Southampton Island, Northwest Territories; Geological Survey of Canada, Open File Report 1285.
1987: Geochemistry of organic-rich sediments on Akpatok and Baffin islands, Northwest Territories; Geological Survey of Canada, Open File Report 1502.

MacLean, B., Williams, G.L., Sanford, B.V., Klassen, R.A., Blakeney, C., and Jennings, A.
1986: A reconnaissance study of the bedrock and surficial geology of Hudson Strait, Northwest Territories; *in* Current Research, Part B, Geological Survey of Canada, Paper 88-1B, p. 617-635.

McCracken, A.D. and Nowlan, G.S.
1989: Conodont paleontology and biostratigraphy of Ordovician carbonates and petroliferous carbonates on Southampton, Baffin and Akpatok islands in the eastern Canadian Arctic; Canadian Journal of Earth Sciences, v. 26, p. 1880-1903.

McGregor, D.C.
1987: Mesozoic and Cenozoic palynomorphs in bedrock samples from the floor of Hudson Bay (NTS D18), submitted for study by B.V. Sanford; Geological Survey of Canada, Fossil Report F1-F-1987-DCM.

Nelson, S.J. and Johnson, R.D.
1976: Oil shales on Southampton Island, northern Hudson Bay; Bulletin of Canadian Petroleum Geology, v. 24, p. 70-91.

Roksandic, M.M.
1987: The tectonics and evolution of Hudson Bay region; *in* Sedimentary Basins and Basin Forming Mechanisms, edited by C. Beaumont and A.J. Tankard, Canadian Society of Petroleum Geologists, Memoir 12, p. 507-518.

Sanford, B.V.
1977: Ordovician rocks of Melville Peninsula, southeastern District of Franklin; *in* T.E. Bolton, B.V. Sanford, M.J. Copeland, C.R. Barnes, and J.K. Rigby, Geology of Ordovician rocks, Melville Peninsula and region, southeastern District of Franklin, Geological Survey of Canada, Bulletin 269, p. 7-21.
1987: Paleozoic geology of the Hudson Platform; *in* Sedimentary Basins and Basin Forming Mechanisms, edited by C. Beaumont and A.J. Tankard, Canadian Society of Petroleum Geologists, Memoir 12, p. 483-505.

Sanford, B.V. and Norris, A.W.
1975: Devonian stratigraphy of the Hudson Platform; Geological Survey of Canada, Memoir 379.

Telford, P.G.
1988: Devonian stratigraphy of the Moose River Basin, James Bay Lowland, Ontario; *in* Devonian of the World, edited by N.J. McMillan, A.F. Embry, and D.J. Glass, Canadian Society of Petroleum Geologists, Memoir 14, p. 123-132.

Telford, P.G. and Long, D.G.F.
1986: Mesozoic geology of the Hudson Platform; *in* Canadian Inland Seas, edited by I.P. Martini, Elsevier Oceanography Series, no. 44, p. 43-54.

Thorpe, J.E.
1988: The Devonian of the Hudson Bay Basin; *in* Devonian of the World, edited by N.J. McMillan, A.F. Embry, and D.J. Glass, Canadian Society of Petroleum Geologists, Memoir 14, p. 133-154.

Trettin, H.P.
1975: Investigations of Lower Paleozoic geology, Foxe Basin, northeastern Melville Peninsula, and parts of northwestern and central Baffin Island; Geological Survey of Canada, Bulletin 251, 175 p.

Wade, J.A., Grant, A.C., Sanford, B.V., and Barss, M.S.
1977: Basement structure of eastern Canada and adjacent areas; Geological Survey of Canada, Map 1400A (4 sheets, 1:2 000 000).

Workum, R.H., Bolton, T.E., and Barnes, C.R.
1976: Ordovician geology of Akpatok Island, Ungava Bay, District of Franklin; Canadian Journal of Earth Sciences, v. 13, p. 157-178.

An airborne gamma-ray soil survey in southern Manitoba

P.B. Holman and R.L. Grasty
Mineral Resources Division

Holman, P.B. and Grasty, R.L., An airborne gamma-ray soil survey in southern Manitoba; in Current Research, Part D, Geological Survey of Canada, Paper 90-1D, p. 31-35, 1990.

Abstract

An airborne gamma-ray survey in southern Manitoba showed that different soil types can be identified by their gamma-ray signature. Clay-rich soils have higher concentrations of potassium, uranium, and thorium. Thorium showed the greatest variation among soil types and proved to be the most useful parameter for soil mapping. The higher uranium concentration of the clays could explain the high radon levels found in homes in Winnipeg.

The airborne measurements also showed that the radon concentrations of the outside air in the vicinity of Winnipeg were among the highest in Canada. These results are consistent with Health and Welfare Canada's radon survey which found some of the highest indoor radon levels in Winnipeg.

Résumé

Il est ressorti d'un levé aérien de rayons gamma dans le sud du Manitoba qu'il était possible d'identifier différents types de sol par la signature produite par les rayons gamma. Les sols très argileux ont des concentrations très élevées en potassium, uranium et thorium. Ce dernier variant beaucoup en fonction du type de sol, il s'est avéré le paramètre le plus utile à la cartographie des sols. La forte teneur en uranium des argiles pourrait expliquer les taux élevés de radon enregistrés dans les habitations de Winnipeg.

Les mesures aériennes ont en outre révélé que les concentrations de radon dans l'atmosphère des environs de Winnipeg étaient les plus élevées au Canada. Ces données correspondent à celles d'un levé sur le radon réalisé par le ministère de la Santé et du Bien-être social qui indiquait que les concentrations de radon dans les habitations à Winnipeg étaient parmi les plus élevées.

INTRODUCTION

There is considerable interest in Canada, in identifying areas where radon levels in homes may be a health concern. The Government of Manitoba has a particular interest, because Winnipeg has been identified by a cross-Canada national survey as having the highest radon levels in Canada (Letourneau et al., 1984).

The principal source of radon in homes is from soil gas, which enters homes through cracks and holes in basement floors and walls. This radon in the soil gas is produced through the decay of uranium in the ground. The concentration of radon in a home depends on many factors, including the concentration of uranium in the soil, the moisture content and permeability of the soil, and various factors that relate to the house construction.

In the mid 1970s, much of Sweden, the United States, and Canada were covered by airborne gamma-ray spectrometry. These surveys measured the uranium concentration in surface soils, by monitoring the gamma-ray emission of decay products in the uranium series. Sweden was the first country to make use of this airborne data to produce maps of radon potential. The maps combine information on soil type, radon concentrations of the soil gas, as well as airborne gamma-ray data. They are frequently produced by the Swedish Geological Company for local communities before any new housing developments.

Several studies have been conducted in the United States to relate radon in homes to airborne gamma-ray measurements. In Virginia, measurements of 2000 homes by George Mason University have shown that airborne radioactivity is the best parameter for predicting radon concentrations in homes (Kline and Mose, 1987). A large study by the New Jersey Department of the Environment of approximately 6000 homes showed a direct correlation between the airborne uranium measurement and radon concentration (New Jersey Department of Environmental Protection, 1988).

In the 1970s', much of Canada was covered by airborne gamma-ray surveys under the Uranium Reconnaissance Program (Darnley et al., 1986). In 1988, the Geological Survey of Canada supported a research project in southwestern Quebec to study the relationship of the airborne gamma-ray measurements carried out during this program to radon in homes. The results of this study are described by Doyle et al. (1990) who found that airborne gamma-ray data could be useful for predicting geographic variations of indoor radon.

Unfortunately, primarily the Precambrian Shield area was covered during Canada's Uranium Reconnaissance Program, since the program was designed specifically for uranium exploration. Consequently, most populated areas such as the Prairies, were not covered.

In 1983, a series of airborne gamma-ray surveys were flown around many of the Canadian cities which had been measured previously for radon by the Department of Health and Welfare (Letourneau et al., 1984). Analyses of the airborne gamma-ray data collected around cities in Manitoba and Saskatchewan indicated that different soil types had characteristic gamma-ray signatures. The clay-rich soils appeared to be distintly higher in uranium concentrations than other types of soil and this could explain the high levels of radon found in homes in Regina and Winnipeg which are both situated on glacial lake clays.

As part of the new GSC Environmental Initiative, a radon research program was initiated with the Manitoba provincial government to investigate the possibility of using provincial soil maps in conjunction with airborne gamma-ray data to produce radon potential maps for Manitoba.

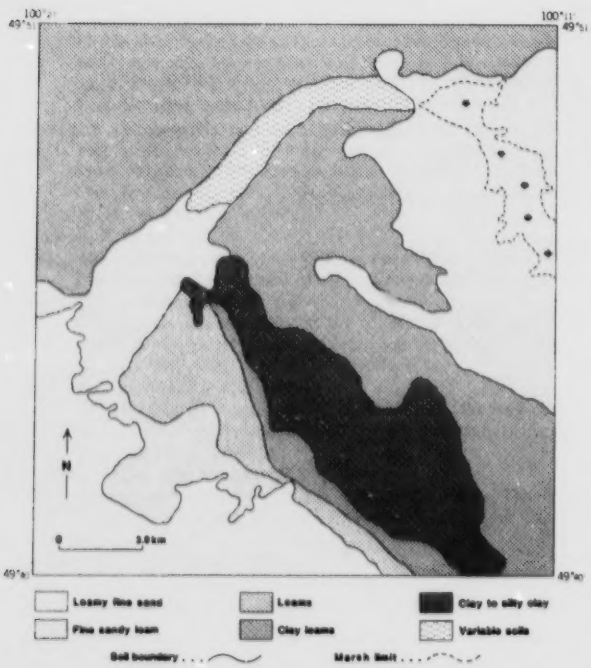

Figure 1. Soil map of study area near Virden, Manitoba.

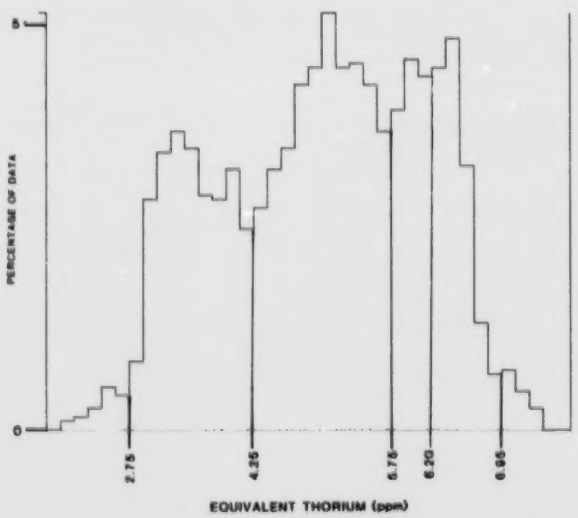

Figure 2. Histogram of thorium ground concentrations.

SELECTION OF TEST AREAS

In order to use soil maps to identify areas of high radon potential, it is necessary to know which soils have high uranium concentration. Results from the 1983 airborne surveys around cities in Manitoba and Saskatchewan indicated that clay soils have the highest uranium concentrations and the more sandy soils are less radioactive. However, these airborne surveys were not planned to characterize the gamma-ray signature of different soils. The flight lines around each of the cities were planned without consideration of variation in soil types. There was therefore a need to carry out airborne gamma-ray surveys specifically for studying gamma-ray variations of soils.

To carry out such a study, the main requirement is to overfly areas which cover a variety of soil types and which are well mapped. It is also helpful if the soil units are well separated so that there is no difficulty in relating the airborne measurements to a particular soil type.

Based on these criteria and with the help of geologists and soil scientists from the Manitoba Department of Energy and Mines and the Department of Agriculture, two areas in Manitoba were selected for study. In the summer of 1989, these two areas, each approximately 20 × 20 km, were flown with a line spacing of approximately 1 km. One area was southeast of Brandon and the other to the east of Winnipeg. This paper describes the airborne gamma-ray survey results for the Virden area near Brandon.

RESULTS

Figure 1 shows the soil types for the area surveyed, taken from the provincial soil map (Ehrlich et al, 1956). It shows a variety of soil types from sandy soils to clay-rich soils.

In producing a gamma-ray map, the airborne measurements of ground concentration of potassium, uranium, and thorium along the aircraft flight path are interpolated to a rectangular grid from which a contour map of ground concentrations is produced. The map is usually contoured with equal concentration intervals and no consideration is given to the distribution of the gridded data to separate particular soil or rock types in the area.

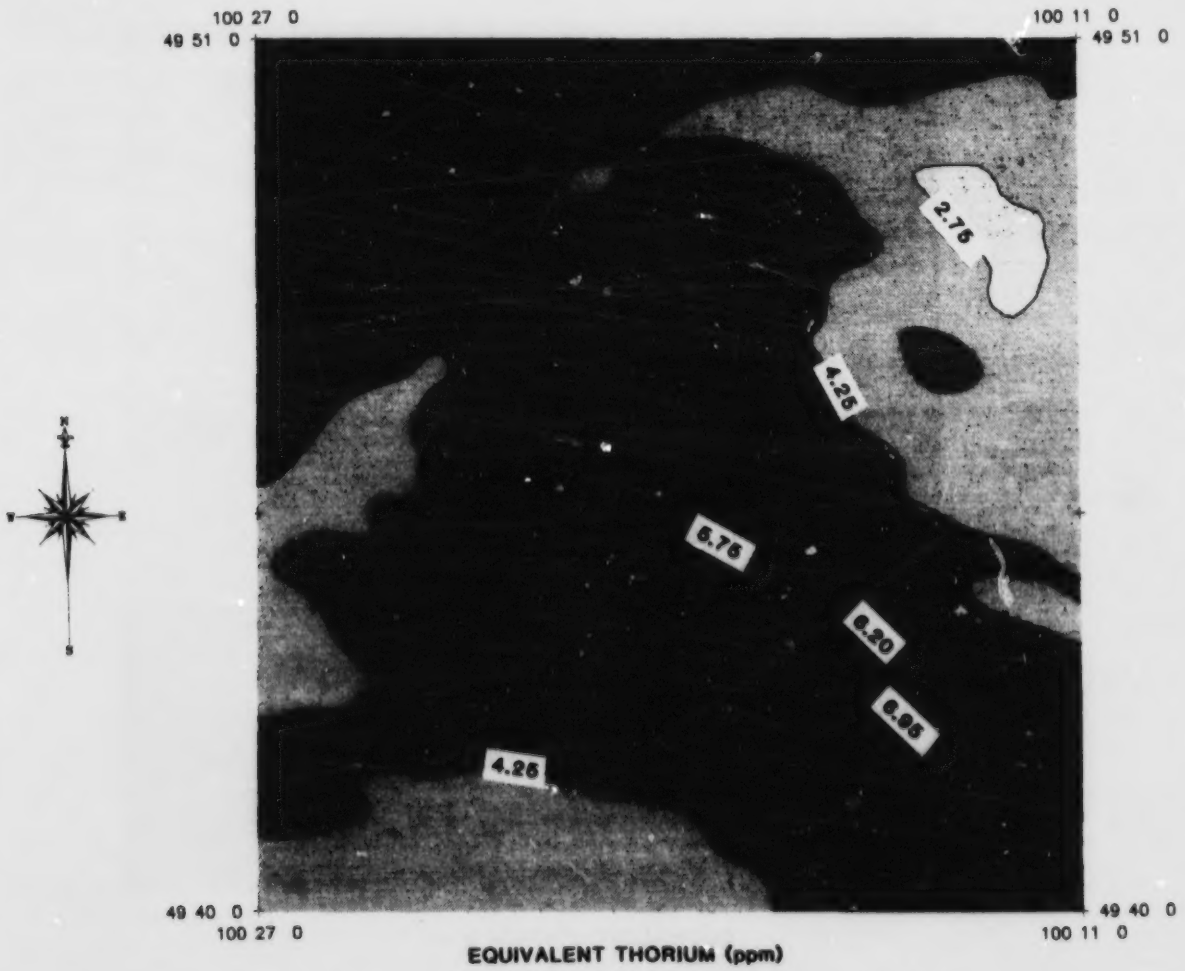

Figure 3. Airborne gamma-ray spectrometer map of study area (thorium).

For the Virden survey, a histogram of the gridded radioactivity data revealed that several populations could be distinguished. Figure 2 shows a histogram of the thorium ground concentrations which suggests that several soil types are present with distinct thorium concentrations. The subdivisions on the histogram were used to define the contour levels on the map in an attempt to separate the different soil types. The resulting thorium map is shown in Figure 3. The uranium map is shown in Figure 4.

DISCUSSION

A comparison of both the thorium and the uranium maps with the soil map shows that the clay soils and the sandy soils can be distinguished by their gamma-ray signatures. Both the thorium and uranium concentrations are highest in the clays and lowest in the sandy soils. The thorium map, however, shows the greatest contrast, varying by a factor of approximately 2 between the two soil types and appears to be the best parameter for mapping these soil types from the air. A more sophisticated mathematical clustering technique such as that described by Harris in press which uses all the measured parameters (potassium, uranium, and thorium) could well improve the distinction of the soil types in the area.

Analyses of airborne gamma-ray data collected during the summer of 1989 in other parts of the Prairies revealed that background radon levels in the vicinity of Winnipeg and Regina are among the highest found anywhere in Canada. These background measurements, which are determined using detectors shielded from the ground, must be removed from the airborne measurements in order to determine the uranium concentration of the ground. Frequently, in the clay-rich areas around Winnipeg and Regina, the gamma-ray signal from radon decay products in the air is many times greater than the signal from uranium on the ground. Because of this high background signal, in these areas, it is difficult to accurately calculate the ground concentration of uranium.

The phenomenom of high atmospheric background in the Winnipeg and Regina areas is of particular interest

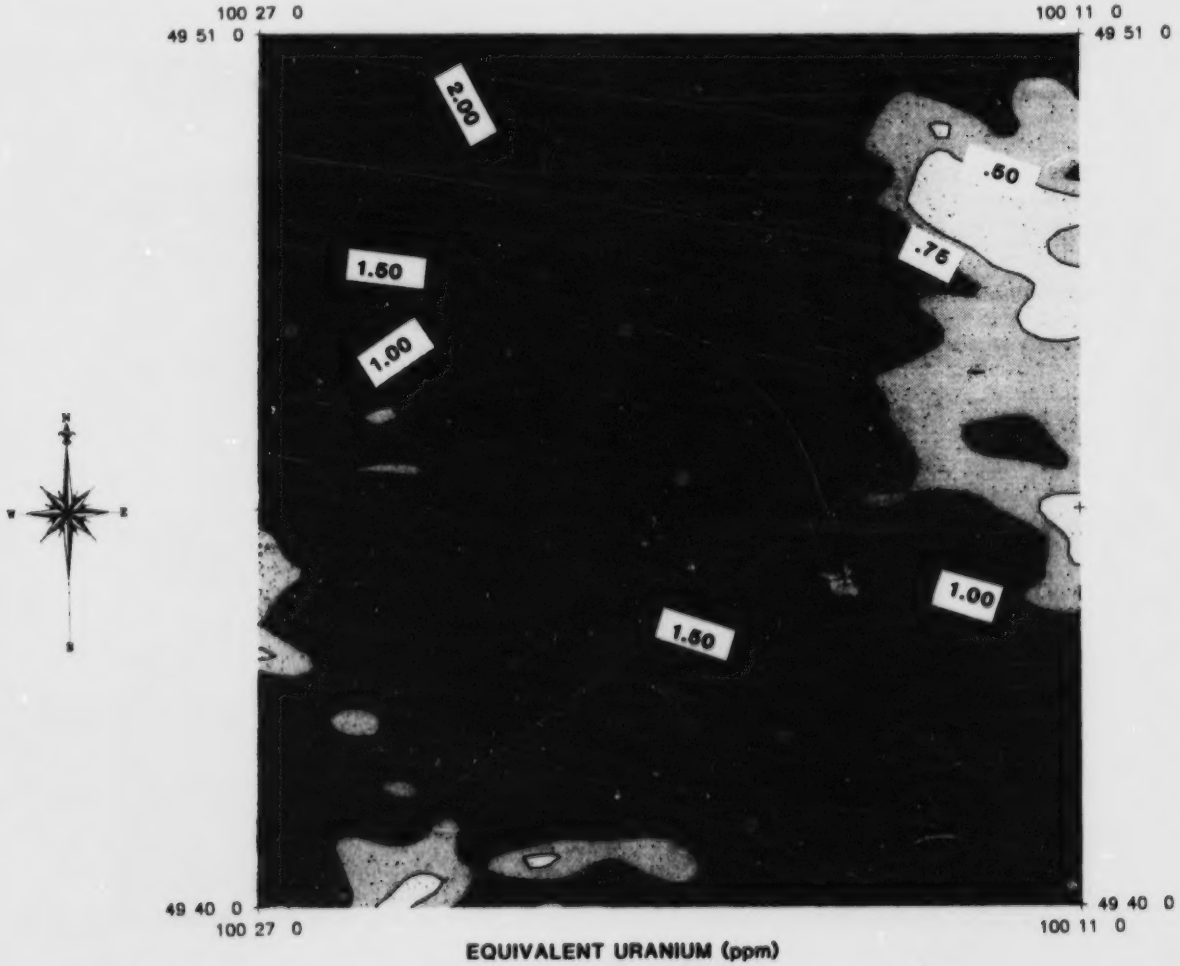

Figure 4. Airborne gamme-ray spectrometer map of study area (uranium).

because the indoor radon levels in these cities are among the highest in Canada. If high levels of radon are found in homes in these cities, high concentrations of radon would also be expected in the outside air. The high level of radon in Winnipeg and Regina is believed to be due to fracturing of the clays, their relatively high radium content, and their emanation efficiency (Grasty, 1989). Together with the dry conditions of the Interior Plains, these related factors could contribute to the high indoor radon levels in Winnipeg and Regina and the adjacent states of North Dakota and Minnesota.

CONCLUSION

Results of an airborne gamma-ray survey near Brandon in southern Manitoba have shown that such surveys can be useful for mapping different soil types. It has been found that within the survey area clay soils are more radioactive than sandy soils and can readily be distinguished by airborne measurements. The thorium map appears to be most useful for separating different soil types but a more sophisticated clustering technique using potassium, uranium, and thorium may prove even more useful.

Airborne gamma-ray measurements in southern Manitoba and Saskatchewan showed that outdoor radon levels in the vicinity of Regina and Winnipeg are among the highest in Canada. These results are consistent with Health and Welfare Canada's cross-Canada surveys which showed that Regina and Winnipeg also had the highest indoor radon levels.

REFERENCES

Darnley, A.G., Richardson, K.A., Grasty, R.L., Carson, J.M., Holman, P.B., and Charbonneau, B.W.
1986: Radioactivity Map of Canada; Geological Survey of Canada, Map 1600A.

Doyle, P.J., Grasty, R.L., and Charbonneau, B.W.
1990: Predicting geographic variations in indoor radon using airborne gamma-ray spectrometry; *in* Current Research, Part A, Geological Survey of Canada, Paper 90-1A (this volume).

Ehrlich, W.A., Pratt, L.E., and Poyser, E.A.
1956: Report of Reconnaissance Soil Survey of Rossburn and Virden map sheet areas; Manitoba Department of Agriculture, Soil Report No. 6.

Grasty, R.L.
1989: The relationship of geology and gamma-ray spectrometry to radon in homes; EOS v. 70, no. 15, p. 496 (abstract).

Harris, J.
in press: Cluster analysis of airborne gamma-ray spectrometer data, Eastern Nova Scotia; *in* Statistical Applications in the Earth Sciences, Proceedings, edited by F.P. Agterberg and G.F. Bonham-Carter, Geological Survey of Canada, Paper 89-9.

Kline, S.W. and Mose, D.G.
1987: Predictive tools for indoor radon studies in Virginia; Geological Society of America, Abstracts with Programs, v. 19, no. 7, Annual Meeting, Phoenix, Arizona.

Létourneau, E.G., McGregor, R.G., and Walker, W.B.
1984: Design and interpretation of large surveys for indoor exposure to radon daughters; Radiation Protection Dosimetry, v. 7, no. 1-4, p. 303-308.

New Jersey Department of Environmental Protection
1988: Task 3 Draft Report; Sampling Design, Data Collection and Analysis, Statewide Scientific Study of Radon.

Petrography and diagenesis of the Middle Devonian Presqu'ile Barrier: implications on formation of dissolution vugs and breccias at Pine Point and adjacent subsurface, District of Mackenzie[1]

Hairuo Qing[2] and E.W. Mountjoy[2]

Qing, H. and Mountjoy, E.W., Petrography and diagenesis of the Middle Devonian Presqu'ile Barrier: implications on formation of dissolution vugs and breccias at Pine Point and adjacent subsurface, District of Mackenzie; in Current Research, Part D, Geological Survey of Canada, Paper 90-1D, p. 37-45, 1990.

Abstract

The Presqu'ile barrier complex consists of various dolomites, the last phases of which host more than 80 Mississippi Valley-type orebodies at Pine Point. The diagenetic features related to the Watt Mountain exposure are preserved mainly in the subsurface Presqu'ile barrier west of Pine Point, whereas at Pine Point they are almost completely destroyed or modified by the effect of late hydrothermal fluids that caused large scale dissolution, dolomitization, and mineralization. Much dissolution occurred in the subsurface after deposition of the Slave Point Formation immediately preceding and during precipitation of saddle dolomite by hydrothermal brines.

Four types of dolomites are recognized: 1) Fine/medium crystalline dolomite, interpreted to have formed penecontemporaneously by evaporitic seawater in the Elk Point basin; 2) Medium crystalline dolomite, which could have occurred a) soon after sedimentation of the Pine Point Formation by evaporitic brines from the adjacent Elk Point basin, or b) during shallow burial by compactional fluids from adjacent evaporite beds, or c) during shallow to intermediate burial by basinal brines derived from sediments downdip in the basin to the west which were compacted by tectonic loading; 3) Coarse crystalline, and 4) saddle dolomites, both of which formed in the subsurface after the deposition of Slave Point Formation.

Résumé

La barrière Presqu'île du Dévonien moyen renferme des gisements de type de la vallée du Mississippi à la pointe Pine. Les caractéristiques diagénétiques liées à l'affleurement du mont Watt ont surtout été conservées dans la barrière souterraine de Presqu'île, à l'ouest de la pointe Pine, tandis qu'à la pointe Pine elles ont été complètement modifiées par des fluides hydrothermaux tardifs qui ont causé une dissolution, une dolomitisation et une minéralisation en profondeur après la mise en place de la formation de Slave Point.

Quatre types de dolomie ont été identifiés: 1) une dolomie cristalline à grain fin à moyen, qui se serait formée pénécontemporainement à l'eau de mer évaporitique dans le bassin de la pointe Elk; 2) une dolomie cristalline à grain moyen a pu se former: a) peu de temps après la sédimentation des saumures évaporitiques du bassin de la pointe Elk adjacent, ou b) durant l'enfouissement à une faible profondeur par des fluides de compaction en provenance de couches évaporitiques adjacentes, ou c) durant l'enfouissement à une profondeur faible à intermédiaire par des saumures de bassin; 3) une dolomie cristalline à grain grossier, et 4) une dolomie d'anticlinal, qui se sont toutes deux formées en profondeur après la mise en place de la formation de Slave Point.

[1] *Contribution to the Canada-Northwest Territories Mineral Development Agreement 1987-91. Project carried by Geological Survey of Canada*

[2] *Department of Geological Sciences, McGill University, 3450 University St., Montreal, PQ, H3A 2A7*

INTRODUCTION

The Pine Point ore bodies are hosted in Middle Devonian Presqu'ile barrier carbonate rocks, which form a linear buildup several hundred kilometres long that extends from outcrops in the Northwest Territories, to northwestern British Columbia in the subsurface (Fig. 1). The maximum thickness of the barrier is about 200 m. It separates two depositional basins: the Mackenzie basin to the north, in which normal marine sediments were deposited; and the Elk Point basin to the south, in which evaporite and carbonates were deposited (Fig. 1). Pine Point is located towards the east end of the barrier, on the south shore of Great Slave Lake (Fig. 1), where various secondary dolomites at different stratigraphic levels host more than 80 individual Mississippi Valley-type (MVT) deposits.

In the Pine Point area, the stratigraphy associated with the Presqu'ile barrier is subdivided as follows (Fig. 2a): 1) a lowermost carbonate platform: the Keg River Formation; 2) a carbonate barrier composed of two formations: the lower Pine Point Formation and the upper Sulphur Point Formation; 3) to the southeast the back-barrier facies of Muskeg dolomites and anhydrites; and 4) to the northwest fore-barrier or slope facies of normal marine shales and carbonates (Buffalo River and Windy Point formations of Rhodes et al., 1984).

The Presqu'ile barrier at Pine Point has undergone a complex history of diagenetic alteration in a variety of diagenetic environments (Jackson and Beales, 1967; Fritz, 1969; Skall, 1975; Kyle, 1981; Rhodes and others, 1984; Krebs and Macqueen, 1984; Morrow et al., 1986; Aulstead et al., 1988). It was invaded by evaporitic brines from the Elk Point Basin, meteoric water during Devonian subaerial exposure, and basinal hydrothermal fluids during burial.

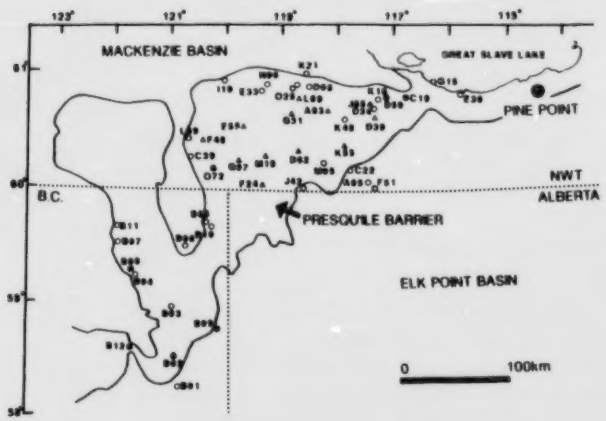

Figure 1. Middle Devonian Presqu'ile barrier and location of the wells studied. Circles and solid dots are wells with core samples. Solid dots indicate wells where dissolution, coarse crystalline and saddle dolomite occur above the Watt Mountain unconformity. Triangles are wells with no cores.

This paper deals with the petrographic and diagenetic features and origin of dissolution vugs of the Presqu'ile barrier. This is part of an ongoing Ph.D. research project with objectives to determine: 1) the origin of dissolution vugs that host MVT deposits; 2) the conditions and times that favoured the formation of massive dolomites; and 3) the relationships between these dolomites and mineralization.

METHODS OF STUDY

A number of open pits and a series of drill holes across the Pine Point barrier were systematically studied, and the spatial distribution of the various dolomites mapped. In order to compare the similarities and/or differences of diagenesis between Pine Point and its subsurface equivalent, cores from the downdip subsurface portion of the Presqu'ile barrier west of Pine Point were also studied. Well history and logs from 45 wells in Northwest Territories were obtained through the Geological Survey of Canada, Institute of Sedimentary and Petroleum Geology, Calgary. Lithological logs were obtained from Canadian Stratigraphic Services, Calgary.

About 160 thin sections were made from samples collected from Pine Point and the subsurface portion of the Presqu'ile barrier west of Pine Point. All thin sections were stained with alizarin red S and potassium ferricyanide.

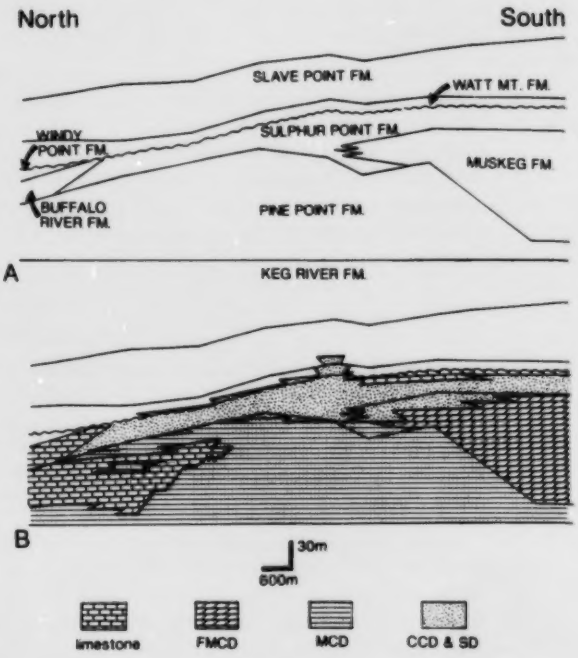

Figure 2. a) Stratigraphy of the Presqu'ile barrier in the western part of Pine Point property (600 m west of open pit N81, along −92 500 geodeparture). b) Spatial distribution of four types of dolomites.

PETROGRAPHY AND DIAGENESIS OF PRESQU'ILE BARRIER

The diagenetic features briefly outlined in this paper are discussed according to their paragenetic sequence (Fig. 3) except for dolomitization, which is presented separately. Overlapping phases are listed according to their first appearance.

Previous studies (e.g. Jackson and Beales, 1967; Fritz, 1969; Skall, 1975; Kyle, 1981; Krebs and Macqueen, 1984; Rhodes et al., 1984) of the Presqu'ile barrier mainly examined the relationship between mineralization and dolomitization. The diagenetic features in the limestones are described herein for the first time. This provides additional information and constraints on the origin of dissolution, dolomitization, and mineralization.

Micrite envelopes

Micrite envelopes form relatively thin micrite rims (40-100 μ on fossil fragments, especially shell fragments (e.g. gastropod and/or brachiopod). In rare cases, however, an entire fossil fragment may be completely micritized. Micrite envelopes are most abundant in skeletal floatstones (Skall's D2 facies; Skall, 1975) of the Sulphur Point Formation.

Syntaxial cement

Syntaxial calcite overgrowths on single crystals of echinoderm fragments occur locally in the upper part of the Sulphur Point Formation. It formed early prior to infilling of micrite.

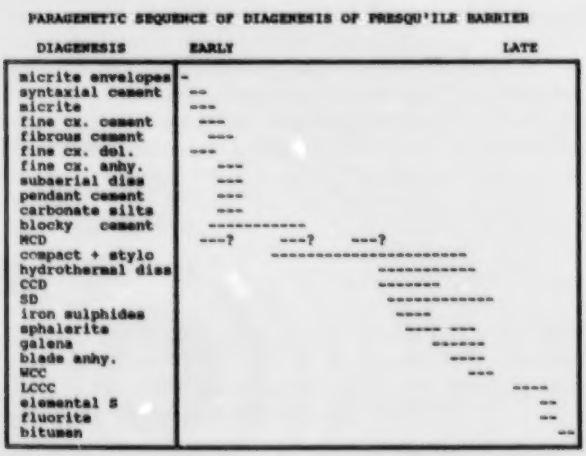

Figure 3. Diagenetic paragenesis of the Presqu'ile barrier (abbreviations: cx. = crystalline; dol. = dolomite; diss = dissolution; MCD = medium crystalline dolomite; compact = compaction; stylo = stylolitization; CCD = coarse crystalline dolomite; SD = saddle dolomite; anhy. = anhydrite; WCC = white coarse crystalline calcite; LCCC = late stage coarse crystalline calcite).

Micrite

Micrite (crystals about 5 μ) occuring as cement and/or lime mud fill pore spaces in peloidal wackestones/packstones and some skeletal wackestones mainly in the Pine Point and Sulphur Point formations. It is the most abundant carbonate that fills pore spaces in the Presqu'ile barrier.

Fine crystalline cement

Fine crystalline cement (equant and anhedral crystals 10 to 30 μ) is common in the limestone portion of the Presqu'ile barrier in the Pine Point and Sulphur Point formations. Most of the primary pore spaces in peloidal wackestones/packstones and skeletal wackestones are cemented by this material, which probably represents a submarine cement precipitated prior to fibrous cements.

Fibrous cement

Fibrous cement (elongate calcite crystals 100 to 600 μ long and 25 to 100 μ wide) occurs only locally in shelter and interparticle pores in skeletal packstones in the Sulphur Point Formation. Most fibrous cements are nonferroan, but some have ferroan bands about 15 μ along the crystal terminations.

Fine crystalline dolomite

See section on Dolomites.

Subaerial dissolution

In the subsurface Presqu'ile barrier west of Pine Point, minor occurrences of dissolution breccia and vugs occur at the top of the Sulphur Point Formation, just below the Watt Mountain unconformity, suggesting that the exposure of the barrier during Watt Mountain emergence caused dissolution. However the scale of dissolution, which could be directly related to the Watt Mountain unconformity, is much smaller than that observed at Pine Point (see sections on Hydrothermal dissolution and Dolomites). The size of the dissolution vugs are usually several millimetres. These vugs and breccias in the Northwest Territories subsurface usually extend less than a few metres below the unconformity and are filled with green mud, carbonate silts, and/or blocky sparry cement. At one place pendant cement was also observed (see below).

Pendant cement

Abundant pendant cement occurs in the dissolution vugs in *Amphipora* rudstone/framestones in well L-59 (about 300 km west of Pine Point) between 1774.5 to 1778.2 m. In a paragenetic sequence, these vugs are filled with: 1) dark brown pendant cement always occurring on the undersides of fossil fragments; 2) carbonate silts and muds that fill the bottom of vugs; 3) milky white calcite cement that follows the pendant cement; and 4) blocky sparry cement in the centre of the pore. Since pendant cements are most likely

related to the Watt Mountain unconformity, which occurs at 1768.4 m, the thickness of this Devonian vadose zone is about 10 m in this part of the Presqu'ile barrier.

Carbonate silts

Carbonate silts are mechanically deposited, uniform silt-sized calcite sediment in solution vugs and/or primary pore spaces. Locally these silts consist of small single crystals of dolomite, varying from 1 to 5 μ No skeletal fragments are recognized in these silts, in contrast to marine internal sediments. These silts are different from internal sediments of Rhodes et al. (1984), which consist of much coarser (200 to 400 μ) dolomite crystals that settled at the bottom of late stage vugs and caves.

Carbonate silts postdate the pendant cement, but predate blocky sparry cement. These silts appear to have resulted from the partial dissolution of carbonate particles as they fill solution vugs as well as primary pore spaces. Carbonate silts are observed both at Pine Point and in the subsurface and occur in the upper part of the Sulphur Point Formation several metres below the Watt Mountain unconformity.

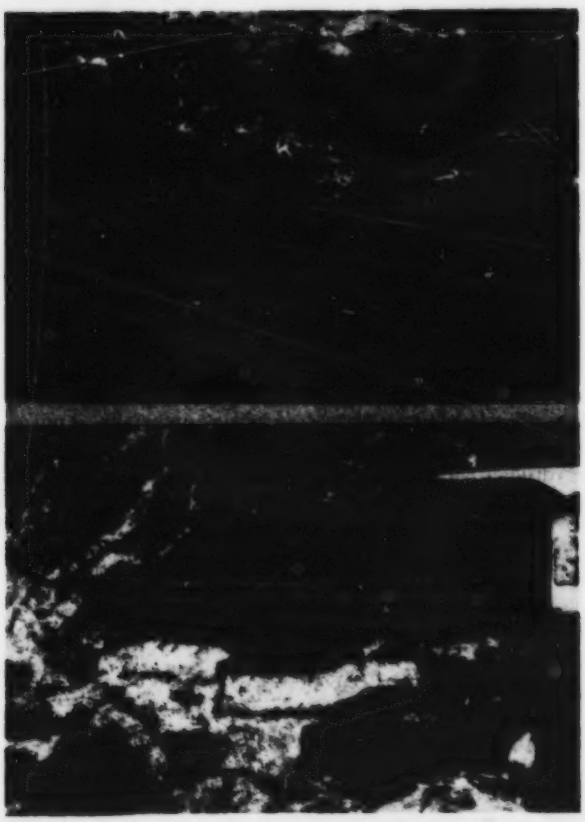

Figure 4. Dissolution and dolomitization above the Watt Mountain unconformity. a) Wall of open pit N-81 (4th bench, Watt Mountain Formation), Pine Point district. The fracturing and dissolution are well developed in the Watt Mountain Formation; Vugs are filled with saddle dolomite, bitumen, and late stage coarse crystalline calcite (hammer for scale, lower right). b) A closer view above the Watt Mountain unconformity shown in a.

Blocky sparry cement

Blocky sparry calcite cement forms limpid to translucent, equant, and usually anhedral crystal (100 to 1000 μ). Blocky sparry cement postdates the micrite, microspar, and fibrous cements, and fills the remaining pore spaces in the skeletal floatstones and peloidal packstones, and fenestral porosity. Most blocky sparry cement is nonferroan. Minor amounts of ferroan blocky sparry cement occur locally in the Presqu'ile barrier.

Medium/coarse crystalline dolomite

See section on Dolomites.

Compaction and stylolitization

With increasing burial, stylolites formed because of pressure solution. Although minor stylolites may have developed in limestones at burial depths of about 300 to 500 m, most stylolites probably formed at burial depths greater than 1000 m. Thus they separate early diagenesis from intermediate to deep burial diagenesis. Coarse crystalline and saddle dolomites postdate stylolitization (see section on Dolomites).

Hydrothermal dissolution

The Presqu'ile barrier was invaded by subsurface and hydrothermal fluids (see Krebs and Macqueen, 1984; Aulstead et al., 1988), resulting in big vugs and caves in the Pine Point area (from several centimetres to a few metres) which are much larger than the subaerial dissolution features. These vugs and caves are filled with saddle dolomite and other late diagenetic products (e.g. sulphide minerals, pyrobitumen, and late stage calcite), differing from diagenetic products in dissolution vugs that were associated with the Watt Mountain unconformity (see section on Subaerial dissolution). Unlike the dissolution vugs that are related to the Watt Mountain unconformity (which are restricted to immediately below the unconformity), the hydrothermal dissolution is closely associated with the occurrence of saddle dolomites. Locally both at Pine Point and in the subsurface large scale dissolution and brecciation occur continuously across the unconformity into Watt Mountain and Slave Point formations where saddle dolomite occurs above the unconformity (Fig. 4). Therefore it is unreasonable to attribute the large scale dissolution that hosts MVT deposits at Pine Point only to the Watt Mountain exposure. The large scale hydrothermal dissolution must have occurred after Watt Mountain exposure.

Coarse crystalline and saddle dolomites

See section on Dolomites

White coarse crystalline calcite (WCC)

In open pits WCC is pure white in colour. It is anhedral and occurs as a thick band (1 to 5 cm) sandwiched between two layers of saddle dolomite (SD). WCC is recognized for the

first time, as previously it has been misidentified as SD. Identification of WCC is difficult, because it looks like the white coarsely crystalline SD. WCC represents a dedolomite since the early stage of SD was replaced locally by WCC and WCC retains typical saddle dolomite textures. WCC is closely associated with the ore bodies and occurs only at Pine Point.

Sulphide minerals

The paragenetic sequence of sulphide minerals at Pine Point is iron sulphides, sphalerite, and galena (Fig. 3; Skall, 1975; Kyle, 1981; Krebs and Macqueen, 1984; Rhodes et al., 1984). These minerals occur as replacement of internal sediments and breccia fragments and/or as open-space fillings in vugs, fractures, and between breccia fragments. The iron sulphides occur as aggregates of fine marcasite (most common) or scattered euhedral pyrite in open spaces. Sphalerite usually occurs as botryoidal bands, followed by crystalline sphalerite. Cubic galena crystals precipitated after botryoidal banded sphalerite, partially filling the remaining pore spaces. Sulphide minerals fill dissolution vugs (meteoric + hydrothermal) in the coarsely crystalline dolomite in the upper part of the barrier, although some orebodies do occur in the fine crystalline dolomite of the back-barrier facies (e.g. X15 and W17). In hand samples, sulphide minerals precipitated either before SD (e.g. marcasite and some botryoidal sphalerite), or coprecipitated with SD (e.g. crystalline sphalerite and galena) which is followed by late stage SD.

Anhydrites

Two types of anhydrites are identified: fine crystalline and bladed cement. Fine crystalline anhydrite, usually white and semitransparent, occurs as nodular masses in vugs and moldic pore spaces and/or laminae interlayered with laminated fine/medium crystalline dolomite in the back-barrier facies of the Muskeg Formation. In thin section fine crystalline anhydrite consists of anhedral crystals about 100 μ In hand samples, it appears pure and homogeneous with floating euhedral dolomite crystals up to 200 μ.

Bladed anhydrite cement consists of white, medium to coarsely bladed anhydrite with euhedral elongate crystals up to 0.5 mm in width and 4.25 mm in length. The contact between the dolomite host rock and the anhydrite cement is sharp. Most of the bladed anhydrite represent a late diagenetic event that postdates saddle dolomite and fills moldic pores, vugs, and some late stage fractures.

Late-stage coarse crystalline calcite (LCCC)

LCCC usually forms semitranslucent or white, rhombohedrons or hexagonal scalenohedrons. Euhedral LCCC is commonly observed in large vugs and caves, fractures or breccia, lining the walls, and encrusting the earlier SD and sulphide minerals. The crystal size varies from a few millimetres to about twenty centimetres. LCCC is found both at Pine Point and in the subsurface Northwest Territories and northeastern British Columbia At Pine Point, LCCC postdates the sulphide minerals and SD.

Elemental sulphur

Elemental sulphur occurs only at Pine Point in minor amounts in vugs and fractures. It is either anhedral, as cement filling dissolution vugs, or occurs as euhedral element sulphur crystals (few millimetres to five centimetres) partially filling vugs and fractures. In both cases, elemental sulphur postdates SD and LCCC.

Fluorite

Massive fluorite (not previously sampled) was sampled along the periphery of pit Z65 close to the Watt Mountain unconformity. It lines the walls of a huge dissolution vug (35 x 60 cm) as a thick band (5 to 10 cm). In hand specimen, it is usually translucent with variable shades of brown. Minor anhedral fluorite is also found in thin sections, replacing LCCC.

Bitumen

Massive black bitumen is common in the Presqu'ile barrier at Pine Point, and has been studied in detail by Macqueen and Powell (1983). It consists of either very fine grained black powdery bitumen, or soft and sticky bitumen. Massive bitumen is the latest diagenetic product, which postdates LCCC, filling some of the remaining vugs and/or caves.

Subaerial or hydrothermal dissolution?

Dissolution vugs and breccias that host MVT deposits are generally interpreted to be mostly of meteoric origin (e.g. Kyle, 1981; Anderson and Macqueen, 1982) although some authors have suggested a hydrothermal origin (e.g. Bogacz et al., 1970; Dzulynski, 1976; Sass-Gustkiewicz et al., 1982; Ohle, 1985; Bakalowicz et al., 1987; Sangster, 1988; Qing and Mountjoy, 1989b). The host carbonates (Middle Devonian Presqu'ile barrier) for MVT deposits at Pine Point were invaded by both meteoric waters and hydrothermal brines. Previously Kyle (1981) suggested that the dissolution at Pine Point was caused by meteoric water during the Watt Mountain exposure (Table 1). However Kyle's (1981) interpretation was based on observations from open pits where the strata above the Presqu'ile barrier were eroded. Later exploration at Pine Point where strata

Table 1. Some proposals on formation of dissolution vugs

AUTHORS	PROPOSED TIME	EVIDENCE	DATA SOURCE
Kyle, 1981	during Watt Mountain exposure	vugs, fractures coarse crystalline dolomite occur below the Watt Mountain unconformity	K57, M40 N204, and others
Krebs and Macqueen, 1984	Pennsylvanian-Permian emergence	vadose silt and "eyebrow texture" indicating influence from meteoric water	7 open pits and personal communication from H. Skall
Rhodes et al., 1984	initiated during Watt Mountain exposure and reactivated later	Slave Point Fm was foundered and collapsed into the karst structures	information from drill holes and open pits

above the unconformity are preserved indicates that dissolution clearly involved strata above the unconformity. Rhodes et al. (1984) suggested that dissolution was initiated during the Watt Mountain exposure and reactivated later (Table 1). Krebs and Macqueen (1984) suggested dissolution occurred during Pennsylvanian-Permian emergence (Table 1), because of the postunconformity dissolution and because this was the next time when fresh water could have caused extensive solution of underlying Presqu'ile barrier. Core examination from the Presqu'ile barrier in the adjacent subsurface shows that dissolution related to the Watt Mountain exposure differs from the dissolution associated with the MVT deposits at Pine Point in at least in three aspects (see sections on Subaerial dissolution and Hydrothermal dissolution):

1. The size of vugs related to the Watt Mountain unconformity is small (usually several millimetres) compared with vugs at Pine Point (a few centimetres to a few metres, or even cave size);

2. Vugs that are related to the unconformity are filled with blocky calcite cements, green shale, or rarely pendant cement, while dissolution vugs at Pine Point are closely associated with saddle dolomite, sulphide minerals, and other late diagenetic products.

3. The dissolution that occurred during the Watt Mountain exposure is minor and is restricted to an interval of about 10 m underneath the unconformity, while hydrothermal dissolution is more extensive and is closely associated with saddle dolomite (Fig. 4). Locally hydrothermal dissolution extends several tens of metres above the unconformity (Fig. 4) into the Slave Point Formation (e.g. open pit N-81 at Pine Point; well C-19, F-24, O-72, and D-50 in subsurface Northwest Territories; and wells B-8 and B-12 in subsurface northeastern British Columbia).

Therefore the role of Watt Mountain exposure has been over-emphasized. The intimate relationship between large scale dissolution and massive occurrence of saddle dolomite suggests that the main dissolution was caused by hydrothermal fluids in the subsurface which precipitated saddle dolomites and dolomitized host limestones (Qing and Mountjoy, 1989b). Fluid inclusion data and stable isotopes indicate that these saddle dolomites were precipitated at temperatures around 100°C (Roedder, 1968; paper in preparation by authors). This clearly indicates a hydrothermal event, because the maximum burial temperature in the Pine Point area was about 60°C (Macqueen and Powell, 1983). However, fluid inclusion temperatures suggest that sphalerite was deposited at temperatures around 50 to 90°C (Roedder, 1968; Kyle, 1981). The reason for this is uncertain, but may be related to the mixing of low temperature basin fluids with hotter hydrothermal fluids.

The timing of the hydrothermal dissolution is uncertain. The main dissolution events clearly postdate the deposition of the Slave Point sediments (late Middle Devonian) because the large scale dissolution extends several tens of metres above the unconformity into the Slave Point Formation. As saddle dolomites postdate stylolitization, saddle dolomites and associated hydrothermal dissolution probably occurred at minimum burial depths of about 500 to 1000 m. The maximum burial depth for hydrothermal dissolution is not clear at present. Among other possibilities, the solution may have occurred: 1) before the end of the Devonian time, as Aulstead et al. (1988) suggested that the Presqu'ile barrier was invaded by hot brines that migrated upward along faults during Devonian time; 2) during Pennsylvanian-Permian emergence as suggested by Krebs and Macqueen (1984); 3) during Cretaceous time as warm brines were expelled to the east during sedimentary and tectonic loading of the western side of the basin (Qing and Mountjoy, 1989a); and 4) during the Tertiary by a gravity-driven groundwater system which developed due to the emergence of the Rocky Mountains (Garven, 1985). Most of these proposals do not satisfactorily explain the available data. For example, in case 2 some fluid inclusions should contain brackish or low salinity fluid due to meteoric influence at shallow burial. However all inclusions from saddle dolomite have high salinities. In case 4, fluid inclusions in the Presqu'ile dolomites do not show gradual increasing temperatures and salinities in the subsurface from west to east as Garven's (1985) model predicts. Likely the hydrothermal fluids were active over a relatively long period of time and had to be sourced downdip in the western part of the basin. At present it is not possible to identify a heat source and more closely limit the timing for these fluids.

The earlier meteoric dissolution, combined with tectonic fracturing (Skall, 1975; Aulstead et al., 1988) and local dissolution of anhydrite (Beales and Hardy, 1980) probably changed the porosity and permeability patterns in the barrier and produced conduits for later hydrothermal fluids. The later subsurface hydrothermal fluids caused large scale dissolution, resulting in vugs and caves that host MVT deposits and associated saddle dolomites at Pine Point. The hydrothermal fluids dissolved large volumes of lithified limestones as well as enhancing earlier porosity and dissolution. The Watt Mountain shale formed a relatively impermeable unit which may have restricted the later hydrothermal fluid flow within the barrier. Generally most dissolution occurred within the Presqu'ile barrier in the Sulphur Point Formation below the Watt Mountain shale. Locally, however, hydrothermal fluids breached the shale cover, resulting in local extensive dissolution and hydrothermal karst in the Watt Mountain and Slave Point formations above the unconformity. These later stages of hydrothermal dissolution and dolomitization have almost completely overprinted and obliterated the earlier unconformity related meteoric solution features.

DOLOMITES

Four types of dolomites recognized in paragenetic sequence are: 1) fine/medium crystalline dolomite (FMCD); 2) medium crystalline dolomite (MCD); 3) coarse crystalline dolomite (CCD); and 4) saddle dolomite (SD). Table 2 compares our classification of dolomite with previous studies (Kyle, 1981; Krebs and Macqueen, 1984; Rhodes et al., 1984). Their fine crystalline dolomite was divided into two types of dolomites, FMCD and MCD, which have different petrographic textures and lithofacies association. The interpretations in the following discussion are based on the

petrography and spatial distribution of the dolomites. Geochemistry is only briefly discussed and will be published elsewhere (paper in preparation by authors).

FMCD

FMCD is either brown or grey in hand sample. Fossils and sedimentary structures are well preserved in FMCD. Dolostones composed of FMCD are generally tight and dense, with very low porosity. Fractures and vugs in these dolostones are usually filled with fine crystalline anhydrite.

Under the microscope, FMCD has well defined crystal boundaries but no undulous extinction. The crystal size of FMCD is bimodal. The finer portion of FMCD consists of subhedral to euhedral dolomite crystals, ranging from 5 to 25 μ (average 8 μ and usually forms dolomite patches and/or laminations within the evaporitic anhydrite in the back-barrier facies (Muskeg Formation, see Fig. 2). Coarser FMCD is composed of anhedral dolomite crystals, varying in size from 100 to 200 μ (average 150 μ). Some coarser crystals have slightly cloudy centres and clear rims. The coarser FMCD occurs in the Muskeg Formation adjacent to orebodies (e.g. X15 and W17) and appears to represent recrystallized FMCD.

FMCD is interpreted to represent limestones that were dolomitized penecontemporaneously by evaporitic seawater in the Elk Point basin because: 1) FMCD is restricted in the back-barrier facies in the evaporitic Elk Point basin and interbedded with evaporitic anhydrites (Fig. 2b); 2) Sr isotopes for FMCD fall on Burke et al.'s (1982) curve for Middle Devonian seawater; and 3) some FMCD have preserved $\delta^{18}O$ signatures that suggest precipitation from evaporated Middle Devonian seawater (δ^{18} −4 to −1.5).

MCD

MCD is medium to dark brown, porous or tight, depending on the presence or absence of intercrystalline porosity. Fossils and sedimentary textures are generally recognizable in MCD. In hand specimen and cores, MCD differs from FMCD in the following: 1) FMCD is associated with evaporitic anhydrite while MCD is not; 2) lamination is locally preserved in FMCD; and 3) MCD consists of coarser and more uniform dolomite crystals. In thin sections, MCD is composed of anhedral to subhedral dolomite crystals (around 200 μ). These crystals have well defined crystal boundaries. Under crossed-nicols, no undulous extinction was observed. Secondary dissolution vugs and fractures are locally developed in MCD dolostones and are usually partially filled with minor amounts of late stage saddle dolomite or anhydrite.

MCD is the most abundant dolomite type in the lower part of the Presqu'ile barrier (Fig. 2b). Thus most of the Pine Point Formation (except in the northern part of the barrier) is composed of MCD (Fig. 2b). In the Pine Point area, there are two layers of very porous sucrosic MCD. One is at the base of the Pine Point Formation, called the B Spongy Member by Rhodes et al. (1984), and the other occurs just below the coarse crystalline dolomite. These porous sucrosic dolomites, however, have not been observed in cores from the subsurface west of the Pine Point property, perhaps due to poor well control and the few cored intervals in the region.

There are at least three possible origins for MCD: (1) soon after sedimentation of the Pine Point Formation, by the evaporitic brines from the adjacent Elk Point basin; (2) at shallow burial by compactional fluids from adjacent evaporite beds (i.e. Muskeg anhydrite and dolomite in the Elk Point basin); or (3) at shallow to intermediate burial by basinal brines derived from sediments downdip in the basin to the west which were compacted by tectonic loading.

Table 2. Classification of dolomites of Presqu'ile barrier

THIS REPORT	PREVIOUS STUDIES
FMCD	fine crystalline dolomite
MCD	fine crystalline dolomite
CCD	Presqu'ile dolomite
SD	white vein dolosparite (Rhodes et al., 1984); white dolomite (Kyle, 1981); coarsely crystalline dolomite (Krebs and Macqueen, 1984)

CCD

CCD is much lighter coloured than FMCD and MCD, being either light brown or buff. The original fabrics in CCD are either destroyed or locally preserved as relics. In contrast to FMCD and MCD, CCD contains a large variety of vugs, cavities, and/or fractures. The vugs and cavities generally range in size from a few millimetres to a few metres which host MVT deposits and other late diagenetic products at Pine Point. In thin section, CCD consist of anhedral dolomite crystals, ranging from 500 μ to 2 mm. The crystal boundaries of CCD are difficult to identify under plane light, in contrast to the FMCD and MCD discussed above. Under cross-polarized light, CCD exhibits undulatory extinction with a single CCD crystal commonly consisting of several domains.

At Pine Point, CCD commonly replaces the lower and middle parts of the Sulphur Point Formation (Fig. 2b), while variable amounts of the upper part of the Slave Point Formation are preserved as limestones. At CCD/limestone contacts, CCD clearly replaces the limestones, precluding the possibility that CCD is a neomorphic modification of earlier dolomites.

CCD, along with vug and fracture filling coarse crystalline saddle dolomite, is termed Presqu'ile dolomites by some geologists. In the early mining days, Presqu'ile dolomite was thought to be a reefal development and was given formation status. It is now known to be an example of secondary dolomitization that crosscuts formation boundaries (e.g. Rhodes et al., 1984). In orebodies in the western part of the Pine Point property (e.g. N18, W85, and G03), CCD extends higher stratigraphically across the unconformity from the Sulphur Point Formation into the Watt Mountain and lower part of the Slave Point formations (Fig. 4). CCD is also observed crosscutting the unconformity in the subsurface of the Northwest Territories (e.g. C-19, D-50, and

O-72) and northeastern British Columbia (e.g. B-8 and B-12). Thin sections made from samples close to CCD/limestone boundaries reveal that CCD replaces blocky sparry cement and other earlier diagenetic products. Locally CCD precipitated along stylolites in limestones, and therefore probably formed below 500 to 1000 m burial depths. The possible origins of CCD and associated SD are discussed below.

SD

In hand specimens, SD has a distinctive white colour, although pink and grey colours also occur locally. SD usually consist of coarse (millimetre-sized) dolomite crystals, and crystal shapes of SD range from rhombohedral, with slightly curved faces through increasing face curvature, to symmetrical saddle forms. In cross-polarized light, SD dolomite crystals have a diagnostic sweeping extinction pattern.

SD mainly occurs in the upper part of the Presqu'ile barrier in the Sulphur Point Formation, as cement in vugs and fractures in CCD. Locally it occurs above the Watt Mountain unconformity (Fig. 4). Minor SD was also observed associated with FMCD and MCD, as a thin rim lining vugs and fractures, postdating these dolomites. SD is usually associated with sulphide minerals at Pine Point. The age relationship of SD with respect to mineralization is complicated. Some SD predates, some is synmineralization because it alternates with sulphide minerals, and some postdates mineralization.

As CCD and SD extend continuously from the Sulphur Point Formation, across the Watt Mountain unconformity, into the lower part of the Slave Point Formation, both dolomites clearly postdate the Watt Mountain emergence. Hence they could not have formed in a mixing zone environment associated with the Watt Mountain Formation, as suggested by Kyle (1981). CCD and SD also occur along stylolites in some limestones, suggesting they formed at burial depths greater than 500 m. CCD occurred as a result of the replacement of the host limestones by dolomitizing fluids, while SD occurred after CCD as a result of direct precipitation of dolomite in open spaces from later dolomitizing fluids. The dolomitizing fluids for CCD and SD were warm basinal brines as fluid inclusions in saddle dolomite indicate filling temperatures of about 100°C. These temperatures of formation are also supported by the depleted $\delta^{18}O$ values for CCD and SD (paper in preparation by authors).

CONCLUSIONS

The diagenetic features related to the Watt Mountain exposure (e.g. subaerial dissolution, pendant cement, and carbonate silts) are observed mainly in the subsurface Presqu'ile barrier west of Pine Point. In the Pine Point area these diagenetic features are almost destroyed by late hydrothermal fluids that caused large scale dissolution, dolomitization, and mineralization. Much dissolution postdated deposition of the Slave Point Formation in the subsurface immediately preceding or during precipitation of SD by warm subsurface brines, although the specific timing of dissolution is still uncertain.

Four types of dolomites recognized are: fine/medium crystalline dolomite; medium crystalline dolomite; coarse crystalline dolomite; and saddle dolomite. The interpretations of dolomitization are based on the petrography and spatial distribution of the dolomites, and their geochemistry (paper in preparation by authors). FMCD is interpreted to represent limestones that were dolomitized penecontemporaneously by evaporitic seawater in the Elk Point basin. There are at least three possible origins for MCD: (1) soon after deposition of the Pine Point Formation by evaporitic brines from the Elk Point basin; (2) during shallow burial by compactional fluids from adjacent evaporite beds (i.e. Muskeg anhydrite and dolomite in the Elk Point basin); or (3) at shallow to intermediate burial by basinal brines derived from sediments downdip to the west compacted by tectonic loading. CCD and SD occurred after the deposition of the Slave Point Formation. CCD and SD also occur along stylolites in some limestones, suggesting a minimum burial depth of about 500 m. CCD occurred as a result of the replacement of the host limestones by the dolomitizing fluids, while SD formed as a result of direct precipitation of dolomite in open pore spaces. The available evidence supports an intermediate to deep subsurface origin for hydrothermal solution and SD.

ACKNOWLEDGMENTS

Financial support for this study came from Canada-Northwest Mineral Development Agreement 1987-91, NSERC Grant A2128 to Professor Mountjoy, and Shell Canada. We appreciate the valuable advice and encouragement from Don Sangster (GSC, Ottawa). We are grateful to Pine Point Mines of Cominco Ltd., especially Ken Carter for information and field assistance during our visits in 1986 and 1987. We thank Shell Canada and Westcoast Petroleum Ltd. for well information, and ISPG (Calgary) and B.C. Core Lab (Fort St. John) for assistance in core examinations.

REFERENCES

Anderson, G.M. and Macqueen, R.W.
1982: Ore deposit models — 6. Mississippi Valley-type lead-zinc deposits; Geoscience Canada, v. 9, p. 108-117.

Aulstead, K.L., Spencer, R.J., and Krouse, H.R.
1988: Fluid inclusion and isotopic evidence on dolomitization, Devonian of Western Canada; Geochimica et Cosmochimica Acta, v. 52, p. 1027-1035.

Beales, F.W. and Hardy, J.L.
1980: Criteria for the recognition of diverse dolomite types with an emphasis on studies on host rocks for Mississippi Valley-type ore deposits; *in* Concepts of Models of Dolomitization, edited by D.H. Zenger, J.B. Dunham, and R.L. Ethington, Society of Economic Paleontologists and Mineralogists, Special Publication No. 28, p. 197-213.

Bakalowicz, M.J., Ford, D.C., Miller, T.E., Palmer, A.N., and Palmer, M.V.
1987: Thermal genesis of dissolution caves in the Black Hills, South Dakota; Geological Society of America Bulletin, v. 99, p. 729-738.

Bogacz, K., Dzulynski, S., and Haranczyk, C.
1970: Ore-filled hydrothermal karst features in the Triassic rocks of the Cracow-Silesian region; Acta Geologica Polonica, v. 20, p. 247-265.

Burke, W.H., Denison, R.E., Hetherington, E.A., Koepnick, R.B., Nelson, H.F., and Otto, J.B.
1982: Variation of seawater $^{87}Sr/^{86}Sr$ throughout Phanerozoic time; Geology, v. 10, p. 516-519.

Dzulynski, S.
1976: Hydrothermal karst and Zn-Pb sulfide ores; Annales de la Société Géologique de Pologne, v. 46, p. 217-230.

Fritz, P.
1969: The oxygen and carbon isotopic composition of carbonates from the Pine Point lead-zinc ore deposits; Economic Geology, v. 64, p. 733-742.

Garven, G.
1985: The role of regional fluid flow in the genesis of the Pine Point deposits, Western Canadian sedimentary basin; Economic Geology, v. 80, p. 307-324.

Jackson, S.A. and Beales, F.W.
1967: An aspect of sedimentary basin evolution: the concentration of Mississippi Valley-type ores during late stages of diagenesis; Bulletin of Canadian Petroleum Geology, v. 15, p. 383-433.

Krebs, W. and Macqueen, R.
1984: Sequence of diagenetic and mineralization events: Pine Point lead-zinc property, NWT, Canada; Bulletin of Canadian Petroleum Geology, v. 32, p. 434-464.

Kyle, J.R.
1981: Geology of Pine Point lead-zinc district; *in* Handbook of Strata-Bound and Stratiform Ore Deposits, edited by K.H. Wolf, New York, Elsevier, v. 9, p. 643-741.

Macqueen, R.W. and Powell, T.G.
1983: Organic geochemistry of the Pine Point lead-zinc ore field and region, Northwest Territories, Canada; Economic Geology, v. 78, p. 1-25.

Morrow, D.W., Cumming, G.L., and Koepnick, R.B.
1986: Manetoe Facies — a gas-bearing, megacrystalline, Devonian dolomite, Yukon and Northwest Territories, Canada; American Association of Petroleum Geologists Bulletin, v. 70, p. 702-720.

Ohle, E.L.
1985: Breccias in Mississippi Valley-type deposits; Economic Geology, v. 80, p. 1736-1752.

Qing, H. and Mountjoy, E.
1989a: Multistage dolomitization in Rainbow buildups, Middle Devonian Keg River Formation, Alberta, Canada; Journal of Sedimentary Petrology, v. 59, p. 114-126.
1989b: Origin of dissolution vugs and breccias in Presqu'ile barrier (Middle Devonian) at Pine Point: meteoric or hydrothermal karst; Geological Society of America, Abstract and Programs, v. 21, no. 6, p. 7a.

Rhodes, D., Lantos, E.A., Lantos, J.A., Webb, R.J., and Owens, D.C.
1984: Pine Point orebodies and their relationship to the stratigraphy, structure, dolomitization, and karstification of the Middle Devonian barrier complex; Economic Geology, v. 79, p. 991-1055.

Roedder, E.
1968: Temperature, salinity, and origin of the ore-forming fluids at Pine Point, Northwest Territories, Canada, from fluid inclusion studies; Economic Geology, v. 63, p. 439-450.

Sangster, D.F.
1988: Breccia-hosted lead-zinc deposits in carbonate rocks; *in* N.P. James, P.W. Choquette, Paleokarst, edited by Springer-Verlag, 416 p.

Sass-Gustkiewicz, M., Dzulynski, S., and Ridge, J.D.
1982: The emplacement of zinc-lead sulfide ores in the Upper Silesian district — a contribution to the understanding of Mississippi Valley-type deposits; Economic Geology, v. 77, p. 392-412.

Skall, H.
1975: The paleoenvironment of the Pine Point lead-zinc district; Economic Geology, v. 70, p. 22-45.

The geology of the Polaris carbonate-hosted Zn-Pb deposit, Canadian Arctic Archipelago[1]

R.N. Randell[2] and G.M. Anderson[3]

Randell, R.N. and Anderson, G.M., The geology of the Polaris carbonate-hosted Zn-Pb deposit, Canadian Arctic Archipelago; in Current Research, Part D, Geological Survey of Canada, Paper 90-1 D, p. 47-53, 1990.

Abstract

This paper reports progress on a study of Polaris, a Mississippi Valley-type Zn-Pb deposit of unusually high grade and compact geometry. Ores comprise veins, disseminations, replacements, and open-space filling. Host Upper Ordovician platform carbonates, the Thumb Mountain Formation, are overlain by impermeable green mudstones and underlain by shales, carbonates, and evaporites, the latter being interpreted from sulphur isotope data to be the source of ore sulphide sulphur. Interpretation of dissolution, host rock, sulphide, and internal sedimentation relationships suggests ore was emplaced prior to the early Devonian folding which deformed the Thumb Mountain Formation, probably between early Silurian and early Devonian time. Ore emplacement probably pre-dates a profound district-wide Lower Devonian unconformity.

Résumé

Le présent document est un rapport sur l'état d'avancement d'une étude de Polaris, gisement à Zn-Pb de type de la vallée du Mississippi, à teneur élevée et à géométrie compacte inhabituelles. Les gisements sont notamment des filons, des disséminations, des substitutions et des remplissages d'espaces ouverts. Les roches carbonatées de plate-forme encaissantes de l'Ordovicien supérieur, la formation de Thumb Mountain, reposent sous des mudstones verts imperméables et recouvrent des schistes argileux, roches carbonatées et évaporites, ces dernières étant, selon des données isotopiques du soufre, la roche d'origine du soufre des minerais sulfurés. L'interprétation des liens entre la dissolution, la roche encaissante, les sulfures et la sédimentation interne indiquent que le minerai a été mis en place avant le plissement du Dévonien inférieur qui a déformé la formation de Thumb Mountain, probablement entre le début du Silurien et le début du Dévonien. La formation du minerai est probablement antérieure à une discordance profonde du Dévonien inférieur qui s'étend sur tout le district.

[1] Contribution to the Canada-Northwest Territories Mineral Development Agreement, 1987-91. Project carried by the Geological Survey of Canada.

[2] Cominco Ltd., #2200, 120 Adelaide St. W, Toronto, Ontario M5H 1T1

[3] University of Toronto, 22 Russell Street, Toronto, Ontario M5S 3B1

INTRODUCTION

Polaris, on Little Cornwallis Island (75°30′N, 96°30′W) in the Canadian Arctic Archipelago (Fig. 1), is a Mississippi Valley-type (MVT) Zn-Pb deposit hosted by Upper Ordovician platform carbonates. A single orebody comprising 22 million tons of 14 % Zn, 4 % Pb, 5 % Fe, and 0.1 oz/t Ag is mined by blasthole stoping methods, with ore being treated at a rate of about 1 million tons annually. Ships load concentrate destined for Europe at the mine site, the shipping season being early August to early November.

Mineralization was discovered in the region 1960 by Bankeno Mines. That company subsequently concluded an agreement with Cominco Ltd. who discovered the ore deposit in 1971. Production commenced in 1981. Muraro (1973), Jowett (1975), Sangster (1974, 1983), and Kerr (1977) have previously referred to this deposit. The regional geology has been described by Thorsteinsson (1958, 1986) and Thorsteinsson and Kerr (1968).

GENERAL GEOLOGY

Polaris ore is confined to the Thumb Mountain Formation, a Middle to Upper Ordovician platform carbonate which is part of a thick sequence of shales, evaporites, and carbonates stretching across much of the Arctic, spanning an interval of time from Cambrian to Devonian. Sedimentation was punctuated in early Devonian time by a major folding event that created the north-trending, northplunging Cornwallis Fold Belt. Signs of this event appeared earlier in the south and later in the north (Miall, 1986; Okulitch et al., 1986). In addition to carbonates, the Devonian succession, which unconformably overlies older rocks, includes a series of clastic sedimentary lobes, developed in response to the mid-Devonian Ellesmerian orogeny (Embry, 1988).

STRATIGRAPHY

At Polaris Mine, the lowest known stratigraphic unit intersected by drillholes, but not by mine openings, is the Bay Fiord Formation, a sequence estimated by Thorsteinsson (1986) to be 440 m thick (Fig. 2). Limestone, dolostone, and minor shale, together with gypsum and anhydrite, are the component lithologies. Only the topmost 70 m has been cored, revealing brown micrites and greenish argillaceous limestones, as well as two distinctive green shaly mudstones.

Conformably overlying the Bay Fiord is a 350 m thick sequence of carbonates ranging in age from Middle to Late Ordovician, the Thumb Mountain Formation. An informal division, employed at Polaris, separates the formation into an upper 90 m of intensely burrowed, richly bioclastic nodular wackestone to argillaceous wackestone, and a lower 260 m of fine grained, dense micritic lime and dolostones, alternating with brown, bituminous, mottled, burrowed, locally intraclastic or pelletal limestones or dolostones. The lower unit displays a cyclical sedimentation pattern, with poorly developed bioclastic components. The upper unit lacks this cyclical pattern. The boundary between the two subunits is sharp, commonly along a stylolite. Two marker beds are recognized in the lower Thumb Mountain Formation, one a worm-burrowed beige micrite, the other apparently an intraclastic rubble bed some 10 to 50 cm thick,

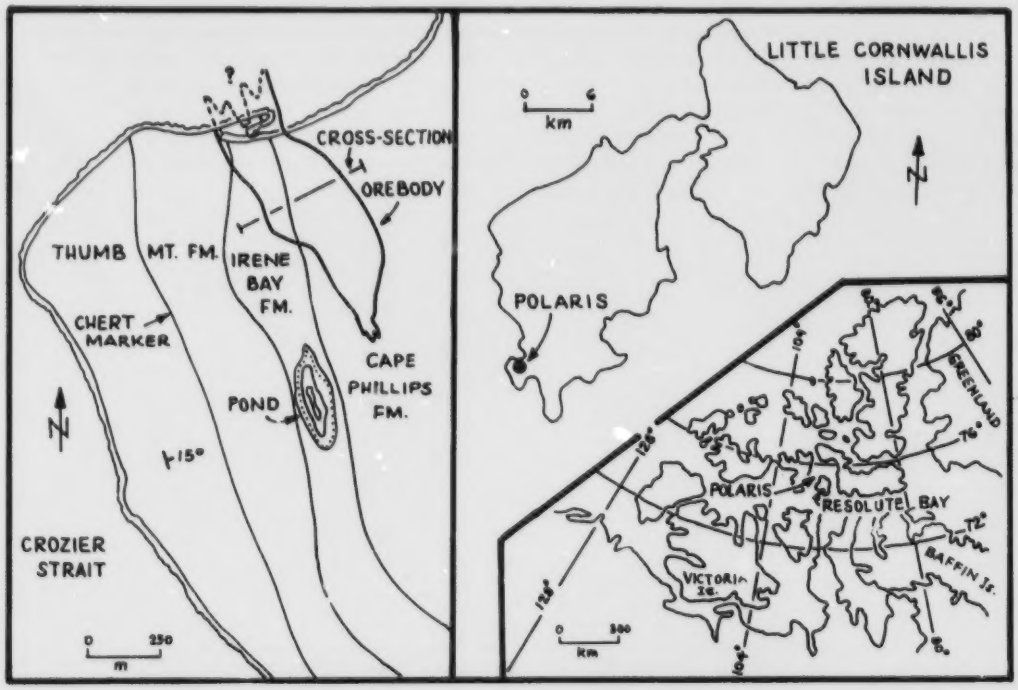

Figure 1. Location of Polaris deposit

possibly a storm deposit. The upper Thumb Mountain Formation contains two markers near the base, one a basal 6 m thickness of nodular chert-bearing dolostone, the other a 10 to 40 cm thick organic algal marker. Algal remains occur as clusters, patches, worm-burrow fill, and stylolite insolubles, presenting a recognizable black mottled or spotted dolostone, always located about 5 m above the nodular chert marker. The topmost 15 to 20 m of the Thumb Mountain Formation tends to be markedly more argillaceous than the rest of the upper 90 m of the formation.

The Irene Bay Formation, 60 m thick and Late Ordovician in age, is a distinctive green mudstone with lenses and intercalated beds of richly bioclastic limestone and argillaceous limestone. It conformably overlies the Thumb Mountain Formation. Its base has been mapped in the field at the base of the lowermost green shale or mudstone. Drill core examination suggests the base might better be placed at the sharp contact between Thumb Mountain argillaceous carbonates (below) and brown, clean, well sorted, richly bioclastic, 2 m thick packstones and grainstones (above) which pass gradationally upward into the distinctive green mudstone of the Irene Bay. This is the same sedimentological relationship as occurs at the base of the succeeding formation.

The Cape Phillips Formation conformably overlies the Irene Bay Formation, and ranges in age from late Ordovician to earliest Devonian. The basal contact, like that of the Irene Bay Formation, is sharp and is overlain by 10 m of bioclastic packstones and grainstones which pass gradationally upward into grey mudstones. The full thickness of the Cape Phillips Formation is not precisely known, but is estimated by Thorsteinsson (1986) to be about 600 m near the Polaris Mine area. Much of the sequence comprises siltstones, fine sandstones, planar laminated, nodular, or micritic carbonates, and cherty equivalents, in addition to shales and mudstones. Bitumen is universally present in the Cape Phillips Formation, which takes on a dark brown to black colour as a result.

No Devonian rocks have been drilled near Polaris. The closest outcrops lie some six kilometres east of the mine. The Disappointment Bay Formation lies with strong angular unconformity upon a sequence of folded pre-Devonian rocks. It is a planar laminated, fenestral porous dolostone, which may intermittently be underlain by a dolomite cobble or chert-chip conglomerate.

MINE GEOLOGY

Underground mapping is hampered by the absence of any water systems to wash walls — the mine operates entirely within permafrost — and by a heavy frost cover for part of the year. Being so far north renders a compass useless.

Structure

Rocks in the vicinity of Polaris dip eastward at angles varying from about 10° to a maximum of perhaps 30°, but averaging about 15°. Dips are commonly steepest at fault zones. The succession strikes north-northwesterly. Faults are most prominently developed along a northwesterly trend, but

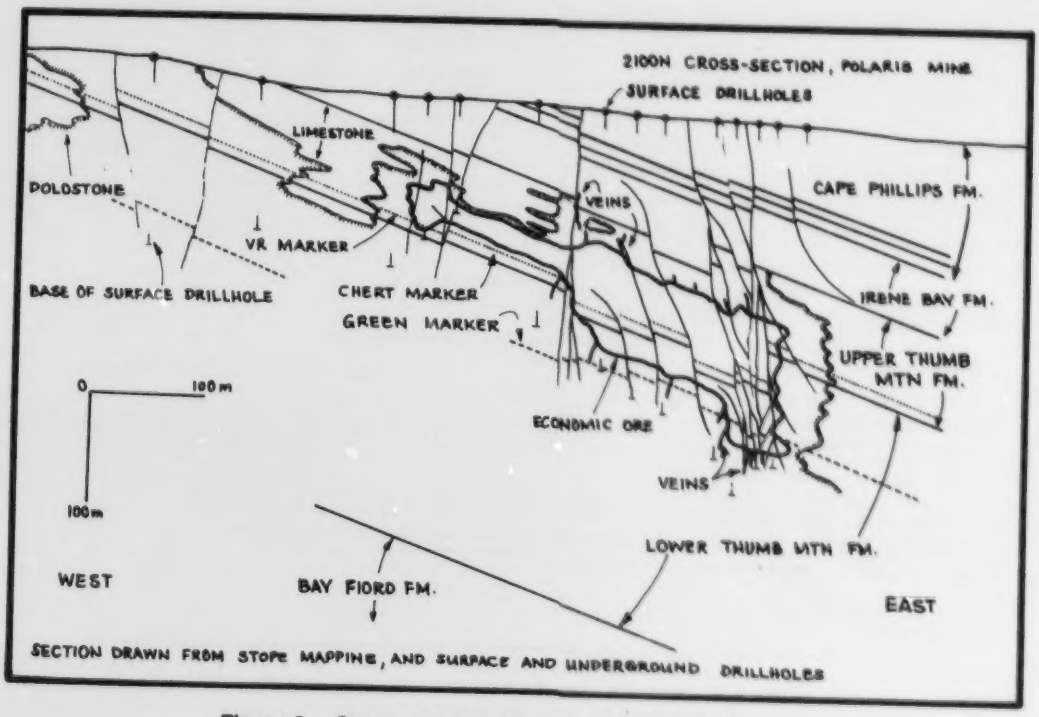

Figure 2. Cross-sectional view of the Polaris orebody on 2100N section

may also be roughly east-west in orientation. Faults may be near-vertical, the most common case (Fig. 2), or may dip at varying angles, some of which are close to or even parallel with bedding planes. Some faults appear to be thrust faults, but normal faults or strike-slip faults are more commonly observed. Some bedding-plane faulting appears to be related to folding responsible for the Cornwallis Fold Belt. Many faults postdate ore, including bedding plane faults. Some faults, on the other hand, pre-date ore, and may indeed have been active during sedimentation. The structural picture at Polaris is, as yet, far from clear.

Sulphides

The Polaris orebody is 300 m wide (east-west), 700 m long (north-south), and ranges in vertical thickness from 30 m in the west to 150 m in the east. The economic ore and mineralization limits are not greatly separated spatially, except in the footwall, where veins and disseminations of sulphides persist well below the economically mineable lower reaches of the orebody. Plan and cross-sectional views of the Polaris orebody are illustrated in Figures 1 and 2, respectively.

Sphalerite and galena are the two ore minerals, accompanied by marcasite, calcite, dolospar, minor barite, and traces of gypsum. Sphalerite occurs as disseminations, as open-space filling or colloform masses, and as veins or veinlets. Galena occurs as disseminations and as open-space filling in vugs and fractures or dolospar veins. Although growth zonation is observed in both colloform and discrete crystals of sphalerite, no uniform "stratigraphy" exists from place to place, and correlation of sphalerite bands even within a few tens of centimetres in a single drillhole is difficult. No signs of dissolution of sphalerite have yet been seen as "unconformities" in layers of colloform sphalerite. However, extensive replacement of sphalerite by galena has been observed. More than one generation of galena is present, with many partly dissolved crystals being commonly observed. Marcasite, too, occurs in two generations: an early phase that replaces host dolostones, and a phase that occurs late in the paragenesis, after all galena and sphalerite precipitation (Fig. 3).

Veins of sphalerite and galena are most easily observed below and above the orebody, but remnant or "ghost" veins also can be located in the highest grade ore where they are surrounded by masses of densely disseminated sphalerite and galena. Multiple dissolution of host dolostone and precipitation of sulphides as coeval or repetitive events appears to have occurred, resulting in the preservation, not only of the "precursor" sulphide veins, but also of a faintly discernible "layering" or "bedding" in the sulphides. Sulphide veins may be traced passing from vertical to bedding-parallel orientations.

Gangue

Sparry dolomite is the predominant gangue mineral. It occurs as early veins prior to much of the dissolution activity, as a recrystallization product of the host dolostone, as vuggy open-space filling in dolostone and sulphides, and as late veins. Late sparry dolomite veins are of two types, both post-main sulphide. The first is a "crackle" network of possible hydraulic fracture origin, the second is usually a planar, sometimes open fracture system.

Calcite is also a common gangue mineral, occurring last in the sequence, together with rare barite and gypsum.

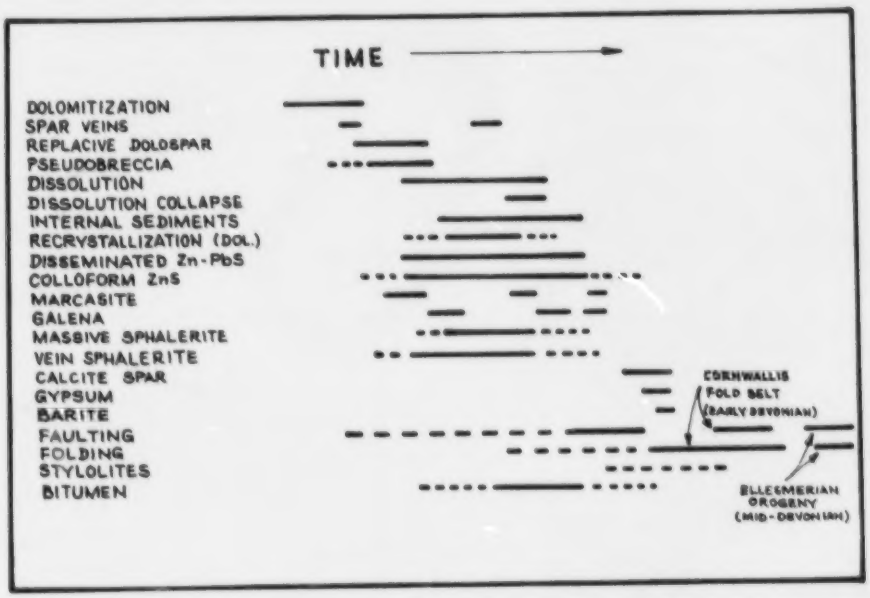

Figure 3. Possible relationships between ore, alteration, internal sedimentation and tectonism at Polaris

Internal sediments

In general, carbonate dissolution, commonly noted in many MVT deposits, either under meteoric karsting conditions related to an erosional surface (unconformity) or under conditions of hydrothermal mineralization unconnected with erosion surfaces, produces open spaces of variable size. Such open spaces may be wholly or partially filled with clastic sediments that may be derived from the adjacent rocks (autochthonous) or from sediments succeeding an unconformity (allochthonous).

Mappable, but volumetrically minor, internal sediments occur at Polaris. These comprise sediments of Thumb Mountain Formation rather than Devonian affinity (see below). All fossil components from the internal sediments are Upper Ordovician.

Although internal sediments occupy space that is discordant to the stratigraphy, the laminations in these internal sediments are everywhere concordant to the bedding of the upper Thumb Mountain Formation, except in areas of faulting and soft-sediment deformation. It may therefore be deduced that internal sedimentation occurred prior to the folding of the host Thumb Mountain Formation.

Fragments of colloform sulphides and of mineralized rock occur as clasts in internal sediments. Within some sequences of internal sediments there are also discrete layers of monomineralic sulphides which may have precipitated onto a planar surface of fine internal clastic sediments during an hiatus in the internal sedimentation history. Internal sediments comprise a series of graded beds, suggestive of successive "pulses" of sedimentation. These relationships are interpreted to mean that sulphide precipitation began before the early Devonian folding events responsible for the creation of the Cornwallis Fold Belt. It is possible that sulphide formation continued during folding, indeed the first remote effects of tectonism may be the mechanism responsible for "driving" fluids.

The absence of any fauna or sediments of recognizable Devonian affinity suggests that none of the internal sediments is related to Devonian (allochthonous) sedimentation which succeeded the profound lower Devonian unconformity.

Marker beds

Several marker beds are preserved in ore, without significant collapse-brecciation displacement. One of these, the VR Marker, is less than 50 cm thick, and comprises flecks and patches of organic algal concentrations in worm burrows and along stylolites. It is invariably present, even in highest grade mineralization comprising 100% sulphide rock. Five other marker horizons are also present in the ore zone, and the informal contact selected by Cominco Ltd. to distinguish the upper 90 m from the lower 260 m of the Thumb Mountain Formation can almost always be precisely located.

Alteration

Included under this title are diverse processes that have altered the original character of the rock.

The first is the alteration of limestone to dolostone which, in the upper Thumb Mountain Formation, forms an envelope around the orebody up to about 100 m in width, but much less in some places. Fault zones also display dolomitization. The extent of dolomitization is much greater in the lower Thumb Mountain Formation.

Dissolution of Thumb Mountain rocks is a notable alteration phenomenon which renders the wackestones and burrowed rock of both the upper and lower Thumb Mountain Formation porous. In the process, rocks show signs of thinning disaggregation and the accumulation of insoluble organic-rich dissolution residuum. These organic-rich parts are sites of sulphide precipitation. At the interval of the Chert Marker, it is possible to map the concentration of chert nodules, which are greater in number within dissolution-altered zones than without. The absence of suitable markers or rock types in much of the succession renders difficult the task of accurately estimating the degree of thinning of Thumb Mountain rocks. This aspect is further complicated by the existence of syndepositional tectonism, which appears to be at least partly responsible for thinning of part of the lower Thumb Mountain Formation.

Recrystallization of the host dolostone is a commonly observed feature in and near ore. In an extreme form, the matrix of early-diagenetic dolomitic burrows becomes completely recrystallized to rhombic dolomite or sparry dolomite. The resultant rocks look like breccias, the "fragments" actually being worm burrows and the "matrix" being neither autochthonous nor allochthonous, but recrystallized upper Thumb Mountain dolostone.

Brecciation is an alteration phenomenon which developed mainly as a result of dissolution. The breccias, though geometrically distinctive, have a relatively small component of translation due to collapse, perhaps measurable in tens of centimetres at most. Other breccias form as a result of repetitive dense vein development of either sparry dolomite or sulphides. Some breccias are clearly early diagenetic or syndepositional gravity "slide" or soft-sediment slump breccias, and are therefore not ore-related alteration phenomena in a direct sense.

The present understanding of the relationships between alteration, mineralization, tectonism, and internal sedimentation are illustrated on the diagram in Fig. 3.

Sulphur isotopes

The δ^{34} sulphur isotope values for sphalerite range from +2.9 to +11.2 per mil, and those for galena, from +1 to +9.4 per mil. Values for the evaporites in the Paleozoic section underlying Polaris are +27 to +29 per mil (Davies and Krouse, 1975). Table shows sulphur isotope values, calculated in per mil relative to the Canon Diablo Troilite Standard. These are plotted in Figure 4.

Table 1. Sulphur isotope values at polaris calculated in per mil, relative to the canon diablo troilite standard

Location	Value
Galena	
P5-425	+7.5
P86-5-157	+4.8
G-stope	+7.3
G-stope	+6.5
(Duplicate	+6.2)
P5-426	+9.4
820-181	+5.3
M-VR	+6.2
730-210	+3.1
A-B Pillar	+4.7
1973 Expl. Drift	+1.2
850-185	+1.0
Sphalerite	
850-189	+11.2
F-ramp	+9.2
A-stope	+8.2
LTM vein	+10.3
G-stope	+8.2
(Duplicate	+8.9)
G-stope	+9.0
LTM vein	+9.3
(Duplicate	+9.0)
850-187 UTM	+8.6
850-187 vein	+9.3
(Duplicate	+8.3)
A-stope Elec. Sub	+8.6
(Duplicate	+8.8)
820-178	+9.7
(Duplicate	+9.8)
850-190	+10.2
(Duplicate	+9.3)
115 x-cut-south	+8.6
790-210	+6.5
730-210	+5.8
B-stope	+4.4
P88-34-148	+6.0
A-B Pillar	+5.8
760-210	+2.9
790 Elec. Sub	+5.9
U86-15-28	+4.1
C-North N	+3.6
Marcasite	
115 x-cut	+7.6
820-185	+6.7
P88-34-131	+6.6

ORIGIN

In Figure 5 are illustrated several features at Polaris that characterize the orebody. Early faults responsible for some lower Thumb Mountain Formation isopach variations possibly acted as plumbing conduits allowing ingress of brines carrying sulphate from evaporites in the Bay Fiord or Baumann Fiord formations, underlying the Thumb Mountain rocks. These brines may also have carried metals. Organic material indigenous to the Thumb Mountain Formation possibly reduced the sulphate thermochemically, whereupon sulphide and metal ions combined to produce ore components. Such reactions probably also contributed to rock dissolution, satisfying the geological observation of an overlap between sulphide precipitation, rock dissolution, and internal sedimentation. In the course of these events, the limestone was dolomitized, with alteration ranging from simple dolomitization to extensive recrystallization or the production of soft, powdery dolomite. Thermal breakdown of organic material possibly produced methane and carbon dioxide, the gases being trapped beneath the impermeable Irene Bay Formation and argillaceous uppermost Thumb Mountain Formation. Carbon dioxide partial pressure variations and sulphate reduction reactions probably jointly controlled the formation of abundant gangue sparry dolomite. Anderson (1983) and Anderson and Garven (1987) have discussed the reactions involved in such a sequence of events.

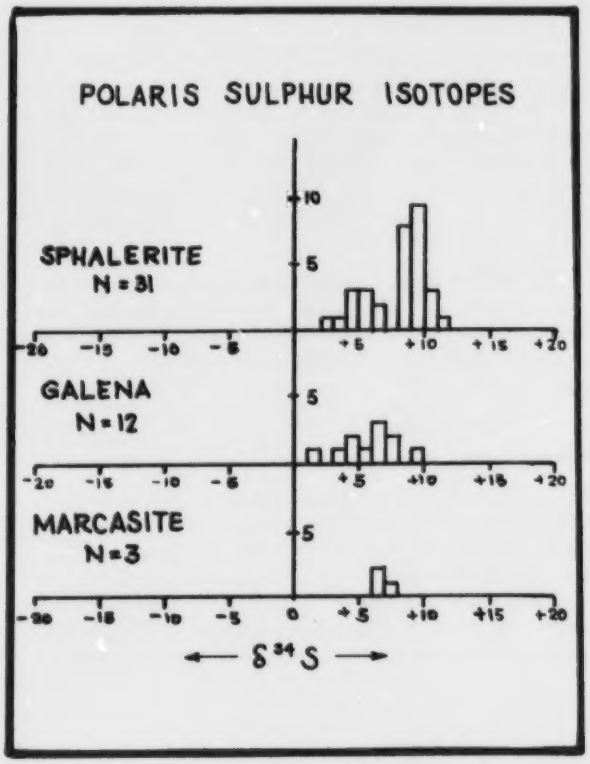

Figure 4. Sulphur isotopes at Polaris (includes duplicates shown in table 1)

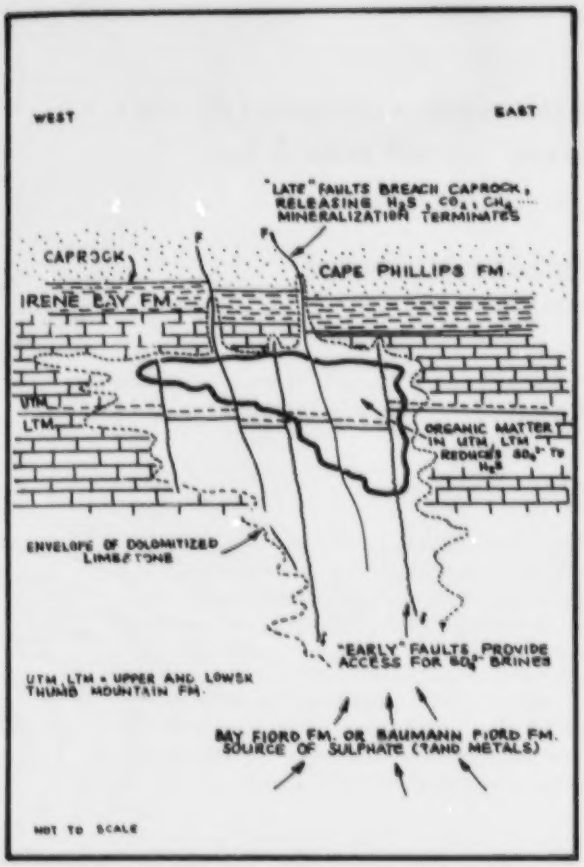

Figure 5. Features contributing to ore formation at Polaris

These events probably began shortly before the major deformation that spawned the Cornwallis Fold Belt and may have overlapped with tectonism. Perhaps advanced tectonism caused the breach of the Irene Bay Formation by faults. The resultant loss of gases may have terminated metal mineralization. Late, though rare, gypsum and barite were the final stages of mineralization. Veins of sulphide in the lowest Cape Phillips Formation suggest earliest Silurian as a possible first date for mineralization. Earliest Devonian folding marks a possible latest date.

ACKNOWLEDGMENTS

Cominco Ltd. allowed this study to be undertaken and provided a leave of absence for RNR, who is presently engaged in research under the guidance of GMA at the University of Toronto. Financial support from NSERC and the University of Toronto is gratefully acknowledged. The Geological Survey of Canada has supported the project through a Mineral Development Agreement which has provided partial funding for analyses. This funding and the generous assistance of D.F. Sangster are gratefully acknowledged. Thanks are due to Polaris Mine for partial funding of analyses and for the provision of summer employment for RNR, and for the cost of shipment of rock samples.

REFERENCES

Anderson, G.M.
1983: Some geochemical aspects of sulphide precipitation in carbonate rocks; *in* International Conference on Mississippi Valley-type Lead Zinc Deposits, Proceedings, edited by G. Kisvarsanyi et al., University of Missouri-Rolla, Rolla, Missouri, p. 61-76.

Anderson, G.M. and Garven, G.
1987: Sulfate-sulfide-carbonate associations in Mississippi Valley-type lead-zinc deposits; Economic Geology, v. 82, p. 482-488.

Davies, G.R. and Krouse, H.R.
1975 Sulphur isotope distribution in Paleozoic sulphate evaporites, Canadian Arctic Archipelago; *in* Current Research, Part B, Geological Survey of Canada, Paper 75-1B, p. 221-225.

Embry, A.F.
1988: Middle-Upper Devonian sedimentation in the Canadian Arctic Islands and the Ellesmerian Orogeny; *in* Canadian Society of Petroleum Geologists, Memoir 14, edited by N.J. McMillan et al., p. 15-28.

Jowett, E.C.
1975: Nature of the ore-forming fluids of the Polaris Lead-Zinc deposit, Little Cornwallis Island, NWT from fluid inclusion studies; Canadian Institute of Mining and Metallurgy Bulletin, v. 68, p. 124-130.

Kerr, J.W.
1977: Cornwallis Lead-Zinc District: Mississippi Valley-type deposits controlled by stratigraphy and tectonics; Canadian Journal of Earth Sciences, v. 14, p. 1402-1426.

Miall, A.D.
1986: Effects of Caledonian tectonism in Arctic Canada; Geology, v. 14, p. 904-907.

Muraro, T.W.
1973: Lead-zinc mining on Little Cornwallis Island; Canadian Society of Exploration Geophysicists National Convention Proceedings, Calgary, p. 230-234.

Okulitch, A.V., Packard, J.J., and Zolnai, A.I.
1986: Evolution of the Boothia Uplift, Arctic Canada; Canadian Journal of Earth Sciences, v. 23, p. 350-358.

Sangster, D.F.
1974: Geology of Canadian lead and zinc deposits; Geological Survey of Canada, Paper 74-1A, p. 141-142.
1983: Mississippi Valley-type deposits: a geological melange; *in* International Conference on Mississipi Valley-type Lead Zinc Deposits, Proceedings, edited by G. Kisvarsanyi et al., University of Missouri-Rolla, Rolla, Missouri, p. 7-19.

Thorsteinsson, R.
1958: Cornwallis and Little Cornwallis islands, District of Franklin, NWT; Geological Survey of Canada, Memoir 294.
1986: Geology of Cornwallis Island and neighbouring smaller islands, District of Franklin, NWT; Geological Survey of Canada, Map 1626A, scale 1:250 000.

Thorsteinsson, R. and Kerr, J.W.
1968: Cornwallis and adjacent smaller islands, Canadian Arctic Archipelago; Geological Survey of Canada, Paper 67-64.

Late Wisconsinan deglaciation of the area south of Dolphin and Union Strait, northern District of Mackenzie

Isabelle McMartin[1] and Denis A. St-Onge
Terrain Sciences Division

McMartin, I. and St-Onge, D.A. Late Wisconsinan deglaciation of the area south of Dolphin and Union Strait, northern District of Mackenzie; in Current Research, Part D, Geological Survey of Canada, Paper 90-1D, p. 55-66, 1990.

Abstract

Late Wisconsinan ice reached the eastern slopes of the Melville Hills just west of Bluenose Lake, District of Mackenzie. Deglaciation from this position to Coronation Gulf has been subdivided into four major retreat phases. These are defined by distinct flow patterns identified from drumlins, flutings and striae, and by ice frontal positions associated with morainic ridges and other ice contact features. The downwasting ice mass gradually retreated from the Melville Hills area and formed distinct lobes flowing northwestward into Dolphin and Union Strait and westward into Richardson River and Rae River basins. Eventually the sea penetrated along a corridor which opened between the ice mass and the mainland extending as far as the upper reaches of Richardson River. Rapid calving into this water body generated numerous minor surges and changes in ice flow direction. The rapid collapse of the Coronation Gulf ice mass resulted in the production of vast quantities of icebergs which scoured the floor of the shallow sea.

Résumé

Les glaces du Wisconsinien supérieur ont atteint les versants orientaux des collines Melville immédiatement à l'ouest du lac Bluenose dans le district de Mackenzie. La déglaciation, de cet endroit jusqu'au golfe Coronation, a été répartie en quatre phases principales de retrait. Celles-ci sont définies en fonction de différentes configurations de l'écoulement glaciaire, telles que déduites de l'examen des drumlins, cannelures et stries, et d'après les positions du front glaciaire associées aux crêtes morainiques et aux autres structures de contact glaciaire. La masse glaciaire en voie de désintégration s'est progressivement retirée de la région des collines Melville, et a formé des lobes distincts qui s'écoulaient vers le nord-ouest, jusque dans le détroit Dolphin et Union et vers l'ouest, jusque dans les bassins hydrographiques de la rivière Richardson et de la rivière Rae. Finalement, la mer s'est introduite dans le corridor qui s'est formé entre la masse glaciaire et la terre ferme, au moins jusqu'au cours supérieur de la rivière Richardson. Le vêlage rapide des glaces dans cette étendue d'eau a produit un grand nombre de crues glaciaires de moindre importance, ainsi que des variations de la direction d'écoulement des glaces. La rapide désintégration de la masse de glace du golfe Coronation a permis la formation de grandes quantités d'icebergs qui ont affouillé le fond de la mer peu profonde.

[1] Département des Sciences de la Terre, Université du Québec à Montréal, Montréal, Québec, H3C 3J7

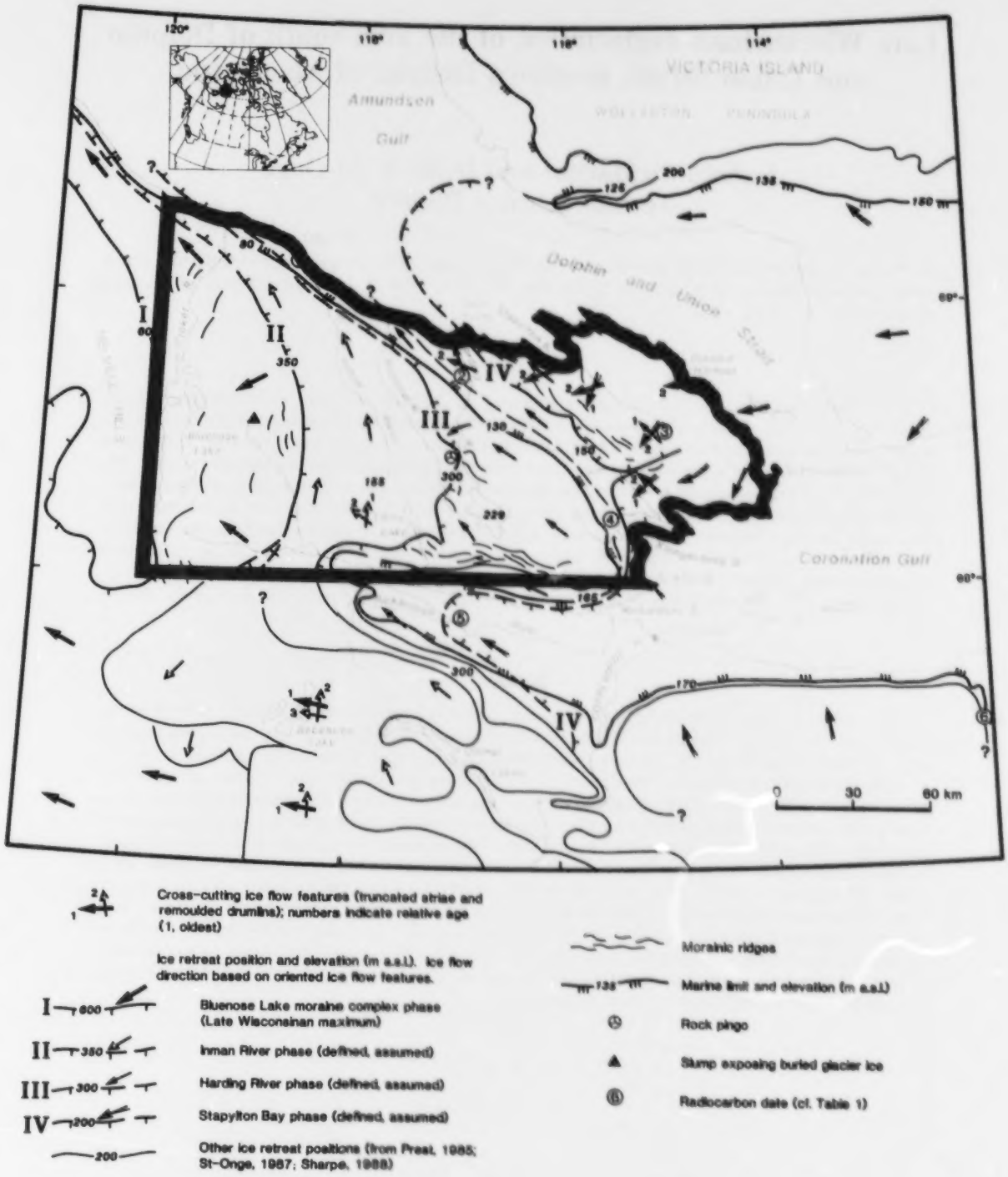

Figure 1. Study area (outlined) and Late Wisconsinan retreat phases south of Dolphin and Union Strait.

INTRODUCTION

Figure 1 is a model for Late Wisconsinan ice retreat in the region south of Dolphin and Union Strait, Northwest Territories. It is based on extensive field work and systematic mapping of surficial deposits since 1986. The study area lies within the Horton Plain of the Interior Plains region and is underlain by subhorizontal lower Paleozoic dolomites and minor dolomitic siltstone and sandstone (Fraser et al., 1960). The southern fringe of the study area, within the Rae River basin, is underlain by a volcano-sedimentary sequence of Proterozoic age (Baragar and Donaldson, 1973). A discontinuous drift cover, up to 30 m thick, mantles large parts of the region; however, bedrock outcrops are common and extensive either along major valley scarps or in areas where the drift has been washed away by glacial meltwaters. St-Onge and McMartin (1987) subdivided the Bluenose Lake region into two sub-regions: the Croker River Hills, part of the Melville Hills, and the Inman River Plateau, which we now propose should be extended easterly to Cape Krusenstern. Deglaciation events have been subdivided into four major retreat phases (Fig. 1). Correlation with deglaciation phases of adjoining areas, particularly to the south and on Victoria Island, are tentatively proposed. No attempt was made to assign definite ages to these phases although existing radiocarbon dates allow for the definition of minimun ages for the deglaciation of the coastal regions.

PREVIOUS WORK

Craig (1960) was the first to propose a pattern of ice retreat for the area south of Dolphin and Union Strait in his brief report based on work done as part of the Geological Survey of Canada's "Operation Coppermine". His mapping of ice flow features suggested that the retreating ice sheet divided into two major lobes. The first, coming from Victoria Island and moving in a southwesterly direction, was responsible for the construction of a series of end moraines south of Stapylton Bay. The second lobe, moving in a northwest direction, overrode at some point features associated with the first lobe. As a result of drawdown into the Richardson River basin, Craig further suggested that the northwestward ice flow was re-oriented in a westerly direction. He thought that the ice margin along Coronation Gulf had been static for a considerable length of time "due to the early entry of the sea between the two major ice lobes as a re-entrant along Dolphin and Union Strait and along the gulf" (Craig, 1960, p. 3).

Mapping in the Richardson River basin, as part of an MA thesis study, led Mercier (1984) to conclude that a glacial lake, which he named glacial Lake Richardson, had occupied the Richardson River and Rae River basins. He further suggested that the eastward retreating ice led to the formation of four distinct glacial lake phases which were controlled by well defined outlets and marked by numerous deltas. Deglaciation of the Richardson River and Rae River basins occurred prior to 10 300 + 240 BP (GSC-3663) Table 1, site 5) based on the age of the oldest shells collected in the area (Mercier, 1984).

A later study by Kerr (1987a) on lithofacies assemblages refined our understanding of the evolution of glacial Lake Richardson and led to a re-evaluation of ice frontal positions. Kerr (1987a, p. 2139) concluded that glacial lakes "remained generally confined to the western end of the ice lobe occupying the basin".

The field and airphoto study of ice flow features, in the area south of Bluenose Lake, led Prest (1985) to identify ice marginal positions with associated glacial lakes in that area. Prest's information is summarized in Figure 1.

Based on extensive work in Coppermine River valley, St-Onge (1987) proposed a model of ice retreat and defined four deglaciation phases associated with ice frontal positions for the regions south of the present study area. The information based on ice flow indicators, moraine ridges and other ice contact features, as well as lithofacies associations is also summarized in Figure 1.

In the western part of the study area, St-Onge and McMartin (1987) identified a major morainic belt which drapes the southeast, east, and northeast slope of the Melville Hills, a high bedrock plateau just west of Bluenose Lake. The "Bluenose Lake moraine", which includes a sequence of major ice-thrust ridges, represents a major ice frontal position. It is a continuation of the ice frontal position which Klassen (1971) considered as the "approximate limit of Late Wisconsinan glaciation"; airphoto interpretation led Vincent (1984) to suggest that this ice limit was probably Early Wisconsinan. The results of our present study as discussed below strongly support a Late Wisconsinan age.

Calving of the lobe occupying Dolphin and Union Strait and parts of Amundsen Gulf created a drawdown which dramatically changed ice flow direction in the low-lying areas

Table 1. Radiocarbon ages pertaining to deglaciation of the study area

Site*	^{14}C age	Lab no.	Elevation (m)	Material	References
1	10 700 ± 100	GSC-4390	61	*Hiatella arctica*	this report
2	10 530 ± 260	I(GSC)-25	74	Marine shells	Craig (1960)
3	9610 ± 90	GSC-4749	105	*Hiatella arctica*	this report
4	11 170 ± 80	TO-1231	125	*Portlandia arctic*	this report
5	10 300 ± 240	GSC-3663	90	*Macoma calcarea*	Mercier (1984)
6	10 215 ± 220	I(GSC)-17	85	*Macoma calcarea*	Craig (1960)

* Locations are shown in Figure 1.

to the east of the Bluenose Lake moraine complex. The active ice now flowed in a northwesterly direction across the Inman River plateau, skirting the high ground to the west. The rapid flow generated by the calving bay produced a spectacular drumlin field with individual drumlins up to 8 km long (St-Onge and McMartin, 1987).

Thinning of the ice mass as a result of rapid extensive flow and subsequent melting and retreat resulted in the formation of two distinct lobes — one in the Richardson River and Rae River basins and one centred in Dolphin and Union Strait and flowing into Amundsen Gulf. The lobe in the first area was fringed by a sequence of narrow ice marginal lakes which are identified by numerous strandlines, ice contact deltas, and thin glacial lacustrine deposits at the western end of the lobe (Kerr, 1987a; St-Onge, 1987, 1988).

LATE WISCONSINAN DEGLACIATION PHASES SOUTH OF DOLPHIN AND UNION STRAIT

The ice frontal positions identified in this report are inferred from the distribution of major continuous morainic ridges, which commonly display thrust features, ice contact meltwater channels, extensively washed surfaces, glaciolacustrine sediments and lake strandlines, and major lithofacies assemblages. No attempt has been made to assign specific ages to any of the ice frontal positions. The whole sequence is assumed to be Late Wisconsinan, and age determinations on marine shells provide minimum ages for the deglaciation of areas covered by the postglacial sea. The trend of intermediate ice frontal positions is also indicated where the presence of morainic or other features permit.

Phase I — Bluenose Lake phase and moraine complex

To the south and west of Bluenose Lake, the limit of Late Wisconsinan active ice is marked by a complex morainic ridge with a steep easterly slope. The ridge is interpreted as glacigenic debris carried along the hanging wall of a thrust-plane at the limit of the actively flowing ice (St-Onge and McMartin, 1987). West of this ridge the drift is thin and is restricted mostly to moulin kames, thin glaciofluvial deposits with collapsed structures to the east, and thin, usually contorted rhythmites also collapsed to the east.

The ice thrust moraine lies at approximately 600 m a.s.l. and marks the western limit of Late Wisconsinan ice advance on the eastern slope of the Melville Hills (Fig. 1). Several lines of evidence support this hypothesis. Sediments exposed along Croker River record a continuous glacial cycle. Pre-last glaciation fluvial gravel and sand at the base, which are overlain by a fining upward sequence of coarse to fine sand, are interpreted as resulting from the blocking of the lower part of the pre-last glaciation Croker River. The glacial lake rhythmites of silt and silty clay are overlain by a massive bouldery diamicton interpreted as a basal till. The till is in turn overlain by rhythmites formed in an early postglacial lake, which are capped by coarse steeply dipping foreset beds of coarse sand and gravel, which on the surface display numerous collapsed structures on the proximal eastern side (St-Onge and McMartin, 1987, p. 98, Fig. 10.7). These delta kame deposits cannot be distinguished in nature, in freshness, or in any other way from a whole flight of similar features which extends from the area just north of Bluenose Lake to the delta kames which mark the marine limit.

The Bluenose Lake moraine also contains numerous small glacial lake basins within major east-facing re-entrants in the hummocky region. Generally speaking, these lacustrine deposits end abruptly to the east where they terminate in drainage channels trending to the north-northwest and ending in the Inman River drumlin field. There is, therefore, a continuity of landforms and lithofacies assemblages between the Bluenose moraine and the drumlin field. It can be further argued that if the limit between the Inman River drumlin field and the Bluenose moraine marked a significant age break, a major northwest trending channel should be found north of Bluenose Lake. This channel would have allowed drainage during the Late Wisconsinan phase when ice would have occupied only the Inman drumlin field and adjacent lowlands. Such is not the case. Indeed, Croker River is superimposed on the drumlin field across which it has carved its valley. This is only possible if it is assumed that the northward flowing river draining the Bluenose Lake basin flowed on top of the ice across part of the Bluenose Lake moraine and across the drumlin field. All the evidence strongly supports the hypothesis that the Bluenose Lake moraine and the Inman drumlin field are part of the same glacial events although they represent distinct ice dynamics within this complex.

Active ice flowing upslope along the east side of the Melville Hills and attaining an elevation of 600 m implies great thickness of ice to the east including southern Victoria Island. Evidence from recent work by Sharpe (1988) indicates that on Wollaston Peninsula the area was covered by active ice during the Late Wisconsinan to more than 325 m a.s.l. elevation. Therefore, our results support the model proposed by Dyke and Prest (1987).

One additional feature of the Bluenose Lake moraine deserves reporting in more detail. Within this arcuate belt of drift, commonly thicker than 30 m, several slumps have recently exposed ice-rich sediments overlain by massive diamicton. This was first mentioned in St-Onge and McMartin (1987, p. 95) but, at that time, the underlying material was not sufficiently exposed to allow speculation on the origin of the icy sediments. The slump, first observed in 1986 (and shown in Fig. 10.4 in St-Onge and McMartin, 1987), was re-examined in 1988 and again in 1989. Between 1986 and 1988 the slump had enlarged substantially (Fig. 2). It now exposes a 25 m high section comprising 15 to 20 m of icy sediments overlain by 2 to 5 m of silty sand and bouldery diamicton (Fig. 3). The icy sediments exhibit folding and complex deformations, and numerous large boulders, cobbles, and pebbles occur in the silty, icy sediment. Some layers also display small subhorizontal sheared ice lenses. The upper contact of the icy sediments and the bouldery diamicton is sharp, planar, and subhorizontal. Reticulate ice, developed in the matrix of the diamicton overlying the unconformity, was observed; the maximum thickness of the active layer is approximately 2 m within the diamicton.

Figure 2. Low level oblique air photograph of the large slump exposing icy sediments within the Bluenose Lake moraine; view towards the northwest. 204982-E.

Figure 3. Ground view of part of the slump shown in Figure 2. Note the sharp contrast between the icy sediments and the overlying diamicton (till), and the numerous clasts within the icy sediments. Figure at right for scale. 204982-A.

It does not correspond to the unconformity between the diamicton and the underlying icy sediment. In the general area where the slump occurs there are many others which also display icy sediments and overlying diamicton. These massive icy sediments are interpreted as basal glacier ice buried by thrusting in an area of compressive flow in the ice frontal zone of an active Late Wisconsinan ice mass (St-Onge and McMartin, 1989).

South of the Bluenose Lake region, in the Bebensee Lake area, the early westward trending ice was also recognized by Prest (1985) who proposed a series of deglacial events with glacier recession generally towards the east.

North of Bluenose Lake, the ice flowed to the northwest into Amundsen Gulf, while south of the lake it skirted the southern limit of the Melville Hills to flow west and eventually to the northwest into Hornaday River basin or to the southwest into Great Bear Lake basin. Following this maximum advance to the Late Wisconsinan ice margin, thinning occurred and drawdown within Amundsen Gulf and Great Bear Lake resulted in numerous surges and redirection of ice flows as explained in the following events.

Phase II — Inman River phase

When the westward flowing ice receded to the Inman River plateau, the compressive flow, typical of the Bluenose Lake phase, was replaced by extensive flow which was redirected towards the calving bay in Amundsen Gulf to the northwest. This high velocity flow moulded drift into large drumlins named the Inman drumlin field by St-Onge and McMartin (1987). The northward trending ice flow observed in the Bebensee Lake area (Prest, 1985) is presumed to be associated with this phase, indicating that the Amundsen Gulf drawdown affected areas up to 250 km inland.

Final ablation of the ice was by massive downwasting as demonstrated by the absence of morainic ridges of any sort. Outwash fans with ice contact features to the east and northeast suggest that the dead ice mass was shrinking towards the lowlands (St-Onge and McMartin, 1987). Several esker ridges, which wind between the drumlins, also suggest downwasting over extensive areas.

North of Bebensee Lake, late surges complicate the deglaciation history. The timing of west and southwest flows (Prest, 1985) is not sufficiently known to be fitted in the sequence described in this report. Thus, the extent of the Inman River Phase, west of Rae River and Richardson River basins, is speculative as shown in Figure 1. In the Coppermine River valley region, St-Onge (1987) defined the Forcier Lake Moraine Phase which is the most westerly ice frontal position recognized in this area. It is possible that this ice frontal position, with an elevation between 325 and 400 m, can be joined with the 350 m ice frontal position during the Inman River Phase. This was suggested by Kerr (1987a, p. 2139, Fig. 2b).

Spectacular rock pingos, which deform the dolomitic bedrock, are scattered in the southern part of the Inman River Plateau near the shores of small, partly drained lakes. The pingos dominate the nearly flat landscape by 5 to 20 m or more. One of these, first identified by Craig (1960), is nearly 22 m high and is composed of slabs of dolomite dipping at 35° to 40° (Fig. 4, 5). Striae are well preserved on some of the tilted bedrock surfaces. The pingo postdates the last ice advance but, at this time, a more precise age is not possible. It could be speculated that like numerous, much smaller features, it also dates from the early deglaciation when permafrost was being re-established (St-Onge et al., 1988).

Phase III — Harding River phase

As a result of rapid thinning, the northwestward flowing ice was divided into two distinct lobes centred in major basins. It is probable that the evidence for westerly and southwesterly flowing ice north of Bebensee Lake represents the early inception of the lobe which was to occupy the Richardson River and Rae River basins. The second lobe that resulted from the shrinking of the main ice mass to lower ground was centred in the channels of Amundsen Gulf and Dolphin and Union Strait.

Figure 4. Location of rock pingo (Fig. 5) and part of the morainic ridge of Phase III interrupted by an outwash complex with collapse structures to the east (OC) and glaciofluvial deltas and fans (D).

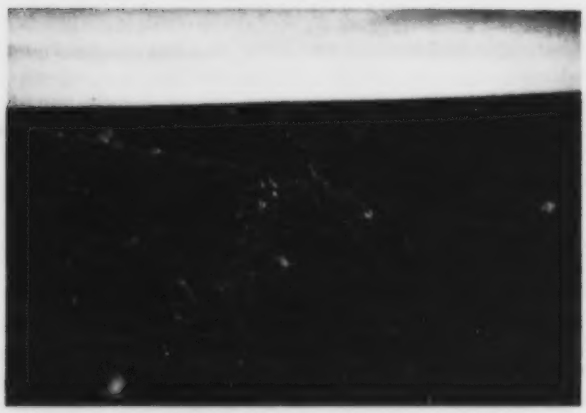

Figure 5. Pingo of pie shaped steeply dipping slabs of dolomite, 22 m high. 204982-B.

West of large unnamed lake from which Harding River originates (Fig. 1, Lake "229"), a major, north-south morainic ridge, averaging 20 m high, occurs at 300 m a.s.l. (Fig. 4, 6). This nearly continuous ridge displays a distinctly steeper east-facing slope and on its western slope some outwash fans and deltas occur. It is interpreted to represent the frontal position of the ice mass occupying the upland area between the two lobes centred in the depressions to the north and south. Two major breaches in this morainic ridge are filled with large outwash terraces of gravel and sand which are bounded by several minor bouldery gravel ridges commonly oriented northwest-southeast (Fig. 4). Drumlins associated with these minor morainic ridges indicate that the major ice front was affected by small surges which frequently crosscut each other. North of Harding River, the ridge strikes towards the northwest and becomes a gravelly kame occupying an extensively washed glaciofluvial corridor which ends abruptly at marine limite at 115 m a.s.l. The drumlins, along the coast, from Hoppner to Croker rivers, are oriented towards the northwest. The ice flow in that area was, thus, identical during both Inman River and Harding River phases.

Figure 6. Southern portion of the morainic ridge and outwash complex of Phase III. Note contrasting texture between Inman River drumlin field west of the ridge and the minor ridges to the east as well as the different orientation of the drumlins. East-west ridges in the southern part of the air photograph are part of a series of major morainic ridges which fringe the northern slopes of the Rae River basin (Fig. 1). See figure 4 for legend.

Between Libby Lake and Lake "229", the ridge extends to the southeast into a pitted outwash complex bordered by collapsed structures (Fig. 6). This results from intense sedimentation between the ice resting on the upland and the Richardson River and Rae River lobe to the south. Numerous ice marginal lakes were formed during this phase; one example is ancestral Lake Libby in which fine sediments were deposited up to 20 m above the present lake level. Surging by the lobe occupying Richardson and Rae river basins into ice marginal lakes at its western extremity, led to the formation of westward and northwestward-trending drumlins (St-Onge, 1988). Sedimentation of till and outwash, along the steep northern slopes of the basin, produced a complex of large morainic ridges trending east-west. These ridges rise from 240 to 280 m a.s.l. and are concentrated in a corridor 70 km long and 10 km wide (Fig. 6). East of Libby Lake, the ridges have not been modified by wave action nor do they comprise glaciolacustrine sediments. Therefore, they represent ice marginal positions prior to the existence of extensive ice marginal lakes or to the incursion of marine waters. At this stage, extensive ice marginal lakes existed only at the western extremity of the lobe (St-Onge and McMartin, 1987). Shrinking of this lobe below elevations of 240 m permitted coalescence and extension of the marginal lakes to a point where they finally surrounded its northern margin, thus accelerating the disintegration of the ice by extensive calving. Glacial lake outlets were identified by Kerr (1987a) at elevations of 240, 210, 180 and 165 m a.s.l. west of Klengenberg Bay, but the extensive stripping of large bedrock surfaces by meltwaters and the large deposits of bouldery gravel at the downstream end of these channels suggest that these corridors were mostly carved by high energy meltwaters flowing from glacier ice to the east resting along the steep slopes west of Cape Kendall.

South of Cape Young, the marine incursion from the northwest led to a minor redirection of the ice flow towards the west-northwest. Numerous northwest striking drumlins have been modified by a west-northwest ice flow (Fig. 7). Intersecting striae show a similar relationship. Craig (1960) originally proposed that a lobe coming from Victoria Island had been overridden by another one moving to the northwest. Evidence from this study, however, suggests that these features are minor fluctuations in the direction of an unstable ice front.

As the lobe occupying Richardson and Rae river basins was shrinking, so was the ice lobe occupying the channel of Amundsen Gulf and Dolphin and Union Strait. Eventually this allowed the sea to invade the isostatically depressed lowlands along a corridor between the land and the ice lobe (St-Onge and McMartin, 1987). The deglaciation of the coast and the synchronous marine invasion occurred prior to 11 170 ± BP (TO-1231), a radiocarbon date obtained from *Portlandia artica* shells collected at 125 m a.s.l. in glaciomarine rythmites overlying subaqueous outwash gravels and sands (Table 1, Site 4). The corridor between sea and ice made it also possible for marine waters to invade the Richardson and Rae river basins from the northeast. The oldest radiocarbon age on marine shells in the basin is 10 300 ± 240 BP (GSC-3663, Table 1) obtained from shells collected at 90 m a.s.l. This elevation is well below the marine limit of approximately 150 m a.s.l. in the west at the head of the basins but which rises to 170 m along Coppermine River to the east (Mercier, 1984). The difference in age is probably due to the absence of an early marine fauna in a marine arm in which large quantities of meltwaters flowed.

During the final stages of the Harding River Phase, the ice front was in contact with the sea, which resulted in large areas near marine limit to be intensively washed and modified by wave and current actions. Sedimentation from meltwaters debouching into the ocean was intensive, resulting in the accumulation of a thick sequence of marine rnythmites (Kerr, 1987b).

Phase IV — Stapylton Bay Phase

This phase marks the beginning of a complete re-orientation of the southeastward retreating ice lobe centred in Dolphin and Union Strait into a southwestward flow coming from Victoria Island to the east. This flow crosscuts the previous northwestward flow (Fig. 1). The entire coastal area in the Dolphin and Union Strait region was deglaciated by the end of this phase which occurred prior to 10 215 ± 220 (I(GSC)-17, Table 1) and age determination obtained from *Macoma calcarea* shells collected at 85 m a.s.l. (Fig. 1, site 6).

The area northeast of an imaginary line passing from Cape Young to Klengenberg Bay, and bordered by Dolphin and Union Strait and Coronation Gulf, lies at elevations below 150 m a.s.l. Glacial landforms in this area were extensively washed by marine waters so that the resulting subdued topography is covered by a lag of coarse material. These lowlands in the Bernard Harbour area (St-Onge et al., 1988) are covered by spectacular swarms of drumlins (Potschin, 1988). They are composed of a silty sand diamicton with numerous dolomitic boulders, pebbles, and cobbles, as well as granitic and gabbroic rocks. These can only have been derived from the south and southeast and are scattered throughout the area. Extensive flutings also occur where the drift is thin. Esker ridges, some as long as 10 km, wind between the drumlins and through the fluted terrain. Kames and kame terraces occur in places at the downstream end of esker ridges. Large bouldery beach ridges have developed on either side of these lanforms, particulary at elevations below 80 m a.s.l.

A complex of discontinuous morainic ridges occurs between Stapylton Bay and Klengenberg Bay. These end moraines, which mark the limit of the southwestward flowing ice and thus are associated with the drumlin fields of the Bernard Harbour area, occur at elevations near or higher than the local marine limit (Fig. 8). They comprise a series of ridges generally arcuate to the southwest and between 5 and 15 m high. As shown in Figure 1, this complex morainic system is divided into two entities by a large re-entrant occupied by ridges and hills of massive bouldery outwash gravel and sand forming an interlobate kame complex. Some of these morainic ridges are made up of a distinct silty diamicton in which the matrix is a reddish silt which is similar to the marine sandy silt, typical of the marine sediments. We suggest that these segments of end moraine and other

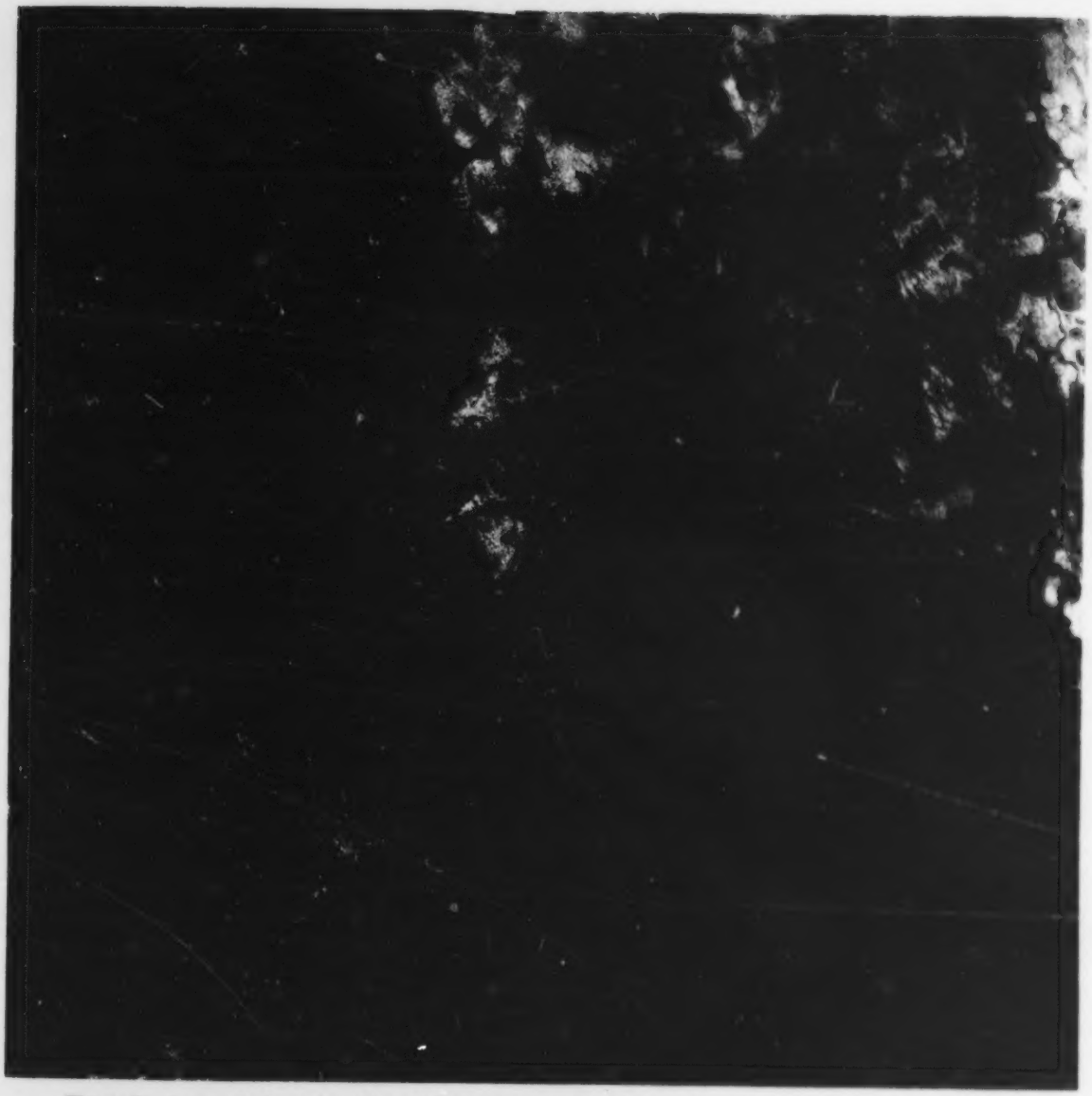

Figure 7. Large glaciomarine delta at 120 m a.s.l. and the limit of marine offlap sediments south of Cape Young. Note remoulding of northwest-striking drumlins by a west-northwest ice flow. See Figure 4 for legend.

minor ridges are the result of minor re-advances of the ice mass into the marine corridor at a time when the ice was calving into the marine bay between the highlands to the southwest and the ice lobe in Dolphin and Union Strait. In the same region to the northeast of the end moraine ridges, numerous minor moraines occur draped over drumlins. These are likely DeGeer moraines formed at the grounded margin of the ice on top of the drumlins (Fig. 9).

This ice front, which terminated into an arm of the sea, was very unstable. Minor surges flowed in various directions as documented by intersecting striae.

On Wollaston Peninsula of Victoria Island, a major lateral moraine complex — the Colville Moraine — was constructed, along with large outwash terraces, deltas and fans before 10 710 ± 100 BP (GSC-3566; Sharpe, 1988). This would suggest that the Colville Moraine was constructed on the north side of the same ice lobe responsible for the construction of end moraines between Klengenberg and Cape Young on its south side. The invasion of the Richardson and Rae river basins by the sea led not only to the rapid disintegration of the Richardson-Rae lobe but also to the collapse of the ice mass occupying Coronation Gulf.

This allowed the postglacial sea to encroach on the south shore of Coronation Gulf where, along the present Coppermine River valley, it reached an elevation of 170 m. a.s.l. (St-Onge and Bruneau, 1982). Following the collapse of the ice mass, the keel of icebergs produced innumerable grooves over the areas that were still covered by the postglacial sea. These shallow scours are generally less than 1 m wide and between 10 and 30 cm deep, with lengths up to several hundreds of metres.

Figure 8. Stapylton Bay (Phase IV) morainic ridges. The east-west ridges are composed of south-dipping beds and lenses of poorly sorted bouldery gravel. The diamicton of the north-south arcuate ridge includes a high percentage of reddish silt similar to the marine sediments to the east. See Figure 4 for legend.

Figure 9. De Geer moraines draped over southwest-striking drumlins northeast of the arcuate moraine ridges shown in Figure 8. These features are generally less than 10 m wide, 40 m long, and not higher than 1 m. 204982-D.

SUMMARY AND CONCLUSIONS

Glacial landforms and lithofacies assemblages provide unambiguous evidence that ice reached the eastern slopes of the Melville Hills in the Bluenose Lake region south of Amundsen Gulf during the Late Wisconsinan. There, westerly flowing ice under compressive flow built a large thrust moraine system within which glacier ice has been preserved.

Following the Late Wisconsinan maximum ice advance, three stages in ice retreat can be defined. Each of these is the result of shrinking ice masses which gradually confined ice lobes to major depressions such as Dolphin and Union Strait to the north and the basin of the Richardson River and Rea River to the south. Flow dynamics were primarily controlled by drawdowns provided by calving bays in Amundsen Gulf and by a glacial lake sequence at the western end of the Richardson River and Rae River lobe. Extensive ice flow conditions led to the moulding of spectacular drumlin fields such as the one in the Inman River region, and the complex, commonly curvilinear swarms of the Bernard Harbour region.

One major conclusion of this study is that early during the Harding River phase of deglaciation, the sea occupied a corridor between the dolomite upland and the ice lobe sitting in the lowlands. It is in this arm of the sea that most of the postglacial marine sedimentation occured. Once the area was completely ice free, sedimentation had all but ceased and marine action was confined to wave washing of progressively emerging landforms such as occurs along the present-day coastline. One major difference, however, is that the rapid disintegration of the ice lobes calving into the sea resulted in pervasive iceberg scouring.

ACKNOWLEDGMENTS

We are indebted to student assistants, who have contributed significantly to the observations and discussions which led to the concepts contained in this paper: R. Avery, H. Beaudet, D. Kerr, M. Potschin, and J. Samson. Their meticulous field observations and keen interest were essential stimulants. Helicopter support from the Polar Continental Shelf Project ensured efficient field logistics. Helicopter and fixed-wing pilots improved the quality of life in the "luxury" accommodations of YSO and Drumlin City. Finally to Rod Stone, the competent and patient radio expeditor, a special thanks for keeping a sense of humour while catering to the often strange requests from numerous field camps. Comments by the critical reader J.S. Vincent significantly improved the original draft of this paper.

REFERENCES

Baragar, W.S., and Donaldson, J.A.
1973: Coppermine and Dismal lakes map-area; Geological Survey of Canada, Paper 71-39, 20 p.

Craig, B.G.
1960: Surficial geology of north-central District of Mackenzie, Northwest Territories; Geological Survey of Canada, Paper 60-18, 8 p.

Dyke, A.S., and Prest, V.K.
1987: Paleogeography of northern North America 18 000-5000 years ago; Geological Survey of Canada, Map 1703A, scale 1:5 000 000.

Fraser, J.A., Craig, B.G., Davidson, W.L., Fulton, R.J., Heywood, W.W., and Irvine, T.N.
1960: Geology, north-central District of Mackenzie, Northwest Territories; Geological Survey of Canada, Map 18-1960, scale 1 inch to 8 miles.

Kerr, D.E.
1987a: Depositional environments during a glaciolacustrine to marine transition in the Richardson-Rae rivers basin, Northwest Territories; Canadian Journal of Earth Sciences, v. 24, p. 2130-2140.
1987b: Preliminary interpretation of the stratigraphy of the marine offlap sequence in the Clifton Point area, District of Mackenzie; *in* Current Research, Part A, Geological Survey of Canada, Paper 87-1A, p. 153-157.

Klassen, R.W.
1971: Surficial geology, Franklin Bay (97 C) and Brock River (97 D); Geological Survey of Canada, Open File 48, scale 1:250 000.

Mercier, A.L.
1984: Glacial lake in the Richardson and Rae river basins, Northwest Territories; Géographie physique et Quaternaire, v. 38, no 1, p. 75-80.

Potschin, M.B.
1988: Drumlin fields of the Bernard Harbour area, Northwest Territories; *in* Current Research, Part D, Geological Survey of Canada, Paper 89-1D, p. 113-117.

Prest, V.K.
1985: Glacial geology of the Bebensee Lake map-area (NTS 86 M), Great Bear Lake region, Northwest Territories; *in* Contributions to the Geology of the Northwest Territories, Volume 2, Indian And Northern Affairs Canada (NAP), p. 63-70.

St-Onge, D.A.
1987: Quaternary geology and geomorphology of the Lower Coppermine River valley, District of Mackenzie; 12th INQUA Congress, International Union for Quaternary Research, Excursion Guide Book A-22, 32 p.
1988: Surficial geology, Coppermine River, District of Mackenzie, Northwest Territories; Geological Survey of Canda, Map 1645A, scale 1:250 000.

St-Onge, D.A. et Bruneau, H.C.
1982: Dépôts meubles du secteur aval de la rivière Coppermine, Territoires du Nord-Ouest; *in* Recherches en cours, partie B, Commission géologiques du Canada, Etude 82-1B, p. 51-55.

St-Onge, D.A. and McMartin, I.
1987: Morphosedimentary zones in the Bluenose Lake region, District of Mackenzie; *in* Current Research, Part A, Geological Survey of Canada, Paper 87-1A, p. 89-100.
1989: Buried glacier ice in the Bluenose Lake moraine (abstract); *in* Abstracts, Second International Conference on Geomorphology, Frankfurt, Germany.

St-Onges, D.A., McMartin, I., and Avery, A.
1988: Rock blisters and other frost-heaved landforms in the Bernard Harbour area, District of Mackenzie, Northwest Territories; *in* Current Research, Part D, Geological Survey of Canada, Paper 89-1D, p. 95-99.

Sharpe, D.R.
1988: Late glacial landforms of Wollaston Peninsula, Victoria Island, Northwest Territories: product of ice-marginal retreat, surge, and mass stagnation; Canadian Journal of Earth Sciences, v. 25, p. 262-279.

Vincent, J-S.
1984: Quaternary stratigraphy of the western Canadian Arctic Archipelago; *in* Quaternary Stratigraphy of Canada — A Canadian Contribution to IGCP Project 24, R.J. Fulton (ed.); Geological Survey of Canada, Paper 84-10, p. 87-100.

Were erratics moved by glaciers or icebergs to Prince Patrick Island, western Arctic Archipelago, Northwest Territories?[1]

D.A. Hodgson
Terrain Sciences Division

Hodgson, D.A. Were erratics moved by glaciers or icebergs to Prince Patrick Island, western Arctic Archipelago, Northwest Territories; in Current Research, Part D, Geological Survey of Canada, Paper 90-1D, p. 67-70, 1990.

Abstract

Clasts scattered to 190 m a.s.l. over outcrop of the sandy fluvial Neogene Beaufort Formation range from granules up to 4 m blocks of crystalline, carbonate, quartzitic, and basic rocks. Sources include the Canadian Shield, which lies 1000 km distant from the south through to the northeast. Other indicators of foreign ice are absent from the island; however, the high elevation of erratics on adjacent Melville Island suggests inundation by a continental ice sheet more extensive and older than Early Pleistocene tills to the south. Size of erratics indicates some ice rafting; the elevations of them do not.

Erratics which likely once covered all landmasses in the western archipelago have been eroded by periglacial processes everywhere except on the well drained Beaufort sand where scarp retreat dominates.

Résumé

Les fragments de roches détritiques disséminés jusqu'à 190 m au-dessus du niveau de la mer, au-dessus de l'affleurement de la formation de Beaufort, formation fluviatile sableuse d'âge néogène, varient de la taille de granules à celle de blocs de 4 m composés de roches cristallines, carbonatées, quartzitiques et basiques. Leur lieu d'origine comprend le Bouclier canadien qui s'étend à 1000 km de distance, du sud jusqu'au nord-est. Il n'existe pas sur l'île d'autres indicateurs de glace allochtone; cependant, la présence de blocs erratiques à haute altitude sur l'île Melville adjacente témoigne d'une inondation par un inlandsis plus étendu et plus ancien que celui qui a déposé les tills du Pléistocène inférieur au sud. Les dimensions des blocs erratiques indiquent qu'il ont pu être transportés dans une certaine mesure par un radeau de glace, mais non leur position en altitude.

Les blocs erratiques qui ont déjà probablement recouvert toutes les îles dans l'ouest de l'archipel ont été érodés par des processus périglaciaires mais tel n'est pas le cas sur le sable bien drainé de Beaufort où le principal processus d'érosion est le recul de l'escarpement.

[1] Contribution to Frontier Geoscience Program

INTRODUCTION

Far travelled erratics have been noted since the mid 19th Century on many islands in the Canadian Arctic Archipelago. Haughton (1859, p. 396-397), using descriptions from the islands, suggested transport by rafting on drifting ice at a time when sea levels were more than 150 m higher than at present. Whereas Dawson (1887, p. 56R-58R), with experience on the mainland, and the glacial theory widely accepted, believed emplacement was by glacial ice moving north. The subsequent variety of opinions on extent of Quaternary glaciers and range of sea levels, summarized by Washburn (1947), indicates how poorly these processes were understood in the area. Quaternary deposits on Prince Patrick Island, and particularly occurrences of erratics, were discussed perceptively by Tozer and Thorsteinsson (1964, p. 34-36). The significance of erratics will be reassessed here because they may be the only indicators of a conjectured pan-archipelago or larger ice sheet reaching Prince Patrick Island (e.g. Craig and Fyles, 1960).

OCCURRENCE AND NATURE OF ERRATICS

Much of the Neogene Beaufort Formation on Prince Patrick Island is overlain by a 1 m layer of sandy gravel in which clasts are distinctly more polymict than in the Beaufort itself. Undisturbed source deposits for erratic clasts have not been recognized. The unconsolidated sandy fluvial deposits which comprise most of the Beaufort Formation cover the west and centre of the island to a maximum elevation of 190 m (Fig. 1). Highest elevations occur at the eastern limit of outcrop towards the east and south of the island. Possibly reworked Beaufort sediments form the western coastal plain. Except where disconformable contact is made with underlying consolidated rock, gravel beds in the formation never include clasts larger than cobble size. These appear to consist of lithologies similar to rock types occurring on eastern Prince Patrick Island and Melville Island. Phanerozoic sediments of varying lithologies and degrees of consolidation outcrop over the remainder of the island, which rises to 280 m a.s.l. in the southeast. Rare occurrences of erratics on bedrock are described in the addendum.

Erratic clasts in the superficial gravel include granites and gneisses (mainly pink, some grey), quartzites, pale buff weathering limestone and dolomite, diabase and gabbro. Closest potential sources of crystalline, carbonate, and basic rocks are shown in Figure 2. Crystalline clasts vary from moderately weathered to spalling and disaggregating. Some formerly large carbonate blocks have split into fragments spread over many square metres. Fine grained intrusive rocks are relatively less weathered and a few bear fine striations. No marine pelecypod valves are found in association with erratics (marine shells occur sporadically in degraded tills on some other islands). Clasts are generally granule to cobble size, though boulders to 4 m in one dimension do occur. These isolated boulder size clasts are found mainly on the higher Beaufort sediments.

On adjacent northwest Melville Island, erratics that occur rarely on the Paleozoic rocks and in scattered patches

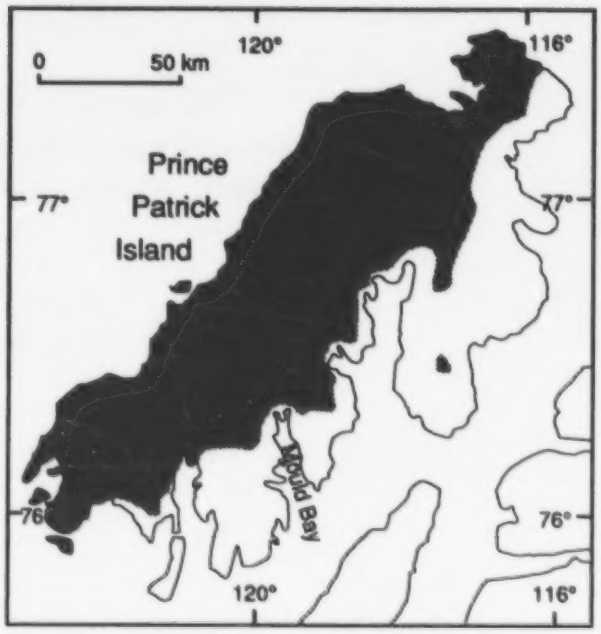

Figure 1. Beaufort Formation (shaded) equals extent of erratics on Prince Patrick Island.

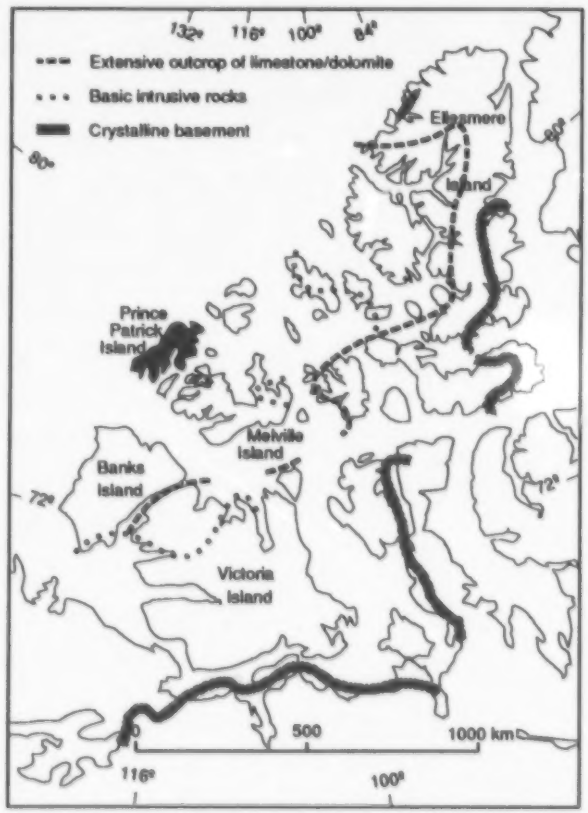

Figure 2. Sources of common erratics on Prince Patrick Island: northwesternmost limits.

of till to elevations > 500 m were believed by Hodgson (in press) to be of southern provenance. Some appear too large to be residuals from a nonglacial deposit. Concentrations near sea level on the southwest coast lie at the northern margin of the Late Wisconsinan Laurentide Ice Sheet (Fig. 3). Shells possibly of Early Pleistocene age found 200 m a.s.l. may have been deposited below contemporary sea level or have been be ice transported. The south coast of Melville Island was overlapped by continental ice up to 300 m a.s.l., leaving Dundas Till which was tentatively correlated (Hodgson et al., 1984) with the Early Pleistocene Banks Glaciation or less extensive Middle Pleistocene Thomsen Glaciation (Vincent, 1984). Crystalline and carbonate erratics occur on Lougheed Island (Fig. 3); they include a 4 m diabase block at 125 m a.s.l.

MODE OF TRANSPORT

Evidence for transport in glacial ice will be weighed against rafting in icebergs or perhaps ice islands.

Glaciers

Glacial indicators are confined to the centre and southeast of Prince Patrick Island. They consist of ice marginal meltwater channels and rare bedrock striations left by local ice of unknown age. Perhaps this ice striated basic erratics left by an earlier event. The high elevation erratics on Melville Island strongly suggest that an ice sheet inundated that island, possibly in the Early Pleistocene or even Pliocene. Such ice would likely have overlapped adjacent and much lower Prince Patrick Island. The source of such a massive ice sheet (possibly twice as large as the Laurentide Ice Sheet) was more likely over continental Canada rather than the eastern archipelago - unless Greenland ice crossed northern Baffin Bay. The edge of the Canadian Shield lies more than 1000 km both to the east and south (Fig. 2), and crystalline erratics are uncommon all the way to central Ellesmere Island. They are relatively common to the south, on Victoria Island, across which ice from the south is known to have flowed at later times. It is notable, however, that on Victoria Island, just a few hundred kilometres from the edge of the Shield, the largest crystalline erratics left by Laurentide ice do not exceed 1 m in diameter. Granitic erratics on Banks Island are never more than 20 cm in diameter (J.-S. Vincent, personal. communication, 1989).

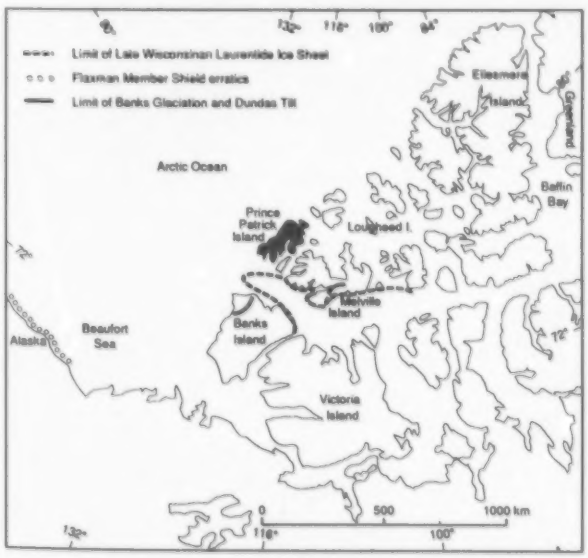

Figure 3. Limits of Quaternary glaciations in the northwest Arctic Archipelago.

Ice rafting

Any ice sheet that reached Victoria Island, or expanded in the eastern archipelago, was a potential source of ice rafted material, though this required movement counter to the present flow of water in a southeast direction through the archipelago. Or glaciers no more extensive than present ones in northern Ellesmere Island could supply crystalline rocks into the southwest drift of the Beaufort Gyre of the Arctic Ocean. To emplace erratics at their present elevations would have required sea level to be at least 190 m higher than at present, plus an allowance of several tens of metres to float icebergs. This is far higher than the > 26 m maximum known for Late Pleistocene sea levels on the island (Lowdon et al., 1967, p.193), or the 60 m maximum elevation of any Pleistocene glacial sea on Banks Island, and is similar to elevations reached inside the margin of the former Laurentide Ice Sheet. Of course, forces other than glacial isostasy may have changed sea levels since the Early Pleistocene (Hodgson, 1981, p. 33). Ice rafting does not comminute debris during transport and can explain the presence of large blocks. A good analogue is the Beaufort Sea coast of Alaska, where the Early Wisconsinan Flaxman Member of the Gubik Formation contains numerous clasts believed to have been ice rafted more than 1000 km from the east (Carter et al., 1986). Nevertheless, Shield erratics are rarely found on the raised shores of islands that lie beyond the limits of Late Wisconsinan Laurentide ice.

Conclusion

Erratics were moved up to 1000 km to Prince Patrick Island in the Early Pleistocene or even Late Pliocene from undefined sources which lay somewhere in an arc of 150° from south to northeast . The most likely process was a continental ice sheet which expanded over the western archipelago prior to the Early Pleistocene Banks Glaciation. On the other hand, the largest erratics are more readily explained in terms of a calving ice front over the Canadian Shield at a time when sea level at Prince Patrick Island was five or ten times higher than that reached in the Late Pleistocene. It seems probable that erratics once were distributed over all of Prince Patrick Island and adjacent landmasses.

ADDENDUM - GEOMORPHIC PROCESSES ERODING BEAUFORT SAND

Tozer and Thorsteinsson (1964, p. 36) suggest that it is anomalous that "The boulders are far more common on the Beaufort Formation than on the Palaeozoic and Mesozoic terrains adjacent to the belt of Beaufort outcrops....if the

boulders are the remains of old moraines it is surprising that the distribution of this morainal material should be related to the distribution of the fluvial Beaufort Formation." I have found erratics only on this formation, or on fans or terraces of material derived, from it with two exceptions. On resistant (but frost fractured) bedrock within a few hundred metres of the retreating eastern margin of the formation, a scattering of boulders remain after complete erosion of the former cover of sand. Numerous erratics also were found on a poorly consolidated outcrop of Mesozoic sandstone east of Mould Bay. The latter deposit lies a hundred metres lower than an adjacent outcrop of Beaufort Formation.

It appears that well drained sand erodes mainly by backwasting scarps, that is, by nivation. This leaves erratics in place until reached by a retreating scarp -- although the finer fraction may be eroded by eolian action. All other materials, whether consolidated or not, undergo extremely active mass wasting. Erratics were deposited on them sufficiently long ago that they have been comminuted or buried in fill in larger valleys.

ACKNOWLEDGMENTS

J.G. Fyles freely made available unpublished observations of surficial materials; he also reviewed the manuscript and made many suggestions for improvements. Field work in 1989 was aided by T.G. Fisher and supported by Polar Continental Shelf Project.

REFERENCES

Carter, L.D., Brigham-Grette, J., and Hopkins, D.M.
1986: Late Cenozoic marine transgressions of the Alaskan Arctic Coastal Plain; *in* Correlation of Quaternary Deposits and Events around the Margins of the Beaufort Sea: Contributions from a Joint Canadian-American Workshop, April 1984, J.A. Heginbottom and J.-S. Vincent (ed.); Geological Survey of Canada, Open File Report 1237, p. 21-26.

Craig, B.G. and Fyles, J.G.
1960: Pleistocene geology of Arctic Canada; Geological Survey of Canada, Paper 60-10, 21 p.

Dawson, G.M.
1887: Notes to accompany a geological map of the northern portion of the Dominion of Canada, east of the Rocky Mountains; Geological Survey of Canada, Annual Report, 1886, Part R, 62 p.

Haughton, S.
1859: Geological account of the Arctic Archipelago, Appendix IV; *in* A Narrative of the Discovery of the Fate of Sir John Franklin and his Companions by F.L. M'Clintock; John Murray, London, p. 372-399.

Hodgson, D.A.
1981: Surficial geology, Lougheed Island, northwest Arctic Archipelago; *in* Current Research, Part C, Geological Survey of Canada, Paper 81-1C, p. 27-34.

Quaternary geology of western Melvile Island; Geological Survey of Canada, Paper 89-21 (in press).

Hodgson, D.A., Vincent, J.-S., and Fyles, J.G.
1984: Quaternary geology of central Melville Island; Geological Survey of Canada, Paper 83-16, 25 p.

Lowdon, J.A., Fyles, J.G., and Blake, W., Jr.
1967: Geological Survey of Canada radiocarbon dates VI; Radiocarbon v.9, p.156-197.

Tozer, E.T. and Thorsteinsson, R.
1964: Western Queen Elizabeth Islands, Arctic Archipelago; Geological Survey of Canada, Memoir 332, 242 p.

Vincent, J.-S.
1984: Quaternary statigraphy of the western Canadian Arctic Archipelago; *in* Quaternary Stratigraphy of Canada - A Canadian Contribution to IGCP Project 24, R.J. Fulton (ed.); Geological Survey of Canada, Paper 84-10, p. 87-100.

Washburn, A.L.
1947: Reconnaissance geology of portions of Victoria Island and adjacent regions, Arctic Canada; Geological Society of America, Memoir 22, 142 p.

Preliminary assessment of selected drainage basins in western Fosheim Peninsula, Ellesmere Island, as sites for global change studies

P.A. Egginton and D. A. Hodgson
Terrain Sciences Division

Egginton, P.A. and Hodgson, D.A. Preliminary assessment of selected drainage basins in western Fosheim Peninsula, Ellesmere Island, as sites for global change studies; in Current Research, Part D, Geological Survey of Canada, Paper 90-1D, p. 71-77, 1990.

Abstract

The four lakes studied on western Fosheim Peninsula, Ellesmere Island have maximum depths between 2 and 46 m and July surface temperatures of 5.5 to 9.5°C. The basin at the head of Slidre Fiord is > 100 m deep and has a surface temperature of only 0.2°C. Cores from lake basins and the fiord may show variation in sedimentation since Late Wisconsinan time at least, recording changes in climate, and thus geomorphic processes.

Records of climatic induced variation in bottom sediments may, however, be obscured by such factors as changes in sediment supply resulting from emergence, iceberg scour (in fiord), local ground-ice induced changes in lake bathymetry, and contamination of datable organics by the abundant old carbon available locally.

Résumé

Les quatre lacs à l'étude dans l'ouest de la péninsule Fosheim (île d'Ellesmere) ont une profondeur maximale variant entre 2 et 46 m et leur température de surface en juillet se situe entre 5,5 et 9,5°C. Le bassin à l'amont du fjord Slidre, dépasse 100 m de profondeur et sa température de surface n'atteint que 0,2° C. Des carottes prélevées dans les bassins lacustres et le fjord pourraient révéler une variation de sédimentation depuis au moins le Wisconsinien supérieur, attestant ainsi des changements climatiques qui se sont répercutés, par conséquent, sur les processus géomorphologiques.

Les indices de variation de sédimentation d'origine climatique pourraient, cependant, être obscurcis par certains facteurs comme des changements d'apport sédimentaire causés par l'émergence, un affouillement par des icebergs (dans le fjord), des changements de bathymétrie des lacs provoqués par la présence de glace dans le sol locale et une contamination des matières organiques datables par l'ancien carbone abondant par endroits.

INTRODUCTION

An integrated study of climate, vegetation and hydrology at Hot Weather Creek, Fosheim Peninsula, Ellesmere Island (Edlund et al., 1989; Woo et al., 1990) could form a nucleus for wider studies of past environmental fluctuations. One of the undertakings will be a study of various components of the hydrological cycle and the documentation of sediment movement in this and possibly other drainage basins. There is a requirement to place current and anticipated future rates of sediment yield and anticipated climatic fluctuations into a geological context. One avenue that may be pursued is the collection and analysis of core from suitable lake basins or downstream fiords (e.g. Blake 1987; Lemmen, 1988; Retelle, 1986; Lemmen et al., 1988). The recovery of datable organics along with pollen and macrofossils may permit a reconstruction of past paleoenvironments and the determination of past sedimentation rates. During summer 1989 while carrying out other field work, a short reconnaissance was undertaken in this area to assess lakes within and adjacent to Slidre River basin and Slidre Fiord as sites for coring.

GEOLOGY

Western Fosheim Peninsula comprises a rolling lowland, underlain by poorly lithified Mesozoic and Cenozoic sediments, and ridges which rise to 1200 m buttressed by more resistant rock including basic dykes and sills. Abundant old carbon is being eroded from Tertiary/Cretaceous coal seams and from high terraces, probably of Neogene age (Fyles, 1989), which contain unlithified wood and peat.

Glacial landforms are rare in western Fosheim Peninsula. Although nonerosive ice may have been present in Late Wisconsinan time, it is more likely that most of the area remained unglaciated. Cores from Slidre Fiord and nearby lakes may possibly record events during the Wisconsinan.

The Late Pleistocene/Holocene marine limit lies at approximately 140 m a.s.l. During marine submergence, a substantial part of the lowland peninsula was inundated (Fig. 1).

METHODOLOGY

The objectives of this reconnaissance were to collect from the chosen water bodies: 1) bathymetric profiles, 2) surface lake temperatures, and 3) subsurface muds to assess the potential of the lake sediments for macrofossil and organic yield. Lakes are rare on the peninsula, as elsewhere in the Queen Elizabeth Islands: the two largest lakes on the western peninsula and two small lakes were sampled (Fig. 1).

Since all sampling was carried out from a floating but nonstationary helicopter there was an emphasis on equipment portability. An Eagle (Mach 1) profiler was used to obtain bathometric profiles. Surface samples were collected for temperature determinations and for later chemical analysis. Bottom waters and muds were sampled using a self sealing cup sampler.

RESULTS

Locations of lakes studied and the surveyed profile along Slidre Fiord are located in Figure 1. Summary data are presented in Table 1. Lake and basin drainage size are given because they influence potential sediment input into the lake. If all else is equal, then a small lake contained within a large drainage area will have relatively high sedimentation rates in comparison with a similar lake and a small drainage area.

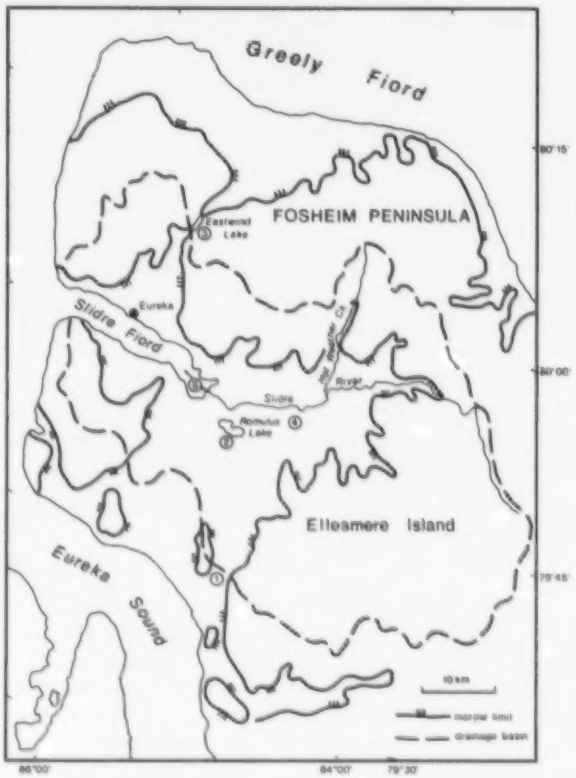

Figure 1. Location of study basins (1-5), western Fosheim Peninsula; including drainage basin for Slidre Fiord and Late Pleistocene/Holocene marine limit.

Table 1. Characteristics of study basins

Water body	Surface temp(°C)	Depth (m)	Area (km^2)	Drainage area (km^2)	Approx elevation (m)
1	6.5	2.1	.6	8	100
2 (Romulus Lake)	5.5	46.0	4.0	31	7
3 (Eastwind Lake)	6.0	2.6	.9	32	150
4	9.5	8.1	.3	2	10
5 (Slidre Fiord)	.2	>100	63.6	1300	0

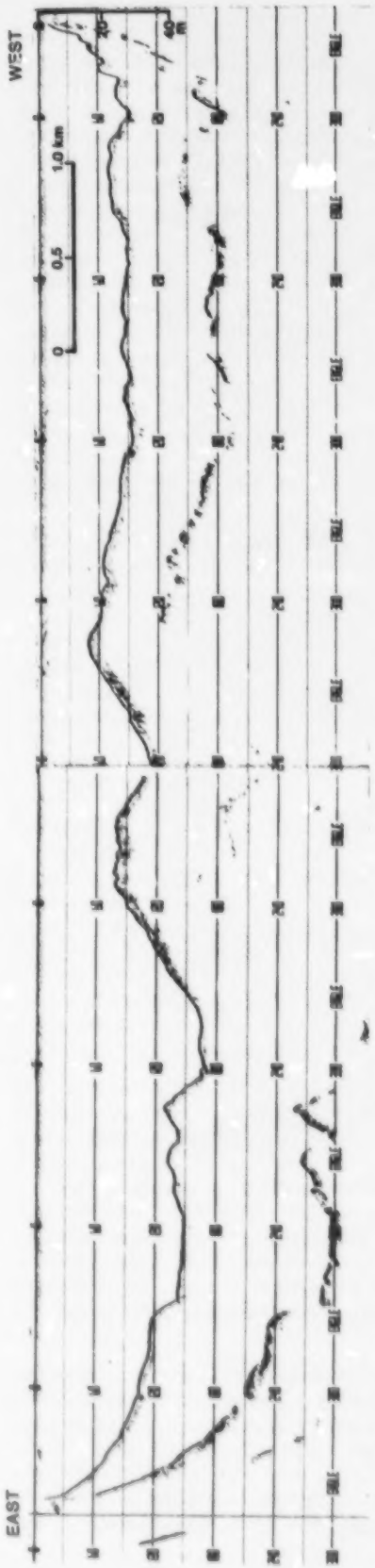

Figure 2. East-west profile through Romulus Lake.

An east-west sounding profile from Romulus Lake is shown in Figure 2; generalized profiles for this and the other lakes are shown in Figure 3a. No profile was run for lake #1. Photographs of the lakes and the adjacent basins are shown in Figure 4.

Romulus Lake (#2)

The lake is located 4 km west of the head of Slidre Fiord at an elevation of 7 m a.s.l (Fig. 1 and 4B). On the basis of regional emergence data, the lake has been above sea level for at least 3,000 years (Hodgson, 1985).

The lake is 46 m deep and several slope breaks are visible on the north and south edges of one profile (Fig. 3a). The east-west profile through the centre-line of the lake displays a bathymetry which changes substantially with distance (Fig. 2). The shallow mid-lake area is congruent with the peninsula on the north side of the lake (c.f. Figs. 2 and 4B). The eastern part of the basin is 'hard' bottomed (multiple echoes) in comparison with the central shallower part of the lake. On the basis of the profile the deepest part of the lake does not contain 'soft' sediments. The cup sampler which was lowered into the deepest part of the basin did not recover or presumably penetrate these sediments. Lake surface temperatures were 5.5°C while bottom temperatures were 0°C (Fig. 3b), reflecting the size and depth of the lake.

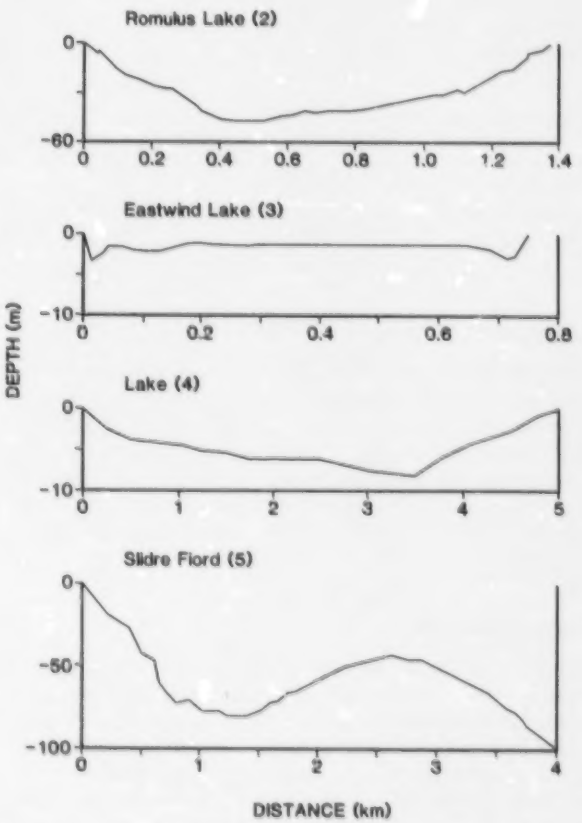

Figure 3a. Computer generated profiles of Romulus Lake, north-south transect; Eastwind Lake; unnamed lake#4; Slidre Fiord, east-west.

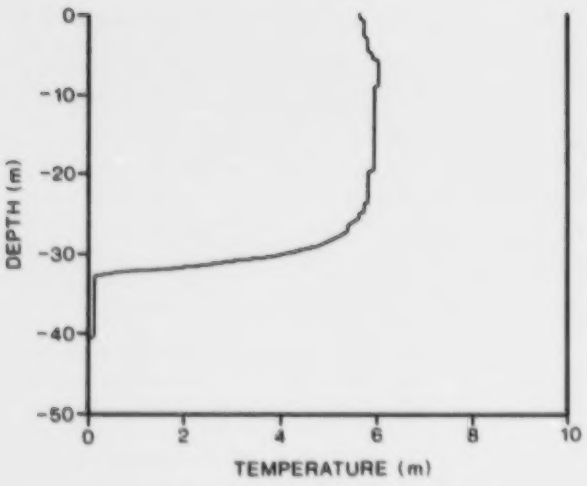

Figure 3b. Temperature profile, Romulus Lake.

Surface water is saline, but no salinity measurements were taken. The origin of the lake is problematical. It could represent an earlier extension of Slidre Fiord which has not been filled by sediment. This would account for its depth. A modern analogue for this may be the north-west corner of Slidre Fiord which is being isolated by two prograding deltas (Fig. 4B). An alternate interpretation may be that the lake has a thermokarst (kettle) origin. This could explain the varied bathymetry.

Eastwind Lake (#3)

Eastwind Lake lies at or above Late Wisconsinan marine limit within a diamicton, probably a till (Fig. 1, 4B). Its surface temperature of 8.0°C is high (Table 1). The lake, however, is shallow, the majority of it is less than 3 m deep (Fig. 3).

Unnamed Lake (#4)

This lake of 1.5 km^2 lies within Slidre River alluvium (Fig. 1 and 4B). Surface temperature was 9.5°C. The lake surface is inset at least 5 m below the surrounding terrain suggesting that the lake has been either partially drained and/or been lowered into the landscape. The profile is asymmetrical with the deeper part (8.1 m) located in the western part of the lake (Fig. 3). The lake may have a kettle or thermokarst origin.

Slidre Fiord (#5)

Slidre Fiord covers 64 km^2 and receives drainage water from an area of 1300 km^2, including some small glaciers in the Sawtooth Mountains. The fiord is composed of two basins each in excess of 80 m depth. The smaller one, which is 1.5 km in length (Fig. 3), receives drainage directly from the Slidre River and is separated from the rest of the fiord by a sill at 50 m depth (Fig. 1 and 3).

DISCUSSION

A schematically represented regional sediment yield between Late Wisconsinan time and present is shown in Figure 5. Although the western Fosheim Peninsula may not have been glaciated in Late Wisconsinan time, deglaciation of the eastern peninsula during the early Holocene would have significantly increased discharge and sediment yield. Ice cores from the Agassiz Ice Cap to the east suggest that Holocene temperatures would have been relatively warm over the interval 10 000 to 4000 BP, with a maximum between 9000 and 7000 BP (Koerner, 1989). Blake (1981) suggested a deterioration in climate to the southeast after 2500 BP. If these latter conditions apply to Fosheim Peninsula, then sediment supply would be expected to remain high during the Hypsithermal over the interval 9000 to 7000 BP when temperatures would have been raised significantly above those at present. During cooler periods such as the Neoglacial, which commenced about 4000 BP, sediment yield would be expected to decline before increasing again when the climate ameliorated.

On a much shorter time frame, during particularly warm years such as the summer of 1988, the upper permafrost may degrade. Retrogressive thaw flow slides initiated or reactivated at this time alter the sediment supply rate to the rivers for several years after the initial thermal disturbance (Fig. 6). These events on the basis of climate records at Eureka (thawing degree days for the month of July) have a return period of about 22 years (Fig. 7). If short term sediment discharges are to be placed into a broader context, then resolution of sediment pulses with a periodicity of about 20 years is required.

Unfortunately these climate related signals may be obscured or obliterated by other geological considerations. For example, the calibre and nature of the sediment supply from Slidre River may have changed significantly over time as lower segments of the river began to contribute sediment as sea level declined. The upper reaches of the river are dominated by bedrock, the lower by older valley fill and marine sediments. In addition, the drainage basin area contributing discharge has increased as relative sea level declined.

Slidre Fiord is ice covered for much of the year. The rivers that drain into the fiord have largely nival regimes, with the bulk of the sediment moved during the short spring freshet. During the short open water period (at least) there are substantial currents within the fiord. Icebergs originating from ice caps to the north of the fiord are constantly moving in and out of the fiord, ploughing and disturbing nearshore sediments. Given their size, scour probably extends to water depths of 70 m or more. Only sediments within the deeper parts of the basin are likely to yield an undisturbed sample.

It is uncertain how much of the finer fraction of sediment entering the fiord is actually deposited in the basins within it. Much of it may be moved out of the fiord during the open water season. Lemmen (1988) found that sedimentation rates in Disraeli Fiord on northern Ellesmere Island were of the order of 5 to 10 cm/1000 years and the impact of major climatic signals, that is, the Hypsithermal or the

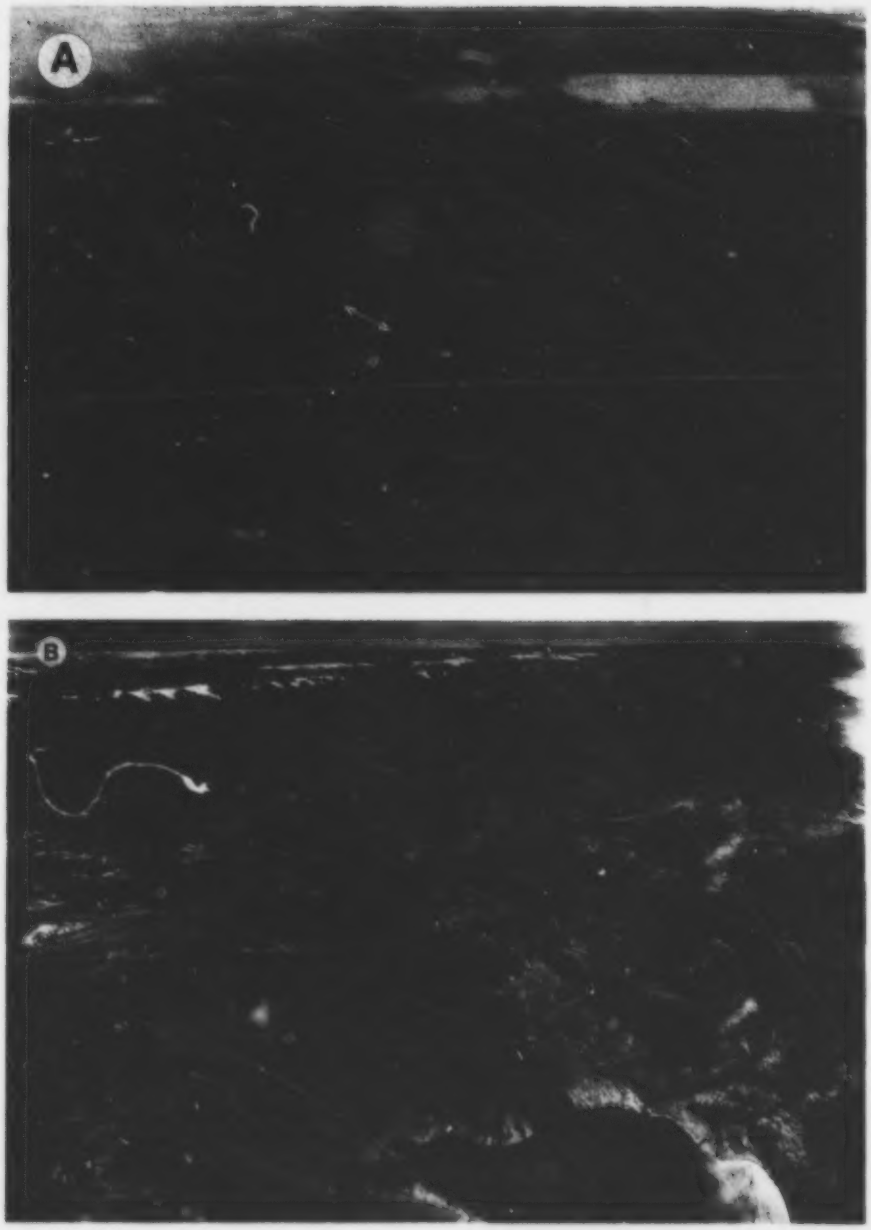

Figure 4A. Eastwind Lake; **B.** Lower Slidre River basin, showing head of Slidre Fiord and profile location, Romulus Lake and profile location, and lake #4. NAPL T49OR-3

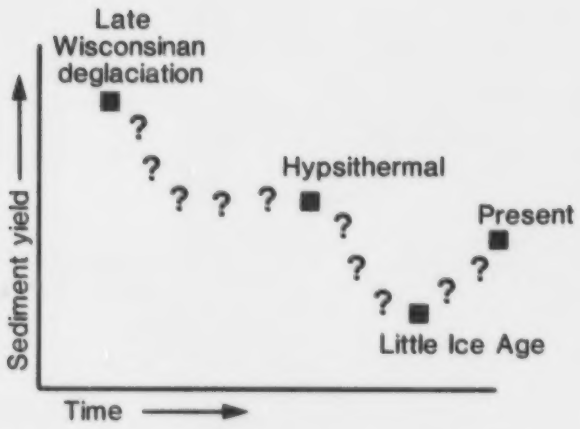

Figure 5. Hypothetical sediment yield curve for the area.

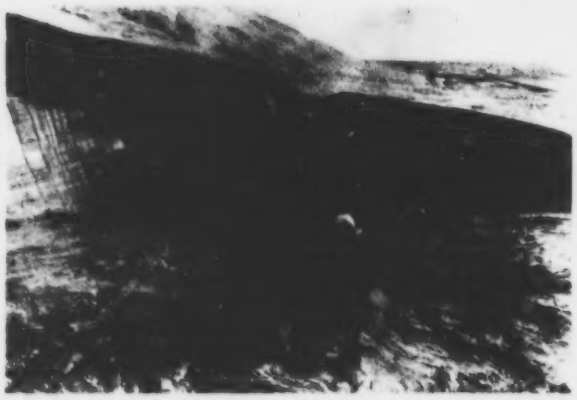

Figure 6. Exposure in a ground ice slump displaying multiple older headwalls. Each headwall is associated with a period of rapid retreat followed by burial and stabilization.

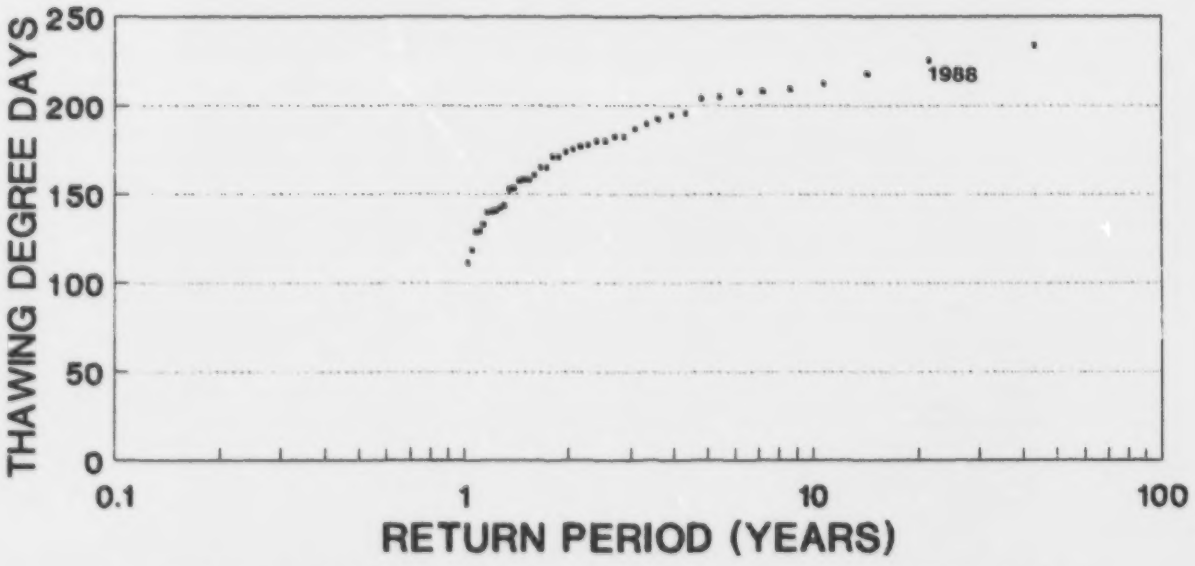

Figure 7. Return periods for July thawing degree days, Eureka. The 1988 event which triggered widespread slumping in the area has a return period of 22 years.

Neoglacial, were poorly resolved. Sediment supply to Slidre Fiord is probably higher than to Disraeli Fiord; a core from the fiord might indicate increased sedimentation at the time of regional deglaciation, as was the case for Disraeli Fiord.

None of the large lakes in the area have significant sediment input (i.e, they are not fed by significant sediment carrying streams). It is unlikely that core thickness and quality will be sufficient to resolve sediment supply variability over short time intervals.

The cup sampler, which has been used successfully farther south to collect bottom organics, did not provide any organic samples.

CONCLUSIONS

The sedimentation rates in the large lake basins remain to be determined but the utility of deep water core for placing short term sedimentation rates into a longer geological context may be limited. An additional difficulty in determining rates of sedimentation in this area arises from the potential problems in dating samples.

Sample lakes in the Fosheim Peninsula were not particularly productive of organics. The cup sampler did not retrieve any organics from the lake basins sampled, only mineral material was encountered. It is likely that the smaller warmer basins which are more easily sampled could be more productive. Old carbon, which incudes coal, unlithified wood, and peat may occur in almost all reworked materials.

ACKNOWLEDGMENTS

Field work was supported by PCSP project 63-84; 32-87 and 88-76. We would like to thank the scientists at Hot Weather Creek for their support. Discussions in the field with T. Bell and B. Luckman were most useful and appreciated. D. Lemmen provided useful comments on this manuscript.

REFERENCES

Blake, W., Jr.
1981: Neoglacial fluctuations of glaciers, southeastern Ellesmere Island, Canadian Arctic Archipelago; Geografiska Annaler, v. 63A, p. 201-218.
1987: Lake sediments and glacial history in the High Arctic; evidence from east-central Ellesmere Island, Arctic Canada, and from Inglefield Land, Greenland; Polar Research, v. 5 n.s., p. 341-343.

Edlund, S.A., Alt, B.T., and Young, K.L
1989: Interaction of climate, vegetation ansd soil hydrology at Hot Weather Creek, Fosheim Peninsula, Ellesmere Island, Northwest Territories; *in* Current Research, Part D, Geological Survey of Canada, Paper 89-ID, p.125-133.

Fyles, J.G.
1989: High terrace sediments, probably of Neogene age, west-central Ellesmere Island, Northwest Territories; *in* Current Research, Part D, Geological Survey of Canada, Paper 89-ID, p. 101-104.

Hodgson, D.A.
1985: The last glaciation of west-central Ellesmere Island, Arctic Archipelago, Canada; Canadian Journal of Earth Sciences, v. 22, p. 347-368.

Koerner, R.M.
1989: Queen Elizabeth Island glaciers; *in* Chapter 6 of Quaternary Geology of Canada and Greenland. R.J. Fulton (ed.); Geological Survey of Canada, Geology of Canada, no.1 (also Geological Society of America, The Geology of North American, v.K-1).

Lemmen, D.S.
1988: The glacial and sea level history of Marvin Peninsula, northern Ellesemere Island, and Ward Hunt Island, High Arctic Canada; unpublished PhD. dissertation, Department of Geography, University of Alberta, Edmonton, 172 p.

Lemmen, D.S., Gilbert, R., Smol, J., and Hall, R.I.
1988: Holocene sedimentation in glacial Tasikutaaq Lake, Baffin Island. Canadian Journal of Earth Sciences, v.25: p. 810-823.

Retelle, M.J.
1986: Stratigraphy and sedimentology of high arctic coastal lacustrine basins, northeast Ellesemere Island, Northwest Territories; Géographie physique et Quaternaire, v. 40, p. 117-128

Woo, M.K., Young, K.L., and Edlund, S.A.
1990: Effects of soil, vegetation and miroclimate on slope hydrology, Hot Weather Creek basin, Ellesmere Island, Northwest Territories; *in* Current Research, Part D, Geological Survey of Canada, Part 90-1D.

Surficial materials associated with glacial Lake McConnell, southern District of Mackenzie

Donald S. Lemmen
Terrain Sciences Division

Lemmen, D.S. Surficial materials associated with glacial Lake McConnell, southern District of Mackenzie; in Current Research, Part D, Geological Survey of Canada, Paper 90-1D, p. 79-83, 1990.

Abstract

Till and glaciolacustrine are the dominant surface materials along the south shore of Great Slave Lake, west of the Slave Delta and below the former limit of glacial Lake McConnell. Beach gravels are the most visible glaciolacustrine deposits and are the most important source of granular material in many areas. Fine grained glaciolacustrine sediments are primarily found in poorly drained sites. These sediments were derived in part through winnowing of the till by waves, whereas the low carbonate content of some deposits suggests that they were transported in suspension from more distant source areas. Although some of these fine grained sediments are laminated, they do not appear to be varved. Wave-cut benches and lags of erratic boulders record wave erosion of the fresh till cover, while unmodified till belies the former existence of the glacial lake in many areas.

Résumé

Le till et les sédiments glacio-lacustres sont les matériaux de surface prédominants observés le long de la rive sud du Grand lac des Esclaves, à l'ouest du delta des Esclaves et au-dessous de l'ancienne limite du lac glaciaire McConnell. Les graviers de plage sont les sédiments glacio-lacustres les plus répandus et constituent la source la plus importante de matériaux granulaires dans de nombreuses zones. Les sédiments glacio-lacustres à grain fin se retrouvent principalement dans les endroits mal drainés. Ces sédiments proviennent en partie du vannage du till par les vagues tandis que la faible teneur en carbonate de certains dépôts indique qu'ils ont été transportés en suspension à partir de zones plus éloignées. Même si certains sédiments à grain fin sont laminaires, ils ne semblent pas être varvés. Les gradins découpés par les vagues et les résidus de blocs erratiques témoignent de l'érosion par les vagues de la couverture de till non altérée tandis que le till non modifié infirme l'existence d'un ancien lac glaciaire dans de nombreuses zones.

INTRODUCTION

Glacial Lake McConnell was an enormous ice marginal lake which formed along the western margin of the retreating Laurentide Ice Sheet during the Late Wisconsinan and filled the ice free portion of the basins now occupied by Great Bear, Great Slave and Athabasca lakes (Fig. 1). The lake was named by Craig (1965) after R.G. McConnell, who first recognized the significance of former high water levels in the Great Slave Basin (see McConnell, 1890). Despite its vast size and its significance with respect to regional deglaciation (Dyke and Prest, 1987), little is known about the history of the lake or the sedimentary associations which document its former existence.

This report discusses the surficial geology of the area south of Great Slave Lake and west of the Slave Delta (Fig. 2), based upon roadwork conducted in 1989. Focus is placed upon the area which lies below the former maximum extent of glacial Lake McConnell. These observations represent the initial stage of a regional project mapping surficial geology (NTS 85A, B, C, and H; Fig. 2). The project was initiated to develop a preliminary data base of till geochemistry and drift dispersal in order to evaluate the local potential for drift prospecting. Because of its location and the nature of the bedrock, the area is a potentially favourable site for stratabound, unconformity controlled, ore bodies. Additionally, this work will provide data on surface materials and distribution of permafrost that will aid in engineering construction and regional development.

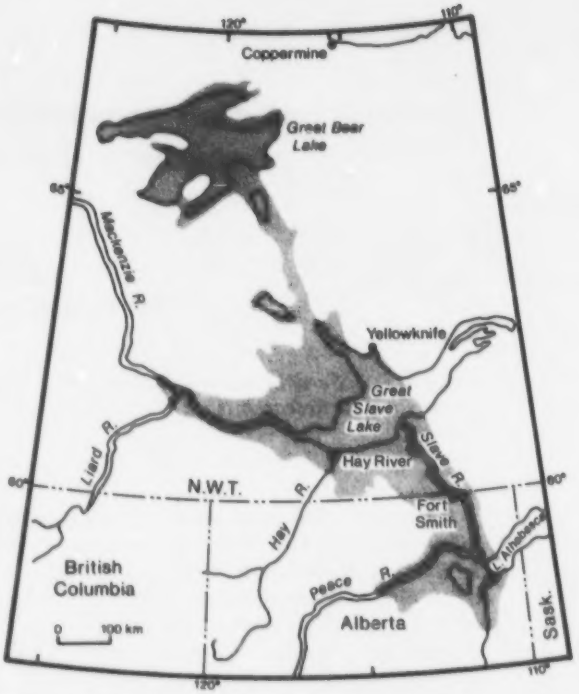

Figure 1. Glacial Lake McConnell (shaded) at its maximum extent, about 10 000 BP (modified from Craig, 1965).

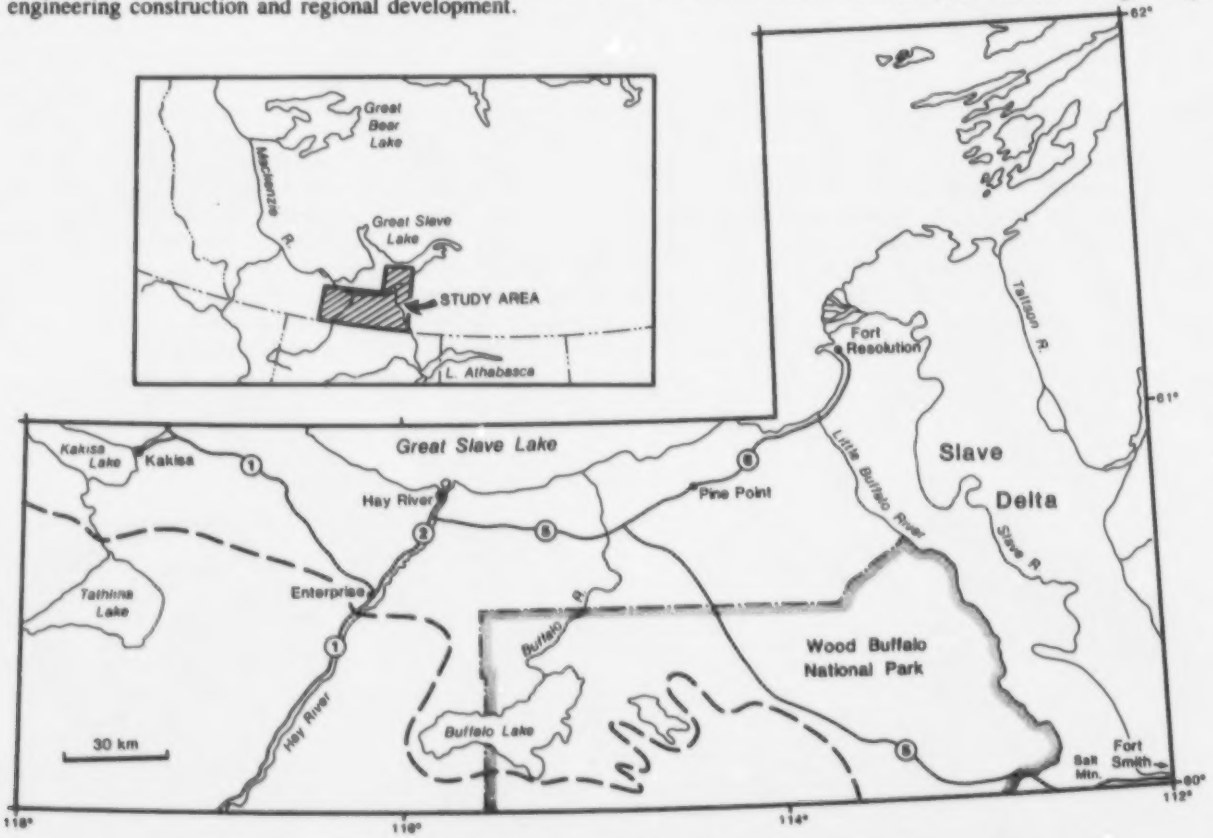

Figure 2. Study area south of Great Slave Lake, Northwest Territories. Approximate upper limit of glacial Lake McConnell shown by dashed line. Road network is shown to illustrate the general distribution of sample points.

Study area

Great Slave Lake straddles two major physiographic regions, the Kazan Region of the Canadian Shield and the Interior Plains (Bostock, 1970). The contact of the Canadian Shield and the Paleozoic rocks underlies thick Quaternary (primarily Holocene) sediments of the Slave Delta (Fig. 2). Field work in 1989 was restricted to the area west of the Slave River. It is an area of nominal local relief lying less than 300 m a.s.l. underlain by horizontally bedded Middle to Upper Devonian rocks (Douglas, 1974; Douglas and Norris, 1974). Gypsum karst forms dominate the Southeastern part of the area within Wood Buffalo National Park. Much of the region is poorly drained and features many lakes and bogs. Streamlined glacial landforms occur in the central and Southwestern part of the study area, recording a former ice flow to the Southwest. Those topographic highs which do not exhibit this Southwest orientation are mostly bedrock controlled.

SURFICIAL MATERIALS

Till

West of the Slave Delta (Fig. 2) the region features a nearly continuous till cover with observed thicknesses ranging from < 1 to > 12 m. Petroleum exploration wells document total drift thicknesses of more than 100 m in some parts of the study area. The till is slightly stony to stony with a calcareous silt to silty-clay matrix. Total carbonate content of the till ranges from 12 to 81 %, with compositional differences primarily related to changes in the underlying bedrock. Shield clasts form a measurable percentage of the gravel fraction in all tills observed.

Below the maximum stand of glacial Lake McConnell, as defined by the highest beaches observed on air photographs, areas of unmodified surface till belie the former presence of the lake. Elsewhere, erosion of fine sediments by waves and associated currents has resulted in the formation of a lag of erratic cobbles and boulders (Fig. 3).

Figure 3. Lag of erratic boulders formed through wave erosion of till. Surface was formerly covered by about 1.5 m of beach gravel which has been excavated to provide aggregate for road construction. (GSC-205020-A)

Unmodified till generally occurs on extensive flat to very gently sloping, moderately well drained sites. Lags are best developed near the base of steeper slopes, and may be recorded morphologically by erosional benches cut into the till by waves.

Fine grained glaciolacustrine sediments

Sand, silt, and clay associated with glacial Lake McConnell are not well exposed in the area. South of Enterprise, along Hay River, and in the Southeastern part of the study area massive, moderately well sorted fine to medium sand attains thicknesses of about 4 m and is probably prodeltaic in origin. Associated finer deposits were rarely observed; about 1.5 m of silt with a few coarse clasts (ice-rafted debris) occurs in section along lower Hay River. At two sites in Wood Buffalo National Park, 80-130 cm of laminated sediments overlie till. The limited occurrences of these sediments suggest isolated pockets of deposition. Current structures are common in sand, while lenses of diamict at one site suggest ice proximal deposition. Individual laminae range from 1-10 mm in thickness; some are normally graded. Severe deformation of the fine grained sediments was observed at one site (Fig. 4), possibly a result of loading by overlying deltaic sands. Neither of these laminated deposits appeared to be varved.

Most of the fine grained sediments deposited in glacial Lake McConnell were deposited in broad shallow basins now occupied by lakes and bogs. Road work biases against the sampling of such sites. Coring in poorly drained sites

Figure 4. Finely laminated glaciolacustrine sediments deformed by loading of overlying deltaic sands. Inclusions of diamict (arrow) suggest deposition occurred at an ice-proximal site. Scale in centimetres. (GSC-205020-C)

invariably penetrated fine sand and/or silt/silty clay, commonly containing small pebbles to produce a slightly stony diamict. These sediments are interpreted as glaciolacustrine owing to the relative scarcity of cobbles and boulders. The carbonate content of the glaciolacustrine sediments is consistently lower than that of the adjacent tills. Some glaciolacustrine sediments likely represent the reworking of till by waves, with the compositional differences being largely a function of differences in texture. However, the occurrence of fine grained sediments with low total carbonate contents (0-10 %) within areas dominated by highly calcareous till (60-80 %) suggests that much of the glaciolacustrine sediment has been derived from non local sources. This sediment was likely transported in suspension after the retreat of the ice sheet, and transgression of the lake, onto the Canadian Shield.

Beaches

Beaches are the most visible glaciolacustrine features in the area. They are of major economic importance as they provide the dominant, and commonly only, source of granular material in most areas (glaciofluvial sediments occur rarely). Beach development was primarily controlled by slope and aspect, with well developed beaches occurring on relatively steeper slopes with a north or east (ie. basinward) aspect. But remarkably evenly spaced strandlines are also common on the gently sloping plain adjacent to Great Slave Lake in the Hay River area.

Beach sediments range from medium sand to boulders dominantly deposited in parallel plane beds (Fig. 5). Total thicknesses of beach deposits approach 5 m at some sites, but 1-2 m is common. Lithologically the beach material reflects the source material, which most commonly was till.

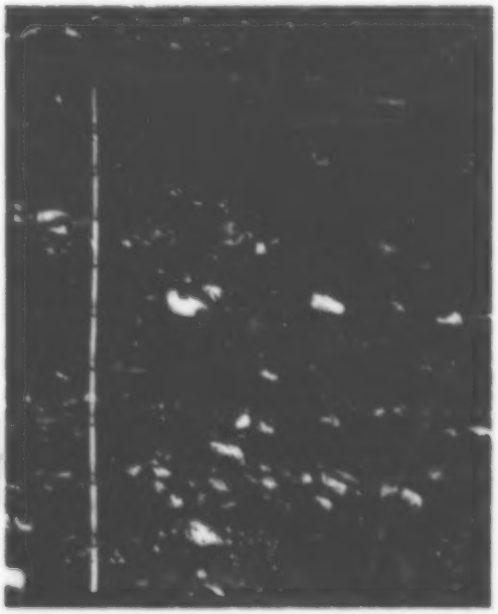

Figure 5. Plane-bedded beach deposits, sand and gravel, exposed in borrow pit. Scale is 1 m. (GSC-205020)

Hence there is generally a relatively high percentage of Shield clasts in beach gravels. Exceptions occur where waves were able to erode bedrock directly, as along the eastern slopes of Salt Mountain (west of Fort Smith) and along a major escarpment west of Enterprise (Fig. 2). The steep paleo-shoreface at these sites resulted in the deposition of gravels >2 m thick, composed almost exclusively of carbonate cobbles. Beaches composed entirely of sand are rare, reflecting the low sand content in the till. Beach deposits overlie bedrock, unmodified till, till lags (Fig. 3) and fine grained glaciolacustrine sediments, recording a regressive lacustrine sequence.

Synthesis

The dominant surficial materials south of Great Slave Lake and west of the Slave Delta are till and glaciolacustrine sediments which were derived in part from the till. Wave activity was the most important geomorphic process controlling the distribution of these surficial materials. Wave energy would have been greatest on steeper slopes with a north and east aspect (those with the greatest potential fetch), and these are the sites where the coarsest and thickest beach deposits are found. Wave-cut benches with a surface till lag record erosion of the paleo-shoreface. The formation of lag surfaces and the deposition of beach gravels, derived exclusively from the till, up to 5 m thick implies extensive erosion of the freshly exposed, saturated till cover. Wave processes were considerably less efficient on very gently sloping terrain, such that the surface material over much of these areas is essentially unmodified till.

Fine grained glaciolacustrine sediments, derived in part from the winnowing of the till, were primarily deposited in broad shallow basins. The textural similarities between the till and glaciolacustrine sediment, as well as the occurrence of the latter in isolated pockets within a regionally ubiquitous till cover, make differentiation of these sediments as distinct map units difficult.

DISCUSSION

An appreciation of these basic sediment associations is fundamental to the interpretation of regional Quaternary history. Through the detailed mapping of these sediments it should be possible to determine more precisely the former extent of glacial Lake McConnell, despite the fact that in many areas the recognition of the highest lacustrine features is difficult (Craig, 1960, 1965; St-Onge and Dredge, 1985). The area investigated appears to have been far from the major sources of sediment input to the glacial lake, which were probably direct inflow at the ice front as well as the Late Pleistocene Peace-Athabasca deltas to the south (Vanderburgh and Smith, 1988). Hence most of the glaciolacustrine deposits in the study area record a relatively low energy environment (excluding wave processes), with deposition occurring primarily through suspension settling. The general scarcity of ice contact deposits is enigmatic, as is the absence of significant volumes of fine grained sediments associated with the paleo-Hay River. As much of the fine grained sediment was derived locally by wave reworking of

unconsolidated glacial deposits, there is limited potential for the recognition of regionally significant paleoclimatic signals in these sediments.

Chronological control of lake history is severely limited. An early phase of the glacial lake complex probably existed in the Great Bear Basin by 11 ka, with the lake near its maximum areal extent by 10 ka (Dyke and Prest, 1987; D. Smith, unpublished data). No material suitable for dating was found during the 1989 season of this study. The fact that most of the surface sediments are till or till derived from till makes it unlikely that they will contain datable material. By 8.5 ka Laurentide ice had retreated east of the Mackenzie drainage divide (Dyke and Prest, 1987), and Great Slave Lake was near its present extent (Vanderburgh and Smith, 1988).

Tilting of glacial Lake McConnell shorelines was recognized by many early workers (e.g. McConnell, 1890; Bell, 1900; Cameron, 1922a,b). As the lake existed at the margin of the actively retreating Laurentide Ice Sheet, the uppermost shorelines must be time transgressive (i.e., older in the west; Craig, 1965); however, differentiation of distinct lake phases remains limited (D. Smith, unpublished data). The fact that many parts of the study area feature continuous flights of raised standlines suggests that the primary control on lake level was isostatic rebound, as opposed to sudden changes in lake level associated with the formation of new outlets.

ACKNOWLEDGMENTS

Capable assistance in the field was provided by R. Glenfield. Thanks to warden J. Mercer, Fort Smith, for her assistance in coordinating research within Wood Buffalo National Park. Discussions in the field with R.J. Fulton were greatly appreciated. The final manuscript has benefited from the comments of L.A. Dredge and D.A. Hodgson.

REFERENCES

Bell, R.
1900: An exploration of Great Slave Lake, N.W.T.; Geological Survey of Canada, Summary Report 1899, p. 103-110.

Bostock, H.S.
1970: Physiographic regions of Canada; Geological Survey of Canada, Map 1254A, scale 1:5 000 000.

Cameron, A.E.
1922a: Hay and Buffalo Rivers, Great Slave Lake, and adjacent country; Geological Survey of Canada, Summary Report 1921, Part B, p. 1-44.
1922b: Post-glacial lakes in the MacKenzie River Basin, N.W.T., Canada; Journal of Geology, v. 30, p. 337-353.

Craig, B.G.
1960: Surficial geology of north-central District of MacKenzie, Northwest Territories; Geological Survey of Canada, Paper 60-18.
1965: Glacial Lake McConnell, and the surficial geology of parts of Slave River and Redstone River map-areas, District of MacKenzie; Geological Survey of Canada, Bulletin 122.

Douglas, R.J.W.
1974: Geology of Trout River, District of MacKenzie; Geological Survey of Canada, Map 1371A, scale 1:500 000.

Douglas, R.J.W. and Norris, A.W.
1974: Geology of Great Slave, District of MacKenzie; Geological Survey of Canada, Map 1370A, scale 1:500 000.

Dyke, A.S. and Prest, V.K.
1987: Late Wisconsinan and Holocene history of the Laurentide Ice Sheet; Géographie physique et Quaternaire, v. 41, p. 237-263.

McConnell, R.G.
1890: Report on an exploration in the Yukon and MacKenzie Basins, N.W.T.; Geological Survey of Canada, Annual Report, v. IV, Part D.

St-Onge, D.A. and Dredge, L.A.
1985: Northeast extension of glacial Lake McConnell in the Dease River Basin, District of MacKenzie; *in* Current Research, Part A, Geological Survey of Canada, Paper 85-1A, p. 181-186.

Vanderburgh, S., and Smith, D.G.
1988: Slave River delta: geomorphology, sedimentology and Holocene reconstruction; Canadian Journal of Earth Sciences, v. 25, p. 1990-2004.

1989 observations of soil, vegetation, and microclimate, and effects on slope hydrology, Hot Weather Creek basin, Ellesmere Island, Northwest Territories

Ming-ko Woo[1], Kathy L. Young[1], and Sylvia A. Edlund
Terrain Sciences Division

Woo, M., Young, K.L., and Edlund, S.A. 1989 observations of soil, vegetation, and microclimate, and effects on slope hydrology, Hot Weather Creek basin, Ellesmere Island, Northwest Territories; in Current Research, Part D, Geological Survey of Canada, Paper 90-1D, p. 85-93, 1990.

Abstract

Field investigation at five study sites in Hot Weather Creek basin during 1989 showed that soil, vegetation and microclimate strongly influence the variability of hydrological responses on a local scale. The abundance of cracks in the silty soil significantly increases infiltration and reduces runoff rates. Vegetation distribution is uneven, and so are precipitation and radiation on slopes of various orientations. The snowmelt rate was greatest on slopes having dirty snow and high radiation input. Surface flow, resulting from a saturated thawed soil layer, occurred during the melt period on the two slopes with greatest snow cover. Groundwater fluctuated considerably even within a small area. Information on the spatial variability of slope hydrology under the present climate will facilitate the detection of future climatic change impacts.

Résumé

Des études sur le terrain réalisées à cinq endroits dans le bassin du ruisseau Hot Weather en 1989 ont révélé que le sol, la végétation et le microclimat influent fortement sur la variabilité à l'échelle locale des réponses hydrologiques. L'abondance de fissures dans le sol silteux augmente considérablement l'infiltration et réduit le ruissellement. La répartition de la végétation est inégale comme le sont les précipitations et le rayonnement sur les talus d'orientation différente. La vitesse de fonte nivale était plus élevée sur les versants recouverts de neige sale et bénéficiant d'un rayonnement élevé. L'écoulement en surface résultant du dégel d'un sol saturé, a été observé pendant la période de fonte sur les deux versants recouverts du manteau nival le plus épais. L'eau souterraine a fluctué considérablement même au sein d'une petite zone. Les données recueillies sur la variabilité spatiale de l'hydrologie des versants sous le climat actuel facilitera la détermination des répercussions des changements climatiques futurs.

[1] Department of Geography, McMaster University, Hamilton, Ontario L8S 4K1

INTRODUCTION

As the atmospheric concentration of carbon dioxide and other trace gases increases, global warming appears to be inevitable (Topping 1989). The permafrost region of northern North America is prone to significant temperature rises and notable increases in precipitation (Schlesinger and Mitchell 1987). Various hydrological activities will undergo changes when the permafrost degrades and when the snow and ice regimes are modified by the future climate (Woo 1990). Hydrological responses are also affected by factors other than the climatic trend; these include edaphic elements, microclimate, and vegetation. Prediction of future impacts requires an understanding of the spatial variations of hydrological attributes under the present climate.

In rugged terrain, slope orientation is an important control of the microclimate (Barry 1981). Consequently, the hydrological responses will vary among slopes, even within a small area. Preliminary observations during summer 1988 suggested that behaviour of the soils in this region is sensitive to changes in hydrological conditions (Edlund et al., 1989). The purpose of this field study in 1989 was to compare and contrast the hydrological responses on slopes of different orientations to local variations in soil, vegetation, and microclimate under a continuous permafrost environment. The result will provide background information to enable the detection of future climatic change impacts.

STUDY AREA AND INSTRUMENTATION

Hot Weather Creek basin (80°N, 84°W) includes the Terrain Sciences Division Global Change observatory site established in June 1988. This small basin, a north-central tributary of Slidre River, is not glacier fed, unlike many other eastern tributaries, which originate in the Sawtooth Range. Instead it is entirely limited to the lowland of northern Fosheim Peninsula. It has moderate relief and a good tundra vegetation cover. Four slopes of different orientation (north, east, south, and west) and a plateau site were chosen for detailed vegetation and hydrological investigation (Fig. 1).

Meteorological observation (net radiation, air and ground temperatures, wind speed, relative humidity, and precipitation) were recorded on hourly or daily intervals and stored in Campbell CR21 data loggers for each of the four slopes and at the plateau site. All sites were less than 500 m from the main automatic weather station whose sensors have been summarized by Edlund et al. (1989). Wind direction and solar radiation were also recorded at the plateau site.

A snow survey was carried out in mid May, using a method described by Woo et al. (1983). Daily snow ablation was obtained by measuring the rate of snow surface lowering and the lowering rate was converted to water equivalent units by multiplying it by the snow surface density. Small lysimeters were placed in the snow on the slopes and on the plateau to measure the sublimation rates between May 23 and June 1. Weekly frost table depths on the plateau and midslopes were obtained by measuring the depth of penetration of a steel rod into the active layer.

On each slope, a network of nine groundwater wells were installed and water level readings were taken daily, whenever possible (Fig. 2) Water level fluctuations at some of these wells were also recorded with Leupold-Stevens Type-F water level recorders. Additional observations, including hydraulic conductivity, specific yield and retention, and infiltration were made at selected locations. Water infiltration rates on a variety of soils were determined using double-ring infiltrometers.

Figure 1. General view of the study area. N, E and S indicate the location of the instrumented slopes with north, east and south aspects.

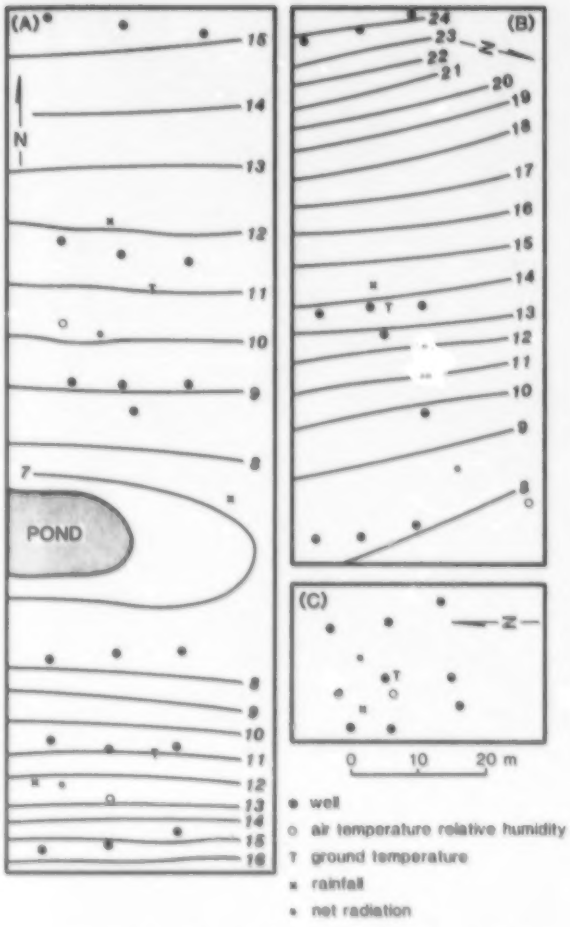

Figure 2. Deployment of groundwater wells and meteorological instruments on studied slopes: (A) north and south slopes (B) east slope (C) west slope.

During the second week of August 1989, measurements of per cent vegetation cover were made along 60 m transects at each site. The transects were parallel to slope on the oriented study sites, but were placed randomly at the nearly level plateau site. Three replicates of entire transects were performed at each site; these involved 1 m^2 quadrat inventories at 5 m intervals along the transects. The study also included a complete survey of the diversity of vascular plants at all sites.

HYDROLOGICAL PROPERTIES OF SOILS

Most hillslopes and plateaus in the study area are blanketed by silty soils whose surfaces have been dissected by high-centre ice-wedge polygons with diameters ranging from 20 to 30 cm. The polygon surfaces are further fissured by desiccation or by frost. Some of the cracks have been enlarged to become small linear depressions surrounding earth hummocks (Fig. 3A). These provide depression storage for surface water and serve as conduits for overland flow during snowmelt and rainstorms. Where hummocks are absent, the cracks may be occupied by the roots of vascular plants, particularly those of *Salix arctica* (Fig. 3B). These cracks, measuring several centimetres wide, allow surface water to enter the silty soil. Small cracks, measured in millimetres, may be sealed by swelling or by coatings of surface sediments during rain, but desiccation after rainstorms soon will re-open a network of fine cracks.

Infiltration is strongly influenced by the soil texture and by cracks in the soil. Figure 4 shows that in the absence of cracks, silt has the lowest infiltration rate, followed by the gravel and silt mixture; slightly sandier materials have a higher infiltration rate. Silty soil with minor cracks will at has an first admit much infiltration rate, but as swelling seals the cracks, the infiltration rate is reduced to a level comparable to that of noncracked silt. Where cracks are wide (over 5 mm), substantial infiltration can be maintained. Thus, despite the low infiltration capacity intrinsic to silty materials, the abundance of cracks facilitates downward seepage of rainwater so that the extent of Hortonian overland flow on silt is limited.

Soils at the four slopes and the plateau site are composed of varying percentages of silt. The east slope has the largest portion of fines. The plateau and the south slope have slightly less silt and clay. The west slope is silty sand. Most parts of north slope consist of sandy materials, but the lower slope is mainly silt. The larger the amount of fines, the lower is the hydraulic conductivity. Pumping tests yielded average hydraulic conductivities of 5.6×10^{-5} m/s for the east slope, 1.0×10^{-5} m/s for the south, and 1.4×10^{-5} m/s for the north slope (west slope remained non saturated throughout summer and no pumping test could be conducted).

The soils have a low specific yield (amount of water released by gravitational drainage) (0.022 +/- 0.017) but large specific retention. The latter averages 0.40 with a standard deviation of 0.04 for the slope soils, but the plateau site averages 0.354 because of its higher clay content. The large water retention values are attributed to the high porosity of the silt and sandy silt materials.

MICROCLIMATE

In contrast to summer 1988 which was exceptionally warm and fairly dry (Edlund et al. 1989), summer 1989 was considerably cooler and much wetter. Figure 5 summarizes climatic conditions at the main Hot Weather Creek automatic weather station on the plateau.

Net radiation

Figure 6 compares the net radiation on the four slopes and the plateau site during the premelt, snowmelt, and snow-free periods. On cloud-free days, net radiation peaks at different times of the day for different slope orientations, as expected (Sellers 1965). The timing contrast is particularly noticeable in the snow-covered period. At this time in late May, the west slope was already bare of snow and had the largest radiation receipt due to its lower albedo. The snow on north slope was covered by eolian deposits and dirt,

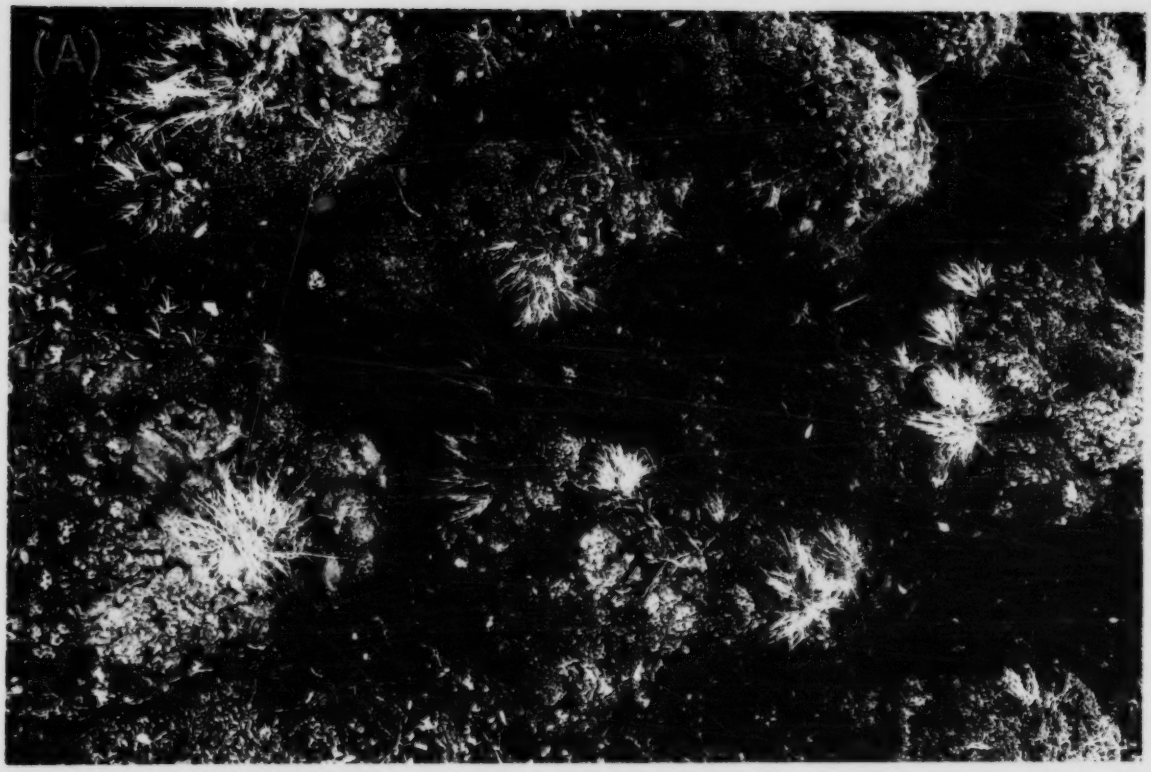
(A)

(B)

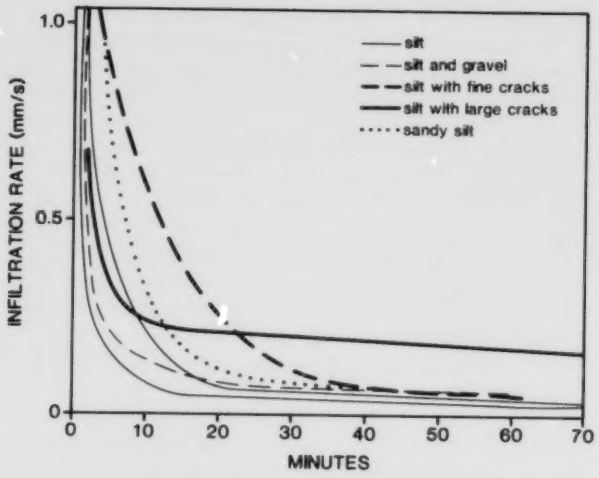

Figure 4. Infiltration curves for silt with gravel, sandy silt, and silty soils with and without cracks.

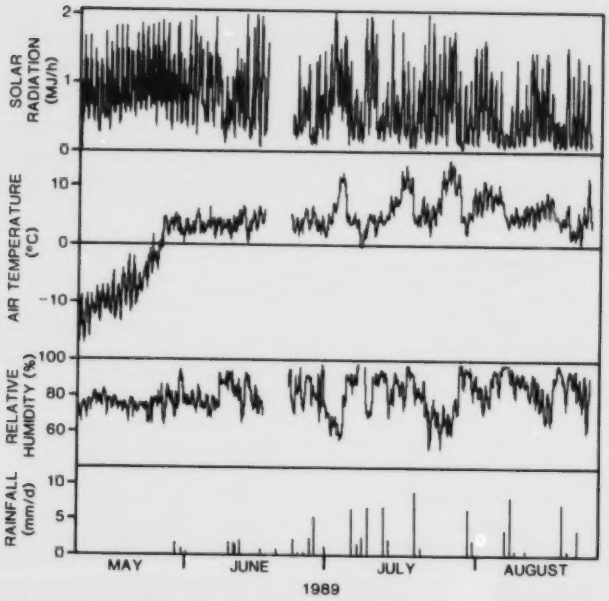

Figure 5. Net radiation, air temperature, relative humidity, and rainfall at the plateau weather station, 1989. The gap in data is due shutdown of the weather station for maintenance.

Figure 3. Cracks in silty soil: (A) Cracks between earth hummocks provide depression storage and serve as conduits for surface flow during rain. (B) Larger cracks exploited by roots of *Salix arctica*, offering seepage channels for surface flow; finer cracks were sealed by swelling clay after 10 mm of rain fell on July 13.

thereby reducing its snow albedo to permit larger radiation inputs. The snow on the plateau and on the south slope was clean and had a high albedo, thus reflecting most of the incoming radiation.

During the melt period, the snow ripened quickly and then ablated. The snow albedo dropped, particularly where the surface was dirty with dust and other deposits (Woo and Dubruil, 1985). Net radiation then increased, as was observed at the study sites. By June 2, the amount of net radiation was similar for all sites, except the plateau and south slope where ripening was slower.

In the snow-free period, the south slope had the largest amount of net radiation and the north slope had the least (e.g., on July 28). This contrast was less on overcast days when diffuse rather than direct beam radiation prevailed.

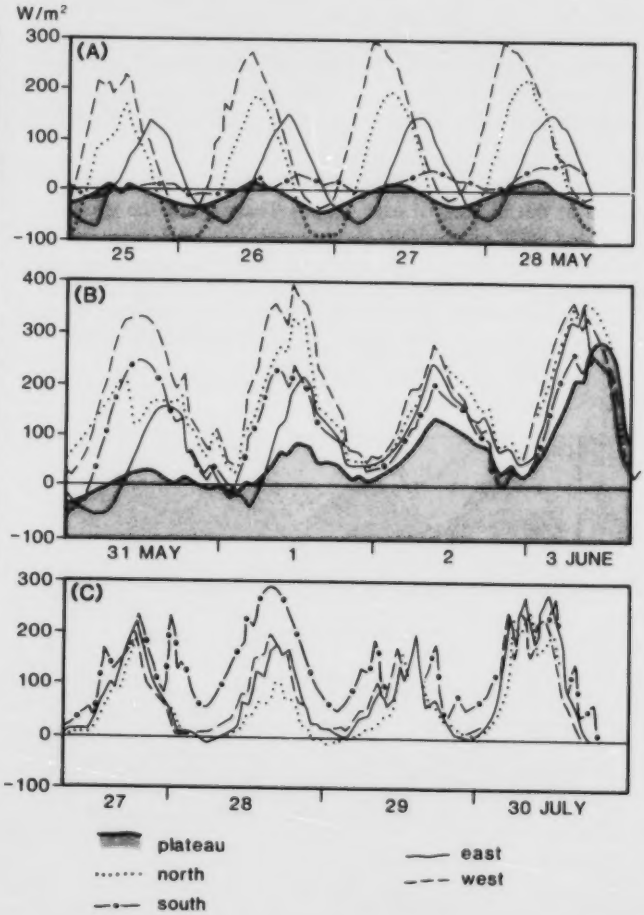

Figure 6. Comparison of net radiation on four slopes and plateau site during (A) premelt (B) melt (C) snow-free periods.

Temperature

Air temperature differences among the slopes were insignificant during the snow-free period, though during the melt season, one slope could be warmer than the other, depending on the distribution of snow and the advection of warmer air from bare ground. For example, the air above the snow on south slope was marginally warmer (about 1°C) than that over the north slope on several occasions in early June. An increase in elevation causes a drop in air temperature, and the plateau site was consistently cooler than the other sites by about 0.5°C (see Table 1 for elevation differences).

Ground temperature at 1 cm below the surface is affected by the ambient air temperature, the snow and vegetation cover. It is an indicator of the heating and cooling of the soil, hence the thawing and freezing of the active layer. During May 25-28, all but the west slope was covered by snow. On warm days, the west slope had higher surface temperature, but on cold days (May 27-28), it had no snow to buffer against heat loss and the surface temperature dropped (Fig. 7). At the snow-covered sites, diurnal temperature cycles were dampened to varying extents, depending on the thickness and degree of ripening of the snow; but the maximum daily temperature could not exceed 0°C. After the melt season, ground surface temperatures at all sites fluctuated according to temperature rhythm of the air. Differences among the slopes may be attributed to their vegetation cover.

Figure 8 shows the depths of the frost table at the plateau and at the middle of each slope. Thawing of the ground started early on the west slope which had little snow even in mid-May. This led to a deeper frost table development than on the south and east slopes. Soils on the plateau and the east slope began to thaw later than the other sites because the snow lingered longer. The plateau thawed more slowly because of its lower air temperature. In contrast, rapid thaw occurred on the north slope because its sandy soil has a higher thermal conductivity than the other siltier soils. By mid-July, its frost table was as deep as that of the west slope site.

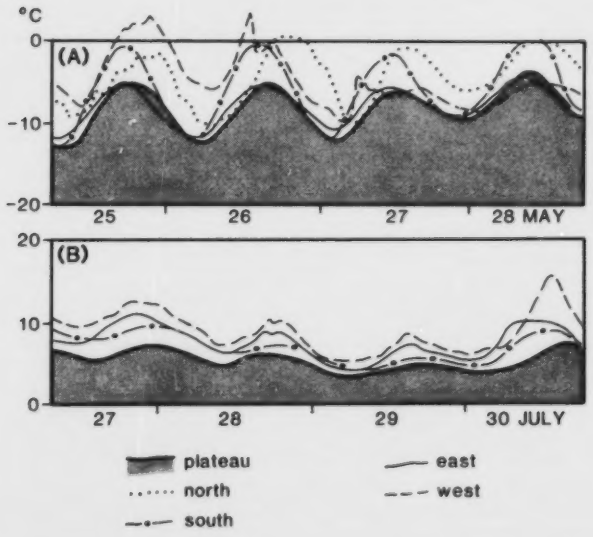

Figure 7. Comparison of soil temperatures (at 1 cm depth) during (A) snowmelt and (B) snow-free periods.

Precipitation

Snow surveys carried out in mid-May 1989 yielded the net snow accumulation for the winter of 1988-89 (Table 1). The snow was densely packed, with densities exceeding 300 kg/m^3. The plateau had 89 mm of snow water equivalent but on the north slope, this amount was doubled. In contrast, the south slope had only 51 mm and the west slope accumulation was minimal (26 mm water equivalent) and was patchy. The disparity in snow accumulation may be attributed to differential snow deposition during precipitation events and subsequent drifting which redistributed the snow. The north slope, which gathered the most snow, was also smeared with eolian deposits so that the snow there was dirty.

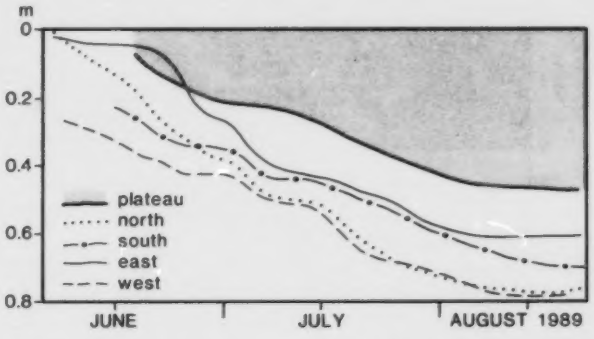

Figure 8. Comparison of frost table development at the middle of four slopes and on the plateau.

Table 1. Precipitation characteristics at the Hot Weather Creek study sites.

	Base	Plateau	North	East	South	West
			Slope			
SNOW						
Mean depth (mm)	—	265	461	320	150	84
Mean density (kg/m^3	—	337	393	339	342	309
Water equivalent (mm)	—	89	181	109	51	26
RAIN						
Rainfall (mm) Jul 1 - Aug 22	74	91	168	94	130	66
Gauge elevation (m above base camp)	0	31	11	15	12	1
Wind direction frequency during rain	—	—	1	2	13	3

Unlike the previous dry summer, 70 mm of rain was recorded at Eureka weather station (about 25 km west of the study site) between June 1 and August 22 1989. Hot Weather Creek basin generally received more rainfall during the same period, with 115 mm recorded at the plateau site. Table 1 shows the rainfall at the study sites between July 1 and August 22. The base camp, situated on a terrace 30 m below the plateau site, had 17 mm less rainfall, suggesting that lower altitudes receive less rainfall. The north slope had the most rain, followed by the south. The west slope received the least amount of rain, and despite its proximity to the base camp, it had less rainfall than on the flat terrace.

The significantly larger amount of rain on the north and the south slope may be related to the prevailing wind direction. Table 1 shows the prevalence of southerly winds (defined here as winds blowing from between 135° and 225° azimuth) on rainy days. In addition, all heavy rainfall (over 15 mm/day) occurred when the wind was from the south. While the south slope received direct impact of the rain, the more sheltered northerly aspect was where much rainfall was collected because of the drop in wind due to the sheltering effect of topography. As the wind funnelled along north-south oriented valleys, the east-and west-facing slopes did not receive as much rain.

VEGETATION

The study sites are all vegetated by woody plant-dominated communities (*Salix-Dryas* tundra) typical of moderately to weel drained, stable silty soils of the lowlands of Fosheim Peninsula and the intermontane zone of the north-central Queen Elizabeth Islands (Edlund and Alt, 1989; Edlund et al., 1989). Although small wetlands exist nearby, no wetland communities were found at the instrumented sites and wetland species are not included in the site inventories. Table 2 shows 28 species that occur at the study sites. Twelve additional species occur on the plateau and on similar slopes in the immediate area, but are found in specialized habitats, such as enriched sites around animal burrows. These were not encountered at the study sites.

Table 2. Per cent cover* of vascular plants at each study site

Species	Plateau	North	East	South	West
		Slope			
Alopecurus alpinus	+	–	+	+	+
Armeria maritima	–	+	–	–	–
Braya purpurescens	+	+	+	+	+
Braya thorild-wulffii	+	–	–	+	–
Carex misandra	–	+	–	–	–
Carex rupestris	–	+	–	+	–
Cassiope tetragona	–	35(b)	–	–	–
Cerastium alpinum	+	–	+	+	–
Draba alpina	+	–	–	–	–
Draba cinerea	+	–	–	+	+
Draba corymbosa	+	–	–	–	–
Dryas intergrifolia	5 – 15	5 – 15	5 – 10	+ – 5	+ – 5
Kobresia myosuroides	–	+	–	–	–
Lesquerella arctica	–	+	–	+	+
Oxyria digyna	+	+	+	+	+
Papaver radicatum	+	+ – 1	+ – 1	+ – 1	+
Pedicularis arctica	+	+ – 1	+	+	+
Pedicularis capitata	–	+	–	–	–
Pedicularis hirsuta	–	–	+	+	–
Pedicularis lanata	+	+	–	–	–
Polygonum viviparum	–	+	+	+	–
Potentilla nivea	+	–	–	–	–
Potentilla rubricaulis	+	–	–	–	–
Puccinellia vaginata	+	–	+	+	–
Salix arctica	25 – 50	10 – 20	40 – 55	30 – 50	15 – 30
Saxifraga oppositifolia	1	1 – 5	1	1	1
Taraxacum hyparcticum	–	+	–	–	+
Vaccinium uliginosum	–	+	–	–	–
Bare Ground	35 – 60	25 – 85	35 – 55	45 – 60	65 – 85

* to the nearest 5%; ranges from top to bottom of slope
+ indicates present in the area but in amounts less than 1% cover
(b) indicates species found only at bottom of slope.

Salix arctica dominates all slopes. It generally roots in shallow troughs, in major cracks between hummocks and in shallow, dished, depressions *Dryas integrifolia*, the most common associate, occurs on more exposed micro habitats and is more abundant on sandier facies. The north slope transect has the greatest diversity of species, because it has includes parts of other communities. A local *Cassiope*-dominated heath community occurs at the foot of the slope. Such heath communities are commonly associated with late-lying snowbeds. The uppermost part of the north slope also has several species more typical of recently disturbed sites. This location corresponds to a band where thin layers of silt, deposited on the winter snow, now drape the slope after the snow has disappeared. The presence of colonizers suggests that the band receives sporadic deposition.

Vascular plants generally average more than 50% cover; however, at each site per cent cover, along with moisture availability, decreases upslope.

HYDROLOGICAL RESPONSES

In response to the spatial variations in soil, vegetation, and microclimate, hydrological quantities are expected to differ among the study sites. In this report, only selected hydrological processes will be discussed as data analysis is still in progress.

Snowmelt

While major snowmelt began towards the end of May, losses by sublimation began earlier. Daily sublimation between May 23 and June 1 was less than 1 mm in most cases, and there was no systematic difference between the slopes. There were several occasions of condensation, and the magnitude was under 0.5 mm.

Snowmelt in the Arctic has been found to be dominated by radiation melt, with sensible heat contribution becoming increasingly important as the snow becomes thin and patchy (Heron and Woo 1978); ablation observed in 1989 confirms this. In late May, daily ablation was in the order of 1 mm. When snow on south slope became dirtier as it ripened, the radiation receipt increased (Fig. 6), and ablation increased rapidly. The snow on the north slope was also covered with eolian silt and ablation was rapid in June. The cleaner snow on east slope and on the plateau ripened slowly and with lower net radiation input (Fig. 6), their ablation rates were retarded. The west slope had little snow and no ablation measurement was taken.

Runoff and groundwater

During snowmelt the shallow, thawed soil layer is frequently saturated by the ample supply of meltwater. When the suprapermafrost water table rises above the ground as a result of saturation, overland flow is generated (Woo and Steer 1986). This mode of surface runoff was observed on two slopes, and between June 4 and 14 (delayed snowmelt) on the east slope. The other slopes, with much less snow available, did not produce surface flow.

After the melt period, a saturated zone was maintained only at the lower segments of the north and the east slopes. The other sites had high soil moisture contents, but no saturated zone, except for a narrow strip along the foot of slopes. Figure 9 shows the water table fluctuations in the lower parts of the north and east slopes. The water table dropped as the frost table fell. The water table rose when it rained.

DISCUSSION

Variation in the hydrology of the study sites have been shown to reflect local differences in the soil, vegetation, and microclimate. Orientation and elevation influence the amount of water and heat fluxes in the Hot Weather Creek basin. The prevalent southerly winds direct more precipitation to north and south slopes, but less so to exposed flat sites and the east and west slopes. This maximizes the water supply contrast between the north or south slopes with the east or west slopes. The higher plateau receives more rain than the valleys below. Energy input is the largest on south-facing slopes, and the lowest on the north. Such difference in heat gained would be expected to be translated into more rapid snowmelt and evaporation on the southerly aspect. However, the soil and vegetation factors are important in governing heat absorption and transfer, while snowmelt is strongly influenced by the depth, dust content and other properties of the snow.

The plateau is colder and has a late snowmelt and a shallow frost table. The west slope, with little snow, a moderate level of radiation and sandier soil, has a deep frost table and a low soil moisture content. The south slope is well supplied with precipitation and energy. The snow stayed longer on the east slope and, with a moderate level of water and energy input, it is more moist than the west slope. The north slope has maximum precipitation and the least energy gain, which result in a saturated lower slope.

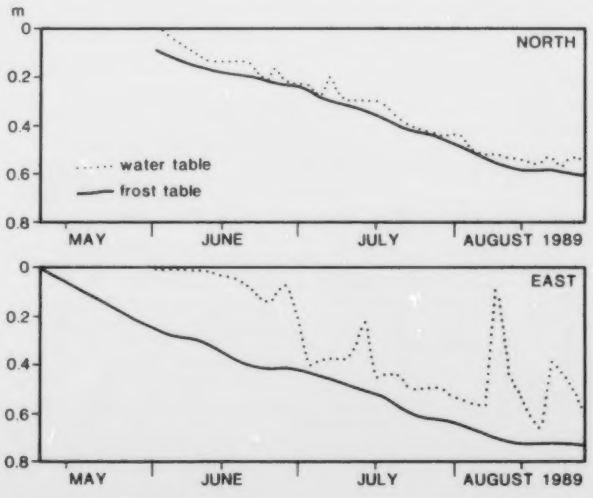

Figure 9. Variations in water table and frost table at the lower segments of north and east slopes.

Where the silty soils of the study area are unfissured, they have high specific retention but low specific yield of water. Where the silty materials have abundant desiccation and frost cracks of varying sizes, infiltration is substantially enhanced.

These differences in soil composition and degree of fissures are reflected in the per cent cover of vegetation. Soils with the least amount of water present in summer, have the lowest per cent cover. This relationship, however, is not simply linear; some plants, such as *Salix artica*, also may themselves alter the infiltration rate of water into the active layer in summer. *Salix* most commonly occurs in cracks and depression where water first collects. Root networks extend into the soil cracks and may provide channels along which water seepage into subsurface soils may be enhanced.

The upward dispersal of water from the base of the active layer also may follow the cracks around plant roots. This is suggested by observations made during the dry summer of 1988. In mid July damp spots reflecting substantial subsurface ice melt started to appear randomly on the plateau and on all but the steepest aspects of slopes (Edlund et al., 1989). The spots first appeared primarily around *Salix* clumps and slowly expanded during the rest of the summer. By early August damp spots also appeared on many unvegetated surfaces. In some places, individual spots enventually coalesced to form an extensive network.

Given the spatial variability of these various factors, nonuniformity of hydrological responses within a small area could be considerable. The large variability of the present climate may generate different spatial patterns of hydrological responses from one year to another. Only through continued monitoring can such variations be documented, and this is a prerequisite to the detection and prediction of long-term climatic change impacts. An ongoing monitoring program is planned for Hot Weather Creek.

Acknowledgments

This work was funded by a research agreement with the Department of Energy, Mines and Resources, by a grant from the Natural Sciences and Engineering Research Council, and by a northern training grant from the Department of Indian and Northern Affairs. The logistical support of the Polar Continental Shelf Project is gratefully acknowledged. We wish to thank Dr. Bea Alt, Miss Sharon Reedyk, and Mr. Tim Siferd for their assistance in the field, and Dr. Harry Baker (National Research Council) and Dr. Philip Marsh (National Hydrology Research Institute) for the loan of several instruments.

References

Barry, R.G.
1981: Mountain Weather and Climate; Methuen, London, 313 pp.

Edlund, S.A. and Alt, B.T.
1989: Regional congruence of vegetation and summer climate patterns in the Queen Elisabeth Islands, Northwest Territories, Canada; Arctic, v. 42, no. 1, p. 3-23.

Edlund, S.A., Alt, B.T., and Young, K.L.
1989: Interaction of climate, vegetation, and soil hydrology at Hot Weather Creek, Fosheim Peninsula, Ellesmere Island, Northwest Territories; *in* Current Research, Part D, Geological Survey of Canada, Paper 89-1D, p. 125-133.

Heron, R. and Woo, M.K.
1978: Snowmelt computation for a High Arctic site; Proceedings, 35th Eastern Snow Conference, Hanover, p. 162-172.

Schlesinger, M.E. and Mitchell, J.F.B.
1987: Climate model simulations of the equilibrium climatic response to increased carbon dioxide; Reviews of Geophysics, v. 25, p. 760-798.

Sellers, W.D.
1965: Physical Climatology; University of Chicago Press, Chicago, 272 p.

Topping, J.C. Jr.
1989: Coping with Climate Change; Proceedings Second North American Conference on Preparing for Climate Change; Climate Institute, Washington, D.C. 696 p.

Woo, M.K.
Consequences of climatic change for hydrology in permafrost zones; American Society of Civil Engineers, Journal. (in press)

Woo, M.K. and Dubreuil, M-A.
1985: Empirical relationship between dust content and Arctic snow albedo; Cold Regions Science and Technology, v. 10, p. 125-132.

Woo, M.K. and Steer, P.
1986: Runoff regime of slopes in continuous permafrost areas; Canadian Water Resources Journal v. 11, p. 58-68.

Woo, M.K., Heron, R., Marsh, P., and Steer, P.
1983: Comparison of weather station snowfall with winter snow accumulation in High Arctic basins; Atmosphere-Ocean, v. 21, p. 312-325.

Geology of the Lucerne east-half map area, Rocky Mountain Main Ranges, Alberta and British Columbia

Roland G. Dechesne[1] and E.W. Mountjoy[1]
Institute of Sedimentary and Petroleum Geology, Calgary

Dechesne, R.G. and Mountjoy, E.W., Geology of the Lucerne east-half map area, Rocky Mountain Main Ranges, Alberta and British Columbia; in Current Research, Part D, Geological Survey of Canada, Paper 90-1D, p. 95-100, 1990.

Abstract

The Lucerne east-half map area straddles the eastern and western Main Ranges. The area is underlain by two major structural panels of upper Proterozoic Miette Group. The upper structural panel contains middle and upper Miette Group overlain by Lower Cambrian Gog Group and capped by Cambro-Ordovician carbonates. These strata were thrust over the lower structural panel, which in the map area contains upper Miette Group and (?)Gog Group, on the Selwyn Range Décollement. Rockingham Creek, Colonel and Moose Pass thrusts represent other early faults in this region. A regional-scale fold, the Mount Robson Syncline, is related to these structures. The Selwyn Range Décollement, Rockingham Creek Thrust and the Mount Robson Syncline were all cut by the later, steep, west-side-up Moose Lake/Chatter Creek Fault.

Résumé

La partie est de la région cartographique de Lucerne chevauche les parties est et ouest des chaînons Main. La zone repose sur deux panneaux structuraux du groupe de Miette du Protérozoïque supérieur. Le panneau structural supérieur contient les parties intermédiaire et supérieure du groupe de Miette sous-jacentes au groupe de Gog du Cambrien inférieur et recouvertes de roches carbonatées cambro-ordoviciennes. Ces couches ont été charriées au-dessus du panneau structural inférieur qui contient, dans la présente région cartographique, la partie supérieure du groupe de Miette et (?) le groupe de Gog, sur le décollement de Selwyn Range. Les chevauchements de Rockingham Creek, Colonel Pass et Moose Pass représentent d'autres failles précoces dans cette région. Un pli d'échelle régionale, le synclinal de Mont Robson, est lié à ces structures. Le décollement de Selwyn Range, le chevauchement de Rockingham Creek et le synclinal de Mount Robson ont tous été par la suite traversés par la faille de Moose Lake et Chatter Creek caractérisée par un compartiment ouest remonté et un pendage abrupt.

[1] Department of Geological Sciences, McGill University, 3450 University St., Montreal, Quebec H3A 2A7

INTRODUCTION

Mapping of the east half of the Lucerne map area (83 D/15, formerly Rainbow) was carried out in 1988 and 1989. The region straddles the Moose Lake/Chatter Creek Fault, which is taken to be the boundary between the eastern and western Main Ranges of the southern Canadian Rocky Mountains in this region (Fig. 1). Exposures of Upper Proterozoic Miette Group (Mountjoy, 1962), Lower Cambrian Gog Group (Mountjoy, 1962) and the Cambro-Ordovician platformal sequence of carbonates were mapped. Regional geology has been summarized by Price and Mountjoy (1970) and Dechesne and Mountjoy (in press).

The map area lies west of the Jasper area (Mountjoy and Price, 1985), and includes unpublished data from work on the 1:250 000 scale Mount Robson sheet (Mountjoy, 1980) and the Bow-Athabasca mapping project (Price and Mountjoy, 1970). McDonough and Simony (1986, 1988) mapped the southern portion of Lucerne west half. Our mapping of Lucerne east half was undertaken to link the mapping of McDonough and Simony with the greater body of mapping across strike to the northeast (Mountjoy, 1962, 1980; Charlesworth et al., 1967; Mountjoy and Price, 1985, 1989; Dechesne and Mountjoy, 1988) as well as to map the Fraser River Antiform in greater detail. South of Lucerne east half, Ptarmigan Creek (83 D/10) comprises part of Project Bow-Athabasca, but polyphase deformation and complex stratigraphic relationships are only now being unravelled (Dechesne, 1990; Mountjoy and Grasby, 1990).

The Lucerne east half map area represents an important link between the stratigraphy and structure of the eastern and western Main Ranges. The deepest known structural levels in the Main Ranges are exposed in the Selwyn Range, which occupies the southwestern portion of the Lucerne east half map area (Fig. 1).

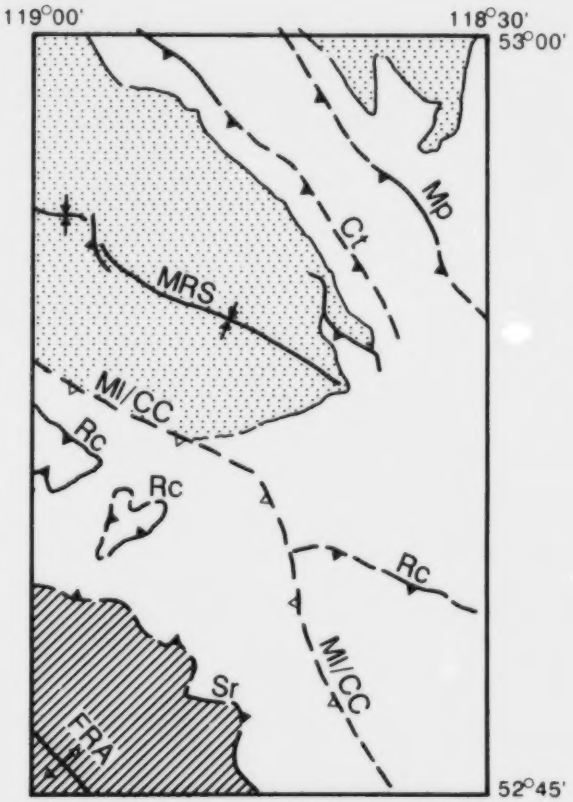

Figure 1. Main tectono-stratigraphic elements of Lucerne east half map area. Hachured zone indicates lower panel, unpatterned is Miette Group of upper panel, dots represent Cambrian strata of upper panel. Solid thrust teeth indicate early thrust faults; hollow teeth, late faults. Dashed lines indicate approximate contacts. MRS, Mount Robson Syncline; FRA, Fraser River Antiform; Mp, Moose Pass Thrust; Ct, Colonel Thrust; MI/CC, Moose Lake/Chatter Creek Fault; Rc, Rockingham Creek Thrust; Sr, Selwyn Range Décollement.

	QUATERNARY	
	Qd	post glacial deposits
	MIDDLE CAMBRIAN	
	CEp	ELDON AND PIKA FORMATIONS: limestone and dolostone, dense, grey, cliff-forming; argillaceous and shale interbeds in upper part
	CTa	TATEI FORMATION: limestone, grey, minor dolostone, argillaceous limestone and calcareous shale
	CCh	CHETANG FORMATION: limestone, grey, thick to medium bedded, interbedded with argillaceous limestone, shale and siltstone
	LOWER CAMBRIAN	
	CHo	HOTA FORMATION: limestone and dolostone, grey massive to thick bedded, locally sandy
		GOG GROUP (CMn - CMa)
	CMa	MAHTO FORMATION: sandstone, quartzose, crossbedded, alternating with thinner beds of siltstone and silty shale
	CMu	MURAL FORMATION: limestone, micritic; dolostone, finely crystalline; grey, with archaeocyathid fragments, massive, interbedded with grey shales
	LOWER CAMBRIAN AND/OR HADRYNIAN	
	CMn	McNAUGHTON FORMATION: sandstone, quartzose, crossbedded, massive; shale, brown to dark grey; feldspathic sandstone and shale at base
	HADRYNIAN	
		WINDERMERE SUPERGROUP
		MIETTE GROUP (PMMl - PMU)
	PMU	UPPER MIETTE GROUP: Upper Unit: pelite, silty, brown to dark grey; calcareous sandstone and feldspathic sandstone; local stromatolitic carbonate; local paraconglomerate with dolomite clasts; Pelite Unit: shale and pelite, silty, brown to dark grey, laminated; minor siltstone; local ridge-forming sandstone, quartzose; carbonate, carbonate conglomerate near base
		MIDDLE MIETTE GROUP (PMMl - PMMu)
	PMMu	UPPER UNIT: ridge-forming grit and sandstone, feldspathic; alternating with shale and siltstone, recessive, dark greyish green; local conglomerate; sandstone and grit generally graded and poorly sorted
	PMMOF	OLD FORT POINT FORMATION: slate with siltstone, green, greenish grey and black; calcareous siltstone, brown; carbonate, brown to buff, black; carbonate conglomerate; minor calcareous sandstone
	PMMl	LOWER UNIT: ridge-forming grit and sandstone, feldspathic; alternating with shale and siltstone, recessive, dark greyish green and black; local conglomerate; sandstone and grit generally graded and poorly sorted; conglomerate at top

Table 1. Stratigraphy of the Lucerne east half map area.

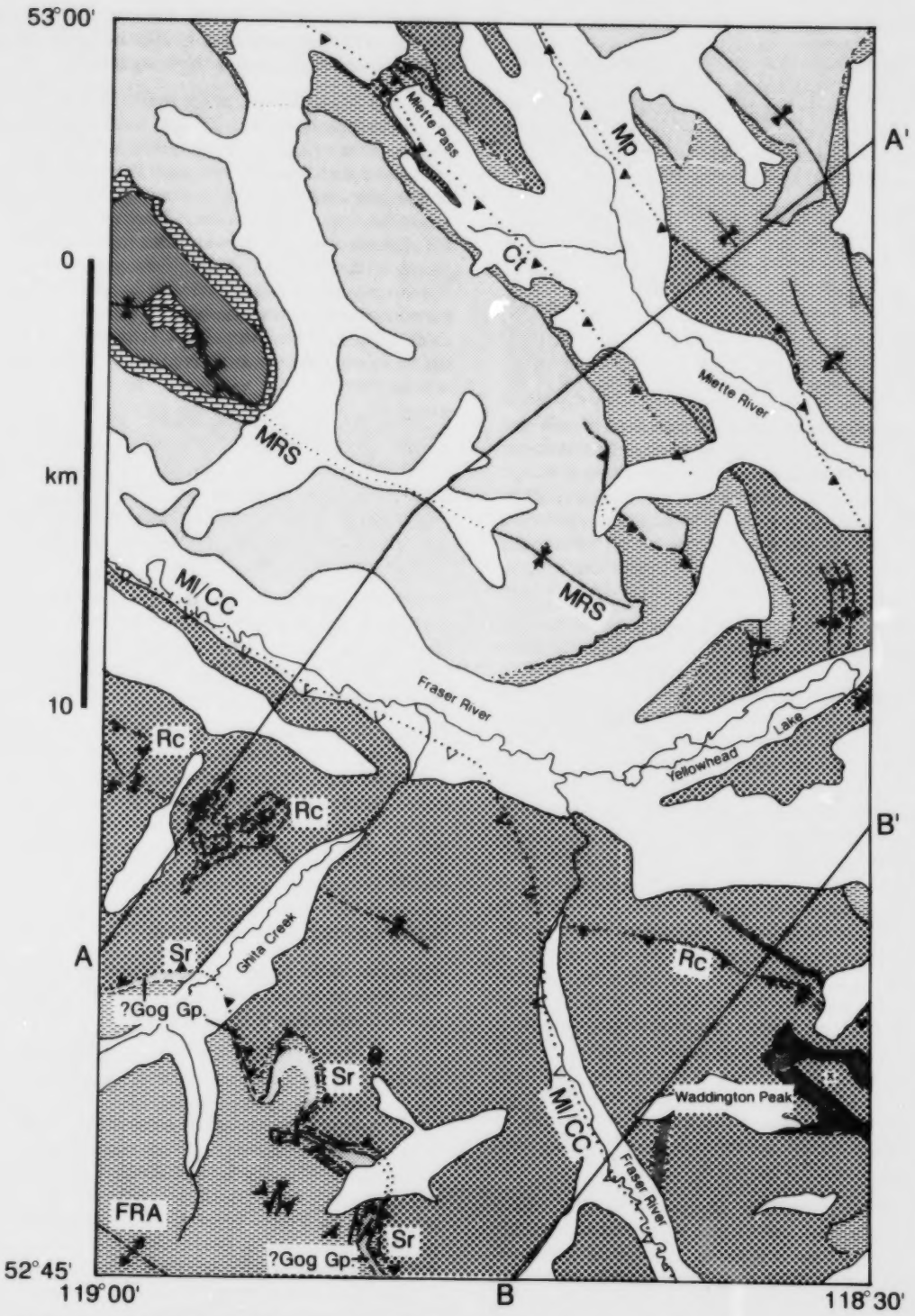

Figure 2. Geological map of Lucerne east half map area. Legend for stratigraphy is in Table 1. Solid thrust teeth indicate early thrust faults; hollow teeth, late faults.

STRATIGRAPHY

New stratigraphic detail was gathered within the Miette Group (Mountjoy, 1962) and is presented briefly below. Major revisions to Miette Group stratigraphy and the upper Miette Group of the lower structural sequence are described in more detail by Dechesne (1990). Descriptions of Cambrian units are included in Table 1.

In the Lucerne map area, two main structural panels of Miette Group are recognised (Fig. 1). The upper panel is continuous with Miette Group strata in the Jasper map area. This upper panel is present in both the eastern and western Main Ranges and is only slightly offset by the out-of-sequence Moose Lake/Chatter Creek Fault. Exposures of the deeper panel are restricted to the Selwyn Range, below the Selwyn Range Décollement. Only the upper two of the three divisions of the Miette Group recognised by Campbell et al. (1973) are definitely present within the Lucerne east half map area (Fig. 2). It was initially thought that lower Miette Group occurred extensively within the Selwyn Range (Mountjoy et al., 1985; Mountjoy and Forest, 1986; McDonough and Simony, 1986, 1988; see also discussion in Dechesne and Mountjoy, in press), but new work (Dechesne, 1990) indicates that most of these strata represent a structural repeat of middle and upper Miette Group.

Middle Miette Group strata are widespread within the upper structural panel within the map area (Fig. 2). Four of five subdivisions recognized regionally (Dechesne, 1990) are present. The lowest stratigraphic unit in the Lucerne east half map area consists of at least 350 m of greenish grey, silty pelites and minor sandstones, and is present only in the Selwyn Range where it sits upon the Selwyn Range Décollement. Regional correlation of this unit is considered in a separate paper by Dechesne (1990). The overlying unit comprises cliff-forming granule conglomerate and sandstone sequences alternating with silty pelite sequences. The Meadow Creek Formation of Charlesworth et al. (1967), if it exists (see discussion in Dechesne and Mountjoy, 1988) would be equivalent to the uppermost portion of this subdivision. The overlying Old Fort Point Formation (Charlesworth et al., 1967) forms a distinctive marker horizon within the middle Miette Group. In the Lucerne map area, the Old Fort Point Formation consists of, from bottom to top, green pelite, brown and orange-buff, thin bedded carbonates, black pelite and grey pelite. The measured thickness of this unit on Waddington Peak is 305 m. Approximately 700 m of alternating sequences consisting of granule conglomerate and sandstone or of silty pelites form the top of the middle Miette Group.

Cliff-forming sequences of the middle Miette Group consist of thick bedded, matrix-rich sandstone and granule to pebble conglomerate containing T_{ab} Bouma sequences and thin bedded, silty pelite turbidite sequences containing T_{cde}. The Old Fort Point Formation also represents turbiditic deposition (Dechesne, 1989a).

Total thickness of the middle Miette Group as measured by Carey and Simony (1985) at Cushing Creek, 110 km to the north, is 2870 m. We derived a minimum thickness of approximately 2400 m, with the base of the sequence carried upon the Selwyn Range Décollement. McDonough and Simony (1988) reported 2300 to 2600 m, but we recognized several thrust faults within their section.

Upper Miette Group in the upper structural panel also outcrops extensively (Fig. 2). This unit is dominated by turbiditic pelites (T_{de}) with rare, thin, graphitic carbonates and associated debris flows near the base. Channelized, quartz-rich sandstone and granule conglomerate occur at the top of the upper Miette Group; local reefoid carbonates of Ediacaran age are also present at the top of the upper Miette Group (Hofmann et al., 1985; Teitz and Mountjoy, 1988). Calcareous debris flows that carried reefal detritus into the surrounding basin are interbedded with thin bedded turbidites at Miette Pass. A thickness estimate of 700 m for the upper Miette Group was derived from detailed mapping at Miette Pass.

Gog Group strata (Mountjoy, 1962), which consist mostly of quartzarenites, generally overlie Miette Group rocks sharply and at least locally unconformably (Aitken, 1969; Te..z and Mountjoy, 1988). Increasing amounts of quartzarenite within the upper portions of the upper Miette Group indicate that the depositional systems of the two groups may be linked, however.

The lower structural panel within the map area (Fig. 1) includes only strata interpreted as upper Miette Group (Fig. 2). To the west and south, interpreted middle Miette Group outcrops beneath this upper Miette Group in the lower structural panel (Dechesne, 1990).

The lower structural panel of upper Miette Group consists dominantly of pelites, semipelites and quartzites. At the top of the upper Miette Group south of Ghita Creek, a 50 m thick, purplish brown quartzite sequence may represent the top of the upper Miette Group or, possibly, basal Gog Group. We have mapped this stratigraphic unit as (?)Gog Group.

STRUCTURE

Structures in the Lucerne east half map area formed during two discrete phases of deformation (Dechesne, 1989b, 1990; Dechesne and Mountjoy, 1988, in press).

Four thrust faults, the Selwyn Range Décollement, Rockingham Creek Thrust, Colonel Thrust and Moose Pass Thrust represent early, low-angle, synmetamorphic thrust faults (timing with respect to metamorphism derived from observations in Ptarmigan Creek map area to the south; Dechesne, 1990). The Selwyn Range Décollement and the Rockingham Creek Thrust are deformed by later, steep structures, the Fraser River Antiform of the Selwyn Range (see Dechesne, 1990; Dechesne and Mountjoy, in press) and the Moose Lake/Chatter Creek Fault, which lies in the Fraser River Valley (Figs. 2, 3). The Moose Lake/Chatter Creek Fault, which has less than 5 km of slip (Fig. 3), is taken to be the boundary between the eastern and western Main Ranges in the Jasper-Yellowhead structural culmination.

The early, low-angle faults are associated with the regional phyllitic cleavage, abundant tight, small-scale folding, and also with large, tight, hanging wall anticlines, all developed in Miette Group strata.

In the Lucerne east half map area, the Selwyn Range Décollement is a northeast-dipping shear zone, approximately 50 m thick (see Dechesne, 1990 for a more complete description of this fault zone). Folding is most common near the shear zone and folds decrease in both size and abundance upward and downward away from the shear zone. In the fault zone, pelites generally show foliation fish (Hanmer, 1984) and northeast-directed crenulation cleavage interpreted as shear bands. Pelites outside of fault zones do not contain either of these two fabrics. As in other regions, later deformation (folding, crenulation and faulting associated with the formation of the Fraser River Antiform) has affected early fault fabrics (cf. Dechesne, 1990; Dechesne and Mountjoy, in press). Dechesne (1990) suggested that the Selwyn Range Décollement is a large, low-angle thrust fault that duplicates about 3 km of stratigraphy, and separates middle Miette Group of the upper structural panel from upper Miette Group and (?)Gog Group of the lower structural panel (Fig. 1-3). Other workers in the region question the presence of a throughgoing shear zone, and interpret the strata as essentially unsheared and conformable (McDonough and Simony, 1986, 1988).

The Selwyn Range Décollement presently outcrops as a 60 x 15 km oval window (Dechesne, 1990; Dechesne and Mountjoy, in press), because it has been folded by the doubly plunging Fraser River Antiform. The hanging wall of Selwyn Range Décollement in the northeastern portion of the Selwyn Range contains a stack of thrust faults, including the Rockingham Creek Thrust, which also occurs in the footwall of the Moose Lake/Chatter Creek Fault.

Both the Selwyn Range Décollement and the Rockingham Creek Thrust are constrained to intersect the Moose Lake/Chatter Creek Fault at high angles. The postmetamorphic Moose Lake/Chatter Creek Fault must cut both of the earlier, folded thrust faults (Fig. 3, Dechesne, 1989b, 1990; Dechesne and Mountjoy, 1988, in press). Eastern equivalents of the Selwyn Range Décollement have not yet been identified, but probably include the Colonel and Moose Pass thrusts and other early thrust faults in the eastern Main Ranges (Dechesne and Mountjoy, 1988; Dechesne, 1989).

The Mount Robson Syncline (Fig. 2, 3) is a prominent, regional-scale fold that involves strata ranging in age from Late Proterozoic to Cambro-Ordovician. This structure is traceable from the McBride map area to the north, where it is somewhat less prominent and is known as the Mount Ryder Syncline (Campbell et al., 1973), southward through the Jasper-Yellowhead structural culmination. Its regional position between successive hanging wall anticlines of early thrust faults suggests that the Mount Robson Syncline is also an early structure (Dechesne and Mountjoy, in press).

The Moose Lake/Chatter Creek Fault offsets part of the western limb of the Mount Robson Syncline. The northwestern portion of the Moose Lake /Chatter Creek Fault roughly parallels early structural trends but the southern segment (which is vertical near Fraser Pass) clearly is oblique to the early structures (Fig. 1, 2).

SUMMARY

The Lucerne east half map area straddles the eastern and western Main Ranges. The area is underlain by two major structural panels of Upper Proterozoic Miette Group. The upper structural panel contains middle and upper Miette Group overlain by lower Cambrian Gog Group and capped by Cambro-Ordovician carbonates. These strata were thrust over the lower structural panel, which here contains upper Miette Group and (?)Gog Group, on the now-folded Selwyn Range Décollement. The fault zone of the Selwyn Range Décollement contains two sets of structures not found outside of the fault zone: foliation fish and low-angle, northeast directed crenulation cleavage. Rockingham Creek, Colonel and Moose Pass thrusts represent other early faults in this

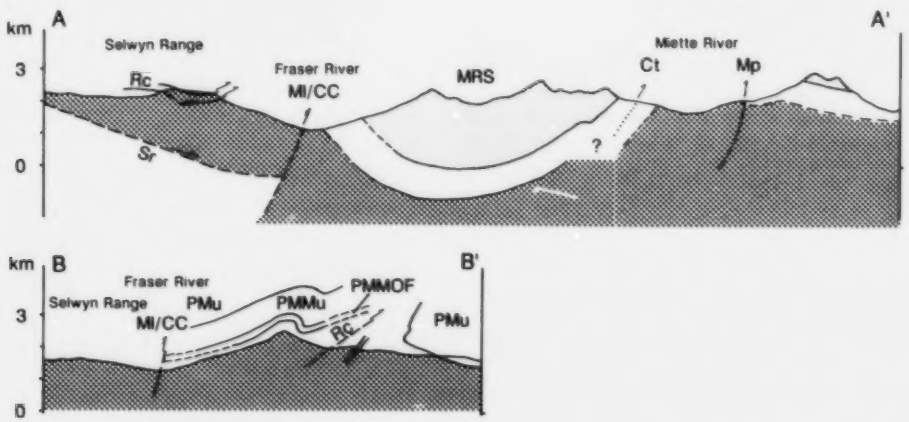

Figure 3. Structural cross-sections of Lucerne east half map area. See Figure 2 for locations. Single arrowheads indicate early thrust faults and double arrowheads represent late faults.

region. A regional-scale fold, the Mount Robson Syncline, is related to these structures. The Selwyn Range Décollement, Rockingham Creek Thrust, and the Mount Robson Syncline were all cut by the later, steep, west-side-up Moose Lake/Chatter Creek Fault.

ACKNOWLEDGMENTS

Financial support for field and laboratory work was provided by EMR research agreement 03SG23294-8-0526 and Mountjoy's NSERC grant A2128. The authors appreciate discussions with M. McDonough and P. Simony. G. Ross, ISPG, provided helpful comments on this manuscript. Special thanks go to Yellowhead Helicopters and B. Hannis for excellent expediting. Field assistance of I. Kirkland and M. Birchard is greatly appreciated.

REFERENCES

Aitken, J.D.
1969: Documentation of the sub-Cambrian unconformity, Rocky Mountain Main Ranges, Alberta; Canadian Journal of Earth Sciences, v. 6, p. 193-200.

Campbell, R.B., Mountjoy, E.W., and Young, F.G.
1973: Geology of the McBride map-area, British Columbia; Geological Survey of Canada, Paper 72-35.

Carey, J.A. and Simony, P.S.
1985: Stratigraphy, sedimentology and structure of Late Proterozoic Miette Group, Cushing Creek area, British Columbia; Bulletin of Canadian Petroleum Geology, v. 33, p. 184-203.

Charlesworth, H.A.K., Weiner, J.L., Akehurst, A.J., Bielenstein, H.U., Evans, C.R., Griffiths, R.E., Remington, D.B., Stauffer, M.R., and Steiner, J.
1967: Precambrian geology of the Jasper region, Alberta; Research Council of Alberta, Bulletin 23, 74 p.

Dechesne, R.G.
1989a: Stratigraphy and sedimentology of the Late Proterozoic Old Fort Point Formation, Miette Group, Jasper, Alberta; Geological Association of Canada, Mineralogical Association of Canada, Annual Meeting, Program with Abstracts, p. A42.
1989b: Tectonic windows at deep structural levels in the Main Ranges of the Rocky Mountains, Jasper-Yellowhead structural culmination, British Columbia; Geological Association of Canada, Mineralogical Association of Canada, Annual Meeting, Program with Abstracts, p. A53.
1990: Geology of the Ptarmigan Creek area, Main Ranges, Rocky Mountains, British Columbia; *in* Current Research, Part E, Geological Survey of Canada, Part 90-1E.

Dechesne, R.G. and Mountjoy, E.W.
1988: Structural geology of part of the Main Ranges near Jasper, Alberta; *in* Current Research, Part E, Geological Survey of Canada, Paper 88-1E, p. 171-176.
in press: Multiple décollements at deep levels of the southern Canadian Rocky Mountain Main Ranges, Alberta and British Columbia. *in* Structural Geology of Fold and Thrust Belts, S. Mitra, (ed.); Dave Elliott Volume, Johns Hopkins University Press.

Hanmer, S.K.
1984: The potential use of planar and elliptical structures as indicators of strain regime and kinematics of tectonic flow; *in* Current Research, Part B, Geological Survey of Canada, Paper 84-1B, p. 133-142.

Hofmann, H.J., Mountjoy, E.W., and Teitz, M.W.
1985: Ediacaran fossils from the Miette Group, Rocky Mountains, British Columbia, Canada; Geology, v. 13, p. 819-821.

McDonough, M.R. and Simony, P.S.
1986: Geology of the northern Selwyn Range, western Main Ranges, Rocky Mountains, British Columbia: preliminary report; *in* Current Research, Part A, Geological Survey of Canada, Paper 86-1A, p. 619-626.
1988: Stratigraphy and structure of Late Proterozoic Miette Group, northern Selwyn Range, Rocky Mountains, British Columbia; *in* Current Research, Part D, Geological Survey of Canada, Paper 88-1D, p. 105-113.

Mountjoy, E.W.
1962: Mount Robson (southeast) map-area, Rocky Mountains of Alberta and British Columbia (83 E/SE); Geological Survey of Canada, Paper 61-31, 114 p.
1980: Mount Robson, Alberta — British Columbia; Geological Survey of Canada, Map 1499A (scale 1:250 000).

Mountjoy, E.W. and Forest, R.
1986: Revised structural interpretation, Selwyn Range between Ptarmigan and Hugh Allan creeks, British Columbia — an antiformal stack of thrusts; *in* Current Research, Part A, Geological Survey of Canada, Paper 86-1A, p. 177-183.

Mountjoy, E.W., Forest, R., and Leonard, R.
1985: Structure and stratigraphy of Miette Group, Selwyn Range, between Ptarmigan and Hugh Allan creeks, British Columbia; *in* Current Research, Part A, Geological Survey of Canada, Paper 85-1A, p. 485-490.

Mountjoy, E.W. and Grasby, S.E.
1990: Revised stratigraphic and structural interpretation of folded décollements, southern Fraser River Antiform, Selwyn Range, British Columbia; *in* Current Research, Part E, Geological Survey of Canada, Paper 90-1E.

Mountjoy, E.W. and Price, R.A.
1985: Jasper (83 D/16) geological map and cross-sections; Geological Survey of Canada, Map 1611A (Scale 1:50 000).
1989: Amethyst Lakes (83 D/9) geological map and cross-sections; Geological Survey of Canada, Map 1657A (Scale 1:50 000).

Price, R.A. and Mountjoy, E.W.
1970: Geological structure of the Canadian Rocky Mountains between Bow and Athabasca rivers — a progress report; *in* Structure of the southern Canadian Cordillera, J.O. Wheeler, (ed.); Geological Association of Canada, Special Paper 6, p. 7-25.

Teitz, M.W. and Mountjoy, E.W.
1988: The Late Proterozoic Yellowhead Carbonate platform west of Jasper, Alberta; *in* Reefs, Canada and adjacent areas. H.J. Geldsetzer et al. (ed.); Canadian Society of Petroleum Geologists, Memoir 13, p. 129-134.

Petrography of silica in upper Paleozoic carbonates of the Sverdrup Basin, Canadian Arctic

Martine Savard[1], Benoit Beauchamp, and Jan Veizer[1, 2]
Institute of Sedimentary and Petroleum Geology, Calgary

Savard, M., Beauchamp, B., and Veizer, J., Petrography of silica in upper Paleozoic carbonates of the Sverdrup Basin, Canadian Arctic; in Current Research, Part D, Geological Survey of Canada, Paper 90-1D, p. 101-109, 1990.

Abstract

Upper Carboniferous (Moscovian) to Lower Permian (Artinskian) shelf carbonate units of the Sverdrup Basin contain silica as a replacive phase as well as cement. Based on their morphology, crystal size, extinction pattern and fabric, seven main silica types have been recognized: 1) splays of lutecite; 2) spherulites and splays of fibrous length-fast chalcedony; 3) spherulites of fibrous length-slow chalcedony; 4) chains of subautomorphic megaquartz; 5) mosaics of xenomorphic megaquartz; 6) mesh of xenomorphic microquartz; and 7) isolated automorphic megaquartz.

Petrographic studies revealed that the silicification products in inner shelf shallow-water carbonates differ from those in deeper-water outer shelf carbonates. Silica precipitates appear to be more diverse in the shallow-water units, probably reflecting: 1) longer duration of the silicification process; and 2) precipitation from more acidic parent waters. Silicification took place relatively early in a shallow burial environment. Thick siliciclastic deposits (marginal facies) and siliceous organisms (shelf-edge facies) could have acted as sources of silica.

Résumé

Diverses phases de silice, des remplacements aussi bien que d'abondants ciments, sont présentes dans les faciès à roches carbonatées de plate-forme datant du Carbonifère supérieur (Moscovien) au Permien inférieur (Artinskien) du bassin de Sverdrup. Sept formes de cristaux s'y distinguent par leurs dimension, forme, arrangement et configuration d'extinction. Il s'agit: 1) d'éventails de lutécite; 2) de sphérolites et d'éventails de quartzine; 3) des sphérolites de chalcédonite; 4) des chaînes de mégaquartz subautomorphes; 5) des mozaïques de mégaquartz xénomorphes; 6) des enchevêtrements de microquartz xénomorphes; et, 7) des mégaquartz automorphes isolés.

Des travaux pétrographiques révèlent que les produits de la silice sont plus diversifiés dans les calcaires provenant de la plate-forme interne que dans ceux provenant des faciès plus profonds de la plate-forme externe. Cette différence découle probablement du fait que la silicification, qui s'est faite relativement tôt en mileux d'enfouissement peu profonds, a duré plus longtemps à la marge du bassin, et qu'elle y a été le produit d'eaux plus acides. D'épais dépôts silicoclastiques en marge du bassin et des organismes siliceux dans les milieux plus profonds ont pu agir comme sources de la silice.

[1] Derry Laboratory, Ottawa-Carleton Geoscience Centre, Ottawa, Ontario K1N 6N5
[2] Institut für Geologie, Ruhr Universität, 4630 Bochum West Germany

INTRODUCTION

Silica has been long known to be a major component of the upper Paleozoic basinal sediments (spiculitic shales and cherts) of the Sverdrup Basin. Silica is also now recognized as a significant diagenetic product in shelf carbonates preceding or postdating the precipitation of carbonate cements. Preliminary petrographic observations of such silica precipitates in Upper Carboniferous to Lower Permian carbonates of the Sverdrup Basin are reported here. This paper: 1) provides a description of the various silica phases; 2) shows that different silica products appear to be associated with different sedimentary environments (inner versus outer shelf); and 3) places these silica products into an early to late paradiagenetic sequence.

GEOLOGICAL SETTING

The Carboniferous and Permian succession of the Sverdrup Basin (Fig. 1) is represented by seven long-term (5 to 5 Ma) transgressive-regressive sequences bounded by major unconformities at the basin margin that pass basinward into equivalent conformities (Fig. 2) (Beauchamp et al., 1989a, b). Three of these sequences, the Serpukhovian to Artinskian sequences 2 to 4, are characterized by very thick, shallow shelf carbonates (Nansen, Antoinette, Tanquary, Canyon Fiord ("middle limestone member"), Belcher Channel, and "unnamed" A formations) that pass laterally into basinal evaporites (Otto Fiord Formation) or mudrocks (Hare Fiord and "unnamed" B formations). Sequences 2 to 4 are also characterized by carbonate buildups of various kinds and shapes that are especially abundant near the shelf edge. Most buildups, as well as some of the non-reefal shelf facies, display spectacular occurrences of early to late diagenetic carbonate cements, which are commonly associated with various silica phases.

Upper Carboniferous to Lower Permian shelf carbonates of the Sverdrup Basin are distributed in a cyclical fashion (Fig. 3). Each cycle is characterized by a basal recessive unit represented by relatively deep-water argillaceous limestone and calcareous shale, passing upward into a resistant, pure, limestone unit displaying features indicative of a shallower-water environment. Based on these sedimentary features, inner shelf and outer shelf cycles are recognized (Beauchamp, 1987). The upper part of inner shelf cycles comprises grainstone or sandstone, indicative of deposition above fairweather wave base (Fig. a). In contrast, the upper part of outer shelf cycles is characterized by muddy facies (lime mudstone, wackestone and packstone) indicating deposition below fairweather wave base (Fig. 4b). Carbonate buildups of various compositions and shapes also occur within outer shelf deposits, and are especially abundant near the shelf-edge.

SAMPLES AND TECHNIQUES

Inner shelf and outer shelf (mostly reef facies) carbonate rocks were examined in this study. These rocks were sampled during the 1985 (Beauchamp), 1987 and 1988 (Savard) field seasons. Inner shelf facies are found in the Canyon Fiord and Belcher Channel formations, and outer shelf facies in the Antoinette, Nansen and "unnamed" A formations. The age of these formations ranges from Moscovian (Late Carboniferous) to Artinskian (Early Permian) (Fig. 2). Most samples come from sections measured in the Blind Fiord and Trold Fiord area, on southwestern Ellesmere Island. Additional samples were collected on Bjorne Peninsula, southwestern Ellesmere Island, and Hamilton Peninsula, west-central Ellesmere Island.

Petrographic examinations (light microscope and cathodoluminescence) were performed on more than 250 thin sections that were previously stained with Alizarin Red S/potassium ferricyanide solutions. Staining helped to differentiate iron-rich and iron-poor dolomites and calcites, as well as to emphasize the presence of silica. Cathodoluminescence aided in timing the silicification episodes relative to the various generations of calcite cements.

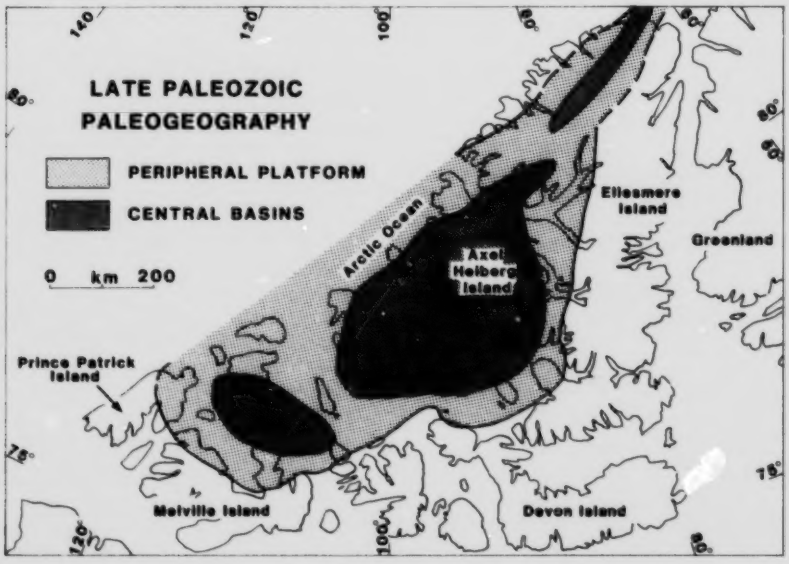

Figure 1. Location map showing outline of Sverdrup Basin in the Canadian Arctic Archipelago.

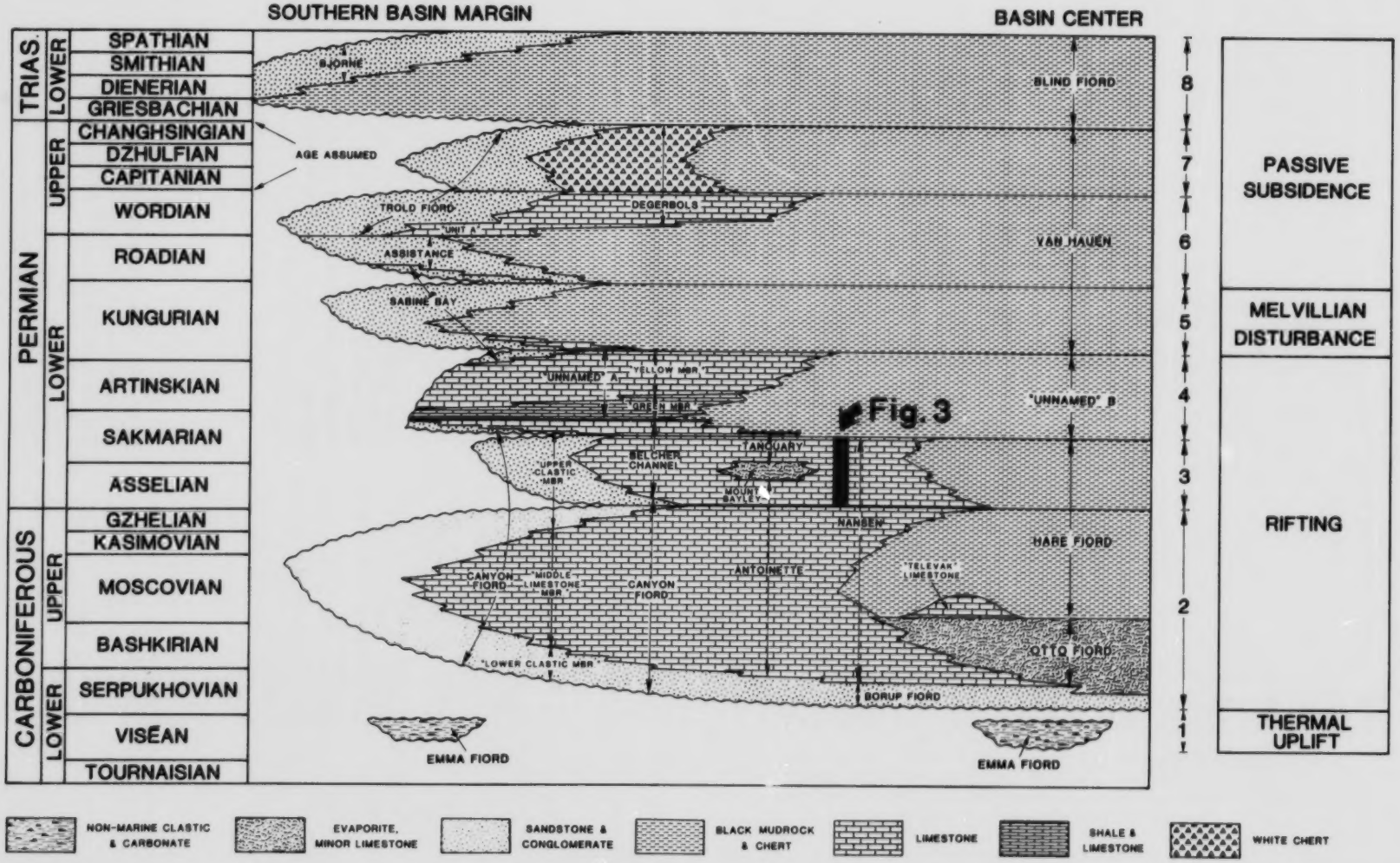

Figure 2. Upper Paleozoic second- and third-order transgressive-regressive sequences in the Sverdrup Basin. (Modified from Beauchamp et al., 1989b). Stratigraphic position of section depicted in Figure 3 is shown.

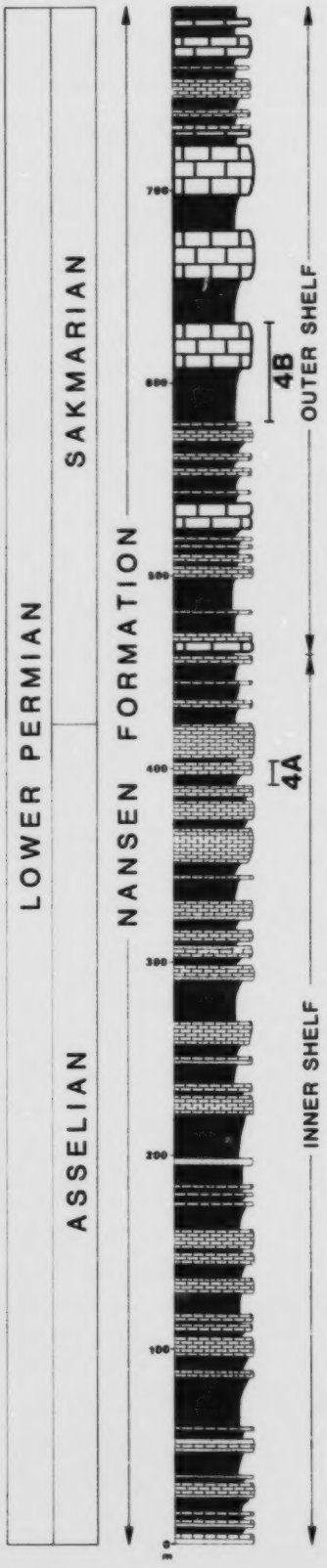

PETROGRAPHY OF SILICA

The descriptive terminology used in this report is that of Roubeault (1963). This terminology, in terms of crystal forms and their arrangement, agrees with general usage (Folk and Pittman, 1971; Arbey, 1980). Examinations of carbonates from shallow to deeper shelf facies led to the recognition of the following seven varieties of silica:

1. Spherulites and splays of wide fibres, with irregular boundaries, that have c-axes parallel to their axes of elongation (length-slow chalcedony or quartzine) (Figs. 5a-c, 6a, h). These crystals display a yellowish hue in plane-polarized light (dark grey tone in Figures 5d, 6b) and are common as replacement of coral skeletons (Figs. 5a, b, 6a) and of early calcite cements (Figs. 5c, d, 6a, b).

2. Splays of coarse, irregularly radiating, wide fibres that have c-axes at approximately 30 from the direction of their elongation (lutecite). The crystals have a yellowish hue in plane-polarized light, are closely associated with quartzine (forming the same crystal layers) and replace coral skeletons (Fig. 5a).

3. Spherulites of perfectly radiating thin fibres that have symmetrical boundaries and c-axes perpendicular to the direction of their elongation (length-fast chalcedony or chalcedonite) (Figs. 5a-e, 6a, b, h). The crystals display a yellow to dark brown hue in plane-polarized light. They appear almost exclusively as cement in intraskeletal cavities or, occasionally, within shelter cavities in mud mounds. Chalcedonite was generally observed growing over replacive quartzine, but in some instances it was growing over corroded bladed crystals of calcite (Fig. 5e).

4. Chains of subautomorph megaquartz (quartz crystals in excess of twenty microns in size) characterized by abundant calcite inclusions (Fig. 5f) and replacing of calcite.

5. Mesh of xenomorphic microquartz (0.03 mm and less), replacing inclusion-rich, early marine, calcite cements along crystalline boundaries (Fig. 5g, h), and in places associated with subautomorphic megaquartz, the latter being a replacement of corals. In shelf-edge carbonate units, microquartz silification does not affect the later generations of inclusion-free calcite, suggesting that microquartz precipitation was an earlier event. Microfractures filled by iron-rich calcite locally cut through the partly silicified early marine cements (Fig. 5g).

Figure 3. Lower Permian (Asselian-Sakmarian) Nansen Formation on the west side of Blind Fiord, southwestern Ellesmere Island. Note intraformational shelf cycles. Black areas depict recessive calcareous shale and argillaceous limestone. Stratigraphic position of individual cycles depicted in Figure 4 is shown.

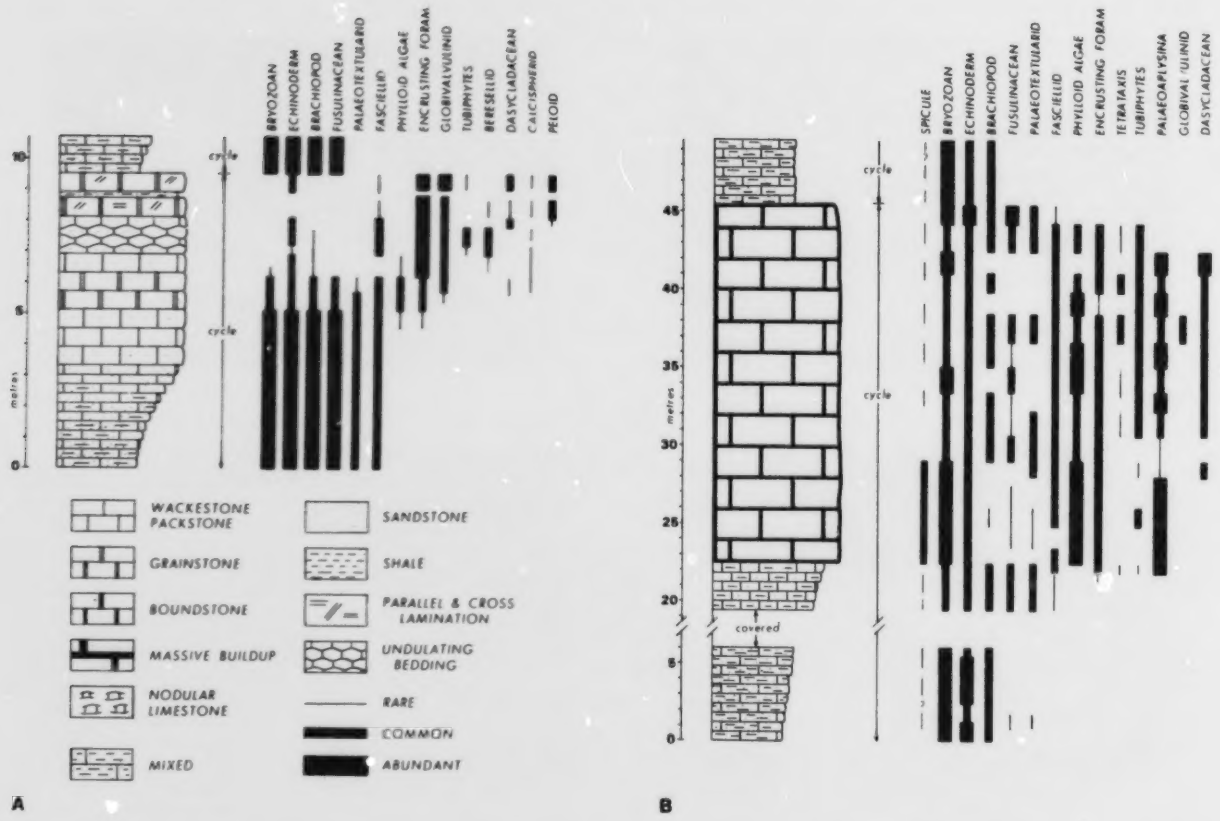

Figure 4. **A.** Upper Asselian inner shelf cycle in Nansen Formation on west side of Blind Fiord. Note dominance of grainstone facies in upper part of cycle. **B.** Sakmarian outer shelf cycle (carbonate buildup) in Nansen Formation on west side of Blind Fiord. Buildup is dominated by wackestones and packstones.

6. Mosaics of equant xenomorphic (locally subautomorphic) megaquartz. These crystals are clear of inclusions, perfectly translucent (Fig. 6b), and appear mostly as pore infills (Fig. 6a, c, d). Wherever both megaquartz and spherulitic chalcedonite occur in the same cavity, the latter invariably postdates the former (Fig. 6a). Xenomorphic megaquartz also postdates iron-poor calcite cement, which may have been previously corroded (Fig. 6e) or preserved in an uncorroded state (Fig. 6f).
7. Isolated automorphic megaquartz with abundant calcite inclusions (Fig. 6g). This form of silica exclusively replaces the fine carbonate sediments in which it is present as disseminated isolated phases.

DISTRIBUTION OF SILICA

Silicification affected both inner and outer shelf upper Paleozoic carbonates in the Sverdrup Basin. In inner shelf packstones and grainstones, silica massively replaces solitary corals (Fig. 5a, c, 6a). It fills up to forty per cent of the primary intraskeletal porosity and, in places, forms chert nodules and chert beds. It also occurs as quartzine, lutecite, chalcedonite, xenomorphic, subautomorphic, and automorphic megaquartz, and as microquartz.

In contrast, only three types of silica were observed in outer-shelf carbonates: isolated automorphic megaquartz replacing carbonate mud, xenomorphic microquartz replacing early marine cements, and pore-filling, xenomorphic megaquartz.

CHRONOLOGICAL SUCCESSION

Inner shelf facies

Many of the inner shelf carbonates display diverse products of silicification that generally appear in the following chronological order, from early to late (Fig. 6a): 1) quartzine and lutecite (mainly relacement); 2) chalcedonite (mainly cement); and 3) mosaic xenomorphic megaquartz (mainly cement).

Silicification postdates iron-poor, bladed calcite cements (shallow burial), but its relationship to later, iron-rich, xenomorphic calcite cements is unclear. Silicification has been observed to either precede (Fig. 6h) or postdate (Fig. 6d) iron-rich calcites. The latter are dull under cathodoluminescence and are interpreted as products of burial environment (Savard, work in progress). Silicification preceded compactional pressure solution, since stylolites

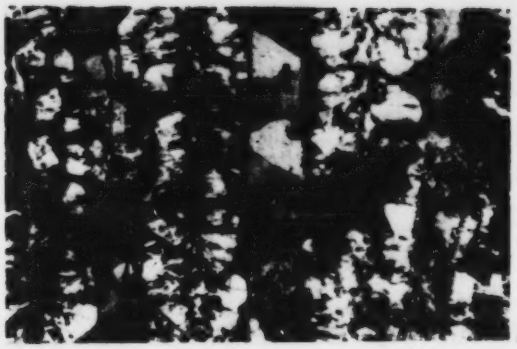
A

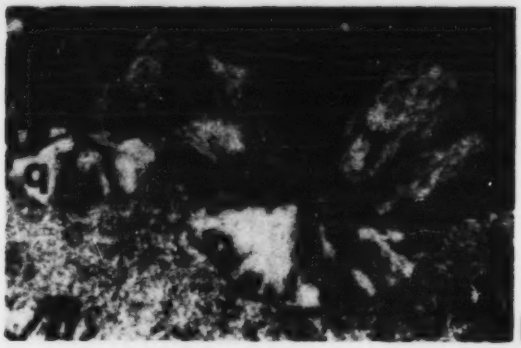

B

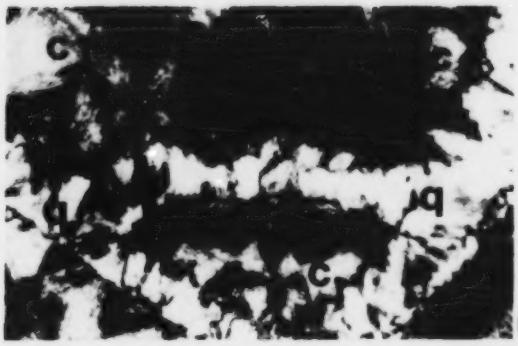

C

D

E

F

G

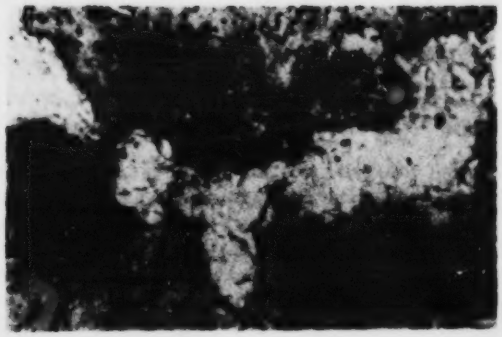
H

can be observed bending around silica crystals. Automorphic megaquartz scattered in the host sediments also preceded stylolitisation; it is otherwise difficult to place in a chronological succession.

Outer shelf facies

All silica types within deeper-water outer shelf carbonates appear to be contemporaneous. Both displacive microquartz and pore-filling megaquartz postdate early marine calcite cementation. Microquartz partly replaces marine calcite cements along their crystal boundaries, whereas the growth of megaquartz in pores followed that of marine calcite fibres (Fig. 6c).

Both types of quartz preceded the iron-rich xenomorphic calcite cements (Fig. 6c), since fractures, cemented by iron-rich calcite, crosscut replacive and pore-filling quartz. Iron-rich calcite is dull under cathodoluminescence and assumed to be of burial origin (Savard, work in progress). Silicification of deeper-water shelf-edge carbonates, however, took place prior to stylolitisation, which can be related to a later burial setting.

DISCUSSION AND IMPLICATIONS FOR DIAGENESIS

As documented above, silica precipitates can pervasively affect carbonate sediments and even noticeably decrease the pore volume, even in the alkaline pore water systems typical of a carbonate sequence. The presence of silica between multiple carbonate precipitates reflects significant changes in the physico-chemical properties of the diagnetic environment. On the one hand, the relative abundance of silica in the inner shelf carbonate units of the basin margin could reflect their proximity to thick siliciclastic deposits and their accessibility to meteoric waters. On the other hand, silica in shelf edge units could be derived from basinal to slope biogenic components, such as siliceous sponge spicules, and could have reached the shallower platform areas through upwelling. Clay diagenesis may also have produced significant amounts of silica, which then circulated in the pore sytsem.

There exist a number of models for the mobilization and precipitation of silica in carbonate rocks. For example, Folk and Pittman (1971) have proposed that the various chert varieties reflect the nature of diagenetic fluids. Lutecite and quartzine form from highly acidic, magnesium- and sulphate-rich waters, chalcedonite from acid to neutral and non-sulphatic waters, and megaquartz from solutions with low silica concentrations. If so, the lutecite/quartzine-chalcedonite-megaquartz succession in the shallow water carbonate units of the Sverdrup Basin probably indicates qualitative changes in the evolving parent waters. These changing waters generated crystals of distinct solubilities, shapes and optical properties.

The various generations of silica have clear, individualistic relationships to the surrounding calcite. Lutecite and quartzine mostly replaced skeletal calcite and early bladed cement, as indicated by their ghosts under plane-polarized light (Fig. 5d, 6b). Chalcedonite generally grew in free

Figure 5. **A.** Coral skeleton partly replaced by quartzine (Q) and lutecite (L). Intraskeletal cavities were filled by chalcedonite (c) and calcite cement (t). Cross-polarized light. Width of photograph is 2 mm. **B.** Spherulite composed of quartzine (q) and chalcedonite (c). The quartzine replaced parts of a coral skeleton, whereas the chalcedonite grew in an empty space. Cross-polarized light. Width of photograph is 0.4 mm. **C.** Coral structure completely replaced by irregular splays of quartzine (q) and lutecite (q). Intraskeletal cavities are occluded by regularly radiating chalcedonite (c) forming perfect spherulites. Cross-polarized light. Width of photograph is 0.64 mm. **D.** Same as in **C** in plane-polarized light, showing ghosts of bladed calcite within quartzine. Note the inclusion-rich nature of both quartzine (q) and chalcedonite (c). Width of photograph is 0.64 mm. **E.** Spherulite of chalcedonite (c) covering corroded bladed cement (t). Cross-polarized light. Width of photograph is 0.32 mm. **F.** Chain of subautomorphic megaquartz, rich in calcite inclusions. Plane-polarized length. Width of photograph is 0.4 mm. **G.** Mesh of microquartz (o) replacing marine calcite cement along fibre boundaries. Iron-rich calcite cement seals a fracture (f) that cuts through silica. Stained sample. Plane-polarized length. Width of photograph is 1.6 mm. **H.** Mesh of microquartz at the junction of three inclusion-rich calcite crystals (a-b-c). Plane-polarized length. Width of photograph is 0.16 mm.

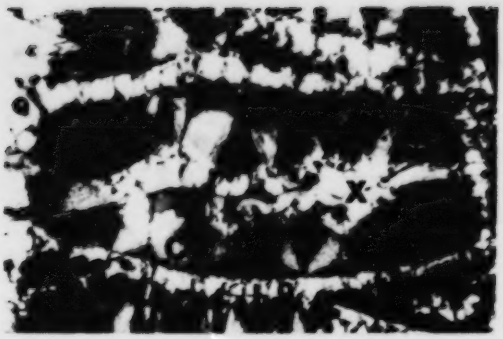
A

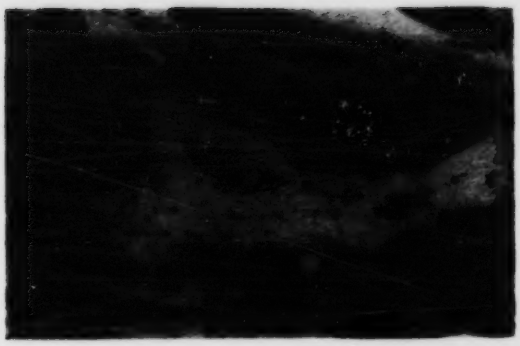
B

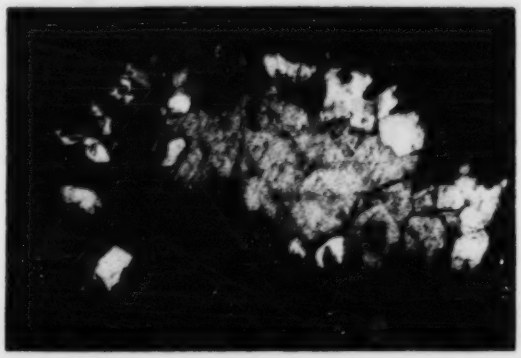
C

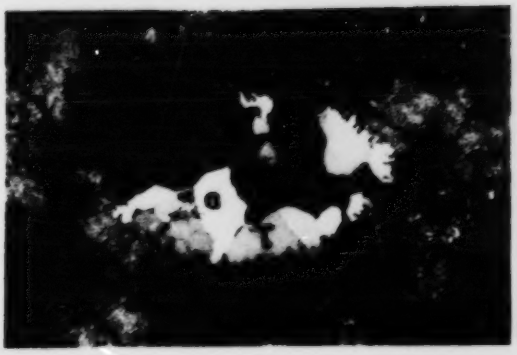
D

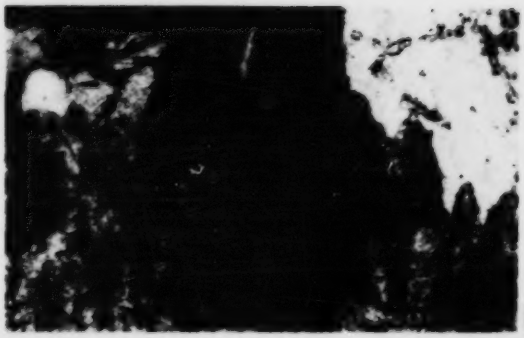
E

F

G

H

space following quartzine precipitation (Fig. 5a-c, 6a, h). The latter, by analogy with xenomorphic megaquartz, could have precipitated over either intact (Fig. 6f) or slightly corroded, bladed, iron-poor calcite (Fig. 5e, 6e). A complete replacement of calcite by lutecite and quartzine might have been a product of more aggressive or acidic waters, whereas alkaline waters could have left the calcite only slightly corroded or intact. In deeper-water shelf-edge carbonate units, the megaquartz phase may reflect the limited aggressivity (acidity) and/or low saturation levels of the parent waters.

The chronological ranking of silica precipitates in the deeper-water outer shelf carbonates, after marine calcite cement but before (iron-rich calcite) burial cements, suggests that silicification occurred during an early burial diagenetic stage. In contrast, silicification of inner shelf carbonate units appears to have taken place over a longer period of time, since in many cases xenomorphic megaquartz postdates the iron-rich burial calcite (Fig. 6d).

Figure 6. **A.** Succession of quarztine (q), chalcedonite (C) and xenomorphic megaquartz (X). Plane-polarized length. Width of photograph is 0.64 mm. **B.** Same as in **A**, under plane-polarized light. Note clarity of the megaquartz (X) in comparison with the chalcedonites (Q and C). Ghosts of replaced coral framework and of balded calcite cement are visible. **C.** Chronological relationships between inclusion-rich fibrous marine calcite cement (m), megaquartz (g) and inclusion-free calcite cement (t) in deeper-water shelf-edge units. The megaquartz grew over fibrous calcite and was in turn overgrown by the inclusion-free calcite. Shelter cavity in mud mound. Plane-polarized length. Width of photograph is 4 mm. **D.** Chronological relationships between inclusion-rich early calcite cement (m), inclusion-free calcite cement (T) and megaquartz (G) in shallow water carbonate units. The inclusion-free calcite grew over fibrous calcite and was in turn overgrown by the megaquartz. Plane-polarized length. Width of photograph is 4 mm. **E.** Magnification of the contact between fibrous calcite cement and megaquartz of **C**. The megaquartz grew over corroded fibres. Plane-polarized length. Width of photograph is 0.8 mm. **F.** Contact between bladed calcite cement and megaquartz. The megaquartz grew over uncorroded blades. Plane-polarized length. Width of photograph is 0.32 mm. **G.** Inclusion-rich, isolated automorphic megaquartz in recrystallized mud. Plane-polarized length. Width of photograph is 0.16 mm. **H.** Inclusion-free calcite cement (T) in the center of a pore postdating the formation of chalcedonite (C) and quartzine (Q). Plane-polarized length. Width of photograph is 0.8 mm.

ACKNOWLEDGMENTS

Fieldwork for this project was facilitated by the Geological Survey of Canada (Frontier Geoscience Program) and by the Polar Continental Shelf Project. We acknowledge the financial support of the Natural Sciences and Engineering Research Council of Canada to J. Veizer (operating grant) and M. Savard (post-graduate scholarship). We are also grateful for the financial support from the "Formation de Chercheurs et l'Aide a la Recherche" of Québec (post-graduate scholarship), and the School of Graduate Studies and Research at the University of Ottawa (postgraduate scholarship to M. Savard). D.W. Morrow kindly reviewed this paper and suggested considerable improvements.

REFERENCES

Arby, F.
1980: Les formes de la silice et l'identification des évaporites dans les formations silicifiées; Bulletin des Centres de Recherches, Exploration-Production Elf-Aquitaine, v. 4, p. 309-365.

Beauchamp, B.
1987: Stratigraphy and facies analysis of the Upper Carboniferous to Lower Permian Canyon Fiord, Belcher Channel and Nansen formations, southwestern Ellesmere Island; Ph.D. thesis, University of Calgary, June, 1987, 370 p.

Beauchamp, B., Harrison, J.C., and Henderson, C.M.
1989a: Upper Paleozoic stratigraphy and basin analysis of the Sverdrup Basin, Canadian Arctic Archipelago: Part 1, time frame and tectonic evolution; *in* Current Research, Part G, Geological Survey of Canada, Paper 89-1G, p. 105-113, 1989.

Beauchamp, B., Harrison, J.C., and Henderson, C.M.
1989b: Upper Paleozoic stratigraphy and basin analysis of the Sverdrup Basin, Canadian Arctic Archipelago: Part 2, transgressive-regressive sequences; *in* Current Research, Part G, Geological Survey of Canada, Paper 89-1G, p. 115-124, 1989.

Folk, R.L. and Pitman, E.F.
1971: Length-slow chalcedony: a new testament for vanished evaporites; Journal of Sedimentary Petrology, v. 41, p. 1045-1058.

Roubault, M.
1 9 6 Détermination des minéraux des roches au microscope polarisant; Deuxieme édition, Editions Lamarre-Poinat, 365 p.

A photoacoustic infrared spectroscopic study to determine variations of the chemical structures of samples from weathered outcrops and fresh coals from Western Canada

R. McFarlane[1] and F. Goodarzi
Institute of Sedimentary and Petroleum Geology, Calgary

McFarlane, R. and Goodarzi, F., A photoacoustic infrared spectroscopic study to determine variations of the chemical structures of samples from weathered outcrops and fresh coals from Western Canada; in Current Research, Part D, Geological Survey of Canada, Paper 90-1D, p. 111-114, 1990.

Abstract

Two suites of samples of a subbituminous and a bituminous coal from Western Canada were analyzed by photoacoustic infrared spectroscopy. The samples were obtained by drilling from outcrop to a depth of about 10 m, parallel to seam orientation, and were originally collected to measure petrological, chemical and rheological effects of weathering. In the present study (photoacoustic IR), variations in the relative intensities of bands due to various C-H, C-O and C-C vibrational modes were observed.

Although no systematic variation in the relative intensities was observed that smoothly parallels the previously determined petrographic, rheological and chemical composition of these samples, this preliminary investigation illustrates the potential of this technique for determining the compositional variation of the surface and near-surface functional groups in weathered and fresh coals.

Résumé

Deux séquences d'échantillons de charbon sub-bitumineux et bitumineux de l'Ouest canadien ont été analysées par spectroscopie infrarouge photoacoustique. Les échantillons ont été prélevés dans un affleurement au moyen d'un forage effectué jusqu'à une profondeur d'environ 10 m, parallèlement à l'orientation de la couche; ils devaient servir, à l'origine, à mesurer les effets pétrologiques, chimiques et rhéologiques de l'altération. Dans la présente étude, on a observé des variations (IR photoacoustiques) des intensités relatives des bandes dues à différents modes de vibration C-H, C-O et C-C.

Bien que l'on n'ait pas observé de variation systématique des intensités relatives qui soit relativement parallèle aux compositions pétrographique, rhéologique et chimique déjà déterminées de ces échantillons, cette analyse préliminaire illustre les possibilités de cette technique au niveau de la détermination de la variation de composition des groupes fonctionnels situés à la surface et près de la surface dans les charbons altérés et non altérés.

[1] Alberta Research Council, Coal Research Centre Devon, One Oil Patch Drive, Devon, Alberta, T0C 1E0

INTRODUCTION

The natural oxidation or weathering of coal is a chemical process that occurs in coals close to the surface of the earth. The physical and chemical properties of coals as they relate to preparation and utilization are very sensitive to change by weathering; for example, swelling (Chandra, 1975; Gray et al., 1976), flotation (Jin and Miller, 1988) and coking (Guyot and Pollard, 1974). Weathering takes place continuously in situ before mining, but further weathering occurs during mining, because the coal seam is further exposed, and also during storage and transportation.

The detection and determination of the degree of weathering is important from an industrial point of view because of its deleterious effects on processing and utilization. Several parameters have been used to detect weathering: maceral reflectance, free swelling index, calorific value, dye adsorption and proximate and ultimate analysis. The use of these parameters has been amply illustrated by Marchioni (1983). A number of studies of the artificial weathering/oxidation of coals using infrared spectroscopy have been reported (e.g., Lynch et al., 1988; Monthioux and Landais, 1988; Kister et al., 1988; Calemma et al., 1988; Gethner, 1987; Fuller and Smyrl, 1985). These oxidations, however, are generally carried out at relatively high temperatures (>100 C) with or without the presence of water vapour. Such investigation may elucidate some aspects of natural weathering. However, because the laboratory conditions are not closely related to natural coal environments, reaction kinetics, mechanisms and ultimately structures may be significantly different.

This report presents preliminary data on naturally weathered coals and also attempts to contrast this natural weathering to laboratory oxidation. To our knowledge, this is the first report on the use of photoacoustic infrared spectroscopy to investigate natural weathering. While no simple correlations exist between these early results and the existing parameters used to determine weathering, the present application does show structural sensitivity from sample to sample, which bodes well for further studies.

The two suites of coal samples studied were collected by Marchioni who previously carried out and reported petrographic, rheological and chemical analyses (Marchioni, 1983). One suite is of a subbituminous coal from Drumheller in southern Alberta and the other a bituminous coal from Sparwood in southeastern British Columbia.

Experimental

Details concerning the coal sampling have been reported by Marchioni (1983). It is sufficient to note here that each suite was obtained from a single coal seam collected from outcrop to a depth of no more than 11 m.

The samples as received for infrared spectroscopic studies were either finely ground or coarse. For all studies the samples were finely ground by hand, under atmospheric conditions, in an agate mortar, to less than 180 microns. All samples were then vacuum dried at 40° C for four hours. Spectra were recorded using an MTEC Model 200 photoacoustic cell with a Nicolet 740 SX spectrometer. The photoacoustic cell was purged with helium and the mirror velocity of the spectrometer was such that the modulation frequency at 4000 cm^{-1} was 2.5 kHz. This high modulation frequency appeared sufficient to reduce photoacoustic saturation effects in the low wavenumber region. Each spectrum was obtained by co-adding 400 double-sided interferograms with a resolution of 8 cm^{-1} and the total measurement time was about five minutes. The spectra of all samples were ratioed against a spectrum of Calgon activated carbon and converted to photoacoustic units.

A sample of each coal obtained at the greatest depth (least weathered) was subjected to oxidation in a humid atmosphere at 110° C for 72 hours in a sealed chamber. After completion of the oxidation, the chamber was cooled to 40° C and evacuated for one hour followed by flooding with nitrogen gas and removal of the sample directly to the photoacoustic cell.

RESULTS

Tables 1 and 2 list the samples and their depth from outcrop. Figures 1 and 2 show the photoacoustic infrared spectra of the two series of coals from Tables 1 and 2, respectively. The spectra are plotted in photoacoustic units, which can be taken as essentially linear with concentration. Both series of spectra show varying concentrations of mineral matter (mainly kaolinite) reflected by bands at 3697, 3668, 3652, 3621, 1040, 934, 913, 547 and 472 cm^{-1}. This fluctuation in concentration of kaolinite could be due either to a real variation in the distribution of kaolinite within the coal seam or a varying concentration in the fines of the coal after grinding. The latter possibility arises because kaolinite is more friable than coal and for this reason, future work would best be performed on coarsely ground samples.

The spectra of the bituminous coal from British Columbia (Fig. 1) show no dramatic changes with depth except in the bands around 1700 and 1440 cm^{-1} which, respectively, decrease and increase in intensity with depth. Bands between 1780 and 1630 cm^{-1} may be assigned to esters, ketones and aldehydes, the presence of which would be expected to decrease with oxidation/weathering. The band at 1440 cm^{-1} can be attributed to asymmetric C-H bending of $-CH_3$ and $-CH_2$ groups and in-plane aromatic C-H deformations because alkyl groups are more reactive than aromatic C-H to weathering. Marchioni (1983) reported that these samples showed the effects of weathering to the maximum depth sampled and that fresh coal was not encountered. With the exception of the outcrop sample, which had the highest oxygen/carbon ratio, the oxygen/carbon ratio was erratic with depth. A similar case was observed for the hydrogen/carbon ratio. Such erratic variation is observed in Figure 1 and measured peak areas in Table 1.

The spectra of the subbituminous coal from Drumheller, Alberta are significantly different from that of the bituminous coal, and the differences are mainly due to the difference in degree of aromaticity. These subbituminous coals exhibit only a very weak band at 3050 cm^{-1} attributable to aromatic C-H stretch, and weaker bands between 900 and 700 cm^{-1} (triplet in Figure 1) which are known to arise

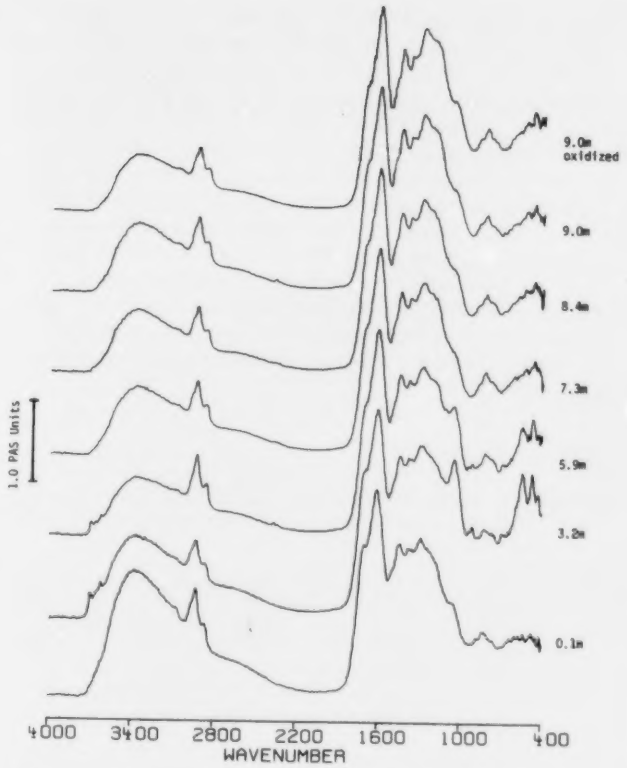

Figure 1. Infrared photoacoustic spectra of bituminous coal from southeastern British Columbia. Spectra have been plotted so that the band at ~1600 cm^{-1} has equal intensity in all spectra. The bar on the left indicates 1.0 photoacoustic unit and the depth of each sample in metres is shown to the left.

Table 1. Sampling depth and infrared photoacoustic intensity ratios for bituminous coal from southeastern British Columbia

Sample	Depth (m)	I(3125-2800) / I(1800-1540)	I(2995-2800) / I(1800-1540)	I(2995-2800) / I(3125-2995)
51/79	0.5	0.13	0.10	3.76
52/79	1.8	0.14	0.11	4.33
53/79	3.2	0.17	0.14	5.03
54/79	5.4	0.14	0.11	3.94
55/79	6.3	0.15	0.12	4.09
56/79	7.8	0.18	0.14	4.18
57/79	9.3	0.14	0.11	4.41
58/79	10.9	0.20	0.16	4.31
58/79[1]	10.9	0.22	0.18	4.00

[1] indicates oxidized sample, see text.
The regions from 3125-2995, 2995-2800 and 1800-1540 cm^{-1} correspond to bands due to aromatic C-H, aliphatic C-H and C-O and aromatic C-C stretching modes, respectively.

Table 2. Sampling depth and infrared photoacoustic intensity ratios for subbituminous coal from Drumheller, Alberta

Sample	Depth (m)	I(2995-2800) / I(1800-1540)
781/78	0.1	0.19
785/78	3.2	0.14
787/78	5.9	0.22
789/78	7.3	0.18
790/78	8.4	0.16
791/78	9.0	0.18
791/78[1]	9.0	0.16

[1] indicates oxidized sample, see text.
The regions from 2995-2800 and 1800-1540 cm^{-1} correspond to aliphatic C-H and C-O and aromatic C-C stretching modes, respectively.

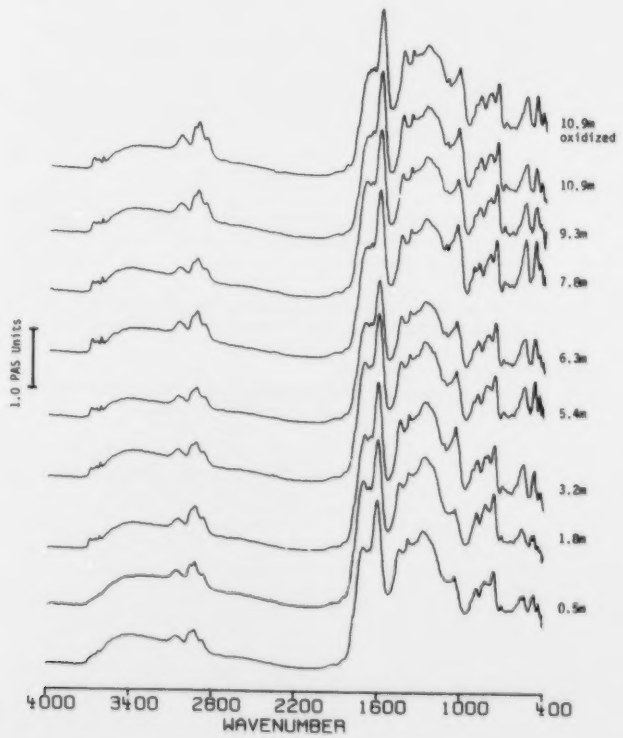

Figure 2. Infrared photoacoustic spectra of subbituminous coal from Drumheller in southern Alberta. All spectra have been plotted such that the bands at ~1600 cm^{-1} have equal intensities. The bar indicates 2.0 photoacoustic units and the depths in metres is indicated to the right of each spectrum.

from out-of-plane bending modes of aromatic C-H. Although the oxygen/carbon ratios of these coals are about twice those of the bituminous coals, the bands around 1700 cm^{-1} do not appear as intense. The region between 1300 and 1100 cm^{-1}, where C-O stretching modes of ethers and alcohols and the O-H bending mode of alcohols occur, show significant variation of intensity with depth. Unfortunately, C-C stretching and $-CH_2$ bending modes also occur in this region of the spectrum, rendering interpretation difficult, but it is suspected that ethers and alcohols may bind some oxygen. The band at 1440 cm^{-1} assigned to $-CH_3$ and $-CH_2$ bending and aromatic C-H in-plane bending modes appears to change in relative intensity with respect to that at 1290 cm^{-1} indicating an increase in $-CH_2$ and $-CH_3$ groups with depth. When spectral subtractions are carried out using the sample farthest from outcrop as the reference, three bands, at approximately 1720, 1550 and 1400 cm^{-1} are observed, and these bands decrease in intensity from outcrop to the penultimate sample. The band at 1720 cm^{-1} can be assigned to an aliphatic ester and that at 1550 cm^{-1} to the anti-symmetrical C-O stretch of a carboxylate anion, which would explain their decrease with depth. The decrease of the band at 1400 cm^{-1} is more difficult to explain since various C-H modes occur near here and would be expected to increase with depth. One explanation may be that this band is due to a coupled mode involving C-O bonds. Unlike the bituminous coal series, Marchioni reports that fresh subbituminous coal was obtained at a depth of 11 m. Our deepest sample was from 9 m where the effects of weathering can still be observed.

When oxidized at 110C for 72 hours in a humid atmosphere, the samples in each series farthest from outcrop showed very little change. This is not surprising in the case of the bituminous coal since Marchioni reported that this sample had been affected by weathering. It is, however, surprising that the subbituminous coal was little changed by oxidation since it was reported close to the region of fresh coal as noted above. It is likely that further oxidation has occurred for all these samples since their original analysis in 1981. Such an occurrence could account for the great similarities between the two series of coals. Despite this, differences, albeit not entirely coincident with the report of Marchioni (1983), have been observed, indicating that the technique may be sensitive enough for the investigation of weathering effects on a controlled sampling of coals from outcrop to fresh coal. Such an investigation is now commencing with the acquisition of recently collected samples.

SUMMARY

A preliminary investigation by photoacoustic infrared spectroscopy of naturally weathered coals, sampled from outcrop to about 10 m depth, indicates that this surface sensitive technique can be applied in conjunction with petrographic and chemical analyses for detailed investigation of weathering. The surface sensitivity of the photoacoustic technique requires that the coal be analyzed soon after collection and the exposure of grain surfaces to atmosphere subsequent to crushing, since weathering will start from the surface and then go inward. This is not a limitation of ultimate analysis, which measures mainly bulk composition. Photoacoustic spectroscopy should offer a sensitivity similar to maceral reflectance and dye adsorption, which are also surface sensitive techniques. Additionally, the ability to identify surface functional groups may offer the possibility of assessing their role in such processes as agglomeration and liquefaction.

REFERENCES

Calemma, V., Rausa, R., Magarit, R., and Girardi, E.
1988: FT-IR study of coal oxidation at low temperature, Fuel, v. 67, p. 764-770.

Chandra, D.
1975: Fundamentals of coal petrology - oxidized coal; *in* Stach's Textbook of Coal Petrology, E. Stach, M.Th., M. Mackowsky, and R. Teichmüller, G.H. Taylor, and D. Chandra ed.; Gebruber-Borntraeger, Berlin-Stuttgart, p. 159-164.

Fuller, Jr., E.L. and Smyrl, N.R.
1985: Chemistry and structure of coals. Diffuse reflectance I.R. spectroscopy equipment and techniques; Fuel, v. 64, p. 1143-1150.

Gethner, J.S.
1987: Kinetic study of the oxidation of Illinois No. 6 coal at low temperatures. Evidence for simultaneous reactions; Fuel, v. 66, p. 1091-1096.

Gray, R.J., Rhodes, A.H., and King, D.T.
1976: Detection of oxidized coal and the effect of oxidation on the technological properties; Society of Mining Engineers, American Institute of Mining Engineers, Transactions, v. 260, p. 334-341.

Guyot, R.E. and Pollard, F.
1974: Effects of oxidation on coal properties related to industrial use; Australia Coal Industry Research Laboratory, Report 74-18.

Jin, Y. Ye. R. and Miller, J.D.
1988: Thermal treatment of low-rank coal and its relationship to flotation response; Coal Preparation, v. 6, p. 1-16.

Kister, J., Guiliano, M., Mille, G., and Dou, H.
1988: Changes in the chemical structure of low rank coal after low temperature oxidation or demineralization by acid treatment. Analysis by FT-IR and U.V. Fluorescence; Fuel, v. 67, p. 1076-1082.

Lynch, B.M., Lancaster, L-I., and MacPhee, J.A.
1988: Detection of carbonyl functionality of oxidized, vacuum-dried coals by Photoacoustic Infrared Fourier Transform (PAIFT) spectroscopy: correlations with added oxygen and with plastic properties; Energy and Fuels, v. 2, p.13-17.

Marchioni, D.L.
1983: The detection of weathering in coal by petrographic, rheologic and chemical methods; International Journal of Coal Geology, v. 2, p. 231-259.

Monthioux, M. and Landais, P.
1988: Natural and artificial maturations of a coal series: Infrared spectrometry study; Energy and Fuels, v. 2, p. 794-801.

The BP Graham C-52 well and upper Paleozoic subsurface stratigraphy in the Canadian Arctic

Benoit Beauchamp and Julie Lamirande[1]
Institute of Sedimentary and Petroleum Geology, Calgary

Beauchamp, B. and Lamirande, J., The BP Graham C-52 well and upper Paleozoic subsurface stratigraphy in the Canadian Arctic; in Current Research, Part D, Geological Survey of Canada, Paper 90-1D, p. 115-122, 1990.

Abstract

A well in the Canadian Arctic, BP Graham C-52 drilled on Graham Island in 1972, was investigated in order to test the recently modified upper Paleozoic stratigraphic framework of the Sverdrup Basin. This well went through 802 m of Permian sediments attributed to the Sakmarian Nansen (or Belcher Channel) Formation (252 m), the Artinskian to lowest Kungurian "unnamed" B formation (267 m), and the Kungurian to post-Wordian(?) Van Hauen Formation (311 m). Microfacies analysis of well cuttings suggests depositional environments ranging from outer shelf (Nansen) to deep water slope and basin ("unnamed" B and Van Hauen). Five (Sequences 3 to 7) of the seven upper Paleozoic second-to third-order transgressive-regressive sequences of the Sverdrup Basin are recognized in the well.

Résumé

Un puits de sursurface de l'Arctique canadien, le BP Graham C-52, foré dans l'Île de Graham en 1972, est ici à l'étude dans le but de mettre à l'essai le canevas stratigraphique, récemment modifié, du Paléozoïque supérieur du bassin de Sverdrup. Le forage a rencontré 802 m de sédiments permiens appartenant à la formation de Nansen (ou Belcher Channel) (252 m; du Sakmarien, (252 m); de la formation « innommée » B (267 m; datant de l'Artinskien au Kungurien inférieur; et Van Hauen (311 m) d'âge kungurien à post-wordien(?). L'analyse des microfaciès de débris de forages semble indiquer des milieux sédimentaires dont le type varie de plate-forme externe (Nansen) à milieu de pente et bassin en eaux profondes (« innommée » B et Van Hauen). Cinq (séquences 3 à 7) des sept grandes séquences transgressives et régressives de deuxième et troisième ordre du Paléozoique supérieur du bassin de Sverdrup sont reconnues dans le puits.

[1] Department of Geology, University of Ottawa, Ottawa, Ontario, K1N 6N5

INTRODUCTION

The recent acquisition of biostratigraphic, lithological and petrographic data has led to a much better understanding of the upper Paleozoic stratigraphy of the Sverdrup Basin. A comprehensive framework that combines chronostratigraphy, lithostratigraphy and sequence stratigraphy was published last year (Beauchamp et al., 1989a, b). Fieldwork in the past few summers has shown that this framework can be used, with confidence, to assess the stratigraphic position of a given unit even with minimal biostratigraphic data. This framework is here tested for the first time on a subsurface well of the Sverdrup Basin: the Graham C-52 well drilled by British Petroleum in 1972 (Fig. 1).

Because the original measurements by British Petroleum were done in feet, depths in the BP Graham C-52 well are provided here in both metres and feet.

GEOLOGICAL SETTING

Seven second- to third-order (5 to 50 Ma) transgressive-regressive sequences have been recognized in the Carboniferous and Permian succession of the Sverdrup Basin (Fig. 2). Each sequence is characterized by a set of formations containing sediments that were deposited either on a shallow-water shelf or in a deeper-water basin (Beauchamp et al., 1989b). Four tectonic phases accompanied late Paleozoic deposition in the Sverdrup Basin (Beauchamp et al., 1989 a): thermal uplift (Viséan), rifting (Serpukhovian to Artinskian), strike-slip deformation (Melvillian Disturbance; Kungurian), and passive subsidence (Roadian to post-Wordian(?)).

Dramatic climatic shifts also occurred during the Carboniferous and Permian in the Sverdrup Basin. Warm and dry, tropical-like climates prevailed from the Viséan to the Sakmarian, cooler and more humid temperate conditions marked the Artinskian, cold climates characterized the Kungurian to Wordian, whereas very cold, polar-like conditions prevailed during the latest Permian (Beauchamp et al., 1989a). This climatic trend is suggested by the transition from highly diversified biogenic assemblages (calcareous algae, foraminifers, ooids and oncoids, reefs) during the Late Carboniferous and Early Permian, to poorly diversified assemblages (sponges, bryozoans, echinoderms and

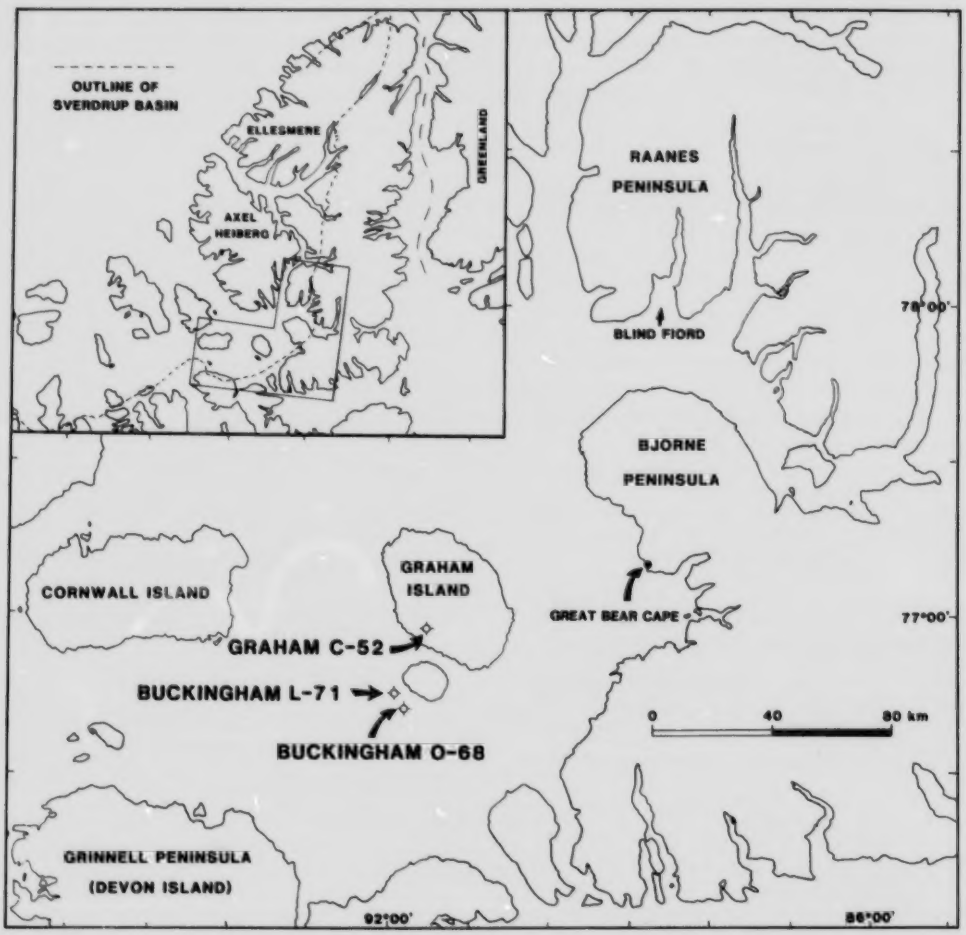

Figure 1. Location map showing BP Graham C-52, Panarctic Buckingham O-68 and Panarctic Buckingham L-71 wells.

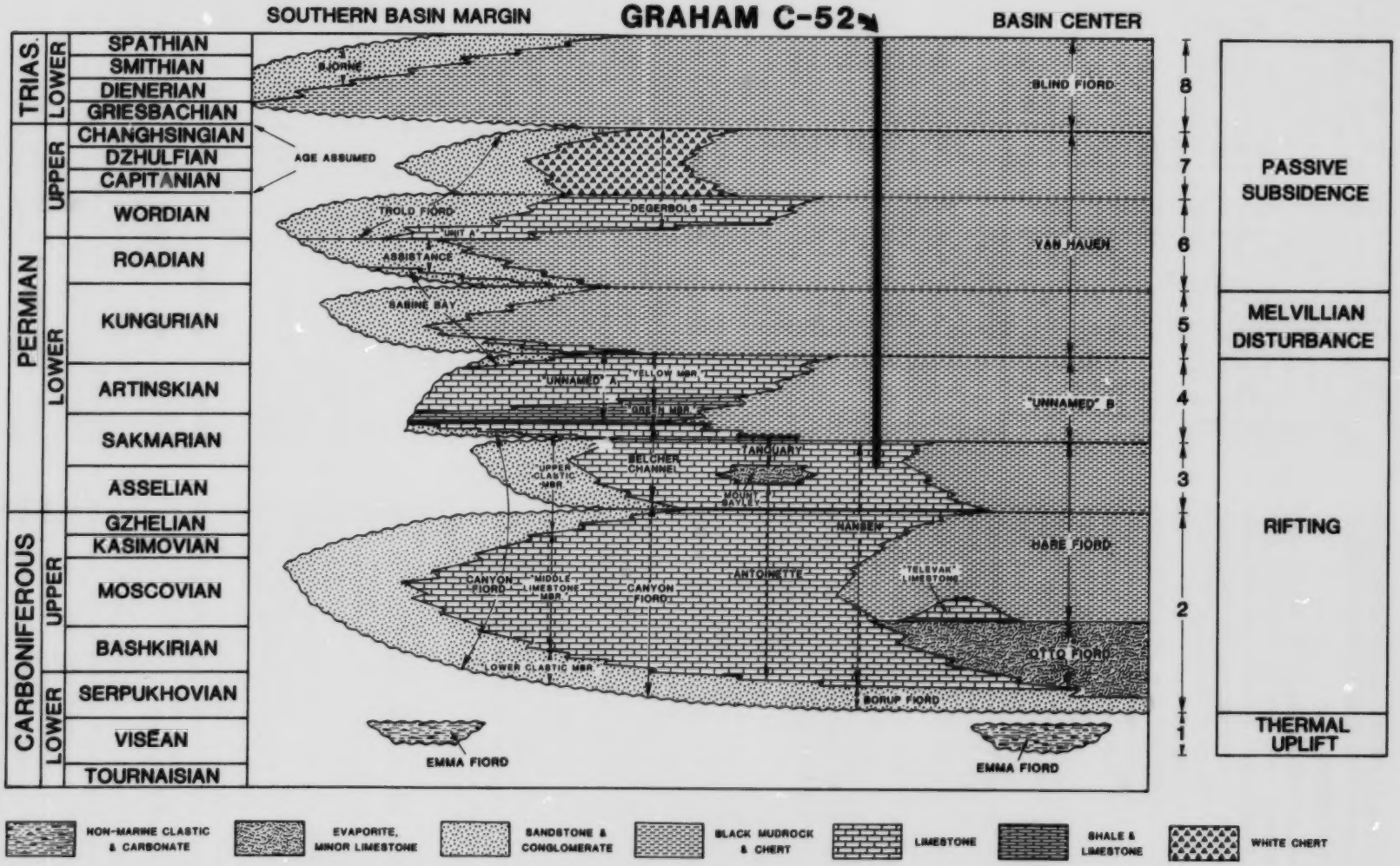

Figure 2. Carboniferous and Permian second- and third-order transgressive-regressive sequences (1 to 7) in the Sverdrup Basin along a schematic proximal-to-distal cross-section. Stratigraphic position of BP Graham C-52 well also is shown. (Modified from Beauchamp et al., 1989b.)

brachiopods) in the younger Early Permian and during the Late Permian. Latest Permian biota comprised essentially nothing but siliceous sponges.

The late Paleozoic paleogeography of the Sverdrup Basin was characterized by a carbonate- and/or clastic-dominated platform surrounding one or several deep water basins (Thorsteinsson, 1974) in which sedimentation took place under anoxic conditions (Beauchamp et al., 1987). The platform-to-basin transition is well exposed in many areas of the Arctic Islands, especially in the Blind Fiord area, where a number of detailed litho- and biostratigraphic studies were carried out (Beauchamp, 1987; Henderson, 1988). The platform-to-basin transition was also the target of three wells drilled in the vicinity of Graham Island at the southern margin of the Sverdrup Basin in 1972 (BP Graham C-52), 1984 (Panarctic Buckingham O-68) and 1986 (Panarctic Buckingham L-71) (Fig. 1). Of these three wells, BP Graham C-52 was drilled the farthest north, and hence penetrated a succession of deeper water sediments.

BP GRAHAM C-52

The BP Graham C-52 well was drilled on Graham Island (7721'14"N, 9051'25"W) from February 21 to May 16, 1972. The well went through 3082 m (10 110 ft.) of Mesozoic and Paleozoic rocks. The boundary between the Mesozoic and Paleozoic here lies at 2128 m (6980 ft.). If one excludes a 117 m (385 ft.) thick diabase sill that lies between 2364 and 2481 m (7755 and 8140 ft.), the well penetrated 807 m (2648 ft.) of Permian sediments. Three Permian cores were recovered from the following intervals: 2235 to 2241 m (7332-7353 ft.), 2671 to 2675 m (8764-8777 ft.), and 3062 to 3068 m (10 045-10 065 ft.). As part of this study, twenty-eight thin sections were made from cuttings selected at key depths.

Based on microfacies analysis, electric log interpretations, and conodont and foraminiferal biostratigraphy, three formations were recognized in the BP Graham C-52 well (Fig. 3). In ascending order they are: the Nansen (or Belcher Channel), the "unnamed" B and the Van Hauen.

Nansen (or Belcher Channel) Formation

A cyclic succession, 253 m (830 ft.) thick, of relatively pure carbonate sediments alternating with mixed shales and carbonates occurs from 2825 m (9270 ft.) to the bottom of the well. It belongs to either the Nansen Formation or the Belcher Channel, but it is impossible to assign it to one or the other because the lithology and age of the underlying, undrilled section is unknown. In the outcrop belt, however, wherever it is overlain by the deeper water "unnamed" B formation, as it is here, this carbonate-dominated succession belongs to the Nansen Formation.

Carbonate microfacies (Fig. 4) of the Nansen(?) Formation contain a wide variety of fossils including: dominant bryozoans, echinoderms, and *Tubiphytes*; common brachiopods, fusulinaceans, smaller foraminifers (Tetrataxids and Nodosarids mostly), encrusting foraminifers (Apterrinellids, Tuberetinids), and red algae

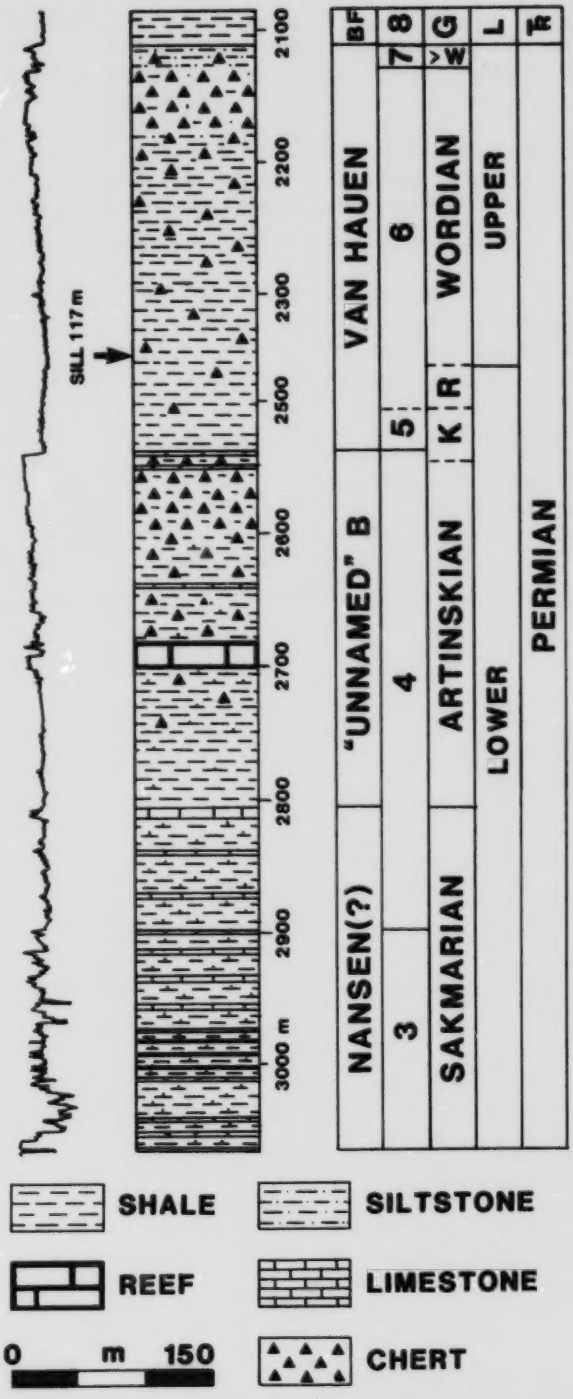

Figure 3. Schematic log of Permian and lowest Triassic sediments in BP Graham C-52, well showing gamma ray signature, lithotypes, formations, sequences (3 to 8), and assumed ages. K, Kungurian; R, Roadian; >W, post-Wordian(?); G, Griesbachian.

(Fasciellids); and accessory phyloid algae, *Palaeoaplysina*, dasycladacean algae, ostracods, gastropods and debris of colonial corals. Depositional fabrics include dominant lime wackestone and packstone, and accessory grainstone. Variably dolomitic facies occur at the base of the succession. The micrite of some of the limestones displays fenestral fabrics and spongiostromid weaves which, in the outcrop belt, are commonly associated with carbonate buildups that characterize the upper Nansen Formation (Beauchamp et al., 1988; Beauchamp, 1988a).

The gamma ray signature of the Nansen(?) Formation, with pronounced variations over short vertical distance, reflects its intraformational cyclicity (Fig. 3). In the field, this cyclicity is expressed as an alternation of recessive and resistant units imparting a banded appearance to the formation. Each recessive-resistant couplet corresponds to a shallowing-upward package, the content of which varies laterally across the depositional axis of the basin. Beauchamp (1987) identified six different types of shelf cycles in the Canyon Fiord-Belcher Channel-Nansen succession. Three cycle types (types 1 to 3) have been interpreted as representing inner shelf sedimentation, and the other three (types 4 to 6) as representing outer shelf sedimentation.

Carbonate facies displayed in the Nansen(?) Formation at Graham C-52 are characteristic of the outer shelf type 4 cycle, which represents deposition of carbonate buildups of various kinds and shapes (Beauchamp, 1987). It is thus likely that the BP Graham C-52 location was close to the shelf edge in Early Permian time. If similar to surface exposures, it is also likely that much larger buildups, such as those exposed on the west side of Blind Fiord (Beauchamp et al., 1989), occur in the vicinity of the well. At Blind Fiord, there is also a single occurrence of a *Tubiphytes*-bryozoan patch reef (Beauchamp, 1988a), the facies of which are remarkably similar to those of the Nansen(?) carbonates in the BP Graham C-52 well.

At BP Graham C-52, the Nansen(?) Formation is Early Permian in age. Conodonts recovered from the 3062 to 3068 m (10 045-10 065 ft.) core yielded a number of species belonging to the upper Sakmarian *Streptognathodus elongatus* zone, or zone P5, of Henderson (in Beauchamp et al., 1989a). The fusulinaceans *Schwagerina whartoni* and *Schubertella* sp. were also identified from the same core (Nassichuk and Wilde, 1977). According to these authors, *S. whartoni* is characteristic of the upper Asselian.

"Unnamed" B formation

From 2825 to 2557 m (9270 to 8390 ft.) the succession consists of a 268 m (880 ft.) thick interval of dark-coloured, siliceous shale that passes upward into relatively pure chert, with minor limestone interbeds (Fig. 3). This succession is assigned to the "unnamed" B formation, an informal stratigraphic unit of the Sverdrup Basin (Beauchamp et al., 1989b) soon to be named (Beauchamp and Henderson, work in progress). The "unnamed" B formation is the deep-water, slope to basinal equivalent of the "unnamed" A formation, a unit of temperate shelf carbonates well exposed along the southern margin of the Sverdrup Basin (Beauchamp et al., 1988b; Beauchamp, 1988b).

The lower part of the "unnamed" B formation comprises variably silty and calcareous shale containing rare fossil debris, mostly bryozoan and sponge spicules. The upper part of the "unnamed" B formation is composed of variably impure, dark coloured, in part organic-rich, spiculitic chert (Fig. 5A), with rare to common silicified debris of echinoderms, bryozoans and brachiopods. Tongues of silicified limestone, with abundant bryozoans, echinoderms and brachiopods, also occur in the upper part of that succession.

The "unnamed" B formation is interpreted as a broad, shallowing-upward package, indicated by both the vertical facies succession and the gamma ray signature (Fig. 3). This gradual trend is interrupted between 2737 and 2697 m (8980-8850 ft.) by stacked carbonate buildups, the presence of which is indicated by marked shifts in the gamma ray signature. These buildups, perhaps three or four of them, comprise bryozoan wackestone, packstone and boundstone, with common echinoderms and ostracods, and accessory brachiopods, encrusting foraminifers and sponge spicules (Fig. 5B-C). The limestone fabrics display variably large fenestrae and cavities, filled by several generations of isopachous radiaxial calcite cement. The micrite matrix is also characterized by a spongiostromid weave, a common feature in most Permian buildups in the Canadian Arctic.

Lower Permian buildups, comprising the same association of fenestellid bryozoans and large, open cavities, have recently been documented from the "unnamed" A formation elsewhere in the Sverdrup Basin (Beauchamp, 1988b). In the Blind Fiord area of southwestern Ellesmere Island, such buildups are shaped like mounds and are as thick as 135 m. Similar buildups also occur at Great Bear Cape, on Bjorne Peninsula, where stacked tabular bodies, not exceeding 5 m in thickness were found in the middle part of the "unnamed" A formation. Based on petrographic evidence, Beauchamp (1988b) has interpreted the open cavities that characterize these buildups as the remnants of calcareous sponges.

The age of the "unnamed" B formation is, at BP Graham C-52, assumed to range from Artinskian to lowest Kungurian, based on: 1) the presence of proven Sakmarian strata below; 2) its correlation with the "unnamed" A formation; and 3) the proven age of the formation elsewhere in the outcrop belt. Unfortunately, no biostratigraphically relevant microfossils were identified from that interval in the studied well.

Van Hauen Formation

The Van Hauen Formation occurs from 2557 to 2127 m (8390-6980 ft.) (Fig.3). It is 312 m (1025 ft.) thick and comprises a variably silty, siliceous and micaceous, dark-coloured shale at the base (Fig. 6A) passing upward into an increasingly siliceous spiculitic shale, then into a relatively pure, light-coloured spiculitic chert (Fig. 6B). Except for some bryozoan and echinoderm debris, microfacies of the Van Hauen Formation are dominated by abundant sponge

Figure 4. Microfacies of the Nansen(?) Formation in BP Graham C-52 well. **A.** Bryozoan (BY) silty wackestone with minor sponge spicules (SP); 2825 to 2850 m (9270-9350 ft.). **B.** Bryozoan (BY) grainstone cemented by radiaxial calcite (arrows); 2825 to 2850 m (9270-9350 ft.). **C.** Tubiphytes (TU), echinoderms (EC), bryozoan (BY) and encrusting foraminiferal (EF) silty packstone; 3030 m (9940 ft.). Scale bar is 1000 microns.

Figure 5. Microfacies of the "unnamed" B formation in BP Graham C-52 well. **A.** Slightly dolomitic spiculitic (SP) chert; 2569 m (8430 ft.). **B.** Bryozoan (BY) wackestone with accessory sponge spicules (SP) and cemented fenestrae (FE); 2710 m (8890 ft.). **C.** Bryozoan (BY), echinoderm (EC) silty packstone; 2710 m (8890 ft.). Scale bars are 400 microns (A) and 1000 microns (B-C).

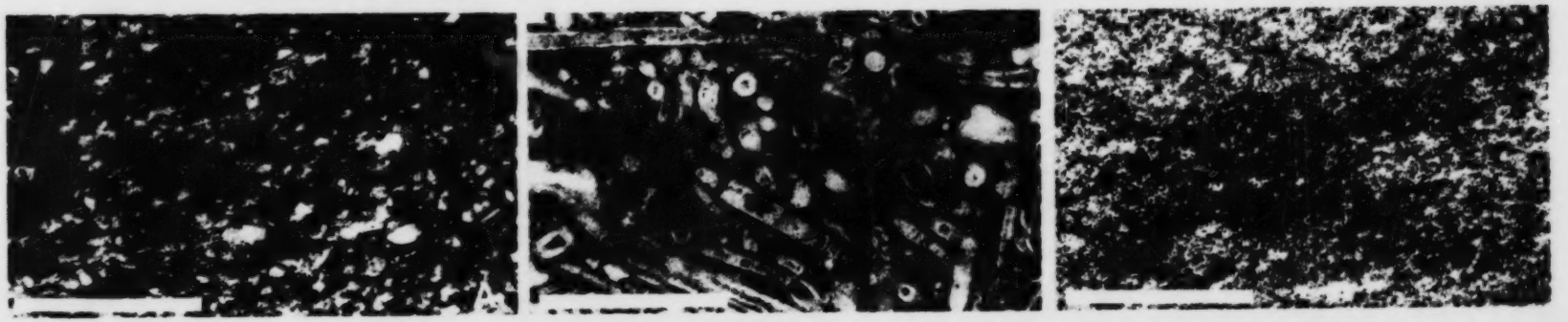

Figure 6. Microfacies of the Van Hauen and Blind Fiord formations in BP Graham C-52 well. **A.** Siliceous silty shale with organic matter stringers; lower Van Hauen Formation; 2222 m (7290 ft.). **B.** Slightly glauconitic spiculitic (SP) chert; upper Van Hauen Formation; 2149 m (7050 ft.). **C.** Micaceous shale; lower Blind Fiord Formation; 2118 m (6950 ft.). Scale bar is 400 microns.

spicules. Glauconite is locally abundant, especially in the upper part of the formation, where the chert becomes purer and lighter coloured.

The vertical succession displayed by the Van Hauen Formation is broadly shallowing-upward, a trend reflected in the smooth, slowly changing gamma ray response (Fig. 3). Both the Van Hauen and underlying "unnamed" B formations display similar sequences of facies, reflecting both an identical environmental setting (deep basin to slope) and a similar shallowing-upward package. The "unnamed" B-Van Hauen contact is, nevertheless, very sharp: deep-water shales of the latter rest in contact with shallower-water cherts of the former. This sharp lithological boundary is expressed as an equally sharp excursion on the gamma ray log (Fig. 3).

A similar lithological change marks the boundary between the Permian Van Hauen Formation and the Triassic Blind Fiord Formation (Fig. 3). The Blind Fiord Formation comprises soft, greenish, micaceous shales (Fig. 6C) that contrast with the black, silty and siliceous shales of the uppermost Van Hauen Formation. This latter facies, which characterizes the uppermost 21 m (70 ft.) of the formation, contrasts rather sharply with the light-coloured spiculitic chert found immediately below. As discussed below, this lithological change in the upper Van Hauen Formation can be associated with the deposition of another, pre-Triassic, sequence.

The age of the Van Hauen Formation at BP Graham C-52 is not substantiated by any biostratigraphic evidence. Based strictly on comparisons with the outcrop belt, it is assumed that the formation ranges from early Kungurian to at least Wordian, and possibly younger Late Permian (post-Wordian).

Sequences

Five (Sequences 3 to 7) of the seven upper Paleozoic transgressive-regressive sequences of Beauchamp et al. (1989b) are recognized in the BP Graham C-52 well (Fig. 2, 3). Sequence 3 (part) occurs in the Nansen(?) Formation, Sequence 4 encompasses the upper Nansen(?) and "unnamed" B formations, and Sequences 5, 6 and 7 occur within the Van Hauen Formation. The Sequence 3-Sequence 4 boundary is believed to occur at 2917 m (9570 ft.) within the Nansen(?) Formation, corresponding to the point where intraformational cycles become much thicker. This increase in cycle thickness probably corresponds to an increase in accommodation and reflects the onset of transgressive conditions. In the field, the Nansen to "unnamed" transition is always characterized by such thicker, deeper-water cycles (Beauchamp, 1987). Sequence 4 is transgressive up to about 2804 m (9200 ft.) in the "unnamed" B formation, above which it is broadly regressive and shallowing-upward, as discussed above.

The Sequence 4-Sequence 5 boundary closely corresponds to the "unnamed" B-Van Hauen contact. Sequence 5 cannot be readily identified in the BP Graham C-52 well, which may be a result of its condensed nature in that part of the basin. Elsewhere in the Sverdrup Basin, Sequence 5 appears to be associated with local, yet important, strike-slip tectonic motions that have been collectively termed the Melvillian Disturbance. As pointed out by Beauchamp et al. (1989a), the Melvillian Disturbance probably created local uplifts and local collapses of sub-basins at the margin of the Sverdrup Basin, resulting in the formation of small, deltaic complexes. These deltas shed significant amounts of clastic sediments (Sabine Bay Formation) in the basin over a relatively short period of time. In some areas of the Sverdrup Basin (e.g., Raanes Peninula), however, there is very little evidence of Melvillian deformation, and no apparent Sequence 5 sedimentation, reflecting non-deposition in areas of tectonic quiescence. The BP Graham C-52 well appears to be located in one of these areas.

Sequence 6 is thus represented by the bulk of the Van Hauen Formation, which displays a small amount of transgressive sediment overlain by a very thick, broadly regressive succession. The upper 21 m of the Van Hauen are, however, lithologically different from the immediately underlying chert, and likely represent the post-Wordian(?) Sequence 7. As indicated by Beauchamp et al. (1989b), Sequence 7 comprises a condensed succession of undated spiculitic chert and siliceous shale lying between dated Wordian (early Late Permian) sediments and dated Griesbachian (Triassic) sediments. These authors raised the possibility that parts, if not all, of the last three Permian stages (Capitanian, Dzhulfian and Changhsingian) might be represented by sediments of Sequence 7. At BP Graham C-52, the siliceous facies of Sequence 7 are overlain by the non-siliceous shale of the Triassic Blind Fiord Formation, the base of which is marked by a sharp kick in the gamma ray signature.

CONCLUSIONS

Three Permian formations are recognized in the BP Graham C-52 well; in ascending order: the Nansen (or Belcher Channel), the "unnamed" B, and the Van Hauen. The assumed ages of these formations range from Sakmarian (Early Permian) to post-Wordian(?) (Late Permian). The Nansen(?) Formation displays a cyclic succession of carbonates that were deposited in an outer shelf setting. Both the "unnamed B" and Van Hauen formations are characterized by dark, siliceous shale and spiculitic chert, which accumulated in a deep water, basinal to slope setting.

This study demonstrates that the upper Paleozoic stratigraphic framework of the Sverdrup Basin, which is based on the analysis of surface strata, can be readily applied to the surbsurface succession as well.

ACKNOWLEDGMENTS

Many thanks to C.M. Henderson for his conodont expertise and to U. Mayr for reviewing the manuscript.

REFERENCES

Beauchamp, B.

1987: Stratigraphy and facies analysis of the Upper Carboniferous to Lower Permian Canyon Fiord, Belcher Channel and Nansen formations, southwestern Ellesmere Island; Ph.D. thesis, University of Calgary, June 1987, 370 p.

1988a: Lower Permian (Sakmarian) Tubiphytes-bryozoan buildup, southwestern Ellesmere Island, Canadian Arctic Archipelago; *in* Reefs

of Canada and Adjacent Areas, H.J. Geldsetzer and D.J. Glass (ed.); Canadian Society of Petroleum Geologists, Memoir 13, p. 585-589.

1988b: Lower Permian (Artinskian) sponge-bryozoan buildups, southwestern Ellesmere Island, Canadian Arctic Archipelago; *in* Reefs of Canada and Adjacent Areas, H.J. Geldsetzer and D.J. Glass (ed.); Canadian Society of Petroleum Geologists, Memoir 13, p. 575-584.

Beauchamp, B., Davies, G.R., and Nassichuk, W.W.

1988: Upper Carboniferous to Lower Permian Palaeoaplysina-phylloid algal buildups, Canadian Arctic Archipelago; *in* Reefs of Canada and Adjacent Areas, H.J. Geldsetzer and D.J. Glass (ed.); Canadian Society of Petroleum Geologists, Memoir 13, p. 590-599.

Beauchamp, B., Harrison, J.C., and Henderson, C.M.

1989a: Upper Paleozoic stratigraphy and basin analysis of the Sverdrup Basin, Canadian Arctic Archipelago: Part 1, time frame and tectonic evolution; *in* Current Research, Part G, Geological Survey of Canada, Paper 89-1G, p. 105-113, 1989.

1989b: Upper Paleozoic stratigraphy and basin analysis of the Sverdrup Basin, Canadian Arctic Archipelago: Part 2, transgressive-regressive sequences; *in* Current Research, Part G, Geological Survey of Canada, Paper 89-1G, p. 115-124, 1989.

Beauchamp, B., Oldershaw, A.E., and Krouse, H.R.

1987: Upper Carboniferous to Lower Permian 13C-enriched primary carbonates in the Sverdrup Basin, Canadian Arctic: comparisons to coeval western North American ocean margins; *in* Isotopes in the Sedimentary Cycle, N. Clauer and S. Chaudhuri (ed.); Chemical Geology (Isotope Geoscience Section), v. 65, p. 391-413.

Henderson, C.M.

1989: Conodont paleontology and biostratigraphy of the Upper Carboniferous to Lower Permian Canyon Fiord, Belcher Channel, Nansen, an unnamed, and Van Hauen formations, Canadian Arctic Archipelago; Ph.D. thesis, University of Calgary, 287 p.

Nassichuk, W.W. and Wilde, G.L.

1977: Permian Fusulinaceans and stratigraphy at Blind Fiord, southwestern Ellesmere Island; Geological Survey of Canada, Bulletin 268.

Thorsteinsson, R.

1974: Carboniferous and Permian stratigraphy of Axel Heiberg Island and western Ellesmere Island, Canadian Arctic Archipelago; Geological Survey of Canada, Bulletin 224.

The life cycle and phyletic affinity of *Gloeocapsomorpha prisca* Zalessky 1917 from Ordovician rocks in the Canadian Williston Basin

L.D. Stasiuk[1] and K.G. Osadetz
Institute of Sedimentary and Petroleum Geology, Calgary

Stasiuk, L.D. and Osadetz, K.G., The life cycle and phyletic affinity of ***Gloeocapsomorpha prisca*** *Zalessky 1917 from Ordovician rocks in the Canadian Williston Basin; in Current Research, Part D, Geological Survey of Canada, Paper 89-1D, p. 123-137, 1990.*

Abstract

The problematic form ***Gloeocapsomorpha prisca*** *Zalessky 1917 dominates Middle and Upper Ordovician petroleum source rocks in Williston Basin and elsewhere.* ***G. prisca*** *occurs in two commonly interlayered, petrographic microfacies that are inferred to be genetically related. Cup-like agglomerations of isolated* ***G. prisca*** *alginite disseminated in a mineral matrix occur in all three facies belts characteristic of cratonic lower Paleozoic depositional systems. The layered microfacies is restricted to deeper subtidal regions of the inner detrital and middle carbonate facies belts and shallower regions of the outer detrital facies belt. The disseminated microfacies is interpreted as representing an initial, non-motile growth stage, with a unicellular form of coccoid organization. A transitional palmella stage, represented in both microfacies, is succeeded by the layered microfacies, a subtidal "stromatolite-like" mat-forming stage. Deep subtidal depositional environments and lack of calcification sharply distinguish* ***G. prisca*** *from intertidal stromatolites both extant and ancient.*

Résumé

La forme problématique ***Gloeocapsomorpha prisca*** *Zalessky 1917 prédomine dans les roches pétrolifères de l'Ordovicien moyen et supérieur du bassin de Williston et d'ailleurs.* ***G. prisca*** *se retrouve dans deux microfaciès pétrographiques généralement interstratifiés qui sont, conclut-on génétiquement liés. Des agglomérations en forme de cuvette d'alginite isolée de* ***G. prisca****, disséminées dans une matrice minérale, se manifestent dans les trois zones de faciès caractéristiques des systèmes de sédimentation cratoniques du Paléozoïque inférieur. Le microfaciès stratifié se limite aux régions infratidales profondes des zones de faciès détritique interne et de roches carbonatées intermédiaires et aux régions moins profondes de la zone de faciès détritique externe. Le microfaciès disséminé est considéré comme un stade de croissance initial non mobile à organisation coccoïde de forme unicellulaire. Un stade palmella de transition, représenté dans les deux microfaciès, est suivi d'un microfaciès stratifié, stade infratidal de formation de tapis de forme stromatolitique.* ***G. prisca*** *se distingue nettement des stromatolites intertidaux, actuels et anciens, par un milieu de sédimentation infratidal profond et une absence de calcification.*

[1] Energy Research Unit and Department of Geology, University of Regina, Regina, Saskatchewan S4S 0A2

INTRODUCTION

Middle and Upper Ordovician petroleum reservoirs in the Mid-Continent and Williston Basin contain oils of distinctive composition (Brooks et al., 1987; Longman and Palmer, 1987; Lenheer and Zumberge, 1987) that are attributed to organic-rich shales and carbonates of similar age (Osadetz et al., 1989; Jacobson et al., 1988; Longman and Palmer, 1987; Kendall, 1976). Oils and source rocks of similar composition (Fowler, in press; Hoffmann et al., 1987; Foster et al., 1986; Fowler et al., 1986; Fowler and Douglas, 1984) occur globally in coeval strata that were deposited in equatorial and subequatorial epicontinental seas (Foster et al., 1986). Numerous studies have related these oils to kukersites (Zalessky, 1917) or kerogenites (Kendall, 1976). These are bituminous "oil shales" (in fact, carbonate mudstones) dominantly composed of *Gloeocapsomorpha prisca* Zalessky 1917 alginite (see Jacobson et al., 1988). This alginite is generally accepted as the dominant source component for Middle and Upper Ordovician oils, although Jacobson et al. (1988) have shown that extractable bitumen composition varies as a function of the organic microfacies and that other organic components, particularly amorphous kerogen, can also be effective source rocks.

PREVIOUS STUDIES

Understanding the depositional environment and accumulation controls for these rich petroleum source rocks is important to oil and gas prospectivity.

Sedimentological, geochemical and petrological techniques have been employed to gain insight into the controls on their accumulation. Recently, controversy has surrounded the life habits of kerogen precursor organisms. Reed et al. (1986) suggested the alga was a non-photosynthetic, prokaryotic, benthic, mat-forming organism; whereas Hoffmann et al. (1987) concluded that the alga was phototrophic, planktonic and possibly eucaryotic. Foster et al. (1989, 1988) have recently suggested that a modern analogue for G. prisca may be *Entophysalis major*; a mat-forming and sometimes stromatolite-forming cyanobacterium.

Several short, commonly cursory, discussions of the petrographic details of Ordovician kerogen assemblages have been published by Combaz and Peniquel (1972), Foster et al. (1986), Jacobson et al. (1988), Foster et al. (1988) and Osadetz et al. (1989). The general emphasis of these studies was to identify *G. prisca* as a component in the source rock kerogen. Jacobson et al. (1988) petrographically examined core samples from three wells in Iowa and distinguished two petrographic assemblages, which they associated with compositional variations in bitumen extracts. Their assemblage A consisted of identifiable *G. prisca* "colonies" that they interpreted as having mechanically accumulated to impart a lamination to the rock. Their assemblage B consisted predominantly of amorphous organic material and lesser organic-walled microfossils, but did not include identifiable *G. prisca*. The detailed petrography of *G. prisca* remains undescribed and unrelated to sedimentologically defined depositional environments, and the life cycle and growth habits of *G. prisca* remain enigmatic.

OBJECTIVES OF THIS STUDY

This study describes spectacularly preserved Ordovician kukersites and other *G. prisca*-bearing lithotypes from southern Saskatchewan. Samples were collected from more than twenty-five well cores in Saskatchewan (Fig. 1). The samples represent a wide range of thermal maturities (Fowler, in press; Osadetz et al.,1989; Stasiuk and Osadetz, work in progress).

Detailed petrographic descriptions are emphasized, and from these the life cycle and growth habit of *G. prisca* is inferred. Specific investigations included the description of both "maceral" component morphology and the depositional, microtextural relationships between organic and inorganic constituents, because petrographic textures can provide valuable information about depositional mechanisms and environments. This paper is the initial report of a developing depositional model for Ordovician petroleum source rocks based on the integration of kerogen composition and microtextural analysis with sedimentological and stratigraphic studies.

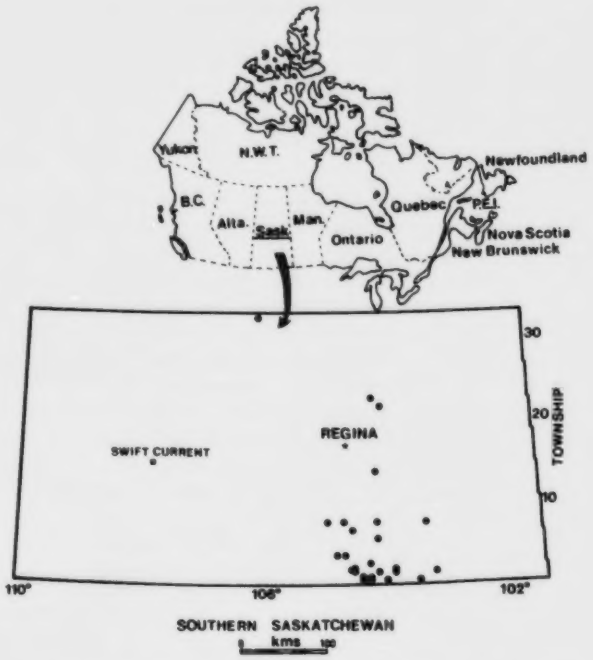

Figure 1. Location map of boreholes in Saskatchewan from which core samples of Upper Ordovician potential source rocks were collected.

STRATIGRAPHIC SETTING

Lower Paleozoic magnafacies belts

Middle and Upper Ordovician strata in Williston Basin (Fig. 2) are remnants of larger continental depositional systems (Osadetz and Haidl, in press). Lithostratigraphic units, commonly of formation rank, are composed of restricted lithofacies assemblages assigned to magnafacies belts that, like the Sauk and Tippecanoe sequences of the Mid-Continent epeiric seaway (Witzke, 1980; Ross, 1976; Ostrom, 1964) and the Paleozoic western cratonic miogeocline (Aitken, 1978, 1966), indicate persistent, broadly similar depositional environments and tectonic settings. The three magnafacies belts include the inner detrital, middle carbonate, and outer detrital belts, which generally indicate progressive distance from the exposed craton.

WILLISTON BASIN SUCCESSION

Each magnafacies belt can be further subdivided into lithofacies assemblages, each representing a distinctive depositional environment. The inner detrital magnafacies belt is commonly subdivided using persistent shoreface (coarse clastic) and shelf (fine clastic) depositional environments (e.g., Vigrass, 1971). The Winnipeg Group (Middle Ordovician) in Williston Basin formed part of the inner detrital magnafacies belt of eastern North America (Fig. 2; Witzke, 1980). It has been subdivided into three parasequence sets, defined by onlap of the fine clastic dominated "shelf water depth" lithofacies onto sandstone dominated "shoreface" and "non-marine" facies (Lefever et al., 1987; Vigrass, 1971).

The Winnipeg Group is succeeded by Yeoman Formation carbonates (Upper Ordovician) of the middle carbonate magnafacies belt. A detailed study of the Big Horn Group (Upper Ordovician) resulted in the recognition of three dominant lithofacies in the Yeoman Formation (Fig. 2; Kendall, 1976). These three included bituminous lime mudstone lithofacies, (kukersites), bioturbated mudstone lithofacies, and pelletal grainstone lithofacies. These represent progressively shallower depositional environments (Fig. 3) and their distribution can be used to map persistent paleogeographic elements within the upper Yeoman Formation (Fig. 4; see also Kendall, 1976, Fig. 24).

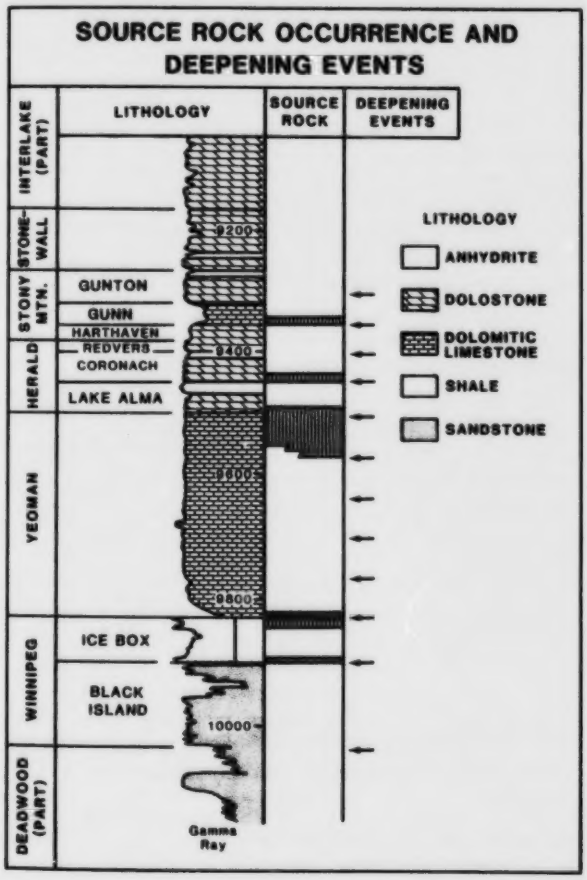

Figure 2. Stratigraphy of lowermost Paleozoic in Saskatchewan; note the stratigraphic position of the Yeoman Formation, which hosts the Gloeocapsomorpha prisca-rich organic microfacies. (From Osadetz et al.,1989.)

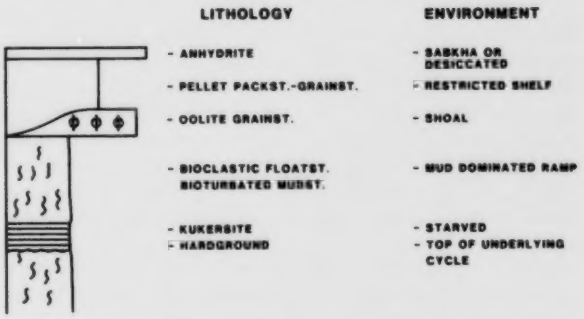

Figure 3. Idealized shallowing-upward parasequence set for the upper Yeoman Formation.

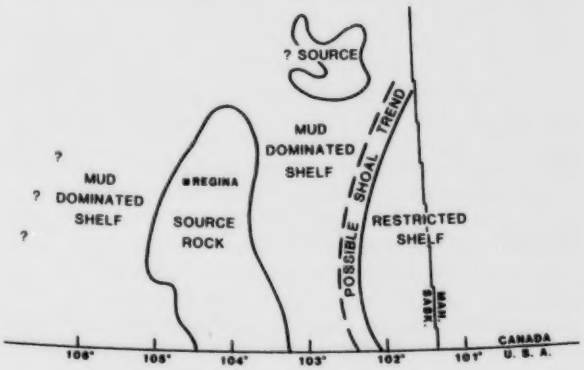

Figure 4. Paleogeographic map of depositional environments in the Upper Yeoman middle carbonate magnafacies belt of southeastern Saskatchewan.

The interpreted late Yeoman paleogeography (Fig. 4) suggests the presence of a north-south trending restricted shelf, probably restricted by oolite shoals (Kendall, 1976), that passes westward into a westward deepening, muddy, carbonate ramp characterized by intensive bioturbation. The deepest portions of this ramp form a trough, the axis of which coincides with the 104th meridian. In this trough, bituminous lime mudstones and kukersites accumulated free of bioturbation below the paleopycnocline. The western margin of the central trough is mapped, but the mirror-image western restricted shelf remains unmapped.

During deposition of the overlying Herald Formation (Upper Ordovician) the central trough of the Yeoman platform was infilled by expansion of the bioturbated mudstone ramp and by sulphate evaporites precipitated by episodic desiccation of the middle carbonate belt (Fig. 2; Kendall, 1976). With deposition of the lower Stony Mountain Formation (Upper Ordovician) (Fig. 2), during the zenith of Tippecanoe onlap, outer detrital belt lithofacies onlapped southeastern parts of Saskatchewan (Osadetz and Haidl, in press).

PETROLEUM SOURCE ROCKS

Osadetz et al. (1989) described the occurrence and pyrolysis characteristics of Ordovician petroleum source rocks in Saskatchewan (Fig. 2, 4). Rich potential petroleum source rocks containing *G. prisca* occur in the Winnipeg Group (Osadetz et al., 1989), particularly at the maximum flooding surface of onlapping parasequence sets defined by Vigrass (1971). Other, generally lean, potential petroleum source rocks occur in black shales and iron-rich (siderite) oolitic greywackes that accumulated in the shelf facies belt. Kukersites that accumulated in the central trough of the Yeoman platform are rich, effective petroleum source rocks dominated by *G. prisca* as elaborated upon below (Fig. 4). In the Herald Formation, rare, thin kukersites accumulated in the same region as those in the Yeoman Formation, commonly interbedded with subtidal, bioturbated lime mudstones. In the Stony Mountain Formation, argillaceous bioclastic floatstones deposited in deeper, subtidal water depths include rare kukersite beds and laminae. Kukersites commonly overlie submarine hardgrounds.

G. prisca is a common, disseminated palynological element in Big Horn Group carbonates (McGregor et al., 1971) and coeval equatorial and subequatorial rocks (Cramer and Diez de Cramer, 1972), but only kukersites and bituminous starved shelf deposits have significant petroleum potential. Present distribution of kukersites in the Big Horn Group reflects control by depositional environments that prevented bioturbation. The contact between bioturbated lime mudstones and kukersites is commonly gradational. Where kukersites are penetrated by burrows, their petroleum potential is completely degraded and the alginite has been consumed (13-23-1-17W2, 10094.5 ft.; Kendall, 1976, p. 108). The accumulation of kukersites in deeper water on the subtidal platform, and the preservation of their organic material, indicate anoxic bottom water conditions hostile to infaunal burrowers. Bottom water anoxia is inferred to have been controlled by high rates of evaporation across the equatorial epeiric sea, resulting in a persistently stratified water column that ponded anoxic saline brines.

This depositional model will be elaborated upon in other work (Osadetz et al., work in progress), yet it is important to emphasize the deeper subtidal depositional environment of kukersites in Williston Basin. This setting must be clearly distinguished from shallower intertidal depositional environments. Although the most extensive kukersites were deposited in a deep subtidal trough on the Yeoman platform (Fig. 4), kukersites also occur in the Herald Formation and the Stony Mountain Formation (Osadetz et al., 1989). Where kukersites occur in the Herald Formation, they too were deposited in deeper subtidal depositional environments (see Kendall, 1976, Plate XXIIIB, p. 162, 3) in regions geographically coincident with the trough mapped in the Yeoman carbonate platform (Fig. 4; Osadetz et al., 1989). Kukersite depositional environments are identical to those interpreted for similar lithologies in strata correlative with the Yeoman Formation in North Dakota and Montana (Kohm and Louden, 1978).

Intertidal depositional environments have been inferred for stromatolitic horizons occurring in parts of the Herald Formation and equivalent strata (Derby and Kilpatrick, 1985; Dombrowski, 1988). The organic petrography of an intertidal stromatolite reveals only amorphous organic material (Foster et al., 1989). The studied core is stained with an oil characteristic of the Ordovician oil source system yet it could be allochthonous, since kukersites occur in the Yeoman Formation in the Cedar Creek Anticline. There is as yet no evidence to support the inference that these intertidal stromatolites are composed of *G. prisca* or that intertidal stromatolites contribute to understanding the phyletic or paleoecological affiliation of *G. prisca*. Neither do the presence of intertidal stromatolites composed of amorphous organic material support an analogy between *G. prisca* and modern stromatolite-forming organisms like *Entophysalis major*, as suggested by Foster et al. (1989). Our conclusions regarding the phyletic affinities of *G. prisca* are similar to those of Foster et al. (1989), but differ significantly in the interpretation of depositional environments.

Oils (see Brooks et al., 1987, Fig. 5) and some solvent extracts from kukersitic source rocks exhibit a predominance of C_{34} pentacyclic terpanes (m/z 191 fragmentograms from gas chromatography-mass spectrometry). The significance of this composition is not clear although it appears to be associated with source rocks from anoxic depositional environments. Evaporation across the equatorial, Ordovician, epeiric carbonate platform and saline brine concentration in troughs provides a suitable model for bottom water anoxia. Despite our inference of their association with highly saline waters and their stratigraphic association with desiccative evaporites, kukersites were definitely deposited in deeper, subtidal portions of the shelf. This conclusion is supported by both sedimentological features and paleogeographic reconstructions (Fig. 3, 4).

ORGANIC PETROGRAPHY OF *GLOEOCAPSOMORPHA PRISCA*

Experimental

Samples were prepared for microscopic examination using procedures similar to those commonly used in coal petrography as described by Mackowsky (1982). Core samples

ground to a 3.0 mm diameter using mortar and pestle were placed in 2.5 cm diameter teflon moulds that were subsequently filled with a mixture of epoxy and hardener and set to cure. Hardened pellets were ground and polished according to the method described in Stasiuk (1988). Several samples were also cut into centimetre-size rectangular blocks and prepared as slabs for microscopic examination.

Pellets and slabs were examined using a Zeiss MPM II, incident light microscope equipped with both white (halogen 12v, 100w) and fluorescent (HBO, 100) light sources. Epiplan-neofluor, oil- immersion objectives (x40, N.A. 0.90: x16, N.A. 0.25) were used in conjunction with optical immersion oils of refractive indices 1.518 and 1.478 at 24 degrees C. Photomicrographs were taken using a Zeiss MC63 photographic system attached to a Leica M35 camera.

Organic petrology involves the microscopic examination of organic matter or kerogen assemblages in fine grained, sedimentary rocks such as shales, marls or carbonates, originally deposited under highly reducing/anoxic conditions. To ensure realistic and thus genetic understanding of the individual organic components or "macerals" that make up the kerogen assemblage, examination of a polished, whole rock sample is essential. Identifying and characterizing microscopic morphology in "macerals" is critical, since it is the cellular floral and/or faunal microscopic organization that enables correlation with similar modern organisms. These observations result in the description of larger scale textural relationships both within the kerogen and between the kerogen and mineral matrix. These textures can provide valuable information about the life mode, ecology and taphonomy of precursor organisms while contributing to the description of depositional environments controlling source rock accumulation.

The kerogen classification used by an organic petrologist depends upon the geological age of the strata being studied. The authors have found "maceral concept" classifications most suitable for sedimentary sequences younger than Middle Devonian. In older kerogen assemblages, a far less complicated system is required because of the lower biological diversity characterizing older rocks. The kerogen classification outlined in Table 1 satisfactorily describes microscopic, morphological characteristics of Ordovician kukersites. Alginite with readily discernible cellular morphology has been broadly classified as telalginite by Cook et al. (1981). The basis for identification of *G. prisca* is an alginite morphology characterized by agglomerations of cup-like structures (approximately 10 μm). Optimal observation is achieved using an ultraviolet light source to irradiate the alginite.

Table 1. Kerogen classification used in petrographic analysis of Ordovician potential hydrocarbon source rocks from Saskatchewan, Canada

Maceral group	Maceral
Alginite	*G. prisca* *Nostoc* *Acritarchs*
Microspores	
Bituminite	
Bitumen	

RESULTS

General mineral-kerogen relationships

The dominant mineral associated with kerogen-rich intervals is dolomite, typically occurring as individually discernible rhombs (5-80 μm). Cryptocrystalline carbonate tends to dominate in organic-poor lithofacies. Pyrite is almost always present in minor amounts, generally as small framboids (< 10 μm) or as highly disseminated euhedral grains. Fine, micritic laminae between kerogenous layers are referred to below as the dolomitic micrite microfacies. Alginite bodies in the Yeoman Formation can be generally subdivided into two main modes of occurrence or "microfacies". Similarly, two associations exist between kerogen components and mineral matter. The two microfacies discussed below occur as interlayered laminae (Plate 1A). Their depositional relationships are inferred to represent a genetic relationship.

Disseminated microfacies

The *G. prisca* disseminated microfacies is characterized by individual alginite bodies (approximately 5-25 per cent by volume) "floating" in a matrix or network of dolomite rhombs (Plate 1B). Depending on the level of thermal maturation of the host rock, and biochemical and geochemical organic homogenization, cellular structure may or may not be microscopically visible.

Remnant cellular structure in these alginites is dominated by agglomerations of 2 to 4 cups or cells (5 μm to 12 μm in diameter) displaying individual cell thickening and generally enclosed by a thin (< 2 μm) oblong to spherical sheath (Fig. 5b). These cell groupings may contain as many as eight individual cups. Larger cell accumulations (at greatest diameter 30-70 μm) occur rarely. The exact number of cells making up this form of *G. prisca* in the disseminated facies is generally obliterated by advanced sheath-development and homogenization (e.g., 3-14-8-20W2, 2577.1 m; Plate 1D). Organizations of four cells enclosed by a rectangular or square sheath have also been noted as rare components of certain samples (Plate 1C). These distinctive organizations may represent another species.

The disseminated microfacies also has been observed in bituminous shales and iron oolitic greywackes of the Icebox Member/Formation of inner detrital belt affinities (Osadetz et al., 1989). The sheathed agglomerations of cells characteristic of the disseminated microfacies are commonly reported as palynological elements in other middle carbonate and outer detrital belt strata (McGregor, 1971; Cramer and Diez de Cramer, 1972). Disseminated microfacies are probably included in unlaminated portions of assemblage A as described by Jacobson et al. (1988). Measurements in the disseminated facies of oblong to spherically sheathed *G. prisca* bodies consisting of four cells, from two locations at different depths give very different average cell

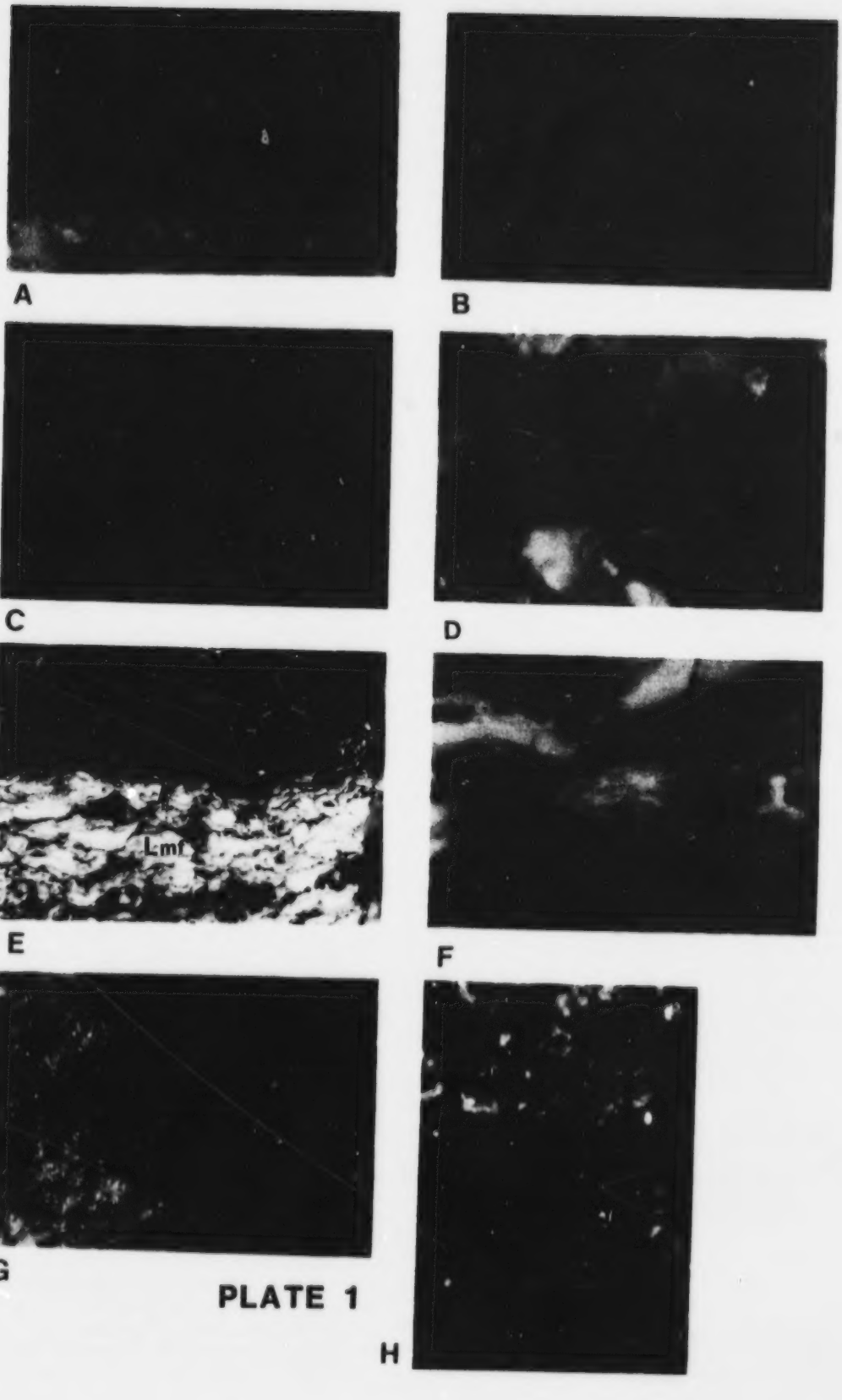

PLATE 1

diameters. The largest average diameter was recorded for the shallowest burial depth and the smallest average diameter from a location with a much greater burial depth (see Table 2). These effects are inferred to be compactional.

Layered microfacies

G. prisca also occurs in the Yeoman Formation as very kerogen-rich laminae (generally <20 per cent by volume mineral matter) where alginite defines the microlamination (Plate 1E). Organic matter in this facies occurs either as lenticularly or linearly shaped alginite bodies displaying faint cell structure (Plate 1F) morphologically similar to *G. prisca* or with identical fluorescence and geometric morphology, but lacking remnant cell structure. Individual alginite bodies touch, creating a stacked, tightly packed network of linear forms (in sections perpendicular to bedding planes) (Plate 1E) that form coalesced networks of rounded to subrounded forms in sections parallel to bedding. The thickness of the layered alginite accumulations ranges from approximately 25 μm to more than 2.0 mm. Repetition of several layered microfacies laminae, up to 2.0 mm thick, are commonly intercalated with dolomite-dominated laminae (up to 0.5 mm thick) containing the disseminated microfacies (e.g., 8-36-2-29w2, 2640.7 m; 16-20-8-10w2, 2445.3 m). Delicate textural features are wholly or partially preserved in this microfacies, particularly at microscopic organic-inorganic boundaries.

The upper portion (approximately 10-50 μm thick) of the layered microfacies may contain filamentous algae (Plate 1G) interwoven with *G. prisca* (e.g., 1-25-23-16w2, 1714.1 m and 8-32-8-16w2, 2458.8 m). Filamentous alginite is tentatively identified as *Nostocales* sp., because of morphological similarities to colonial, filamentous cyanophytes. Filaments vary in length from less than 20 μm to 100μm. They are composed of individual cells approximately 5 μm in diameter. Larger individual cells with thickened cell walls are also present within filaments. These probably represent heterocysts (Plate IG), enlarged cells in filaments that are released as spores during asexual reproductive fission (South and Whittick,1987). Paleozoic *Nostoc* algae have been reported in several studies; for example, from the Cambrian of India (Sastri et al.,1972). Modern Nostocaceae have variable ecological habits ranging from planktonic to benthic. They also form minor components of marine algal mats (e.g., *Nodularia*; Golubic,1976).

Table 2. Average diameter of *Gloeocapsomorpha prisca* cells in the disseminated facies from 2 boreholes with very different present-day burial depths. Measurements were made on alginite bodies consisting of four cells. Both samples from the Yeoman Formation.

Location	Depth (m)	Average cell size (μm)	Range
1-25-23-16W2	1714.8	8.6	7.5-9.5
16-20-8-10W2	2445.3	6.3	6.0-7.0

PLATE 1

All photomicrographs were taken using incident light and oil immersion objectives.

Figure 1A. Micro-interlayering of the two dominant organic microfacies in the Yeoman Formation; (Dmf) Gloeocapsomorpha prisca disseminated microfacies and (Lmf) G. prisca layered microfacies.

Figure 1B. The disseminated G. prisca microfacies illustrating coccoid alginite morphology (Gp) of individual bodies "floating" in a matrix of predominantly dolomite (D). Also note the cell wall thickening and development of an enclosing, thin sheath around cell agglomerations (S). This microfacies is interpreted as representing the initial, non-motile growth stage.

Figure 1C. An example of alginite (Ae) with square to rectangular individual cells; a cellular morphology unlike that of G. prisca. This morphology is very similar to the extant, coccoid cyanophyte Eucapsis.

Figure 1D. Extensive and advanced stage of sheath development and homogenization in the disseminated G. prisca microfacies. This probably represents a colonial growth period in the life cycle and a transitional period to a mat-forming stage.

Figure 1E. Alginite-defined microlaminae in the layered microfacies, (Lmf). The texture preserved at the organic-inorganic interface (arrow) is indicative of simple, flat mat, algal accumulation. The linearity results from the orientation of the section, perpendicular to bedding.

Figure 1F. G.prisca alginite morphology (Gp) faintly visible in high magnification image of flat mat texture in layered microfacies. A portion of field of view from E above.

Figure 1G. Filamentous alginite (arrows) associated with G. prisca algal mat. The morphology of the filamentous alginite is similar to modern Nostocales.

Figure 1H. Algal mat pinnacles (P) located at the interface between dolomite-rich, disseminated microfacies (Dmf) and layered microfacies (Lmf).

A

B

C

D

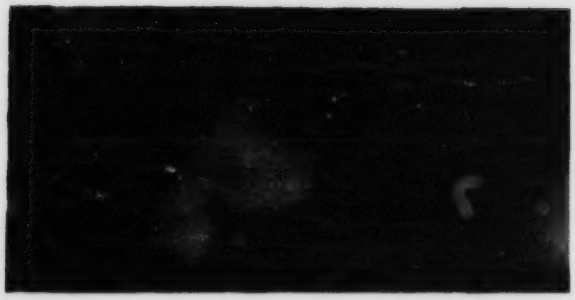

E

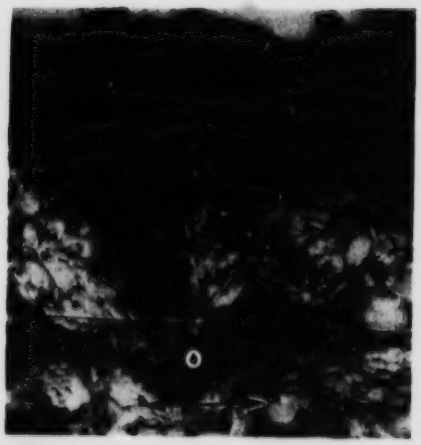

F

G

PLATE 2

Layered microfacies also occur in the Gunn Member of the Stony Mountain Formation kukersites (Osadetz et al., 1989) and are inferred to occur in the fine clastic facies of the Icebox Formation of the Winnipeg Group in the American part of the basin. This inference is based upon the composition of solvent extract chromatograms reported by Williams (1974). These solvent extracts have pronounced odd predominance (C_{15} to C_{19} n-alkanes) and low abundances of n-alkanes of carbon number greater than 19, features characteristic of solvent extracts from kukersites (Jacobson et al., 1988; Reed et al., 1986). The layered microfacies is interpreted to include laminated portions of assemblage A as described by Jacobson et al. (1988).

Microtextures in the layered microfacies

The most commonly preserved texture is simple flat lamination (Plate 1E) forming mats of alginite. Mats occur encrusting submarine hardgrounds. Contortion resulting from alginite bodies conforming to, or "wrapped around" associated dolomitic grains, is also apparent. Disturbed flat laminae have also been noted where ripped-up clasts of the layered microfacies, enclosed by dolomitic micrite, occur inclined to bedding (e.g., borehole 1-14-1-17w2; 3108.4 m). Hypautochthonous transport and oxidation of flat laminated alginite is indicated by drastically reduced fluorescence intensity and significant colour shift toward the red spectral region when compared with the fluorescent properties of undisturbed flat laminated alginite in the same sample.

Pinnacles are preserved in the layered microfacies. They commonly occur at the contact between alginite-rich layered microfacies and dolomitic micrites of the disseminated microfacies (Plate 1H). Maximum pinnacle height is 230 µm (16-20-8-10w2, 2445.25 m; 6-32-8-16w2, 2458.8 m) in mats that attain a maximum thickness of 2.3 mm. Interpinnacle regions are cemented or infilled by dense, cryptocrystalline white carbonate (e.g., 15-9-2-14w2; 3070.9 m) (Plate 2A). Flat laminated alginite textures pass gradationally upward into pinnacle mat texture. Textures are similar to those in stromatolitic microbial mats (Kinsman and Park,1976; Golubic ,1976) (Plate 1H).

Pustular textures or mat pustules also occur at the kerogen-dolomite contact (Plate 2B). The height from the roof of pustules to renewed horizontal alginite laminae ranges from approximately 45 to 240 µm. Alginite-forming pustules are generally not oriented parallel to underlying flat laminae but display some orientation, commonly "pointing" toward the roof of the pustule or apex of the pinnacle (Plate 2C).

Textural features similar to "mat pustules" are observed and bear a striking morphological similarity to "algal heads" presently forming in the intertidal zone on Andros Island, Bahamas (Black,1933). Similar textures in the Yeoman Formation are herein referred to as "algal heads" (Plate 2D). Exceptionally well preserved examples of "algal heads" are present in the Yeoman layered microfacies in boreholes 3-26-4-20w2 (2832.1 m) and 6-32-8-16w2 (2458.8 m). A dense, cryptocrystalline, white carbonate occurs between algal heads as fissure infillings.

A unique, intimate textural association between alginite in the layered microfacies and carbonate grains is shown in Plate 2E. Dolomite grains are "trapped" within alginite mats by an upward "growing", sieve-like network

PLATE 2

All photomicrographs were taken using incident light and oil immersion objectives.

Figure 2A. Inter-pinnacle region (Ip) probably caused by syneresis or gas expulsion during diagenesis and subsequently infilled by a white (viewed in plane polarized light), very dense, cryptocrystalline carbonate (C).

Figure 2B. Algal mat pustules (P) preserved at the interface between the dolomite-rich, disseminated microfacies and the layered microfacies.

Figure 2C. An example of algal mat texture displaying directional orientation (arrows), with long axes of alginite aligned approximately perpendicular to the roof of a pustule, or apex of a pinnacle (Pr).

Figure 2D. Exceptionally well preserved "algal head" (AH) from the Yeoman Formation. This texture compares favourably with algal heads from the intertidal zone, Andros Island, Bahamas (Black,1933).

Figure 2E. Small-scale, domal stromatolite associated with carbonate grains (C) "trapped" within the mesh-like network of alginite.

Figure 2F. Vertically oriented alginite interlayered with horizontally laminated alginite probably resulting from phototaxis, a characteristic of photosynthetic organisms that during daylight produce vertically erect bundles and, during the night, horizontal laminae.

Figure 2G. Degraded upper portion of layered Gloeocapsomorpha prisca microfacies (De). Note the marked decrease in alginite fluorescence intensity and shift in colour toward the red region of the spectrum, relative to fluorescence of underlying undegraded alginite.

(15-9-2-14w2; 3070.9 m). These structures are strikingly similar to accreting, sediment-trapping, small-scale stromatolites.

A rather uncommon texture in the layered microfacies consists of vertically oriented alginite/bituminite resting upon horizontally laminated alginite/bituminite (Plate 2F; 15-9-2-14w2, 3070.9 m). The contact between the perpendicularly oriented habits is sharp. Similar vertical growth tendencies exist in some textures described above, but they are not as pronounced as in this texture. These textures are interpreted as being indicative of phototacticity and resemble algal growth controlled by light, where erect algal bundles grown during the day are interlayered with thinner, horizontal organic laminae developed during the night (Gebelein,1969; Monty,1976). Plate 2F indicates strong similarities to modern, phototactic algal microtextures from Andros Island, Bahamas (c.f. Monty,1976). This texture is strong evidence of photosynthetic activity in *G. prisca*.

Degradation textures

The upper portion (approximately 25-100 μm) of the layered microfacies (Plate 2G), nearest the contact with the micritic dolomite microfacies, is often characterized by changes in optical properties compared with underlying alginite. These changes include: significantly decreased fluorescence intensity, fluorescence colours shifted toward the red region of the spectrum, and increased reflectance (%Ro) not accompanied by disruption in textural fabric. All these changes also occur where textural fabric and orientation are disrupted. They are accompanied by decreased average alginite particle size (e.g., 15- 9-2-14w2, 3075.7 m).

Similar degraded optical features are associated with lenses, inclusions, or shapeless masses of tightly packed, equidimensional, alginite/bituminite in the micritic dolomite microfacies. These degraded areas range in size from 20 x 130 μm to 300 x 150 μm, while the shapeless masses of tightly packed, equidimensional alginite/bituminite are generally <10 μm. Larger *G. prisca* particles exhibiting cellular morphology have been noted as rare inclusions within these organic lenses and masses (e.g., 16-20-8-10w2; 2445.5 m). These obviously degraded, textural features are interpreted as representing physically, biologically and chemically degraded organic matter originally deposited as layered microfacies. Evidence of burrowing infaunal activity (Osadetz et al.,1989) and oxidative processes are now preserved as degraded microtextures.

DISCUSSION

Life cyle hypothesis

Textural and stratigraphic association of the two organic microfacies defined above are inferred to represent two distinctive stages in the life cycle of *Gloeocapsomorpha prisca* (Fig. 5). Such ontological changes are not uncommon. "Many algae exhibit great morphogenetic plasticity in

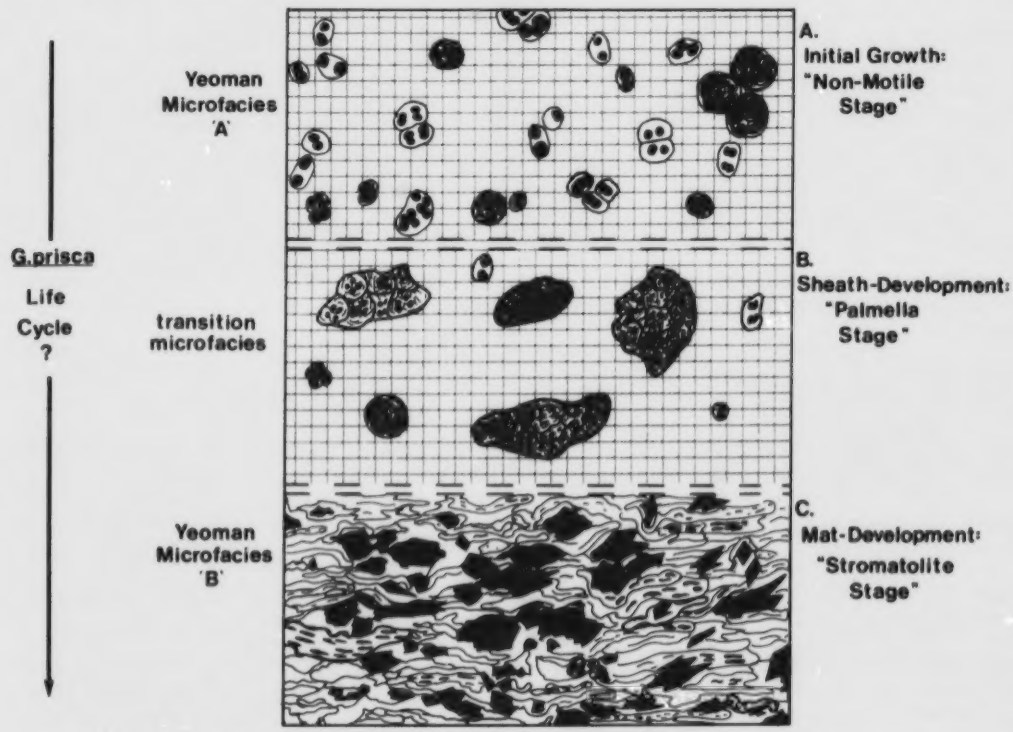

Figure 5. Proposed life cycle scenario for Gloeocapsomorpha prisca alginite in Upper Ordovician, Yeoman Formation, Saskatchewan. See text for explanation of the relationship between preserved alginite microfacies and growth stages of G. prisca.

response to environmental factors and may possess two or more entirely different morphologies at different stages in their life history" (South and Whittick,1987).

Non-motile stage

G. prisca in the disseminated microfacies,(stage A in Fig. 5) displays morphological characteristics of coccoid organization of unicellular alga during a period when motility is restricted or entirely absent (see South and Whittick,1987). Minor amounts of square to rectangular alginite resemble the non-motile growth of an extant cyanophyte *Eucapsis* (Fig. 6). The complete lack of *G. prisca* flagella in the disseminated facies also suggests preservation of a non-motile growth stage.

Agglomerations of two to eight cells with a thin enclosing sheath (Plate 1B and Plate 1C) typify early coccoid algal growth stages (Padmaja,1972) and are restricted to reproductive stages in some algae (South and Whittick,1987). Assuming that flagella would be occasionally preserved if they were present in the non-motile growth stage and noting that delicate flagella are frequently preserved in associated acritarchs, it is inferred that *G. prisca* did not possess flagella. It is inferred that the widespread occurrence of the non-motile life stage in lithofacies representing diverse environments indicates a planktonic, upper water column life mode. A planktonic life mode is compatible with photosynthetic activity, a characteristic also suggested by other evidence discussed below.

Palmelloid sheath development stage

It is inferred that the non-motile stage is followed by transformation from a unicellular, coccoid form to a palmelloid form. This growth stage (Fig. 5) is clearly evident in larger colonial *G. prisca* alginite and occurs in both organic microfacies (Plate 1D, F) (Fig. 5d, f) but predominantly in the disseminated facies. Coccoid unicellular algae can enter a palmella stage, where the algae undergo successive vegetative divisions while embedded in a common gelatinous matrix. Detailed studies of modern coccoid "blue-green algae" by Padmaja (1972) have shown that colonies congregate during this colonial stage of sheath development and are then surrounded and enclosed by a gelatinous, balloon-shaped sheath.

Stromatolite-like mat development stage

Textures in and the stratigraphic setting of the layered microfacies (Plate 2B, E) indicate periods when *G. prisca* formed a component of noncalcareous, stromatolite-like, subtidal benthic mats (Table 5) (Till, 1978; Playford and Cockbain, 1976; Logan et al., 1970, 1974) that are preferentially preserved in the deepest portions of the subtidal platform. The presence of filamentous algae (Plate 1G) at the mineral/stromatolite interface, indicates that at least two species of algae were responsible for the construction of stromatolite-like structures in the Yeoman Formation. It is inferred that such mats formed throughout the the subtidal, mud-dominated platform but were generally reworked by infaunal burrowers. Mats are preserved only in deeper portions of the platform, below the pycnocline, where persistent bottom water anoxia suppressed infaunal activity.

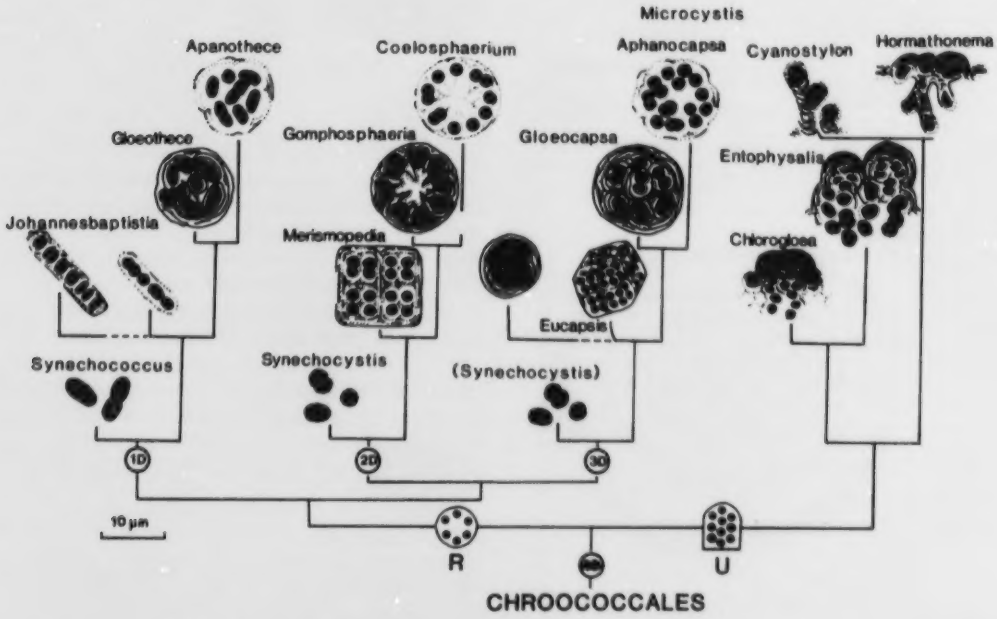

Figure 6. Morphology of modern Chroococcales or coccoid cyanophytes. (From Golubic, 1976.) Growth of coccoids can either be radial (R) or unidirectional (U), and in one-(1D), two-(2D), or three- dimensional (3D) outward growth.

Calcareous sediments were mechanically trapped or bound within prostrate microbial communities. The interlayering of vertical growth and horizontally laminated alginite, mimicking stromatolitic textures (Plate 2F), suggests that the original organism was photosynthetic. This life stage is, however, fundamentally different from intertidal stromatolites because of its exclusively subtidal depositional environment and the absence of calcification. Features like fissures and pustules must be attributed to other processes, as neither desiccation nor exposure are consistent with the sedimentology or paleogeography of these strata.

Whether this algal growth habit of *G. prisca* truly represents an advanced stage in the life cycle, as depicted in Figure 5, or developed as a consequence of environmental pressures, is a matter for further investigation.

PHYLETIC AFFILIATION

Algae are broadly classified into Prokaryota and Eucaryota, depending on whether a nucleolus, chromosomes and plastids are present. Prokaryotes lack all three and include the bacteria Cyanophycota ("blue-green algae") and Prochlorphycota, whereas eucaryotic forms include four divisions of algae (Table 3). Divisions and classes of algae have been divided on the basis of principal pigments, food reserves, chloroplast features, cell wall construction and presence or absence of flagella (Parker,1982). Most groups of algae possess flagella at some stage in their development, a feature inferred here not to be characteristic of *Gloeocapsomorpha prisca*. Prokaryotes and the eucaryotic rhodophycotes do not have flagella during the non-motile growth stage. Unicellular or coccoid forms are extremely rare in rhodophycotes, whose cell walls are made up of cellulose.

Table 3. A general classification of algae (in part from Parker, 1982).

KINGDOU		DIVISION
Plantae	Prokaryota	Cyanophycota
		Prochlorophycota
	Eukaryota	Rhodophycota
		Chromophycota
		Eugleophycota
		Chlorophycota

Table 4. Summary of levels of organization in algae

Organizational type	Forms
Unicellular	Coccoid Rhizopidial Flagellate
Colonial	Palmelloid Coenobial
Filamentous	Simple Branched Heterotrichous
Psuedoparenchymatous	Multiaxial Parenchymatous Siphonocladous Siphonous

Modern-day stromatolite-builders are almost exclusively prokaryotic cyanophytes with minor contributions from eucaryotes and other bacteria (Golubic, 1976; Brock, 1976). While the majority of modern stromatolites are built by cyanobacteria, other organisms, including eucaryotic algae and fungi, can participate in their formation, although this is very rare (Awramik,1984). We conclude that *G. prisca* was a photosynthetic, prokaryotic organism because: 1) it lacks flagella; and 2) it had a coccoid, non-motile life stage. It also had stromatolite-like textures during its mat-forming life stage and exhibits features compatible with phototrophism during both the non-motile and mat-forming life-cycle stages. It is likely that *G. prisca* has affinities with chroococcales, prokaryotic photosynthesizers that include the extant genera *Gloeocapsa* and *Entophysalis* (Fig. 6).

Different levels of algal organization or structural morphology are also considered by classifications (Table 4). The alga *G. prisca* achieved two levels of organization, unicellular and colonial, during its life cycle. The coccoid form of G. prisca dominated the unicellular organization period, and the palmelloid form dominated the colonial period. Recognition of these two forms and their textural relationships have been employed above to formulate the life cycle of *Gloeocapsomorpha prisca*. Holocene mat-forming coccoid cyanophytes (e.g., *Aphanothece* sp., Gulf of Elat, Sinai Peninsula; Potts,1980) have life cycles similar to that interpreted for *G. prisca*. They produce large amounts of gel, which provides a coherent sediment coating (Golubic, 1976) enabling sediment-trapping in modern subtidal and intertidal depositional environments.

G. prisca colonized both submarine hardgrounds and loose substrate on the subtidal, mud-dominated, Yeoman carbonate ramp during its mat-forming stage. It exhibits a large tolerance for variations in water column chemistry. Mats are believed to have formed both in oxic water columns, where it is inferred that they were not preserved because of pervasive infaunal bioturbation, and beneath anoxic water columns where they escaped browsing. During its non-motile stage, *G. prisca* was tolerant of oxic open marine conditions, and its association with chitinozoa in the Winnipeg Formation (Osadetz et al., 1989) suggests tolerance for brackish as well as hypersaline waters.

CONCLUSIONS

Our conclusions fall between two current hypotheses concerning this organism. Reed et al. (1986) suggested *Gloeocapsomorpha prisca* was a "non-photosynthetic, prokaryotic, benthic and mat-forming, aerointolerant chemoautotroph". Hoffmann et al. (1987) suggested that

Table 5. Summary of the main alginite-related textures present in the Yeoman Formation. Their preservation potential and preferential position of formation is based on comparison with textural studies of Holocene algal mats/stromatolites in peritidal depositional areas (see text for specific references).

Mat texture	Preservation potential	Holocene depositional environment
flat lamination	excellent	intertidal; but also subtidal in high salinity areas
pinnacles	fair	intertidal
pustular	low	middle and lower intertidal
algal heads	poor to excellent	intertidal
small, domal stromatolites	good	sub-littoral to lower intertidal

"*G. prisca* was probably planktonic, photosynthetic and very possibly eucaryotic...". Both of these studies are largely based on geochemical evidence. As cited above, previous petrographic studies are either cursory (e.g., Jacobson et al., 1988) or comment on inappropriate lithologies (Foster et al., 1989).

Detailed sedimentological and stratigraphic analyses (Osadetz et al., work in progress), combined with petrographic studies described herein, lead to the recognition of two microfacies and the inference of a life cycle including both planktonic and benthic life stages. This reconciles the conclusions of earlier studies. We conclude that specific taphonomic environments are required to ensure that the benthic mat-forming stage escapes destruction by infaunal organisms. The prokaryotic affinities of the organism, based on lack of flagella and similarities to stromatolite-forming cyanophytes, are well founded in spite of the obvious contrasts between depositional environments. Numerous examples of sedimentary, microscopic textures of the layered *G. prisca* microfacies occurring in the Yeoman Formation are strikingly similar to textures described and detailed from modern stromatolite/algal mat-forming environments (Table 5) (e.g., Black, 1933; Logan et al., 1970; Park,1976; Golubic, 1976; Kinsman and Park, 1976; Bauld, 1984). Conclusions that this organism was aerointolerant or chemoautotrophic appear unfounded when the distribution of the non-motile stage is considered. This is consistent with chemical characteristics outlined by Hoffmann et al. (1987).

Despite recent progress in understanding the life cycle and phyletic affinities of *G. prisca*, important work remains to be done, particularly on the geochemistry and diagenesis of these source rocks (Fowler, in press; Hoffmann et al., 1987). Stromatolitic lithotypes from intertidal depositional environments in associated strata should be examined, as have the subtidal kukersites, in order to understand the differences between kukersites and stromatolites. Both the economic and biogeochemical significance of these organisms provide strong motivation for such studies.

ACKNOWLEDGMENTS

This project is funded by the Office of Energy Research and Development (O.E.R.D.), Energy Mines and Resources, Canada. The Government-Industry Review Committee is responsible for the guidance of this activity, O.E.R.D. Project 6.1.1.04 (Quantitative Aspects of Petroleum Origin in the Western Canada Sedimentary Basin), and the authors are grateful for this assistance. The authors would also thank E.M.V. Nambudirri, of the Energy Research Unit at the University of Regina, and M.G. Fowler and J.D. Aitken, Institute of Sedimentary and Petroleum Geology, Calgary, for their comments and assistance.

REFERENCES

Aitken, J.D.
1978: Revised models for depositional grand cycles, Cambrian of the southern Rocky Mountains, Canada; Bulletin of Canadian Petroleum Geology, v. 26, p. 515-542.
1966: Middle Cambrian to Middle Ordovician cyclic sedimentation, southern Rocky Mountains, Alberta; Bulletin of Canadian Petroleum Geology, v. 14, p. 405-411.

Awramik, S.M.
1984: Ancient stromatolites and microbial mats; *in* Microbial Mats: Stromatolites, Y.C. Cohen, R.W. Castenholtz, and H.O. Halvorson (ed.); MBL Lectures in Biology, v. 3, Alan R. Liss Inc., New York, p.1-22.

Bauld, J.
1984: Microbial mats in marginal marine environments: Shark Bay, Western Australia, and Spencer Gulf, South Australia; *in* Microbial Mats: Stromatolites, Y.C. Cohen, R.W. Castenholtz, and H.O. Halvorson (ed.); MBL Lectures in Biology, v. 3, Alan R. Liss Inc., New York, p. 39-58.

Black, M.
1933: The algal sediments on Andros Island, Bahamas; Royal Society of London Philosophical Transactions, Series B, v. 222, p. 165-192

Brock, T.D.
1976: Environmental microbiology of living stromatolites; *in* Stromatolites, M.R. Walter (ed.); Developments in Sedimentology 20, Elsevier Scientific Publishing Company, p. 141-148.

Brooks, P.W., Snowdon, L.R., and Osadetz, K.G.
1987: Families of oils in southeastern Saskatchewan; *in* Proceedings of the Fifth International Williston Basin Symposium, C.G. Carlson and J.E. Christopher (ed.); Bismark, North Dakota, June 15-17, 1987, Saskatchewan Geological Society, Special Publication no. 9, p. 253-264.

Combaz A. and Peniquel,G.
1972: Etude palynostratigraphique de l'Ordovician dans quelques sondage du Bassin de Canning (Australie Occidentale); Bulletin Centre de Recherche, SNPA, v. 6, p.121-167.

Cook, A.C., Hutton, A.C., and Sherwood, N.R.
1981: Classification of oil shales; Bulletin Centre de Recherche, Exploration Production, Elf Aquitaine, Pau, p. 353- 381.

Cramer F.H. and Diez de Cramer M.D.C.R.
1972: North American Silurian palynofacies and their spatial arrangement: acritarchs; Palaeontographica Abt. B, v. 138, p. 107-180.

Derby, J.R. and Kilpatrick, J.T.
1985: Ordovician Red River dolomite reservoirs, Killdeer Field, North Dakota; *in* Carbonate Petroleum Reservoirs, P.O. Roehl and P.W. Choquette (ed.); Springer-Verlag, p. 61-69.

Dombrowski, A.
1988: Generation of calcrete with chalky porosity in Upper Ordovician Red River grainstone reservoirs, Cedar Creek anticline, southwestern Williston Basin; (Abstract.); American Association of Petroleum Geologists Bulletin, v. 72, p. 179.

Foster, C.B., Reed, J.D., Wicander, R., and Summons, R.
1989: Anatomy of an Ordovician oil-prone maceral: Gloeocapsomorpha prisca Zalessky 1917; *in* Proceedings of the Macerals '89 Symposium, C.G. Thomas and M.G. Strachan (ed.); CSIRO Division of Coal Technology, North Ryde, New South Wales, Part 16, p. 1-9.

Foster, C.B., O'Brien, G.W., and Watson, S.T.
1986: Hydrocarbon source potential of the Goldwyer Formation, Barbwire Terrace, Canning Basin, Western Australia; Australian Petroleum Exploration Journal, p. 142-155.

Foster, C.B., Reed, J.D., and Wicander, R.
1988: Gloeocapsomorpha prisca Zalessky, Gen. Et Sp. Nov.: A restudy -taxonomy, geochemistry, and paleoecology (Abstact.); *in* Paleozoic abstracts of papers presented at the American Asociation of Stratigraphic Paleontologists Houston meeting, November 1988, p. 6.

Fowler, M.G.
in press: Organic geochemistry of oils and organic-rich rocks of Late Ordovician age from Canada; *in* Proceedings of the 9th Alfred Wegener Conference, Early Organic Evolution: Implications for Mineral and Energy Resources, M. Schidlowski et al. (ed.); Springer Verlag.

Fowler, M.G. and Douglas, A.G.
1984: Distribution and structure of hydrocarbons in four organic-rich Ordovician rocks; Organic Geochemistry, v. 6, p. 105-114.

Fowler, M.G., Abolins, P., and Douglas, A.G.
1986: Monocyclic alkanes in Ordovician organic matter; Organic Geochemistry, v. 10, p. 815-823.

Gebelein, C.D.
1969: Distribution, morphology, and accretion rate of Recent subtidal algal stromatolites, Bermuda; Journal of Sedimentary Petrology, v. 39, p. 49-69.

Golubic, S.
1976: Organisms that build stromatolites; *in* Stromatolites, M.R. Walter (ed.); Developments in Sedimentology 20, Elsevier Scientific Publishing Company, p. 113-126.

Hoffman, C.F., Foster C.B., Powell T.G., and Summons, R.E.
1987: Hydrocarbon biomarkers from Ordovician sediments and fossil alga *G.prisca* Zalessky 1917; Geochimica et Cosmochimica Acta, v. 51, p. 2681-2697.

Jacobson, S.R., Hatch, J.R., Teerman C.S., and Askin, A.A.
1988: Middle Ordovician organic matter assemblages and their effect on Ordovician-derived oils; American Association of Petroleum Geologists, Bulletin, v. 72, p. 1090-1100.

Kendall, A.C.
1976: The Ordovician carbonate succession (Bighorn Group) of southern Saskatchewan; Saskatchewan Department of Mineral Resources, Report 180, 185 p.

Kinsman, D.J.J. and Park, R.
1976: Algal belt and coastal sabkha evolution, Trucial Coast, Persian Gulf; *in* Stromatolites, M.R. Walter (ed.); Developments in Sedimentology 20, Elsevier Scientific Publishing Company, p. 421-434.

Kohm, J.A. and Louden, R.O.
1978: Ordovician Red River of eastern Montana and western North Dakota: relationships between lithofacies and production; *in* 1978 Williston Basin Symposium - the Economic Geology of the Williston Basin; Proceedings of the Montana Geological Society, 24th Annual Conference, Billings, Montana, p. 99-117.

Leenheer, M.J. and Zumberge, J.E.
1987: Correlation and thermal maturity of Williston Basin crude oils and Bakken source rocks using terpane biomarkers; *in* Williston Basin: anatomy of a cratonic oil province, M.W. Longman (ed.); Rocky Mountain Association of Geologists, Denver, Colorado, p. 2870-298.

Lefever, R.D., Thompson, S.C., and Anderson, D.B.
1987: Earliest Paleozoic history of the Williston Basin in North Dakota; *in* Proceedings of the Fifth International Williston Basin Symposium, C.G. Carlson and J.E. Christopher (ed.); Bismark, North Dakota, June 15-17, 1987, Saskatchewan Geological Society, Special Publication no. 9, p. 22-36.

Logan, B.W., Hoffman, P., and Gebelein, C.D.
1974: Algalmats, cryptalgal fabrics and structures, Hamelin Pool, Western Australia; American Association of Petroleum Geologists, Memoir 22, p. 140-194.

Logan, B.W., Davies, G.R., Read, J.F., and Cebulski, D.E.
1970: Carbonate sedimentation and environments, Shark Bay, Western Australia; American Association of Petroleum Geologists, Memoir 13, p.38-84.

Longman, M.W. and Palmer, S.E.
1987: Organic geochemistry of Mid-continent Middle and Late Ordovician oils; American Association of Petroleum Geologists, Bulletin, v. 71, p. 938-950.

Mackowsky, M.-Th.
1982: Methods and tools of examination; *in* Stach's Textbook of Coal Petrology, E. Stach et al. (ed.); Gebruder Borntraeger, Berlin, p. 295-299.

McGregor, D.C., Cramer, F.H., Flower, R.H., and Rigby, J.K.
1971: Fossils of the Ordovician Red River Formation (Cat Head Member), Manitoba; Geological Survey of Canada, Bulletin 202.

Monty, C.L.V.
1976: The origin and development of cryptalgal fabrics; *in* Stromatolites, M.R. Walter (ed.); Developments in Sedimentology 20, Elsevier Scientific Publishing Company, p. 193-250.

Neumann, A.C., Gebelein, C.D., and Scoffin, T.P.
1970: The composition, structure and erodibility of subtidal mats, Abaco, Bahamas; Journal of Sedimentary Petrology, v. 40, p. 274-297.

Osadetz, K.G. and Haidl, F.M.
in press: Tippecanoe Sequence: Middle Ordovician to lowest Devonian: vestiges of a great epeiric sea; Chapter 8 *in* Western Canada Sedimentary Basin A Case Study, B.D. Ricketts (ed.); Canadian Society of Petroleum Geologists, Calgary.

Osadetz,.K.G., Snowdon, L.R., and Stasiuk, L.D.
1989: Association of enhanced hydrocarbon generation and crustal structure in the Canadian Williston Basin; *in* Current Research, Part D, Geological Survey of Canada, Paper 89-1D, p. 35-47.

Ostrom, M.E.
1964: Pre-Cincinnatian Paleozoic cyclic sediments in the upper Mississippi Valley: a discussion; *in* Symposium on Cyclic Sedimentation, D.F. Merriam (ed.); State Geological Survey of Kansas and the University of Kansas, Bulletin 169, p. 381-398.

Padmaja, T.D.
1972: Studies on coccoid blue-green algae II; *in* Taxonomy and Biology of Blue-Green Algae, T.V. Desikachary (ed.); The Bangalore Press, Bangalore, p. 75-127.

Park, R.
1976: A note on the significance of lamination in stromatolites; Sedimentology, v. 23, p. 379-393.

1977: The preservation potential of some recent stromatolites; Sedimentology, v. 24, p. 485-506.

Parker, S.P.
1982: Synopsis and Classification of Living Organisms, Volumes 1 & 2; *in* 1982: Introduction to Phycology, G.R. South and A. Whittick (ed.), Blackwell Scientific Publications, Oxford, 341 p.

Playford, P.E. and Cockbain, A.E.
1976: Modern algal stromatolites at Hamelin Pool, a hypersaline barred basin in Shark Bay, Western Australia; *in* Stromatolites, M.R. Walter (ed.); Developments in Sedimentology 20, Elsevier Scientific Publishing Company, p. 389-412.

Potts, M.
1980: Blue-green algae (Cyanophyta) in marine coastal environments of the Sinai Peninsula, distribution, zonation, stratification and taxonomic diversity; Phycologia, v. 19, p. 60-73.

Reed, J.D., Illich, H.A., and Horsfield, B.
1986: Biochemical evolutionary significance of Ordovician oils and their sources; Organic Geochemistry, v.10, p. 347-358.

Ross, R.J.
1976: Ordovician sedimentation in the western United States; *in* The Ordovician System: proceedings of a Palaeontological Association symposium, M.G. Bassett (ed.); Birmingham, September 1974, University of Wales Press and National Museum of Wales, p. 73-105.

Sastri, V.V., Venkatachala, B.S., and Desikachary, T.V.
1972: A fossil Nostocaceae from India; *in* Taxonomy and Biology of Blue-Green Algae, T.V. Desikachary (ed.); The Bangalore Press, Bangalore, p. 159-160.

South, G.R. and Whittick, A.
1987: Introduction to Phycology; Blackwell Scientific Publications, Oxford, 341 p.

Stasiuk, L.D.
1988: Thermal maturation and organic petrology of Mesozoic strata of southern Saskatchewan; M.Sc. thesis, University of Regina, Regina, Saskatchewan, 178 p.

Till, R.
1978: Arid shorelines and evaporites; *in* Sedimentary Environments and Facies, H.G. Reading (ed.); Elsevier, New York, p. 178-206.

Vigrass, L.W.
1971: Depositional framework of the Winnipeg Formation, Manitoba and eastern Saskatchewan; Geological Association of Canada, Special Paper no. 9, p. 225-234.

Williams, J.A.
1974: Characterization of oil types in Williston Basin; American Association of Petroleum Geologists, Bulletin, v. 58, p. 1243-1252.

Witzke, B.J.
1980: Middle and Upper Ordovician paleogeography of the region bordering the Transcontinental arch; *in* Paleozoic paleogeography of the west-central United States, T.D. Fouch and E.R. Magathan (ed.); Society of Economic Paleontologists and Mineralogists Rocky Mountain Section, West Central Paleogeography Symposium 1, p. 1-18.

Zalessky, J.E.
1917: On marine sapropelite of Silurian age formed by a blue-green alga; Izvestiia imperatorskoi Akademii Nauk IV, ser. no.1, p. 3-18.

Field investigation of the Mount Bayley Formation, a Lower Permian evaporite in the Canadian Arctic

Carol A. Wallace[1] and Benoit Beauchamp
Institute of Sedimentary and Petroleum Geology, Calgary

Wallace, C.A. and Beauchamp, B., Field investigation of the Mount Bayley Formation, a Lower Permian evaporite in the Canadian Arctic; in Current Research, Part D, Geological Survey of Canada, Paper 90-1D, p. 139-146, 1990.

Abstract

Four stratigraphic sections of the Mount Bayley Formation, a Lower Permian evaporite of the Sverdrup Basin, were measured on west-central Ellesmere Island. The thickness of the formation ranges from 58 to 162.5 m. Alternating evaporite and carbonate units occur in these sections. Depositional and diagenetic features of the evaporites (gypsum and anhydrite) include: undisturbed, varve-like laminae, discontinuous nodules, bedded mosaics, mosaics, and anhydrite pseudomorphs after halite hopper crystals. Carbonates vary from fossiliferous to unfossiliferous, varve-like dolostones. The Mount Bayley Formation appears to have been deposited in a relatively deep water, subaqueous environment.

Résumé

Quatre sections stratigraphiques de la formation de Mount Bayley, une évaporite datant du Permien inférieur du bassin de Sverdrup, ont été mesurées au centre-ouest de l'île d'Ellesmere. L'épaisseur de la formation varie de 58 à 162,5 m. Les sections sont caractérisées par une alternance d'unités d'évaporites et de roches carbonatées. Les faciès sédimentaire et diagénétique observés dans les évaporites (gypse et anhydrite) comprennent: lamines intactes ressemblant à des varves, nodules discontinus, mosaïques litées, mosaïques et pseudomorphes anhydritiques de cristaux de halite. Les roches carbonatées comprennent, ou bien des dolomies ressemblant à des varves, ou bien des dolomies fossilifères. La sédimentation de la formation de Mount Bayley s'est faite dans un milieu marin relativement profond.

[1] Department of Geology and Geophysics, The University of Calgary, Calgary, Alberta, T2N 1N4

INTRODUCTION

The Lower Permian Mount Bayley Formation is an evaporite unit exposed along the eastern margin of the Sverdrup Basin, a major depocentre of the Canadian Arctic Archipelago. It outcrops irregularly in a narrow band, over 200 km long, on west-central Ellesmere Island (Fig.1). Stratigraphic and sedimentological information about the Mount Bayley Formation has been limited to the original description by Thorsteinsson (1974). A more detailed study was begun in the summer of 1989 in order to expand our knowledge of this formation. The results of our field observations are presented here. This information provides important clues to the understanding of the origin of the Mount Bayley Formation and also provides a base for further biostratigraphic, geochemical and petrographic work (Wallace, work in progress).

GEOLOGICAL SETTING

Sverdrup Basin sedimentation was initiated in the Early Carboniferous following rift-induced collapse of Devonian and older rocks of the Franklinian basement (Thorsteinsson and Tozer, 1970; Trettin, 1989). A nearly continuous succession of sedimentary rocks and minor volcanics accumulated during the remainder of the late Paleozoic, the Mesozoic and the early Tertiary. Sediments of the Sverdrup Basin were affected by the Eurekan Orogeny, a middle Tertiary tectonic event probably associated with the opening of the North Atlantic Ocean (Kerr, 1981). This event produced prominent mountain ranges in the eastern Arctic, where the Mount Bayley Formation is well exposed.

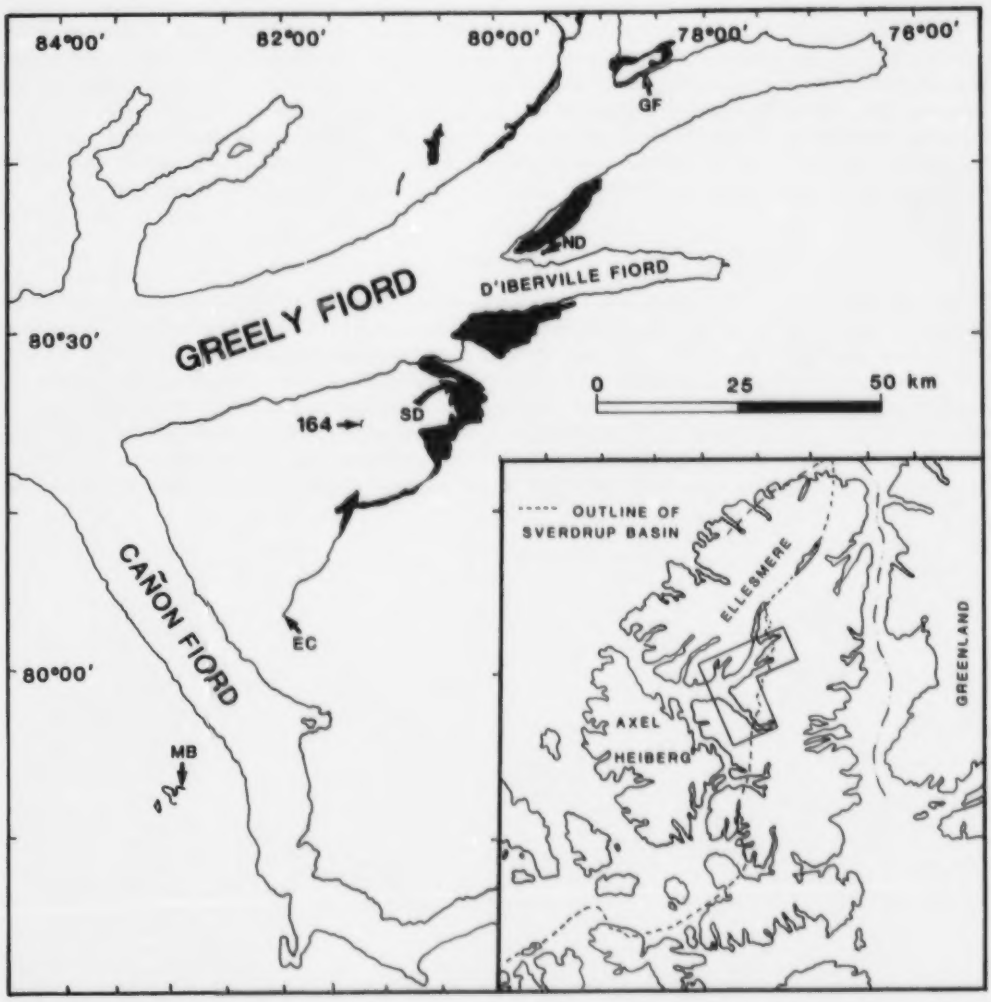

Figure 1. Location of measured sections and outcrop distribution (black areas) of Mount Bayley Formation on west-central Ellesmere Island. Measured sections are: (**MB**) Mount Bridgman, (**EC**) East Cape River, (**SD**) South D'Iberville, (**GF**) Greely Fiord. Location of North D'Iberville (**ND**) outcrop and locality 164 of Thorsteinsson (1974) also are shown.

The Mount Bayley Formation is a Lower Permian deposit (Thorsteinsson, 1974). A recently processed conodont sample from the base of the overlying Tanquary Formation at Mount Bridgman has yielded a species of Adetognathus, which is known to range from late Asselian to middle Sakmarian (C.M. Henderson, pers. comm., 1989). S. Pinard (pers. comm., 1989) also identified an advanced form of "Calcidiscus" from 14.5 m below the top of the Mount Bayley Formation at Mount Bridgman. This foraminifer has only been found in uppermost Asselian to Sakmarian strata elsewhere in the Sverdrup Basin (Pinard, work in progress).

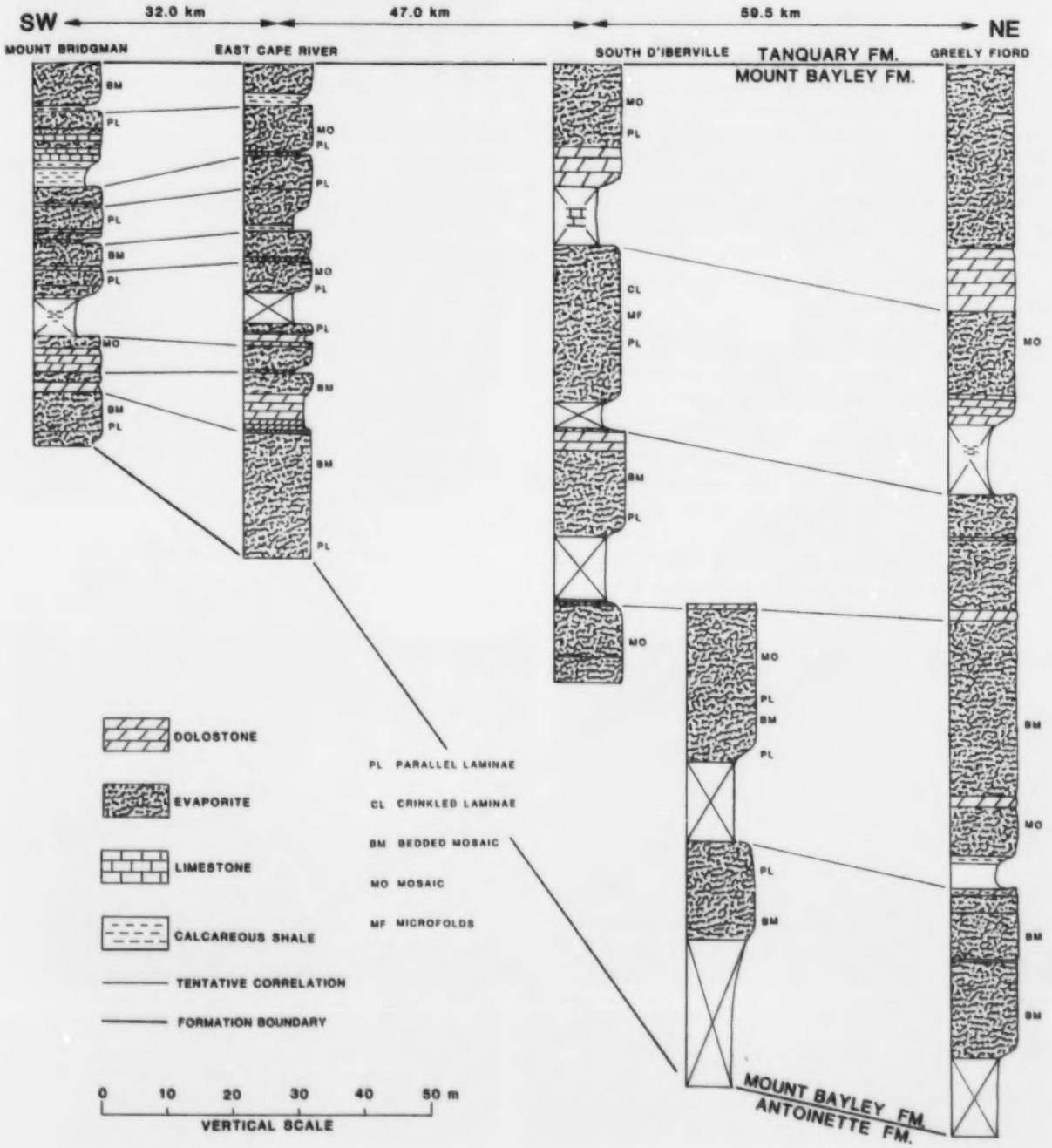

Figure 2. Cross-section (SW-NE) of the Mount Bayley Formation with tentative correlations. See text for further explanation.

Seven second- to third-order transgressive-regressive sequences have been documented in the Carboniferous and Permian succession of the Sverdrup Basin (Beauchamp et al., 1989b). Each sequence is characterized by shallow-water carbonate and/or clastic shelf sediments that pass basinward into lower Upper Carboniferous evaporites (Otto Fiord Formation; Nassichuk and Davies, 1980), and into younger Carboniferous and Permian deep-water mudrocks (Hare Fiord, "unnamed" B, and Van Hauen formations; Beauchamp et al., 1989b). A very thick succession of shelf carbonates, with abundant biogenic buildups, reflecting tropical-like conditions, developed in the Late Carboniferous to Early Permian. Active block-faulting and rifting affected the eastern margin of the basin during this time resulting in the formation of a number of sub-basins (Beauchamp et al., 1989a). Deposition of the Mount Bayley Formation probably resulted from the dry, evaporative climatic setting in conjunction with the creation of enclosed or semi-enclosed sub-basins at the southern margin of the main Sverdrup Basin.

The Mount Bayley is enclosed within carbonate strata: it is underlain by the Antoinette Formation, overlain by the Tanquary Formation, and passes laterally into either the Nansen or the Belcher Channel formations (Thorsteinsson, 1974). These units contain a variety of carbonate-dominated sediments, with minor evaporites. The Antoinette and Tanquary formations consist of multiple intraformational cycles. Each cycle is characterized by a shallowing-upward package comprising a recessive, shale-dominated unit at the base that passes upward into purer and more resistant fusulinid-rich wackestone and packstone. Such cycles, referred to as "type 4" by Beauchamp (1987), were shown to represent sedimentation in a relatively deep-water, outer shelf setting.

MEASURED SECTIONS

Four stratigraphic sections, spread over 138 km, were measured in 1989 (Fig. 1, 2): Greely Fiord section, South D'Iberville Fiord section, East Cape River section and Mount Bridgman section. Mount Bayley evaporites on the north shore of D'Iberville Fiord were also examined. Although no sections were measured there because of structural complexity, this outcrop displays a vast array of remarkably well-preserved evaporite fabrics showing outstanding examples of microfolds, varve-like laminae, nodules of various sizes, and pseudomorphs after halite hoppers.

Greely Fiord section

The Greely Fiord section (Fig. 3A) is the type-section of the Mount Bayley Formation (Thorsteinsson, 1974). The section is located on the north shore of Greely Fiord at lat. 8052' N, long. 7837'W. The Mount Bayley Formation is 162.5 m thick at the Greely Fiord section (Fig. 2). It comprises dominant anhydrite, locally rehydrated to gypsum, and minor amounts of variably silty dolostone. The anhydrite facies are generally poorly preserved because of tectonic deformation, which altered the depositional and early diagenetic fabrics. Better preserved surfaces display bedded mosaic anhydrite and millimetre-scale parallel laminae (carbonate-sulphate couplets) that resemble varves (as in Fig. 4). Most of these laminae typically display a crinkled outline, reflecting the pervasive shearing at that section.

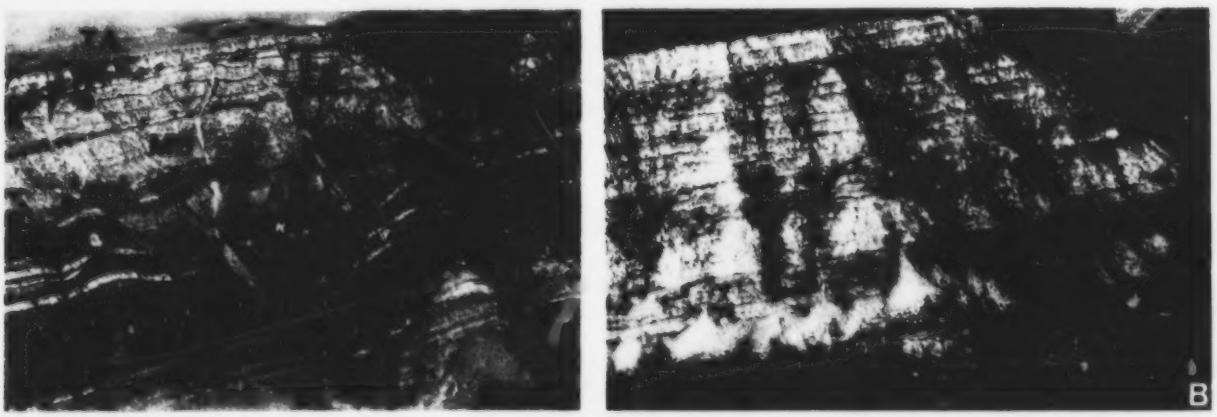

Figure 3. Exposures of the Mount Bayley Formation on west-central Ellesmere Island. **A.** Greely Fiord section. Upper Antoinette (**AN**), Mount Bayley (**MB**) and lower Tanquary (**TA**) formations are shown. Note dolostone (arrows) and evaporite (white bands) horizons within Antoinette Formation and carbonate horizons (dark bands) within Mount Bayley Formation. Sediments above dashed line in Antoinette Formation comprise porous dolostones. **B.** Mount Bridgman Section. Note multiple carbonate layers (dark bands) interstratified with evaporites.

The Greely Fiord section also contains minor proportions of carbonate rocks (Fig. 2). Eight relatively thin units of dolostone occur in the section. Carbonate units are closely associated with a distinctive, unconsolidated green calcareous mud. The dolostones are platy and display varve-like parallel laminae. Fossils are present locally: fusulinids are the most common; solitary corals and brachiopods are rare and occur only in the thicker units near the top of the formation. Dolostone units represent only a minor fraction of the formation and form darker bands that contrast markedly with the evaporites (Fig. 3A). The alternation of dark carbonate bands and thicker evaporite units appears to reflect some sort of cyclicity within the Mount Bayley Formation.

South D'Iberville section

The Mount Bayley Formation is 154.5 m thick at the South D'Iberville section (lat. 80°26′N, long. 80°17′W), which was measured in two segments as shown in Figure 2. Evaporites characterize the formation with minor amounts of carbonates and unconsolidated calcareous mud. The section comprises five broad units, ranging in thickness from 25 to 37 m. Each unit consists of a basal recessive and covered interval overlain by cliff-forming evaporites. Carbonates associated with green calcareous mud occur at the bases of these units. These carbonates are organic-rich, variably sandy and dolomitic. A much thicker (6 m) carbonate horizon occurs in the upper part of the formation. It is composed of thick bedded, fusulinid-rich, in part gypsiferous dolomite with enigmatic, algal-like stringers.

A wide variety of fabrics characterizes the evaporites, which consist of anhydrite and its rehydrated product, gypsum. Millimetre thick, varve-like laminae, which occur immediately above the recessive intervals, are the most conspicuous sedimentary structures. Other features include a wide spectrum of crinkled laminae, bedded mosaics, mosaics (as in Fig. 5B), and discontinuous nodules (as in Fig. 4B). The most spectacular features of the South D'Iberville section are microfolds of deformed anhydrite (Fig. 6B).

A section located 18 km west of the South D'Iberville section (loc. 164 in Fig. 1) was reported to contain up to 249 m of Mount Bayley strata, which represents the thickest known occurrence of the formation. According to Thorsteinsson (1974), sandstone predominates in the lower 90 m of the Mount Bayley Formation with lesser silty limestone and siltstone interstratified with subordinate anhydrite, whereas anhydrite predominates in the upper 159 m of the formation.

East Cape River section

The Mount Bayley Formation is 74 m thick (Fig. 2) at East Cape River (lat. 80°05′N, long. 81°48′W). It is composed of alternating evaporites and subordinate dolostones. A relatively thick unit (19 m) of evaporite marks the base of the section. It contains varve-like laminae passing upward into bedded mosaics and mosaics. The overlying evaporite units are thinner, ranging in thickness from 4 to 8 m, displaying either laminated or nodular fabrics.

The intervening carbonate units range in thickness from less than 1 m to 6 m. Gypsiferous dolostone interbedded with dark shale constitutes the dominant carbonate lithology. Limestones are also present. The dolostone commonly displays fossil-barren, varve-like laminae. Thin units of green unconsolidated calcareous mud occur throughout the section as recessive intervals.

Mount Bridgman section

The Mount Bayley Formation is 58 m thick at Mount Bridgman (lat. 79°50′N, long. 82°38′W). It consists of alternating evaporites and minor carbonates (Fig. 3B). Carbonates are present in greater proportions than in the other sections. Evaporite units range from less than 2 m to 6 m thick. A complex spectrum of varve-like laminated facies and mosaic anhydrite occurs throughout these units with sharp contacts between these facies. Dark, organic-rich, fetid dolostone units characterized by remarkably well developed varve-

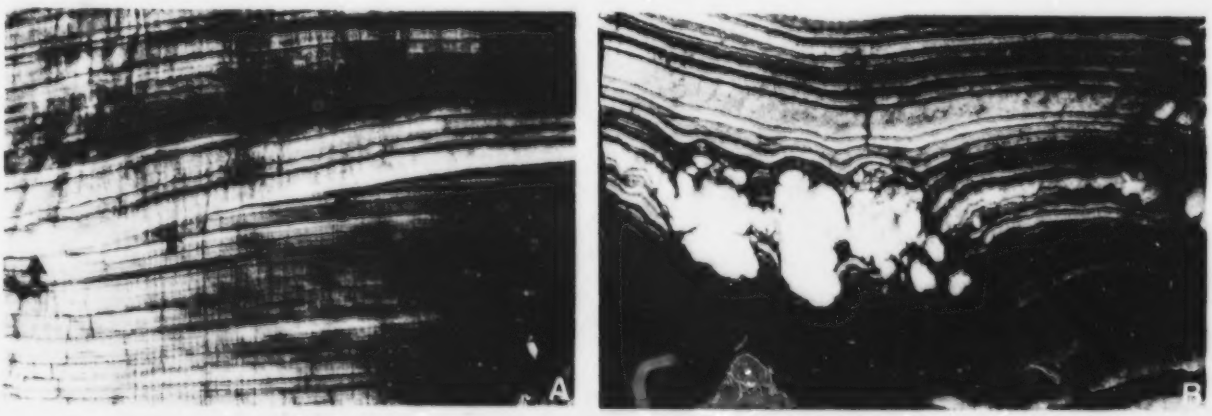

Figure 4. Varve-like laminae in Mount Bayley Formation, North D'Iberville outcrop. **A.** Laminae truncated by erosional surface (arrows) resembling submarine slump scar. **B.** Discontinuous nodules diagenetically grown within laminae. Lens cap is 5 cm wide.

like laminae occur throughout the section. In addition, thinner fossiliferous carbonate units occur. These contain fusulinids and possible algal material. Recessive units of unconsolidated green calcareous mud are associated with the carbonates (Fig. 2).

HYPOTHESES

A number of hypotheses can be advanced regarding the stratigraphic, environmental and diagenetic significance of the Mount Bayley Formation.

Correlations

The top of the Mount Bayley Formation is used as a datum in the cross-section depicted in Figure 2. It is assumed that the upper surface is synchronous throughout the study area. This assumption, although not yet substantiated by biostratigraphic evidence, appears reasonable considering that an identical number of Tanquary shelf cycles were observed above the Mount Bayley Formation at both Mount Bridgman and Greely Fiord. These cycles likely represent timeequivalent packages that can be correlated across the entire Sverdrup Basin (Beauchamp et al., 1989b). The Mount Bridgman and East Cape River sections appear to correlate fairly well, because a similar number of carbonate-evaporite couplets can be recognized in both sections (Fig. 2). The same is true for the South D'Iberville and Greely Fiord sections. However, the latter sections do not readily correlate with the former sections.

The formation may be synchronous throughout the study area, indicating a much thicker development of the Mount Bayley at South D'Iberville and Greely Fiord than at Mount Bridgman and East Cape River. The thickness difference possibly reflects the shallower depositional environment of the Mount Bridgman and East Cape River sections. However, this scenario appears unlikely as intraformational correlations between the East Cape River section and the South D'Iberville section cannot be drawn with confidence. Alternatively, the Mount Bayley Formation may be diachronous throughout the study area. This would imply that lower Mount Bayley strata are correlative with upper Antoinette strata. This possibility is reasonable considering the presence of interbedded evaporites within the Antoinette Formation at Greely Fiord and South D'Iberville.

Biostratigraphy may help to decipher which possibility, if any, is correct. Future research may actually show that the Mount Bayley was deposited in more than one sub-basin, and that none of the above hypothetical correlations is valid.

Depositional environment

The regional stratigraphic setting of the Mount Bayley Formation (totally enclosed within shelf carbonates belonging to the Nansen, Belcher Channel, Antoinette and Tanquary formations), the absence of exposure features, and the presence of marine fossils, suggest that the Mount Bayley Formation was deposited in a subaqueous environment. Some lines of evidence further suggest that most of the Mount Bayley Formation accumulated in relatively deep water. These include: the pervasiveness of undisturbed varve-like laminae both in the carbonate and evaporite facies; the absence of wave-generated sedimentary structures and bottom growth fabrics; and the presence of outer shelf carbonates immediately below and above the formation.

However, as discussed above, the possibility exists of lateral bathymetric variations, with the thicker (and likely deeper) development of the Mount Bayley Formation around the D'Iberville Fiord area. In contrast, the East Cape River and Mount Bridgman sections appear to contain a shallower succession as indicated by the presence of thinner units of evaporites in addition to the occurrences of fossiliferous algal-rich carbonate sediments. Vertical bathymetric variations may also be indicated by the alternation of evaporites, carbonates and calcareous muds in each section. These variations may reflect some sort of cyclicity within the Mount Bayley Formation, the causes of which are uncertain at this stage.

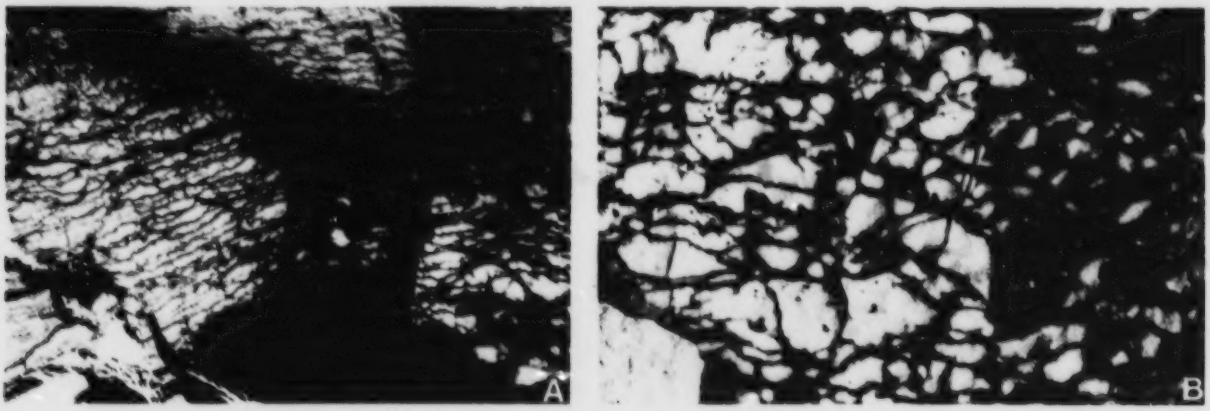

Figure 5. Diagenetic fabrics in Mount Bayley Formation, North D'Iberville outcrop. **A.** Bedded mosaic anhydrite. Thickness of evaporite layers averages 2 cm. **B.** Mosaic anhydrite. Lens cap is 5 cm wide.

Diagenesis

A wide spectrum of diagenetic features are present within the anhydrite of the Mount Bayley Formation. These reflect a rather complex postdepositional history. Some of these features can be related to the well documented episodes of dehydration of gypsum and rehydration of anhydrite that accompany burial and subsequent uplift of evaporite deposits (Blatt et al., 1980). Other features, however, appear to have formed very early in the diagenetic history of the evaporite sediments. These include a variety of nodules that grew superimposed on the primary depositional fabrics. Field observations have revealed a continuum of nodular fabrics ranging from isolated nodules in varve-like anhydrite (discontinuous nodules in Fig. 4B) to nodular mosaics showing no remnants of the primary laminae (Fig. 5B).

Other diagenetic features observed include anhydrite pseudomorphs after halite hopper crystals (Fig. 7). These probably formed very early, because of high salinities in the near-surface diagenetic environment. Perhaps the most spectacular postdepositional feature of the Mount Bayley Formation evaporites are the microfolds, which occur at a variety of scales and intensities of folding (Fig. 6). The origin of these folds is unclear, although interpretations ranging from tectonism to synsedimentary deformation to geochemically-induced folding have been proposed for similar features in other basins.

COMPARISONS

The Mount Bayley Formation appears to differ substantially from the other major upper Paleozoic evaporite of the Sverdrup Basin, the Otto Fiord Formation. Although both formations were deposited in a subaqueous environment, the pervasiveness of varve-like laminae and microfolds along with the scarcity of interstratified fossiliferous limestone and the absence of bottom-grown gypsum crystals in the Mount Bayley Formation, suggest a somewhat different environment of deposition than that of the Otto Fiord Formation. The Otto Fiord Formation, at least in the outcrop belt, is characteristically interstratified with thick,

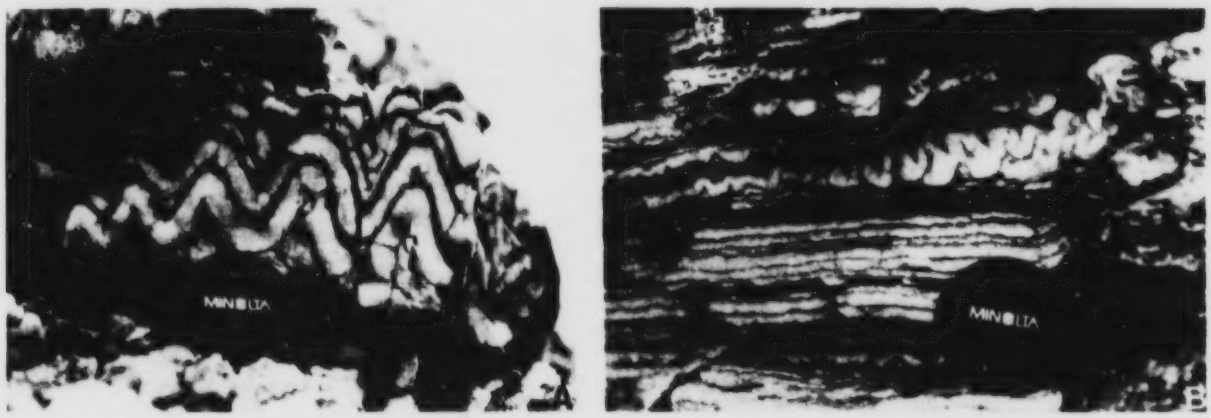

Figure 6. Microfolds in Mount Bayley Formation. **A.** Multiple folded anhydrite laminae; North D'Iberville outcrop. **B.** Tightly folded gypsum layer; South D'Iberville section. Note lateral disappearance of folds. Lens cap is 5 cm wide.

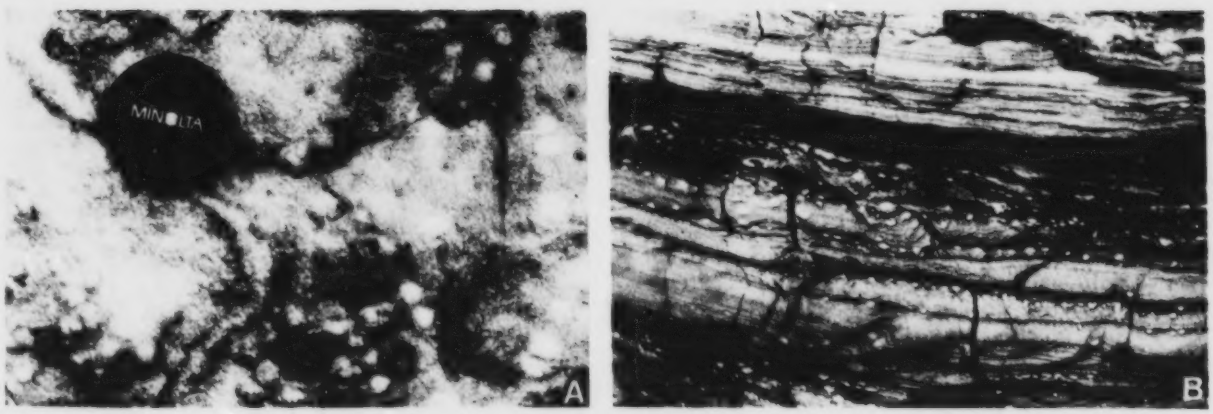

Figure 7. Pseudomorphs of halite hoppers in Mount Bayley Formation, North D'Iberville outcrop. **A.** Close-up view of bedding plane showing range of hopper preservation. **B.** Abundant hoppers superimposed on varve-like laminae. Lens cap is 5 cm wide.

fossiliferous, in part reefal (Nassichuk and Davies, 1980; Davies and Nassichuk, 1988) limestones that contain abundant green algae indicating fairly shallow water deposition. The Otto Fiord Formation is also, in places, interstratified with sandstone units displaying sedimentary structures indicative of shallow water deposition. Varve-like laminae are locally developed in the Otto Fiord Formation but never to the same extent as in the Mount Bayley. Microfolds are not reported from the Otto Fiord Formation. Similar diagenetic nodules do occur in both formations.

The Mount Bayley Formation appears to be very similar to one of the most studied evaporite deposits of the world, the Permian Castile Formation of west Texas. The Castile Formation has been interpreted by many, not only as a subaqueous deposit, but as one of the very best examples of a deep-water evaporite (Udden, 1924; Anderson et al., 1972). Among other features, the Castile comprises well developed undisturbed laminae, which were first interpreted as annual varves by Udden (1924), an idea expressed in recent years as well (Dean and Anderson, 1982). These varves have been correlated across the Delaware Basin for distances exceeding 100 km (Dean and Anderson, 1982). Moreover, microfolds, very similar to the Mount Bayley Formation microfolds, have been documented in the Castile Formation. Intraformational packages, interpreted as salinity cycles, also occur within the Castile (Dean and Anderson, 1978). These cycles resemble the packages observed within the Mount Bayley Formation, especially at South D'Iberville.

Clearly, the Castile and the Mount Bayley formations share many of the same features. Further in-depth research will determine whether the two formations were deposited in the same depositional environment.

CONCLUSIONS

Preliminary study of the Mount Bayley Formation indicates that this evaporite formed subaqueously in a relatively deep-water environment. This is suggested by the regional setting of the formation, the absence of exposure and shallow-water features, and the presence of undisturbed, varve-like laminae.

The top of the Mount Bayley Formation appears to be synchronous throughout the study area. Whether the base of the formation is synchronous or diachronous is yet to be determined. Intraformational correlations can be drawn between the adjacent Mount Bridgman and East Cape River sections, and South D'Iberville and Greely Fiord sections. However, all four sections cannot be easily correlated.

Alternations of varve-like laminae, bedded mosaics, and mosaics within the Mount Bayley Formation suggest a complex depositional and diagenetic history. Recurring carbonate-evaporite packages in the Mount Bayley Formation appear to reflect some sort of cyclicity.

ACKNOWLEDGMENTS

We are grateful to P. Larson for providing us with invaluable comments in the field, to C. M. Henderson and S. Pinard for their paleontological expertise, and to R. Spencer for reviewing an early version of the manuscript and suggesting considerable improvements.

REFERENCES

Anderson, R.Y., Dean, W.E. Jr., Kirkland, D.W., and Snider, H.I.
1972: Permian Castile varved evaporite sequence, west Texas and New Mexico; Geological Society of America, Bulletin, v. 83, p. 59-86.

Beauchamp, B.
1987: Stratigraphy and facies analysis of the Upper Carboniferous to Lower Permian Canyon Fiord, Belcher Channel and Nansen formations, southwestern Ellesmere Island; Ph.D. thesis, University of Calgary, June 1987, 370 p.

Beauchamp, B., Harrison, J.C., and Henderson, C.M.
1989a: Upper Paleozoic stratigraphy and basin analysis of the Sverdrup Basin, Canadian Arctic Archipelago: Part 1, time frame and tectonic evolution; *in* Current Research, Part G, Geological Survey of Canada, Paper 89-1G, p. 105-113.
1989b: Upper Paleozoic stratigraphy and basin analysis of the Sverdrup Basin, Canadian Arctic Archipelago: Part 2, transgressive-regressive sequences; *in* Current Research, Part G, Geological Survey of Canada, Paper 89-1G, p. 115-124.

Blatt, H., Middleton, G., and Murray, R.
1980: Origin of Sedimentary Rocks (Second Edition.); Prentice-Hall, Englewood Cliffs, New Jersey, 1980, 782 p.

Davies, G.R. and Nassichuk, W.W.
1988: Upper Carboniferous tubular algal boundstone reefs in Otto Fiord Formation, Canadian Arctic Archipelago; *in* Reefs of Canada and Adjacent Areas, H.J. Geldsetzer and D.J. Glass (ed.); Canadian Society of Petroleum Geologists, Memoir 13, p. 649-657.

Dean, W.E. and Anderson, R.Y.
1978: Salinity cycles: evidence for subaqueous deposition of Castile Formation and lower part of Salado Formation, Delaware Basin, Texas and New Mexico; New Mexico Bureau of Mines and Mineral Resources, Circular 139, p. 15-20.

Dean, W.E. and Anderson, R.Y.
1982: Continuous subaqueous deposition of the Permian Castile evaporites, Delaware, Texas and New Mexico; Society of Economic Paleontologists and Mineralogists, Core Workshop no. 3, p. 324-353.

Kerr, J.Wm.
1981: Evolution of the Arctic Islands: a transition between the Atlantic and the Arctic oceans; *in* The Ocean Basins and Margins, Volume 5, The Arctic Ocean, A.E. Nairn, M. Churkin, Jr., and F.G. Stehli (eds.); Plenum Press, New York, p. 105-199.

Nassichuk, W.W. and Davies, G.R.
1980: Stratigraphy and sedimentation of the Otto Fiord Formation — a major Mississippian-Pennsylvanian evaporite of subaqueous origin in the Canadian Arctic Archipelago; Geological Survey of Canada, Bulletin 286, 87 p.

Thorsteinsson, R.
1974: Carboniferous and Permian stratigraphy of Axel Heiberg Island and western Ellesmere Island, Canadian Arctic Archipelago; Geological Survey of Canada, Bulletin 224.

Thorsteinsson, R. and Tozer, E.T.
1970: Geology of the Arctic Archipelago; *in* Geology and Economic Minerals of Canada, R.J.W. Douglas (ed.); Geological Survey of Canada, Economic Report no. 1, 5th ed., p. 548-590.

Trettin, H.P.
1989: The Arctic Islands; *in* The Geology of North America-An Overview, A.W. Bally and A.R. Palmer (ed.); Boulder, Colorado, Geological Society of America, The Geology of North America, v. A, p. 349-370.

Udden, J.A.
1924: Laminated anhydrite in Texas; Geological Society of America Bulletin, v. 35, p. 347-354.

Middle Ordovician sedimentary and volcanic rocks at Fire Bay, Emma Fiord, northwestern Ellesmere Island

H.P. Trettin and G.S. Nowlan
Institute of Sedimentary and Petroleum Geology, Calgary

Trettin, H.P. and Nowlan, G.S., Middle Ordovician sedimentary and volcanic rocks at Fire Bay, Emma Fiord, northwestern Ellesmere Island; in Current Research, Part D, Geological Survey of Canada, Paper 90-1D, p. 147-151, 1990.

Abstract

Volcanogenic sediments and minor flows of felsic composition (dacite, rhyolite, etc.), radiolarian chert, and slate at Fire Bay have associated with them lenticular carbonate bodies interpreted as olistostromes (shelf deposits transported into deeper water by sliding). These carbonate lenses have yielded conodonts of early Middle Ordovician (Whiterockian) age. The entire volcanic-sedimentary assemblage was previously included in the Silurian Lands Lokk Formation (type area of member B and adjacent part of member A) but evidently represents a fault block of older rocks. It is comparable to the Mount Rawlinson assemblage of northeastern Ellesmere Island, also composed of felsic volcanics, carbonates, and radiolarian chert, which has a Middle Ordovician U-Pb (zircon) age.

Résumé

À la baie Fire, les sédiments d'origine volcanique et les coulées secondaires de composition felsique (dacite, rhyolite, etc.), le chert radiolaire et l'ardoise sont associés à des massifs carbonatés de forme lenticulaire que l'on considère être des olistostromes (sédiments de plate-forme transportés vers des eaux plus profondes par glissement). Ces lentilles carbonatées ont produit des conodontes datant du début de l'Ordovicien moyen (Whiterockien). Cet assemblage volcano-sédimentaire a été dans le passé entièrement inclus dans la formation silurienne de Lands Lokk (zone type du membre B et partie adjacente du membre A), mais il représente sans conteste un bloc faillé de roches plus anciennes. Il est comparable à l'assemblage du mont Rawlinson dans le nord-est de l'île d'Ellesmere qui est également composé de roches volcaniques felsiques, de roches carbonatées et de chert radiolaire dont l'âge établi par géochronologie U-Pb (appliquée aux zircons) remonte à l'Ordovicien moyen.

INTRODUCTION

An inlier of lower Paleozoic sedimentary and volcanic rocks at Fire Bay, Emma Fiord, northwestern Ellesmere Island, was discovered by R. Thorsteinsson in 1957 during an extensive sledge expedition. The inlier was further investigated by Trettin for a few days in 1961, in the course of a reconnaissance of the pre-Carboniferous geology of northern Axel Heiberg and northwestern Ellesmere islands (Trettin, 1969). The lower Paleozoic rocks of northwestern Ellesmere Island are generally too structurally complex for systematic stratigraphic section work, but lithological observations, combined with sparse graptolite collections, have permitted the definition of a few major units. Most strata in the vicinity of Emma Fiord were assigned to the Lands Lokk Formation, which was divided into three informal members. Member A, of late Llandovery or Wenlock to early Ludlow age, comprised mudrock with local occurrences of volcanic arenite and tuff. Member B, recognized only at Fire Bay and in a small area east of Emma Fiord, comprised tuff, volcanic conglomerate, siltstone, and minor lenses of limestone. No fossils were found in this unit, but proximity to a graptolite occurrence in member A (discovered by Thorsteinsson in 1957) suggested an early Ludlow age. Member C, also placed in the early Ludlow, was composed of mudrock, sandstone and minor conglomerate with flysch-like primary structures.

The Lands Lokk Formation has subsequently been traced throughout northern Ellesmere Island, from Emma Fiord to Clements Markham Inlet. A re-examination of the type area around Emma Fiord was begun in 1986, when critical exposures of members C and A were restudied (Trettin, 1987). The examination continued for a few days in 1988, when the area east and southeast of Fire Bay was revisited. The main purpose of this work was to investigate the origin of the limestones and to obtain samples for conodont analysis (not available in the early sixties when the initial work was carried out). Conodonts were retrieved, but their identification, by Nowlan, indicated an early Middle Ordovician rather than a Silurian age. The suite of rocks that must now be re-assigned to the Middle Ordovician is here informally referred to as the Fire Bay assemblage (Fig. 1). It underlies the entire area originally assigned to member B of the Lands Lokk Formation and also an adjacent area assigned to member A, but does not include Thorsteinsson's graptolite locality (cf. Trettin, 1969, Fig. 8). It is likely that the Fire Bay assemblage is separated from the Lands Lokk Formation by a major fault, but additional fieldwork is required to verify this.

LITHOLOGY AND MODE OF ORIGIN

The Fire Bay assemblage is divisible into two suites of rocks: 1) a recessive suite composed of thinly interstratified dark grey chert and slate and minor tuff with rare carbonate lenses, and 2) a cliff-forming suite composed mainly of volcanogenic sediments with rare volcanic flows and some carbonate lenses. Both suites are complexly folded and faulted and their stratigraphy is difficult to establish. Suite 2 overlies Suite 1 in a structural sense but the contact is mostly covered and may be faulted. Suite 2 has a minimum thickness of 70 m but may be more than 100 m thick.

The chert contains abundant inclusion-free spheres, 0.05 to 0.25 mm in diameter, which are interpreted as recrystallized radiolarian tests because of their resemblance to better preserved radiolarians in similar deposits; for example, in the Mount Rawlinson assemblage and in the Hazen Formation (see below). This kind of chert is indicative of deep water environments with very low sedimentation rates.

The volcanogenic sediments range in size grade from silt to cobble conglomerate and are mainly medium sand to fine pebble grade. The volcanic material consists of crystals of feldspar and lithic fragments of felsic composition. Whole-rock X-ray diffraction analyses show that the feldspar is largely or entirely albite. The lithic fragments studied in thin section are felsic in composition, commonly dacite or andesite. A relatively unaltered specimen of mixed fragmental rock has the overall chemical composition of a "calc-alkaline dacite, K-poor series" (computer analysis, based on the major-element classification of Irvine and Baragar, 1971). Some volcanogenic conglomerates also include carbonate clasts.

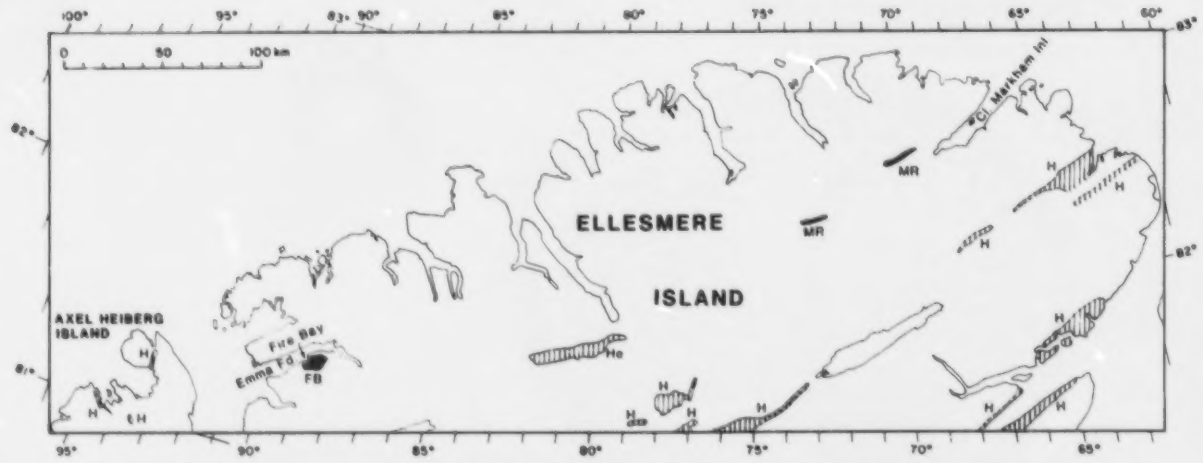

Figure 1. Generalized outcrop areas of Fire Bay (FB) and Mount Rawlinson (MR) assemblages, Hazen Formation (H), and Hazen Formation equivalent (He).

The volcanogenic deposits occur mainly in thick or massive beds that rarely show lamination. Their association with radiolarian chert and carbonate olistostromes (see below) suggests deposition in a deep water setting, possibly by concentrated sediment gravity flows, but it is unknown whether they are of detrital or pyroclastic origin.

One specimen of a flow rock consists of feldspar phenocrysts in a matrix of microfelsite. The feldspar is largely or entirely albite according to a whole-rock X-ray diffraction analysis. The rock is classified as "calc-alkaline rhyolite, K-poor series" on the basis of its major-element chemical composition (computer analysis, based on Irvine and Baragar, 1971).

The carbonate bodies, as mentioned, occur both in the chert suite and in the volcanogenic suite. They form lenses that are metres in length and thickness, but one body is about 100 m long. They are generally massive, but some are brecciated and others conglomeratic in texture, with carbonate cobbles embedded in a carbonate matrix. Samples studied in thin section show recrystallized lime mudstone, skeletal wackestone, skeletal grainstone, pelletal packstone and microcrystalline dolostone. Identifiable skeletal material was derived from bryozoans, echinoderms, trilobites, and algae, including Girvanella. These sediments originated in shelf environments (perhaps on volcanic edifices) and probably were redeposited in deep water settings by sliding and slumping.

AGE

Eight samples for conodont studies were taken from five different carbonate bodies (see Appendix). All of these produced conodont elements, but yields were small, ranging from two to nine specimens per sample. A total of only 31 identifiable specimens was recovered.

Diagnostic faunas are present in C-97241 and C-97242 (see Appendix): the presence of "*M*". *marathonensis* is suggestive of an early to middle Whiterockian age for C-97241, whereas the presence of *H. holodentata* suggests a late Whiterockian age for C-97242. Both are from the same small outcrop area, suggesting that it contains blocks of different ages. The fauna from C-97244 is suggestive of an early Whiterockian age based on the presence of *O. multicorrugatus*. It should be pointed out that Whiterockian is used herein as originally defined (Cooper, 1956) and not as revised to Series level by Ross et al. (1982). The remaining samples can be less precisely dated, but they could all be of Whiterockian age and are certainly no younger. The most common form recovered from the samples is "*Scolopodus*" *gracilis* Ethington and Clark. This species is not very biostratigraphically diagnostic, ranging in age from Early Ordovician (mid-Canadian) to early Middle Ordovician (Whiterockian).

The conodont Colour Alteration Index (CAI) varies from sample to sample (see Appendix) with a low of 2.5 and a high of 4, but 5 out of 7 samples that have been assigned indices are in the range 3 to 3.5. This relatively high variability within a small area (4 km^2 or less) may be due to the local effects of diabase dyke intrusion, folding, and faulting.

The limestones, because they are redeposited, could be slightly older than the associated chert and volcanogenic deposits, but large age discrepancies between resedimented limestones and the enclosing strata have never been encountered in the Franklinian deep water basin.

REGIONAL RELATIONSHIPS

The lower Paleozoic rocks of northern Ellesmere Island have recently been assigned to two major tectonic or depositional elements: the Pearya Terrane on the north coast of Ellesmere Island, and the Franklinian deep water basin on the southeast. The latter, in turn, is divisible into a northwestern sedimentary and volcanic subprovince (corresponding to the Clements Markham Fold Belt) and a southeastern sedimentary subprovince (corresponding to some extent to the Hazen Fold Belt) (cf. Trettin et al., 1987, Fig. 2). The two subprovinces are in fault contact and there is some evidence suggesting that the Clements Markham Fold Belt was involved in the sinistral strike slip inferred for Pearya (Trettin, 1987). Fire Bay lies within the sedimentary-volcanic subprovince (Clements Markham Fold Belt). Previously, the only Ordovician unit known to be exposed in that subprovince was the Mount Rawlinson assemblage of northeasternmost Ellesmere Island, (Fig. 1), which consists of volcanics, radiolarian chert, and carbonates (Trettin et al., 1987). The volcanics comprise altered flows and tuffs, classified as andesite, rhyodacite-dacite, and trachyandesite, on the basis of stable trace elements. One sample yielded a U-Pb (zircon) age of 454.7 + 9.7/- 4.5 Ma, early Caradoc (medial Ordovician) with confidence limits in the Llandeilo (Chazyan) and early Caradoc according to the time scale of Harland et al., 1989. The Mount Rawlinson assemblage is in fault contact with the Lands Lokk and Imina formations. It thus is broadly comparable to the Fire Bay assemblage in age, lithology and structural setting. Combined, the Fire Bay and Mount Rawlinson assemblages suggest a sediment-starved, deep water basin, receiving radiolarian chert, with arc- type volcanic edifices that locally were capped by carbonate shelves.

The Fire Bay and Mount Rawlinson assemblages are correlative with a part of the Hazen Formation, which in Ellesmere Island represents the sedimentary subprovince of the Franklinian deep water basin. It ranges in age from latest Early Cambrian to Early Silurian (middle Llandovery) and consists of radiolarian chert, resedimented carbonates, and mudrock. During the Middle Ordovician, chert and minor claystone dominated deposition in the northern and central parts of the subprovince, and resedimented carbonates the southern part, but the facies boundary cannot be delineated precisely because of limited age control. The formation also occurs in northern Axel Heiberg Island. There it also is nonvolcanic but lies within a belt that contains older and younger volcanics.

In conclusion, the new fossil evidence from Fire Bay has added a significant control point to the regional facies map for the Middle Ordovician. Further fieldwork is required to delineate the contact between the Fire Bay assemblage and the Lands Lokk assemblage in the Fire Bay inlier and to establish whether other occurrences of felsic volcanic rocks

in the Emma Fiord region are part of the Lands Lokk Formation - as previously assumed - or fault slices of Ordovician rocks.

ACKNOWLEDGMENTS

We are indebted to U. Mayr for improvements to the manuscript, and to T. Uyeno for a preliminary inspection of the conodonts; he was the first to recognize their Middle Ordovician age.

REFERENCES

Cooper, G.A.
1956: Chazyan and related brachiopods; Smithsonian Miscellaneous Collection, v. 127, two parts, 1245 p.

Harland, W.B., Armstrong, R.L., Cox, A.V., Craig, L.E., Smith, A.G., and Smith, D.G.
1989: A geologic time scale 1989; Card published by The British Petroleum Company (by arrangement with Cambridge University Press); first edition July, 1989

Irvine, T.N. and Baragar, W.R.A.
1971: A guide to the chemical classification of the common volcanic rocks; Canadian Journal of Earth Sciences, v. 8, p. 523-548.

Ross, R.J., Jr., Adler, F.J., Amsden, T.W., Bergstrom, D., Bergström, S.M., Carter, C., Churkin, M., Cressman, E.A., Derby, J.R., Dutro, J.T., Jr., Ethington, R.L., Finney, S.C., Fisher, D.W., Fisher, J.H., Harris, A.G., Hintze, L.F., Ketner, K.B., Kolata, D.L., Landing, E., Neuman, R.B., Sweet, W.C., Pojeta, J., Jr., Potter, A.W., Rader, E.K., Repetski, J.E., Shaver, R.H., Thompson, T.L., and Webers, G.F.
1982: The Ordovician System in the United States; International Union of Geological Sciences Publication no. 12, 73 p.

Trettin, H.P.
1969: Pre-Mississippian geology of northern Axel Heiberg and northwestern Ellesmere islands, Arctic Archipelago; Geological Survey of Canada, Bulletin 171, 82 p.
1987: Investigations of Paleozoic geology, northern Axel Heiberg and northwestern Ellesmere islands; *in* Current Research, Part A, Geological Survey of Canada, Paper 87-1A, p. 357-367.

Trettin, H.P., Parrish, R., and Loveridge, W.D.
1987: U-Pb age determinations of Proterozoic to Devonian rocks from northern Ellesmere Island, Arctic Canada; Canadian Journal of Earth Sciences, v. 24, p. 246-256.

APPENDIX OF LOCALITIES AND FAUNAL LISTS

(Identifications by G.S. Nowlan)

All localities are within a few kilometres east, northeast, or southeast of the head of Fire Bay (Cape Stallworthy map area, NTS 560 D). A detailed map or enlarged air photograph of this area will be published when the fieldwork has been completed.

Field station no. 88-TM-203A; about 1 km ENE of head of Fire Bay; UTM Zone 16X, 9045600mN, 473300mE. A small area (metres in diameter) with carbonate outcrops, is sourrounded by poorly exposed radiolarian chert, siliceous submarine tuff, etc. Both limestone samples are skeletal grainstones with fragments of echinoderms, bryozoans and algae, including *Girvanella*.

C-97241: field sample no. 88-TM-203A-1; outcrop; mass dissolved: 3285 g (97 % breakdown). Fauna: (CAI 2.5) *Erraticodon*? sp.; "*Microzarkodina*" *marathonensis* (Bradshaw); *Parapanderodus striatus* (Graves and Ellison); *Protopanderodus* sp.; "*Scolopodus*" *asymmetricus* (Barnes and Poplawski)

C-97242: field sample no. 88-TM-203A-2; outcrop; mass dissolved: 2842 g (91 % breakdown). Fauna: (CAI indeterminate) *Histiodella holodentata* Ethington and Clark; *Loxodus*? *curvatus* Stouge

Field station no. 88-TM-203E; about 2 km ENE of head of Fire Bay; UTM Zone 16X, 9045000mN, 473300mE; limestone lens, roughly 100 m long, partly brecciated; intercalated between volcanogenic sediments.

C-97243: field sample no. 88-TM-203E; talus; mass dissolved: 3237 g (95 % breakdown). Fauna: (CAI 3.5) ?*Drepanodus arcuatus* Pander; *Histiodella*? sp. "*Scolopodus*" *gracilis* Ethington and Clark; oistodontiform element indeterminate

Field station no. 88-TM-203F; about 3 km E of head of Fire Bay; UTM Zone 16X, 9044700mN, 474300mE; carbonate lens, tens of metres long, lying between volcanogenic sediments (above) and recessive chert etc. (below); nature of contacts uncertain; limestone samples are skeletal grainstones with fragments of bryozoans, trilobites, echinoderms and algae, including *Girvanella*.

C-97244: Field sample no. 88-TM-203F-1; outcrop; mass dissolved: 2270 g (91 % breakdown). Fauna: (CAI 4) *Erismodus*? sp.; *Oistodus multicorrugatus* Harris; "*Scolopodus*" *gracilis*

C-97245: Field sample no. 88-Tm-203F-3; talus; mass dissolved: 1283 g (94 % breakdown) Fauna: (CAI 3) *Parapanderodus striatus* (Graves and Ellison); "*Scolopodus*" *gracilis* Ethington and Clark

C-97246: Field sample no. 88-TM-203F-2; talus; mass dissolved: 1458 g (77 % breakdown). Fauna: (CAI 3?) *Ansella* sp.; "*Scolopodus*" *gracilis* Ethington and Clark

Field station 88-TM-204A; about 2 km ESE of head of Fire Bay; UTM Zone 16X, 9043400mN, 473300mE; lens of limestone conglomerate/breccia, metres in diameter, enclosed in radiolarian chert and slate; sample consists of brecciated, variably recrystallized lime mudstone with some fragmants of echinoderms and trilobites.

C-97247: Field sample no. 88-TM-204A; outcrop; mass dissolved: 2109 g (81 % breakdown). Fauna: (CAI 3.5) *Protopanderodus* sp.; "*Scolopodus*" *gracilis* Ethington and Clark

Field station 88-TM-204H; about 1.5 km ENE of head of Fire Bay; UTM Zone 16X, 9045600mN, 473300mE; limestone lens, metres in diameter, enclosed in volcanogenic sediments; sample consists of pelletal packstone with rare fragments of algae, trilobites and echinoderms.

C-97248: Field sample no. 88-TM-204H; outcrop; mass dissolved: 2011 g (77 % breakdown). Fauna: (CAI 3.5?) "*Scolopodus*" *gracilis* Ethington and Clark

Winnipegosis Pinnacle Reef play in Williston Basin, Saskatchewan and North Dakota: oil compositions and effects of oil-based drilling muds on exploration geochemistry

K.G. Osadetz, F. Goodarzi, L.R. Snowdon, P.W. Brooks, and S. Fayerman[1]
Institute of Sedimentary and Petroleum Geology, Calgary

Osadetz, K.G., Goodarzi, F., Snowdon, L.R., Brooks, P.W., and Fayerman, S., Winnipegosis Pinnacle Reef play in Williston Basin, Saskatchewan and North Dakota: oil compositions and effects of oil-based drilling muds on exploration geochemistry, in Current Research, Part D, Geological Survey of Canada, Paper 90-1D, p. 153-163, 1990.

Abstract

Understanding thermal maturity patterns in the developing Winnipegosis Pinnacle Reef oil play allows play fairway definition and prediction of oil density, two factors important to economic success. Maximum organic geochemical information can be obtained only if solvent extract compositions from stains and sources can be relied upon. Solvent extracted stains from the Alvstad and Golden pinnacles are compositionally similar to the Winnipegosis oil-source system. Information from these wells is used to outline the Winnipegosis Pinnacle Reef play fairway in the United States. Stains from the Steelman 2-14 well are contaminated by an oil-based drilling fluid. Petrographically their thermal maturity conforms to the regional pattern, but solvent extract saturate fraction hydrocarbon compositions have been drastically altered. Until thermal maturity and oil density patterns are better established, oil-based drilling fluids should be avoided.

Résumé

La détermination du rôle joué par les configurations de maturité thermique dans la formation de la zone pétrolière du pinacle récifal de Winnipegosis permet de définir le passage de la zone pétrolière et de prévoir la masse volumique du pétrole, deux facteurs d'importance économique. Pour obtenir tous les renseignements géochimiques organiques possibles, il faut que les compositions obtenues par extraction au solvant de taches et de roches mères soient exactes. Les taches extraites au solvant des pinacles d'Alvstad et de Golden sont de composition semblable à celle des roches mères de Winnipegosis. Les données recueillies dans ces puits sont utilisées pour délimiter le passage de la zone pétrolière du pinacle récifal de Winnipegosis aux États-Unis. Les taches du puits Steelman 2-14 sont contaminées par un fluide de forage à base d'huile. Pétrographiquement, leur maturité thermique correspond à celle de la configuration régionale, mais la composition des hydrocarbures de la fraction saturée extraite au solvant a été considérablement altérée. Jusqu'à ce que les configurations de maturité thermique et de masse volumique du pétrole soient davantage précisées, il faudra éviter d'utiliser des fluides de forage à base de pétrole.

[1] Exploration Geology, Gulf Canada Resources Inc., 401 - 9th Avenue S.W., P.O. Box 130, Calgary, Alberta T2P 2H7

INTRODUCTION

Explorationists can gain important information from organic geochemistry studies. Organic geochemistry can be used to identify potential petroleum source rocks, to correlate oils with their sources and to determine source rock and oil thermal maturities. Source rock characterization and oil-source correlations are used by explorationists in play fairway identification and prospect appraisal. Comprehensive hydrocarbon generation models (Powell and Snowdon, 1984) also associate hydrocarbon compositions and material characteristics of petroleum with thermal maturity and source rock type. Crude oil material characteristics including density (A.P.I. gravity) have important effects on engineering considerations and economic value.

Continuing exploration developments in the Winnipegosis Pinnacle Reef (Middle Devonian) play in southeastern Saskatchewan and western North Dakota indicate that oil density is important to economic success. The oil density variation pattern is not yet well known but densities are controlled primarily by the thermal maturity of source rocks charging a pool. Understanding the thermal maturity variations of oil pools and stains could contribute to the identification of a migration pathway and migration timing while at the same time predicting oil engineering qualities and economic values in untested prospects.

It is also important to determine the source of oils in Winnipegosis reservoirs . Effective source rocks occur in both the Winnipegosis Formation and the underlying Big Horn Group (Upper Ordovician) (Stasiuk and Osadetz, this volume; Osadetz et al., 1989). Winnipegosis prospects containing Ordovician-sourced oil (Leenheer and Zumberge, 1987) may indicate potential in deeper horizons in the same prospect. These analyses depend on reliable compositional characterization of both oils and solvent extracts from stained cores.

Spatial variations in reef porosity and complex lithostratigraphic relationships (Rosenthal, 1987) between Winnipegosis reefs and anhydrite rock bodies surrounding them demand precise well locations and increase the risk that targets will be reached in unfavorable facies, often narrowly missing production. Drilling in the Tablelands area (Table 1) illustrates these risks. Two unsuccessful wells were drilled at 16-15-2-9W2 and 6-27-2-9W2 before an oil discovery was completed in 6A-27-2-9W2. It is imperative to obtain the most useful geochemical information about source rocks and oil density, from dry wells, particularly if they are stained.

This paper compares solvent extract compositions from cores drilled with water-based muds to those drilled with oil-based mud to illustrate the effect that mud choice has on geochemical information obtained from cores. When water-based muds are employed, stains retain oil-source system compositional characteristics. Oil-based muds adversely contaminate cores and cuttings, preventing reliable use of organic geochemical techniques.

SETTING

Williston Basin is a cratonic petroleum province that dominates the central North American craton. Its major oilfields in Canada (Saskatchewan and Manitoba) and the United States (North Dakota, South Dakota and Montana) are significant petroleum resources.

WILLISTON BASIN SUCCESSION

The stratigraphic column is composed of six successions bounded by inter-regional unconformities. The oldest succession is Middle Cambrian to Lower Ordovician, predominantly Inner Detrital belt clastic sediments, deposited on the early Paleozoic miogeocline of western North America (Lefever et al., 1987). This succession is onlapped from the east by Middle Ordovician clastics and Upper Ordovician and Silurian carbonates, evaporites and minor clastics deposited in the epeiric seaway of eastern North America (Kendall, 1976; Vigrass, 1971).

After a significant erosional interval in the Late Silurian and Early Devonian, sedimentation resumed in the Middle Devonian (Wardlaw and Reinson, 1971; Edie, 1959) and continued without significant interruption into the Mississippian. Devonian and Mississippian strata consist of two stratigraphic successions, each exhibiting a distinctive style and pattern of deposition, and separated by a thin, uppermost Devonian shale, the Bakken Formation (Sandberg et al., 1983). Persistent basinal lithofacies are rare in the Williston Basin Paleozoic carbonate succession. Only in the later Middle Devonian, latest Devonian and earliest Mississippian are persistent basinal lithofacies developed.

The Upper Carboniferous and Permian succession present in American Williston Basin is generally absent in Canada. During Triassic and Jurassic time, the entire basin formed a depositional re-entrant on the western North American cratonic margin during its transformation from a miogeocline into an orogenic foreland. Succeeding Cretaceous and Tertiary formations, Columbian and Laramide orogenic foreland successions represent the final significant depositional episode (Stott, 1984). Except for the latest Cretaceous and Paleocene formations, the foreland successions are dominated by basinal lithofacies.

Tectonic setting controls both source rock deposition and thermal maturity (Osadetz et al., 1989). These differences make petroleum exploration in northern Williston Basin fundamentally different from that in the Alberta Basin. Potential petroleum source rocks in the Foreland successions are widespread but thermally immature in southeastern Saskatchewan. Paleozoic source rocks have limited distributions that, except for Ordovician strata, commonly mimic the distribution of persistent Paleozoic basinal lithofacies. Source rocks are rare because the basin is situated high in the central North American craton. Intrabasinal structures, unconformity bounded stratigraphic plays and

Table 1. Locations of oils, sources, and stains discussed in this paper

Oils

GSC NO.	POOL NAME	DEPTH (m)	LOCATION	ZONE
0466	No pool name	1080.3	05-33-010-32W1	Birdbear
0546	Freda Lake	1703.3	16-30-004-18W2	Ratcliffe
0551	Hummingbird	2313.5	10-26-002-19W2	Birdbear
0552	Kisbey	1620.5	07-27-007-06W2	Birdbear
0553	Hummingbird	2226.0	05-26-002-19W2	Bakken
0558	Hoffer	1940.0	05-30-001-15W2	Ratcliffe
0568	Hoffer	1944.5	09-27-001-15W2	Ratcliffe
0577	Flat Lake	1975.0	06-05-001-16W2	Ratcliffe
0755	Tableland	2601.0	04-36-002-10W2	Winnipegosis
0756	Tableland	2581.0	08-22-002-09W2	Winnipegosis
0802	Bienfait	2436.0	12-31-003-06W2	Winnipegosis
0841	Oxbow	2327.0	10-24-002-03W2	Winnipegosis
0842	Oxbow	2310.0	10-24-002-03W2	Winnipegosis
1009	Beaver Lodge		SW NE 19-156N-095W	Duperow
1011	Beaver Lodge		SW/4 01-155N-096W	Silurian
1017	Ambrose		SW NE 14-163N-099W	Duperow
1021	Dolphin		SW NE 29-161N-095N	Souris River
1093	Moraine		SW NW 36-161N-098W	Winnipegosis
6899	Golden	2532.0	SW SE 34-161N-087W	Winnipegosis
6903	Alvstad	3059.0	NW NE 29-157N-088W	Winnipegosis

Sources

#	Formation	Depth(m)	Location	Lithology
6744	Winnipegosis	2700.7	04-18-001-21W2	Kerogenous laminite
6785	Winnipegosis	2422.6	09-31-004-08W2	Biotb. limestone
6786	Winnipegosis	2560.4	08-01-004-09W2	Biotb. limestone
6854	Winnipegosis	88.1	14-12-045-26W1	Kerogenous laminite
6908	Winnipegosis	974.4	03-15-107-10W4	Kerogenous laminite
7100	Winnipegosis	2614.2	06-27-002-09W2	Biotb. dolowackestone
7097	Winnipegosis	2638.5	16-15-002-09W2	Kerogenous laminae
7098	Winnipegosis	2638.3	16-15-002-09W2	Kerogenous laminae
7099	Winnipegosis	2615.5	06-27-002-09W2	Laminated dolostone

Stains

#	Formation	Depth(m)	Location	Lithology
6742	Winnipegosis	2764.7	12-24-001-10W2	Dark brown laminite
6751	Winnipegosis	2017.0	03-03-001-11W2	Lam. dolst. & anhyd.
6752	Winnipegosis	2014.0	03-03-001-11W2	Lam. dolst. & anhyd.
6784	Winnipegosis	2336.3	07-24-004-05W2	Laminated limestone
6902	Winnipegosis	3135.2	NENE-05-161-95	Kerogenous laminite
6909	Winnipegosis	3674.2	NENW-35-156-93	Kerogenous laminite
7202	Winnipegosis	2269.0	02-14-05-05W2	Migrabitumen stain
7203	Winnipegosis	2275.5	02-14-05-05W2	Migrabitumen stain
7204	Winnipegosis	2276.5	02-14-05-05W2	Migrabitumen stain
####	Mud		02-14-05-05W2	Drilling mud

complex stratigraphic/diagenetic traps form the major oilfield trends in Williston Basin. This differs from the stratigraphic reef traps in basinal magnafacies that dominate Paleozoic exploration in Alberta. A persistent basinal magnafacies, like that common in the Alberta Basin, occurred in Williston Basin during Middle Devonian time.

WINNIPEGOSIS PETROLEUM PLAYS

During Upper Elk Point Group deposition (Middle Devonian) a major baselevel rise drowned much of the Lower Winnipegosis carbonate platform in Williston Basin. The Upper Winnipegosis lithosome is differentiated into three depositional settings. A carbonate platform undofacies dominates the area south of the fiftieth latitude. The edge of this carbonate platform is controlled by anomalous subsidence along the Ancestral Nesson Structure coinciding approximately with the 103rd meridian (Fig. 1). This large embayment separates the Winnipegosis and Elm Point platforms in Saskatchewan and Manitoba, respectively. North of the platform undofacies lies a starved basin, with pinnacle reefs, which accumulated a rich bituminous lime mudstone fondofacies. Lime mudstone clinofacies are sporadic, being best developed in the North Dakota portions of the basin (Ehrets and Kissling, 1987).

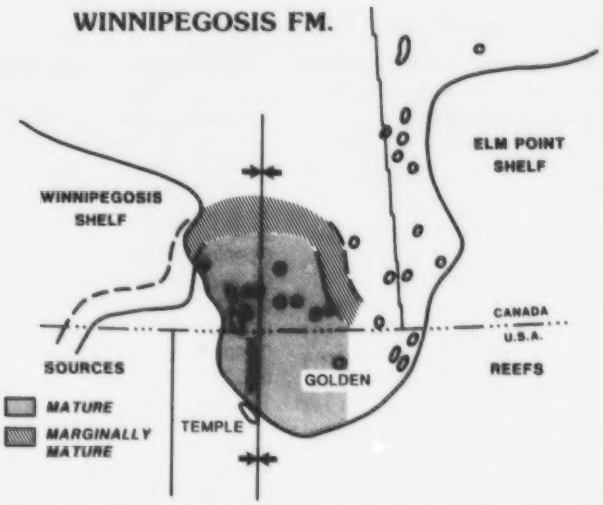

Figure 1. Upper Winnipegosis Formation shelf edge in Williston Basin and limits of thermal maturity for basinal fondofacies source rocks. Weyburn Embayment separates the Winnipegosis and Elm Point carbonate platforms.

Different Winnipegosis magnafacies have differing source rock potential. The richest source rocks occur in the bituminous, starved basin fondobeds. Informally known as the "Brightholme" member, these beds have excellent petroleum potential. They average 7.38 per cent Total Organic Carbon (TOC) and are inferred to have an initial hydrocarbon potential of approximately 615 kg/tonne (Osadetz and Snowdon, work in progress). Rosenthal (1987) indicated that this facies is between 1 and 15 m thick in Manitoba, whereas beds in cores from the Weyburn Embayment, the large embayment in the Upper Winnipegosis platform (Fig. 1), are up to 1 m thick, but average only 60 cm. There is a good possibility of thicker source rock intervals in the Weyburn Embayment because exploration practice attempts to avoid locating wells in, or coring sections of, basinal fondofacies.

In contrast, the lime mudstone clinofacies are very thick but have poor source rock potential, with only 0.59 per cent TOC on average. Thin beds of rich source rocks have been found at the maximum flooding surface between the Upper and Lower members of the Winnipegosis Formation. These 'platform' source rocks are inferred to be thin and extensive and have an unestablished petroleum potential.

Anomalous subsidence of the ancestral Nesson Structure localized rich Winnipegosis source rocks and pinnacle reefs in deeply buried parts of Williston Basin. Anomalous crustal heat flows associated with this structure enhanced hydrocarbon generation in this region, commonly elevating the oil window by more than 700 m (Fig. 1; Osadetz et al., 1989). Rich source rocks, pinnacle reef reservoirs and enhanced thermal maturity make an interesting exploration play where thermally mature source rocks cover more than four times the area of Rainbow, Zama and Shekilie sub-basins combined (including the American region). Using conservative source rock thickness estimates (60 cm to 1 m) and an expulsion efficiency of only 25 per cent, the oil expelled into secondary migration pathways is estimated to be up to approximately 317 million cubic metres (approximately two billion barrels).

The Winnipegosis Pinnacle Reef play (Edie, 1959), served as the stratigraphic model for the discoveries at Rainbow in northwestern Alberta (Bill Hyrhor, pers. comm., 1989). Following success at Rainbow, a renewed exploration effort in Saskatchewan, the Pheasant program, attempted to reevaluate Winnipegosis pinnacle reef potential. Most lands explored by this program were well north or west of the Weyburn embayment, the region now known to be thermally mature. Dome Petroleum Limited made a Winnipegosis reef discovery in the Tablelands area in 1976 (11-14-2-9W2), but the well was a poor producer, hampered by the precipitation of salt at the well bore, and was abandoned. Home Oil Company exploration exploited the initial Dome discovery in December 1986 by completing the (8-22-2-9W2) well and initiating current activities. Other important wells were drilled in North Dakota. The Shell Golden well and three other pinnacles were drilled but could not establish sustained commercial production (Ehrets and Kissling, 1987). Discoveries in combination plays at the updip edge of the Upper Winnipegosis shelf, characterized by Temple Field, North Dakota and in structures in the platform, such as at Raymond Field, Montana, have indicated additional important plays in the platform (Figs. 1, 2).

WINNIPEGOSIS OIL-SOURCE SYSTEMS IN WILLISTON BASIN

Winnipegosis source rocks (Fig. 3) produce compositionally distinctive oils (Fig. 2) (Brooks et al., 1988; Snowdon and Osadetz, 1988). These oils are particularly characterized by their low ratios of C_{23} tricyclic/C_{30} pentacyclic and tricyclic/tetracyclic terpanes (Table 2). These compositional characteristics are commonly accompanied by a predominance of C_{34} pentacyclic terpanes, generally attributed

Table 2. Select compositional characteristics of oils, sources, and stains

GSC No.	PROD. ZONE	%HC	S/A	Pr/Ph	23/30	Ts/Tm	D/R	S/R	bb/R	
OILS										
0466	Birdbear	91.1	1.49	1.47	0.04	0.47	1.21	0.59	0.74	
0546	Ratcliffe	36.5	0.81	0.86	0.25	0.34	0.51	0.88	1.38	
0551	Birdbear	90.7	1.37	1.20	0.08	0.44	1.51	1.01	1.08	
0552	Birdbear	91.1	1.32	1.17	0.07	0.48	1.14	0.94	1.17	
0553	Bakken	87.2	1.04	1.03	0.21	0.41	0.77	0.83	0.87	
0558	Ratcliffe	87.0	1.19	0.97	0.19	0.94	1.53	0.93	1.62	
0568	Ratcliffe	81.4	0.97	0.75	0.09	0.97	1.56	1.07	0.80	
0577	Ratcliffe	65.8	1.59	1.05	0.14	0.94	1.90	1.10	0.83	
0755	Winnipegosis	89.5	2.59	0.62	0.08	1.12	1.58	1.17	1.34	
0756	Winnipegosis	93.6	2.51	0.75	0.09	1.16	1.73	1.09	1.30	
0802	Winnipegosis	86.3	1.51	0.83	0.12	0.69	0.95	0.78	0.73	
0841	Winnipegosis	59.6	1.02	0.81	0.04	0.42	0.57	0.74	0.81	
0842	Winnipegosis	71.1	1.10	0.79	0.03	0.30	0.69	0.77	0.60	
1009	Duperow	97.0	3.46	0.96	0.37	8.69	5.42	1.79	1.87	
1011	Silurian	95.9	7.34	0.83	CRACKED					
1017	Duperow	93.5	1.56	1.39	0.24	0.94	4.42	1.25	0.80	
1021	Souris River	95.8	3.29	0.55	1.21	17.62	7.76	1.10	0.66	
1093	Winnipegosis	94.0	2.69	1.23	0.96	10.77	6.50	1.34	1.28	
6899	Winnipegosis	66.8	1.90	0.50	0.09	0.70	1.17	1.25	0.70	
6903	Winnipegosis	23.0	0.60	1.18	0.02	0.45	3.47	0.90	0.97	
SOURCE ROCK SOLVENT EXTRACTS										**TOC**
6854	Winnipegosis	10.9	0.24	0.78	0.12	0.73	0.10	0.12	0.28	1.75
6908	Winnipegosis	20.2	0.16	0.59	0.59	0.12	0.82	0.75	0.86	17.53
6785	Winnipegosis	17.1	0.32	1.90	0.18	0.87	5.28	1.24	1.54	2.24
6786	Winnipegosis	29.5	0.77	2.22	0.34	0.86	6.33	0.95	1.09	0.86
7100	Winnipegosis	29.0	0.46	0.74	0.24	1.81	2.56	2.05	2.18	1.96
7099	Winnipegosis	42.5	0.94	0.83	0.20	1.60	2.06	1.32	1.22	0.40
7098	Winnipegosis	36.0	0.64	0.92	0.41	2.67	5.04	1.12	1.16	0.64
7097	Winnipegosis	20.3	0.27	1.10	0.48	2.18	3.75	1.36	1.08	2.36
6744	Winnipegosis	31.7	0.69	0.65	0.04	0.61	1.02	1.07	0.36	4.68
STAINS										
7202	Winnipegosis	67.2	1.60	1.64	1.68	0.48	7.33	1.22	1.78	
7203	Winnipegosis	38.2	0.70	1.45	0.73	0.29	4.47	0.98	1.13	
7204	Winnipegosis	63.4	1.50	1.27	1.28	0.50	6.30	0.90	1.03	
#### Mud				1.47	2.20	1.22	6.00	0.82	1.63	
6752	Winnipegosis	50.8	2.00	0.67	0.07	3.27	4.17	1.22	1.22	
6751	Winnipegosis	73.0	2.58	0.41	1.04	51.70	2.64	1.09	1.00	
6784	Winnipegosis	25.2	1.06	0.78	0.07	0.52	0.42	0.75	0.33	
6742	Winnipegosis	55.3	2.46	0.84	0.30	3.02	3.67	1.26	1.60	
6902	Winnipegosis	73.8	3.05	0.90	3.04	2.10	5.54	0.17	0.63	
6909	Winnipegosis	51.8	2.06	1.88	1.38	6.86	7.09	1.11	1.28	

to hypersaline depositional environments, a feature present in oils from pinnacle reefs (Table 2), but not always developed in 'platform' source rocks (Table 2). Winnipegosis terpane distributions are similar to Upper Ordovician Big Horn Group kukersitic source rocks and their oils (Brooks et al., 1987). Fortunately, the Ordovician oil-source system has a distinctive C_{15}+ Saturate Fraction Gas Chromatogram (SFGC) and oils from Ordovician sources can be distinguished from Winnipegosis oils by their lack of pristane and phytane accompanying both a pronounced even/odd predominance in n-alkanes in the range C_{17}-C_{20} and a low abundance of higher molecular weight n-alkanes (ibid.). Winnipegosis sourced oils have SFGC compositions overlapping Lodgepole and Bakken oil compositions. Some oils now assigned to a Winnipegosis source (Table 1) were originally associated with Bakken-sourced oils, although their distinctive compositions were recognized by Brooks et al. (1987).

Using these compositional criteria, it has been possible to identify 13 oil pools or stained reservoirs from Winnipegosis source rocks in Williston Basin (Table 1). Four other pools can be inferred to be sourced by Winnipegosis source rocks, even though their biological markers (terpanes) are thermally cracked (Table 1). The possibility that these oils are from Ordovician source rocks can be discounted because their SFGC's are not diagnostic of the Ordovician oil-source system and there is an absence of other identified, effective

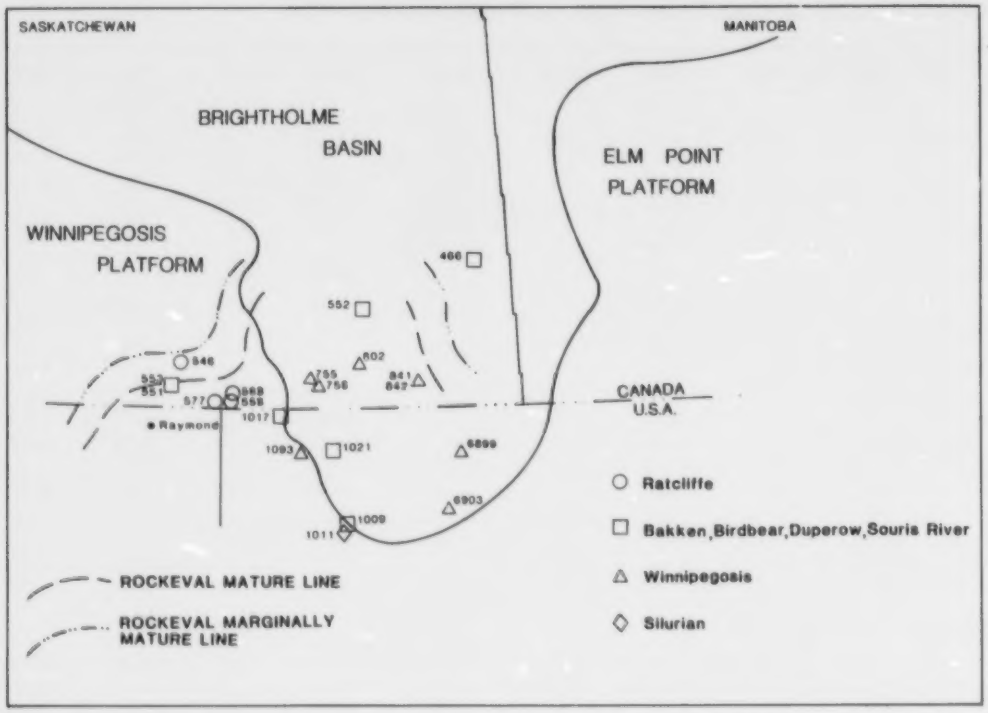

Figure 2. Location and stratigraphic position of oils and stains from reservoirs attributed to Winnipegosis source rocks mentioned in this study. Limits of fondofacies source rock thermal maturity and shelf edge from Figure 1.

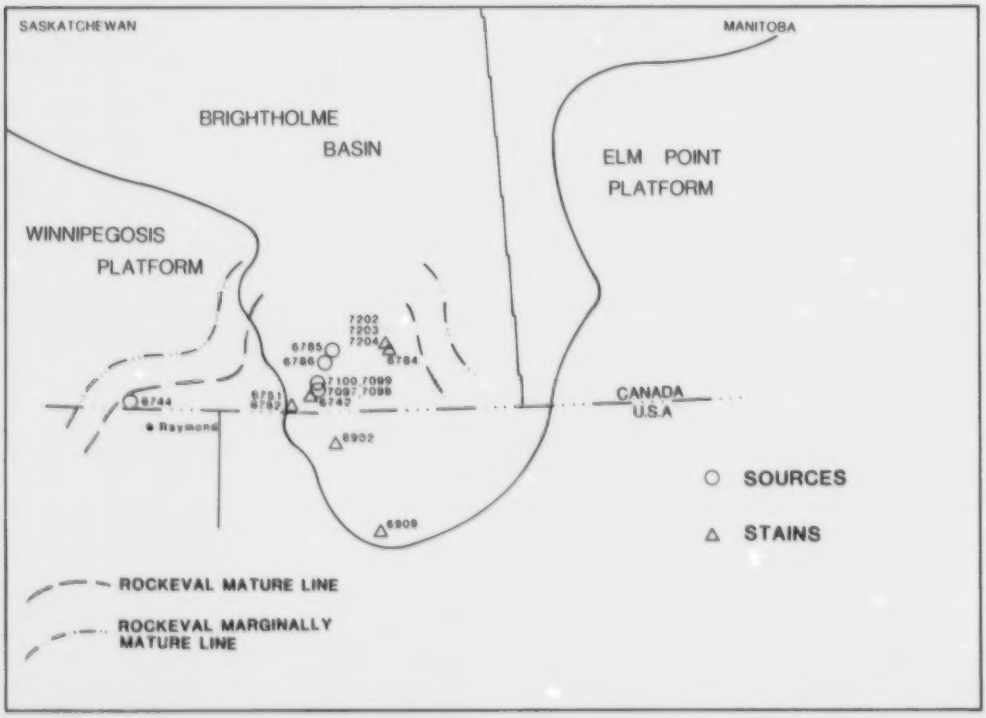

Figure 3. Location of source rocks and stains solvent extracted for this study. Limits of fondofacies source rock thermal maturity and shelf edge from Figure 1.

source rocks within this stratigraphic interval. The Winnipegosis pool in a platform structure at Raymond, Montana has an SFGC composition identical to Ordovician oils (Leenheer and Zumberge, 1987).

EXPERIMENTAL

Oil gross compositions were determined using techniques similar to those discussed by Snowdon (1978). Gasoline fractions and $C_{15}+$ saturate fractions were analyzed chromatographically. Gasoline range compositional analysis followed techniques similar to those outlined by both Thompson (1979) and Snowdon and Powell (1979). $C_{15}+$ saturate fractions were examined by capillary column gas chromatography (GC) using a VARIAN 3700 gas chromatographer equipped with a 25 m fused-silica column coated with OV-1, and temperature programmed from 50 to 280°C at a heating rate of 4 degrees per minute (using He as the Carrier gas). $C_{15}+$ saturate fraction capillary column gas chromatography-mass spectrometry (GC-MS) of oils and solvent extracts was performed using either a KRATOS MS-80RF mass spectrometer under the control of a DS-55 data system or a VG 70SQ hydbrid gas chromatography-mass spectrometer-mass spectrometer (GC-MS-MS) to duplicate GC-MS conditions. GC-MS conditions were typically: J and W 25m DB5 column temperature programmed from 50 to 320 degrees C at 4 degrees per minute, and coupled directly to the source of the mass spectrometer, a 300 microA filament emission current and 70 eV ionization potential. Data were collected by either full mass spectra scanning or by multiple ion detection (M.I.D.), monitoring ions at m/z 177.1638, 191.1794, 217.1950, 218.2028, 231.2106, and 259.2262.

Source rocks were identified and characterized using Rock-Eval/TOC anhydrous pyrolysis. TOC from stains was also analyzed by Rock-Eval/TOC. Bituminous material was extracted from source rocks and stains using Soxhlet technique and fractionated using packed column chromatography following a method effectively similar to that published by Snowdon (1978). Extracts from stains include both oil pool reservoirs that were used to characterize oil pools for which a fluid sample could not be obtained and residual stains on migration pathways. Extracts from unstained source rocks were used to characterize source rocks. Various fractions obtained from packed column fractionations were used to characterize the solvent extract gross compositions. Saturate fractions were further characterized by SFGC and GC-MS or GC-MS-MS following methods similar to those used to characterize the $C_{15}+$ saturate fraction of oils.

Binocular and organic petrographic observation of three core samples from the Steelman well were performed to determine the nature of the bitumen occurrence and its thermal maturity. The composition of these three stains was characterized in the same way as the other stains, as was the hydrocarbon composition of oil-based mud used during the drilling of the Steelman well.

STAINS IN THE GOLDEN AND ALVSTAD PINNACLES

Sustained commercial production of oil from Winnipegosis pinnacle reefs remains to be established in North Dakota. Oil stained samples were collected from wells coring the pinnacle reef facies at Golden (6899) and Alvstad (6903) in North Dakota (Table 1; Fig. 2). Although the mud system composition is unknown in both cases, the solvent extracts from these stains are compositionally similar to oils in commercially producing Winnipegosis reefs in Canada (Table 1; Fig. 2). In particular, these stains have low ratios of C_{23} tricyclic/C_{30} pentacyclic terpanes, low ratios of tricyclic/tetracyclic terpanes and a marked predominance of C_{34} pentacyclic terpanes (Table 2; Fig. 4). A Winnipegosis source rock for these stains is confirmed by inspection of the SFGC, the only way to distinguish Winnipegosis sourced oils from those sourced by Ordovician kukersites.

These stains were instrumental in defining the play fairway in the American part of the basin (Fig. 1). The oil at Golden is only marginally mature, essentially comparable to oils at Oxbow (841 and 842). Regions shallower than Golden are expected to be thermally immature. When combined with data from Canadian source rocks and oils they define a huge, thermally mature, prospective area that is approximately 4 times that included by the Rainbow, Zama, and Shekilie sub-basins of northwestern Alberta.

STAINS IN THE STEELMAN 2-14 WELL

Types of staining

The use of an oil-based mud for the drilling of Gulf et al. Steelman 2-14 (02-14-005-05W2) (Table 1; Fig. 3) provided an opportunity to study the extent to which an oil-based mud affects exploration geochemistry. Two types of staining are obvious. The first is a pervasive, light coloured, volatile stain of similar odour to the drilling fluid. The second type of stain is a very dark brown to black, viscous bitumen, staining stylolites and pores.

Organic petrology

Organic petrology results are listed in Table 3. The light, volatile stain coats the entire rock except nonporous portions that remain unstained on fresh broken surfaces. This stain is attributed to the drilling fluid. The dark stains restricted to stylolites and larger pores is a migrated bitumen (Jacob, 1984). Observation 5, sample 7203 (2275.5 m) contains liptodetrinite, and several samples contain fluorescing acritarchs and Tasmanales. Some bitumens indicate thermal maturity of this material; for example, sample 7202 (2269 m) and the first observation on sample 7204 (2276.5 m). The observed bitumen reflectances (Rb), 0.517 and 0.512 (Table 3) are related to equivalent vitrinite reflectances (Rv), by the relation (Jacob, 1985):

$$Rv = 0.618(Rb) + 0.400$$

Using this relation, the inferred equivalent vitrinite reflectances are:

Rb = 0.512 => Rv = 0.716
Rb = 0.517 => Rv = 0.720

Saturate fraction of extractable hydrocarbons

Three migrated bitumen samples were isolated from the core and extracted using the Soxhlet technique (Table 1; Fig. 3). Sample 7203 (2275.5 m) comes from a thick seam in a stylolite that was cleanly separated from other rock material. The other two samples included stains both on stylolitic surfaces and in intercrystalline porosity and could not be cleanly separated from the rock matrix.

Table 3. Organic petrography

Depth	Observation	#	Rmin	Rmax	Rmean	sigma²
2269	1	14	0.492	0.573	0.517	0.026
2275.5	1	2	0.378	0.390	0.384	0.008
2275.5	2	10	0.507	0.567	0.539	0.017
2275.5	3	9	0.618	0.666	0.637	0.018
2275.5	4	18	0.777	0.858	0.815	0.022
2275.5	5	12	0.864	1.009	0.926	0.051
2276.5	1	5	0.504	0.525	0.512	0.007
2276.5	2	13	0.621	0.666	0.639	0.015

# = number of measurements
Rmin = minimum reflectance
Rmax = maximum reflectance
Rmean = mean reflectance
sigma² = standard deviation

The select saturate fraction compositional characteristics of extracts from these stains are listed in Table 2 with the mud and other stains. A stain from a well, sample 6784, in the township adjacent to the Steelman 2-14 well is also important. The Steelman stains are characterized by high ratios of pristane/phytane, tricyclic/pentacyclic terpanes and diasteranes/regular steranes. The values of these ratios are consistently lower in sample 7203 although even 7203 has much higher values than the nearby stain 6784. All of these differences suggest contamination of the Steelman 2-14 solvent extracts.

DISCUSSION

The compositions of stains from the Steelman 2-14 well can be compared with those of the oils, sources and other stains to determine the effects of using oil-based drilling fluid on saturate fraction organic geochemistry (Table 2). Critical compositional characteristics have been cross-plotted (Figs. 4, 5) to illustrate compositional variation among these samples. Most samples of oils and source rocks fall into fields defined by diasterane/regular sterane <5.00, C_{23} tricyclic/C_{30} pentacyclic terpane <0.30 and $0.50 <$ bb/R <2.00 (Figs. 4, 5). Two immature source rocks and one immature stain have values of a C_{29} sterane thermal maturity indicator, bb/R, <0.50, but otherwise fall within the

Figure 4. Cross-plot of diasterane/regular sterane ratio and C_{23} tricyclic/ C_{30} pentacyclic terpane ratio for oils, stains and source rocks from Table 2. Notice both the distribution of samples into fields following critical ratios discussed in the text and the position of samples from the Steelman 2-14 well with respect to the nearby stain 6784 and nearby oils from Bienfait (802) and Oxbow (840 and 841).

compositional fields characteristic of the Winnipegosis oil-source system. This compositional group, including the two immature samples, includes all samples with a C_{34} pentacyclic terpane predominance.

Another distinctive set of samples lies in the fields defined by diasterane/regular sterane >5.00 and 0.50 < bb/R <2.00 (Figs. 4, 5). Most of these samples generally have independent evidence of thermal cracking that has altered biological marker compositional ratios. Others, like 6785, a source rock in the Lower member of the Winnipegosis Formation, are from uncommon source rock facies and may not conform to the compositional traits of the fondobed source rocks. Two of the Steelman 2-14 stains also lie in this field.

A third, poorly populated field is characterized by ratios of diasterane/regular sterane <5.00 and C_{23} tricyclic/C_{30} pentacyclic terpane >0.30 (Figs. 4, 5). Of the four samples in this field one is a source rock from the Alberta part of the basin, far removed from the Weyburn Embayment, two are samples that are part of pairs of samples whose geographic counterparts lie in another field and one, 7203, is a stain from the Steelman 2-14 well.

Of these three compositional groups, those falling in the field defined by ratios of diasterane/regular sterane < 5.00 and C_{23} tricyclic/C_{30} pentacyclic terpane < 0.30 are characteristic of the Winnipegosis oil-source system. Those in the field defined by ratios of diasterane/regular sterane >5.00 are in general thermally cracked, and those in the final field, with ratios of diasterane/regular sterane <5.00 and C_{23} tricyclic/C_{30} pentacyclic terpane >0.30, are of other affinities.

The three stains from the Steelman 2-14 well are compositionally distinct from both nearby oils (Figs. 2, 3), in the Bienfait and Oxbow pools (802, 841 and 842) and the stain 6784. The composition of those oils and that stain are generally similar. All have low C_{23} tricyclic/C_{30} pentacyclic ratios, C_{34} pentacyclic terpane predominance, and S/R sterane ratios, a thermal maturity indicator, between 0.74 and 0.78 (Table 2; Fig. 6). In contrast, the Steelman stains have S/R sterane ratios greater than 0.90.

Although not yet well defined, thermal maturity and oil variations in pinnacle reef pools show indications of systematic variation (Fig. 6). Both oils in deeper parts of the basin and those closer to the hinge of the Nesson Anticline have greater thermal maturity. Although vertically migrated oils like the Kisbey Birdbear pool (552) do not conform to this pattern, the thermal maturity in pinnacle reef oils appears to conform (Fig. 6). Within current understanding it appears that pinnacle reefs are relatively locally sourced. As of yet no discoveries of oil have been made in pinnacle reefs updip of the region of thermally mature source rocks. It is, therefore, expected that stains in the vicinity of Bienfait (802) and Oxbow (841 and 842) oil pools should have similar thermal maturities to those pools. This is true of the stain 6784 but not for the three stains from the Steelman 2-14 well.

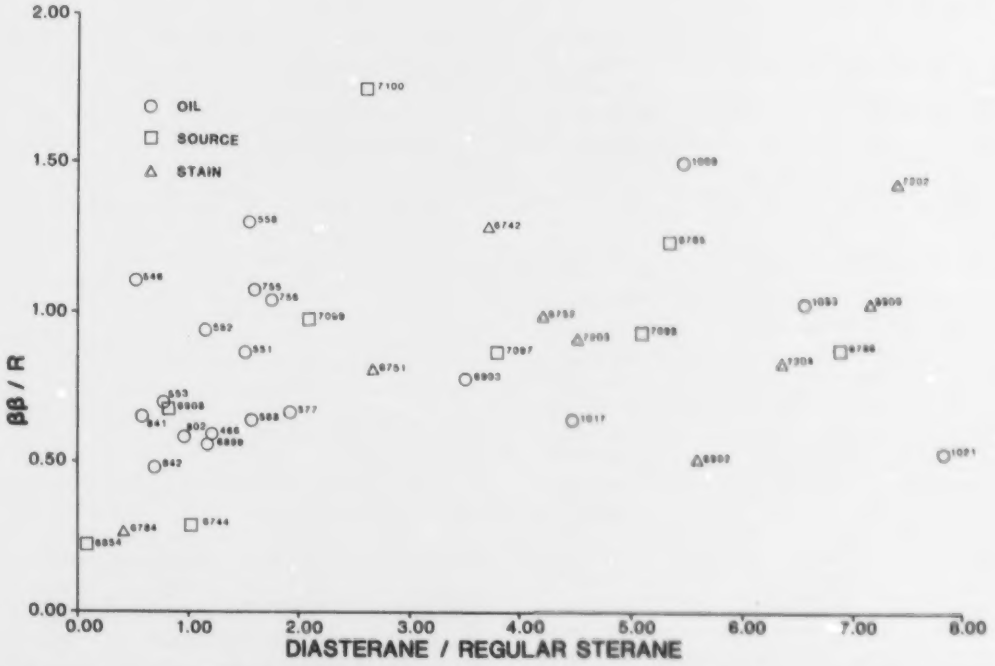

Figure 5. Cross-plot of diasterane/regular sterane ratio and C_{29} beta beta/R sterane thermal maturity indicator for oils, stains and source rocks from Table 2. Notice both the distribution of samples into fields following critical ratios discussed in the text and the position of samples from the Steelman 2-14 well with respect to the nearby stain 6784 and nearby oils from Bienfait (802) and Oxbow (840 and 841).

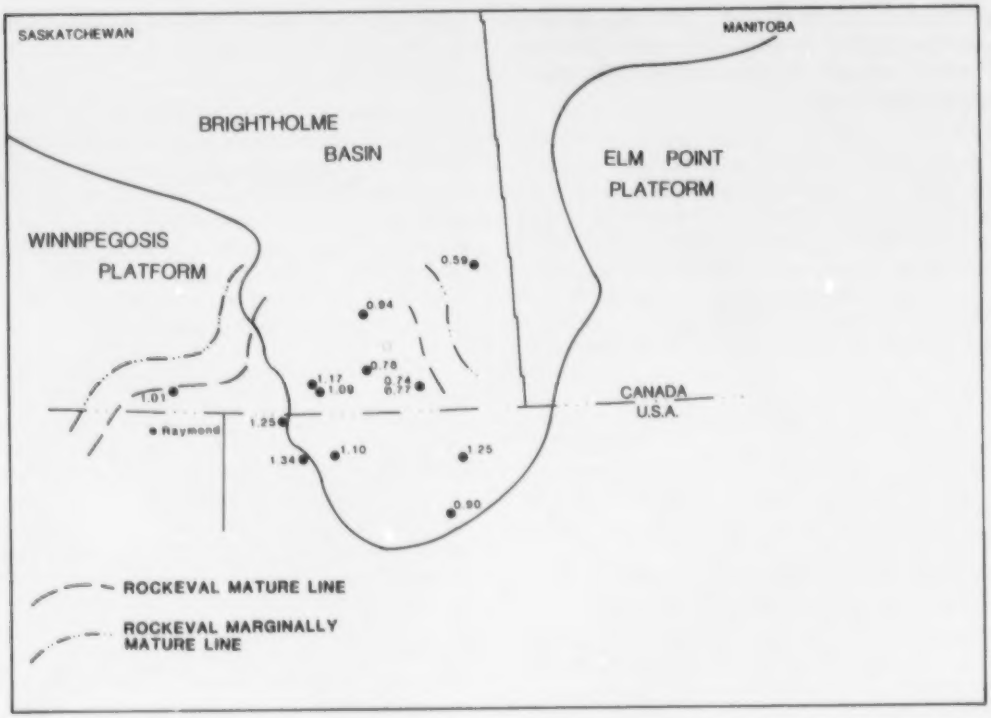

Figure 6. Geographic variation of C_{29} S/R sterane thermal maturity indicator for oils (closed circles). The figure also indicates the location of the Steelman well (open circle). Limits of fondofacies source rock thermal maturity and shelf edge from Figure 1.

We believe that the stains in the Steelman 2-14 well actually conform to this pattern of short distance migration and thermal maturity but that they have been contaminated by the drilling fluid. This can be demonstrated with reference to the petrographic characteristics of the Steelman 2-14 migrabitumen (Table 3). Bein and Sofer (1987) employ a relation, attributed to Zumberge, between Rv and the C_{29} S/R sterane ratio:

$$Rv = 0.487\ (20S/20R) + 0.333$$

Rearrangement of this relationship allows inference of what the 20S/20R ratio for these stains should be, based upon their petrographic characteristics. Using the reflectance determined here, the 20S/20R ratios for these stains should be approximately 0.79. The 20S/20R ratio inferred from petrographic properties is consistent with the value obtained from oil pools and stains closest to the Steelman 2-14 well but significantly different from the solvent extract of these samples.

We conclude that the lack of agreement between the petrographic thermal maturity of stains from Steelman 2-14 and the biological marker thermal maturity indicators indicates contamination of the saturate fraction of the Steelman 2-14 stains by the drilling fluid. The possibility that these compositional traits result from a different source rock are unlikely, because the terpanoid alkanes of Ordovician source rocks and the other effective source of oils for Winnipegosis reservoirs resemble those of Winnipegosis source rocks. No other effective source rocks are known to supply oils to this stratigraphic interval. Pristane/phytane ratios of the Steelman stains more closely resemble the drilling fluid than Winnipegosis oils in the same area.

Notably, sample 7203, which could be most effectively physically isolated from the pervasive, light coloured, volatile stain that contaminates the core, has a composition that is closest to the field of Winnipegosis oils on the cross-plot of diasterane/regular sterane versus C_{23} tricyclic/C_{30} pentacyclic terpanes (Fig. 4), even though there is a strong mismatch of thermal maturity indicators (Table 2; Fig. 5). This suggests that the effects of contamination can be reduced but not eliminated by physical isolation of different modes of bitumen occurrence.

The favorable conditions that allowed the physical separation of bitumens in this well cannot always be expected. Nor could indigenous bitumen compositions be inferred using a simple mixing model with the drilling fluid. The sterane S/R ratios for the stains in the Steelman well are not intermediate in value between those characteristic of Winnipegosis oils in that region and the composition of the drilling fluid. Similarly, the Ts/Tm thermal maturity indicators do not appear to have been altered using a simple mixing rule.

CONCLUSIONS

The Winnipegosis oil-source system in the Weyburn Embayment is best characterized by its terpanoid alkane composition. Although the terpanoid alkane compositions of Ordovician source rocks and their oils are similar to those of Winnipegosis oils and their source rocks, the Ordovician oils and sources can be distinguished from the Winnipegosis oils and sources using the $C_{15}+$ SFGC composition. Solvent-extracted saturate fractions from stains in the Golden and Alvstad pinnacles are comparable in composition to the oils and provide useful information that can be used to extend the play fairway into the United States. Three migrabitumens in the Steelman 2-14 well are contaminated by the drilling fluid. The correlation of these stains to their source rocks is not determinable from their solvent extract saturate fraction compositions. If the Williston Basin oil-source systems were less well understood it would be unlikely that these contaminated stains could have been correlated to their source rocks. Had it not been for petrographic techniques, the correct migrabitumen thermal maturities could not have been determined. Thermal maturity appears to control oil density. The best estimates of oil density are made from either petrographic observations or saturate fraction molecular compositions. Saturate fraction molecular compositions can be determined unambiguously if water-based drilling fluids are used but are obscured when oil-based drilling fluids are used. Until the pattern of oil density and thermal maturity is better established, we recommend avoidance of oil-based drilling fluids.

REFERENCES

Bein, A. and Sofer, Z.
1987: Origin of oils in Helez region, Israel — Implications for exploration in the eastern Mediterranean; American Association of Petroleum Geologists, Bulletin, v. 71, no. 1, p. 65-75.

Brooks, P.W., Osadetz, K.G., and Snowdon, L.R.
1987: Families of oils in southeastern Saskatchewan; *in* Proceedings of the Fifth International Williston Basin Symposium, ed. C.G. Carlson and J.E. Christopher; Bismark, North Dakota, June 15-17, 1987, Saskatchewan Geological Society, Special Publication no. 9, p. 253-264.
1988: Geochemistry of Winnipegosis discoveries near Tablelands, Saskatchewan; *in* Current Research, Part D, Geological Survey of Canada, Paper 88-1D, p. 11-20.

Edie, R.W.
1959: Middle Devonian sedimentation and oil possibilities, central Saskatchewan, Canada. American Association of Petroleum Geologists, Bulletin, v. 43, no. 5, p. 1026-1057.

Ehrets, J.R. and Kissling D.L.
1987: Winnipegosis platform margin and pinnacle reef reservoirs, northwestern North Dakota; *in* Core Workshop Volume, Fifth International Williston Basin Symposium, ed. D.W. Fischer; June, 1987, North Dakota Geological Survey, Miscellaneous Series 69, p. 1-31.

Jacob, H.
1984: Migrabitumen. International committee for coal petrology, Commission II Session, Calgary, 1984, 11 p.
1985: Dispersed solid bitumens as an indicator for migration and maturity in prospecting for oil and gas; Erdöl und Kohle Erdgas Petrochemie, v. 8, p. 356.

Kendall, A.C.
1976: The Ordovician carbonate succession (Bighorn Group) of southern Saskatchewan. Saskatchewan Department of Mineral Resources, Report 180, 185 p.

Leenheer, M.J. and Zumberge, J.E.
1987: Correlation and thermal maturity of Williston Basin crude oils and Bakken source rocks using terpane biomarkers; *in* Williston Basin: anatomy of a cratonic oil province, ed. M.W. Longman; Rocky Mountain Association of Geologists, Denver, Colorado, p. 2870-2898.

Lefever, R.D., Thompson, S.C., and Anderson, D.B.
1987: Earliest Paleozoic history of the Williston Basin in North Dakota; *in* Proceedings of the Fifth International Williston Basin Symposium, ed. C.G. Carlson and J.E. Christopher; Bismark, North Dakota, June 15-17, 1987, Saskatchewan Geological Society, Special Publication no. 9, p. 22-36.

Osadetz, K.G., Snowdon, L.R., and Stasiuk, L.D.
1989: Association of enhanced hydrocabon generation and crustal structure in the Canadian Williston Basin; *In* Current Research, Part D, Geological Survey of Canada, Paper 89-1D, p. 35-47.

Powell, T.G. and Snowdon, L.R.
1984: A composite hydrocarbon generation model: implications for evaluation of basins for oil and gas; Erdöl und Kohle Erdgas Petrochemie, Bd. 36, Heft 4, p. 163-170.

Rosenthal, L.R.
1987: The Winnipegosis Formation of the northeastern margin of the Williston Basin; *in* Proceedings of the Fifth International Williston Basin Symposium, ed. C.G. Carlson and J.E. Christopher; Bismark, North Dakota, June 15-17, 1987, Saskatchewan Geological Society, Special Publication no. 9, p. 37-46.

Sandberg, C.A., Gutschick, R.C., Johnson, J.G., Poole, F.G., and Sando, W.J.
1983: Middle Devonian to late Mississippian history of the overthrust belt region, western United States; Rocky Mountain Association of Geologists, Geologic Studies of the Cordilleran Thrust Belt, v. 2, p. 691-719.

Snowdon, L.R.
1978: Organic geochemistry of the Upper Cretaceous/Tertiary delta complexes of the Beaufort Mackenzie Sedimentary Basin; Geological Survey of Canada, Bulletin 291.

Snowdon, L.R. and Osadetz, K.G.
1988: Geological processes interpreted from gasoline range analyses of oils from southeast Saskatchewan and Manitoba; *in* Current Research, Part D, Geological Survey of Canada, Paper 88-1D, p. 33-40.

Snowdon, L.R. and Powell, T.G.
1979: Families of crude oils and condensates in the Beaufort-Mackenzie Basin; Bulletin of Canadian Petroleum Geology, v. 27, no. 2, p. 139-162.

Stasiuk, L.D. and Osadetz, K.G.
1990: The life cycle and phyletic affinity of Gloeocapsomorpha prisca Zalessky 1917 from Ordovician rocks in Canadian Williston Basin; *in* Current Research, Part D. Geological Survey of Canada, Paper 90-1D.

Stott, D.F.
1984: Cretaceous sequences of the Foothills of the Canadian Rocky Mountains; *In* The Mesozoic of Middle North America, ed. D.F. Stott and D.J. Glass; Canadian Society of Petroleum Geologists, Memoir 9, p. 85-107.

Thompson, K.F.M.
1979: Light hydrocarbons in subsurface sediments; Geochimica et Cosmochimica Acta, v. 43, no. 5, p. 657-672.

Vigrass, L.W.
1971: Depositional framework of the Winnipeg Formation Manitoba and eastern Saskatchewan; Geological Association of Canada, Special Paper no. 9, p. 225-234.

Wardlaw, N.E. and Reinson, G.E.
1971: Carbonate and evaporite deposition and diagenesis, Middle Devonian Winnipegosis and Prairie evaporite formations of south-central Saskatchewan; American Association of Petroleum Geologists, Bulletin, v. 55, p. 1759-1786.

Paleogeothermal gradients and changes in the geothermal gradient field of the Alberta Plains

Kirk G. Osadetz, David E. Pearson[1], and Laverne D. Stasiuk[2]
Institute of Sedimentary and Petroleum Geology, Calgary

Osadetz, K.G., Pearson, D.E., and Stasiuk, L.D., Paleogeothermal gradients and changes in the geothermal gradient field of the Alberta Plains; in Current Research, Part D, Geological Survey of Canada, Paper 90-1D, p. 165-178, 1990.

Abstract

Changes in the pattern and magnitude of the geothermal gradient field in the Alberta Plains can be inferred by comparing the present geothermal gradient field with coalification data. Ideally, well profile coalification gradients could be compared to near surface coalification data to corroborate the relationship proposed by Hacquebard between the equilibrium moisture content of near surface coals and erosion. Unfortunately, the large uncertainties commonly associated with well profile coalification gradients prevent this. Paleogeothermal gradients inferred using the Hacquebard relation to estimate erosion compare favorably with other constraints on paleogeothermal gradients. Both the pattern and magnitude of the geothermal gradient field have changed little since the end of the Laramide Orogeny indicating that hydrodynamically controlled advective heat transfer dominated the late orogenic geothermal gradient field as it does now. Changes are greatest where changes in geological structure have occurred.

Résumé

Les changements de configuration et d'amplitude du champ de gradient géothermique dans les plaines de l'Alberta peuvent être déterminés par inférence en comparant le champ de gradient géothermique actuel avec les données de houillification. L'idéal serait que les gradients de houillification du profil de puits pourraient être comparés aux données de houillification relevées près de la surface et ainsi corroborer le lien proposé par Hacquebard entre la teneur en humidité d'équilibre des charbons situés près de la surface et l'érosion.

Malheureusement, le degré élevé d'incertitude habituellement associé aux gradients de houillification du profil de puits empêche cette comparaison. Les gradients paléogéothermiques déduits par l'application de la relation d'Hacquebard pour évaluer l'érosion se comparent avantageusement à d'autres gradients établis par d'autres méthodes. La configuration et l'amplitude du champ de gradient géothermique ont peu changé depuis la fin de l'orogène laramien indiquant qu'un transfert de chaleur d'advection à contrôle hydrodynamique a caractérisé le champ de gradient géothermique de la fin de l'orogène comme c'est le cas actuellement. Les changements sont plus importants là où la structure géologique a été modifiée.

[1] David E. Pearson and Associates Ltd., 4277 Houlihan Place, Golden Head, Victoria, British Columbia, V8N 3T2
[2] Department of Geology, University of Regina, Regina, Saskatchewan, S4S 0A2

INTRODUCTION

The present geothermal gradient field of the western Canadian Plains, as characterized by analysis of bottom hole temperatures recorded during the wireline logging of petroleum exploration wells, indicates differences between the pattern and magnitude of average geothermal gradients in the clastic dominated Mesozoic foreland succession and the carbonate and evaporite dominated Paleozoic succession (Majorowicz et al., 1985a, 1985b, 1986). In western portions of the Plains, near the Cordilleran Structural Province, average gradients in the foreland succession are low and those in the Paleozoic succession are higher. In eastern portions of the basin, where topography is low, near the Canadian Shield, the geothermal gradients variation with depth is generally reversed. Higher gradients characterize the foreland succession and lower gradients occur in the Paleozoic succession. Accounting for the differences in thermal conductivity between these two successions, vertical variation in average geothermal gradients has been interpreted to represent hydrodynamically controlled, advective heat transfer (Majorowicz et al., 1985a). In topographically high areas, regional meteoric water recharge depresses the heat flow in shallower foreland rocks. Heat is advectively transferred by hydrodynamically circulating formation waters to topographically low regions of regional hydraulic discharge where average geothermal gradient variations characterize decreasing heat flow with depth (Majorowicz, 1985b).

The relative topographic profile of the basin has not changed since the Cordilleran orogenies (Upper Jurassic to Paleogene) when the Cordillera was uplifted and eroded, the sediments being deposited in foreland basins (Stott, 1984). It is therefore reasonable to speculate that advective heat transfer dominated the geothermal field of the Laramide Foreland Basin at the end of Laramide Orogeny as it does today. If this is true, western portions of the foreland basin should have low paleogeothermal gradients and paleogeothermal gradients in the foreland succession should increase eastward.

TECHNIQUES FOR PALEOGEOTHERMAL GRADIENT DETERMINATION

Coalification is the most commonly used constraint on paleogeothermal history in the Foreland Basin. Commonly, paleogeothermal gradients have been estimated by matching predicted coal ranks from burial and geothermal history calculations of Time-temperature index (Lopatin, 1971) to observed coal ranks. The transformation of Time-temperature indices to calculated coal ranks generally involves using a global relationship between Time-temperature index and coalification (Waples, 1980) allowing spot coal rank observations to be matched to models of burial and geothermal history. Until now only local studies or profiles have been modeled and the general paleogeothermal gradient field of the Foreland Basin remains to be described.

Paleogeothermal gradient inference from coalification gradient data is preferred over matching single coalification measurements using Time-temperature index models. Coalification gradients are generally more reliable than spot observations. Coalification gradient techniques also allow alternative techniques for inferring the paleogeothermal gradient to be employed. These techniques are computationally simpler than burial history calculations and require fewer assumptions than the geothermal gradient matching approach. Such techniques are ideally suited to reconnaissance paleogeothermal gradient field description.

Middleton (1982) and Buntebarth (1979) suggested that the paleogeothermal gradient can be estimated from the coalification (reflectance) gradient or both the coalification gradient and the burial rate. Middleton's (1982) technique suggests that geothermal gradient is proportional to logarithmic reflectance gradient, where the paleogeothermal gradient is the product of the logarithmic reflectance gradient (log %Ro/km) and 194.8 (ibid.). Buntebarth's (1979) technique suggests a functional relationship between linear reflectance gradient and burial rate. In this method, a natural logarithm is taken of a product of a constant value, the linear reflectance gradient and the square root of subsidence rate. This commonly results in negative gradient values because of the low burial rates in the Foreland succession. For this reason, Middleton's (1982) technique is preferred in this geological setting.

Burial and geothermal history matching studies have indicated that the greatest portion of coal rank was acquired by Foreland Basin strata during the time of maximum burial and maximum temperature at the end of Laramide Orogeny (Majorowicz and Jessop, 1981; Majorowicz et al., 1985c; Rahman et al., 1985; England and Bustin, 1986; Kalkreuth and McMechan, 1984). The coalification gradient field in foreland sediments will reflect the geothermal field at the end of the Laramide Orogeny. Kalkreuth and McMechan (1984) have suggested that the uplift of the Foreland Basin could have coincided with uplift of the Omineca Crystalline Belt, and they used an age of 48 Ma (Middle Eocene) as the time of maximum burial. Comparison with the present geothermal gradient field allows inference of changes in the pattern and magnitude of the geothermal field since the end of the Laramide Orogeny.

SOURCES OF COALIFICATION DATA

There are numerous sources of coalification data in the southern Interior Platform Structural Province. Surface coalification characteristics, including equilibrium moisture content of near surface coals, are restricted to outcropping Mesozoic foreland strata in Alberta (Fig 1; Nurkowski, 1984; Hacquebard, 1977). Reflectance studies of specific stratigraphic units and coalification gradients are the most common source of coalification data from the subsurface. Hacquebard (1977) made an initial study of Mannville Group samples and important studies of coalification and coalification gradient have been made in the northwestern Plains of Alberta and British Columbia (Kalkreuth and McMechan, 1984), and the southern Alberta Plains (England and Bustin, 1986). Cameron (in press) studied reflectance of Tertiary coals in southeast Saskatchewan.

Studies funded by this project have examined the coalification characteristics and organic petrography of the Mesozoic succession in Saskatchewan (Stasiuk, 1988) and

Upper Devonian and younger strata, although primarily the foreland succession, of the Alberta Plains (Pearson, 1985a; 1985b). Only Mannville Group and observations from equivalent strata are employed in this discussion (Fig. 2; Tables 1, 2). Much of the data used here are new, including all of the observations in Saskatchewan and the six regionally distributed, east-west profiles (Fig. 2) that provide the basis of observations in Alberta.

WELL PROFILES AND ESTIMATES OF EROSION

Coalification gradients can be determined from studies of well profiles. Well profile reflectance data were collected by Kalkreuth and McMechan (1984), England and Bustin (1986), and Stasiuk (1988). These studies are independent of assumptions and have quantifiable uncertainties. Unfortunately, the number of well profile studies in the Canadian Great Plains is few. There are numerous data from spot observations of a single stratigraphic horizon. The most numerous spot observations are from the Mannville Group, the strata of which are commonly the lowermost in the foreland succession of the plains. Estimates of both erosion and the coalification gradient are available directly from well profiles. This method provides an independent estimate of erosion by extrapolating well profile logarithmic coalification gradients to zero coalification (Dow, 1977). This technique is dependent only on the coalification gradient and the estimate of zero coalification (Fig. 3). As it employs the direct measurement of well profile coalification gradients, few calculations of this type can be made because of the limited number of well profile studies. Alternatively, coalification gradients can be be estimated using independent estimates of erosion and zero coalification with a single value of reflectance with depth. The equilibrium moisture content of near surface coals is well known in Alberta (Fig. 1) and erosion can be estimated using the relationship between the equilibrium moisture content of near surface coals and depth proposed by Hacquebard (1977) (Fig. 4).

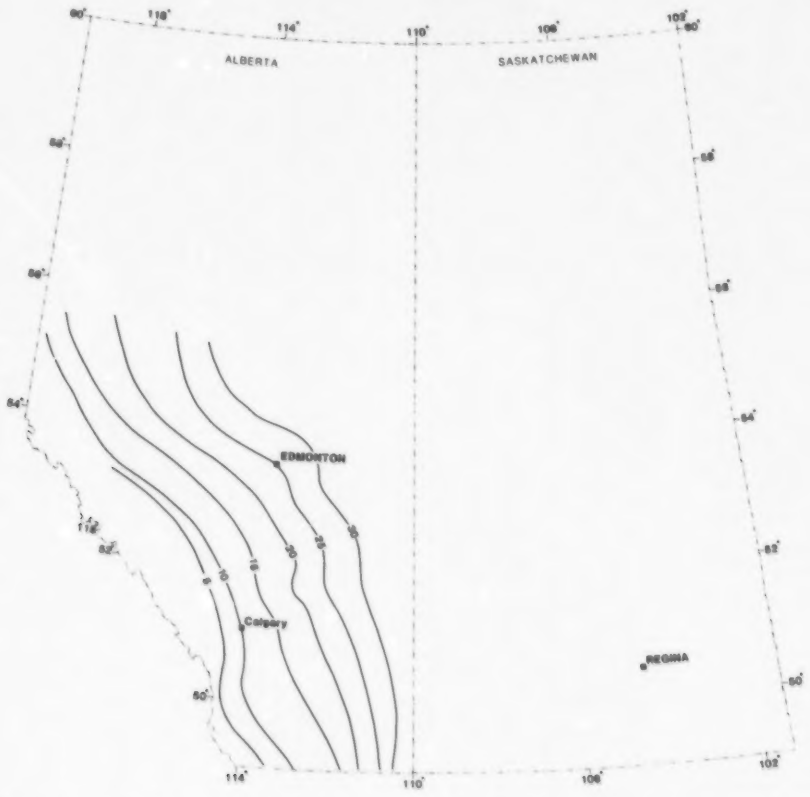

Figure 1. Equilibrium moisture content of near surface coals. (From Hacquebard, 1977.)

Table 1. Coalification data for Mannville Group and other Lower Cretaceous formations in the Alberta Plains

LOCATION	Ro	DEPTH	ELEVATION	ZONE
01-19-014-33W1	.37	603.5	-11.9	MAN
14-07-003-03W2	.36	993.7	-416.7	MAN
05-32-008-11W2	.33	1011.9	-407.5	MAN
16-08-009-21W2	.35	1036.3	-260.0	MAN
02-07-001-28W3	.38	1042.4	-199.3	MAN
09-18-003-03W3	.40	1319.8	-326.5	MAN
06-10-003-18W3	.36	1172.0	-234.4	MAN
01-01-005-25W3	.40	1222.3	-260.0	MAN
14-07-005-27W3	.38	1149.1	-175.6	MAN
15-11-006-20W3	.40	1286.3	-300.3	MAN
11-20-013-13W3	.52	1071.3	-189.5	MAN
14-06-015-19W3	.36	986.0	-205.1	MAN
01-06-039-26W3	.31	790.0	-84.0	MAN
03-07-039-26W3	.34	778.0	-76.7	MAN
14-32-039-26W3	.33	740.0	-64.3	MAN
04-01-039-27W3	.34	796.0	-81.6	MAN
11-07-040-25W3	.37	735.5	-68.0	MAN
14-03-040-26W3	.37	733.0	-58.9	MAN
10-04-040-26W3	.34	746.0	-65.1	MAN
02-21-040-26W3	.31	776.0	-72.9	MAN
10-28-042-25W3	.31	654.0	-35.5	MAN
03-29-042-25W3	.38	650.0	-21.8	MAN
09-29-042-25W3	.31	649.0	-29.7	MAN
06-07-043-24W3	.31	711.0	-22.6	MAN
15-34-047-23W3	.40	508.0	83.3	MAN
06-06-050-23W3	.37	519.0	106.1	MAN
15-01-050-24W3	.40	502.0	110.8	MAN
07-08-004-04W4	.42	1116.5	-83.2	BLMR
10-30-004-04W4	.46	1056.1	-81.7	BLMR
02-03-005-04W4	.42	1145.5	-89.9	BLMR
04-06-005-04W4	.44	1077.5	-86.0	BLMR
03-27-006-28W4	.64	2975.0	-1829.6	MAN
03-22-007-24W4	.59	1895.0	-878.0	MAN
02-18-008-25W4	.63	2105.0	-1901.8	MAN
06-06-008-27W4	.65	2550.0	-1550.1	MAN
15-03-010-10W4	.50	929.6	-60.7	BLMR
08-01-010-11W4	.67	912.0	-74.1	BLMR
02-35-010-13W4	.40	914.4	-98.8	BLMR
08-26-010-15W4	.67	917.4	-121.0	BLMR
06-26-010-21W4	.63	1236.0	-330.1	BLMR
10-28-010-23W4	.86	1447.8	-484.0	BLMR
08-06-010-27W4	.75	2470.0	-1471.5	MAN
10-24-010-27W4	.70	2115.0	-1120.6	MAN
16-31-011-13W4	.46	902.2	-153.3	BLMR
06-29-011-18W4	.64	1092.7	-231.0	BLMR
10-30-011-18W4	.51	1113.1	-257.6	BLMR
06-16-012-27W4	.66	2190.0	-1177.4	MAN
13-16-012-28W4	.64	2602.0	-1459.7	MAN
06-06-013-15W4	.51	930.0	-139.2	MAN
08-03-013-28W4	.78	2465.0	-1407.1	MAN
06-11-014-29W4	.75	3025.0	-1696.8	MAN
08-11-015-28W4	.82	2400.0	-1294.4	MAN
10-25-015-29W4	.65	2572.5	-1470.2	MAN
06-32-015-29W4	.71	2675.0	-1607.6	MAN
08-14-016-27W4	.79	2085.0	-1061.6	MAN
06-04-016-29W4	.75	2682.5	-1505.3	MAN
14-01-018-13W4	.46	992.7	-239.6	BLMR
07-16-018-14W4	.43	1007.7	-251.5	BLMR
09-09-018-15W4	.57	1047.0	-247.5	BLMR
01-16-018-15W4	.59	1053.0	-261.5	BLMR
06-21-018-19W4	.53	1325.9	-400.5	BLMR
06-29-018-20W4	.69	1391.0	-434.0	BLMR
07-35-018-21W4	.66	1452.0	-474.6	BLMR
14-05-019-08W4	.49	971.1	-172.2	BLMR
06-29-020-06W4	.57	1022.0	-186.5	BLMR
06-09-020-07W4	.44	943.1	-174.7	LMAN
06-10-020-07W4	.43	937.6	-186.9	LMAN
12-28-020-08W4	.44	944.6	-182.3	LMAN
01-22-020-12W4	.44	977.8	-229.2	BLMR
11-32-020-16W4	.57	1062.8	-300.5	BLMR
08-06-020-22W4	.63	1673.4	-607.8	BLMR
10-11-020-24W4	.64	1741.9	-706.5	BLMR
11-12-020-26W4	.62	1869.9	-785.2	BLMR
07-17-020-27W4	.66	2057.4	-976.3	BLMR
04-17-020-28W4	.50	1873.9	-835.8	BLMR
10-25-021-10W4	.49	963.8	-192.3	BLMR
11-23-022-09W4	.53	894.9	-171.9	BLMR
10-03-022-20W4	.59	1212.8	-351.1	MAN
07-18-024-18W4	.52	1321.0	-412.7	BLMR
06-07-024-19W4	.55	1339.6	-416.1	BLMR
07-32-024-19W4	.50	1285.3	-364.2	BLMR
16-23-025-12W4	.61	1009.5	-266.7	BLMR
10-28-026-21W4	.66	1431.3	-530.4	MAN
06-02-027-20W4	.55	1360.3	-474.3	BLMR
07-26-027-20W4	.60	1322.2	-490.7	BLMR
06-15-027-23W4	.69	1481.3	-630.9	BLMR
11-17-028-18W4	.69	1230.2	-425.2	MAN
06-10-028-20W4	.66	1344.8	-499.9	BLMR
06-34-030-08W4	.44	931.5	-167.0	BLMR
07-08-030-12W4	.46	1086.5	-278.3	BLMR
07-17-030-18W4	.62	1272.9	-412.4	MAN
12-19-031-09W4	.41	1048.1	-283.2	BLMR
02-36-031-14W4	.50	1122.3	-278.3	BLMR
12-34-031-15W4	.45	1106.4	-297.2	BLMR
10-34-031-17W4	.53	1241.5	-379.8	BLMR
04-10-031-18W4	.60	1310.6	-420.6	BLMR
15-14-031-22W4	.62	1457.2	-596.9	BLMR
11-01-031-23W4	.66	1562.1	-644.3	BLMR
11-03-031-23W4	.72	1553.0	-674.5	BLMR
07-30-031-26W4	.74	1886.2	-925.4	BLMR
02-18-031-27W4	.63	1972.1	-1011.9	BLMR
08-20-032-17W4	.58	1250.6	-390.1	MAN
06-22-032-17W4	.60	1231.4	-390.5	MAN
07-20-032-19W4	.53	1336.5	-467.0	BLMR
06-06-032-21W4	.60	1403.9	-572.4	MAN
04-11-033-14W4	.47	1200.6	-325.8	BLMR
08-28-035-17W4	.57	1130.2	-298.3	BLMR
10-31-035-17W4	.53	1171.3	-333.8	BLMR
10-20-035-21W4	.64	1422.8	-576.2	MAN
11-09-035-23W4	.74	1575.8	-664.5	BLMR
10-34-036-04W4	.41	721.5	-53.3	BLMR
07-12-036-18W4	.63	1132.6	-301.1	BLMR
08-18-036-19W4	.66	1266.9	-410.3	MAN
06-14-038-10W4	.56	935.7	-163.7	BLMR
07-26-038-18W4	.56	1251.8	-432.8	MAN
16-19-038-20W4	.68	1322.8	-502.9	MAN
12-14-038-21W4	.62	1306.1	-486.2	BLMR
04-32-038-22W4	.61	1407.3	-573.3	MAN
07-10-039-06W4	.42	830.9	-134.7	MAN
08-26-039-20W4	.67	1290.8	-471.5	MAN
12-22-039-21W4	.65	1341.1	-521.8	BLMR
10-22-039-22W4	.71	1361.8	-552.6	BLMR
06-29-039-22W4	.66	1369.5	-570.6	BLMR
10-33-039-23W4	.65	1437.1	-615.1	MAN
13-15-040-01W4	.30	755.6	-78.3	BLMR
15-21-040-01W4	.32	768.1	-75.3	BLMR
10-06-040-04W4	.28	794.6	-110.6	BLMR
06-21-040-07W4	.31	815.6	-123.4	BLMR
12-27-040-07W4	.36	822.7	-131.7	BLMR
08-26-040-08W4	.31	870.2	-126.2	BLMR
06-28-040-08W4	.42	903.4	-141.1	BLMR
03-27-040-10W4	.32	873.3	-166.7	BLMR
01-28-040-10W4	.35	883.0	-185.2	BLMR
07-11-040-16W4	.61	1014.1	-269.7	BLMR
07-14-040-16W4	.39	1082.0	-344.1	BLMR
13-10-040-18W4	.62	1204.0	-431.6	BLMR
10-17-040-20W4	.73	1325.0	-514.5	BLMR
06-07-040-24W4	.79	1567.0	-684.3	BLMR
06-27-040-26W4	.65	1658.7	-769.3	BLMR
10-34-040-27W4	.97	1708.1	-821.4	BLMR
05-16-041-01W4	.32	871.4	-114.6	BLMR
02-17-041-01W4	.36	829.1	-77.4	BLMR
06-03-041-03W4	.29	786.5	-94.2	BLMR
16-20-041-12W4	.35	903.0	-200.6	BLMR
02-22-041-12W4	.36	921.4	-197.8	BLMR
15-29-041-12W4	.42	909.0	-212.4	BLMR
16-30-041-12W4	.35	907.1	-207.9	BLMR
05-32-041-12W4	.37	898.3	-203.0	BLMR
10-18-041-14W4	.50	977.2	-255.7	BLMR
10-19-041-20W4	.45	1370.1	-576.4	BLMR
04-29-042-02W4	.35	630.0	-1.5	BLMR
10-33-042-02W4	.43	679.7	0.0	BLMR
16-24-042-03W4	.42	630.9	6.1	BLMR
10-18-042-12W4	.46	887.3	-192.9	MAN
06-29-043-05W4	.42	688.8	-26.0	BLMR
10-25-044-04W4	.50	624.2	24.4	BLMR
12-14-045-08W4	.51	639.8	40.2	MAN
05-32-045-08W4	.45	697.7	11.3	MAN
09-19-046-05W4	.41	692.6	79.2	BLMR
11-05-046-06W4	.42	687.4	20.0	MAN
04-08-046-06W4	.44	645.5	27.5	MAN
04-17-046-06W4	.48	655.8	21.2	MAN
10-15-046-23W4	.66	1278.6	-527.0	BLMR
11-18-047-04W4	.44	608.1	6.4	BLMR
06-19-047-04W4	.44	597.4	6.1	BLMR
08-20-047-04W4	.40	689.0	3.4	BLMR
06-25-048-06W4	.41	698.8	11.6	BLMR
03-15-048-21W4	.50	1263.7	-506.0	BLMR
06-31-048-21W4	.66	1176.5	-400.8	BLMR
11-04-049-01W4	.43	547.3	121.6	BLMR
03-13-049-01W4	.45	586.7	71.0	BLMR
14-35-049-01W4	.53	532.8	131.4	BLMR
11-21-049-02W4	.39	597.5	84.4	BLMR
05-11-049-04W4	.39	621.8	71.9	BLMR
15-26-049-07W4	.43	576.1	53.3	BLMR
07-06-049-09W4	.43	786.3	-32.0	BLMR
11-22-049-11W4	.42	626.2	43.3	BLMR
08-27-049-11W4	.41	653.5	22.6	BLMR
07-26-049-13W4	.47	742.2	-51.2	BLMR
14-22-049-23W4	.50	1272.5	-510.2	BLMR
15-15-049-25W4	.57	1335.0	-582.6	BLMR
04-10-049-26W4	.60	1382.5	-609.9	BLMR
11-02-049-27W4	.71	1450.8	-686.3	BLMR
05-09-050-01W4	.48	576.1	93.0	BLMR
12-15-050-02W4	.40	752.9	-55.8	BLMR
08-04-050-11W4	.52	709.3	-38.4	BLMR
09-18-050-18W4	.55	978.4	-278.0	BLMR
04-15-050-21W4	.41	1207.0	-436.8	BLMR
11-33-051-14W4	.50	772.4	-125.6	BLMR
07-31-052-12W4	.39	662.9	10.1	BLMR
14-36-053-06W4	.49	530.4	124.4	BLMR
08-06-055-04W4	.38	473.0	145.4	BLMR
07-08-055-04W4	.38	480.0	149.0	BLMR
11-20-055-15W4	.55	585.8	50.3	BLMR
06-04-056-08W4	.41	497.7	130.5	BLMR
10-01-056-14W4	.47	580.6	79.2	BLMR
05-16-060-02W4	.38	442.0	150.6	BLMR
10-09-060-03W4	.42	395.3	226.5	BLMR
12-11-060-04W4	.48	408.4	202.7	BLMR
13-29-060-05W4	.44	396.2	190.6	BLMR
03-16-060-09W4	.37	539.5	90.2	BLMR
13-03-060-11W4	.44	513.0	144.8	BLMR
10-08-060-15W4	.41	571.5	115.2	BLMR
11-25-060-16W4	.41	548.6	132.6	BLMR
11-08-060-17W4	.39	492.3	122.2	BLMR
15-31-060-20W4	.36	608.1	59.4	BLMR
09-13-060-25W4	.45	712.6	-92.7	BLMR
01-22-060-26W4	.43	963.2	-311.8	BLMR
01-27-060-26W4	.36	944.6	-294.4	BLMR
08-23-060-27W4	.46	759.6	-130.1	BLMR
08-22-064-26W4	.39	676.7	27.1	BLMR
07-15-072-17W4	.43	432.5	139.9	BLUE
03-15-007-03W5	.88	0.0	1500.0	BLMR
15-20-007-03W5	1.08	0.0	1500.0	BLMR
08-03-008-04W5	.79	0.0	1500.0	BLMR
02-14-011-04W5	.93	0.0	1500.0	BLMR
07-26-014-05W5	.95	0.0	2000.0	BLMR
06-21-016-05W5	1.06	0.0	1700.0	BLMR
01-32-016-05W5	.94	0.0	2000.0	BLMR
11-10-017-01W5	.75	2780.0	-1612.3	MAN
08-36-017-01W5	.88	2472.5	-1321.9	MAN
04-02-026-05W5	.90	2757.8	-1490.5	BLMR
08-16-028-06W5	1.58	3406.1	-2015.3	MAN
08-15-033-03W5	.96	2407.6	-1371.3	MAN
10-33-033-03W5	.97	2362.0	-1355.4	BLMR
11-30-034-03W5	.96	2375.9	-1363.4	MAN
10-28-035-04W5	.81	2246.4	-1548.4	BLMR
08-11-035-06W5	.94	2859.0	-1671.2	BLMR
10-18-036-04W5	.92	2386.7	-1407.0	BLMR
10-12-036-05W5	.89	2442.1	-1453.5	BLMR
12-21-037-03W5	.79	2238.0	-1273.1	BLMR
03-36-037-03W5	.80	2106.5	-1168.7	MAN
11-27-037-08W5	1.31	3107.4	-1919.0	BLMR
12-31-037-08W5	1.29	3148.6	-1935.5	BLMR
10-04-038-03W5	.58	2172.3	-1245.1	BLMR
10-20-038-04W5	.74	2278.2	-1281.7	BLMR
11-22-038-04W5	.93	2231.7	-1251.2	BLMR
02-29-038-04W5	.52	2289.0	-1300.0	BLMR
10-29-038-04W5	.59	2295.4	-1317.3	BLMR
04-31-038-04W5	.78	2300.6	-1302.1	BLMR
10-36-038-05W5	.66	2342.4	-1339.9	BLMR
08-26-038-08W5	1.24	2784.5	-1746.5	BLMR
04-18-039-03W5	.61	2128.7	-1202.7	BLMR
14-18-039-03W5	.56	2183.9	-1219.5	BLMR
10-19-039-03W5	.59	2152.2	-1207.6	BLMR
09-26-039-03W5	.62	2082.3	-1135.7	BLMR
02-05-039-04W5	.62	2285.4	-1308.5	BLMR
12-05-039-04W5	.68	2256.4	-1283.8	BLMR
10-06-039-04W5	.76	2302.8	-1336.5	BLMR
10-08-039-04W5	.87	2239.4	-1278.9	BLMR
10-09-039-04W5	.83	2241.6	-1269.8	BLMR
02-24-039-04W5	.62	2174.4	-1219.5	BLMR
02-01-039-05W5	.85	2316.5	-1315.5	BLMR
12-11-039-05W5	.84	2317.1	-1325.9	BLMR
10-12-039-05W5	.85	2238.8	-1436.5	BLMR
16-16-039-05W5	.91	2302.2	-1333.5	BLMR
14-21-039-05W5	.78	2284.5	-1339.9	BLMR
10-11-040-02W5	.77	1918.7	-1010.1	BLMR
04-09-041-02W5	.65	1993.1	-1041.2	BLMR
04-18-041-03W5	.80	2066.5	-1104.8	MAN
07-32-041-03W5	.74	2149.8	-1138.6	BLMR
11-15-042-04W5	.81	2095.5	-1139.0	MAN
04-18-042-04W5	.88	2112.0	-1146.6	MAN
10-35-042-04W5	.90	2045.8	-1060.1	BLMR
01-30-043-01W5	.73	1758.0	-844.1	MAN
10-17-043-03W5	.67	2006.6	-1048.2	BLMR
08-21-044-04W5	.83	2040.0	-1078.8	LMAN
08-14-044-08W5	1.26	2345.0	-1322.0	UMAN
11-01-044-09W5	1.30	2277.2	-1309.4	BLMR
06-29-048-04W5	.62	1784.0	-933.9	BLMR
04-32-048-04W5	.73	1772.4	-942.4	BLMR
13-33-048-04W5	.64	1821.5	-972.9	BLMR
04-11-049-01W5	.71	1496.6	-739.1	BLMR
15-11-049-02W5	.70	1560.6	-787.0	BLMR
11-25-049-03W5	.58	1554.5	-789.1	BLMR
10-35-049-13W5	.89	2415.0	-1419.5	BLMR
07-20-049-15W5	1.23	2840.7	-1743.2	BLMR
16-18-052-05W5	.55	1642.6	-843.1	BLMR
15-02-052-10W5	.72	1951.6	-1058.8	BLMR
11-20-054-11W5	.86	1865.0	-1053.4	BLMR
07-26-055-20W5	1.15	2766.4	-1571.5	BLMR
10-19-056-11W5	.74	1898.0	-960.4	BLMR
06-32-056-11W5	.64	1819.7	-934.8	BLMR
07-33-056-11W5	.63	1822.7	-936.3	BLMR
16-04-059-05W5	.77	1204.0	-537.7	BLMR
15-04-060-12W5	.74	1533.8	-832.4	BLMR
02-18-062-18W5	.72	1825.7	-1044.5	CDMN
10-25-064-19W5	.67	1431.0	-852.6	BLMR
10-14-064-20W5	.67	1553.0	-734.6	BLMR
07-16-065-22W5	.49	1844.0	-1108.0	BLUE
12-16-075-15W5	.38	754.4	-170.1	GETH
14-15-075-22W5	.38	954.0	-379.5	GETH
06-23-075-22W5	.39	945.2	-377.7	BLUE
10-07-077-23W5	.46	786.3	-358.6	GETH
11-30-080-23W5	.40	741.6	-167.3	BLUE
10-22-083-10W6	1.86	3430.0	-1943.0	FALH
07-21-084-07W6	.70	2588.0	-1534.4	CDTT
06-06-085-02W6	.78	2338.1	-1483.1	SRIV
10-16-085-02W6	.67	2201.6	-1387.5	BLUE
07-34-085-03W6	.97	2262.3	-1483.2	BLUE
03-16-085-04W6	.72	2463.4	-1595.6	GETH
05-12-085-05W6	.83	2477.1	-1635.9	SRIV
10-23-085-05W6	.60	2086.0	-1298.4	SRIV
10-04-087-10W6	1.28	2485.0	-1619.7	FALH
07-15-087-10W6	1.23	2535.0	-1542.6	FALH
08-12-070-05W6	.88	1743.0	-1089.8	GETH
10-25-070-08W6	.91	1840.1	-943.4	FALH
10-08-070-09W6	1.19	2183.9	-1488.8	GETH
11-10-070-09W6	.93	1779.1	-1083.3	FALH
08-22-070-09W6	.67	1774.9	-1080.4	FALH
06-05-070-10W6	.77	1917.2	-1198.3	FALH
11-28-070-11W6	1.00	1873.4	-1155.9	FALH
13-20-075-02W6	.50	1182.0	-536.7	GETH
06-05-075-13W6	1.37	1875.1	-1055.9	GETH
07-21-080-06W6	.66	1017.5	-410.6	GETH
06-35-085-04W6	.55	1016.5	-178.3	GETH

Table 2. Average reflectances of samples from the Mannville Group and other Lower Cretaceous formations in the Alberta Plains

LOCATION	Ro	DEPTH	ELEVATION	ZONE
01-19-014-33W1	.35	621.8	-30.2	MAN
14-07-003-03W2	.36	993.7	-416.7	MAN
05-32-006-11W2	.36	1015.0	-410.6	MAN
16-08-009-21W2	.35	1036.3	-269.0	MAN
02-07-001-29W3	.40	1060.7	-217.6	MAN
09-18-003-03W3	.37	1350.3	-357.0	MAN
06-10-003-18W3	.36	1172.0	-234.4	MAN
01-01-005-25W3	.37	1244.8	-282.5	MAN
14-07-005-27W3	.38	1148.1	-175.6	MAN
15-11-006-20W3	.40	1286.3	-300.3	MAN
11-20-013-13W3	.52	1071.3	-189.5	MAN
14-08-015-19W3	.36	986.0	-206.1	MAN
01-06-039-26W3	.31	780.0	-84.0	MAN
03-07-039-26W3	.34	778.0	-76.7	MAN
14-32-039-26W3	.33	740.0	-84.3	MAN
04-01-039-27W3	.34	796.0	-81.6	MAN
11-07-040-25W3	.37	735.5	-68.0	MAN
14-03-040-26W3	.37	733.0	-58.9	MAN
10-04-040-26W3	.34	746.0	-65.1	MAN
02-21-040-26W3	.31	776.0	-72.9	MAN
10-28-042-25W3	.31	654.0	-35.5	MAN
03-29-042-25W3	.38	650.0	-21.8	MAN
09-29-042-25W3	.31	649.0	-29.	7MAN
06-07-043-24W3	.31	711.0	-22.6	MAN
15-34-047-23W3	.40	508.0	83.3	MAN
08-06-050-23W3	.37	519.0	108.1	MAN
15-01-050-24W3	.40	502.0	110.8	MAN
07-06-004-04W4	.42	1116.5	-83.2	BLMR
10-30-004-04W4	.46	1056.1	-81.7	BLMR
02-03-005-04W4	.42	1145.5	-89.9	BLMR
04-06-005-04W4	.44	1077.5	-86.0	BLMR
03-27-008-28W4	.64	2975.0-1829.6		MAN
03-32-007-24W4	.61	1705.0-	740.4	MAN
02-18-008-25W4	.63	2105.0-1901.9		MAN
06-08-008-27W4	.67	2775.0-1775.1		MAN
15-03-010-10W4	.50	929.6	-80.7	BLMR
08-01-010-11W4	.67	91z.0	-74.1	BLMR
02-35-010-13W4	.40	914.4	-98.8	BLMR
08-26-010-15W4	.67	917.4	-121.0	BLMR
06-28-010-21W4	.63	1236.0	-330.1	BLMR
10-28-010-23W4	.66	1447.8	-484.0	BLMR
08-08-010-27W4	.66	2524.5-1526.0		MAN
10-24-010-27W4	.72	2215.0-1220.6		MAN
16-31-011-13W4	.46	902.2	-153.3	BLMR
08-29-011-18W4	.57	1108.9	-247.2	BLMR
10-36-011-26W4	.76	2385.0-1370.8		MAN
06-16-012-27W4	.69	2363.6-1351.0		MAN
13-16-012-28W4	.64	2602.0-1459.7		MAN
06-06-013-26W4	.72	2035.0-1006.0		MAN
08-03-013-28W4	.78	2485.0-1407.1		MAN
06-11-014-29W4	.75	3025.0-1696.8		MAN
08-11-015-28W4	.82	2400.0-1294.4		MAN
10-25-015-29W4	.69	2702.5-1600.2		MAN
08-32-015-29W4	.84	2950.0-1682.6		MAN
08-14-016-27W4	.79	2085.0-1081.6		MAN
08-04-016-29W4	.77	2735.0-1557.8		MAN
14-01-018-13W4	.46	992.7	-239.6	BLMR
07-16-018-14W4	.43	1007.7	-251.5	BLMR
09-09-018-15W4	.57	1047.0	-247.5	BLMR
01-16-018-15W4	.59	1053.0	-261.5	BLMR
08-21-018-19W4	.53	1325.9	-400.5	BLMR
06-29-018-20W4	.69	1391.0	-434.0	BLMR
07-35-018-21W4	.66	1452.0	-474.6	BLMR
14-05-019-08W4	.49	971.1	-172.2	BLMR
06-29-020-08W4	.57	1022.0	-186.5	BLMR
06-09-020-07W4	.44	943.1	-174.7	LMAN
06-10-020-07W4	.43	937.6	-186.9	LMAN
12-28-020-08W4	.44	944.6	-182.3	LMAN
01-22-020-12W4	.44	977.8	-229.2	BLMR
11-32-020-16W4	.57	1082.8	-300.5	BLMR
08-08-020-22W4	.63	1673.4	-807.8	BLMR
10-11-020-24W4	.64	1741.9	-798.5	BLMR
11-12-020-26W4	.62	1889.9	-785.2	BLMR
07-17-020-27W4	.66	2057.4	-976.3	BLMR
04-17-020-28W4	.69	2202.2-1164.0		BLMR
10-25-021-10W4	.49	983.8	-192.3	BLMR
11-23-022-09W4	.48	v20.8	-197.8	BLMR
10-03-022-20W4	.59	1212.8	-351.1	MAN
07-18-024-18W4	.54	1323.7	-415.4	BLMR
06-07-024-19W4	.55	1339.6	-416.1	BLMR
07-32-024-19W4	.55	1286.3	-365.2	BLMR
16-23-025-12W4	.61	1009.5	-268.7	BLMR
10-28-026-21W4	.62	1431.6	-530.7	BLMR
06-02-027-20W4	.55	1360.3	-474.3	BLMR
07-26-027-20W4	.60	1322.2	-490.7	BLMR
06-15-027-23W4	.69	1481.3	-630.9	BLMR
11-17-028-18W4	.69	1230.2	-425.2	MAN
08-10-028-20W4	.66	1344.8	-499.9	BLMR
08-34-030-08W4	.44	931.5	-167.0	BLMR
07-09-030-12W4	.46	1066.5	-278.3	BLMR
07-17-030-18W4	.62	1272.9	-412.4	MAN
12-19-031-08W4	.41	1046.1	-263.2	BLMR
02-36-031-14W4	.59	1122.3	-278.3	BLMR
12-34-031-15W4	.45	1106.4	-267.2	BLMR
10-34-031-17W4	.53	1241.5	-379.8	BLMR
04-10-031-18W4	.60	1310.6	-420.6	BLMR
15-14-031-22W4	.62	1457.2	-565.9	BLMR
11-01-031-23W4	.66	1562.1	-644.3	BLMR
11-03-031-23W4	.72	1553.0	-674.5	BLMR
07-30-031-26W4	.74	1865.2	-925.4	BLMR
02-18-031-27W4	.63	1972.1-1011.9		BLMR
08-20-032-17W4	.58	1250.6	-390.1	MAN
06-22-032-17W4	.60	1231.4	-390.5	MAN
07-20-032-19W4	.53	1336.5	-467.0	BLMR
08-08-032-21W4	.67	1416.1	-584.6	BLMR
04-11-033-14W4	.47	1200.6	-325.8	BLMR
08-28-035-17W4	.59	1142.7	-301.8	BLMR
10-31-035-17W4	.53	1171.3	-333.8	BLMR
10-20-035-21W4	.64	1422.8	-576.2	MAN
11-09-035-23W4	.74	1575.8	-684.5	BLMR
10-34-036-04W4	.41	721.5	-53.3	BLMR
07-12-036-18W4	.58	1147.0	-315.5	BLMR
08-18-036-19W4	.58	1287.2	-410.6	BLMR
06-14-038-10W4	.49	940.3	-168.2	BLMR
07-26-038-18W4	.55	1251.8	-432.8	MAN
16-19-038-20W4	.66	1322.8	-502.9	MAN
12-14-038-21W4	.62	1306.1	-486.2	BLMR
04-32-038-22W4	.61	1407.3	-573.3	MAN
07-10-039-06W4	.34	830.9	-134.7	BLMR
08-26-039-20W4	.67	1290.8	-471.5	MAN
12-22-039-21W4	.65	1341.1	-521.8	BLMR
10-22-039-22W4	.71	1361.8	-552.6	BLMR
08-29-039-22W4	.63	1374.3	-575.5	BLMR
10-33-039-23W4	.65	1437.1	-615.1	MAN
13-15-040-01W4	.30	755.6	-78.3	BLMR
15-21-040-01W4	.32	768.1	-75.3	BLMR
10-06-040-04W4	.28	794.6	-110.6	BLMR
06-21-040-07W4	.31	815.6	-123.4	BLMR
12-27-040-07W4	.36	822.7	-131.7	BLMR
08-26-040-08W4	.31	870.2	-126.2	BLMR
06-28-040-08W4	.42	903.4	-141.1	BLMR
03-27-040-10W4	.32	873.3	-166.7	BLMR
01-28-040-10W4	.39	883.0	-165.2	BLMR
07-11-040-16W4	.61	1014.1	-268.7	BLMR
07-14-040-16W4	.39	1082.0	-344.1	BLMR
13-10-040-18W4	.62	1204.0	-431.6	BLMR
10-17-040-20W4	.73	1325.0	-514.5	BLMR
06-07-040-24W4	.79	1567.0	-684.3	BLMR
06-27-040-26W4	.69	1680.6	-771.1	BLMR
10-34-040-27W4	.97	1708.1	-821.4	BLMR
06-16-041-01W4	.32	871.4	-114.6	BLMR
02-17-041-01W4	.29	828.1	-77.4	BLMR
08-03-041-03W4	.29	786.5	-94.2	BLMR
16-20-041-12W4	.35	903.0	-200.6	BLMR
02-29-041-12W4	.41	904.0	-203.0	BLMR
15-29-041-12W4	.42	909.0	-212.4	BLMR
16-30-041-12W4	.35	907.1	-207.9	BLMR
05-32-041-12W4	.37	880.3	-203.0	BLMR
10-18-041-14W4	.43	952.0	-271.6	BLMR
10-19-041-20W4	.45	1370.1	-576.4	BLMR
04-29-042-02W4	.35	630.0	-1.5	BLMR
10-33-042-02W4	.43	679.7	0.0	BLMR
16-24-042-03W4	.42	630.9	-6.1	BLMR
10-18-042-12W4	.49	888.5	-194.2	MAN
08-29-043-05W4	.42	688.9	-29.0	BLMR
10-25-044-04W4	.50	624.2	24.4	BLMR
12-14-045-06W4	.51	639.8	40.2	MAN
05-32-045-06W4	.45	697.7	11.3	MAN
09-19-046-05W4	.42	693.2	78.6	MAN
11-05-046-06W4	.42	687.4	20.0	MAN
04-09-046-06W4	.44	645.5	27.5	MAN
04-17-046-08W4	.48	665.8	21.2	MAN
10-15-046-23W4	.66	1278.6	-527.0	BLMR
11-18-047-04W4	.44	606.1	6.4	BLMR
06-19-047-04W4	.44	597.4	6.1	BLMR
08-20-047-04W4	.40	589.0	3.4	BLMR
08-25-048-08W4	.41	588.8	11.6	BLMR
03-15-048-21W4	.50	1293.7	-508.0	BLMR
06-31-048-21W4	.66	1176.5	-400.8	BLMR
11-04-049-01W4	.43	547.3	121.6	BLMR
03-13-049-01W4	.45	586.7	71.0	BLMR
14-35-049-01W4	.46	535.2	126.9	BLMR
11-21-049-02W4	.39	597.5	94.4	BLMR
05-11-049-04W4	.39	621.8	71.9	BLMR
15-28-049-07W4	.43	576.1	53.3	BLMR
07-08-049-08W4	.43	798.3	-32.0	BLMR
11-22-049-11W4	.42	628.2	43.3	BLMR
06-27-049-11W4	.41	653.5	22.6	BLMR
07-28-049-13W4	.47	742.2	-51.2	BLMR
14-22-049-23W4	.50	1272.5	-510.2	BLMR
15-15-049-25W4	.57	1335.0	-582.8	BLMR
04-10-049-26W4	.60	1382.5	-609.9	BLMR
11-02-049-27W4	.71	1450.8	-698.3	BLMR
05-09-050-01W4	.48	576.1	93.0	BLMR
12-15-050-02W4	.40	752.9	-55.8	BLMR
08-04-050-11W4	.52	709.3	-38.4	BLMR
09-18-050-18W4	.55	978.4	-278.0	BLMR
04-15-050-21W4	.41	1207.0	-436.8	BLMR
11-33-051-14W4	.50	772.4	-125.6	BLMR
07-31-052-12W4	.39	662.9	10.1	BLMR
14-36-053-08W4	.48	530.4	124.4	BLMR
06-06-055-04W4	.39	473.0	145.4	BLMR
07-06-055-04W4	.39	480.0	149.0	BLMR
11-20-055-15W4	.55	585.8	50.3	BLMR
06-04-056-08W4	.41	487.7	130.5	BLMR
10-01-056-14W4	.47	580.6	79.2	BLMR
05-16-060-02W4	.39	442.0	150.6	BLMR
10-09-060-03W4	.42	395.3	226.5	BLMR
12-11-060-04W4	.44	411.5	199.6	BLMR
13-29-060-05W4	.44	396.2	190.3	BLMR
03-16-060-09W4	.37	539.5	90.2	BLMR
13-03-060-11W4	.44	513.0	144.8	BLMR
10-08-060-15W4	.41	571.5	115.2	BLMR
11-25-060-16W4	.45	635.5	45.7	BLMR
11-08-060-17W4	.39	492.3	122.2	BLMR
15-31-060-20W4	.38	761.1	-93.6	BLMR
09-13-060-25W4	.47	938.8	-318.8	BLMR
01-22-060-26W4	.43	963.2	-311.8	BLMR
01-27-060-26W4	.36	944.6	-294.4	BLMR
08-23-060-27W4	.48	758.6	-130.1	BLMR
09-22-064-26W4	.39	676.7	27.1	BLMR
07-15-072-17W4	.43	432.5	139.9	BLUE
03-15-007-03W5	.89	0.0	1500.0	BLMR
15-20-007-03W5	1.06	0.0	1500.0	BLMR
08-03-008-04W5	.70	0.0	1500.0	BLMR
02-14-011-04W5	.93	0.0	1500.0	BLMR
07-26-014-05W5	.95	0.0	2000.0	BLMR
05-21-016-05W5	1.06	0.0	1700.0	BLMR
01-32-016-05W5	.94	0.0	2000.0	BLMR
11-10-017-01W5	.75	2760.0-1612.3		MAN
08-36-017-01W5	.73	2605.0-1454.4		MAN
04-02-026-05W5	.90	2757.8-1490.5		BLMR
06-16-028-06W5	1.58	3406.1-2015.3		MAN
06-15-033-03W5	.96	2407.6-1371.3		MAN
10-33-033-03W5	.97	2362.0-1355.4		BLMR
11-30-034-03W5	.95	2375.9-1363.4		MAN
10-28-035-04W5	.91	2246.4-1546.4		BLMR
06-11-035-06W5	.94	2859.0-1671.2		BLMR
10-18-036-04W5	.92	2305.7-1407.0		BLMR
10-12-036-05W5	.89	2442.1-1463.5		BLMR
12-21-037-03W5	.79	2238.0-1273.1		BLMR
03-36-037-03W5	.80	2108.5-1188.7		MAN
11-27-037-09W5	1.31	3107.4-1919.0		BLMR
12-31-037-09W5	1.26	3148.6-1835.5		BLMR
10-04-038-03W5	.59	2172.3-1245.1		BLMR
10-20-038-04W5	.74	2276.2-1281.7		BLMR
11-22-038-04W5	.93	2231.7-1251.2		BLMR
02-29-038-04W5	.52	2289.0-1300.0		BLMR
10-29-038-04W5	.58	2295.4-1317.3		BLMR
04-31-038-04W5	.78	2300.6-1302.1		BLMR
10-36-038-05W5	.66	2342.4-1339.9		BLMR
06-26-038-08W5	1.24	2784.5-1746.5		BLMR
04-18-039-03W5	.61	2128.7-1202.7		BLMR
14-18-039-03W5	.58	2183.9-1219.5		BLMR
10-19-039-03W5	.59	2152.2-1207.6		BLMR
08-28-039-03W5	.82	2082.3-1135.7		BLMR
02-05-039-04W5	.62	2285.4-1308.5		BLMR
12-05-039-04W5	.66	2256.4-1263.8		BLMR
10-06-039-04W5	.75	2308.9-1342.6		BLMR
10-08-039-04W5	.70	2243.9-1263.5		BLMR
10-09-039-04W5	.83	2241.8-1269.8		BLMR
02-24-039-04W5	.62	2174.4-1219.5		BLMR
02-01-039-05W5	.77	2350.6-1349.7		BLMR
12-11-039-05W5	.84	2317.1-1325.9		BLMR
10-12-039-05W5	.85	2238.8-1436.5		BLMR
16-16-039-05W5	.91	2302.2-1333.5		BLMR
14-21-039-05W5	.78	2284.5-1339.9		BLMR
10-11-040-02W5	.77	1918.7-1010.1		BLMR
04-09-041-02W5	.65	1983.1-1041.2		BLMR
04-18-041-03W5	.80	2086.5-1104.6		MAN
07-32-041-03W5	.74	2149.8-1136.6		BLMR
11-15-042-04W5	.81	2095.5-1139.0		MAN
04-18-042-04W5	.88	2112.0-1146.6		MAN
10-35-042-04W5	.90	2045.8-1080.1		BLMR
01-30-043-01W5	.73	1758.0	-844.1	MAN
10-17-043-03W5	.67	2006.6-1048.2		BLMR
08-21-044-04W5	.83	2040.0-1078.6		LMAN
08-14-044-08W5	1.26	2345.0-1322.0		UMAN
11-01-044-09W5	1.30	2277.2-1309.4		BLMR
06-29-048-04W5	.62	1784.0	-933.9	BLMR
04-32-048-04W5	.73	1772.4	-942.4	BLMR
13-33-048-04W5	.64	1821.5	-972.9	BLMR
04-11-049-01W5	.71	1496.6	-739.1	BLMR
15-11-049-02W5	.70	1580.6	-787.0	BLMR
11-25-049-03W5	.58	1554.5	-789.1	BLMR
10-35-049-13W5	.89	2415.0-1419.5		BLMR
07-20-049-15W5	1.23	2840.7-1743.2		BLMR
16-18-052-05W5	.55	1642.6	-843.1	BLMR
15-02-052-10W5	.72	1951.6-1058.6		BLMR
11-20-054-11W5	.86	1885.0-1053.4		BLMR
07-26-055-20W5	1.15	2786.4-1571.5		BLMR
10-19-056-11W5	.74	1886.0	-980.4	BLMR
06-32-056-11W5	.64	1819.7	-934.8	BLMR
07-33-056-11W5	.63	1822.7	-938.3	BLMR
16-04-059-05W5	.77	1204.0	-537.7	BLMR
15-04-060-12W5	.74	1533.8	-832.4	BLMR
02-18-062-18W5	.72	1925.7-1044.5		CDMN
10-25-064-19W5	.67	1431.0	-652.6	BLMR
10-14-064-20W5	.67	1553.0	-734.6	BLMR
07-16-065-22W5	.49	1844.0-1108.0		BLUE
12-16-075-15W5	.38	754.4	-170.1	GETH
14-15-075-22W5	.36	954.0	-379.5	GETH
08-23-075-22W5	.39	945.2	-377.7	BLUE
10-07-077-23W5	.46	786.3	-358.8	GETH
11-30-080-23W5	.40	741.6	-167.3	BLUE
16-22-053-10W6	2.21	3530.0-2043.0		FALH
07-21-084-07W6	.70	2586.0-1534.4		CDTT
08-06-085-02W6	.78	2338.1-1463.1		SRIV
10-16-065-02W6	.67	2201.6-1387.5		BLUE
07-34-065-03W6	.97	2282.3-1483.2		BLUE
03-16-065-04W6	.72	2483.4-1595.6		GETH
05-12-065-05W6	.83	2477.1-1635.9		SRIV
10-23-065-05W6	.60	2086.0-1286.4		SRIV
10-04-067-10W6	1.26	2485.0-1619.7		FALH
07-15-067-10W6	1.23	2535.0-1582.8		FALH
06-12-070-05W6	.69	1743.0-1088.8		GETH
10-25-070-08W6	.91	1640.1	-943.4	FALH
10-08-070-09W6	1.19	2183.9-1468.8		GETH
11-10-070-09W6	.93	1779.1-1083.3		FALH
08-22-070-09W6	.67	1774.9-1080.4		FALH
08-05-070-10W6	.77	1917.2-1198.3		FALH
11-28-070-11W6	1.00	1873.4-1155.9		FALH
13-20-075-02W6	.50	1182.0	-536.7	GETH
05-05-075-13W6	1.37	1875.1-1055.9		GETH
07-21-080-06W6	.66	1017.5	-410.6	GETH
08-35-085-04W6	.55	1016.5	-178.3	GETH

Hacquebard (1977) provided few details about the derivation of this relationship and no discussion of the errors associated with the determination of it. For this reason his technique for estimating erosion could be considered suspect. However, Nurkowski (1984), in a comprehensive study of Alberta near-surface coals, found statistically significant relationships between equilibrium moisture content and both dry ash and moist mineral-matter-free calorific values, over the limited range of the calorific values in coals that outcrop in the Alberta Plains. As reflectance is also related to coal rank (e.g., Kalkreuth and McMechan, 1984) it is reasonable to assume that a relationship exists between logarithmic reflectance gradient, amount of erosion and surface equilibrium moisture content (Fig. 5). Ideally it should be possible to employ coalification gradient data to determine the validity of Hacquebard's relationship. Unfortunately, this cannot be done because of uncertainties associated with coalification gradients. If logarithmic coalification gradients from well profiles are extrapolated to zero coalification, 0.25 % Ro (Fig. 5), then an estimate of erosion and the uncertainty in that estimate resulting from uncertainty in the logarithmic reflectance gradient is obtained. This can be compared directly with the independent estimate of the eroded section using its geographic location and near surface equilibrium moisture content (Fig. 1).

This was done for several wells that have reflectance profiles (England, 1984; Kalkreuth and McMechan, 1984; Stasiuk, 1988). The results from extrapolated well profile coalification gradients are plotted (Fig. 6) such that the erosion estimate and its accompanying uncertainty, shown as an error bar, is the abscissa value (axis labeled "depth of burial" in Figure 6 and representing the depth of burial of the present surface at the time of maximum burial), and the ordinate value is the equilibrium moisture content of near surface coals (axis labeled "bed moisture") as estimated from geographic position of the well profile study (Fig. 1).

It is clear that the large uncertainties and the rapid geographic variations in well profile erosion estimates cannot be used to corroborate the relationship proposed by Hacquebard (1977), nor can they be used to formulate an independent relationship between erosion and surface coal properties. Hence the relationship between erosion and bed moisture is employed without increased confidence.

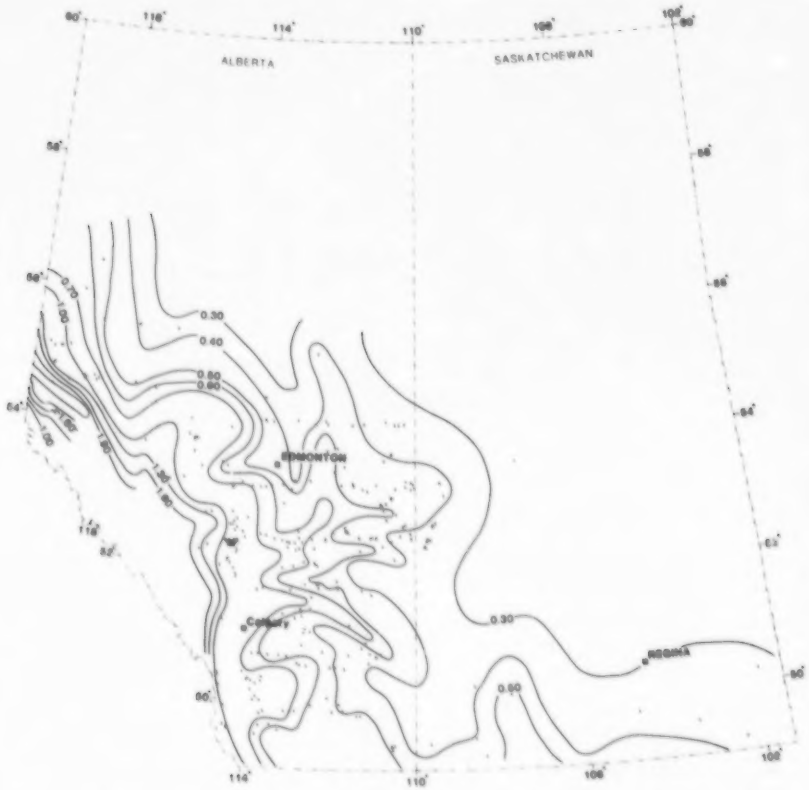

Figure 2. Reflectance of Mannville Group sediments. Plains data from various sources mentioned in the text. On the northwestern portion of the map, that area west of the 118th meridian, the isoreflectance contours are taken from Kalkreuth and McMechan (in press) and are drawn on the Gething Formation, approximately equivalent to the Mannville Group.

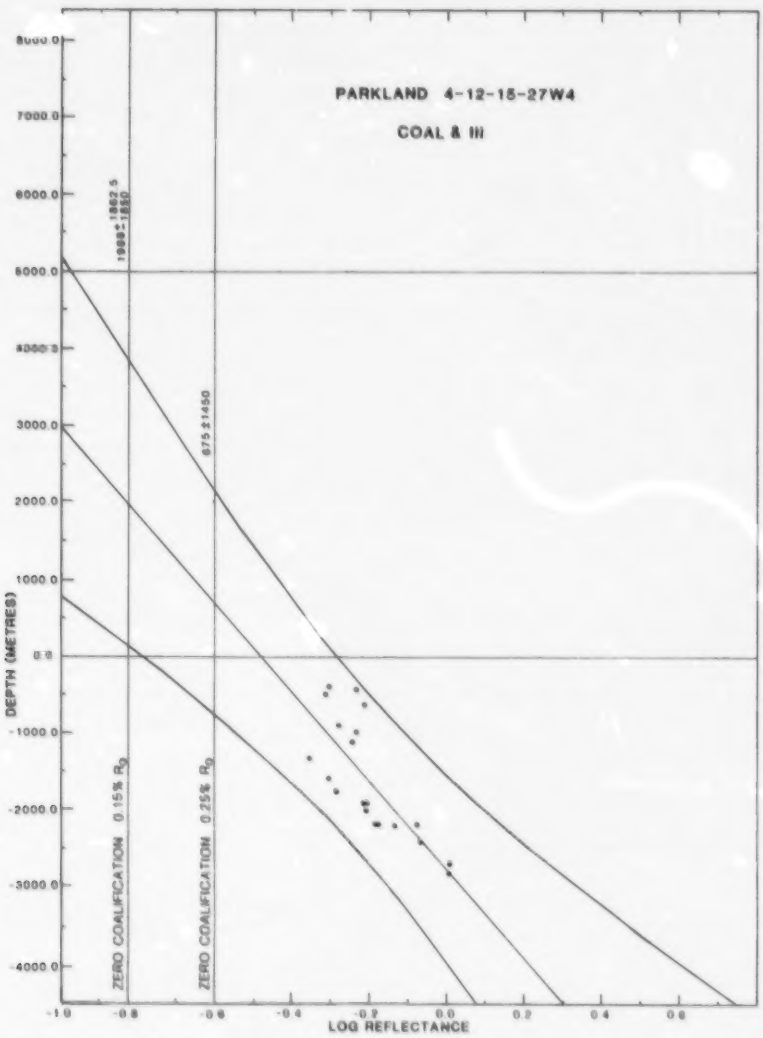

Figure 3. Dependence of logarithm of reflectance on depth in core samples of coals and Type III organic material from the Parkland well 4-12-15-27W4 (L.D. Stasiuk, analyst). The regressed coalification gradient (log %Ro/km) and 2 sigma error envelope are shown as the hyperbolic envelope to the best fit line. The dependence of the estimate of erosion as a function of both the model of zero coalification (both 0.15% and 0.25% Ro models are indicated) and the uncertainty in the coalification gradient are shown by the two estimates of 675 + /- 1450 m (0.25%Ro zero coalification model) and 1988 + 1862.5/-1850 m (0.15%Ro zero coalification model).

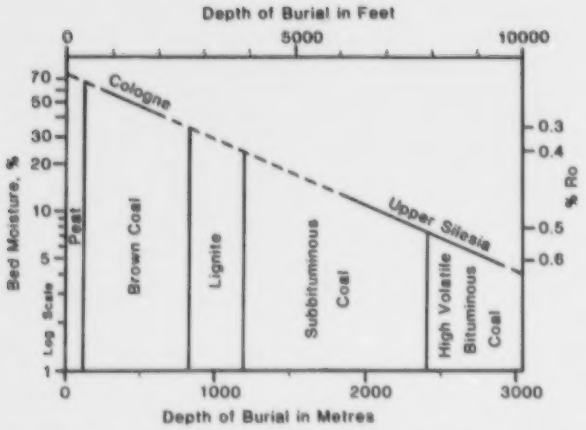

Figure 4. Nurkowski's (1984) expression of Hacquebard's (1977) relationship between maximum burial depth and equilibrium moisture content of coals.

FORELAND PALEOGEOTHERMAL GRADIENTS

Calculation of the paleogeothermal gradient field

We assume that it is possible to estimate erosion since the time of maximum burial from Hacquebard's relationship (Fig. 1). This can be combined with a map of the thickness of remaining Cretaceous and Tertiary sediments on the Plains (e.g., Masters, 1984) to estimate the thickness of the Foreland succession at the end of Laramide Orogeny (Fig. 7). Knowing the reflectance variation of Mannville Group coals and organic material (Fig. 2), the thickness of the Foreland succession on the Plains (Fig. 7), and using a reflectance of 0.25 %Ro to represent zero coalification, it is possible to calculate both logarithmic coalification gradients and the paleogeothermal gradient using Middleton's (1982) technique (Fig. 8).

Many of the data used to make the reflectance map for the Mannville Group (Fig. 2, Tables 1, 2) are new and were assembled specifically for this project. The extreme northwest portion of this map is taken from a map of reflectance on the Gething Formation (from Kalkreuth and McMechan, 1988). That portion is consistent with the Mannville Group data in the adjoining portions of the map.

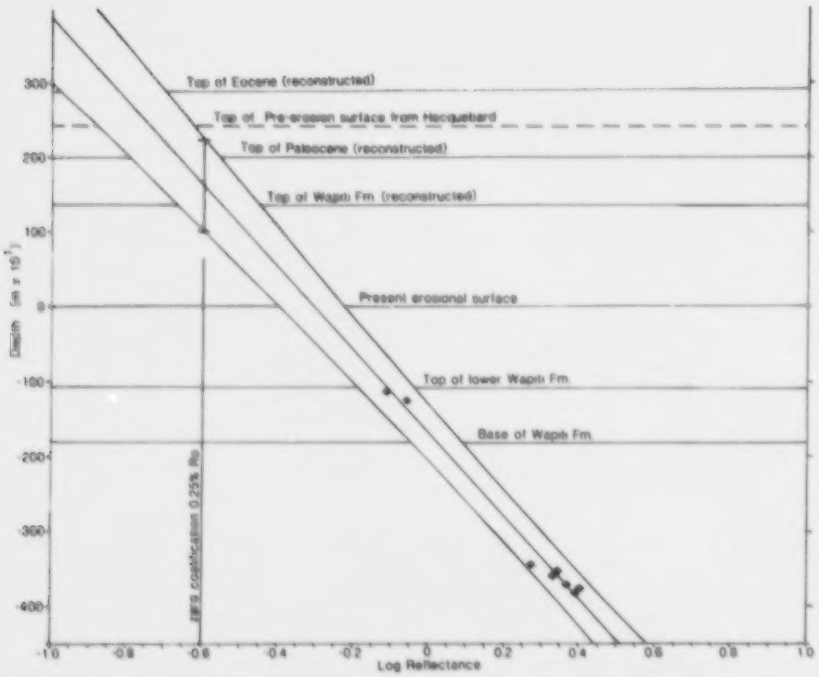

Figure 5. Dependence of logarithm of reflectance on depth in the well Husky et al., Cutbank 16-22 (data from Kalkreuth and McMechan, 1984). Tops of known and inferred stratigraphic layers indicated. The regressed coalification gradient (log%Ro/km) and 2∂ error envelope are employed to infer the effective paleogeothermal gradient (Middleton, 1982) and consistency of the reflectance gradient with the stratigraphic model when the former is extrapolated to a level of zero coalification (0.25%Ro).

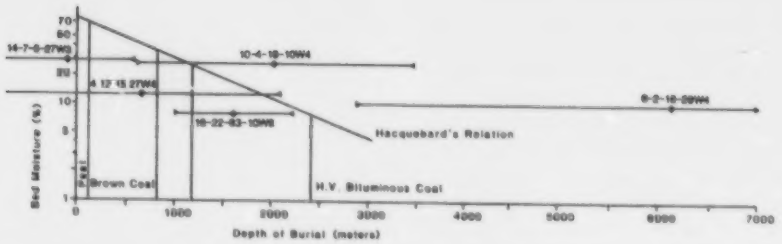

Figure 6. Plot comparing estimates of erosion as derived from both surface equilibrium moisture content of coal, and extrapolation of several coalification gradients to zero coalification. Errors on the extrapolated reflectance gradients are defined by the intersection of the 2∂ error envelopes with 0.25%Ro.

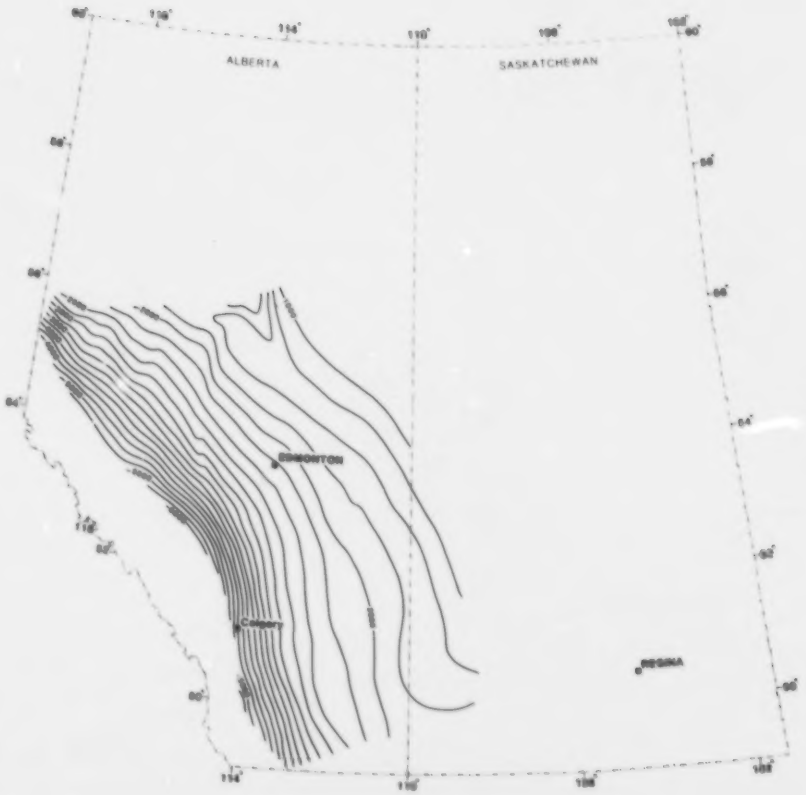

Figure 7. Depth to the base of the Cretaceous succession (commonly Mannville Group) in the Plains at the end of the Laramide Orogeny in the Middle Eocene. See text for construction technique.

Like a map by Masters (1984), this map (Fig. 2) is characterized by a general increase in reflectance toward the west. Reflectances range from less than 0.3 %Ro on the northeastern margin of the basin, to approximately 2.0 %Ro in its deepest portions. Unlike Master's map (1984, Fig. 18, p. 17) this map suggests that isoreflectance contours do not conform well with burial depth contours, indicating a more complex paleogeothermal gradient field. Figure 2 is characterized by prominent intrusions of the 0.7 %Ro contour into the Plains. The more northerly of these features is poorly delineated. The southern feature forms a bifurcating set of ridges that penetrate the Plains, one looping from Calgary toward Brooks, and the other trending northeast toward Edmonton, where the ridge bifurcates toward Lloydminster and Lac La Biche. A major extension of the 0.50 %Ro contour lies in the keel of the Shaunavon Syncline in southwestern Saskatchewan at approximately the 108th meridian of longitude.

COMPARISON TO OTHER CONSTRAINTS

The pattern and magnitude of paleogeothermal gradients calculated (Fig. 8) using Mannville Group coal rank and an independent erosion estimate using the surface equilibrium moisture content of coals can be compared to other constraints on paleogeothermal gradients. There is general agreement, within a few mK/m, to data from the Garrington and Pembina oil pool areas, where independent temperature estimates for the time of maximum burial were made using fluid inclusions (Currie and Nwachukwu, 1974; recalculated using depths of burial suggested by Hacquebard's (1977) relation for consistency) and isotopic geothermometry (Longstaffe, 1986). There is also a general agreement between paleogeothermal gradients calculated from this study and those from the western three quarters of a profile (Beaumont et al., 1985) where paleogeothermal gradients were calculated using hydrocarbon aromatization and isomerization reactions.

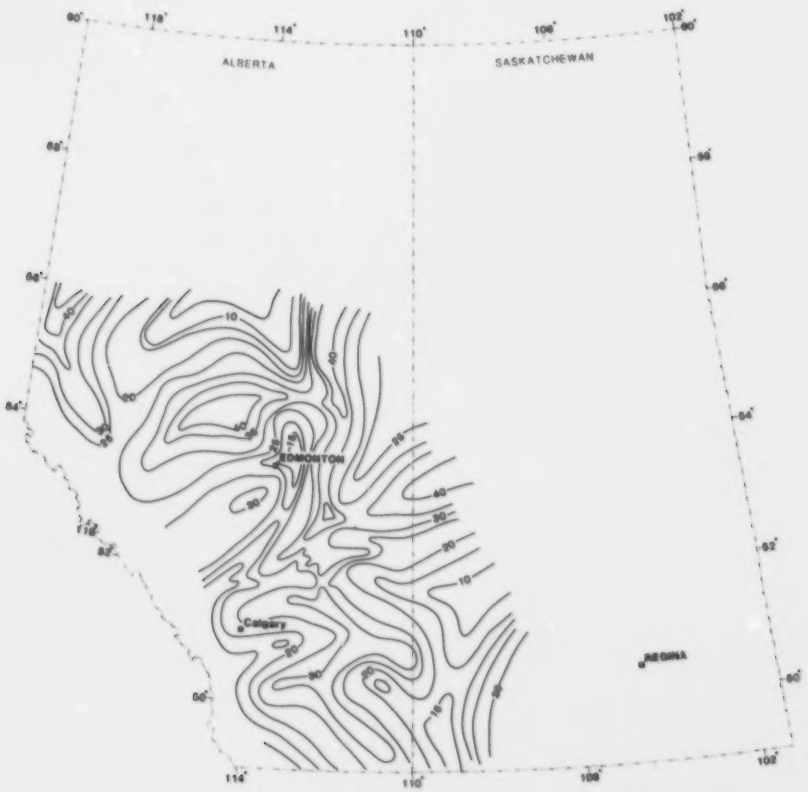

Figure 8. Inferred Middle Eocene geothermal gradient field based on analysis of Mannville Group reflectance and maximum burial depth, using the technique of Middleton (1982) as mentioned in the text.

SIMILARITIES TO THE PRESENT GEOTHERMAL GRADIENT FIELD

The paleogeothermal gradient map (Fig. 8) exhibits both similarities to and differences from the present geothermal gradient map (Fig. 9). Present geothermal gradients are strikingly similar to paleogeothermal gradients in both pattern and magnitude. Like the present gradient, paleogeothermal gradients tend to increase eastward toward regions of lower topography, suggesting that hydrodynamically controlled advective heat transfer dominated the late orogenic geothermal field as it does currently. Another striking similarity is the large region of the Plains where the geothermal gradient is inferred not to have changed significantly. The similarity between the two maps is particularly evident in southern Alberta, where the 30 mK/m isogradient contours are generally coincident. The ridge of higher geothermal gradients that extends from Canmore to Calgary can be seen on both maps, as well as the lower geothermal gradients in the western part of the southern Plains adjacent to the Foothills. The pronounced ridge of high geothermal gradients northeast of Edmonton remains a feature of the present gradient field, with gradients even higher now than they were in the past.

DIFFERENCES FROM THE PRESENT GEOTHERMAL GRADIENT FIELD

The differences between the two maps can be associated with specific geological features postdating the time of maximum burial (Fig. 10). Several regions exist where significant increases in the magnitude of the geothermal gradient have occurred. A region of higher present gradients coincides with the present outcrop of Lower Cretaceous aquifers, an area of regional hydraulic discharge. These outcrop patterns are a post-Middle Eocene feature of the basin.

Geothermal gradient values from the map (Fig. 8) compare well with values calculated by Beaumont et al. (1985) along the western three quarters of a profile in which paleogeothermal gradients were studied using aromatization and isomerization reactions in hydrocarbon extracts. However, the paleogeothermal gradients calculated using coalification data that coincide with the eastern portion of this profile were generally less than 30 mK/m, whereas aromatization and isomerization data suggest that geothermal gradients in this area may have exceeded 60 mK/m (ibid.). The present geothermal gradients in this region lie between 35 and 40 mK/m. The reason for these differences is uncertain. Also

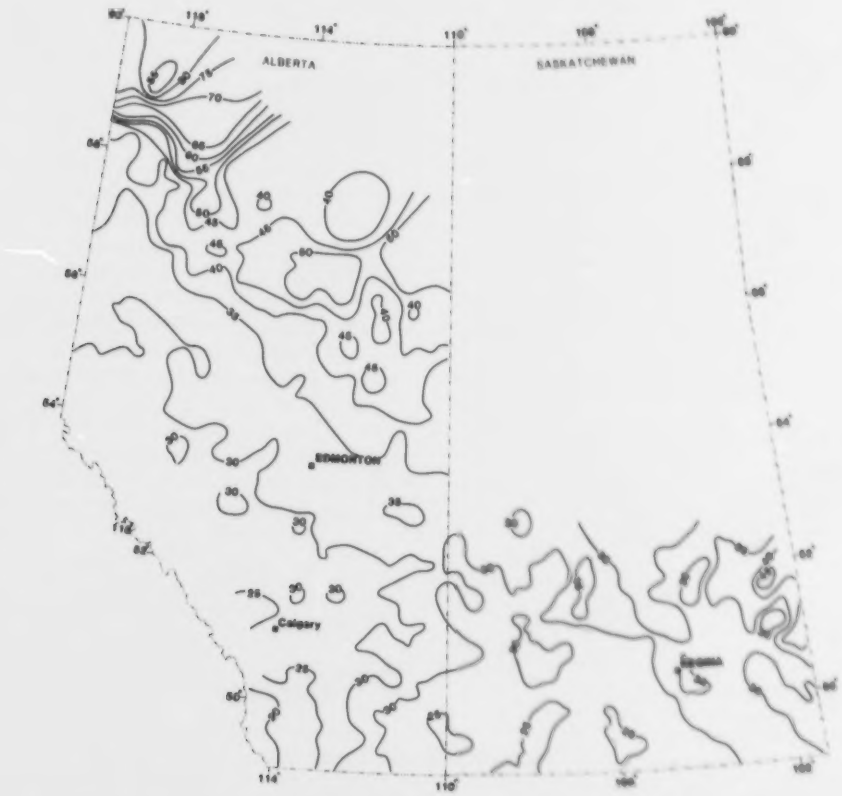

Figure 9. Present geothermal gradient field (mK/m) within the Foreland Basin succession. (After Majorowicz et al., 1985b; 1986.)

uncertain is a plausible mechanism for the high gradients calculated for the easternmost aromatization-isomerization samples. Possibly they may reflect local high geothermal gradient anomalies analogous to those identified in Devonian strata by Aulstead and Spencer (1985).

Specific changes in the gradient field elsewhere can be attributed to changing geological structure affecting hydraulic recharge and discharge. One example occurs in southwestern Saskatchewan along the interprovincial boundary (Fig. 10). These changes follow meteoric water circulation commonly attributed to hydraulic recharge in the Bearpaw and Little Rocky mountains of eastern Montana. These uplands are related to a Miocene volcanic centre, and the geothermal gradient changes are associated with geological features formed after the end of the Laramide Orogeny. The ridge of greatest change in the geothermal gradient associated with this feature coincides with the subcrop of the Madison Group (Mississippian carbonates) immediately below the Mannville Group and with a pattern of fresher formation waters. Formation water salinity studies have previously suggested that the Madison and Three Forks (uppermost Devonian and Lower Mississippian) groups act as a conduit for meteoric waters from the uplifts in eastern Montana. These waters would be heated during their passage through Paleozoic strata and be discharged into Cretaceous strata along the subcrop edge of the Madison Group.

This information can be used to corroborate ideas of timing of hydrocarbon accumulations and biodegradation. Throughout this region, oils are progressively biodegraded following a geographic pattern similar to that of the greatest change in geothermal gradients. It has commonly been assumed that the biodegradation of oils accompanied the appearance of the Bearpaw and Little Rocky mountains in the Miocene and the introduction of fresh, bacteria-bearing waters in these recharge areas. Such models are consistent with changes in the pattern of the geothermal gradient field.

Increase in geothermal gradients is also observed along the southwestern margin of the Plains. These increases can be attributed to a loss of efficiency in the hydrodynamic recharge system following the erosional decay of topography (Fig. 10).

Figure 10. Map of the differences between the Middle Eocene paleogeothermal gradients and the Present geothermal gradients formed by subtracting the paleogeothermal gradient map from the present geothermal gradient map. Positive contour lines indicate an increase in geothermal gradient values since the end of the Laramide Orogeny. See discussion in the text of features on this map.

OTHER CHANGES IN THE GEOTHERMAL GRADIENT FIELD

Strong evidence indicates that the geothermal gradient has decreased elsewhere in the Foreland succession. North of the hinge of the Nesson Anticline (103rd meridian of longitude) the present geothermal gradient in the foreland succession conforms with the regional pattern. Along this trend the geothermal gradient in the underlying Paleozoic succession is high (Majorowicz et al., 1986) and lignites in Tertiary strata overlying the same region have higher reflectances than those at similar stratigraphic levels away from this region (Cameron, in press). Price et al. (1984) described a thermal maturity anomaly along the crest of the Nesson Anticline. Osadetz et al. (1989) extended this maturation anomaly north into Canada beyond the closure of the present anticline to define a larger and longer-lived structural feature. The elevated reflectance of Tertiary lignites in this region indicates that high geothermal gradients must have persisted in the Foreland succession at least until Paleocene time, although they are currently suppressed (Fig. 9) (Majorowicz et al., 1986).

CONCLUSIONS

Paleogeothermal gradients can be calculated in the foreland succession for the time of maximum burial using an independent estimate of the eroded section, an assumed reflectance at zero coalification and a map of reflectance of the Mannville Group. Calculated paleogeothermal gradients generally agree with gradients estimated from fluid inclusion, isotopic geothermometers and aromatization-isomerization reactions in hydrocarbon extracts. Unfortunately, the large uncertainties associated with coalification gradients from well profiles make it impossible to determine if estimates of erosion and the inferred paleogeothermal gradients agree with the paleogeothermal gradients determined directly from well profile data. The paleogeothermal gradient field compares favorably with the present geothermal gradient field. This suggests that hydrodynamically controlled advective heat transfer dominated the paleogeothermal gradient field at the end of the Laramide Orogeny in a manner analogous to that inferred currently. Large changes in the geothermal gradient field since the end of the orogeny reflect changes in the pattern of hydrodynamic water flow that are controlled by post-Eocene structural features in the Interior Platform Structural Province.

REFERENCES

Aulstead, K.L. and Spencer, R.J.
1985: Diagenesis of the Keg River Formation, northwestern Alberta: Fluid inclusion evidence; Bulletin of Canadian Petroleum Geology, v. 33, no. 2, p. 167-183.

Beaumont, C., Boutilier, R., Mackenzie, A.S., and Rullkotter, J.
1985: Isomerization and aromatization of hydrocarbons and the paleothermometry and burial history of the Alberta Foreland basin; American Association of Petroleum Geologists, Bulletin, v. 69, no. 4, p. 546-566.

Buntebarth, G.
1979: The degree of metamorphism of organic matter in sedimentary rocks as a paleo-geothermometer, applied to the upper Rhine Graben; Paleogeophysics, v. 117, p. 83-91.

Cameron, A.R.
in press: Regional patterns of reflectance distribution in lignites of the Ravenscrag Formation, Saskatchewan, Canada.

Currie, J.B. and Nwachukwu, S.O.
1974: Evidence on incipient fracture porosity in reservoir rocks at depth; Bulletin of Canadian Petroleum Geology, v. 22, no. 1, p. 42-58.

Dow, W.G.,
1977: Kerogen studies and geological interpretation; Journal of Geochemical Exploration, v. 7, p. 79-99.

England, T. D. J. and Bustin, R.M.
1986: Thermal maturation of the western Canadian Sedimentary Basin south of the Red Deer River: I) Alberta Plains, Bulletin of Canadian Petroleum Geology, v. 34, no. 1, p. 71-90.

Hacquebard, P. A.
1977: Rank of coal as an index of organic metamorphism for oil and gas in Alberta; *in* The origin and migration of petroleum in the western Canadian Sedimentary basin, Alberta — A geochemical and thermal maturation study, G. Deroo, T.G. Powell, B. Tissot and R.G. McCrossan; Geological Survey of Canada, Bulletin 262, p. 11-22.

Kalkreuth, W. and McMechan, M.E.
1984: Regional pattern of thermal maturation as determined from coal-rank studies, Rocky Mountain Foothills and Front Ranges north of Grande Cache, Alberta — implications for Petroleum exploration; Bulletin of Canadian Petroleum Geology, v. 32, no. 3, p. 249-271.
1988: Coal rank, burial histories and thermal maturity, Rocky Mountain Foothills and Foreland, east-central British Columbia and adjacent Alberta, Canada; American Association of Petroleum Geologists, Bulletin.

Lopatin, N.V.,
1971: Temperature and geologic time as factors in coalification. Akademia Nauka USSR, Yzv. Ser. Geol. 3, p. 95-106.

Majorowicz, J.A. and Jessop, A.M.
1981: Regional heat flow patterns in the western Canadian sedimentary basin; Tectonophysics, v. 74, p. 209-238.

Majorowicz, J.A., Jones, F.W., and Jessop, A.M.
1986: Geothermics of the Williston basin in Canada in relation to hydrodynamics and hydrocarbon occurrences; Geophysics, v. 51, no. 3, p. 767-779.

Majorowicz, J.A., Jones, F.W., Lam, H.L., and Jessop, A.M.
1985a: Terrestrial heat flow and geothermal gradients in relation to hydrodynamics in the Alberta basin, Canada; Journal of Geodynamics, v. 4, p. 265-283.
1985b: Regional variations of heat flow differences with depth in Alberta, Canada; Geophysical Journal of the Royal Astronomical Society, v. 81, p. 479-487.

Majorowicz, J.A., Rahman, M., Jones, F.W., and McMillan, N.J.
1985: The paleogeothermal and present thermal regimes of the Alberta basin and their significance for petroleum occurrences; Bulletin of Canadian Petroleum Geology, v. 33, no. 1, p. 12-21.

Masters, J.A.
1984: Lower Cretaceous oil and gas in Western Canada. *in* Elmworth — case study of a deep basin gas field, ed. J.A. Masters; American Association of Petroleum Geologists, Memoir 38, p. 1-34.

Middleton, M.F.
1982: Tectonic history from vitrinite reflectance; Royal Astronomical Society, Geophysical Journal, v. 68, p. 121-132.

Nurkowski, J.R.
1984: Coal quality, coal rank variation and its relation to reconstructed overburden, Upper Cretaceous and Tertiary Plains coals, Alberta, Canada; American Association of Petroleum Geologists, Bulletin, v. 68, p. 285-295.

Osadetz, K.G., Snowdon, L.R., and Stasiuk, L.D.
1989: Association of enhanced hydrocarbon generation and crustal structure in the Canadian Williston Basin; *in* Current Research, Part D, Geological Survey of Canada, Paper 89-1D, p. 35-47.

Pearson, D.E.,
1985a: Source rock maturity of the Alberta Plains: a database of vitrinite reflectance for oil and gas exploration planning. Manuscript Final Report to Department of Supply and Services contract OSG84-00100. Institute of Sedimentary and Petroleum Geology, Calgary.

1985b: Source rock maturity over the Peace River Arch. Manuscript Final Report to Department of Supply and Services contract OSG85-00184. Institute of Sedimentary and Petroleum Geology, Calgary.

Price, L.C., Ging, T., Daws, T., Love, A., Pawlewicz, M., and Anders, D.

1984: Organic metamorphism in the Mississippian-Devonian Bakken shale, North Dakota portion of the Williston Basin; *in* Hydrocarbon source rocks of the greater Rocky Mountain region, eds. J. Woodward, F.F. Meissner, and J.L. Clayton; Rocky Mountain Association of Geologists, Denver, p. 83-134.

Rahman, M., Majorowicz, J.A., Bosse, V., and Jones F.W.,

1985: Some implications of organic maturation modelling in south-central Alberta; Bulletin of Canadian Petroleum Geology. v. 33, p. 396-409.

Stasiuk, L.D.

1988: Thermal maturation and organic petrology of Mesozoic sediments of southern Saskatchewan; unpublished M.Sc. thesis, University of Regina, Regina, 172 p.

Stott, D.F.

1984: Cretaceous sequences of the Foothills of the Canadian Rocky Mountains; *in* The Mesozoic of Middle North America, ed. D.F. Stott and D. J. Glass; Canadian Society of Petroleum Geologists, Memoir 9, p. 85-107.

Waples, D.W.,

1980: Time and temperature in petroleum formation: application of Lopatin's method to petroleum exploration; American Association of Petroleum Geologists, Bulletin, v. 54, p. 916-926.

Stratigraphy of Cretaceous — Tertiary rocks of North Bylot Trough, Bylot Island, N.W.T.

P. H. Benham[1] and E. T. Burden[1]
Atlantic Geoscience Centre

Benham, P.H. and Burden, E.T., Stratigraphy of Cretaceous — Tertiary rocks of North Bylot Trough, Bylot Island, N.W.T.; in Current Research, Part D, Geological Survey of Canada, Paper 90-1D, p. 179-185, 1990

Abstract

Cretaceous and Tertiary strata of the North Bylot Trough at Maud Bight on Lancaster Sound are divided into 6 lithostratigraphic units encompassing 3 depositional and tectonic phases. In detail, quartz arenites and shales roughly correspond with the lithologies for Hassel and Kanguk formations of the Eclipse Group in nearby Eclipse Trough on southwest Bylot Island. Tertiary strata containing Paleocene plant fossils are markedly different from Tertiary beds of the Eclipse Group. North Bylot rocks include a coarsening-upward cycle of shale, lithic greywacke and boulder conglomerate beds more than 200 m thick. Lithostratigraphic correlation of North Bylot Trough with Eclipse Trough indicates that these two areas became separated when the Byam Martin Mountains formed in the Maastrichtian. Deformed Tertiary strata indicate renewed tectonic activity corresponding with the opening of Baffin Bay to the east and the Lancaster Aulacogen to the north.

Résumé

Les couches crétacés et tertiaires de la dépression de North Bylot, à la baie Maud, dans le détroit de Lancaster, ont été divisées en six unités lithostratigraphiques englobant trois phases sédimentaires et tectoniques. Les arénites à quartz et schistes argileux correspondent en gros aux lithologies des formations de Hassell et de Kanguk du groupe d'Eclipse contenues dans la dépression voisine d'Eclipse, dans le sud-ouest de l'île Bylot. Les couches tertiaires contenant des fossiles de plantes paléocènes sont nettement différentes des couches tertiaires du groupe d'Eclipse. Les roches de North Bylot sont composées, entre autres, d'une séquence négative de couches de schiste argileux, de grauwacke lithique et de couches de conglomérat à blocs de plus de 200 m d'épaisseur. La corrélation lithostratigraphique de la dépression de North Bylot avec la dépression d'Eclipse indique que ces deux zones ont été séparées lorsque les monts Byam Martin se sont formés pendant le Maastrichtien. La déformation de couches tertiaires témoigne d'une reprise de l'activité tectonique correspondant à l'ouverture de la baie de Baffin, à l'est, et à l'aulacogène de Lancaster, au nord.

[1] Department of Earth Sciences, Memorial University, St. John's, Newfoundland, A1B 3X5

INTRODUCTION

Regional geological syntheses of the Mesozoic and Cenozoic history of northern Baffin Island and Bylot Island show that as Baffin Bay opened in the Cretaceous and early Tertiary, extensional faulting in the Lancaster Sound region generated an aulacogen filled with at least 6 km of strata (Kerr, 1980). Little of this rock is found onshore; consequently, little is known about the style of deposition, the tectonism, age and resource potential of this area.

A short distance south on Bylot Island lies North Bylot Trough, an area where Cretaceous and Tertiary rocks from the rim of the Lancaster Aulacogen extend onshore (Fig. 1). This area is our only direct link to the submarine geology of the Lancaster Aulacogen. Here, faulted and downthrown blocks of Proterozoic strata are covered, over an area of approximately 120 km^2, with Cretaceous and Tertiary clastic sediments having a composite total thickness of about 500 m.

Our studies are aimed at refining the stratigraphy, age and paleoenvironments for the Cretaceous and Tertiary rocks of this exposed part of the Lancaster Aulacogen. Due to the proximity of Eclipse Trough (Fig. 1), one would expect similar strata in North Bylot Trough; we present evidence which shows different, albeit tectonically related strata.

Previous Work

Little geological fieldwork has been reported on the Cretaceous and Tertiary strata of this area; the area remained largely unexplored until 1968, when the Geological Survey of Canada launched Operation Bylot, a helicopter supported reconnaissance mapping project (Jackson, 1969). In that study the Cretaceous and Tertiary rocks of the Maud Bight area were divided into Cretaceous orthoquartzites and undifferentiated, unconsolidated Cretaceous to Tertiary sandstone and shale of variable colour, texture and bedding thickness (Jackson and Davidson, 1975). In the mid-seventies interest in the geology and petroleum potential of Lancaster Sound was increased as seismic and other regional geophysical studies showed a thick sedimentary fill containing structures which might hold several billion barrels of recoverable hydrocarbons (Keen *et al.* 1972; Daae and Rutgers, 1975; Beh, 1975). Petroleum companies sent geologists to examine and collect strata from the Maud Bight area (McWhae, 1981); however, research emphasis on stratigraphy and sedimentology remained with the more accessible rocks of Eclipse Trough (Jackson *et al.* 1975; Miall *et al.*, 1980).

Regional tectonic and stratigraphic syntheses by Jackson *et al.* (1975), Kerr (1980), Jackson and Iannelli (1981) and Jackson and Sangster (1987) show that the north Baffin

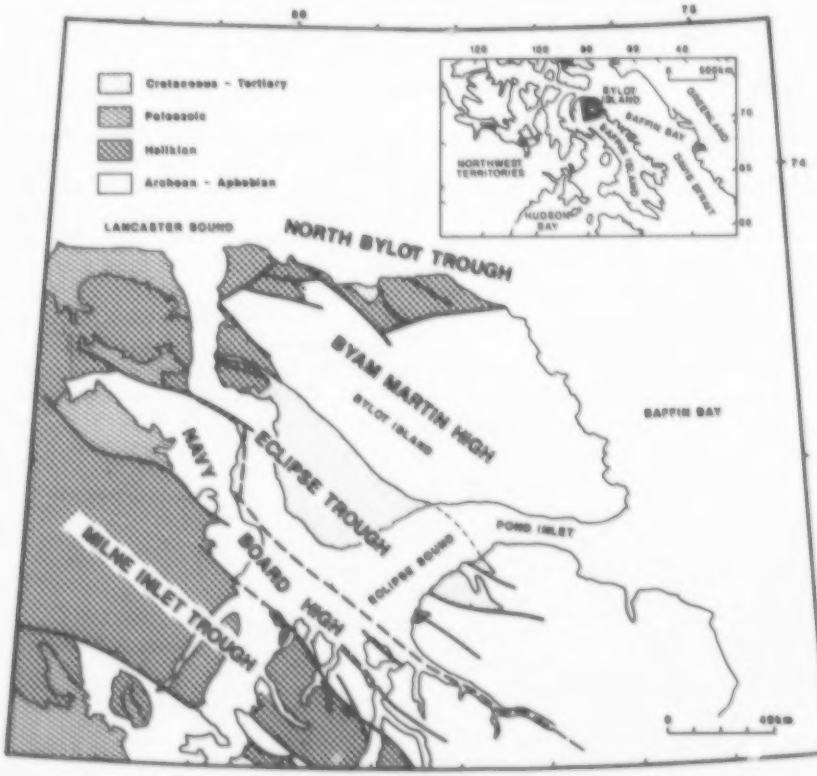

Figure 1. Regional setting for North Bylot Trough (after Jackson and Davidson, 1975).

region is composed of a number of fault bounded, northwest- plunging basins and structural highs truncated by the North Baffin Fault, an east- and northeast- striking fault on the southern margin of the Lancaster Aulacogen. Strata in the basins consist of unconformity bounded "sequences" (Kerr, 1980) or groups (Jackson and Sangster, 1987). These sequences indicate recurring extensional tectonic activity during the last 2 Ga.

FIELDWORK

The area containing the best exposures of Cretaceous and Tertiary rocks is the coastal plain immediately south of Maud Bight (Fig. 2). The plain is bordered on the south and west by faulted and uplifted Precambrian granitic and metasedimentary rocks of the Byam Martin Mountains and on the east by faulted and uplifted carbonates and evaporites of the Precambrian Victor Bay Formation; the northern margin, about 10 km offshore in Lancaster Sound, is the North Baffin Fault.

Cretaceous and Tertiary rocks consisting of flat lying or gently dipping, poorly consolidated conglomerate, sandstone, siltstone and shale, are best exposed in cliffs along the seashore and on the banks of glacial streams. Elsewhere, strata are covered with a thin veneer of glacial debris. Cretaceous and Tertiary rocks from near the south and east margins of the North Bylot Trough are steeply inclined, complexly folded and faulted by both normal and reverse faults.

Sections containing thick deposits of laterally extensive strata were measured and sampled for sedimentology and palynology. Other smaller sections were identified from ground and helicopter traverses and plotted on air photographs.

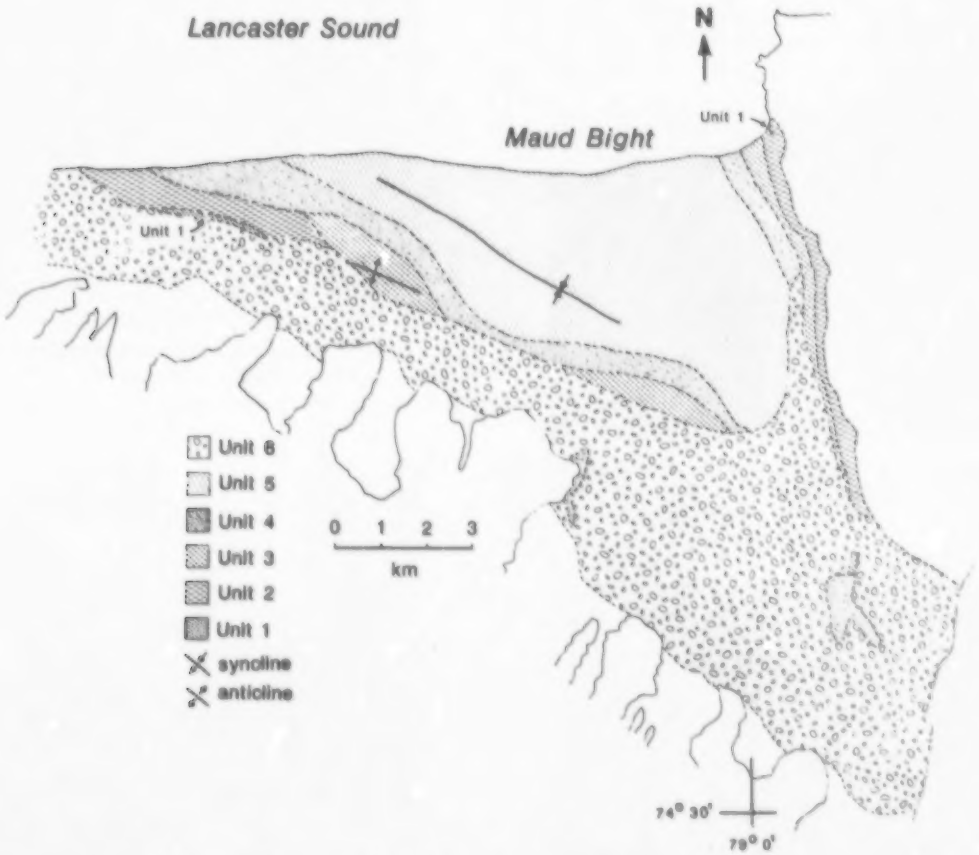

Figure 2. Distribution of Cretaceous and Tertiary rock units in North Bylot Trough at Maud Bight.

STRATIGRAPHY

The Mesozoic-Cenozoic strata of North Bylot Trough have been divided into six lithostratigraphic units (Fig. 2, 3).

Unit 1, measuring no more than 8 m in thickness (Fig. 3), is exposed along the western margin of the trough and in fault bounded sections out cropping along sea cliffs in the northeast corner of the map area (Fig. 2). In the east the unit consists of a massive, white, mature, coarse grained quartz arenite lying upon several metres of kaolinitic and calcite cemented regolith of the Precambrian Victor Bay Formation. Irregular shaped, greenish, pyritic concretions and yellow (jarosite?) bands are locally present in this uncemented rock. The western margin, not well exposed, consists of white quartz arenite with boulders of Precambrian Adams Sound Formation.

Unit 2 is a friable, grey to black sulphurous laminated and massive shale, streaked with yellow (jarosite?) bands and with local concretions (Fig. 3). It occurs near the fault bounded eastern margin of the basin, along the north coast and in a structurally complex area near the middle of the area (Fig. 2). Where sections have been undisturbed by faulting, the shale lies with a sharp contact on either the Victor Bay Formation, Precambrian migmatites or unit 1. Mottling and Chondrites type trace fossils occur in many of the grey shale bands. Possible thin or incomplete sections around the faulted margin contain about 20 m of shale; the thickest section, in a sea cliff, is more than 80 m thick (Fig. 4).

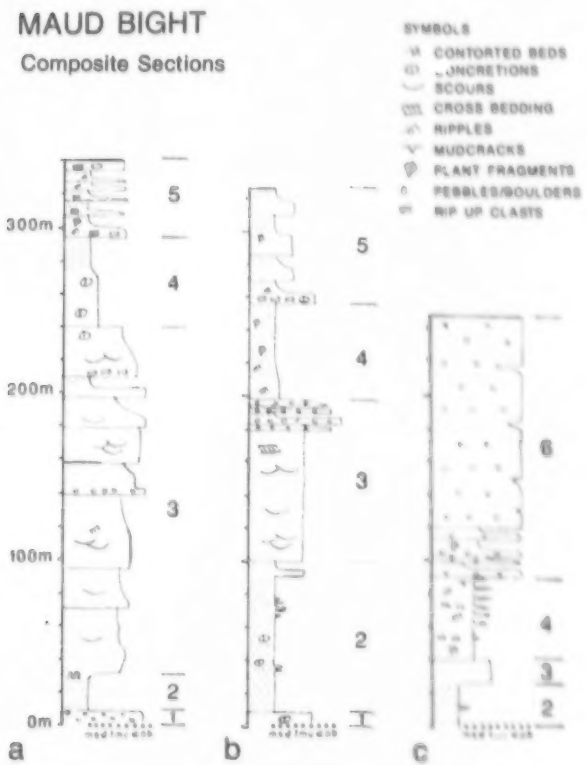

Figure 3. Maud Bight: composite stratigraphic sections. (a) the northwest corner, (b) the coastal section in the northeast corner and (c) the southern margin near the Byam Martin Mountains. Grain size is indicated with symbols (m -mudstone, s - siltstone, vf - very fine sandstone, f - fine sandstone, m - medium sandstone, c - coarse sandstone, vc -very coarse sandstone, p - pebble conglomerate, b - boulder conglomerate).

Unit 3 (Fig. 2) is a complex of lithologies forming a coarsening-upward succession. The base, consisting of shale with siltstone and sandstone interbeds, is overlain by thick beds of white to greenish (glauconitic?), massive, medium- to very coarse-grained quartz arenite. At the top there lies massive and crossbedded, very coarse grained sandstone and conglomerate containing cobbles derived from the Adams Sound Formation. In some sections unit 3 is more than 100 m thick (Fig. 3). The contact of unit 3 with overlying Tertiary sediments is a gently inclined angular unconformity.

Sedimentary structures from near the base of unit 3 include burrowed silty sandstones and thin beds of mixed siltstone and cobbles (debris flows). The overlying sandstones of unit 3 are predominantly unconsolidated and massive; curving, moderately cemented, sideritic bands may be scours. The trace fossil Skolithos is uncommon. The upper part of unit 3 (Fig. 5) contains trough and low angle planar crossbeds with concentrations of magnetite and other heavy minerals and metre- thick gravel bars with megaripples.

Unit 4 ranges from an interbedded fine grained sandstone and siltstone in the south to entirely siltstone in the north (Fig. 3). In the south, the "coarse" lithology is light grey to green, centimetre to decimetre interbeds of fine grained lithic greywacke and siltstone with isolated well rounded pebbles; in the north, the "fine" lithology is a grey, burrowed siltstone with secondary calcitic concretions (Fig. 6). Lithic fragments (notably red metamorphic rocks) and feldspar grains with accessory garnets are common in the greywackes, as are rip-up clasts and wood fragments (including logs). Sedimentary structures include ripples and

Figure 4. Approximately 30 m thick section of grey and black laminated and massive shale of unit 2.

lamination in the coarse- and fine-grained sediments respectively. Beds tend to fine up from a lithic, poorly cemented sandstone with ripple based scours and rip-up clasts to a burrowed black siltstone or shale with minor lenticular beds of fine grained sandstone.

Unit 4 is widespread and reaches 50 m thickness in some sections. It rests unconformably on the shales and sandstones of units 2 and 3 respectively, and is overlain both gradationally and unconformably by the rocks of units 5 and 6.

Unit 5 is light grey to green, medium- to coarse- grained lithic sandstone deposited as a repetitive series of lensoid channel fill and tabular interchannel deposits (Fig. 7). Typical channel fill deposits contain multiple scours overlain with rip-up clasts and granitic and migmatitic boulders. Channel sandstones contain planar crossbeds, trough crossbeds and ripple marks. Plant fragments are common in the interchannel sandstones and at several localities there are mud cracks.

Figure 5. Approximately 30 m thick section of coarse grained sandstone and conglomerate beds of the upper part of unit 3.

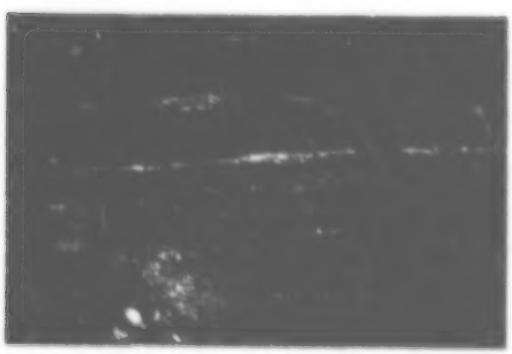

Figure 6. Typical exposure of interbedded siltstone with fine and medium-grained sandstone of the fine grained end member of unit 4. Shovel is about 75 cm in length.

Unit 5 unconformably overlies units 2 and 3 and grades up from the siltstones of unit 4 (Fig. 3). In places the contact with unit 4 is scoured. Unit 5 covers much of the northern half of the study area (Fig. 2) where it reaches a thickness of about 50 m. It appears to have been removed from the southern portions of the basin before the overlying conglomerate (unit 6) was deposited.

Unit 6 is a flat lying conglomerate containing minor sandstone and siltstone beds. Clasts are angular to subrounded and range up to 2 m in diameter (Fig. 8). They are composed of migmatites, foliated granites, augen gneisses, quartzite sandstones and rare basaltic boulders. Individual beds are 1 to 5 m thick, lensoid and contain abundant large wood fragments. The lithic sandstone in the matrix and in separate beds appears to be lithologically similar to, though generally coarser than, the rocks of unit 5. In addition, there are rare, grey, laminated siltstone beds, especially near the base of this unit. One bed has produced many well preserved plant macrofossils (*Equisetum* sp., *Metasequoia occidentalis* (Newberry) Chaney 1951 and *Trochodendroides arctica* (Heer) Berry 1926 in a low diversity assemblage of probable early to middle Paleocene age (Basinger, pers. comm., 1988). The sediments are poorly to moderately cemented with calcite.

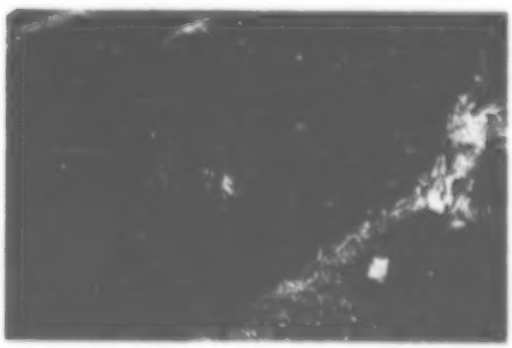

Figure 7. Section of unit 5 approximately 20 m thick showing channel sandstone deposits with adjacent interbedded sandstone and siltstone.

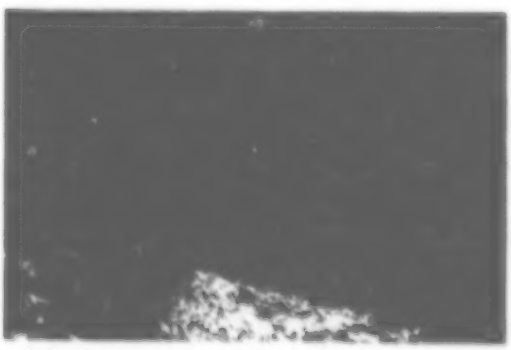

Figure 8. Beds of boulder conglomerate of unit 6 lying on unit 4.

The total thickness of the conglomerate could not be accurately measured; it has been estimated at more than 200 m on the flanks of the Byam Martin Mountains in the southern part of the trough and thins towards the coast. It unconformably overlies units 2, 3 and 4 (Fig. 9). The contact with unit 5 is not as clear; in some sections it appears to be erosional, whereas elsewhere there may be a gently inclined angular unconformity.

DISCUSSION

The Cretaceous and Paleogene depositional and tectonic history of the onshore extension of the North Bylot Trough can be divided into three unconformity bounded tectonostratigraphic phases which correlate with the rocks of Eclipse Trough (Fig. 10). The first phase containing unit 1, is lithologically similar to some outcrops of the Hassel Formation in Eclipse Trough; there, Miall *et al.* (1980) proposed a fluviatile origin for the Hassel Formation. Kerr (1980) postulated an extension of Hassel Formation north into Lancaster Sound where, before the formation of Baffin Bay and the Lancaster Aulacogen, a sheet of fluviatile sediments was deposited on the low lying craton. Our unit 1 sediments at Maud Bight support this line of reasoning and point to the possibility that Hassel strata lie beneath Lancaster Sound.

Phase 2 includes units 2 and 3, which were deposited during a marine transgression. The nature of unit 2 shales suggests a marine environment which is like the interpretation for the grey mudstone of the lower member (Campanian) of the Kanguk Formation in Eclipse Trough (Figure 10) and elsewhere (Miall *et al.*, 1980; Miall 1986).

The shale grades up into the glauconitic sandstone and conglomerate of unit 3. These rocks are interpreted as marine foreshore and beach deposits derived from exposures of the Precambrian Adams Sound Formation. This unit does not compare compositionally with the inferred equivalent strata in Eclipse Trough; upper Kanguk (early Maastrichtian) sandstones in Eclipse Trough contain granitic boulders, cobbles and dinosaurs. Unit 3 and upper Kanguk formation strata show a similar coarsening upward trend. If correlated correctly, this sequence likely marks the uplift of the Byam Martin Mountains and the isolation of Eclipse Trough from the North Bylot Trough and Lancaster Aulacogen. The end of phase 2 in North Bylot Trough is marked by a gently inclined angular unconformity.

The third phase contains rocks of probable early Paleocene age formed during a period of renewed tectonism in North Bylot Trough. Folding and faulting of these beds corresponds with rifting and volcanism in Baffin Bay (Pierce, 1982; Srivastava and Tapscott, 1986); it may also reflect tectonic activity in Lancaster Sound. Beh (1975) suggested that the main rifting phase in Lancaster Sound is in the middle Eocene; Kerr (1980) indicated that rifting began in the latest Cretaceous and by the Miocene/Pliocene all major faulting had ended. Our data suggest that tectonism in North Bylot Trough ended in the Paleocene with the deposition of flat lying unit 6 conglomerates. This suggests that the separation of North Bylot Trough from the Lancaster Aulacogen occurred in the Paleocene when North Baffin Fault formed offshore.

Phase 3 strata resting unconformably on older strata in North Bylot Trough are inferred to represent a transition from distal to proximal alluvial fan environments. These beds are correlated with, but not equated to, the shales and sandstones of the Mount Lawson and Mokka Fiord formations of the Eureka Sound Group in Eclipse Trough (Fig. 10). Distal equivalents of lithostratigraphic units 4 and 5 should be found in Lancaster Sound.

The Tertiary conglomerates at Maud Bight can easily be mistaken for Quaternary glacial deposits. It is possible that the fossil wood reported from Eclipse Trough in Bernier (1912) and Tremblay (1921) may simply represent logs eroding from elevated remnants of a similar Paleogene alluvial fan complex. A search of the elevated borders of Eclipse and North Bylot troughs might turn up other Tertiary strata containing well preserved plant macrofossils.

Figure 9. Approximately 100 m thick section showing the pronounced erosional truncation of unit 4 before deposition of unit 6.

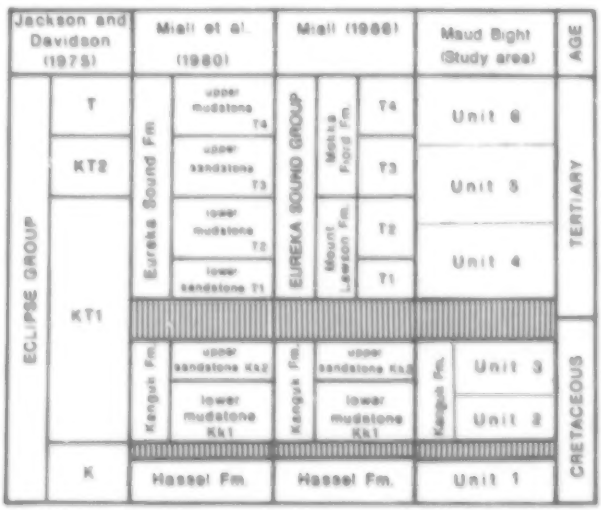

Figure 10. Correlation of Maud Bight strata with lithostratigraphic units described for Eclipse Trough.

CONCLUSIONS

A map containing 6 lithological units for the Cretaceous and Tertiary rocks of the Maud Bight area is interpreted as indicating three tectonostratigraphic phases in the development of the North Bylot Trough. These correlate with events in Eclipse Trough to show a general pattern for sedimentation and tectonism in this region as Baffin Bay and the Lancaster Aulacogen formed. Differences in stratigraphy between the North Bylot and Eclipse troughs are probably a function of basin morphology, the proximity to and provenance of adjacent uplands and different tectonic histories during the late stages of development.

ACKNOWLEDGMENTS

Financial and logistical support was provided by the Geological Survey of Canada (Research Agreement Number 88-144), Natural Sciences and Engineering Research Council, Polar Continental Shelf Project, Department of Indian Affairs and Northern Development — Northern Scientific Training Program, Northern Heritage Society — Science Institute of the Northwest Territories Northerner Employment Training, Employment and Immigration - Challenge 89 and Texaco Canada. Accommodation in Pond Inlet was provided by the Arctic Research Establishment. Helen Gillespie, Terry Wiseman, Robert Rowsell, Joshua Enookoolook and Joseph Maktar assisted in the field. Garth Jackson and Rod Klassen of the GSC Ottawa provided information on access to Maud Bight and on enigmatic boulder beds identified during their exploration of this area; Jim Basinger of the University of Saskatchewan provided plant macrofossil identifications. Dale Russell and Clayton Kennedy of the National Museum of Canada (Ottawa) were helpful and aimable companions in our early attempts to gain access to and from this foggy coast. Graham Williams and Brian MacLean of the Atlantic Geoscience Centre in Halifax formally reviewed this work.

REFERENCES

Beh, R.L.
1975: Evolution and geology of western Baffin Bay and Davis Strait, Canada; *in* Canada's Continental Margins and Offshore Petroleum Exploration, ed. C.J. Yorath, E.R. Parker, and Glass, Canadian Society of Petroleum Geologists, Memoir 4, p. 453-476.

Bernier, J.E.
1912: The "Arctic" Expedition 1910. Report of the Dominion Government Expedition to the northern waters and Arctic Archipelago of the D.G.S. "Arctic" in 1910; Department of Marine and Fisheries, p. 161.

Daae, H.D. and Ratgers, A.T.C.
1975: Geological History of the Northwest Passage; *in* Canada's Continental Margins and Offshore Petroleum Exploration; ed. C.J. Yorath, E.R. Parker, and Glass, Canadian Society of Petroleum Geologists, Memoir 4, p. 477-500.

Jackson, G.D.
1969: Reconnaissance of north-central Baffin Island; *in* Report of Activities, April to October, 1968, Geological Survey of Canada, Paper 69-1, Part A, p. 171-176.

Jackson, G.D. and Davidson, A.
1975: Bylot Island map-area, District of Franklin; Geological Survey of Canada, Paper 74-29, 12 p.

Jackson, G.D. and Iannelli, T.R.
1981: Rift-related cyclic sedimentation in the Neohelikian Borden, northern Baffin Island; *in* Proterozoic Basins of Canada, ed. F.H.A. Campbell; Geological Survey of Canada, Paper 81-10, p. 269-302.

Jackson, G.D. and Sangster, D.F.
1987: Geology and resource potential of a proposed national park, Bylot Island and northwest Baffin Island, Northwest Territories; Geological Survey of Canada, Paper 87-17, p. 31.

Jackson, G.D., Davidson, A., and Morgan, W.C.
1975: Geology of the Pond Inlet map-area, Baffin Island, District of Franklin; Geological Survey of Canada, Paper 74-25, 31 p.

Keen, M.J., Johnson, J., and Park, I.
1972: Geophysical and geological studies in eastern and northern Baffin Bay and Lancaster Sound; Canadian Journal of Earth Sciences, v. 9, no. 6, p. 698-708.

Kerr, J.W.
1980: Structural Framework of Lancaster Aulacogen, Arctic Canada; Geological Survey of Canada, Bulletin 319, 24p.

McWhae, J.R.H.
1981: Structure and spreading history of the northwestern Atlantic region from the Scotian Shelf to Baffin Bay; *in* Canadian Society of Petroleum Geologists, Memoir 7, p. 299-332.

Miall, A.D.
1986: The Eureka Sound Group (Upper Cretaceous Oligocene), Canadian Arctic Islands; Bulletin of Canadian Petroleum Geology, v. 34, p. 240-269.

Miall, A.D., Balkwill, H.R., and Hopkins, W.S., Jr.
1980: Cretaceous and Tertiary sediments of Eclipse Trough, Bylot Island area, Arctic Canada, and their regional setting, Geological Survey of Canada, Paper 79-23, 20p.

Pierce, J.W.
1982: The evolution of the Nares Strait lineament and its relation to the Eurekan orogeny; *in* Nares Strait and the Drift of Greenland: A Conflict in Plate Tectonics, ed. P.R. Dawes and J.W. Kerr; Meddelelser om Grønland, Geoscience, v. 8, p. 237-252.

Srivastava, S.P. and Tapscott, C.R.
1986: Plate kinematics of the North Atlantic; *in* The Geology of North America, Volume M, The Western North Atlantic Region, Chapter 23, The Geological Society of America, p. 379-404.

Tremblay, A.
1921: Cruise of the Minnie Maud; The Arctic Exchange and Publishing Ltd., Quebec, Canada, p. 573.

Petrographic study of Upper Cretaceous brackish-water coals from Vesta Mine, east-central Alberta

Thomas Gentzis[1], Fariborz Goodarzi, and Kanwal Lali[1]
Institute of Sedimentary and Petroleum Geology, Calgary

Gentzis, T., Goodarzi, F., and Lali, K., Petrographic study of Upper Cretaceous brackish-water coals from Vesta Mine, east-central Alberta; in Current Research, Part D, Geological Survey of Canada, Paper 90-1D, p. 187-193, 1990.

Abstract

Substantial quantities of Upper Cretaceous coal occur in the Battle River coalfield, Alberta Plains. Petrographic analysis of two sections taken from seam 3, Vesta Mine, indicates that the coal is low in mineral matter, except for the upper part of section 1. The coal is rich in huminite, and humocollinite and humotelinite are the dominant macerals. Humodetrinite is present in low to moderate amounts (2-20 % mmf) and is more abundant in section 1.

The high content of huminite points to a relatively reducing depositional environment, whereas the high inertinite content of some intervals points to subaerial exposure of the peat surface, oxidation, and/or fire.

Reflectance measured on humotelinite (eu-ulminite B) ranges from 0.39 to 0.52 % Ro, indicating that the coal is of subbituminous C-A rank. Total sulphur is less than 0.6 per cent and boron values range from 150 to 270 ppm. The latter indicates a possible interaction of organic matter with brackish waters in a marginal marsh environment.

Résumé

Des quantités importantes de charbon du Crétacé supérieur se trouvent dans le champ houiller de Battle River dans les plaines de l'Alberta. L'analyse pétrographique de deux plaques minces prélevées dans le filon n° 3 de la mine Vesta indique que le charbon a une faible teneur en matières minérales, à l'exception de la partie supérieure de la plaque n° 1. Le charbon a une teneur élevée en huminite et les principaux macéraux sont l'humocollinite et l'humotélinite. Des quantités de faible à moyenne (de 2 à 20 % mmf) d'humodétrinite ont été relevées mais cette teneur est supérieure dans la plaque n° 1.

La haute teneur en huminite témoigne d'un milieu sédimentaire relativement réducteur tandis que la haute teneur en inertinite de certains intervalles révèle qu'il y a eu affleurement subaérien de la surface de la tourbe, oxydation ou incendie, ou les deux.

La réflectance de l'humotélinite (eu-ulminite B) varie de 0,39 à 0,52 % Ro, indiquant que le charbon est de rang sub-bitumineux C-A. Le soufre total s'élève à moins de 0,6 % et les concentrations en bore varient de 150 à 270 ppm. Ces dernières concentrations indiquent une interaction possible des matières organiques avec des eaux saumâtres dans un milieu marécageux marginal.

[1] *Alberta Research Council, Coal Research Centre Devon, One Oil Patch Drive, Devon, Alberta, T0C 1E0*

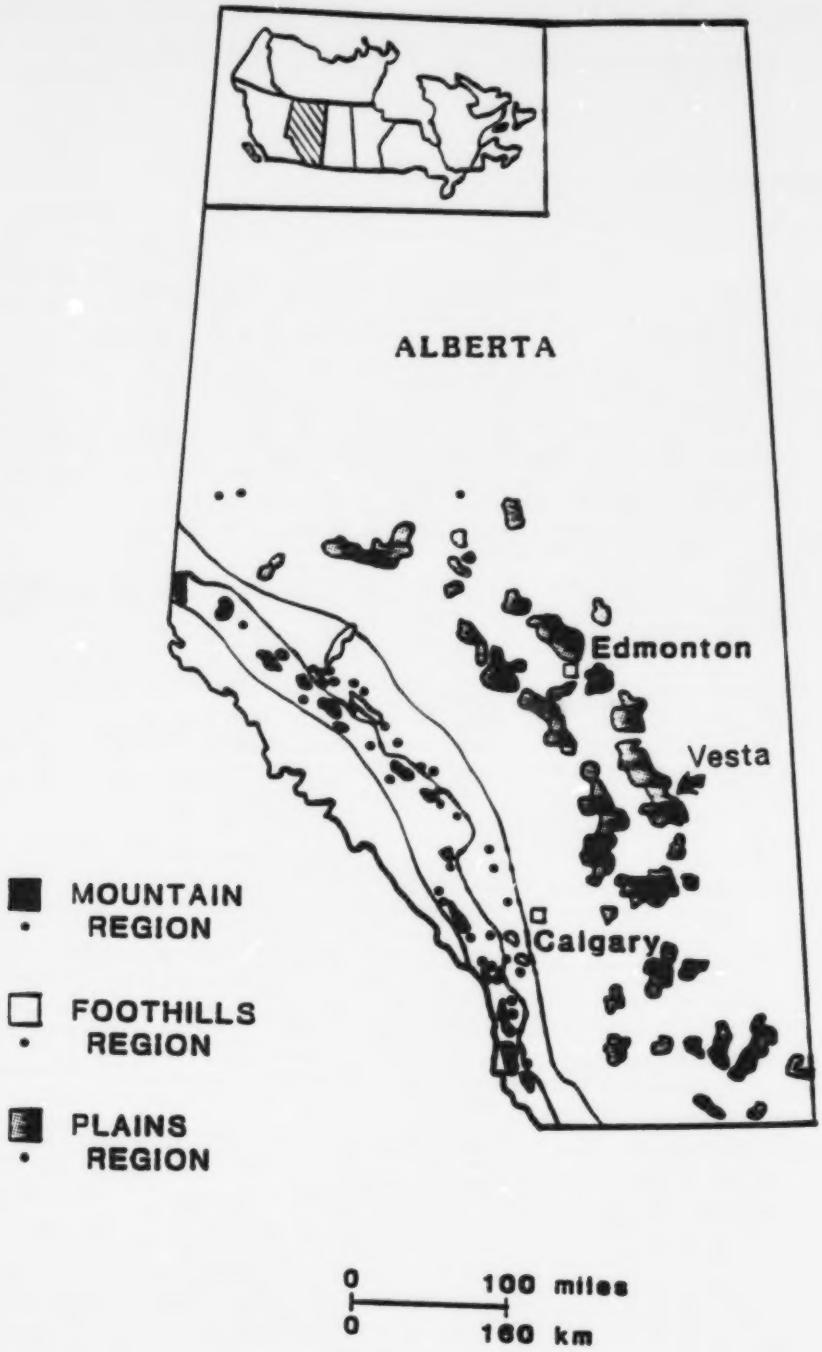

Figure 1. Map of Alberta showing the location of Vesta Mine.

INTRODUCTION AND GEOLOGICAL SETTING

Vesta Mine is an open-pit mine located within the Battle River coalfield in east-central Alberta (Fig. 1). The coal occurs in the Horseshoe Canyon Formation, which constitutes the lower part of the Upper Cretaceous/Tertiary Edmonton Group (Fig. 2). There are in excess of 1000 megatonnes of subbituminous coal present in the coalfield, and the coal is being used for electric power generation (Dawson et al., 1989).

The depositional history of the Upper Cretaceous/Lower Tertiary succession in the central Alberta Plains has been investigated by numerous workers (Irish, 1970; Shepheard and Hills, 1970; Gibson, 1977). Strata of the Horseshoe Canyon Formation are part of an eastward-thinning wedge of mainly fluvio-deltaic sediments, deposited along the western margin of the Late Cretaceous Bearpaw Sea (Gibson, 1977). The Horseshoe Canyon Formation (Irish, 1970) consists of nonmarine, fluvio-deltaic sandstone, siltstone, shale, mudstone and claystone (Gibson, 1977). The formation conformably overlies marine mudstone, siltstone and shale of the Bearpaw Formation (Fig. 2). The lower part of the Horseshoe Canyon Formation, which is in close contact with the Bearpaw Formation, contains marine to brackish water strata (Gibson, 1977).

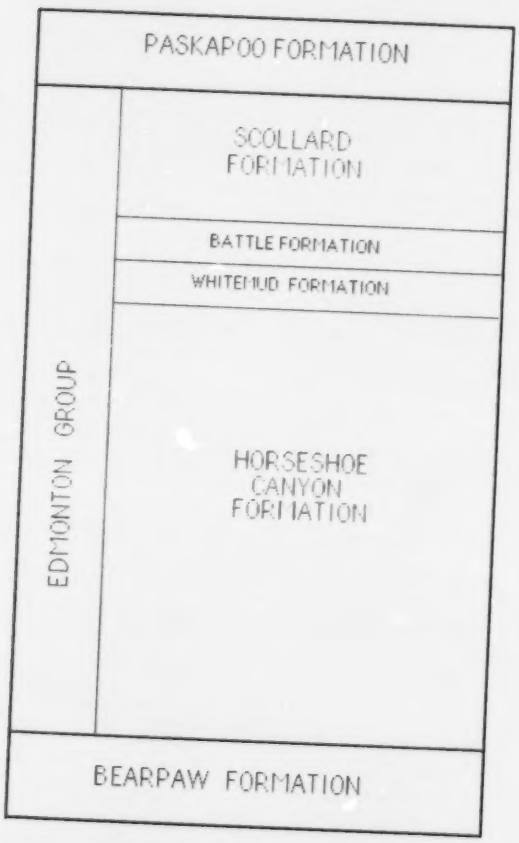

Figure 2. Stratigraphic section of the Upper Cretaceous/Lower Tertiary in the Alberta Plains. (after Gibson, 1977.)

The Battle River coalfield most likely contains the greatest resource potential in the east-central region of the Alberta Plains (Dawson et al., 1989). Ten individual coal beds, several of which range up to 2.8 m in thickness, have been recognized within the coalfield.

ANALYTICAL METHODS

Optical microscopy

A series of samples was collected for petrographic analysis from outcrop sections of seam 3, and trenches were dug to remove the weathered material. Natural sedimentological breaks, such as partings, were used as sample boundaries.

All coal samples were analysed for reflectance values and maceral types. The material was crushed to −20 mesh (850 μm), moulded in pellets with epoxy resin and polished according to standard procedures (ASTM, 1979). A Zeiss MPM II microscope, equipped with both white (halogen) and UV light sources and attached to a Zonax microcomputer and printer, was used for reflectance measurements.

The maceral nomenclature used was that recommended by the International Committee for Coal Petrology (ICCP, 1971). Huminite was divided into humotelinite (material retaining the original woody tissue structure), humocollinite (material that has no tissue structure preserved or has passed through a colloidal, gel-like stage), and humodetrinite (finely fragmented and partly gelified huminitic material). Liptinite and inertinite macerals are essentially the same for both low and high rank coals (ICCP, 1971).

Reflectance values (Ro random) represent an average of 50 measurements per sample. Maceral quantities were determined by point counting (500 points per sample) using a Swift Model F automatic point counter, and then calculated to per cent values.

RESULTS AND DISCUSSION

Organic petrology

Figures 3 and 4 show the vertical maceral and reflectance profiles of sections 1 and 2. Nearly all samples are uniformly rich in huminite, containing over 80 per cent huminite on a mineral-matter-free basis. This agrees with petrographic results obtained by Parkash et al. (1985) and Dawson et al. (1989).

Humotelinite and humocollinite are present in almost equal amounts in section 1 (average 35.0 per cent and 40.0 per cent, respectively), whereas in section 2 there is a predominance of humocolinite over humotelinite (15.0 per cent versus 45.0 per cent) (Fig. 3, 4). Humodetrinite is more abundant in section 1 but never exceeds 15.0 per cent. Liptinite is relatively low in most samples, averaging about 5.0 per cent and never exceeding 10.0 per cent, whereas total inertinite averages 13.0 per cent in section 1 and 18.0 per cent in section 2 (Fig. 3, 4).

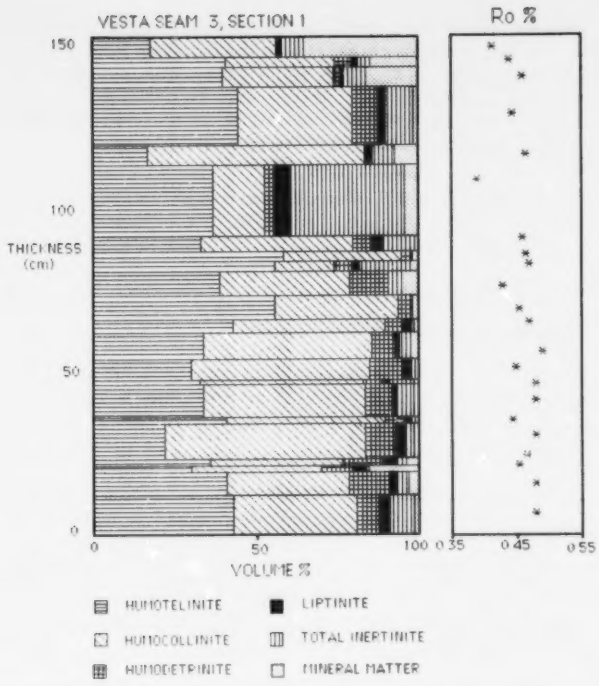

Figure 3. Maceral and reflectance profile, seam 3, section 1.

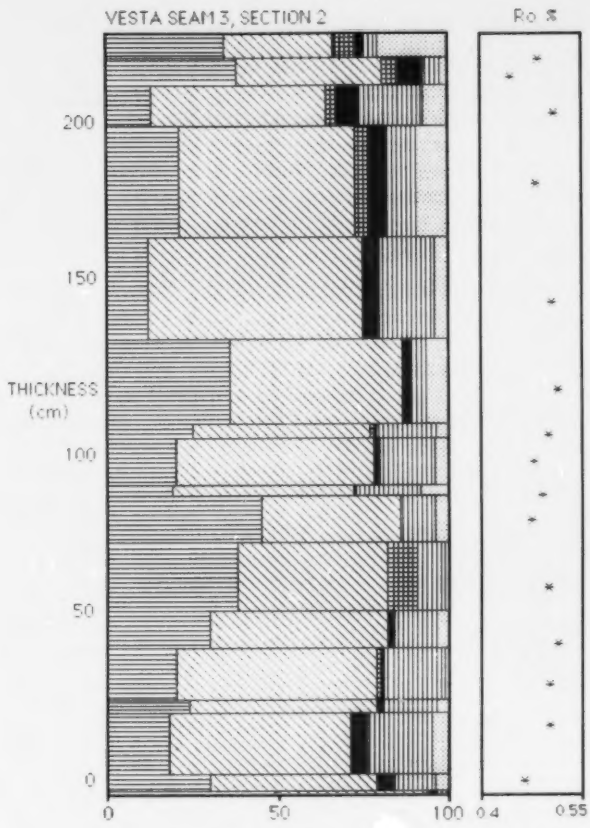

Figure 4. Maceral and reflectance profile, seam 3, section 2.

PLATE 1

All photomicrographs taken in black and white, reflected light, oil immersion

Long axis of each photo is 180 μm.

a) Alternation of eu-ulminite A (dark) (E_A) and eu-ulminite B (light) (E_B) bands.

b) Texto-ulminite (TU) and corpohuminite (C).

c) Association of eu-ulminite B (E_B) and phlobaphinite (PH).

d) Cutinite (CU) and inertodetrinite (ID) in a humodetrinite matrix.

e) Bands of eu-ulminite B (E_B) and humodetrinite (HD). The cracks perpendicular to the bands are filled by exsudatinite (EX).

f) Eu-gelinite (G) showing characteristic desiccation cracks and gel-like appearance.

g) Corpohuminite (C), fusinite (F) showing bogen structure, sporinite (SP) and macrinite (M).

h) Sclerotinite (SC) with its cells being filled by exsudatinite (EX) associated with inertodetrinite (ID) and liptodetrinite (LD) in a densinite groundmass.

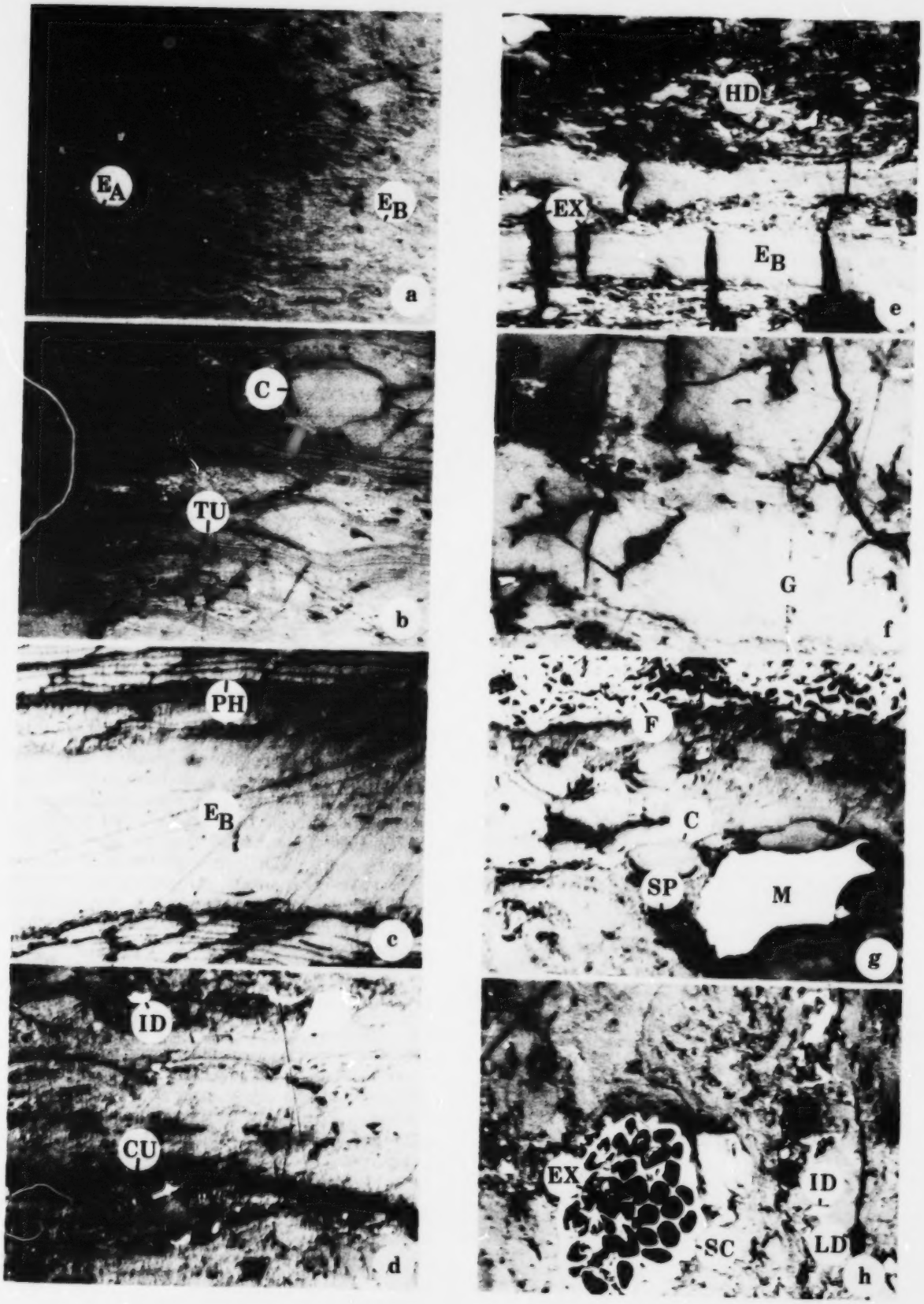
EA
EB
a
C
TU
b
PH
EB
c
ID
CU
d
HD
EX
EB
e
G
f
F
C
SP
M
g
EX
ID
SC
LD
h

Huminite is made up of eu-ulminite A and B, gelinite, phlobaphinite and minor densinite (Plate 1), whereas sporinite, resinite, cutinite, liptodetrinite and minor exsudatinite are the most abundant liptinite macerals (Plate 1). Inertinite consists mainly of fusinite, semifusinite, macrinite and minor sclerotinite and inertodetrinite (Plate 1).

Random reflectance values of Vesta coal range from 0.39 to 0.52 per cent with the majority being around 0.45 per cent, indicating a subbituminous C-A rank (Teichmüller and Teichmüller, 1982). Similar reflectance values (0.47-0.53 per cent) have been reported by Dawson et al. (1989) for Battle River coal samples near the study area.

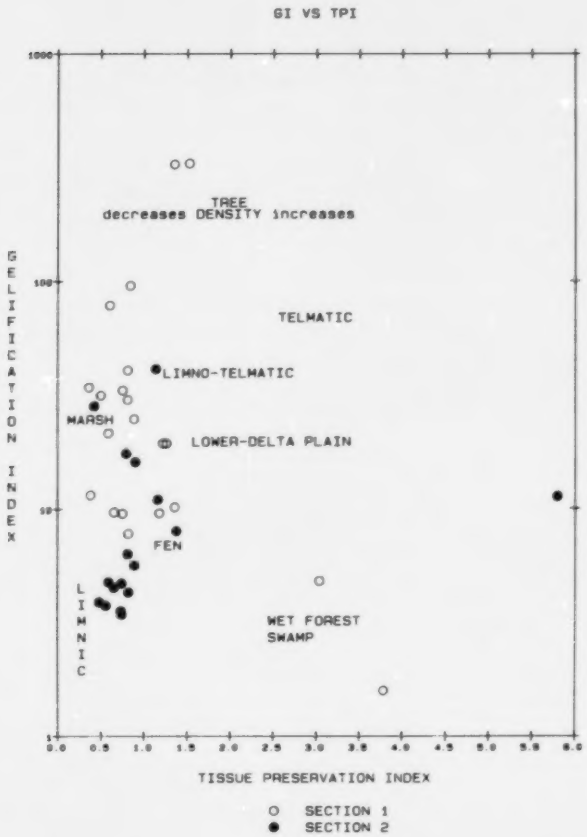

Figure 5. Coal facies and depositional environment of Vesta Mine coal (after Diessel, 1986).

ENVIRONMENT OF DEPOSITION

A model relating petrographic composition of coal to differences in swamp types has been proposed by Diessel (1986). Two indices, the Tissue Preservation Index (TPI) and the Gelification Index (GI) are used to determine the degree to which plant tissue structure is preserved or destroyed.

The GI and TPI are calculated from the maceral data (mmf) as follows:

$$GI = \frac{\text{Total huminite and macrinite}}{\text{semifusinite, fusinite and inertodetrinite}}$$

$$TPI = \frac{\text{humotelinite, semifusinite and fusinite}}{\text{humocollinite, humodetrinite, macrinite and inertodetrinite}}$$

Figure 5 shows the relationship between maceral composition and possible depositional environments. It should be noted that the GI is uniformly high, indicating generally wet conditions of deposition (lower delta-plain environment). In addition, samples from both sections have similar TPI values, an indication that the peat was deposited in a marsh-type environment occupied by herbaceous plant communities rather than in a swamp with high tree density. Dawson et al. (1989) arrived at a similar conclusion for their samples.

The boron (150-270 ppm) and total sulphur (0.3-0.6 per cent) values show that the Vesta coals may have been affected by brackish waters. This conclusion agrees with sedimentological studies conducted in the area, showing that the lower part of the Horseshoe Canyon Formation has been influenced by brackish waters (Dawson et al., 1989).

CONCLUSION

Vesta coal in east-central Alberta is rich in huminite, less so in inertinite and liptinite. Reflectance on eu-ulminite B ranges from 0.39 to 0.52 per cent, indicating a subbituminous C-A rank. Total sulphur is 0.6 per cent, and boron content ranges from 150 to 270 ppm. The boron values are indicative of possible interaction of the organic matter with brackish waters, in agreement with sedimentological evidence. A marginal marine marsh type of depositional environment is indicated by the petrological characteristics of the Vesta coal.

ACKNOWLEDGMENTS

The authors are appreciative of the help provided by the geological staff of the Vesta Mine regarding permission for sample collection and access to areas within the mine. The authors would also like to thank B. McDougall of W.J. McDougall Consultants Ltd. for critically reviewing this paper and J. Moir, Coal and Hydrocarbon Processing Department, Alberta Research Council for typing it.

REFERENCES

ASTM (American Society for Testing and Materials)
1979: Annual book of ASTM standards, part 26. Gaseous Fuels; Coal and Coke; Atmospheric Analysis; American Society for Testing and Materials, Philadelphia, Pa.

Dawson, F.M., Cameron, A.R., and Jerzykiewicz, T.
1989: Distribution and character of coal in the Battle River Coalfield, east-central Alberta; Contributions to Canadian Coal Geoscience, Geological Survey of Canada, Paper 89-8, p. 49-62.

Diessel, C.F.K.
1986: On the correlation between coal facies and depositional environments; Proceedings of the 29th Newcastle Symposium, University of Newcastle, Australia, p. 19-22.

Gibson, D.W.
1977: Upper Cretaceous and Tertiary coal-bearing strata in the Drumheller-Ardley region, Red Deer River Valley, Alberta; Geological Survey of Canada, Paper 76-35, 41 p.

ICCP (International Committee for Coal Petrology)
1971: International Handbook of Coal Petrography, First Supplement to Second Edition; Centre National de la Recherche Scientifique, Paris, France.

Irish, E.J.W.
1970: The Edmonton Group of south-central Alberta; Bulletin of Canadian Petroleum Geology, v. 18, no. 2, p. 125-155.

Parkash, S., Lali, K., and Cameron, A.R.
1985: Petrography of subbituminous coals from Alberta (Canada) Plains; Journal of Coal Quality, v. 4, no. 1, p. 84-91.

Shepheard, W.W. and Hills, L.V.
1970: Depositional environments Bearpaw-Horseshoe Canyon (upper Cretaceous) transition zone, Drumheller "Badlands", Alberta; Bulletin of Canadian Petroleum Geology, v. 18, no. 2, p. 166-215.

Teichmüller, M. and Teichmüller, R.
1982: The geological basis of coal formation; *in* Coal Petrology, 3rd edition, E. Stach, M.Th. Mackowsky, M. Teichmüller, G.H. Taylor, D. Chandra, and R. Teichmüller (ed.); Gebruder Borntraeger, Berling-Stuttgart, p. 5-85.

Petrology of the Arbour and Val D'or coal seams at Coalspur, Alberta

Thomas Gentzis[1], Fariborz Goodarzi, and Tomasz Jerzykiewicz
Institute of Sedimentary and Petroleum Geology, Calgary

Gentzis, T., Goodarzi, F., and Jerzykiewicz, T., Petrology of the Arbour and Val D'or coal seams at Coalspur, Alberta; in Current Research, Part D, Geological Survey of Canada, Paper 90-1D, p. 195-200, 1989.

Abstract

Ten samples taken from the Arbour and Val D'or coal seams in the Alberta Foothills have been examined petrologically. The coals are high in vitrinite and low in inertinite. The maceral variation is between telinite and collinite, indicating that the coals were formed in an alluvial floodplain under wet conditions.

The rank of the coal is high-volatile bituminous C (% Ro random is 0.60-0.64) and the presence of a burning coal zone above the two seams has not affected their rank. Based on maceral composition and rank, the coals could be used as feedstock for combustion/gasification and liquefaction.

Résumé

Dix échantillons prélevés dans les couches de charbon d'Arbour et de Val d'Or dans les contreforts de l'Alberta ont fait l'objet d'une analyse pétrologique. Ils ont une teneur élevée en vitrinite et une teneur faible en inertinite. Les macéraux varient de telinite à collinite indiquant que les charbons se sont formés dans une plaine d'inondation alluviale, donc dans des conditions humides.

Il s'agit de charbon de rang bitumineux C à teneur élevée en matières volatiles (le % Ro aléatoire est de 0,60 à 0,64) et la présence d'une zone de charbon de combustion au-dessus des deux couches n'a pas modifié leur rang. Compte tenu de leur composition en macéraux et de leur rang, les charbons pourraient être utilisés comme charge pour les processus de combustion et gazéification et de liquéfaction.

[1] *Alberta Research Council, Coal Research Centre Devon, One Oil Patch Drive, Devon, Alberta, T0C 1E0*

INTRODUCTION

The Val D'or and Arbour seams are the youngest and thickest coal seams within the Coalspur coal zone, which forms the upper member of the Coalspur Formation (Jerzykiewicz, 1985). The Coalspur coal zone is one of the most important sources of low-sulphur coal in the Alberta Foothills, and is being mined in the Coal Valley Mine some 25 km southeast of Coalspur. The Coalspur Formation (previously known as the Coalspur beds) was deposited in an alluvial plain environment during the Early Paleocene (Jerzykiewicz and McLean, 1980). The Coalspur coal zone is laterally continuous along the outer Foothills between Athabasca River to the northwest and Red Deer River to the southeast. Correlative coal-bearing strata occur farther northwestward between Hinton and Grande Cache and even farther to the north within the Wapiti Group, where they are known as the Kakwa coal zone. Gradual thinning of the Coalspur coal zone southeastward along the Foothills and its termination between the Red Deer River and Waiparous Creek sections (Jerzykiewicz, work in progress) is due to paleoclimatic differences between north-central and southern Alberta in the Late Cretaceous (Jerzykiewicz and Sweet, 1988; Jerzykiewicz, work in progress).

This paper deals with coal samples collected in the type locality of the Coalspur coal zone at Coalspur (Fig. 1) and represents only a preliminary study of Coalspur coals. A more detailed, regional study of the Coalspur coal zone is underway.

EXPERIMENTAL

Ten samples from the Coalspur Formation were selected to study the petrological composition of the coal seams and the possible effect of the burning coal zone on the seams. Figure 2 illustrates the location of the samples collected. Samples were embedded in an epoxy resin and were ground and

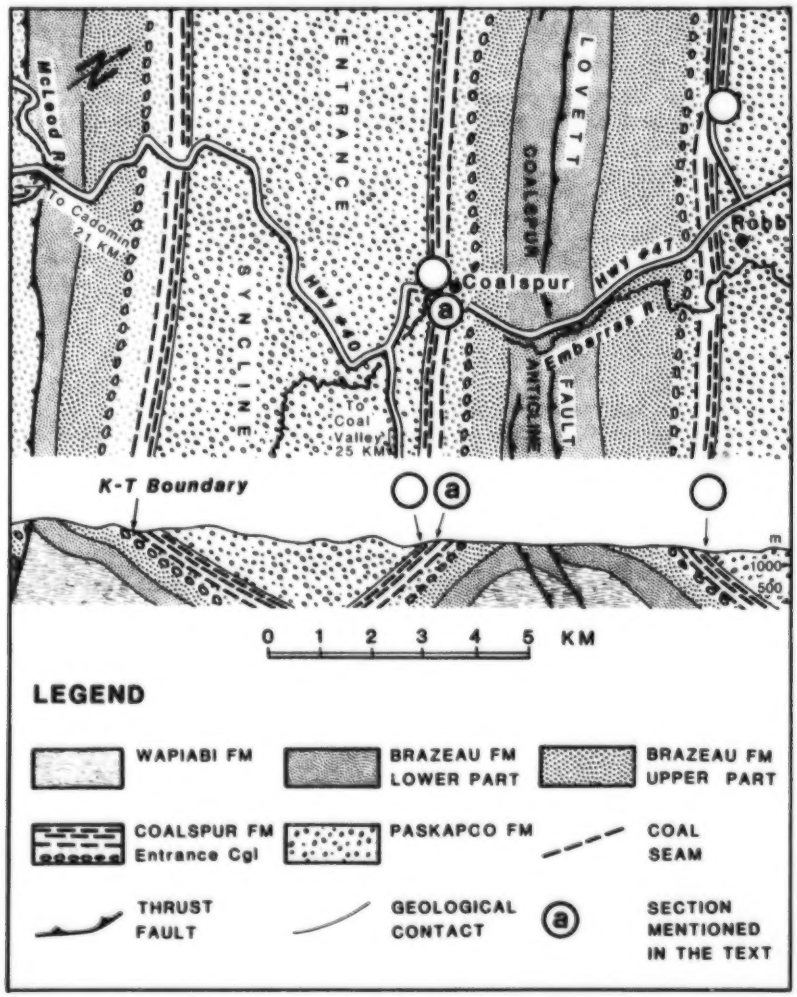

Figure 1. General location map, Alberta Foothills.

polished according to the method of Mackowsky (1982). A Zeiss MPM II reflected light microscope, fitted with white (halogen) and fluorescent light (HBO) sources, connected to a Zonax microcomputer and printer were used for reflectance measurements and maceral analysis.

PETROLOGY

Vitrinite is the most abundant maceral group in the coal seams and the variation of maceral content is basically related to the variation of vitrinite macerals. In this maceral group the variation is between telinite and collinite (Plate 1a, b). Telinite ranges from a minimum of 20.0 per cent to a maximum of 68.0 per cent (Table 1). Collinite has a range of 17.6 to 48.0 per cent, whereas vitrodetrinite is the least abundant and occurs in the range of 1.0 to 14.7 per cent (Table 1).

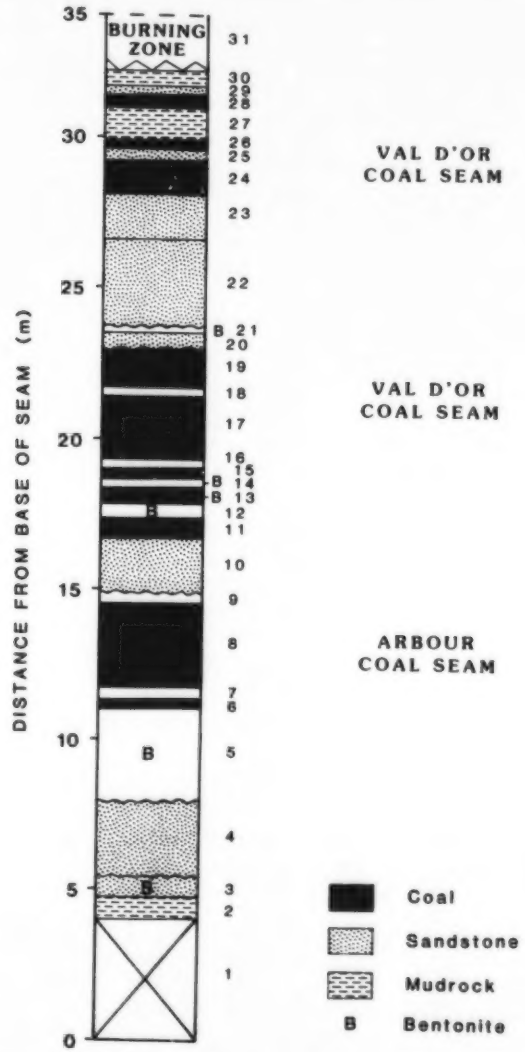

Figure 2. Stratigraphic section of the Coalspur roadcut showing sample locations.

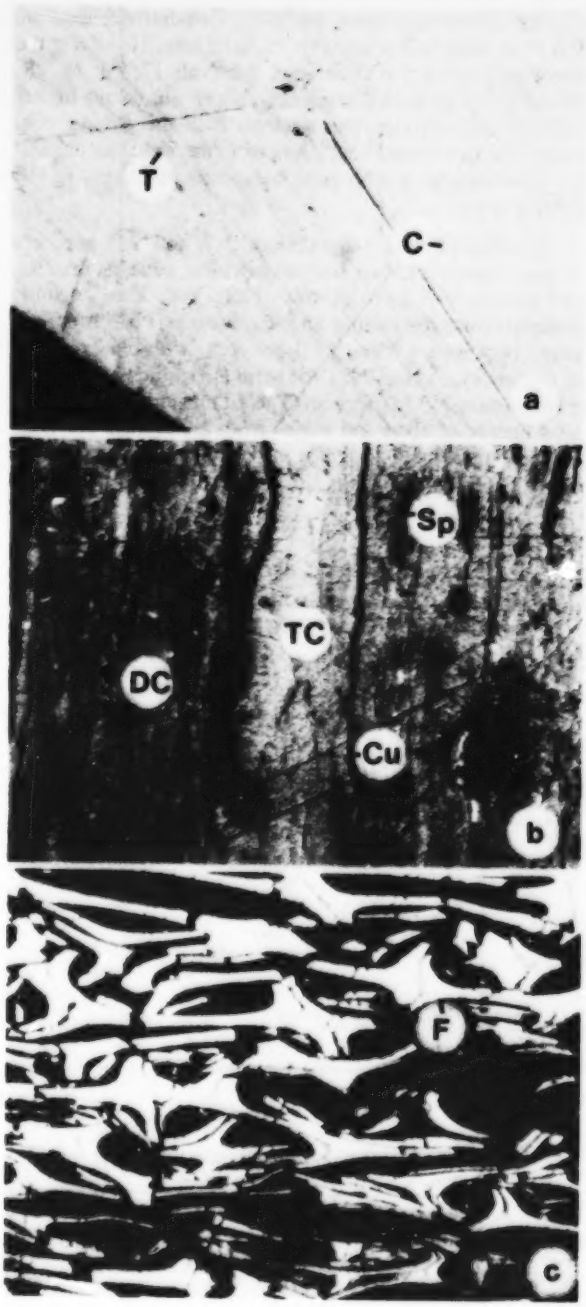

PLATE 1

All photomicrographs taken in black and white, under oil immersion. Magnification is 500x.

a) Telinite (T) showing faint cell structure grading to collinite (C), sample 26.

b) Telocollinite band (TC) and desmocollinite (DC) enclosing sporinite (Sp), cutinite (Cu) and liptodetrinite (Ld) (sample 6).

c) Broken fusinite (F) showing 'bogen' structure and high relief (sample 19).

The Arbour coal seam has lower vitrodetrinite than the Val D'or seam and it contains more telinite. However, the upper part of the Val D'or seam (intervals 17, 19, 26, 28, 30 and 31) (Fig. 2) has, in general, lower telinite and higher collinite and vitrodetrinite contents than the Arbour coal seam. The two lowest coal intervals in the Val D'or (13 and 15) have similar petrological compositions to that of the Arbour seam.

Liptinite content ranges from 1.7 and 9.0 per cent (Table 1) and consists mainly of sporinite, cutinite, resinite, exsudatinite and liptodetrinite (Plate 1b). The inertinite macerals comprise fusinite and semifusinite (Plate 1c). They range betweeen 4.0 and 14.0 per cent, with the exception of one interval in the Val D'or seam (19) which has an inertinite content of 37.0 per cent (Table 1). Mineral matter consists mainly of clays and varies from 2.0 to 12.3 per cent. Mineral matter is the highest in interval 30 underneath the burning coal zone (Table 1).

Reflectance (% Ro random) is 0.60 to 0.64, indicating that the coal is of high-volatile bituminous C rank. Heat generated from the burning coal zone above has not increased the reflectance of vitrinite in the Arbour and Val D'or seams.

Diessel (1986) developed a model that relates variations in petrological composition of coal to differences in the swamp types in which the peats were deposited. Two indices, the Tissue Preservation Index (TPI) and the Gelification Index (GI) are calculated from the maceral composition in the following manner and are then graphically expressed as a crossplot:

$$TIP = \frac{\text{Telinite, semifusinite and fusinite}}{\text{vitrodetrinite, fusinite and inertodetrinite}}$$

$$GI = \frac{\text{Total vitrinite and macrinite}}{\text{Semifusinite, fusinite and inertodetrinite}}$$

Table 1. Maceral and reflectance analyses.

Sample interval	Telinite	Collinite	Vitro-detrinite	Liptinite	Semi-fusinite	Fusinite	Mineral matter	Random reflectance (%)	Maximum reflectance (%)	GI	TPI
Val D'or Seam											
31	27.7	48.0	3.0	4.7	6.0	6.3	12.3	0.64	0.71	6.4	0.79
30	24.0	48.0	4.3	4.0	-	10.0	7.0	0.64	0.70	7.6	0.65
28	25.3	50.7	6.0	5.0	1.7	6.7	4.7	0.63	0.66	9.9	0.6
26	34.7	29.3	14.7	4.0	10.7	4.3	2.3	0.63	0.71	5.3	1.13
19	20.0	29.3	8.7	1.7	17.0	19.7	3.7	0.64	0.70	1.58	1.49
17	22.7	42.0	12.3	6.0	6.7	8.0	2.3	0.60	0.66	5.25	0.69
15	68.0	17.6	1.0	7.3	4.0	-	2.0	0.60	0.67	21.6	3.8
13	50.0	19.0	7.7	9.0	4.3	2.0	8.0	0.60	0.68	12.3	2.1
Arbour Sea											
8	59.3	17.0	1.7	3.0	7.0	7.0	5.0	0.63	0.70	5.6	3.9
6	54.3	19.0	4.0	5.7	6.0	2.7	8.7	0.61	0.67	8.9	2.7

Table 2. Proximate/ultimate analyses.

Sample interval	Moisture %	Ash	VM	FC	%C	%H	%N	%S	CV(cal/gr)
Val D'or Seam									
31	3.4	4.6	37.3	54.7	71.4	4.8	0.84	0.34	6884
30	3.0	4.0	34.8	57.2	72.7	4.8	0.86	0.33	6991
28	3.4	6.6	36.8	53.2	69.8	4.9	0.81	0.32	6792
26	3.5	9.6	37.7	49.2	66.1	4.5	0.76	0.53	6350
19	3.3	12.5	31.3	52.9	66.1	4.3	0.70	0.36	6315
17	3.0	11.4	35.5	50.1	67.1	4.7	0.72	0.29	6513
15	4.1	2.7	37.4	55.8	73.6	5.0	0.56	0.38	7162
13	3.6	8.9	35.3	52.2	68.5	4.8	0.76	0.43	6684
Arbour Seam									
8	4.1	3.8	33.2	58.9	71.7	4.7	0.68	0.39	6888
6	4.2	8.5	34.3	53.0	68.9	4.9	0.82	0.69	6724

The GI versus TPI plot is shown in Figure 3. All samples have uniformly high GI and low TPI values, which indicates the dominance of unstructured material (collinite and vitrodetrinite) over structured vitrinite (telinite).

CHEMICAL PROPERTIES

The proximate and ultimate analyses of the samples studied are given in Table 2. The low-rank coals from the Arbour and the Val D'or seams are low in ash (2.7-11.4 per cent), the sulphur content is relatively low (0.29-0.69 per cent) and the nitrogen and hydrogen contents are moderate (0.56-0.86 per cent and 4.3-5.0 per cent, respectively) (Table 2).

It has been known for some time that the technological properties of coals can be related to rank and maceral composition. The work of Given et al. (1975) and Davis et al. (1976) has shown that a relationship exists between rank and composition of coal and its conversion during liquefaction. This relationship, for the coals studied, is shown in Figure 4. The rectangle indicates the area of optimum properties for liquefaction, the reflectance limits correspond to high-volatile bituminous coals (0.5-1.0% Ro), and the total amount of reactive macerals (vitrinite and liptinite) must exceed 70.0 per cent by volume.

Considering the rank and maceral composition of the coals and their chemistry, they should be good feedstock for liquefaction and combustion/gasification.

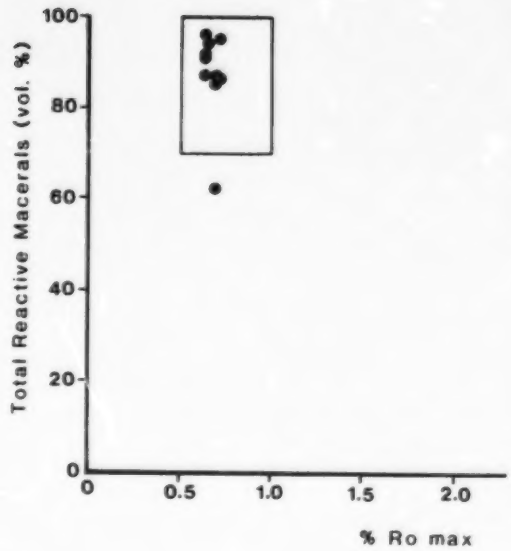

Figure 4. Predicted liquefaction potential of Coalspur coal based on maximum reflectance (Ro max) and total reactive macerals (mmf). (Modifed from Davis et al., 1976.)

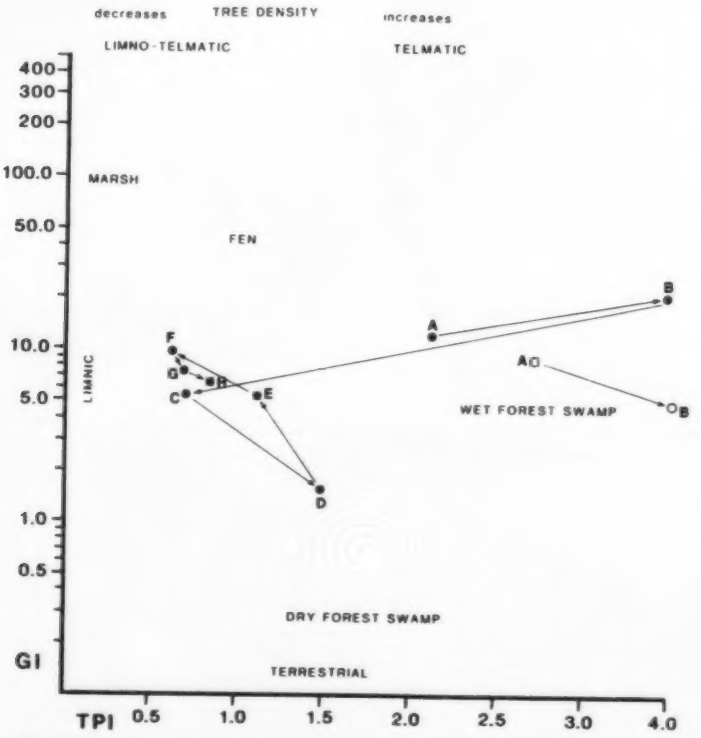

Figure 3. Relationship between maceral composition data and possible depositional environments. (Modified from Diessel, 1986.) (•) Arbour seam, (O) Val D'or seam.

CONCLUSIONS

1. The coals are rich in vitrinite and low in inertinite. They formed under wet conditions, in an alluvial floodplain depositional environment.
2. The rank of the Val D'or and Arbour coal seams has not been affected by the presence of a burning coal zone above the two seams.
3. The coals are good feedstock for liquefaction and combustion/gasification based on rank and composition.

ACKNOWLEDGMENTS

The authors wish to thank K. Lali of the Coal and Hydrocarbon Processing Department, Alberta Research Council, for performing some of the reflectance measurements, and J. Moir for typing the manuscript.

REFERENCES

Davis, A., Spackman, W., and Given, P.
1976: The influence of properties of coal on their conversion into clean fuels; Energy Sources, v. 3, no. 1, p. 55-81.

Diessel, C.F.K.
1986: On the correlation between coal facies and depositional environments; Advances in the study of the Sydney Basin, Proceedings of the 12th Symposium, Department of Geology, University of Newcastle, Australia, p. 19-22.

Given, P., Cronauer, D., Spackman, W., Lovell, H., Davis, A., and Biswas, B.
1975: Dependence of coal liquefaction behaviour on coal characteristics; Fuel, v. 54, p. 40-49.

Jerzykiewicz, T.
1985: Stratigraphy of the Saunders Group in central Alberta Foothills — a progress report; *in* Current Research, Part B, Geological Survey of Canada, Paper 85-1B, p. 247-258.

Jerzykiewicz, T. and McLean, J.R.
1980: Lithostratigraphical and sedimentological framework of coal-bearing Upper Cretaceous and lower Tertiary strata, Coal Valley area, central Alberta Foothills; Geological Survey of Canada, Paper 79-12, p. 47.

Jerzykiewicz, T. and Sweet, A.R.
1988: Sedimentological and palynological evidence of regional climatic changes in the Campanian to Paleocene sediments of the Rocky Mountain Foothills, Canada; Sedimentary Geology, v. 59, p. 29-76.

Mackowsky, M-Th.
1982: Methods and tools of examination; *in* Stach's Textbook of Coal Petrology, Stach, E., Mackowsky, M-Th., Teichmüller, M., Taylor, G.H., Chandra, D., and Techmüller R. (ed.); Gebruder Borntraeger, Berlin, p. 295.

Models of organic maturation and hydrocarbon potential: application to Lougheed Island drillholes, Sverdrup Basin, Canadian Arctic Islands

D.N. Skibo, K.G. Osadetz, and F. Goodarzi
Institute of Sedimentary and Petroleum Geology, Calgary

Models of organic maturation and hydrocarbon potential: application to Lougheed Island drillholes, Sverdrup Basin, Canadian Arctic Islands; in Current Research, Part D, Geological Survey of Canada, Paper 90-1D, p. 201, 1990.

Abstract

A vitrinite reflectance profile for the Skybattle C-15 borehole has a logarithmic coalification gradient of 0.11 +/−.02 log % Ro/km. The coalification gradient suggests the erosion of 1900 (+900/−815) m of strata. This erosion estimate is somewhat greater than an estimated range of 600 to 800 m of erosion determined from stratigraphic considerations. Below 700 m depth, the best fit line to observed reflectance data agrees with the calculated reflectance for a thermal history model with an average paleo-heat flow of 50 mW/m² and can be clearly distinguished from 40 and 60 mW/m² models.

From theoretical models relating vitrinite reflectance gradient and effective geothermal gradient (Middleton model and MATOIL results) it is inferred that the present reflectance profile was acquired in an effective geothermal gradient of approximately 20 mK/m. This is in agreement with current geothermal gradient estimates for the well of 24 +/−4 mK/m.

As a first approximation, thermal maturation estimates for this part of the basin can be made through use of constant heat flow models constrained by current geothermal conditions.

Résumé

Un profil de réflectance de la vitrinite du trou de sondage Skybattle C-15 donne un gradient de houillification logarithmique de 0,11 ± 0,02 log %Ro/km. Le gradient de houillification indique une érosion de 1900 (+900/−815)m des couches. Ces valeurs sont un peu plus élevées que l'intervalle de 600 à 800 m d'érosion déterminé à partir de données stratigraphiques. Au-delà de 700 m de profondeur, la droite de meilleur ajustement des données de réflectance observées correspond à la réflectance calculée pour un modèle d'évolution thermique dont l'écoulement paléothermique est de 50 mW/m² se distinguant nettement des modèles de 40 et de 60 mW/m².

À partir de modèles théoriques établissant un lien entre le gradient de réflectance de la vitrinite et le gradient géothermique réel (modèle de Middleton et données de MATOIL), on en a déduit que le profil de réflectance actuel a été enregistré dans un gradient géothermique réel d'environ 20 mKm⁻¹. Cette valeur correspond aux estimations du gradient géothermique du puits, soit 24 ± 4 mKm⁻¹.

En première approximation, les estimations de la maturation thermique dans cette partie du bassin peuvent être faites en recourant au modèle de flux thermique constant ayant comme limite les conditions géothermiques actuelles.

INTRODUCTION

Lougheed Island is situated in the west-central part of the Queen Elisabeth Islands, Canadian Arctic Archipelago. To date, thirteen boreholes have been drilled in the area (Fig. 1).

Under the Frontier Geoscience Program of the Geological Survey of Canada, a series of studies are being made to determine levels of organic maturity and hydrocarbon potential in the Lougheed Island area of the Sverdrup Basin. The evaluation of the utility and accuracy of thermal maturation/burial history computer models in attaining these objectives is an integral part of these studies. For the estimation of timing of hydrocarbon generation, paleotemperature reconstructions and kinetic models must be accurately calibrated.

The IFP (Institut français du Pétrole) has developed and marketed a numerical simulation program for personal computers (MATOIL (r)). This paper reports some results obtained using this program. These results are compared and correlated to measured organic maturity parameters obtained for the SUN K.R. Panarctic Skybattle Bay C-15 exploration drillhole on Lougheed Island. Sample material comprised cores, bulk-rock cuttings, and hand-picked samples. The maturity data (Table 1) consist of sets of vitrinite reflectance measurements obtained under outside contract and through routine laboratory pyrolysis measurements made using the Rock-Eval facility of the Geochemistry Subdivision, ISPG (Institute of Sedimentary and Petroleum Geology, Calgary).

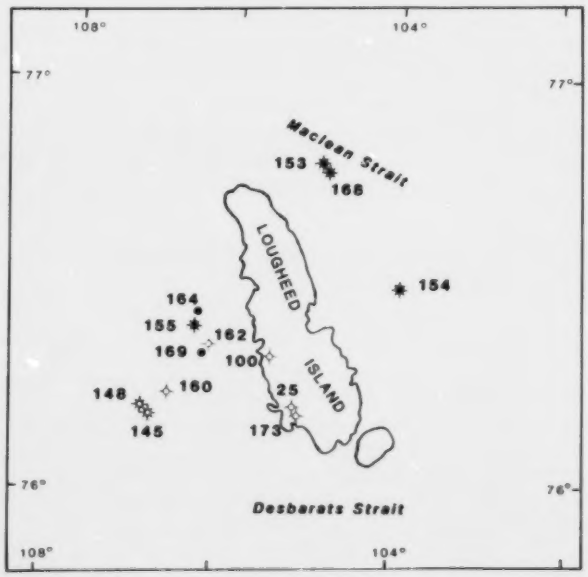

Figure 1. Location map showing wells used in this study. Well location key:

25 SUN K.R. Panarctic Skybattle Bay C-15
100 Panarctic Tenneco et al. Pat Bay A-72
145 Panarctic AIEG Whitefish H-63
148 Panarctic AIEG Whitefish 2h-63
153 Panarctic AIEG PPC Dome Skate B-80
154 Panarctic AIEG PPC Dome Maclean I-72
155 Panarctic AIEG PRC PPC Cisco B-66
160 Panarctic et al. Whitefish A-26
162 Panarctic et al. Cisco C-42
164 Panarctic et al. Cisco K-58
168 Panarctic et al. Skate C-59
169 Panarctic et al. Cisco M-22
173 Panarctic et al. Skybattle Bay M-11

COMPUTER MODEL INPUT

The main data input to the MATOIL program is a specification of:

1. A table of formations for which either lithotypes or measured physical properties (porosities, thermal conductivity and heat capacity) are given. In addition, depths and ages are specified. Neither lithology nor physical properties are entered in the case of unconformities or eroded sections.
2. Present thermal data (heat flow, or temperature gradient or temperature/depth data) which can be used for calibration of the calculated thermal history.
3. Thermal history for the cases exhibiting variable surface paleotemperature, variable or constant heat flow, or rift-model heat flow.
4. Source rocks, according to depth, kerogen type and total organic carbon.

INPUT PARAMETERS: SKYBATTLE BAY C-15 DRILLHOLE

The well was spudded in the Upper Cretaceous Hassel Formation. Thus it is inferred that considerable section has been eroded, particularly during and following the Paleogene-Eurekan Orogeny. Balkwill et al. (1982) gave thicknesses and approximate mean accumulation rates for Triassic through Cretaceous clastic sedimentary rocks on Lougheed Island. The missing Cretaceous-Tertiary section in the Skybattle C-15 well consists of perhaps one third (100 m) of the Hassel Formation, all of the Kanguk Formation (200 m) and all of the Eureka Sound Group (300-475 m). These values give an estimated missing section thickness of from 600 to 775 m. This estimate is probably an upper limit since the estimate for missing known section thickness is only 320 + m.

The lithostratigraphy and chronostratigraphy of the observed section follows the work of A.F. Embry (Table 2), taken from the Regional Well Database at the ISPG, and from Embry (in press). Lithology was determined from the CANSTRAT log for the well and is also available in Balkwill et al. (1982). Ages of the geological stages are taken from Haq et al. (1987). Timing of the Eurekan Orogeny is also obtained from the work of Reideger et al. (1984).

HEAT FLOW MODELS

Additional input parameters required for the MATOIL model involve present- and paleo-thermal data. As noted above, several options are available. However, existing

Table 1. Maturity data for the SUN KR Panarctic Skybattle Bay C-15 well.

A. VITRINITE REFLECTANCE DATA

Depth (m)	Ro(%) average	Number of measurements	Range (%)	Formation-Member /comment
215	0.39	50	0.37-0.41	Hassel
270	0.46		0.40-0.51	Christopher
290	0.37		0.28-0.50	Christopher
335	0.41	3	0.39-0.42	Christopher
381	0.37	4	0.40-0.41	Christopher
533	0.40	2	0.40-0.41	Christopher
594	0.38	2	0.37-0.39	Christopher
605	0.48		0.45-0.51	Christopher
762	0.42	11	0.40-0.49	Christopher
869	0.42	12	0.40-0.46	Christopher
	0.32	8	0.29-0.34	Christopher/stained
1097	0.42	27	0.39-0.45	Isachsen
1189	0.48	21	0.46-0.51	Isachsen
1195	0.60		0.50-0.72	Isachsen
1219	0.50	10	0.48-0.52	Isachsen
	0.37	15		Isachsen/stained
1280	0.57		0.51-0.70	Deer Bay
1326	0.51	7	0.49-0.55	Deer Bay
1370	0.60		0.51-0.70	Deer Bay
1448	0.50	5	0.48-0.51	Deer Bay
1707	0.65	15	0.51-0.66	McConnel
1760	0.61		0.50-0.71	McConnel
1830	0.67			Jameson
1900	0.59		0.55-0.65	Jameson
2030	0.68		0.66-0.70	Lougheed
2039	0.72	3	0.70-0.76	Maclean
2080	0.70			Grosvenor
2195	0.72	2	0.71-0.73	Barrow
2200	0.75		0.60-0.80	Barrow
2240	0.76	3	0.75-0.77	Barrow
2270	0.77		0.72-0.82	Barrow
2301	0.78	3	0.77-0.79	Barrow
2320	0.75		0.69-0.76	Pat Bay
2463	0.73	4	0.71-0.73	Pat Bay
2470	0.82	1		Pat Bay
2561	0.77	5	0.75-0.79	Eden Bay
2604	0.82	6	0.79-0.85	Eden Bay
	0.81	2		Eden Bay
2804	0.79	2	0.78-0.79	C. Caledonia
	0.83	4		C. Caledonia
2865	0.84	2	0.82-0.86	Murray Harbor
2956	0.90	3	0.87-0.91	Murray Harbor

B. ROCK-EVAL ANALYSES

Source rock horizons, Schei Point Group

Depth (m)	Tmax deg C	S1 (mg	S2 /	S3 gSR)	TOC wt.%	HI	OI	PC	PI
EDEN BAY FORMATION									
2591	439	.93	13.79	.82	2.35	586	34	1.22	.06
2594-2603	437	.68	10.29	.45	1.83	562	24		.06
2609	441	1.29	21 42	.90	3.45	620	26	1.89	.06
2603-2612	438	.69	14.94	.77	2.48	602	31		.04
2743-2752	437	1.14	34.06	1.19	4.98	683	23		.03
CAPE CALEDONIA FORMATION									
2743-2752	438	.09	.75	.42	.35	214	120		.11
2783-2795	438	.69	14.08	.69	2.78	506	24		.05
2804	446	2.86	27.21	.76	4.90	555	15	2.50	.10
2801-2810	444	1.94	22.92	1.00	4.07	563	24		.08
2810-2819	445	1.92	24.88	1.10	4.22	589	26		.07

Important Rock-Eval parameters are:

Tmax — temperature (deg.C) corresponding to maximum hydrocarbon generation (peak S2 during pyrolysis)

TOC — total organic carbon (weight %)

S1 — free and adsorbed hydrocarbons distilled during pyrolysis (typically for 3 min.) at 300 deg. C [mg/g rock (—source rock, generally)]

S2 — hydrocarbons generated during pyrolysis at constant heating rate (typically 25 deg. C/min.) between 300 and 600 deg. C (mg/g rock)

S3 — CO_2 liberated/generated from kerogen during pyrolysis between 300 and 390 deg. C (mg/g rock)

HI — Hydrogen Index = (S2/TOC) × 100

OI — Oxygen Index = (S3/TOC) × 100

PC — Pyrolyzable Carbon = 0.83 × (S1 + S2)/10 (weight %)

PI — Production Index = S1/(S1 + S2)

reflectance data are only precise enough to justify maturity models with a constant assumed heat flow for formations older than about 110 Ma (Isachsen and older). Three cases were computed using constant heat flow from 240 Ma up to 110 Ma and a variable near-surface temperature (constant through geological time at 20°C prior to the Eurekan Orogeny [Eocene-Oligocene], and then decreasing to zero at present).

Further, in order to provide an adequate model of thermal history following the renewed rifting during Late Cretaceous time, a relationship given by Royden (1986) was used. Heat flow, assumed constant prior to 110 Ma was then increased (or diminished) according to the relation:

$$q = \text{Constant} + 0.13 \times dZ/dt$$

where q is heat flow (mWm-2) and dZ/dt is subsidence (or upift/erosion) rate in m/Ma. The constant or base value of heat flow was varied to find the best model to account for pre-Isachsen reflectance measurements and also to provide a satisfactory match to estimates of present heat flow (where dZ/dt is approximately zero). Use of this relationship gave an increase of about 10 per cent above base (constant) heat

Table 2. Formation Table: Skybattle Bay C-15/300C157720105000

Number Formations/Oldest Penetrated: 35/Bjorne Formation

Line	Formation	Depth (ft.)	Elev (ft.)	Depth (m)	Elev (m)
1	HASSEL FM	31.0	79.0	9.4	24.1
2	CHRISTOPHER FM	692.0	-582.0	210.9	-177.4
3	MACDOUGALL PT MBR	692.0	-582.0	210.9	-177.4
4	INVINCIBLE POINT MBR	2,091.0	-1,981.0	637.3	-603.8
5	ISACHSEN FM	3,033.0	-2,923.0	924.5	-890.9
6	WALKER ISLAND MBR	3,033.0	-2,923.0	924.5	-890.9
7	RONDON MBR	3,490.0	-3,380.0	1,063.8	-1,030.2
8	PATERSON ISLAND MBR	3,645.0	-3,535.0	1,111.0	-1,077.5
9	DEER BAY FM	4,145.0	-4,035.0	1,263.4	-1,229.9
10	AWINGAK FM	5,145.0	-5,035.0	1,568.2	-1,534.7
11	RINGNES FM	5,492.0	-5,382.0	1,674.0	-1,640.4
12	MCCONNELL ISLAND FM	5,612.0	-5,502.0	1,710.5	-1,677.0
13	SANDY POINT FM	5,797.0	-5,687.0	1,766.9	-1,733.4
14	JAMESON BAY FM	5,850.0	-5,740.0	1,783.1	-1,749.6
15	SNOWPATCH MBR	5,850.0	-5,740.0	1,783.1	-1,749.6
16	CAPE CANNING MBR	6,131.0	-6,021.0	1,868.7	-1,835.2
17	HEIBERG GRP	6,340.0	-6,230.0	1,932.4	-1,898.9
18	KING CHRISTIAN FM	6,340.0	-6,230.0	1,932.4	-1,898.9
19	LOUGHEED ISLAND FM	6,556.0	-6,446.0	1,998.3	-1,964.7
20	MACLEAN STRAIT FM	6,701.0	-6,591.0	2,042.5	-2,008.9
21	GROSVENOR ISLAND FM	6,829.0	-6,719.0	2,081.5	-2,048.0
22	SKYBATTLE FM	6,904.0	-6,794.0	2,104.3	-2,070.8
23	SCHEI POINT GRP	7,083.0	-6,973.0	2,158.9	-2,125.4
24	BARROW FM	7,083.0	-6,973.0	2,158.9	-2,125.4
25	SKATE MBR	7,083.0	-6,973.0	2,158.9	-2,125.4
26	SCALLON POINT MBR	7,250.0	-7,140.0	2,209.8	-2,176.3
27	PAT BAY FM	7,600.0	-7,490.0	2,316.5	-2,283.0
28	HOYLE BAY FM	8,452.0	-8,342.0	2,576.2	-2,542.6
29	EDEN BAY MBR	8,452.0	-8,342.0	2,576.2	-2,542.6
30	ROCHE POINT FM	8,609.0	-8,499.0	2,624.0	-2,590.5
31	GORE POINT MBR	8,609.0	-8,499.0	2,624.0	-2,590.5
32	CHADS POINT MBR	8,880.0	-8,770.0	2,706.6	-2,673.1
33	CAPE CALEDONIA MBR	8,932.0	-8,822.0	2,722.5	-2,688.9
34	MURRAY HARBOUR FM	8,932.0	-8,822.0	2,722.5	-2,688.9
35	BJORNE FM	9,758.0	-9,648.0	2,974.2	-2,940.7
	BOTTOM TD	12,000.0	-11,890.0	3,657.6	-3,624.1

flow value at mid-Eocene time, which was then followed by a decrease toward the base value of heat flow at the present.

It was found that calibration to the observed temperature profile (Fig. 2) and thermal conductivity profile (Fig. 3, calculated by the Matoil program from input lithology), gave a calculated present heat-flow of 48 mW/m^{-2}. Jones et al. (1989, Table 1) gave a heat flow value of 43 mW/m^{-2} calculated from an average temperature gradient of 24 mK/m and a thermal conductivity of 1.8 W/m/K. The agreement of our results with their estimate is well within the uncertainty of both methods. Base (constant) heat flow values of 40, 50, and 60 mW/m^{-2} bracketing these values, were used in the trial calculations presented here.

The procedure gave better estimates of confidence limits in the modelling method used here, and was used to find the best match (least-squares sense) to all vitrinite reflectance measurements available for this well. The three test cases were run without calibration to present temperature observations — a procedure used to allow for uncertainty in bottom-hole temperature corrections.

RESULTS

The observed reflectance profile is given in Figure 4 and has been made from the data given in Table 1. The sample range is from 270 to 2820 m and the measured vitrinite reflectances range from 0.46 per cent at 270 m to 0.82 per cent at 2470 m, with lower values of 0.72 to 0.80 per cent through the rest of the interval (2615-2820 m) Figure 4 also gives the best-fit log (% Ro) gradient, which is 0.11 +/−0.02 log (% Ro)/km. Extrapolation of the best-fit log-linear gradient to the present surface gives a value of 0.41 +/0.02 per cent. The initial maturity level was taken as 0.25 per cent, a starting Ro deduced from studies across several Arctic regions (L.R. Snowdon, pers. comm.). If the observed log (% Ro) gradient from the deeper part of the section can be validly extrapolated through the missing section, then an estimate may be made of the thickness of the eroded section. The ninety-five per cent confidence interval

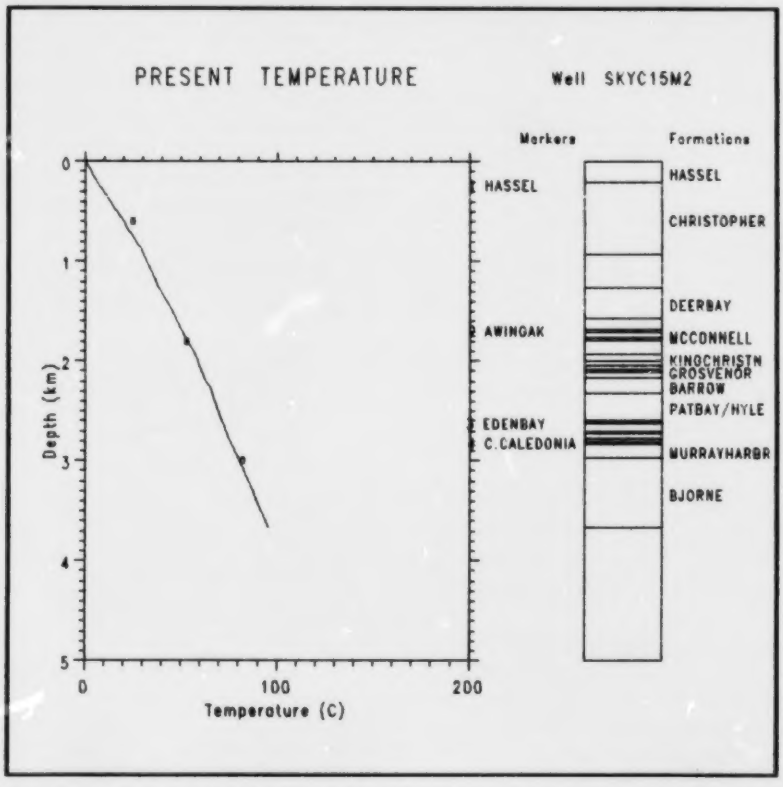

Figure 2. Skybattlebay C-15 well. Calculated present temperature variation with depth (solid line) compared to corrected bottomhole temperature (symbols). Present temperature is calculated for thermal conductivity distribution given in Figure 3 and an assumed basal heat flow of q = 48.16 mW/m^{-2}

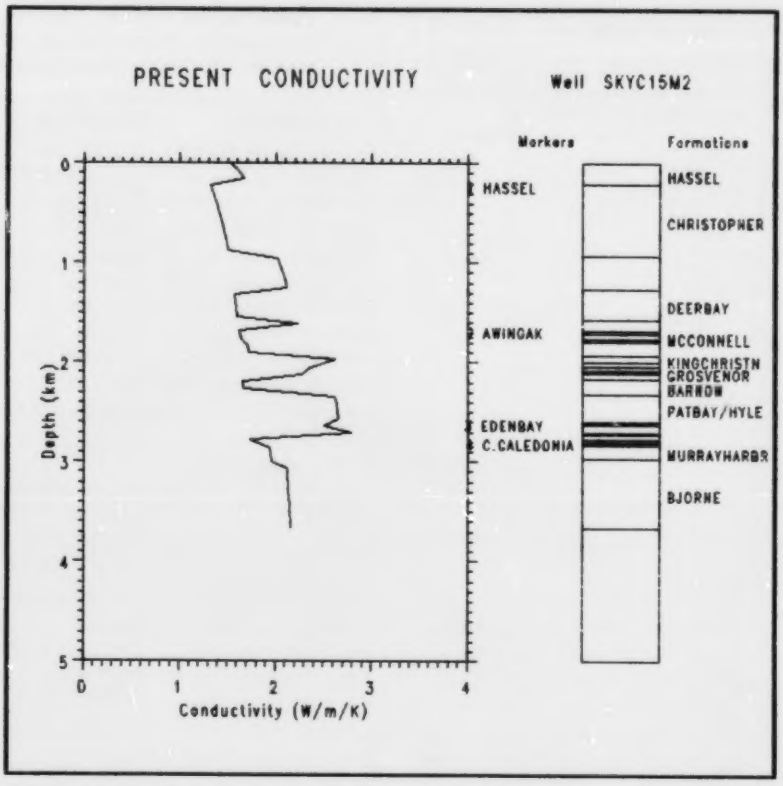

Figure 3. Skybattle Bay C-15 well. Present thermal conductivity distribution calculated by MATOIL program for observed lithology (used to calculate mean solid conductivity) and using average present porosity distribution obtained from the relationship:

$$1/[\text{porosity}(Z)] = L \times Z + 1/[\text{porosity}(Z = 0)]$$

where Z = depth (km), L = compaction factor (km^{-1})
$L = 1.741\ km^{-1}$ and porosity ($Z = 0$) = 0.56 (i.e. surface porosity = 56%).

is also plotted for the log-linear fit and gives an estimate of erosion of 1900 (+900/−815)m at an Ro of 0.25 per cent. The estimate of missing section from the data of Balkwill et al. (1982) of 500 to 700m is seen to lie outside of this range. However, it remains unclear as the whether a log-linear extrapolation from deeper horizons is valid for fitting a trend to reflectance values at depths of less than about 1000 m. Another possible complication is the observation that for many of the wells in the Sverdrup Basin, near-surface Ro values are typically high, in the 0.4 to 0.5 per cent range, as compared to the 0.20 to 0.25 per cent range of values expected for near surface vitrinites. This may indicate a substantial amount of missing eroded section; alternatively, a reworked component in the measured reflectance may be indicated. In addition, iron-carbonates (siderite concretions) are commonly found in surface (and deeper) formations (A.F. Embry, pers. comm.). Oxidative alteration by association with the carbonates is then suggested as a possible cause of the high near-surface Ro values.

Vitrinite reflectance grade evolution in near-surface sediments probably occurs under conditions of higher temperature gradients than for deeper horizons. In a study of over thirty wells, in a profile across the Sverdrup Basin, Jones et al. (1989, Fig. 6) have found a systematic change in temperature gradient with depth. At depths shallower than about 800 m, temperature gradients are as high as 45 mK/m, gradually decreasing to about 20 mK/m at depths of about 3000 m. This could be due in part to the expected increase in thermal conductivity with increasing depth. Such a variation is modelled in the MATOIL calculations presented in the next section. Since an average porosity-depth function, decreasing from about 60 per cent at the surface to about 10 per cent at total depth, is used in MATOIL to calculate thermal conductivity, thermal conductivity (Fig. 3) is seen to increase with depth over and above changes due to changes in lithology. Accordingly, the calculated temperature gradient varies from about 20 mK/m at depth to about 35 mK/m at the present surface.

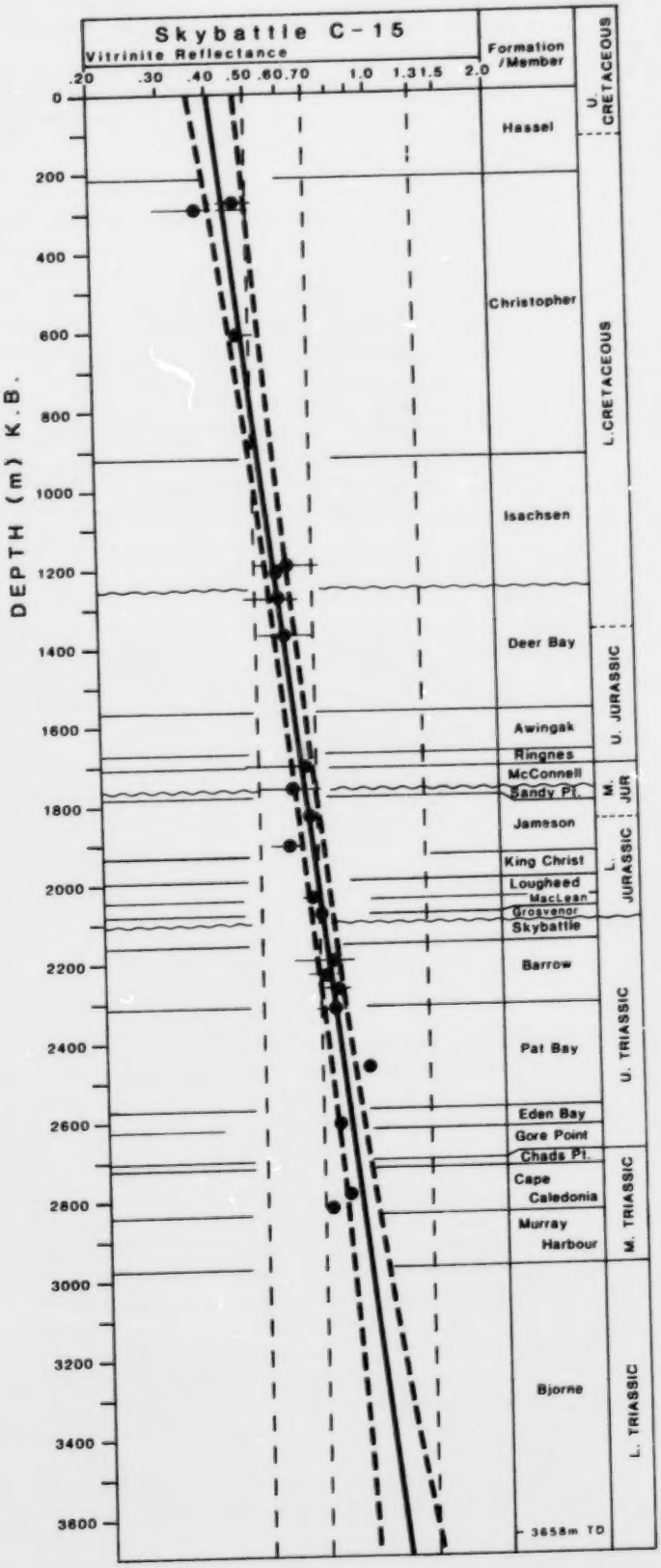

Table to accompany Figure 4. From Mesozoic Stratigraphic Nomenclature, Western and Central Sverdrup Basin. Embry (in press)

GROUP	FORMATION	MEMBER
Eureka Sound		
	Hassel	
	Christopher	MacDougall Point, Invincible Point
	Isachsen	Walker Island,
	Deer Bay	Rondon, Patterson
	Awingak	Island
	Ringnes	
	McConnel Island	
	Sandy Point	
	Jameson Bay	Snowpatch, Cape Canning
Heiberg		
	King Christian	
	Lougheed Island	
	Maclean Strait	
	Grosvenor Island	
Schei Point		
	Barrow	
	Pat Bay	
	Hoyle bay	Eden Bay
	Roche Point	Gore Point
		Chads Point
		Cape Caledonia (Eldridge Bay equiv.)
	Murray Harbour	
	Bjorne	

Figure 4. Observed vitrinite reflectance vs. depth, Panarctic et al. Skybattle Bay C-15 drillhole. The log-linear least squares fit to the data is shown (solid line) and the 95 per cent confidence limits are given by the dashed lines.

MATOIL MODELS

Three cases were calculated for the input conditions previously described. Results were calculated for three values of time-invariant component of heat flow. These results are plotted in Figure 5. For comparison, Table 3 is a summary of log-linear trends (95 per cent confidence level) fitted to these three solutions. The 40 mW/m^2 case can be rejected on the grounds that the present surface value, Ro, is far outside the 95 per cent confidence interval for a log-linear fit to observed values, while the 60 mW/m^2 case is seen to give a log-reflectance gradient steeper than that of sample measurement. The 50 mW/m^2 case satisfies these criteria and also, as mentioned, is a value in reasonable accord with estimates of bottom-hole temperatures, thermal conductivity estimates and calculated heat-flow from Jones et al. (1989).

Table 3. Least-squares coalification gradients

Observed			
Log-Reflectance Gradient (km^{-1}) : 0.11 +/− .02			
Ro (%) value:			
at present surface : 0.41 +/− .04			
at 1200 m : 0.53 +/− .06			
at 3658 m (T.D.) : 1.04 +/− .12			
Calculated			
MATOIL Models			
Base heat flow (mW/m^{-2})	40	50	60
Log Reflectance Gradient (km^{-1}) :	0.10	0.13	0.18
(+/−)	(.005)	(.005)	(.005)
Ro(%) value:			
at present surface :	0.34	0.37	0.39
(+/−)	(.005)	(.004)	(.010)
at 1200 m :	0.44	0.54	0.64
(+/−)	(.005)	(.005)	(.012)
at 3659 m (T.D. :	0.78	1.12	1.71
(+/−)	(.005)	(.005)	(.012)

HYDROCARBON GENERATION: KINETIC MODELS

The MATOIL program models the primary cracking of kerogen to oil + gas + residue and simultaneous secondary cracking of the hydrocarbon phase to gas plus residual oil. The primary cracking reaction is characterized by up to twelve parallel elementary reactions, according to the first-order kinetics model for kerogen types of Tissot amd Espitalie (1975). Each reaction is modelled according to a constant activation energy and an initial hydrocarbon potential, with the same frequency factor (Arrhenius constant) for all reactions. The secondary cracking of oil into gas is modelled by a single first-order reaction with a constant activation energy and frequency (Arrhenius) factor and a reaction yield (mg/g hydrocarbon) that depends upon kerogen type (the reaction also includes condensate cracking). All of these mentioned maturation reactions may be calibrated against laboratory experiments (e.g., Rock-Eval, closed capsule, or hydrous-pyrolysis measurements). In particular, the kinetic parameters of the primary cracking reaction may be obtained from specially processed Rock-Eval analyses; for example, use can be made of the OPTIM procedure of Ungerer and Pelet (1987) performed on immature samples of source rocks. For this report, we have used the given default data file of parameters for standard types of organic matter, as first defined by Tissot and Espitalié (1975) and recalibrated in the MATOIL program for three source rock samples considered representative of the three main types of organic matter. In addition, use was made of the default data file of average values for secondary cracking parameters, thought valid in a first approximation for every organic matter type, and recalibrated by the IFP from laboratory and geochemical data for the three kerogen

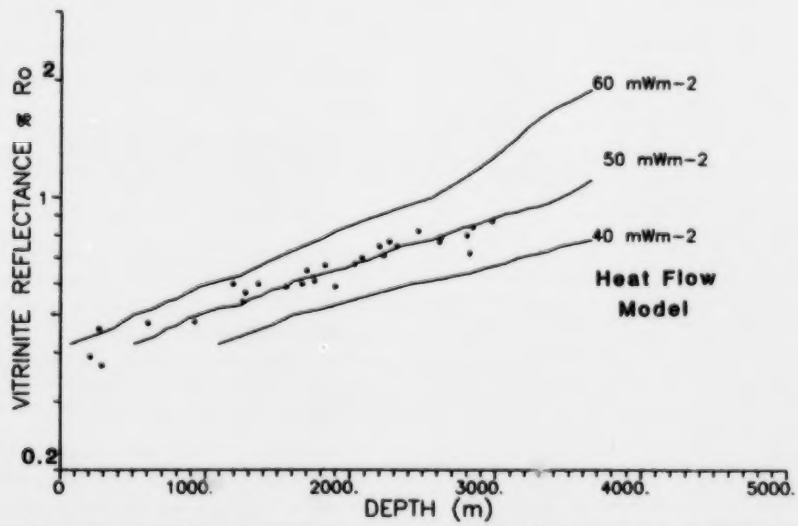

Figure 5. Calculated coalification gradients using Matoil solutions. Calculated vitrinite reflectance vs. depth for three cases of constant basal heat flow (solid lines).

classes considered. For calculation of vitrinite reflectance grade and as a standard for all formations chosen for the computation of the oil window, we have used the Type IV, twelve-component kinetic model (vitrinite, Lower Jurassic, North Sea) plus the correlation between TR (Transformation Ratio) of Type IV kerogen and vitrinite reflectance as given by the MATOIL default data file. (Transformation Radio is defined as the fraction of reacted kerogen at a given level of thermal maturity.)

Using the kinetic parameters for Type IV kerogen and the reflectance correlation discussed above and given in Table 4, the oil window is calculated and plotted on the burial history plot, for selected marker horizons of the Skybattle C-15 well, in Figure 6. As shown on the figure, the main source-rock horizons, the Eden Bay and Cape Caledonia, entered the oil window at bout 69 and 75 Ma, respectively. Peak oil generation (about 50 per cent conversion of kerogen to oil) has not been attained by the Eden Bay horizon and is only approached at present by the somewhat older and more productive (11 kg/t source rock at present) Cape Caledonia source rock. Although the two source rock are of comparable quality and richness, the older horizon has attained a greater level of maturation and hence present productivity.

Table 4. Parameters for calculation of vitrinite reflectance from thermal history[1]

Kinetic parameters for Type IV kerogen diagenesis		Correlation: Transformation ratio (TR) Type IV kerogen vs. Ro %	
Primary Cracking:			
Activation energy (kcal/mole)	Initial petroleum potential	Ratio: HC/OM (per cent)	Vitrinite reflectance Ro (%)
48	4	1.00	0.40
50	4	2.50	0.47
52	5	5.00	0.55
54	10	10.00	0.68
56	28	15.00	0.76
58	20	20.00	0.83
60	13	25.00	0.88
62	9	30.00	0.93
64	7	35.00	0.99
66	5	40.00	1.04
68	4	45.00	1.10
70	4	50.00	1.18
		60.00	1.45
Total:	113	65.00	1.65
		70.00	1.87
Arrhenius factor = Ai		75.00	2.10
all Ai = 0.596 E + 15		80.00	2.35
		90.00	3.25
		95.00	4.20
Secondary cracking:			
Activation energy = 57 kcal/mole			
Arrhenius factor = 3.0 E + 14s-1			
Reaction yield = 550 mg gas/g HC			
(includes condensate cracking)			

[1] In J. Espitalié. Use of Tmax as a maturation index for different types of organic matter. Comparison with vitrinite reflectance; *in* Thermal Modelling in Sedimentary Basins (1986) J. Burrus (ed.), Ed. Technip, p. 475-496.

Results from the calculations for MATOIL default kinetic parameters used can be compared to Rock-Eval data given in Table 1. Calculated Transformation Ratio or equivalently, Hydrogen Index can be plotted as a function of calculated vitrinite reflectance grade. Such a plot is given in Figure 7. Measured values are plotted for the Skybattle C-15 well as well as the remainder of the drillholes in the Lougheed Island area. It can be seen that the majority of the source rock observations fall within the Type I — Type II kerogen trends. However, the results in Figure 7, and Matoil model calculations for Types I and II kerogens, indicate a conversion of between about 20 per cent for Type I to about 50 per cent for Type II kerogen. Therefore it could be expected that a substantial quantity of hydrocarbons should have been generated (i.e., the size of the S1 measurements should be from 25 per cent to 100 per cent of the S2 peaks for the Rock-Eval measurements in Table 1.)

The low values for Production Index or for the S1 peak in Table 1, do not agree with model predictions nor with the remainder of the experimental data. Further work is in progress to establish whether this apparent deficiency of generated hydrocarbons coule be due to expulsion and migration of generated hydrocarbons out of the source rock.

DISCUSSION

The best-fit line to reflectance data is generally coincident with the predicted reflectance profile for heat-flow of 50 mW/m^2. However, the slope of the observed log-linear trend is shallower than calculated model trends, particularly at shallow depths. For the observed data, the best-fit line intersects the line predicted by the 60 mW/m^2 model at approximately 100 m depth. In addition, the prediction of the 60 mW/m^2 model enters the 95 per cent confidence envelope of the observed data for depths of less than 700 m.

The 40 mW/m^2 model does not intersect the 95 per cent confidence envelope of the observed data over the depth range of the observed data and so accordingly is rejected.

It is concluded that 50 mW/m^2 represents a reasonable model of the observed data for values below 700 m current depth.

If the effective paleogeothermal gradient is calculated from the Middleton (1982) relation (Z = depth)

$$dT/dZ = 194.8^* \, d[\log(\%\ Ro)]/dZ$$

then the effective paleogeothermal gradient for the observed coalification gradient of 0.11 km^{-1} is 21.4 +/−3.9 deg. C/km. This value is on the lower range of one geothermal gradient estimate for the Skybattle C-15 well of 24 +/−4 mk/m (Jones et al., 1989), but nonetheless is surprisingly close in view of the uncertainties in interpretation of both vitrinite reflectance and bottom-hole temperature data.

Although a 10 per cent variation in heat flow about an assumed base value has been included in thermal histories considered here, work in progress on regional variation in coalification gradients in the Lougheed Island area (not reported here) indicates that the degree of coalification often

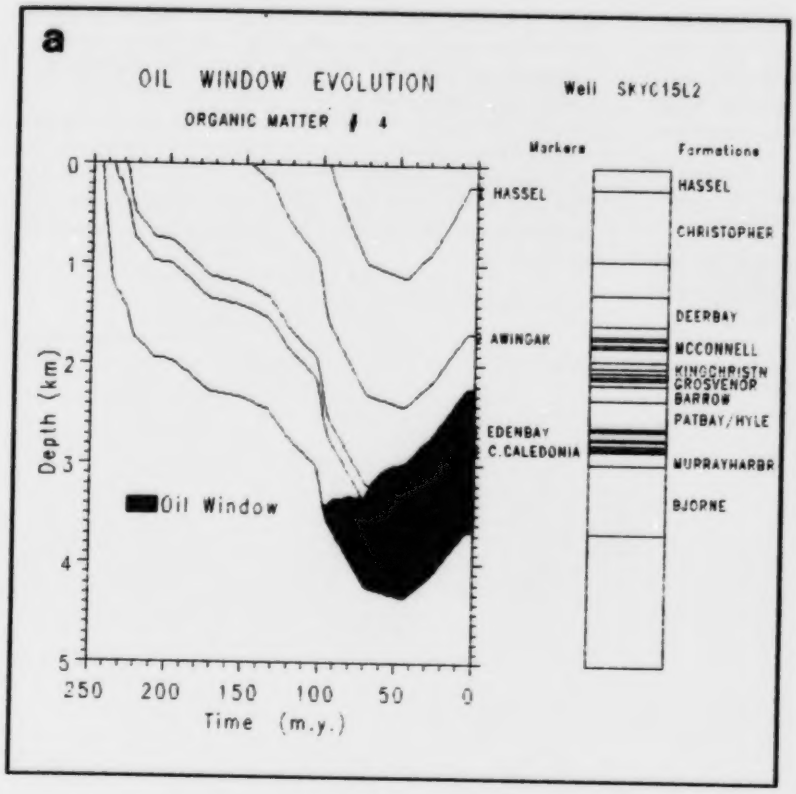

Figure 6. Skybattle Bay C-15 drillhole MATOIL results: **(a)** Geological subsidence history (burial history): selected marker horizons. Oil window calculated according to vitrinite reflectance grade evolution using kinetic parameters in Table 4. **(b)** Fraction of initial kerogen converted to hydrocarbons as a function of time for source rock horizons and kerogen types indicated.

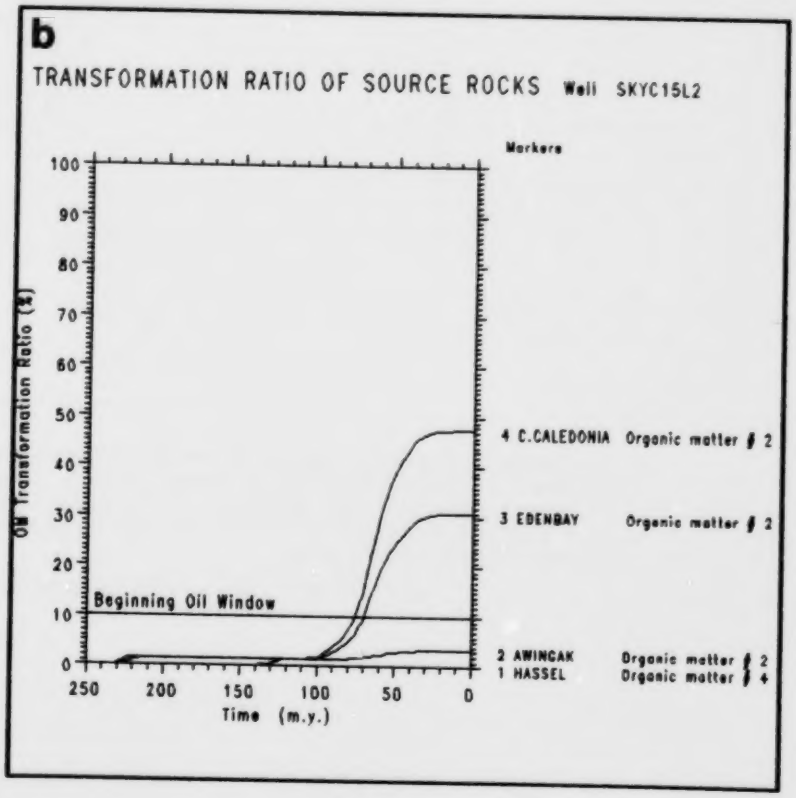

follows stratigraphic contacts and so was probably acquired at the time of maximum burial. Thus we can infer that geothermal gradients have changed only in accord with changes in subsidence rate and thermal conductivity, while heat flow has changed little since the time of maximum burial.

ACKNOWLEDGMENTS

It is a pleasure to acknowledge the work of B. Gorham, and R. Fanjoy at the ISPG in providing Rock-Eval data and computer processed data files and graphics, as well as the work of Carol Boonstra and the staff of the Cartography and Photomechanical Sections, ISPG, in producing the figures. Constructive and valuable reviews were provided by D. Issler and A.F. Embry. We wish to especially acknowledge the long standing support to this project from A.F. Embry, L.R. Snowdon and T. Gentzis. We are especially grateful to K.R. Stewart, Arctic Geochem Consultants, Calgary, for his work and essential contributions made during all stages of this project.

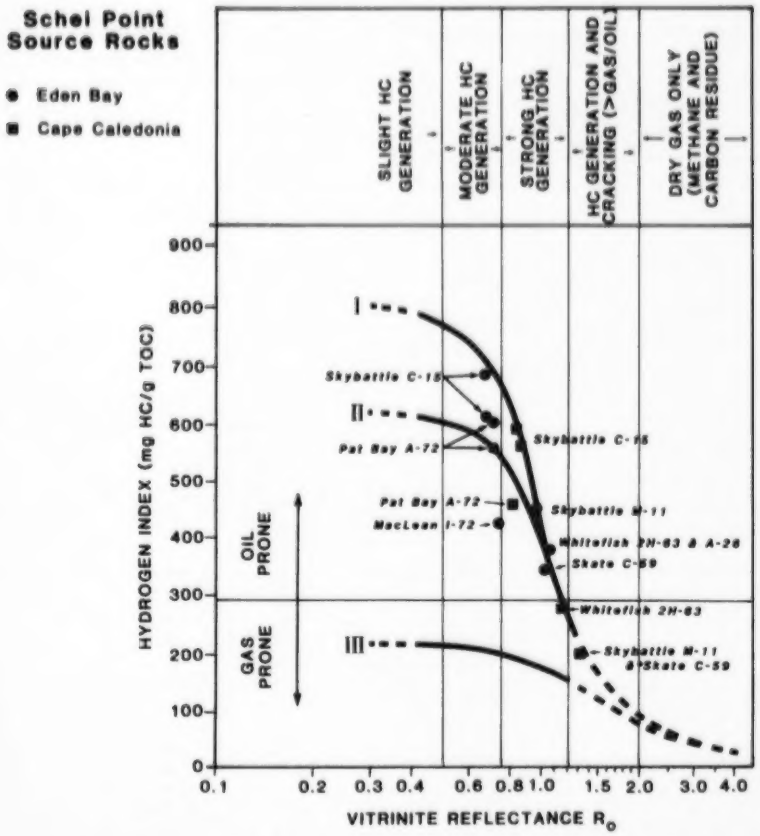

Figure 7. Hydrogen Index (HI) vs. vitrinite reflectance grade shown for two major source rock horizons for Lougheed Island area drillholes. Trends of the three kerogen types (solid lines) are from Orr (1981). Dashed lines give the calculated trends from MATOIL kinetic models. The relation between Transformation Ratio (TR) and HI is:

$$HI = (1\text{-}TR)HIo,\ HIo = \text{initial Hydrogen Index.}$$

REFERENCES

Balkwill, H.R., Hopkins, W.S. Jr., and Wall, J.H.
1982: Geology of Lougheed Island and nearby small islands, District of Franklin; Geological Survey of Canada, Memoir 395.

Embry, A.F.
in press: Mesozoic history of the Arctic Islands; *in* Innuitian Orogen and Arctic Platform: Canada and Greenland, H.P Trettin, (ed.); Geological Survey of Canada, Geology of Canada, no. 3.

Haq, B.U., Hardenbol, J., and Vail, P.R.
1987: Chronology of fluctuating sea levels since the Triassic; Science, v. 235, p. 1156-1167.

Jones, F.W., Majorowics, J.A., and Embry, A.F.
1989: A heat flow profile across the Sverdrup Basin, Canadian Arctic Islands; Geophysics, v. 54, p. 171-180.

Middleton, M.F.
1982: Tectonic history from vitrinite reflectance; Geophysical Journal of the Royal Astronomical Society, v. 68, p. 121-132.

Orr, W.L.
1981: Comments on pyrolytic hydrocarbon yields in source-rock evaluation; Advances in Organic Geochemistry, 1981, p. 775-787.

Reideger, C.L., Bustin, R.M., and Rouse, G.E.
1984: New evidence for the chronology of the Eurekan Orogeny from south-central Ellesmere Island; Canadian Journal of Earth Sciences, v. 21, p. 1286-1295.

Royden, L.
1986: A simple method for analyzing subsidence and heat flow in extensional basins; *in* Thermal modelling in Sedimentary Basins, J. Burrus (ed.); Editions Technip, Paris, p. 49-73.

Tissot, B. and Espitalié, J.
1975: L'évolution thermique de la matière organique des sédiments: applications d'une simulation mathématique; Revue Institute français du Pétrole, v. 30, p. 743-777.

Ungerer, P. and Pelet, R.
1987: Extrapolation of the kinetics of oil and gas formation from laboratory experiments to sedimentary basins; Nature, v. 327, no. 6117, p. 52-54.

Correlation of the lower Middle Devonian *Elenisporis biformis* spore subzone in Arctic Canada and the U.S.S.R.

A.D. Arkhangelskaya[1], D.C. McGregor, and J.B. Richardson[2]
Institute of Sedimentary and Petroleum Geology, Ottawa

*Arkhangelskaya, A.D., McGregor, D.C., and Richardson, J.B., Correlation of the lower Middle Devonian **Elenisporis biformis** spore subzone in Arctic Canada and the U.S.S.R.; in Current Research, Part D, Geological Survey of Canada, Paper 90-1D, p. 213, 1990.*

Abstract

Early Devonian spores typical of the Elenisporis biformis *Subzone of A.D. Arkhangelskaya occur in an upper tongue of the Strathcona Fiord Formation on southwestern Ellesmere Island, Arctic Canada. This discovery enables direct biostratigraphic correlation to be made for the first time at the subzonal level between lower Eifelian terrigenous strata of the Canadian Arctic and the European U.S.S.R., and between units of the independently developed Russian and non-Russian spore zonal scales. The* E. biformis *Subzone includes the upper Biya (probably) and lower Afonino horizons of the Urals, and the upper Ryazhsk and lower Morsovo horizons of the central region of the Russian Plate. It correlates with the lower part of the* velata-langii *Zone.*

Résumé

Des spores du Dévonien inférieur, typiques de la sous-zone à Elenisporis biformis *de A.D. Arkhangelskaya se trouvent dans un biseau supérieur de la formation de Strathcona Fiord dans le sud-ouest de l'île d'Ellesmere (Arctique canadien). Cette découverte permet d'établir pour la première fois une corrélation biostratigraphique directe au niveau de la sous-zone entre des couches terrigènes de l'Eifélien inférieur de l'Arctique canadien et de l'URSS européen et entre des unités des échelles de zonation des spores élaborées isolément en Russie et ailleurs. La sous-zone à* E. biformis *comprend les couches supérieures de Biya (probablement) et inférieures d'Afonino, dans l'Oural, et les couches supérieures de Ryazhsk et inférieures de Morsovo de la région centrale de la plaque russe. Elle correspond à la partie inférieure de la zone à* velata-langii.

[1] All-Union Scientific Research Institute of Petroleum and Geological Exploration, (VNIGNI), shosse Entuziastov 124, 105275 Moscow, U.S.S.R.

[2] British Museum (Natural History), Cromwell Road, London SW7 5BD, England

INTRODUCTION

Spores are widely used for local, interregional and intercontinental biostratigraphic correlation of Devonian rocks. This report concerns an example of intercontinental correlation, made possible by the recent discovery of the lowest Middle Devonian spore subzone of the Russian Plate in Devonian strata of Arctic Canada.

In October 1986, at a workshop at the British Museum (Natural History) in London, the authors compared Devonian spore assemblages of the U.S.S.R. and Canada. One of the results was the discovery of the *Elenisporis biformis* Subzone in the Strathcona Fiord Formation in the Queen Elizabeth Islands of Arctic Canada (Fig. 1).

THE *ELENISPORIS BIFORMIS* SUBZONE

The *E. biformis* Subzone is part of the first palynological zonal scale established for the upper Emsian and the Eifelian of the European U.S.S.R. by Arkhangelskaya (1972, 1985). This zonation was developed to assist in resolving the disputed question of interregional correlation of Devonian deposits of many facies in the central and eastern regions of the Russian Plate. For this purpose, the stratigraphic ranges of selected species were determined and traced across the Russian Plate. Quantitative differences in species content related to lithofacies and geographic position were also analyzed.

PLATE 1

Figures d, i, and k, x500; others, x750. The name of the species is followed by the slide number, England Finder coordinates, and GSC type number. All specimens are from GSC locality C-084874.

Figure a. *Elenisporis biformis* (Arkhangelskaya) Arkhangelskaya 1985; 24, R70/3, GSC 96771.
b. *Apiculiretusispora gaspiensis* McGregor 1973; 25, L53/1, GSC 96772.
c. *Camptozonotriletes aliquantus* Allen 1965; 25, P68/3, GSC 96773.
d. *Auroraspora aurora* Richardson 1960, 11, R67/4, GSC 96774.
e. *Emphanisporites annulatus* McGregor 1961; 25, J59/3, GSC 96775.
f. *Emphanisporites schultzii* McGregor 1973; 11, 68U/3, GSC 96776.
g. *Gneudnaspora divellomedium* (Chibrikova) Balme 1988; 11, V41/1, GSC 96777.
h. *Lophotriletes portentosus?* Arkhangelskaya 1972; 25, S41/4, GSC 96778.
i. *Periplecotriletes tortus* Egorova 1974; 1, Q61/4, GSC 96779.
j. *Retusotriletes rugulatus* Riegel 1973; 25, 071, GSC 96780.
k. *Grandispora velata* (Eisenack) Playford 1971; 24, 049/1, GSC 96781.
l. *Sinuosisporis sinuosus* (V. Umnova) Arkhangelskaya 1985; 25, T49/1, GSC 96782.
m. *Rhabdosporites mirus* Arkhangelskaya 1985; 25, F45, GSC 96783.
n. *Reticulatisporites vulgaris* (Arkhangelskaya) Arkhangelskaya 1985; 1, N45/3, GSC 96784.

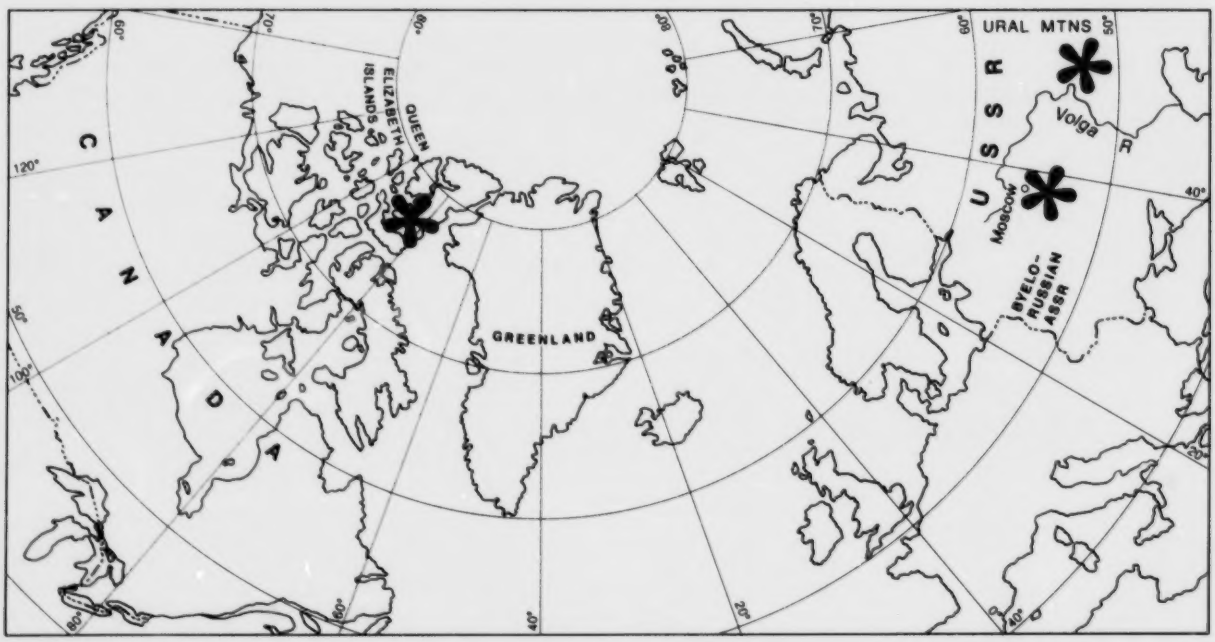

Figure 1. Geographic location of strata containing spores of the *Elenisporis biformis* Subzone. The Canadian site is GSC locality C-084874.

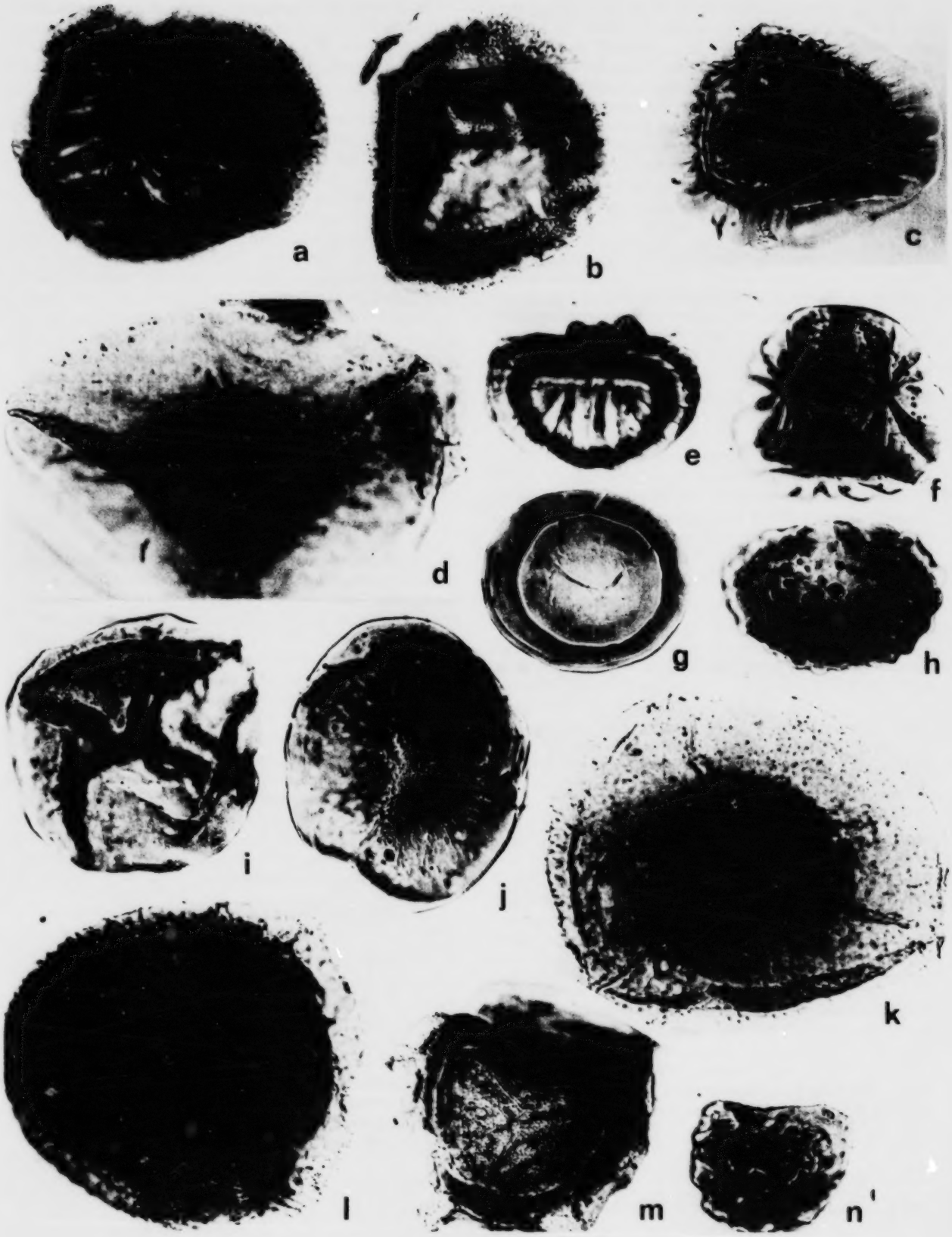
a
b
c
d
e
f
g
h
i
j
k
l
m
n'

For the first time in the study of the Devonian of the U.S.S.R., qualitative changes in species content have been used for spore zonation at the subzonal level. Previously, the palynologists of the U.S.S.R. used changes in the abundance of predominant spore species as indicators for subdivision and correlation. However, correlations based on quantitative methods have not proved totally effective, and in some instances have resulted in mistakes, because spore abundance may vary in different facies owing to sedimentary, taphonomic and other factors. Consequently, the results may not accurately indicate stratigraphic position or synchroneity.

The *E. biformis* Subzone is the lower part of the *Periplecotriletes tortus* Zone. It is both a range zone of the eponym *E. biformis* (Arkhangelskaya) Arkhangelskaya 1985, and a concurrent range zone consisting of the species *Auroraspora aurora* Richardson 1960, *Grandispora velata* (Eisenack) Playford 1971[1], *Retusotriletes fragosus* Arkhangelskaya 1972, *R. rugulatus* Riegel 1973, and *Sinuosisporis sinuosus* (V. Umnova) Arkhangelskaya 1985, which first appear in the subzone; and *Apiculiretusispora gaspiensis* McGregor 1973, *Brochotriletes triquetrus* Arkhangelskaya 1972, *Camptozonotriletes aliquantus* Allen 1965, *Emphanisporites annulatus* McGregor 1961, *E. schultzii* McGregor 1973, *Lophotriletes portentosus* Arkhangelskaya 1972, *Reticulatisporites vulgaris* (Arkhangelskaya) Arkhangelskaya 1985, and *Rhabdosporites mirus* Arkhangelskaya 1985, which have not been discovered above this subzone.

In the eastern region of the Russian Plate, between the Volga River and the Urals (Fig. 1), spores of the *E. biformis* Subzone have been discovered in boreholes in the Udmurtian and Bashkirian Soviet Autonomous Republics, as well as in Orenburg Province: boreholes Zhuravlyevo-Stepanovka No. 3, 2500-2504 m; Zaglydino No. 137, 2443-2449 m; Shalty No. 19, 2212-2217 m; Arkhaevska No. 71, 2030-2034 m; Ermikeyevo No. 11, 1976-1982 m; Stakhanovo-Baltapkan No. 13, 1940-1946 m; Syumsi No. 310, 1785-1796 m; and others.

In this region, the *E. biformis* Subzone accords with the upper part of the Biya Horizon (probably) and the lower part of the Afonino Horizon. At present the conodont data for this interval are limited (Khalymbadzha et al., 1985; Baryshev, 1983). The *E. biformis* Subzone may correlate with part of the stratigraphic interval from the upper *patulus* Zone to the *costatus* Zone in the Urals, and thus be close to the Lower/Middle Devonian boundary.

In the central region of the Russian Plate, between the Volga River and the Byelorussian ASSR (Fig. 1), spores of the *E. biformis* Subzone were found in sections from the following boreholes in Tula, Moscow, and Ryasan provinces: Tula No. 121400, 923-928 m; Serpukhov No. 1, 1051-1058 m; Novobasovo No. 3, 928-943 m; Ryazhsk No. 1, 912-920 m; and others.

In this region the subzone includes the upper, thinner part of the Ryazhsk Horizon and the lower part of the Morsovo Horizon as originally defined by Filippova (in Filippova et al., 1958). These deposits do not contain definitive faunas.

The spore assemblage of the *E. biformis* Subzone in the central and eastern regions comprises more than 80 species, among them numerous species of the genera *Acinosporites* Richardson 1965, *Apiculiretusispora* Streel 1964, *Dibolisporites* Richardson 1965, *Hymenozonotriletes* Naumova ex Mehta 1944 (sensu Potonié 1958), *Periplecotriletes* Naumova ex Ishchenko 1952, *Retusotriletes* Naumova emend. Streel 1964, and *Sinuosisporis* Arkhangelskaya 1985. The eponymous (index) species, the concurrent species listed above, and *Gneudnaspora divellomedium* (Chibrikova) Balme 1988 and *Knoxisporites bonus* (Arkhangelskaya) Arkhangelskaya 1985, are in the minority. *Camptozonotriletes aliquantus* and *Emphanisporites schultzii* are rare. In the eastern part of the Russian Plate, small spores, such as *Granulatisporites muninensis* Allen 1965 and *Lophotriletes devonicus* (Naumova ex Chibrikova) McGregor and Camfield 1976, constitute a considerable percentage of the assemblage in comparison with the assemblage from the central region of the plate.

OCCURRENCE IN ARCTIC CANADA

A taxonomically diverse spore assemblage containing most of the characterizing species of the *E. biformis* Subzone of the Russian Plate occurs in a thin tongue of the Strathcona Fiord Formation 8 m above its contact with the Bird Fiord Formation. The studied sample was collected by R. Thorsteinsson 2 km east of the Bird Formation type section, east of Bird Fiord on southwestern Ellesmere Island in the Queen Elizabeth Islands, at Geological Survey of Canada locality C-084874 (Fig. 1). The following species characteristic of the *E. biformis* Subzone are present: *E. biformis*, *Apiculiretusispora gaspiensis*, *Auroraspora aurora*, *Brochotriletes triquetrus*, *Camptozonotriletes aliquantus*, *Emphanisporites annulatus*, *E. schultzii*, *Gneudnaspora divellomedium*, *Grandispora velata*, *Lophotriletes portentosus?*, *Periplecotriletes tortus* Egorova 1974, *Reticulatisporites vulgaris*, *Retusotriletes rugulatus*, *Rhabdosporites mirus*, and *Sinuosisporis sinuosus*.

Of the species that are used to define the *E. biformis* Subzone in the U.S.S.R., only *Knoxisporites bonus* and *Retusotriletes fragosus* have not yet been found in Canada.

No age-diagnostic faunas were found with the spores at locality C-084874. However, conodonts abut 200 m above the base of the Bird Fiord Formation 77 km to the southwest are in the interval of the *serotinus* to *costatus* zones (upper Emsian or lower Eifelian), and conodonts 165 to 194 m above the base of the Strathcona Fiord Formation 80 km to the east-northeast probably are referable to the *costatus* or *australis* zones (early or mid Eifelian; T.T. Uyeno, pers. comm., 1985 and 1986).

[1] JBR prefers Calyptosporites velatus (Eisenack) Richardson 1962

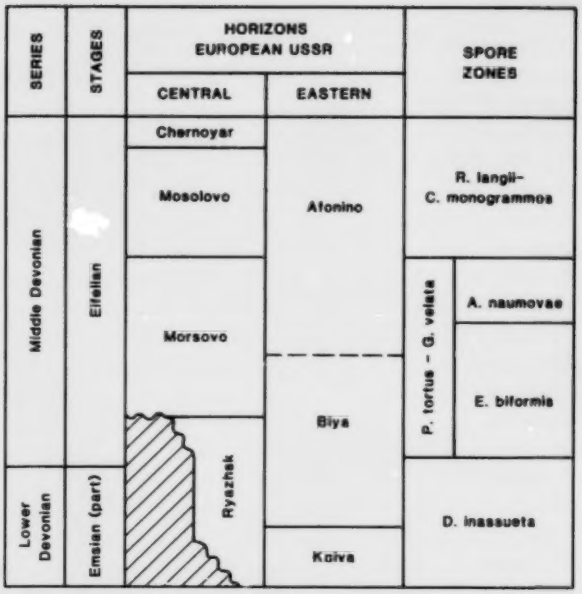

Figure 2. Correlation of horizons and spore zones of the central and eastern parts of the European U.S.S.R. Spore zones of Arkhangelskaya (1985).

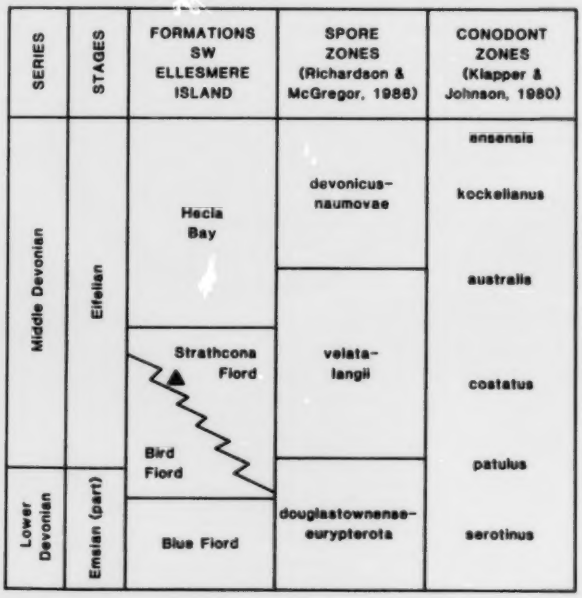

Figure 3. Biostratigraphic correlation of Emsian and Eifelian rocks, southwestern Ellesmere Island. The triangle indicates the approximate stratigraphic position of the sample from GSC locality C-084874.

CONCLUSIONS

The degree of similarity of the spore assemblages makes it possible to confirm the presence of the *E. biformis* Subzone in Arctic Canada. The position of this subzone in the northern hemisphere spore zonal scale of Richardson and McGregor (1986) may be fixed approximately. On the basis of present knowledge, the occurrence of *Grandispora velata* and the absence of *Rhabdosporites langii* and *Densosporites* spp. suggest a correlation with the lower part of the *velata-langii* Zone (Fig. 2). The base of the *E. biformis* Subzone probably is early Eifelian (Fig. 3), not late Emsian as assumed by Arkhangelskaya (1985) from the work of Tiwari and Schaarschmidt (1975).

The results of this work have enabled us for the first time to directly correlate terrigenous strata close to the Lower/Middle Devonian boundary in northern Canada and the European U.S.S.R. It is reasonable to expect that it will be possible to use spores to further correlate Devonian rocks of these two countries with a similar degree of temporal resolution.

REFERENCES

Arkhangelskaya, A.D.
1972: Palinologicheskaya kharakteristika nizhnikh gorizontov srednego devona vostochnoi chasti Russkoi platformy; Trudy VNIGRI 83, Paleontologicheskii Sbornik 4, Moskva, "Nedra", p. 124-143, 240.
1985: K utochneniyu granits otdelov, yarusov i pogorizontnoi mezhregional'noi korrelyatsii nizhnei chasti devona Russkoi platformy; *in* Srednii devon SSSR, ego granitsy i yarusnoe raschlenenie; Moskva, "Nauka", p. 173-178.
Baryshev, V.N.
1983: Konodonty srednego devona zapadnogo sklona Yuzhnogo Urala; *in* Srednii devon SSSR, ego granitsy i yarusnoe raschlenenie. Tezisy dokladov, Ufa, RTP BFAN SSSR, p. 19-20.
Filippova, M.F., Aronova, S.M., Afremova, M.F., et. al.
1958: Devonskie otlozheniya tsentral'nykh oblastei Russkoi platformy; Gostoptekhizdat, p. 405.
Khalymbadzha, N.G., Chernysheva, N.G., Baryshev, V.H.
1985: Biostratigrafiya srednego devona zapadnogo sklona Urala po konodontam; *in* Srednii devon SSSR, ego granitsy i yarusnoe raschlenenie. Moskva, "nauka", p. 69-74.
Klapper, G. and Johnson, J.G.
1980: Endemism and dispersal of Devonian conodonts; Journal of Paleontology, v. 54, p. 400-455.
Richardson, J.B. and McGregor, D.C.
1986: Silurian and Devonian spore zones of the Old Red Sandstone continent and adjacent regions; Geological Survey of Canada, Bulletin 364, 79 p.
Tiwari, R.S. and Schaarschmidt, F.
1975: Palynological studies in the Lower and Middle Devonian of the Prüm Syncline, Eifel (Germany); Abhandlungen der Senckenbergischen Naturforschenden Gesellschaft, v. 534, p. 1-129.

AUTHOR INDEX

Anderson, G.M. 47
Arkhangelskaya, A.D. 213
Beauchamp, B. 101, 115, 139
Benham, P.H. 179
Bower, M.E. 11
Brooks, P.W. 153
Burden, E.T. 179
Dechesne, R.G. 95
Edlund, S.A. 85
Eggington, P.A. 71
Fayerman, S. 153
Forsyth, D. 11
Gentzis, T. 187, 195
Goodarzi, F. 111, 153, 187, 195, 201
Grant, A.C. 17
Grasty, R.L. 31
Hardwick, C.D. 11
Hodgson, D.A. 67, 71
Holman, P.B. 31
Jerzykiewicz, T. 195
Lali, K. 187
Lamirande, J. 115
Lemmen, D.S. 79
Macnab, R. 1, 11
Marcotte, D.L. 11
McFarlane, R. 111
McGregor, D.C. 213
McMartin, I. 55
Mountjoy, E.W. 32, 95
Nelson, J.B. 11
Nowlan, G.S. 147
Osadetz, K.G. 123, 153, 165, 201
Pearson, D.E. 165
Qing, H. 37
Randell, R.N. 47
Richardson, J.B. 213
Sanford, B.V. 17
Savard, M. 101
Skibo, D.N. 201
Snowdon, L.R. 153
Srivastava, S.P. 1
St-Onge, D.A. 55
Stasiuk, L.D. 123, 165
Teskey, D. 11
Thorning, L. 11
Trettin, H.P. 147
Veizer, J. 101
Verhoef, J. 1
Wallace, C.A. 139
Woo, M. 85
Young, K.L. 85

Geological Survey of Canada, Paper 90-1, Current Research is published as six parts, listed below, that can be purchased separately.

Recherches en cours, une publication de la Commission géologique du Canada, Étude 90-1, est publiée en huit parties, énumérées ci-dessous; chaque partie est vendue séparément.

Part A, National and general programs
Partie A, Programmes nationaux et généraux

Part B, Eastern and Atlantic Canada
Partie B, Est et région atlantique du Canada

Part C, Canadian Shield
Partie C, Bouclier canadian

Part D, Interior Plaines and Arctic Canada
Partie D, Plaines intérieures et région arctique du Canada

Part E, Cordillera and Pacific Margin
Partie E, Cordillère et marge du Pacifique

Part F, Frontier Geoscience Program, Cordilleran and offshore basins, British Columbia
Partie F, Programme géoscientifique des régions pionnières, bassins de la Cordillère et extracôtiers, Colombie-Britannique